

Dynamics of Asia's and Australasia's forests in a changing world

Edited by

Nophea Sasaki, Ling Zhang, John Meadows,
Jeong-Wook Seo and Hans Juergen Boehmer

Published in

Frontiers in Forests and Global Change



FRONTIERS EBOOK COPYRIGHT STATEMENT

The copyright in the text of individual articles in this ebook is the property of their respective authors or their respective institutions or funders. The copyright in graphics and images within each article may be subject to copyright of other parties. In both cases this is subject to a license granted to Frontiers.

The compilation of articles constituting this ebook is the property of Frontiers.

Each article within this ebook, and the ebook itself, are published under the most recent version of the Creative Commons CC-BY licence. The version current at the date of publication of this ebook is CC-BY 4.0. If the CC-BY licence is updated, the licence granted by Frontiers is automatically updated to the new version.

When exercising any right under the CC-BY licence, Frontiers must be attributed as the original publisher of the article or ebook, as applicable.

Authors have the responsibility of ensuring that any graphics or other materials which are the property of others may be included in the CC-BY licence, but this should be checked before relying on the CC-BY licence to reproduce those materials. Any copyright notices relating to those materials must be complied with.

Copyright and source acknowledgement notices may not be removed and must be displayed in any copy, derivative work or partial copy which includes the elements in question.

All copyright, and all rights therein, are protected by national and international copyright laws. The above represents a summary only. For further information please read Frontiers' Conditions for Website Use and Copyright Statement, and the applicable CC-BY licence.

ISSN 1664-8714
ISBN 978-2-8325-5590-3
DOI 10.3389/978-2-8325-5590-3

About Frontiers

Frontiers is more than just an open access publisher of scholarly articles: it is a pioneering approach to the world of academia, radically improving the way scholarly research is managed. The grand vision of Frontiers is a world where all people have an equal opportunity to seek, share and generate knowledge. Frontiers provides immediate and permanent online open access to all its publications, but this alone is not enough to realize our grand goals.

Frontiers journal series

The Frontiers journal series is a multi-tier and interdisciplinary set of open-access, online journals, promising a paradigm shift from the current review, selection and dissemination processes in academic publishing. All Frontiers journals are driven by researchers for researchers; therefore, they constitute a service to the scholarly community. At the same time, the *Frontiers journal series* operates on a revolutionary invention, the tiered publishing system, initially addressing specific communities of scholars, and gradually climbing up to broader public understanding, thus serving the interests of the lay society, too.

Dedication to quality

Each Frontiers article is a landmark of the highest quality, thanks to genuinely collaborative interactions between authors and review editors, who include some of the world's best academicians. Research must be certified by peers before entering a stream of knowledge that may eventually reach the public - and shape society; therefore, Frontiers only applies the most rigorous and unbiased reviews. Frontiers revolutionizes research publishing by freely delivering the most outstanding research, evaluated with no bias from both the academic and social point of view. By applying the most advanced information technologies, Frontiers is catapulting scholarly publishing into a new generation.

What are Frontiers Research Topics?

Frontiers Research Topics are very popular trademarks of the *Frontiers journals series*: they are collections of at least ten articles, all centered on a particular subject. With their unique mix of varied contributions from Original Research to Review Articles, Frontiers Research Topics unify the most influential researchers, the latest key findings and historical advances in a hot research area.

Find out more on how to host your own Frontiers Research Topic or contribute to one as an author by contacting the Frontiers editorial office: frontiersin.org/about/contact

Dynamics of Asia's and Australasia's forests in a changing world

Topic editors

Nophea Sasaki — Asian Institute of Technology, Thailand

Ling Zhang — Jiangxi Agricultural University, China

John Meadows — University of the Sunshine Coast, Australia

Jeong-Wook Seo — Chungbuk National University, Republic of Korea

Hans Juergen Boehmer — University of the South Pacific, Fiji

Citation

Sasaki, N., Zhang, L., Meadows, J., Seo, J.-W., Boehmer, H. J., eds. (2024). *Dynamics of Asia's and Australasia's forests in a changing world*. Lausanne: Frontiers Media SA. doi: 10.3389/978-2-8325-5590-3

Table of contents

- 06 **Editorial: Dynamics of Asia's and Australasia's forests in a changing world**
Nophea Sasaki, Ling Zhang, John Meadows, Jeong-Wook Seo and Hans Juergen Boehmer
- 09 **Potential effects of surface ozone on forests in Gangwon Province, South Korea, based on critical thresholds**
Myeong-Ju Kim and Sang-Deok Lee
- 20 **Monoculture plantations impede forest recovery: Evidence from the regeneration of lowland subtropical forest in Hong Kong**
Huilong Zhu, Jinlong Zhang, Mang Lung Cheuk, Billy C. H. Hau, Gunter A. Fischer and Stephan W. Gale
- 34 **Perspective: Improving the accuracy of plant phenology observations and land-cover and land-use detection by optical satellite remote-sensing in the Asian tropics**
Nagai Shin, Chifuyu Katsumata, Tomoaki Miura, Narumasa Tsutsumida, Tomoaki Ichie, Ayumi Kotani, Michiko Nakagawa, Kho Lip Khooon, Hideki Kobayashi, Tomo'omi Kumagai, Shunsuke Tei, Runi anak Sylvester Pungga, Taizo Yamada, Akihiro Kameda, Masayuki Yanagisawa, Kenlo Nishida Nasahara, Hiroyuki Muraoka, Kazuhito Ichii and Yuji Tokumoto
- 50 **Dynamic variation of non-structural carbohydrates in branches and leaves of temperate broad-leaved tree species over a complete life history**
Kaibo Wang, Guangze Jin and Zhili Liu
- 62 **Mixed planting improves soil aggregate stability and aggregate-associated C-N-P accumulation in subtropical China**
Yaqin He, Qianchun Zhang, Chenyang Jiang, Yahui Lan, Han Zhang and Shaoming Ye
- 75 **Radiation and temperature dominate the spatiotemporal variability in resilience of subtropical evergreen forests in China**
Jinghua Chen, Shaoqiang Wang, Hao Shi, Bin Chen, Junbang Wang, Chen Zheng and Kai Zhu
- 87 **Bacterial and fungal inhibitor interacted impacting growth of invasive *Triadica sebifera* and soil N₂O emissions**
Xiaoqin Lai, Laicong Luo, Haifu Fang, Ling Zhang, Nasir Shad, Jian Bai, Aixin Li, Xi Zhang, Yadi Yu, Hao Wang and Evan Siemann
- 97 **Research on subsidy standards for public welfare forests based on a dynamic game model—Analysis of a case in Jiangxi, China**
Na Ding, Da Li, Shaowen Zhang, Kankan Shi and Wei Chen

- 106 **Elevation, aspect, and slope influence woody vegetation structure and composition but not species richness in a human-influenced landscape in northwestern Yunnan, China**
Zhongqian Cheng, Tuomas Aakala and Markku Larjavaara
- 118 **Influence of hydrothermal factors on a coniferous forest canopy in the semiarid alpine region of Northwest China**
Yonghong Zhao, Weijun Zhao and Huijun Fang
- 127 **Responses of economic and anatomical leaf traits to soil fertility factors in eight coexisting broadleaf species in temperate forests**
Mingyue Jin, Guangze Jin, Qingxi Guo and Zhili Liu
- 137 **Five-year measurement data along a 1200 m elevational gradient reveals that global warming increases soil respiration**
Soichiro Takeda, Ryota Majima, Naoki Makita and Koichi Takahashi
- 149 **Optimization of tropical rainforest ecosystem management: implications from the responses of ecosystem service values to landscape pattern changes in Hainan Tropical Rainforest National Park, China, over the past 40 years**
Xiaofu Lin and Hui Fu
- 166 **Are farmers willing to enter the forestry property market? Evidence from collective forest areas in southern China**
Yaqing Han, Qiangqiang Wang and Yuanzhu Wei
- 179 **Spatiotemporal approach for estimating potential CO₂ sequestration by reforestation in the Korean Peninsula**
Sle-gee Lee and Hyun-Jun Kim
- 189 **Soil uptake of isoprenoids in a *Eucalyptus urophylla* plantation forest in subtropical China**
Zhaobin Mu, Jianqiang Zeng, Yanli Zhang, Wei Song, Weihua Pang, Zhigang Yi, Dolores Asensio, Joan Llusà, Josep Peñuelas and Xinming Wang
- 199 **Intra-annual dynamic of opposite and compression wood formation of *Pinus massoniana* Lamb. in humid subtropical China**
Chunsong Wang, Zhuangpeng Zheng, Feifei Zhou, Xinsheng Liu, Patrick Fonti, Jiani Gao and Keyan Fang
- 209 **Mixed *Eucalyptus* plantations in subtropical China enhance phosphorus accumulation and transformation in soil aggregates**
Yuhong Cui, Yu Yan, Shengqiang Wang, Han Zhang, Yaqin He, Chenyang Jiang, Rongyuan Fan and Shaoming Ye
- 226 **Fire frequency, intensity, and burn severity in Kalimantan's threatened Peatland areas over two Decades**
Andres Schmidt, Lisa M. Ellsworth, Grace A. Boisen, Nisa Novita, Anjelita Malik, Adi Gangga, Israr Albar, Ati Dwi Nurhayati, Rasis Putra Ritonga, Adibtya Asyhari and J. Boone Kauffman

- 242 **Summer climate information recorded in tree-ring oxygen isotope chronologies from seven locations in the Republic of Korea**
En-Bi Choi, Jun-Hui Park, Masaki Sano, Takeshi Nakatsuka and Jeong-Wook Seo
- 252 **Modeling branch attributes and biomass for *Catalpa bungei* plantations under various fertilization regimes**
Zhuizhui Guan, Qingbin Zhang, Tiaozi Xu, Dong Chen, Yizeng Lu, Qingjun Han, Ningning Li, Wenjun Ma, Junhui Wang, Yan Su, Jiyue Li, Quan Qiu and Qian He



OPEN ACCESS

EDITED AND REVIEWED BY
Heather R. McCarthy,
University of Oklahoma, United States

*CORRESPONDENCE
Hans Juergen Boehmer
✉ boehmer@geobotanik.uni-hannover.de

RECEIVED 02 August 2024
ACCEPTED 17 September 2024
PUBLISHED 08 October 2024

CITATION
Sasaki N, Zhang L, Meadows J, Seo J-W and
Boehmer HJ (2024) Editorial: Dynamics of
Asia's and Australasia's forests in a changing
world. *Front. For. Glob. Change* 7:1474882.
doi: 10.3389/ffgc.2024.1474882

COPYRIGHT
© 2024 Sasaki, Zhang, Meadows, Seo and
Boehmer. This is an open-access article
distributed under the terms of the [Creative
Commons Attribution License \(CC BY\)](#). The
use, distribution or reproduction in other
forums is permitted, provided the original
author(s) and the copyright owner(s) are
credited and that the original publication in
this journal is cited, in accordance with
accepted academic practice. No use,
distribution or reproduction is permitted
which does not comply with these terms.

Editorial: Dynamics of Asia's and Australasia's forests in a changing world

Nophea Sasaki^{1,2}, Ling Zhang³, John Meadows⁴,
Jeong-Wook Seo⁵ and Hans Juergen Boehmer^{6,7*}

¹Natural Resources Management Program, Asian Institute of Technology, Klong Luang, Pathum Thani, Thailand, ²Sasin School of Management, Chulalongkorn University, Bangkok, Thailand, ³Jiangxi Key Laboratory of Subtropical Forest Resources Cultivation, College of Forestry, Jiangxi Agricultural University, Nanchang, China, ⁴Tropical Forests and People Research Centre, Forest Research Institute, University of the Sunshine Coast, Sippy Downs, QLD, Australia, ⁵Department of Wood and Paper Science, Chungbuk National University, Cheongju-si, Chungcheongbuk-do, Republic of Korea, ⁶Institute of Earth System Sciences (IESW) - Geobotany Section, Leibniz University Hannover, Hanover, Germany, ⁷School of Geography, Earth Science and Environment, University of the South Pacific, Suva, Fiji

KEYWORDS

air pollution, biodiversity conservation, climate change, carbon sequestration, forest fragmentation, forest soils, plantation forests, tree phenology

Editorial on the Research Topic

Dynamics of Asia's and Australasia's forests in a changing world

The world's forests are under extraordinary pressure. Increasingly frequent droughts (Alizadeh et al., 2020), more extreme heat (Hammond et al., 2022), more frequent and severe storms (Senf and Seidl, 2021; Seidl and Turner, 2022), tree decline and dieback from increased insect pressures (Sallé and Bouget, 2020), and other effects of global warming are taking their toll, as well as anthropogenic disturbance which is affecting pristine forests at an unprecedented speed (Stibig et al., 2014; Ferrante and Fearnside, 2020). Biological invasions contribute to the complexity of interacting challenges (Seebens et al., 2023). At the same time, foresters and the forest economy in total struggle to adapt to rapidly changing conditions to achieve sustainability (Raj et al., 2024).

When precipitation patterns, temperatures and light availability suddenly deviate significantly from the usual values, this can, for instance, result in increased tree mortality (Hartmann et al., 2018), reduced reproductive success and a shift in species and ecosystem ranges (Pouteau et al., 2018; O'Sullivan et al., 2021). Consequently, some forest ecosystems have become particularly vulnerable through synergistic effects of climate change (Boehmer, 2011), and provision of their ecosystem services such as freshwater retention and disaster risk reduction is likely to become more and more limited (Sudmeyer-Rieux et al., 2021). Additionally, long-term analysis by Schmidt et al. underscores the significant impact of fire frequency, intensity, and burn severity on Kalimantan's peatland areas, highlighting the need for comprehensive fire management strategies. Forest structure and dynamics under these conditions have now become one of the research fronts of ecology (Ehbrecht et al., 2021; Hammond et al., 2022; Boehmer and Galvin, 2024), and what is being worked out is as interesting as it is concerning (Engert et al., 2024).

Meanwhile, the Global Agreement reached at the 26th Conference of the Parties (COP26) to the UNFCCC, signed by over 100 world leaders, represents a significant commitment to restore forests by 2030. This landmark pledge, endorsed by countries representing 85% of the world's forests, aims to halt and reverse forest loss and land degradation. Such initiatives are crucial for addressing deforestation and promoting sustainable land use practices. They leverage the latest research in forest ecology,

conservation biology, and environmental science to ensure that forest management strategies are both sustainable and effective (UNFCCC, 2021). Thus, scientific research underpins these global agreements and initiatives, providing essential data and methodologies to guide effective policy and practice.

The Research Topic entitled “The Forest Science Regional Spotlight: Asia and Australasia” provides a snapshot of current research on forest ecosystems in this region where major issues have been highlighted since the 1970s (Collins et al., 1991; Huettl and Mueller-Dombois, 1993). The Research Topic of 21 articles explores various dimensions of forest science, offering critical insights that align with international efforts to combat deforestation, enhance biodiversity, and promote sustainable land use practices.

The Research Topic begins with a focus on carbon sequestration and the impact of climate change on forests. For instance, Mu et al. explore the role of soil in absorbing isoprenoids in a *Eucalyptus urophylla* plantation in subtropical China. This study highlights the importance of soil chemistry in carbon storage processes. Similarly, Lee and Kim examine the potential for reforestation to sequester CO₂ on the Korean Peninsula, offering a spatiotemporal approach that underscores reforestation’s role in mitigating climate change.

Ecosystem management and restoration practices are prominently featured in the Research Topic. Lin and Fu provide a comprehensive study on optimizing tropical rainforest ecosystem management in Hainan Tropical Rainforest National Park, China. Their research tracks changes in ecosystem service values over the past 40 years, providing valuable insights for future management practices. In a related study, Zhu et al. investigate the challenges posed by monoculture plantations in the regeneration of lowland subtropical forests in Hong Kong, advocating for more diverse planting strategies to enhance the recovery of this biologically important forest community. Guan et al. model the branch attributes and biomass for *Catalpa bungei* plantations under various fertilization regimes, offering insights into the impacts of fertilization on forest growth.

The intricate relationships between environmental factors and biological processes are examined in several studies. Takeda et al. reveal how global warming increases soil respiration across a 1200-meter elevational gradient, highlighting broader climate change impacts on soil processes. In addition, Lai et al. explore the complex interplay between microbial activity and the growth of the invasive plant *Triadica sebifera*, illustrating the multifaceted nature of ecosystem interactions. A study by Wang C. et al. examines the dynamics of opposite wood and compression wood formation in *Pinus massoniana*, revealing how mechanical stress influences xylem cell division and wood formation under varying climatic conditions. Moreover, the study by Choi et al. utilizes tree-ring oxygen isotope chronologies to reveal significant regional climate differences and their correlations with temperature and precipitation across the Korean Peninsula, providing a valuable reference for understanding rainfall variations in East Asia. Chen et al. show how radiation and temperature dominate the spatiotemporal variability in resilience of subtropical evergreen forests in China, emphasizing the influence of climatic factors on forest health.

Socioeconomic perspectives and policy implications are addressed through research on economic incentives and market dynamics. Han et al. analyze the willingness of farmers to enter the forestry property market in southern China, shedding light on the economic motivations behind forest conservation. Complementing this, Ding et al. present a dynamic game model to determine effective subsidy standards for public welfare forests in Jiangxi, China, providing a useful framework for designing sustainable forestry policies.

Biodiversity and ecosystem health are critical themes throughout the collection of this Research Topic. Cheng et al. study the effects of elevation, aspect, and slope on woody vegetation structure in northwestern Yunnan, China, providing insights into biodiversity conservation in human-altered landscapes. Meanwhile, Wang K. et al. examine the dynamic variation of non-structural carbohydrates in temperate broad-leaved trees, offering a deeper understanding of tree physiology and its response to environmental changes. Research by Jin et al. analyzes further into the responses of economic and anatomical leaf traits to soil fertility factors in eight coexisting broadleaf species in temperate forests, further contributing to our understanding of forest ecology.

The Research Topic also explores the effects of mixed planting and species interactions on forest health. He et al. demonstrate that mixed planting improves soil aggregate stability and aggregate-associated C-N-P accumulation in subtropical China, suggesting benefits for soil health and nutrient cycling. Cui et al. report that mixed *Eucalyptus* plantations enhance phosphorus accumulation and transformation in soil aggregates, underscoring the potential of mixed-species plantations for sustainable forest management.

Additional research highlights the influence of atmospheric conditions on forest ecosystems. For example, Kim and Lee investigate the potential effects of surface ozone on forests in Gangwon Province, South Korea, based on critical thresholds, revealing the impact of air pollution on forest health. Zhao et al. explore the influence of hydrothermal factors on a coniferous forest canopy in the semiarid alpine region of Northwest China, providing insights into the adaptive strategies of forests under varying climatic conditions. Finally, Shin et al. emphasize the importance of improving the accuracy of plant phenology observations and land-cover and land-use detection by optical satellite remote-sensing in the Asian tropics, showcasing the role of advanced technologies in forest monitoring and management.

This Research Topic underscores the importance of interdisciplinary approaches to understanding and managing forests in Asia and Australasia. From carbon sequestration to biodiversity conservation, these studies provide valuable knowledge that can help inform policy, guide sustainable management practices, and address the pressing challenges of climate change and ecological degradation.

We hope this Research Topic inspires further research and action toward preserving the vital forests of this region for future generations. The diversity and depth of these studies demonstrate the dynamic interplay between natural processes and human activities, highlighting the critical role forests play in maintaining ecological balance and supporting human well-being. Further, by aligning with global agreements such as the Paris Agreement and

the Sustainable Development Goals, this Research Topic aims to contribute to international efforts in environmental conservation and sustainable development.

Explore these insightful articles and join the ongoing conversation about forest science in Asia and Australasia [here](#).

Author contributions

NS: Writing – original draft, Writing – review & editing. LZ: Writing – review & editing. JM: Writing – review & editing. J-WS: Writing – review & editing. HJB: Writing – original draft, Writing – review & editing.

Funding

The author(s) declare that no financial support was received for the research, authorship, and/or publication of this article.

References

- Alizadeh, M. R., Adamowski, J., Nikoo, M. R., Kouchak, A. A., Dennison, P., and Sadegh, M. (2020). A century of observations reveals increasing likelihood of continental-scale compound dry-hot extremes. *Sci. Adv.* 6:eaz4571. doi: 10.1126/sciadv.aaz4571
- Boehmer, H. J. (2011). “Vulnerability of tropical montane rain forest ecosystems due to climate change,” in *Coping with Global Environmental Change, Disasters and Security – Threats, Challenges, Vulnerabilities and Risks*, eds. H. G. Brauch, Ü. Oswald Spring, C. Mesjasz, J. Grin, P. Kameri-Mbote, B. Chourou, et al. (Cham: Springer), 789–802.
- Boehmer, H. J., and Galvin, S. (2024). Climate-induced forest decline in the tropical Pacific islands – what do we really know? *Pacific Sci.* 77, 139–161. doi: 10.2984/77.2.2
- Collins, N. M., Sayer, J. A., and Whitmore, T. C. (1991). *The Conservation Atlas of Tropical Forests: Asia and the Pacific*. London: Macmillan Publishers Ltd.
- Ehbrecht, M., Seidel, D., Annighöfer, P., Kreft, H., Köhler, M., Zemp, D. C., et al. (2021). Global patterns and climatic controls of forest structural complexity. *Nat. Commun.* 12, 519. doi: 10.1038/s41467-020-20767-z
- Engert, J. E., Campbell, M. J., Cinner, J. E., Ishida, Y., Sloan, S., Supriatna, J., et al. (2024). Ghost roads and the destruction of Asia-Pacific tropical forests. *Nature* 629, 370–375. doi: 10.1038/s41586-024-07303-5
- Ferrante, L., and Fearnside, P. M. (2020). The Amazon’s road to deforestation. *Science* 369, 634. doi: 10.1126/science.abd6977
- Hammond, W. M., Williams, A. P., Abatzoglou, J. T., Adams, H. D., Klein, T., López, R., et al. (2022). Global field observations of tree die-off reveal hotter-drought fingerprint for Earth’s forests. *Nat. Commun.* 13, 1761. doi: 10.1038/s41467-022-29289-2
- Hartmann, H., Schuldt, B., Sanders, T. G. M., Macinnis-Ng, C., Boehmer, H. J., Allen, C. D., et al. (2018). Monitoring global tree mortality patterns and trends. Report from the VW symposium “Crossing scales and disciplines to identify global trends of tree mortality as indicators of forest health.” *New Phytologist* 217, 984–987. doi: 10.1111/nph.14988
- Huettl, R. F., and Mueller-Dombois, D. (1993). *Forest Decline in the Atlantic and Pacific Region*. Berlin, Heidelberg: Springer-Verlag.
- O’Sullivan, K. S. W., Ruiz-Benito, P., Chen, J.-C., and Jump, A. S. (2021). Onward but not always upward: individualistic elevational shifts of tree species in subtropical montane forests. *Ecography* 44, 112–123. doi: 10.1111/ecog.05334
- Pouteau, R., Giambelluca, T. W., Ah-Peng, C., and Meyer, J.-Y. (2018). Will climate change shift the lower ecotone of tropical montane cloud forests upwards on islands? *J. Biogeog.* 45, 1326–1333. doi: 10.1111/jbi.13228
- Raj, A., Jhariya, M. K., Banerjee, A., Lal, B., Mecherui, T., Devi, A., et al. (2024). “Forest for sustainable development,” in *Land and Environmental Management through Forestry*, 293–311.
- Sallé, A., and Bouget, C. (2020). Victims or perpetrators: Contribution and response of insects to forest diebacks and declines. *Ann. Forest Sci.* 77:104. doi: 10.1007/s13595-020-01009-0
- Seebens, H., Meyerson, L. A., Rahlao, S. J., Lenzner, B., Tricarico, E., Aleksanyan, A., et al. (2023). *IPBES Invasive Alien Species Assessment: Chapter 2. Trends and status of alien and invasive alien species: Thematic Assessment Report on Invasive Alien Species and their Control of the Intergovernmental Science-Policy Platform on Biodiversity and Ecosystem Services. (IPBES Invasive Alien Species Assessment)*.
- Seidl, R., and Turner, M. G. (2022). Post-disturbance reorganization of forest ecosystems in a changing world. *Proc. Nat. Acad. Sci.* 119:e2202190119. doi: 10.1073/pnas.2202190119
- Senf, C., and Seidl, R. (2021). Storm and fire disturbances in Europe: distribution and trends. *Global Change Biology* 27, 3605–3619. doi: 10.1111/gcb.15679
- Stibig, H.-J., Achard, F., Carboni, S., Raši, R., and Miettinen, J. (2014). Change in tropical forest cover of Southeast Asia from 1990 to 2010. *Biogeosciences* 11, 247–258. doi: 10.5194/bg-11-247-2014
- Sudmeyer-Rieux, K., Arce-Mojica, T., Boehmer, H. J., Doswald, N., Emerton, L., Friess, D. A., et al. (2021). Scientific evidence for ecosystem-based disaster risk reduction. *Nat. Sustainab.* 4, 803–810. doi: 10.1038/s41893-021-00732-4
- UNFCCC (2021). *COP26: Pivotal Progress Made on Sustainable Forest Management and Conservation*. Available at: <https://unfccc.int/news/cop26-pivotal-progress-made-on-sustainable-forest-management-and-conservation>

Conflict of interest

The authors declare that the research was conducted in the absence of any commercial or financial relationships that could be construed as a potential conflict of interest.

The author(s) declared that they were an editorial board member of Frontiers, at the time of submission. This had no impact on the peer review process and the final decision.

Publisher’s note

All claims expressed in this article are solely those of the authors and do not necessarily represent those of their affiliated organizations, or those of the publisher, the editors and the reviewers. Any product that may be evaluated in this article, or claim that may be made by its manufacturer, is not guaranteed or endorsed by the publisher.



OPEN ACCESS

EDITED BY

Jeong-Wook Seo,
Chungbuk National University,
South Korea

REVIEWED BY

Sanjeevi Nagalingam,
University of California, Irvine,
United States
Eva Yvonne Pfannerstill,
University of California, Berkeley,
United States

*CORRESPONDENCE

Sang-Deok Lee
sdlee@kangwon.ac.kr

SPECIALTY SECTION

This article was submitted to
Forests and the Atmosphere,
a section of the journal
Frontiers in Forests and Global Change

RECEIVED 18 July 2022

ACCEPTED 31 August 2022

PUBLISHED 20 September 2022

CITATION

Kim M-J and Lee S-D (2022) Potential
effects of surface ozone on forests
in Gangwon Province, South Korea,
based on critical thresholds.
Front. For. Glob. Change 5:996859.
doi: 10.3389/ffgc.2022.996859

COPYRIGHT

© 2022 Kim and Lee. This is an
open-access article distributed under
the terms of the [Creative Commons
Attribution License \(CC BY\)](#). The use,
distribution or reproduction in other
forums is permitted, provided the
original author(s) and the copyright
owner(s) are credited and that the
original publication in this journal is
cited, in accordance with accepted
academic practice. No use, distribution
or reproduction is permitted which
does not comply with these terms.

Potential effects of surface ozone on forests in Gangwon Province, South Korea, based on critical thresholds

Myeong-Ju Kim¹ and Sang-Deok Lee^{2*}

¹Department of Forest Environment System, Kangwon National University, Chuncheon, South Korea, ²Division of Forest Science, Kangwon National University, Chuncheon, South Korea

High hourly concentrations of ozone, a secondary pollutant produced from the photochemical reactions of primary precursors, have been increasing in South Korea, bringing potential adverse effects on vegetation. Deforestation caused by high ozone concentrations has been investigated in China and Japan. Using ozone measurements from East and West, Gangwon Province, South Korea, from 2001 to 2018, this study compared changes in surface ozone concentrations and analyzed the influences of meteorological factors and air pollutants. This study calculated accumulated ozone exposure over a threshold of 40 ppb (AOT40) and investigated the possibility of ozone affecting deforestation. Monthly average surface ozone concentrations increased rapidly in both regions from 2009. Although the daily total insolation (a meteorological factor that significantly impacts photochemical reactions) of West Gangwon and East Gangwon did not differ significantly, the ozone concentration was lower in East Gangwon than in West Gangwon (1.5 times lower from 2001 to 2018) owing to local strong winds. Moreover, there was a negative correlation between nitrogen dioxide and ozone generation. AOT40 in West Gangwon was about twice that in East Gangwon and exceeded 10,000 ppbh, the critical level for forests, every year since 2003. Potential damage from high concentrations of ozone was higher in West Gangwon than in East Gangwon.

KEYWORDS

surface ozone, forest, daily total insolation, AOT40, critical level

Introduction

Ozone (O₃) is a secondary pollutant generated from photochemical reactions by ultraviolet rays when precursors, nitrogen oxides (NO_x) and volatile organic compounds (VOCs), are present in the atmosphere. NO_x is generated during fossil fuel combustion. In the Seoul metropolitan area, 57% of NO_x emissions come from road transportation

pollution sources, such as automobiles (Ministry of the Environment Metropolitan Air Quality Management Office, 2022). VOCs easily evaporate in the atmosphere owing to their low boiling point, and 72% come from the use of organic solvents, such as in chemical and pharmaceutical factories and plastic drying processes (Ministry of the Environment Metropolitan Air Quality Management Office, 2022). Owing to rising emissions of NO_x and VOCs from anthropogenic sources, O₃ concentrations have been steadily increasing (Volz and Kley, 1988) and are expected to further increase in the future with rising anthropogenic pollutant emissions (Vingarzan, 2004; Meehl et al., 2007).

Although primary air pollutants play a role in the generation of high O₃ concentrations, meteorological conditions, such as temperature, insolation, relative humidity, and wind speed, are also key factors (Osrodka and Swiech-Skiba, 1997; Treffeisen and Halder, 2000; Walczewski, 2005). Among meteorological conditions, O₃ tends to rise in proportion to insolation and temperature and decreases with increasing cloud and rain (Ferretti et al., 2003). When the temperature rises, emissions of volatile hydrocarbons increase and solar radiation increases, thereby increasing photochemical processes, accelerating the formation of O₃ (Fiala et al., 2003).

According to the Seoul Metropolitan Area Atmospheric Environment Agency (2005) published by the Metropolitan Air Environment Agency of the Korean Ministry of Environment, meteorological conditions in which high concentrations of O₃ occur can be largely categorized as follows: (1) temperature of 25°C or higher, (2) relative humidity of 75% or lower, (3) continuous wind speed of 4 m/s or less, (4) total insolation from sunrise to noon of 6.4 MJ/m² or more, and (5) continuous strong insolation and no clouds in sunny weather. When high concentrations of O₃ occur, if the atmosphere is stable and convection does not occur owing to frontal or subsidence inversion, then anthropogenic air pollutants emitted by anthropogenic activities become trapped near the earth's surface with the surrounding air, which can adversely impact human health and forest ecosystems. It is necessary to monitor the interaction between weather factors and air pollutants for a long time to identify the condition of the atmosphere and the degree of air pollutants and establish air pollution policies.

High concentrations of O₃ adversely impact the human body and are highly toxic to plants and the degree of damage varies with the O₃ concentration and period of exposure. During gas exchange between leaves and the environment, O₃ penetrating through open stomata (Rich et al., 1970) can lead to acute damage, such as necrosis and spots, and chronic damage, such as pigmentation and dieback (Krupa and Manning, 1988). Long-term exposure to high O₃ concentrations adversely impacts crop yields, forest growth, and species composition (Ashmore, 2005).

The critical level of O₃ for vegetation was first defined in Germany in 1988 (ECE, 1988). This was further developed and

the concept of accumulated exposure to O₃ above the critical level for a given time was adopted. The indicator for the impact of O₃ exposure on vegetation is accumulated O₃ exposure over a threshold of 40 ppb (AOT40), which set a concentration of 40 ppb (0.04 ppm) for the AOT_x indicator widely used in Europe. The average AOT40 in East Asia is steadily increasing, and damage from ozone is expected to increase (Chang et al., 2017). In order to manage the damage caused by ozone in the long term, it is necessary to study at a local level.

As forests occupy approximately 63% of the total land in South Korea (Korea Forest Service Home, 2022), forest damage caused by O₃ is expected to grow in severity. Recently, high O₃ concentrations are frequently occurring in South Korea and the number of O₃ warnings issued is increasing (Air Korea, 2022).

As climate change becomes serious, the function of forests in carbon absorption is being discussed as a means of responding to climate change. However, there are concerns about the decline of forests owing to air pollutants (Takahashi et al., 2020). To prevent forest reduction, it is necessary to study the regional critical level and create and manage forests accordingly. As such, there is a growing need for studies on the impacts of O₃ on forests, but such research is insufficient. The primary aim of this study is to investigate the possibility of O₃ adversely impacting the productivity of forests in South Korea. Long-term changes in O₃ concentration and AOT40 were calculated and analyzed using national data on surface O₃ concentrations in East Gangwon and West Gangwon, Gangwon Province, from 2001 to 2018.

Materials and methods

Monitoring sites

Gangwon Province, South Korea, has a total area of 16,875 km², approximately 17% of the country's total land area. About 81% (13,716 km²) of Gangwon Province's total area is forest, making it the largest forest area in South Korea [approximately 21.6% of national forest cover (Korea Forest Service, 2021)]. Gangwon Province is divided into East Gangwon and West Gangwon by the Taebaek Mountains, the longest mountain range in South Korea, stretching from South Hamgyong Province in North Korea to Busan in South Korea, known as the backbone of the Korean Peninsula. The Taebaek Mountains crossing Gangwon Province consist of a continuously connected high and wide mountain range with an average elevation of 800–1,000 m above sea level. They act as a boundary, separating cultures within the province and causing distinct climates.

Regarding general meteorological characteristics, in East Gangwon, the steep slopes of the mountain range are connected to the sea and form a narrow and long topography along the coastline with barely any plains. Consequently,

the region has many meteorological characteristics associated with oceanic climates, such as heavy rain and heavy snowfall during northeasterly currents. It also experiences warm winters and relatively cool summers for its latitude, so the annual temperature difference is relatively small (Gangwon Regional Meteorological Administration, 2011).

In West Gangwon, there is a gradual distribution of mountain ranges and basins to the west, plains are more developed than in East Gangwon, and springs from the Gwangju, Charyeong, and Sobaek Mountains gather to become the source of the Han River and other major rivers. Owing to its central inland location, West Gangwon has characteristics closer to a continental climate, with less precipitation than East Gangwon (Gangwon Regional Meteorological Administration, 2011).

Changes in O₃ can be clearly observed in Gangwon Province depending on the region when diverse variables are considered, such as meteorological conditions and air pollutant emission concentrations. Accordingly, to compare East Gangwon and West Gangwon centered around the Taebaek Mountains, this study selected Gangneung-si (East Gangwon) and Wonju-si (West Gangwon) as the monitoring sites (Figure 1). From the monitoring network, measurement data from Okcheon-dong [2179 Gyeonggang-ro, Gangneung-si, Gangwon-do (37°45′36.6″N 128°54′10.6″E)] were used for East Gangwon and measurement data from Myeongnyundong [171 Dangu-ro, Wonju-si, Gangwon-do (37°21′12.6″N 127°56′54.7″E)] for West Gangwon.

Database and data processing

Since 2021, the public website Air Korea has provided real-time air pollution information for South Korea consisting of air quality standard data measured from 600 urban atmospheric monitoring networks installed in 228 cities and counties nationwide, roadside atmospheric monitoring networks, national baseline concentration monitoring networks, suburban atmospheric monitoring networks, and port atmospheric monitoring networks. In this study, national data that conducted QA/QC according to Korea's air pollution measurement network operating guidelines were used, and a total of two urban air measurement stations were used, one each in Gangneung and Wonju.

The measurement methods of each air quality standard item vary; O₃ is measured hourly and daily using the UV photometric method. Observational data from nationwide air-quality monitoring stations were collected and converted to the maximum daily 8 h ozone average (MDA8O3). To calculate MDA8O3 for a given calendar day, we selected the highest value among 24 possible 8 h rolling mean concentrations from the hourly ozone data observed at each station. If >25% of hourly data for a given day were not valid, MDA8O3 was not calculated

for those days and was excluded from further analysis. Yearly MDA8O3 averages were calculated from daily values. This study used hourly O₃ measurements from January 2001 to December 2018 from the urban atmospheric monitoring networks and calculated the annual and monthly average O₃ concentrations based on 8 hours during the daytime (9:00 to 17:00), when photosynthesis is active.

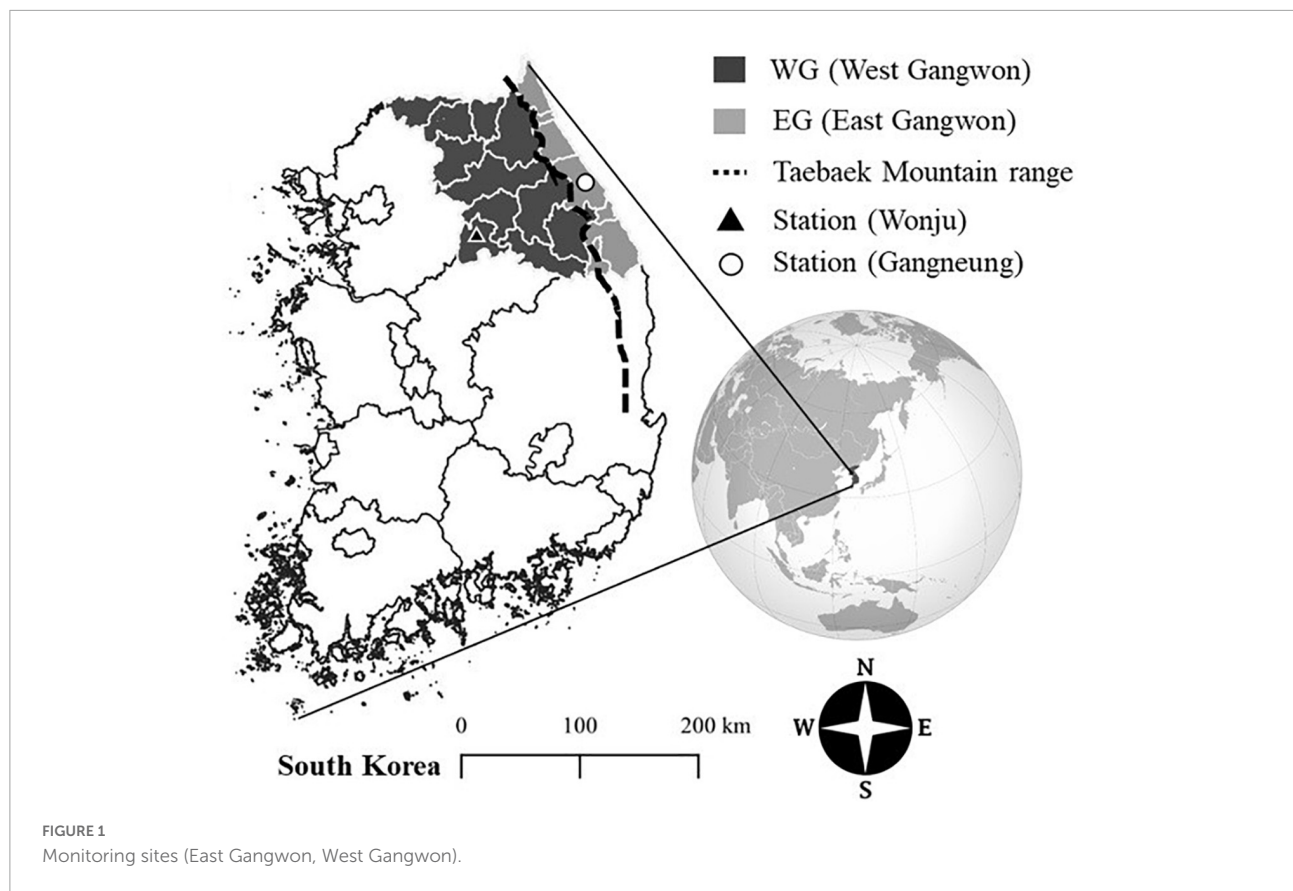
To analyze the O₃ concentrations according to meteorological factors and primary pollutants, this study used public national data on nitrogen dioxide (NO₂) concentrations and meteorological factors, including average temperature, average relative humidity, average wind speed, average cloud cover, and daily total insolation. As daily total insolation is a major factor affecting the O₃ concentrations according to photochemical reactions (Massambani and Andrade, 1994; Ellis et al., 2000; Kumar et al., 2010), this study analyzed its correlation using meteorological data from the same regions as the O₃ monitoring stations.

Ozone exposure indices

Two indices for analyzing the long-term effects of O₃ exposure on vegetation (e.g., crops and trees) are AOT40, which is mainly used in Europe, and SUM60, which is mainly used in the US (Tong et al., 2009). AOT40 and SUM60 are similar evaluation measures, but in the case of AOT40, experimental data on trees or crops exist. In this study, AOT40 was used to determine the biological relevance according to the O₃ concentration.

$$AOT40 = \sum_{i=1}^n [C_{O_3} - 40] \text{ i for } C_{O_3} \geq 40 \text{ ppb} \quad (1)$$

AOT40 refers to the accumulated quantity of O₃ exceeding a concentration of 40 ppb in a specific period. Studies have reported that forest production declines by over 10% when the AOT40 value from April to September, the growth period of trees, exceeds 10,000 ppbh, which was defined as the O₃ critical level for forests (Loibl et al., 2004; Kohno et al., 2005). Deciduous tree species, such as ash (*Fraxinus excelsior*) and black alder (*Alnus glutinosa*), have higher sensitivity to O₃ (Ozolincius et al., 2005), and based on the O₃ exposure index, a study showed that the growth of beech (*Fagus sylvatica*) considerably decreased when AOT40 exceeded 10,000 ppbh (Braun and Flückiger, 1995). Given that vegetation mainly absorbs O₃ during the daytime when the stomata are open, only the period when solar radiation energy exceeds 50 W/m² should be considered when calculating AOT40 (World Health Organization [WHO], 2000). As such, to calculate AOT40, this study extracted only O₃ concentrations of 40 ppb or higher during 8 h in the daytime (9:00 to 17:00) from the hourly O₃ concentration measurement data from 1 January 2001 to 31 December 2018. Additionally, the daily averages were calculated and AOT40 of East Gangwon



and West Gangwon was obtained using the accumulated sum of 6 months (180 days). For 2001, data for calculating AOT40 were available starting from July. The changes in AOT40 by year were observed by dividing the research period into 2001–2008 and 2009–2018. This divide was chosen because O_3 concentrations surged in 2009.

Results and discussion

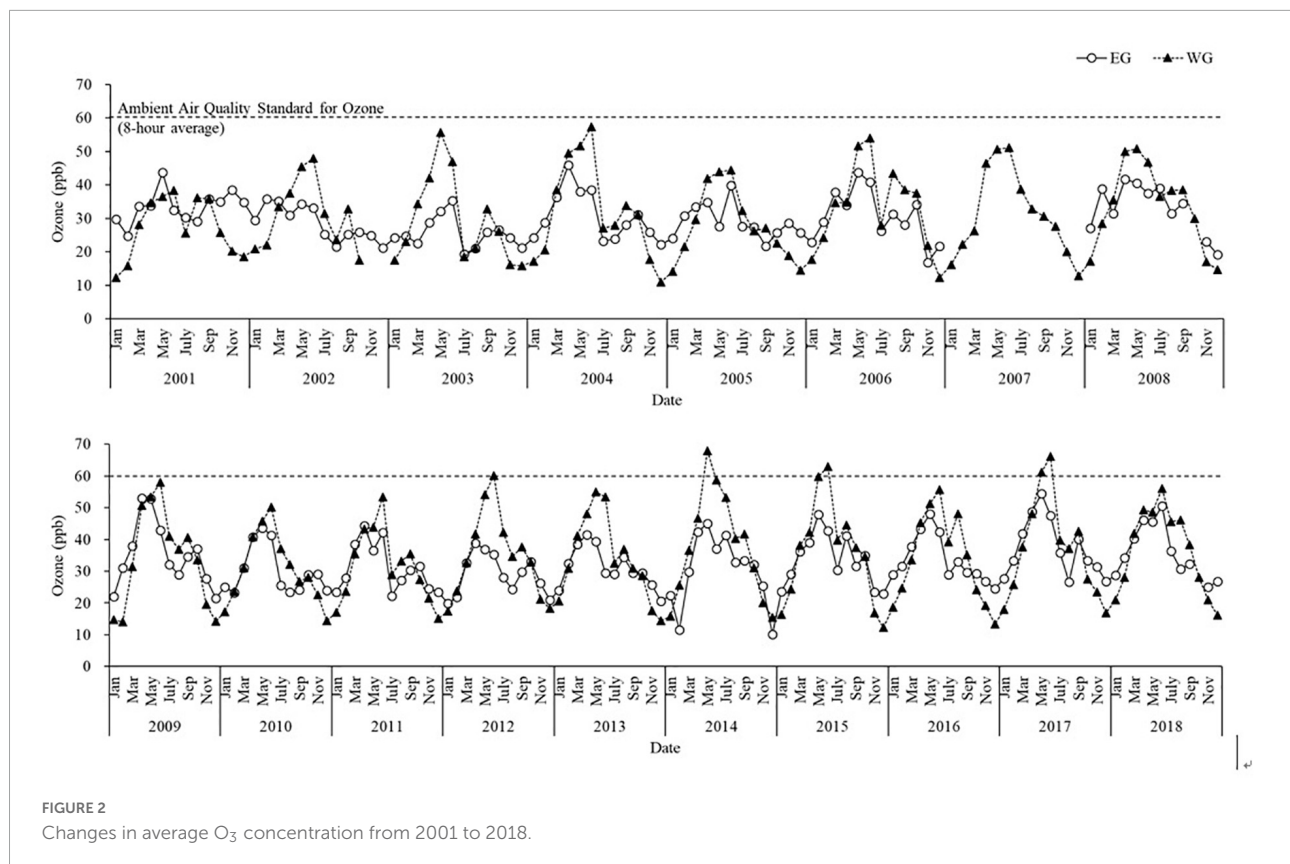
Comparison of ozone concentrations in East Gangwon and West Gangwon

Figure 2 compared yearly atmospheric O_3 concentrations in East Gangwon and West Gangwon from 2001 to 2018 and South Korea's O_3 air quality standard of 60 ppb is indicated by the dotted line. Owing to the absence of measurement data for 2007 in East Gangwon, we could not confirm measurement data from April to June, when high O_3 concentrations are expected, so this period was excluded from the study. The average O_3 concentration over 18 years was confirmed to be higher in West Gangwon (32.63 ppb) than in East Gangwon (29.85 ppb). The average annual O_3 concentration was highest in 2009 (35.18 and 34.00 ppb in East Gangwon and West Gangwon, respectively;

Supplementary Table 1). The average O_3 concentrations in East Gangwon and West Gangwon were 30.10 ± 2.77 and 30.73 ± 2.32 ppb from 2001 to 2008 and 32.75 ± 2.83 and 34.65 ± 2.27 from 2009 to 2018, respectively, indicating that the O_3 concentrations rose in both regions from 2009.

According to a comparison of the average monthly O_3 concentrations in the two regions by year, the highest in East Gangwon was 54.48 ppb, measured in May 2017 and the highest in West Gangwon was 67.87 ppb, measured in May 2014. In terms of the maximum average monthly O_3 concentrations per year from 2001 to 2018, in East Gangwon, maximum concentrations were observed once in February, six times in April, seven times in May, and three times in June, indicating that O_3 concentrations frequently peaked in April and May. In West Gangwon, maximum concentrations were observed four times in May and 14 times in June, indicating that O_3 generation peaked in May and June (**Supplementary Table 1**).

To clearly observe the changes in O_3 concentration from 2001 to 2018, the period was divided into two (2001–2008 and 2009–2018). The overall O_3 concentration rose more from 2009 to 2018 than from 2001 to 2008 in both regions, though O_3 concentrations declined from December to February from 2009 to 2018 (**Figure 3**). East Gangwon showed the largest increase in April–May, whereas West Gangwon showed the largest increase in June–July. West Gangwon showed higher monthly



average O₃ concentrations than East Gangwon and tended to show higher concentrations from April–September, when the meteorological conditions for high O₃ concentration were met. In contrast, from October–March, East Gangwon showed higher O₃ concentrations than West Gangwon. This is likely because the average winter temperature in East Gangwon is higher than that in West Gangwon, providing better conditions for the generation of O₃ (Gangwon Province, 2022).

Changes in ozone concentration according to meteorological factors and air pollutants

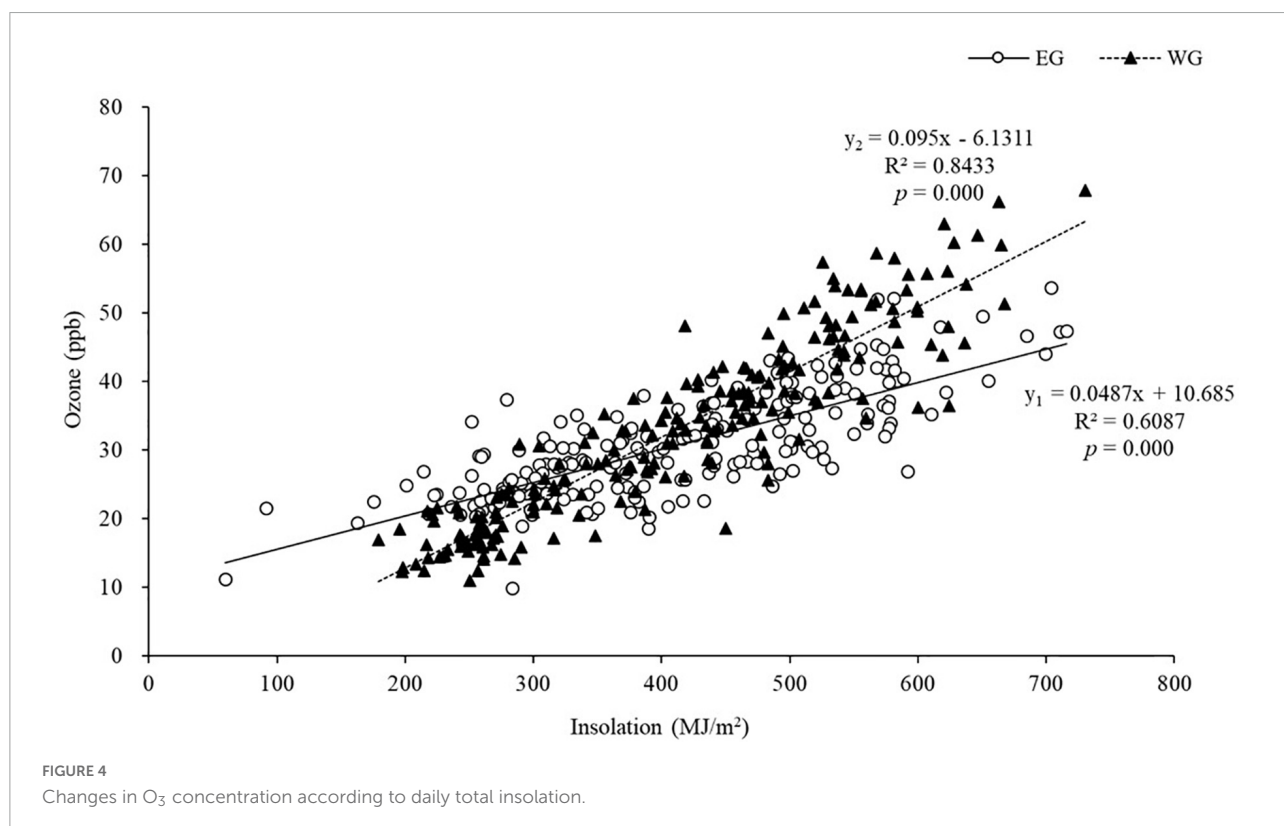
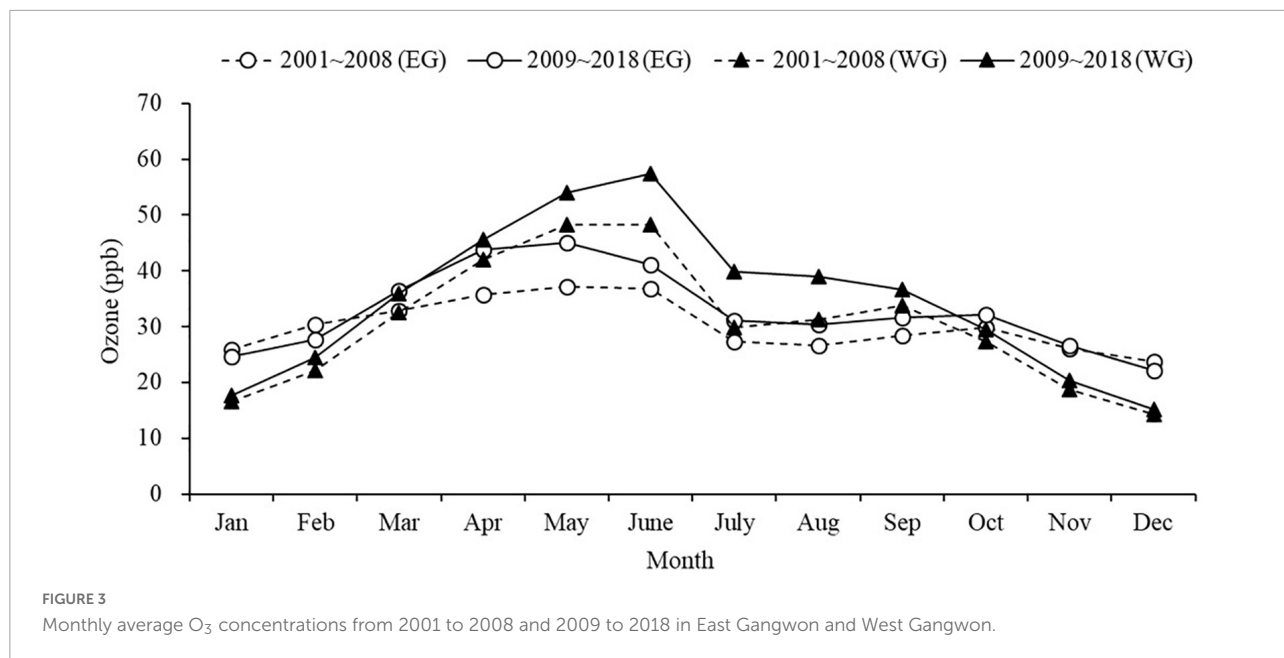
Meteorological factors

Ozone is a secondary pollutant generated from the photochemical reactions of primary pollutants in the atmosphere. Therefore, insolation, which is directly related to the photochemical reactions, is a major meteorological factor affecting O₃ generation. General linear regression analysis between insolation and O₃ in East Gangwon and West Gangwon achieved R^2 of 0.61 (y_1) and 0.84 (y_2), respectively (Figure 4). Insolation and O₃ showed a positive correlation in both regions; however, surface O₃ was more influenced by insolation in West Gangwon than in East Gangwon, as

high O₃ concentrations of 60 ppb or more were generated as insolation increased. In general, O₃ is actively generated and deposited in a stable atmosphere (Jacob et al., 1992; Helmig et al., 2008, 2012; Xing et al., 2017; Karle et al., 2020). In East Gangwon, a regional meteorological phenomenon occurs in which a continuous wind current in the central inland region crosses the Taebaek Mountains and reaches East Gangwon, forming a temperature inversion layer on the downwind side and producing dry strong winds (Lee, 2003). Therefore, the relatively low R^2 between insolation and O₃ in East Gangwon despite the identical insolation can be attributed to the reduced generation of O₃. Accordingly, given that East Gangwon and West Gangwon in Gangwon Province have different climatic characteristics, including average temperature, average wind speed, and insolation owing to the Taebaek Mountains' unique geographical characteristics, O₃ management measures should consider individual microclimate (Gangwon Province, 2022).

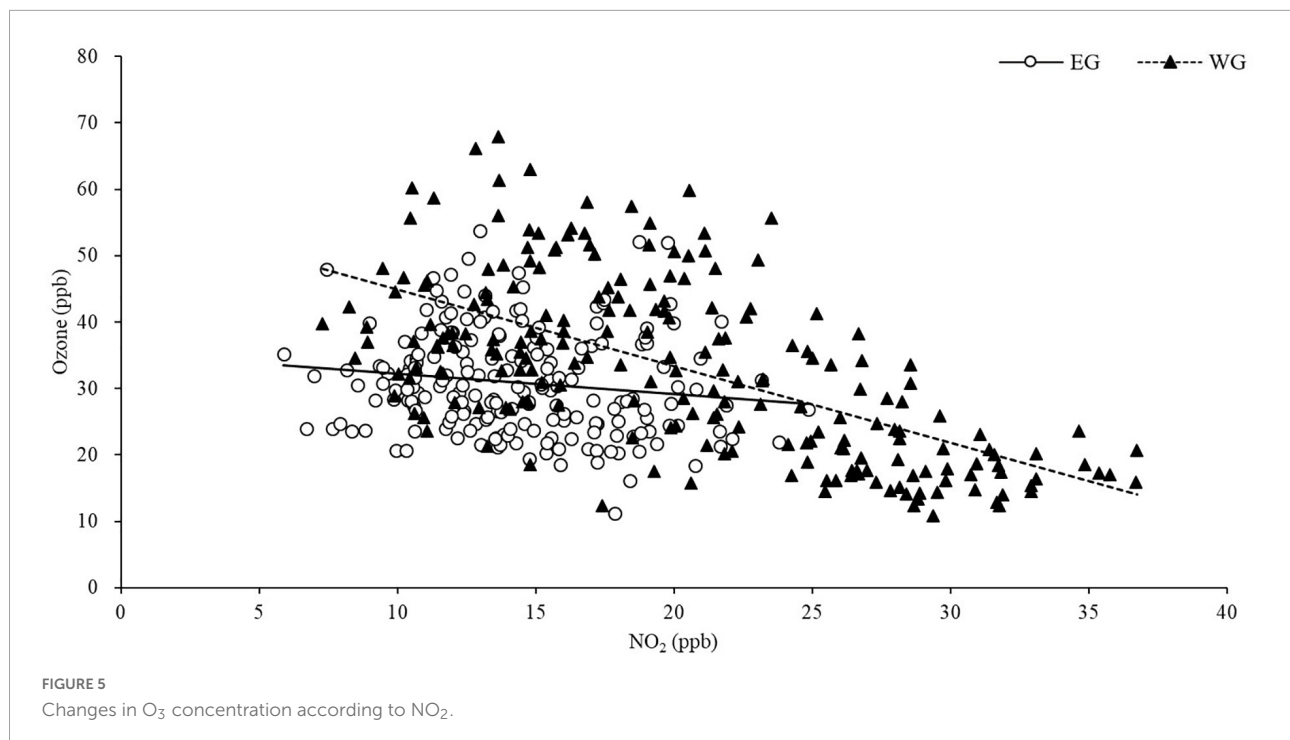
Air pollutants

Nitrogen oxides are a major determinant of atmospheric O₃ concentrations (Grewe et al., 2012; He et al., 2013). In West Gangwon, there was a negative correlation between NO₂ and O₃, which can be explained by seasonal effects and the effects of VOCs-limited regime in the heavily polluted urban areas (National Research Council, 1992). In West Gangwon,



from April to June, O₃ concentrations were high and NO₂ concentrations were low, with O₃ then decreasing from July and NO₂ increasing from September (Figure 6). During July and August at the monitoring sites, intensive rainfall occurred and insolation decreased, whereas insolation was highest from April to June (Isaksen et al., 1978). As insolation rises owing

to seasonal factors, solar radiation increases, photochemical reactions become active, NO₂ is converted to O₃, and the concentration of atmospheric NO₂ declines (Yienger et al., 1999; Liu and Shi, 2021), whereas that of O₃ rises (Sillman, 1999; Yienger et al., 1999; Chang et al., 2017). In addition, unlike other air pollutants, O₃ has non-linear efficiency, so the reduction of



NO_x can exacerbate O₃ in the short term. As O₃ concentrations change according to the ratio of atmospheric VOCs and NO_x (Sillman and He, 2002; Jeon et al., 2017), it is important to control NO_x and VOCs to reduce O₃ concentrations. Generally, regions with a VOCs/NO_x ratio of 6 or less are classified as VOCs-limited regions, which applies to large cities with heavy traffic such as Seoul, Busan, and Wonju. Researchers have reported that in Seoul, NO_x is already saturated and VOCs act as a limiting factor for O₃ generation (Korean Statistical Information Service, 2022a). Therefore, in large cities with high NO_x emissions, control of VOCs is necessary for the effective integrated management of O₃.

In contrast, NO₂ concentrations throughout the year were lower in East Gangwon than in West Gangwon, and there were no large differences by month (Figure 6B). In this regard, as East Gangwon has a smaller population [as of 2021: East Gangwon 215,322 and West Gangwon 361,056 (Korean Statistical Information Service, 2022a)], traffic volume [registered vehicles as of 2022: East Gangwon 115,464 and West Gangwon 186,896 (Korea Industrial Complex Corporation, 2022)], and industrial complex size (total area of general industrial complexes as of 2015: East Gangwon 2.144 km² and West Gangwon 2.198 km²) (Matsumura, 1997), NO₂ emissions from non-point and point sources were lower than those in West Gangwon. Figures 4, 5 show that in East Gangwon, changes in O₃ concentration were barely influenced by NO₂ and were mainly influenced by meteorological factors, such as insolation. In East Gangwon, the atmospheric NO₂ concentration is low and the atmosphere is unstable owing to its topographical

features. Hence, East Gangwon had lower O₃ concentrations from April to June and smaller fluctuations in O₃ throughout the year than West Gangwon (Figure 6B). On the other hand, East Gangwon had higher O₃ concentrations from November to February than West Gangwon (Figure 6B).

Calculation of accumulated ozone exposure over a threshold of 40 ppb and impact assessment

When trees are exposed to high O₃ concentrations over long periods, damage can occur, such as leaf necrosis, browning, and spots (Günthardt-Goerg and Vollenweider, 2007). If damage accumulates, tree growth can be inhibited and species diversity reduced, leading to a decline in forest productivity. Therefore, this study observed AOT40 in East Gangwon and West Gangwon based on AOT40 10,000 ppbh, the critical level for forests reported by WHO. In South Korea, high O₃ concentrations of 40 ppb and higher occur from April to June and the AOT40 accumulated over the previous 6 months was highest from July to September (Figure 7). Figure 7 shows the changes in East Gangwon and West Gangwon by year for 6 months from April to September. AOT40 in both regions fluctuated every year according to pollution and meteorological conditions in the region but there were clear differences between East Gangwon and West Gangwon. The average AOT40 in West Gangwon over the 18 years (10,106 ppbh) was about twice that of East Gangwon (5,383 ppbh). In East Gangwon, the

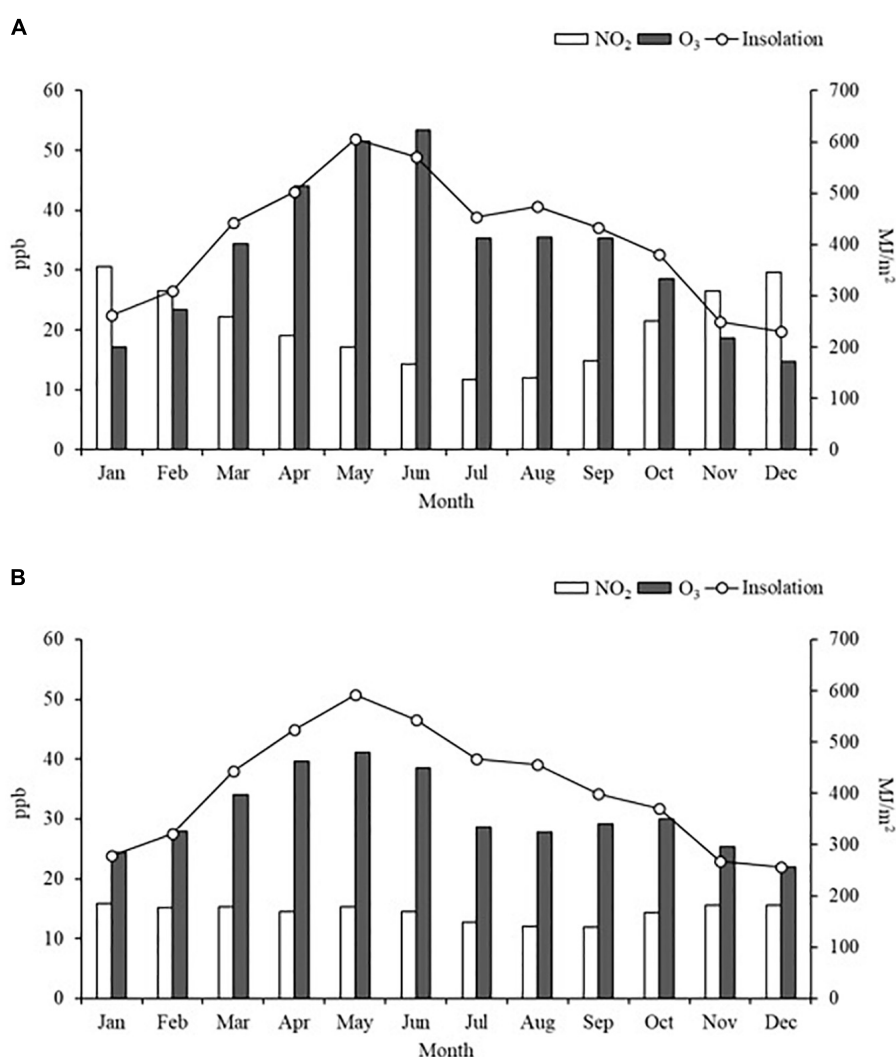


FIGURE 6
Monthly average NO₂ and O₃ concentrations and insolation from 2001 to 2018: (A) West Gangwon; (B) East Gangwon.

critical level was first exceeded in 2009 (September: 12,546 ppbh) and then decreased, but starting in 2012, it showed a steady increase every year. AOT40 exceeded the critical level from 2017 (September: 12,984 ppbh) to 2018 (September: 12,483 ppbh). In West Gangwon, AOT40 began to approach the critical level from 2002 and then exceeded the critical level from July to September every year from 2003 to 2018. AOT40 rose particularly quickly in 2009 (September: 19,039 ppbh) and peaked across the whole study period in 2014 (September: 23,804 ppbh). From 2014 to 2018 in West Gangwon, the average AOT40 in September was 20,714 ppbh, more than twice the critical level. This value is higher than the average AOT40 (19,600 ppbh) in summer in East Asia (Chang et al., 2017). As such, there is a greater concern in West Gangwon than in East Gangwon about declining forest productivity from long-term exposure to high surface O₃ concentrations.

Nevertheless, it is important to note that there is uncertainty regarding applying the AOT40 critical level, which was developed for Europe, in South Korea. Although this study matched the AOT40 calculation formula and critical level with the guidelines for Europe (World Health Organization [WHO], 2000), differences in forest biodiversity between Europe and East Asia and the air pollution tolerance index for each tree species lead to uncertainty in the assessment of O₃ exposure in South Korea. In the neighboring country of Japan, based on a study on the O₃ exposure of 16 representative native tree species (Izuta et al., 2001), researchers suggested that the AOT40 critical level for forest protection in Japan may range from 8,000 to 21,000 ppbh (Li et al., 2016). Moreover, owing to high background O₃ concentration levels in East Asia (Sillman, 1999; Pochanart et al., 2002) and increased photosynthetic activity at lower

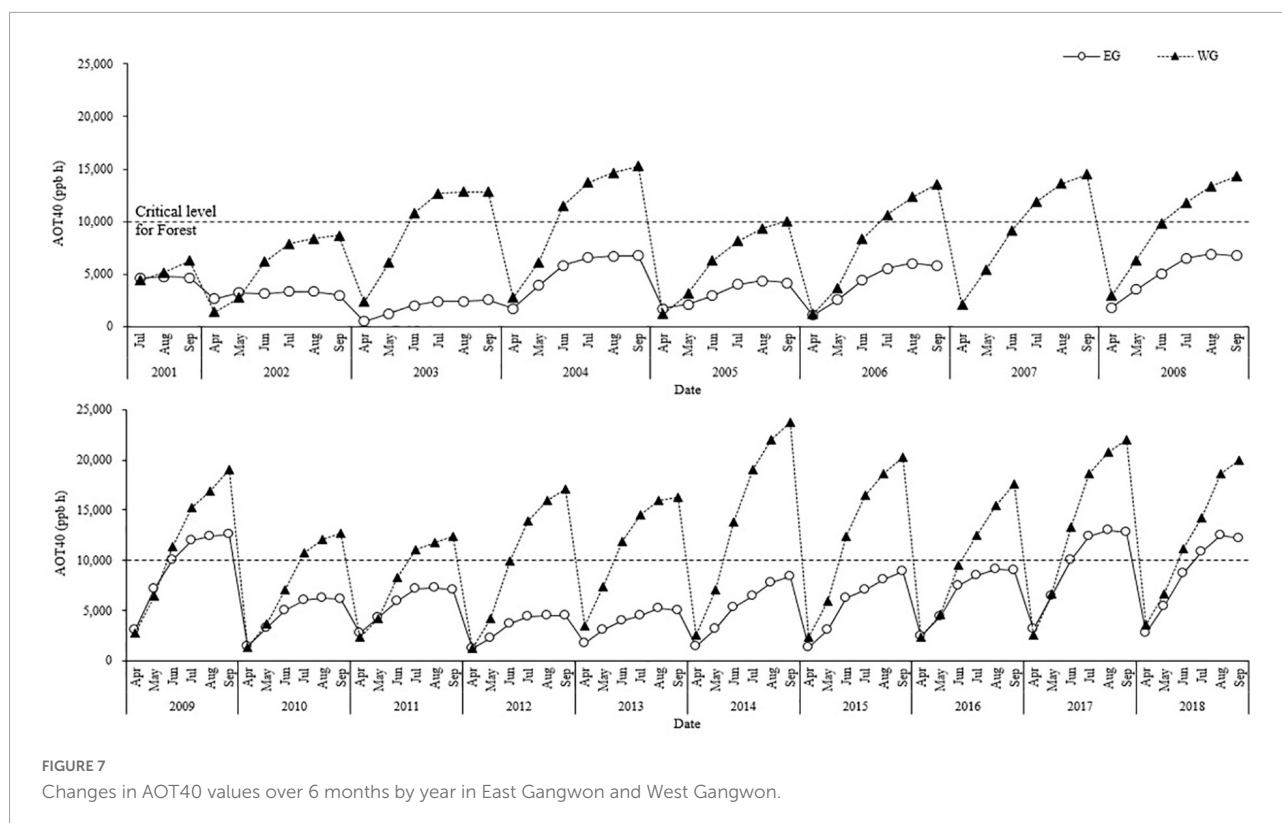


FIGURE 7
Changes in AOT40 values over 6 months by year in East Gangwon and West Gangwon.

latitudes compared with Europe, high O_3 values from early spring to fall can influence forest damage (Chang et al., 2017).

Although there are limitations in applying AOT40 to South Korea owing to uncertainty, it is judged to be valuable as an index showing changes in atmospheric O_3 concentrations. To set O_3 concentration indices suitable for a specific region, there is a need for more research and long-term monitoring to identify the long-term effects of O_3 concentrations.

Conclusion

West Gangwon showed substantially higher average O_3 concentrations than East Gangwon, and in terms of maximum O_3 concentrations, there were frequent occurrences of high O_3 concentrations close to 60 ppb, the Korean O_3 air quality standard. Both regions showed sharp increases in O_3 concentrations in 2009 and long-term rising trends began from that year.

Insolation showed a positive correlation with O_3 , whereas NO_2 showed a negative correlation. O_3 concentrations increased as insolation increased in both regions but was less influenced by insolation in East Gangwon than in West Gangwon, even with identical insolation, owing to local meteorological phenomena, such as strong winds caused by the Taebaek Mountains. In West Gangwon, O_3 and NO_2 showed

a completely inversely proportional relationship, which is attributed to seasonal effects and the fact that the region is VOCs-limited. Moreover, because East Gangwon has a lower population density, traffic volume, and industrial complex size than West Gangwon, NO_2 concentration had a smaller influence. West Gangwon had a much higher AOT40 than East Gangwon. Although the critical level for forests (10,000 ppbh) was exceeded three times in East Gangwon (2009, 2017, and 2018), in West Gangwon, the AOT40 critical level was exceeded every year from 2003. Particularly, in West Gangwon, from 2014 to 2018, the average AOT40 in September was 20,714 ppbh, more than twice the critical level. As high O_3 concentrations occurred more frequently and AOT40 values were much higher in West Gangwon than in East Gangwon, forests are expected to decline faster in West Gangwon.

Even within the same administrative zone of Gangwon Province, the O_3 concentrations are not homogeneous owing to geographical features and climatic differences. As such, it is necessary to establish regional measures for managing O_3 . To examine the specific long-term effects of O_3 on forests, it is necessary to conduct research to determine an AOT40 critical level appropriate for forest tree species in South Korea. Particularly, given that biotic factors and abiotic stresses are important factors in forest ecosystems, there is a need for research that considers diverse meteorological factors and tree stress factors in addition to air pollutants.

Data availability statement

The datasets presented in this study can be found in online repositories. The names of the repository/repositories and accession number(s) can be found below: www.airkorea.or.kr.

Author contributions

S-DL: supervision and writing—review and editing. M-JK: writing—original draft, investigation, and data curation. Both authors read and agreed to the final version of the manuscript.

Funding

This study was supported by the “Experts Training Graduate Program for Particulate Matter Management,” from the Ministry of Environment, Korea, and the Basic Science Research Program through the National Research Foundation of Korea (NRF) funded by the Ministry of Education (NRF-2021R1F1A1062524).

References

- Air Korea (2022). Available online at: https://www.airkorea.or.kr/eng/O3Alert?pMENU_NO=162 (Accessed on August, 13 2022).
- Ashmore, M. R. (2005). Assessing the future global impacts of ozone on vegetation. *Plant Cell Environ.* 28, 949–964. doi: 10.1111/j.1365-3040.2005.01341.x
- Braun, S., and Flückiger, W. (1995). Effects of ambient ozone on seedlings of *Fagus sylvatica* L. and *Picea abies* (L.) Karst. *New Phytol.* 129, 33–44. doi: 10.1111/j.1469-8137.1995.tb03007.x
- Chang, K.-L., Petropavlovskikh, I., Cooper, O. R., Schultz, M. G., Wang, T., Helmig, D., et al. (2017). Regional trend analysis of surface ozone observations from monitoring networks in eastern North America, Europe and East Asia. *Elem. Sci. Anthropocene* 5:50. doi: 10.1525/elementa.243
- ECE (1988). *ECE Critical Levels Workshop*. Bad Harzburg: ECE, 14–18.
- Ellis, A. W., Hildebrandt, M. L., Thomas, W. M., and Fernando, H. (2000). Analysis of the climatic mechanisms contributing to the summertime transport of lower atmospheric ozone across metropolitan Phoenix, Arizona, USA. *Clim. Res.* 15, 13–31. doi: 10.3354/cr015013
- Ferretti, M., Alianiello, F., Amoriello, T., Amorini, E., Buffoni, A., Bussotti, F., et al. (2003). *Assessment of Ozone Exposure and Effects on Forest Vegetation Through Routine Monitoring Programmes—A Risk Analysis in Italy*. Raleigh, NC: Swedish Water And Air Pollution Research Laboratory—Publications-IVL B, 351–362.
- Fiala, J., Cernikovskiy, L., de Leeuw, F., and Kurfuerst, P. (2003). *Air Pollution by Ozone in Europe in Summer 2003. Overview of Exceedances of EC Ozone Threshold Values During the Summer Season April–August 2003*. Copenhagen: European Environment Agency, 33.
- Gangwon Province (2022). Available online at: https://www.provin.gangwon.kr/gw/eng/sub01_03_02 (Accessed on August, 13 2022).
- Gangwon Regional Meteorological Administration (2011). *Regional Climate Change Report*. Gangwon: Gangwon Regional Meteorological Administration Press.
- Grewe, V., Dahmann, K., Matthes, S., and Steinbrecht, W. (2012). Attributing ozone to NO_x emissions: Implications for climate mitigation measures. *Atmos. Environ.* 59, 102–107. doi: 10.1016/j.atmosenv.2012.05.002
- Günthardt-Goerg, M. S., and Vollenweider, P. (2007). Linking stress with macroscopic and microscopic leaf response in trees: new diagnostic perspectives. *Environ. Pollut.* 147, 467–488. doi: 10.1016/j.envpol.2006.08.033
- He, H., Hemberck, L., Hosley, K. M., Canty, T. P., Salawitch, R. J., and Dickerson, R. R. (2013). High ozone concentrations on hot days: The role of electric power demand and NO_x emissions. *Geophys. Res. Lett.* 40, 5291–5294. doi: 10.1002/grl.50967
- Helmig, D., Boylan, P., Johnson, B., Oltmans, S., Fairall, C., Staebler, R., et al. (2012). Ozone dynamics and snow-atmosphere exchanges during ozone depletion events at Barrow, Alaska. *J. Geophys. Res.* 117:15. doi: 10.1029/2012JD017531
- Helmig, D., Johnson, B., Oltmans, S. J., Neff, W., Eisele, F., and Davis, D. D. (2008). Elevated ozone in the boundary layer at South Pole. *Atmos. Environ.* 42, 2788–2803. doi: 10.1016/j.atmosenv.2006.12.032
- Isaksen, I. S. A., Hov, O., and Hesstvedt, E. (1978). Ozone generation over rural areas. *Environ. Sci. Technol.* 12, 1279–1284. doi: 10.1021/es60147a011
- Izuta, T., Matsumura, H., Kohno, Y., and Shimizu, H. (2001). Experimental studies on the effects of ozone on forest tree species. *Taiki Kankyo Gakkaishi* 36, 60–77. doi: 10.11298/taiki1995.36.2_60
- Jacob, D. J., Fan, S.-M., Wofsy, S. C., Spiro, P. A., Bakwin, P. S., Ritter, J. A., et al. (1992). Deposition of ozone to tundra. *J. Geophys. Res.* 97, 16473–16479. doi: 10.1029/91JD02696
- Jeon, E. M., Cho, H. S., Kim, Y. J., Kwon, E. H., Seo, K. S., Gwon, M. H., et al. (2017). Statistical quality assurance and quality control methods for volatile organic compounds and their major emission sources. Seoul Metropolitan Government. *Inst. Health Environ. Rep.* 53, 168–177.
- Karle, N. N., Mahmud, S., Sakai, R. K., Fitzgerald, R. M., Morris, V. R., and Stockwell, W. R. (2020). Investigation of the successive ozone episodes in the El Paso–Juarez region in the summer of 2017. *Atmosphere* 11:532. doi: 10.3390/atmos11050532

Conflict of interest

The authors declare that the research was conducted in the absence of any commercial or financial relationships that could be construed as a potential conflict of interest.

Publisher’s note

All claims expressed in this article are solely those of the authors and do not necessarily represent those of their affiliated organizations, or those of the publisher, the editors and the reviewers. Any product that may be evaluated in this article, or claim that may be made by its manufacturer, is not guaranteed or endorsed by the publisher.

Supplementary material

The Supplementary Material for this article can be found online at: <https://www.frontiersin.org/articles/10.3389/ffgc.2022.996859/full#supplementary-material>

- Kohno, Y., Matsumura, H., Ishii, T., and Izuta, T. (2005). "Establishing critical levels of air pollutants for protecting East Asian vegetation—A challenge," in *Plant Responses to Air Pollution and Global Change*, eds K. Omasa, I. Nouchi and L. J. De Kok (Berlin: Springer), 243–250.
- Korea Forest Service (2021). *Forest Basic Statistics 2020*. Daejeon: Korea Forest Service Press, 23.
- Korea Forest Service Home (2022). Available online at: https://english.forest.go.kr/kfswb/kfi/kfs/cms/cmsView.do?cmsId=FC_001679&mn=UENG_01_03 (Accessed on April, 15 2022).
- Korea Industrial Complex Corporation (2022). *Overview of Korean Industrial Complexes: Gangwon-do*. Daegu: Korea Industrial Complex Corporation.
- Korean Statistical Information Service (2022a). Available online at: https://kosis.kr/statHtml/statHtml.do?orgId=211&tblId=DT_211N_B00100&conn_path=I2 (Accessed on April, 26 2022).
- Korean Statistical Information Service (2022b). Available online at: https://kosis.kr/statHtml/statHtml.do?orgId=116&tblId=DT_MLTM_5498&conn_path=I2 (Accessed on April, 26 2022).
- Krupa, S. V., and Manning, W. J. (1988). Atmospheric ozone: Formation and effects on vegetation. *Environ. Pollut.* 50, 101–137. doi: 10.1016/0269-7491(88)90187-x
- Kumar, R., Naja, M., Venkataramani, S., and Wild, O. (2010). Variations in surface ozone at Nainital: A high-altitude site in the central Himalayas. *J. Geophys. Res.* 115:D16302. doi: 10.1029/2009JD013715
- Lee, J. G. (2003). A numerical study of the orographic effect of the Taebak mountains on the increase of the downslope wind speed near Gangnung area. *Int. J. Environ. Sci.* 12, 1245–1254. doi: 10.5322/IJES.2003.12.12.1245
- Li, J., Yang, W., Wang, Z., Chen, H., Hu, B., Li, J., et al. (2016). Modeling study of surface ozone source-receptor relationships in East Asia. *Atmos. Res.* 167, 77–88. doi: 10.1016/j.atmosres.2015.07.010
- Liu, C., and Shi, K. (2021). A review on methodology in O₃-NO_x-VOC sensitivity study. *Environ. Pollut.* 291:118249. doi: 10.1016/j.envpol.2021.118249
- Loibl, W., Bolhär-Nordenkamp, H. R., Herman, F., and Smidt, S. (2004). Modelling critical levels of ozone for the forested area of Austria modifications of the AOT40 concept. *Environ. Sci. Pollut. Res. Int.* 11, 171–180. doi: 10.1007/BF02979672
- Massambani, O., and Andrade, F. (1994). Seasonal behavior of tropospheric ozone in the Sao Paulo (Brazil) metropolitan area. *Atmos. Environ.* 28, 3165–3169. doi: 10.1016/1352-2310(94)00152-B
- Matsumura, H. (1997). "Effects of ozone and/or sulfur dioxide on tree species," in *Proceedings of the CRIEPI International Seminar on Transport and Effects of Acidic Substances November 28–29, 1996*, Tokyo, 190–205.
- Meehl, G. A., Stocker, T. F., Collins, W. D., Friedlingstein, P., Gaye, A. T., Gregory, J. M., et al. (2007). *Global Climate Projections. Chapter 10*. Geneva: IPCC.
- Metropolitan Area Atmospheric Environment Agency (2005). *Area Atmospheric Environment Information*. Gwacheon: Metropolitan Area Atmospheric Environment Agency press, 3–4.
- Ministry of the Environment Metropolitan Air Quality Management Office (2022). Available online at: <https://me.go.kr/mamo/web/index.do?menuId=590> [Accessed on April, 12 2022].
- National Research Council (1992). *Rethinking the Ozone Problem in Urban and Regional Air Pollution*. Washington, DC: National Academies Press.
- Osrodka, L., and Swiech-Skiba, J. (1997). Klimatologiczne aspekty powstawania smogu letniego na obszarze Gornoslaskiego Okregu Przemyslowego. *Wiadomości Instytutu Meteorologii i Gospodarki Wodnej* 20, 113–128.
- Ozolincius, R., Stakenas, V., and Serafinavičiute, B. (2005). Meteorological factors and air pollution in Lithuanian forests: Possible effects on tree condition. *Environ. Pollut.* 137, 587–595. doi: 10.1016/j.envpol.2005.01.044
- Pochanart, P., Akimoto, H., Kinjo, Y., and Tanimoto, H. (2002). Surface ozone at four remote island sites and the preliminary assessment of the exceedances of its critical level in Japan. *Atmos. Environ.* 36, 4235–4250. doi: 10.1016/S1352-2310(02)00339-4
- Rich, S., Waggoner, P. E., and Tomlinson, H. (1970). Ozone uptake by bean leaves. *Science* 169, 79–80. doi: 10.1126/science.169.3940.79
- Sillman, S. (1999). The relation between ozone, NO_x and hydrocarbons in urban and polluted rural environments. *Atmos. Environ.* 33, 1821–1845. doi: 10.1016/S1352-2310(98)00345-8
- Sillman, S., and He, D. (2002). Some theoretical results concerning O₃-NO_x-VOC chemistry and NO_x-VOC indicators. *J. Geophys. Res. Atmos.* 107, ACH-26–21–ACH-26–15. doi: 10.1029/2001JD001123
- Takahashi, M., Feng, Z., Mikhailova, T. A., et al. (2020). Air pollution monitoring and tree and forest decline in East Asia: A review. *Sci. Total Environ.* 742:140288. doi: 10.1016/j.scitotenv.2020.140288
- Tong, D. Q., Mathur, R., Kang, D., Yu, S., Schere, K. L., and Pouliot, G. (2009). Vegetation exposure to ozone over the continental United States: Assessment of exposure indices by the Eta-CMAQ air quality forecast model. *Atmos. Environ.* 43, 724–733. doi: 10.1016/j.atmosenv.2008.09.084
- Treff Eisen, R., and Halder, M. (2000). Spatial and temporal variation of ozone concentrations at high altitude monitoring sites in Germany. *Environ. Monit. Assess.* 65, 139–146. doi: 10.1023/A:1006405420701
- Vingarzan, R. (2004). A review of surface ozone background levels and trends. *Atmos. Environ.* 38, 3431–3442. doi: 10.1016/j.atmosenv.2004.03.030
- Volz, A., and Kley, D. (1988). Evaluation of the Montsouris series of ozone measurements made in the nineteenth century. *Nature* 332, 240–242. doi: 10.1038/332240a0
- Walczewski, J. (2005). Meteorologiczne i klimatyczne warunki rozprzestrzeniania się zanieczyszczeń powietrza. *Prz. Geofiz.* 3–4, 177–193.
- World Health Organization [WHO] (2000). *Air Quality Guidelines for Europe*. Copenhagen: WHO Regional Publications.
- Xing, J., Wang, J., Mathur, R., Wang, S., Sarwar, G., Pleim, J., et al. (2017). Impacts of aerosol direct effects on tropospheric ozone through changes in atmospheric dynamics and photolysis rates. *Atmos. Chem. Phys.* 17, 9869–9883. doi: 10.5194/acp-17-9869-2017
- Yienger, J. J., Klonecki, A. A., Levy, H., Moxim, W. J., and Carmichael, G. R. (1999). An evaluation of chemistry's role in the winter-spring ozone maximum found in the northern midlatitude free troposphere. *J. Geophys. Res.* 104, 3655–3667. doi: 10.1029/1998JD100043



OPEN ACCESS

EDITED BY
Nophea Sasaki,
Asian Institute of Technology, Thailand

REVIEWED BY
Bhoj Raj Ghimire,
Nepal Open University, Nepal
Yan Gao,
Universidad Nacional Autónoma de México,
Mexico

*CORRESPONDENCE
Jinlong Zhang
✉ jlzhang@kfbg.org
Stephan W. Gale
✉ stephangale@kfbg.org

SPECIALTY SECTION
This article was submitted to
Planted Forests,
a section of the journal
Frontiers in Forests and Global Change

RECEIVED 15 November 2022
ACCEPTED 05 January 2023
PUBLISHED 01 February 2023

CITATION
Zhu H, Zhang J, Cheuk ML, Hau BCH,
Fischer GA and Gale SW (2023) Monoculture
plantations impede forest recovery: Evidence
from the regeneration of lowland subtropical
forest in Hong Kong.
Front. For. Glob. Change 6:1098666.
doi: 10.3389/ffgc.2023.1098666

COPYRIGHT
© 2023 Zhu, Zhang, Cheuk, Hau, Fischer and
Gale. This is an open-access article distributed
under the terms of the [Creative Commons
Attribution License \(CC BY\)](https://creativecommons.org/licenses/by/4.0/). The use,
distribution or reproduction in other forums is
permitted, provided the original author(s) and
the copyright owner(s) are credited and that the
original publication in this journal is cited, in
accordance with accepted academic practice.
No use, distribution or reproduction is
permitted which does not comply with
these terms.

Monoculture plantations impede forest recovery: Evidence from the regeneration of lowland subtropical forest in Hong Kong

Huiling Zhu¹, Jinlong Zhang^{1*}, Mang Lung Cheuk¹,
Billy C. H. Hau², Gunter A. Fischer^{1,3} and Stephan W. Gale^{1*}

¹Flora Conservation Department, Kadoorie Farm and Botanic Garden, Tai Po, Hong Kong SAR, China, ²School of Biological Sciences, The University of Hong Kong, Pokfulam, Hong Kong SAR, China, ³Missouri Botanical Garden, St. Louis, MO, United States

Anthropogenic disturbance has led to widespread clearance and degradation of tropical forests, and tree planting has been promoted as an effective solution for recovery. However, trees have been overwhelmingly planted in monocultures or low-diversity mixes and this is expected to have profound, lasting impacts on forest structure, diversity, and functioning. In this study, we tested the extent to which historical vegetation transition types (VTTs) constrain forest recovery in a secondary tropical landscape in Hong Kong, South China. To do so, we overlaid vegetation types (forest, shrubland, pine plantation, grassland) identified in aerial photographs taken in 1956 and 1963 of a 20-ha plot situated in Tai Po Kau Nature Reserve, allowing us to define six historic VTTs, namely: FF (forest to forest), GP (grassland to plantation), GS (grassland to shrubland), SS (shrubland to shrubland), SF (shrubland to forest), and SP (shrubland to plantation). We compared present-day forest structure and species diversity among these VTTs, as determined from a census conducted in 2015, using incidence- and abundance-based rarefaction and extrapolation, and we assessed species' association within VTTs using a torus translation test. Our results reveal that stem density and species diversity in naturally regenerated forests were more similar to those of old-growth forest, whereas species diversity in areas occupied by pine plantations was significantly lower as compared with naturally regenerated areas. Despite 60 years of recovery, pine plantations were characterised by a significantly greater proportion of negatively associated species, and lateral species were still predominantly confined to old-growth patches. Present-day species distribution is chiefly explained by the combined effects of topography and VTT (17.1%), with VTT alone explaining 4.4%. Our study demonstrates that VTT has a significant long-term impact on forest regeneration and community assembly and, importantly, that monocultural plantations (forest plantation) can greatly impede forest recovery. Remnant old-growth forest patches merit priority protection, and active restoration, including thinning and enhancement planting, is necessary to facilitate forest succession.

KEYWORDS

subtropical forest, land-use history, biodiversity, aerial photograph, torus translation test, succession, forest restoration, vegetation transition types

1. Introduction

The occurrence of tree species within forest communities is defined by an interplay of environmental variables and historic disturbance (Hermý and Verheyen, 2007). Key environmental variables that contribute to the establishment and survival of a tree within its habitat include topographic factors, light availability, moisture, humidity, and soil properties (Harms et al., 2001; Comita et al., 2007; Zuleta et al., 2020). A habitat-association relationship of this sort has been confirmed by a number of studies conducted in forest dynamic plots in the tropics (Gunatilleke et al., 2006; Lai et al., 2009; Bin et al., 2016; Guo et al., 2016). However, as most forest dynamic plots are established in primary forest, these studies overwhelmingly focus on quantifying the relative importance of various environmental factors and tend to disregard the role of anthropogenic disturbances (Uriarte et al., 2004; Thompson et al., 2007). Indeed, forest plots in primary forest do not generally account for a human disturbance dimension and may therefore not be suitable for testing the relative contribution of historic disturbance regimes in limiting species distributions (Davies et al., 2021).

However, more than half of all tropical moist forests globally are at various stages of secondary regrowth following human-induced impact and conversion (Wright, 2005; Brancalion et al., 2019). Such disturbance may not only lead to the loss of canopy cover and biodiversity, but also fundamentally alter environmental conditions and constrain the forest's capacity to regenerate (Chazdon, 2003). Depending on the degree of degradation and specific land-use history, secondary forests (Brown and Lugo, 1990; Corlett, 1994; Dent and Wright, 2009) undergo contrasting successional pathways (Norden et al., 2011; Arroyo-Rodríguez et al., 2017). The particular pathway taken and the rate of succession will both be closely related to the initial composition during succession (Egler, 1954) and the same factors that govern the distribution of species in communities, that is, environmental variables and land-use history (Arroyo-Rodríguez et al., 2017). Both factors determine the remaining species pool (Karger et al., 2015), which comprises the species present *in situ* and/or those able to disperse out of remnant forest fragments nearby, as well as those represented in the soil seed bank (de Medeiros-Sarmento et al., 2021). Because the scale and intensity of disturbance dictates which species survive and remain locally able to reproduce, disperse and recruit, it also characterises the species pool available for recolonisation and succession (Brown and Boutin, 2009; Chase, 2003; Rozendaal et al., 2019).

Species pool is often greatly reduced after a clear-cut event and may only be able to partially recover (Xu et al., 2015). However, subsequent land-use type is also an important determining factor. In mountainous parts of South China, for example, where landscape-level forest clearance for agriculture dates back thousands of years, species survive in small, isolated, remnant forest fragments, or in secondary associations, forming small pockets of native biodiversity (Turner and Corlett, 1996). These pockets often conserve a significant proportion of the original species pool, some of which may be able to recolonise adjacent areas and thus contribute to the regeneration of continuous canopy cover given enough time (Turner and Corlett, 1996).

Whilst the remnant species pool determines which species are available to recolonise, the precise species composition of newly regenerated secondary communities at a given location is primarily defined by priority effect (Fukami, 2015; Fukami et al., 2016). This

is an aggregate ecological mechanism that allows those species that remain present in the soil seed bank, or which arrive at a disturbed site sooner, to attain dominance at an early stage of succession, thus enabling them to replace themselves repeatedly from seed where no competing late-seral species are present to initiate species turn-over (Ashton et al., 2001; Paul et al., 2004; Goldsmith et al., 2011). This can lead to arrested succession (Goldsmith et al., 2011; Young and Peffer, 2010). Priority effects have a significant impact not only on the dynamics of forest ecosystems, but also on the properties of the active species pool (Fukami, 2015). As the recovery of tree species diversity and community composition is often a long-term process (Osazuwa-Peters et al., 2015), historic disturbance and subsequent priority effect can constrain succession for decades or centuries to come. It is thus hypothesised that the signature of different disturbance regimes can be detected in forest communities even over exceptionally long timespans (Johnstone et al., 2016).

Planting trees is considered an effective approach to overcome priority effects (Weidlich et al., 2021) and thereby facilitate natural succession of degraded tropical lands (Lugo, 1992; Lamb et al., 2005; Crouzeilles et al., 2017; Meli et al., 2017). It has generally been argued that biodiversity and ecosystem functioning are better restored *via* tree planting (i.e., active restoration) than by natural succession (i.e., passive restoration) alone (Crouzeilles et al., 2017; Atkinson and Bonser, 2020). However, whether this is true or not in all cases remains contentious (Reid et al., 2019). Monocultures and plantation forest comprising exceptionally low diversity (Food and Agriculture Organization of the United Nations, 2018) may hamper natural succession as the species pool will be limited and regeneration capacity thereby constrained through priority effects (Maestre and Cortina, 2004; Holl et al., 2013; Liu et al., 2018). Indeed, whether or not active restoration is more effective than natural regeneration will depend on the degree of disturbance and the remaining species pool, as well as the selection of species planted and method of restoration (Chazdon, 2003; Reid et al., 2019). An inappropriate restoration method—for example, the use of a limited species mix or of species not suited to the modified environment—often results in lower diversity and delayed succession (Reid et al., 2019). Exotic tree plantations often further exacerbate the degradation of ecological functioning, *via* accelerated soil erosion, the promotion of pest outbreaks, and suppression of recovery in other dependent taxa, such as birds (Maestre and Cortina, 2004). In this sense, tree planting could actually delay or stall recovery. Indeed, analyses in Hong Kong revealed that, at the landscape level, secondary succession of tropical forest can be much faster in naturally regenerated areas as compared to areas planted with monocultural stands of exotic *Eucalyptus*, *Pinus*, and *Acacia* species (Abbas et al., 2019).

In the present study, we sought to assess the impact of different disturbance regimes caused by historic land-use changes on the current distribution of tree species in South China's secondary forest communities. To do so, we established a 20-ha forest dynamic plot following ForestGEO standards (Anderson-Teixeira et al., 2015; Davies et al., 2021) in Hong Kong. All trees inside the plot with a DBH (Diameter at Breast Height) ≥ 1 cm were mapped and identified, and their DBH was measured. To determine changes in forest cover over time and characterise specific vegetation transition types, we mapped historic vegetation cover as inferred from a time series of historic black and white aerial photographs. We hypothesise that the spatial distribution of species recovery will reflect historic disturbance regimes and that areas with the highest species diversity today will therefore be associated with small pockets of remnant old-growth

forest. We test the correlation between present forest structure [standing tree stem density and above-ground biomass (AGB)], diversity, species composition, and species-vegetation associations with different historic disturbance regimes to address the following questions: (i) do species richness, diversity and the presence/absence of indicator species differ among present-day vegetation types characterised by different disturbance regimes, and (ii), what are the relative influences of disturbance regime and environmental factors on present-day species composition? We discuss our findings in the context of the regenerative potential of degraded tropical lands and the potential for active restoration to overcome inherent barriers to secondary succession.

2. Materials and methods

2.1. Study site

Hong Kong is located on the coast of South China and has a marginally tropical climate with an annual average rainfall of 2,325 mm and an annual mean temperature of 23°C (Abbas, 2017). The zonal vegetation is usually considered evergreen broad-leaved forest (Zhuang and Corlett, 1997). However, due to widespread anthropogenic activities over the past several centuries, no primary forest remains in the territory (Zhuang and Corlett, 1997; Corlett, 1999). Our study site is located in the Tai Po Kau Nature (henceforth, TPK) Reserve, which is situated in Hong Kong's New Territories with an area of 460 ha and a steep, hilly topography. Despite the prevalence of plantations containing a mixture of native (*Castanopsis fissa*, *Cinnamomum camphora*, and *Pinus massoniana*) and exotic (*Acacia confusa*, *Eucalyptus tereticornis*, and *Lophostemon confertus*) species planted between 1956 and 1963, TPK's numerous remote, narrow gullies have protected small fragments of old-growth forest that pre-date WWII. As such, the reserve is regarded as one of the most biologically important secondary lowland woodlands in the territory (Nicholson, 1996).

A 400 × 500 m 20-ha plot was established inside TPK (22.42°N, 114.17°E) in 2012 (Figure 1A). The elevation of the plot ranges from 214 to 344 m, and the incline of the slope varies from 0.9 to 33.6° (Figure 1B). A full tree census (Condit, 1998; Anderson-Teixeira et al., 2015) was undertaken in the plot in 2015. A total of 81,019 individual trees (117,203 stems, including branches) with DBH ≥ 1 cm were recorded, belonging to 172 species, 111 genera and 53 families. The most abundant species was the shrub *Psychotria asiatica* with 26,646 individuals, which accounted for 33% of all individuals (Supplementary Table 1). Data pertaining to dead trees (1,876 stems or branches) were removed, including one species that was represented by a single individual, leaving 171 species for further analysis.

2.2. Classification of historic vegetation types and change in vegetation transition type over time

We obtained three black-and-white aerial photographs of TPK from the Lands Department of the Hong Kong SAR Government, one from 1956 (Supplementary Figure 1A) representing the initial degraded state, one from 1963 (Supplementary Figure 1B)

representing the early regeneration state, and one from 1983 (Supplementary Figure 1C) representing the closed canopy state. As the entire area was forested by 1983, the following assignment of vegetation to transition types was conducted for 1956 and 1963 only. The aerial photographs for these 2 years were firstly geo-referenced, co-registered and resampled to the same 1 m resolution for comparison. Then, we used the “segment mean shift” algorithms (Comaniciu and Meer, 1999) in ArcGIS 10.7 (ESRI, 2019, Redlands, California, USA) to delineate vegetation parcels with similar texture and grey tone. Segmented vegetation parcels were then divided into three groups based on the K-means clustering of averaged grey tone values within each parcel (Yadav and Sharma, 2013). Finally, manual refinements were made by considering the spatial continuity of each vegetation type.

Four vegetation types were identified in the aerial photographs: grassland, shrubland, pine plantation, and mixed natural forest. Whereas in 1956 the site comprised grassland, shrubland, and mixed natural forest (Supplementary Figure 1D), by 1963 the grassland had been substituted by pine plantation and shrubland (Supplementary Figure 1E). We overlaid the classified vegetation types in both images to derive six vegetation transition types (VTTs; Figure 2), namely, forest to forest (FF), grassland to pine plantation (GP), grassland to shrubland (GS), shrubland to shrubland (SS), shrubland to forest (SF), and shrubland to pine plantation (SP). Each VTT was regarded as reflecting a distinct vegetation change history. Because the FF VTT represented the occurrence of the oldest canopy cover in the plot, this vegetation was taken as reference old-growth forest. Whereas the GS, SS, and SF VTTs represented natural transitions were thus considered passive restoration, the GP VTT entailed management intervention was thus regarded as active restoration. The resulting vegetation transition map was converted to 20 m resolution (500 20 × 20 m subplots, Figure 2) based on the dominant rule (in which each grid cell was classified according to the VTT that accounted for the largest area within it) for further analyses. Since the area of SP (including six 20 × 20 m subplots, Figure 2) was <1 ha, this VTT was excluded from subsequent analysis.

2.3. Data analysis

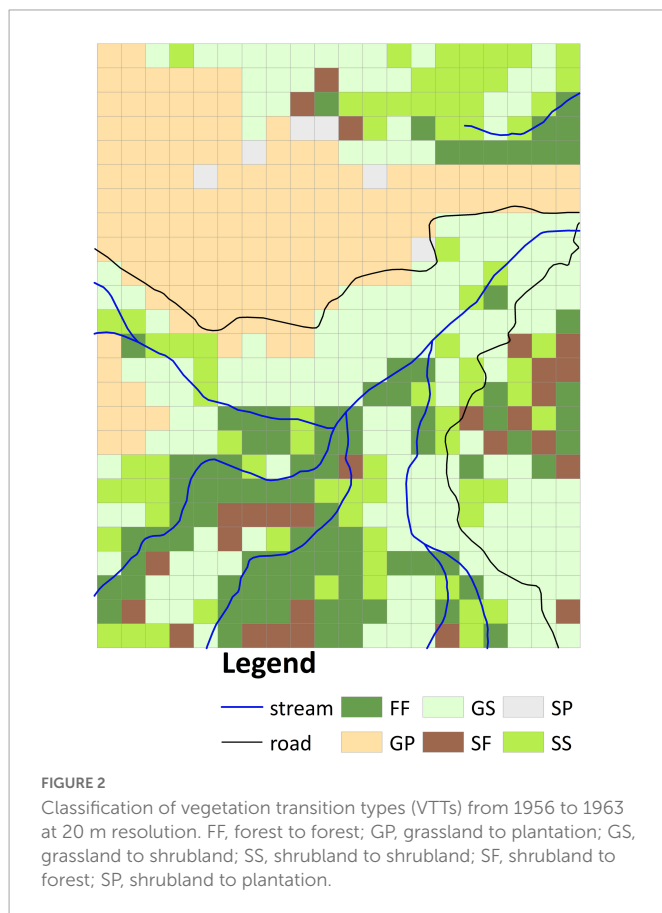
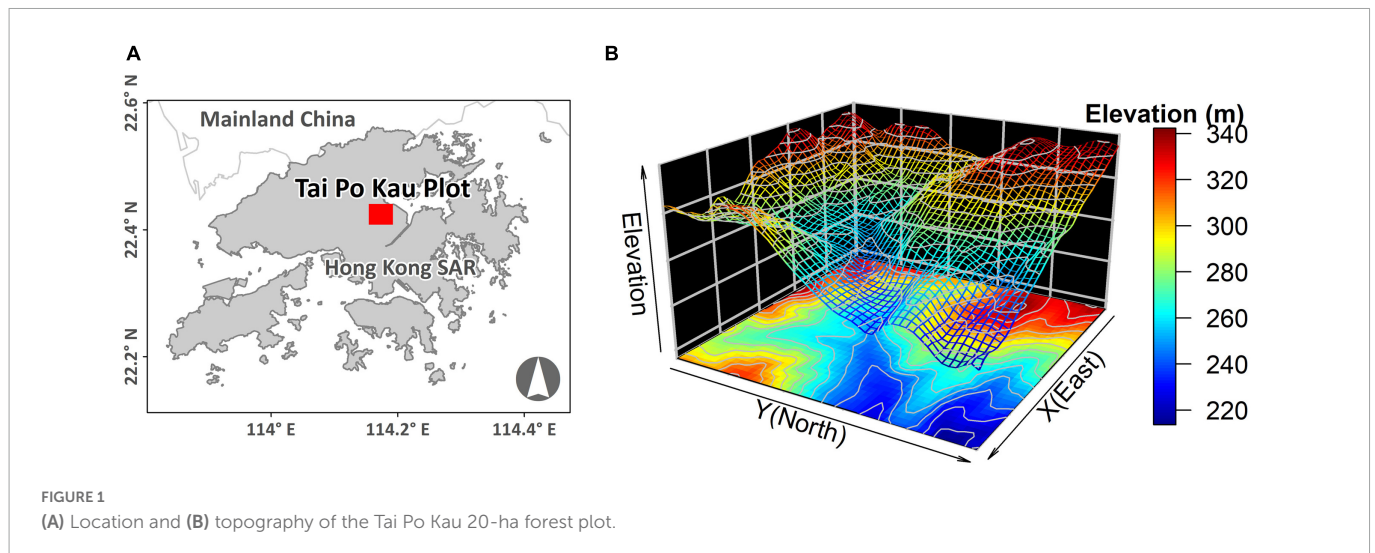
2.3.1. Comparison of stem density and above-ground biomass among VTTs

We used stem density and AGB to compare present-day forest structure, as determined by the 2015 census, between VTTs. We calculated AGB in kg based on DBH for all the species occurring in each VTT following Chave et al. (2005), using the following equation:

$$\text{AGB}_{\text{est}} = \rho \times \exp[-1.499 + 2.148 \ln(D) + 0.207 [\ln(D)]^2 - 0.0281 [\ln(D)]^3] \quad (1)$$

Where ρ is wood density (g/cm^3) and D is DBH (cm).

Wood densities were mainly compiled from studies conducted in Dinghushan (Zhang et al., 2018) and Heishiding (Yin et al., 2021), which represent the two closest ForestGEO plots to Hong Kong. Where data for certain species were not available from these sources, we obtained them from the R package BIOMASS (Réjou-Méchain et al., 2017). Where no wood density data were available, a mean value was derived from all other congeners, or from all species belonging to the same family, present in the plot.



We tested for significant differences in stem density and AGB between VTTs using resampling, which can reduce the effect of differences due to environmental factors and variable sample size (Chao and Jost, 2012; Chao et al., 2014). Twenty-five 20×20 m quadrats (total 1 ha) were randomly sampled for each VTT, and indices for both metrics were calculated in each quadrat. This procedure was repeated 1,000 times with replacement. 95% confidence intervals (CIs) were generated from the 2.5 and 97.5% quantiles, corresponding to significance at the 0.05 level (Goldsmith et al., 2006).

2.3.2. Comparison of diversity using rarefaction and extrapolation with Hill's numbers

We used Hill's numbers curves to determine the effect of VTT on biodiversity (Jost, 2007; Chao and Jost, 2012; Chao et al., 2014). The first three Hill's numbers are: (1) species richness ($q = 0$), (2) the exponential of Shannon's entropy index ($q = 1$), and (3) the inverse of Simpson's concentration index ($q = 2$) (Hill, 1973). These values were calculated using both incidence-based and abundance-based data for each VTT using the "iNEXT" package in R (Hsieh et al., 2016). The equation for abundance-based Hill's numbers is:

$${}^qD = \left(\sum_{i=1}^S p_i^q \right)^{\frac{1}{(1-q)}} \quad (2)$$

And the equation for incidence-based Hill's numbers is:

$${}^q\Delta = \left[\sum_{i=1}^S \left(\frac{\pi_i}{\sum_{j=1}^S \pi_j} \right)^q \right]^{\frac{1}{(1-q)}} \quad (3)$$

Where S is the number of species; p_i is the relative abundance of the i th species; and π_i is the relative incidence of the i th species. Incidence was calculated based on occurrence in the 20×20 m quadrats.

2.3.3. Species turnover in different VTTs

In comparing Hill's numbers among different vegetation types, we also tested if species turnover differs among VTTs (Wilson and Shmida, 1984; Koleff et al., 2003). Species turnover was visualised using an RGB colour map derived from non-metric multidimensional scaling (NMDS) (Thessler et al., 2005). To do so, we computed Bray-Curtis dissimilarities (Bray and Curtis, 1957) between all 20×20 m quadrats and constrained the results to three axes using the function "metaMDS" in the "vegan" package (Oksanen et al., 2022). The scores of the first three axes were converted to hexadecimal colour values for red, blue, and green, respectively. As the value of RGB colours must be positive integers, we added a constant (1.0) to the NMDS ordination axis scores to make them positive, multiplied them by 100 and then rounded the product. The red, green, and blue layers of each quadrat were overlaid and visualised to create an RGB colour map in ArcGIS (Thessler et al., 2005). Using this map, we were able to compare

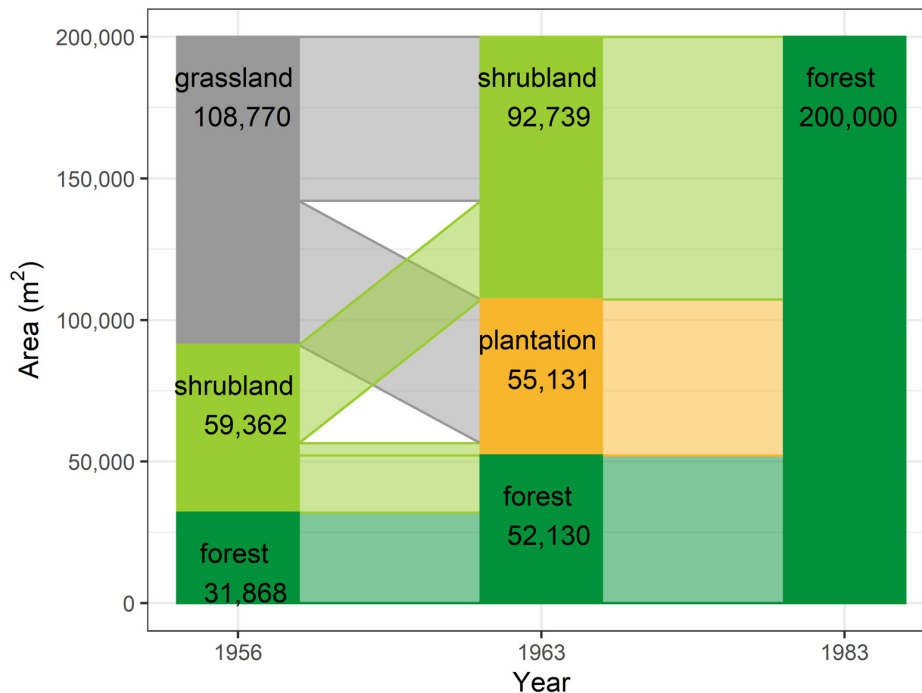


FIGURE 3

Schematic representation of the area accounted for by each vegetation type within the TPK plot at each time point.

species composition chromatically (Thessler et al., 2005; Hogan et al., 2016), with greater similarity in colour being indicative of greater similarity in the range of species present.

2.3.4. Quantifying the relative importance of VTT and topography

We recorded elevation, slope incline, curvature and aspect in each 20×20 m quadrat. These variables have been widely used to define topography in other forest dynamic plots (Harms et al., 2001; Lai et al., 2009; Guo et al., 2017; Davies et al., 2021). All variables were standardised through *z*-score standardisation (see R code in [Supplementary material](#)). We then used variation partitioning to quantify the relative importance of VTT and topography in explaining species turnover (Legendre, 2008; Legendre and Legendre, 2012; Peres-Neto et al., 2006). This was carried out using the function “varpart” (Borcard et al., 1992; Legendre and Legendre, 2012) in *vegan* (Oksanen et al., 2022).

2.3.5. Species–VTT association using torus translation test

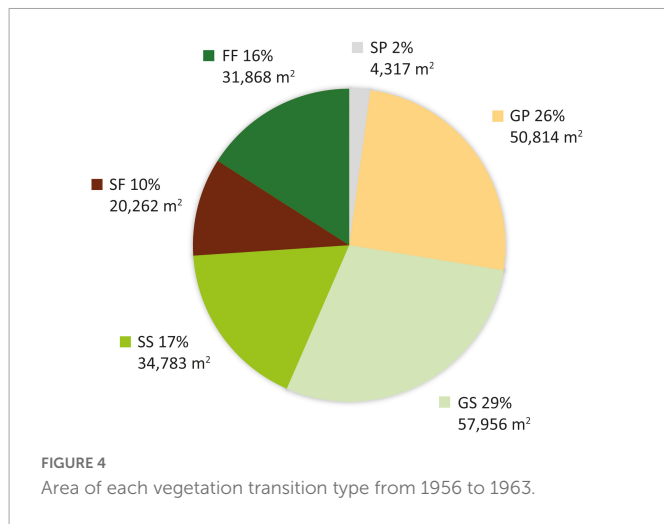
We used a torus translation test to evaluate the strength of association between species and VTT (Harms et al., 2001; Zuleta et al., 2020). This approach allowed us to compare the observed relative densities of a species with the expected densities generated from simulated habitat maps for each vegetation type (Harms et al., 2001; Comita et al., 2007; Lai et al., 2009). We shifted the observed vegetation map by 20 m increments in the four cardinal directions and calculated a relative density for each species. We then ran the torus translation procedure for three simulated maps based on the original map: mirror image, 180° rotation and 180° rotation of the mirror image. As the TPK plot has 500 (20×25) 20 m cells, we generated 1999 ($500 \times 4 - 1$) simulated maps. If the

relative density of a species determined from the original vegetation map deviated from 97.5% of the simulated relative densities (i.e., 0.05 significance for a two-tailed test), the species was judged to be statistically associated (either positively or negatively) with that VTT (Harms et al., 2001). Sixty-three species represented by <20 individuals were excluded for the purpose of this analysis, leaving 108 species (of a total of 171). Analyses were conducted with *fgeo.habitat* (Lepore, 2018) in R (see R code in [Supplementary material](#)).

3. Results

3.1. Change in vegetation type over time

The study area was found to have gradually transformed from a grassland-dominated landscape to a forest-dominated one as a result of natural succession and active restoration over the study period (Figure 3). Whereas 54.4% (108,770 m²) of the plot was grassland in 1956, with scattered patches of mixed natural forest occurring only in ravines along streams and accounting for just 15.9% of the total area (Figure 3), forests occupied 26.1% of the plot in 1963 and 100% in 1983. This transformation was mainly achieved through expansion of remnant natural forest from the streams. However, nearly half (GP: 50,814 m²) of the area occupied by grassland in 1956 had been replaced by pine plantation in 1963, with the remaining half (GS: 57,956 m²) becoming shrubland (Figure 4). More than half of the shrubland present in 1956 was still shrubland in 1963 (SS: 34,783 m²). Only a very small fraction (SP: 4,317 m²) of shrubland had been replaced by pine plantation in 1963.



3.2. Stem density and above-ground biomass among VTTs

Stem density was highest in SF and lowest in FF, and whilst there was no significant difference among GS, SS, and FF, it was significantly higher in GP than in SS and FF (Figure 5A). A similar pattern was observed in AGB, although the differences among VTTs were smaller, with that associated with GP being almost the same as for GS (Figure 5B). Differences in stem density were mainly caused by smaller trees (DBH 1–5 cm), while differences in AGB were mainly contributed by the trees with intermediate or large diameters (DBH ≥ 10 cm) (Supplementary Figure 2).

3.3. Comparing Hill's numbers among VTTs

Numbers of species and individuals associated with different VTTs are shown in Table 1. *Psychotria asiatica* was the dominant species in all vegetation types (Supplementary Table 2). Whereas FF was ascribed the highest values for all Hill's numbers, diversity curves were the lowest for GP (Figures 6A–F). GS was significantly higher and closer to FF than it was to GP. For the abundance-based curves, Hill's numbers for richness ($q = 0$) declined in the order FF > SS > GS > SF > GP. However, 95% CIs overlapped for GS, SS, and FF, indicating no significant difference. Hill's numbers for the exponential of Shannon's entropy index ($q = 1$) and for the inverse of Simpson's concentration index ($q = 2$) declined in the order FF > SS > SF > GS > GP. In both cases, most curves were widely separated from one another, apart from GS and SF for $q = 1$ (Figures 6B,C). In the incidence-based curves, whereas the 95% CIs for GS, SS, and SF overlapped with one another and were close to those for FF, those for GP were much lower and clearly separated (Figures 6D–F). Coverage of sample size approximated to one for both abundance (Figure 6G) and incidence data (Figure 6H).

3.4. Species turnover in different VTTs

Species composition was closely correlated with topography and varied across VTTs (Figure 7). Meanwhile, compositional differences

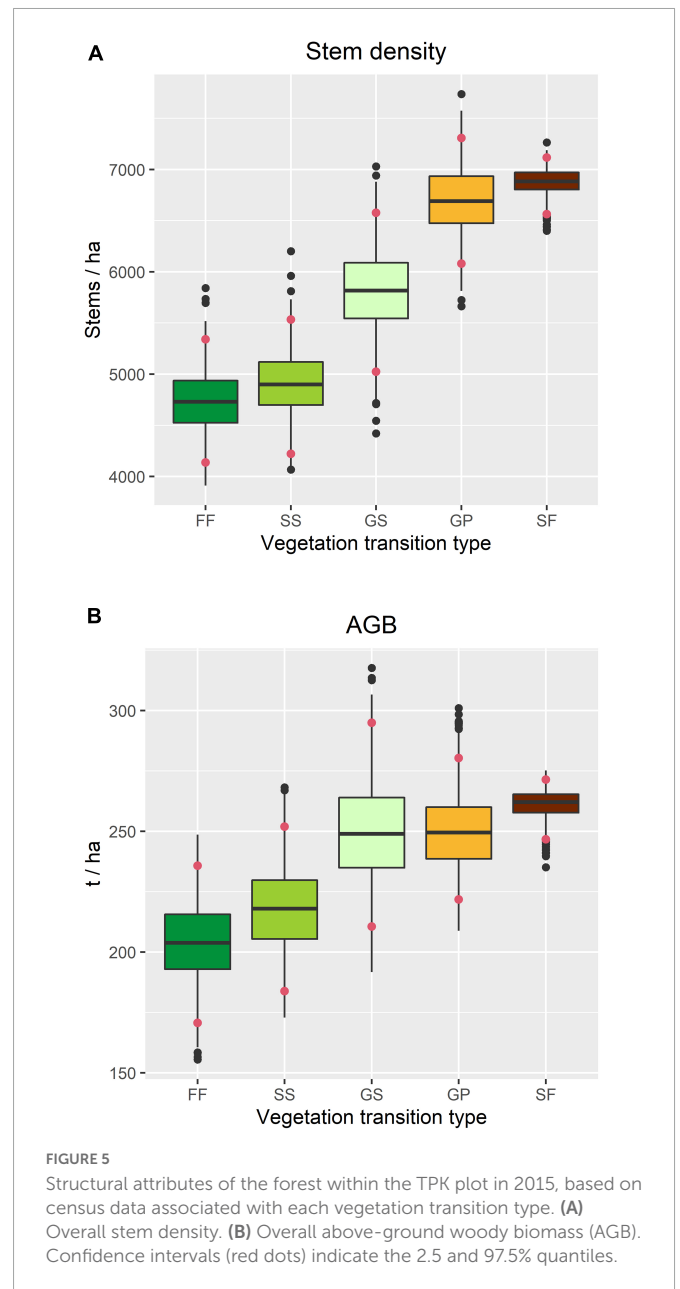


TABLE 1 Number of species and individuals in each vegetation transition type (see main text for definition of each acronym).

| Type | GS | GP | FF | SS | SF | SP |
|--------------------|--------|--------|--------|--------|-------|-----|
| No. of species | 152 | 123 | 143 | 135 | 106 | 60 |
| No. of individuals | 27,733 | 24,683 | 11,146 | 10,351 | 5,137 | 763 |

were captured along the elevational gradient in all VTTs except for the area of pine plantation represented by GP (Figure 7).

3.5. The relative importance of VTT and topography

Variation partitioning showed that VTT and topography accounted for 17.1% of total variation in species composition. Whereas VTT alone explained 4.4% of total variance and topography

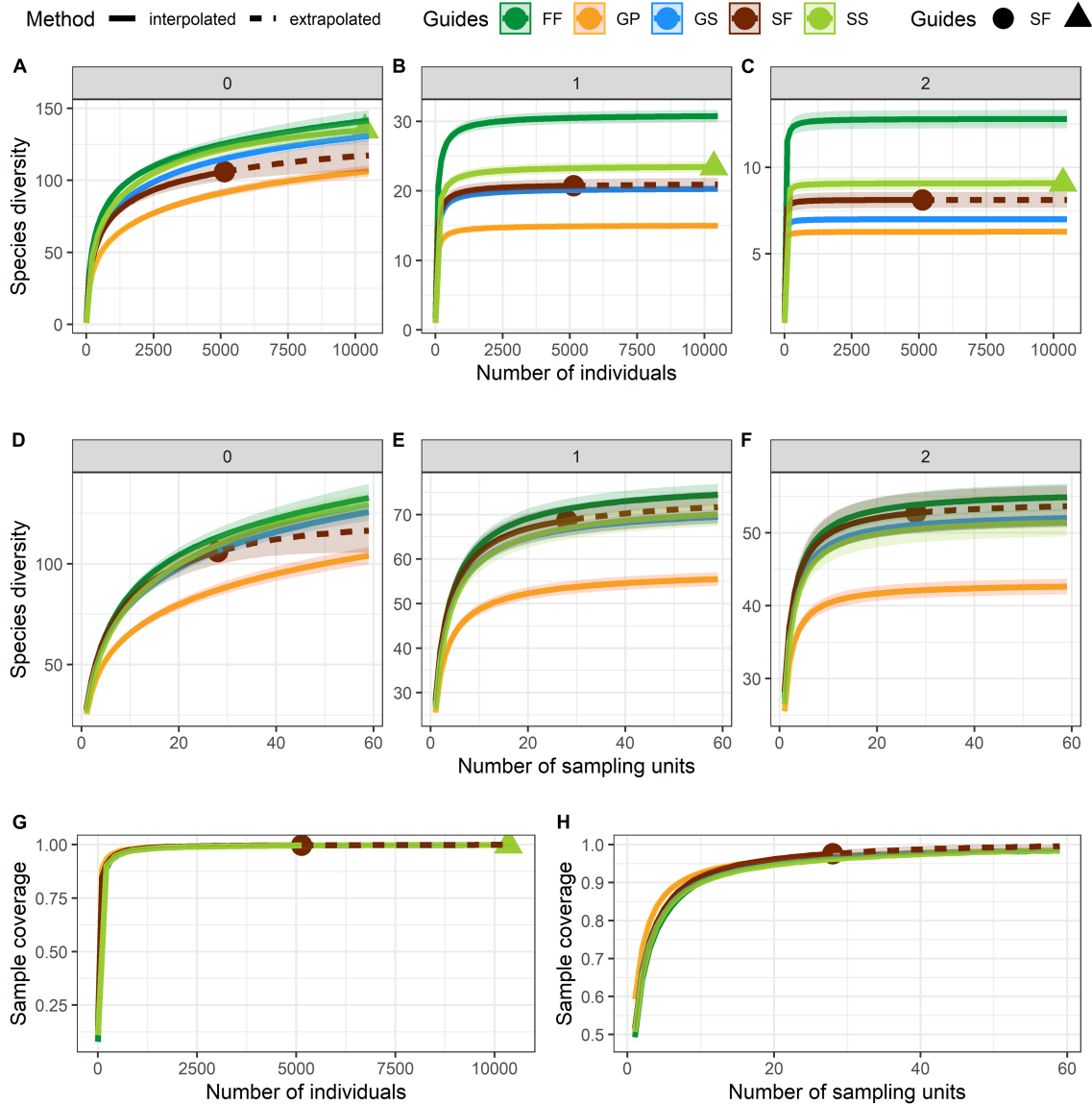


FIGURE 6
 Curves of Hill's numbers for each vegetation transition types (VTTs). (A–C) Abundance-based Hill's numbers. (D–F) Incidence-based Hill's numbers. In panels (A) and (D): $q = 0$ (species richness); in panels (B) and (E): $q = 1$ (exponential of Shannon's entropy index); in panels (C) and (F): $q = 2$ (inverse of Simpson's concentration index). (G) Sample completeness (sample-coverage) curve for abundance data. (H) Sample completeness (sample-coverage) curve for incidence data. 95% confidence intervals (CIs) were indicated by the shade areas above and below each curve and were obtained by bootstrapping 1,000 replicates. The sampling unit is 400 m² (20 × 20 m quadrat) in the incidence-based analyses.

alone explained 9.7%, both factors together explained 2.9% of variance (Figure 8).

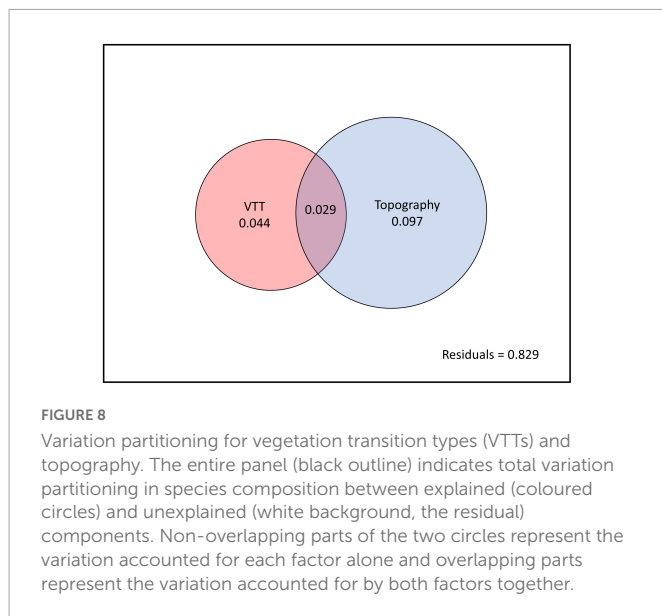
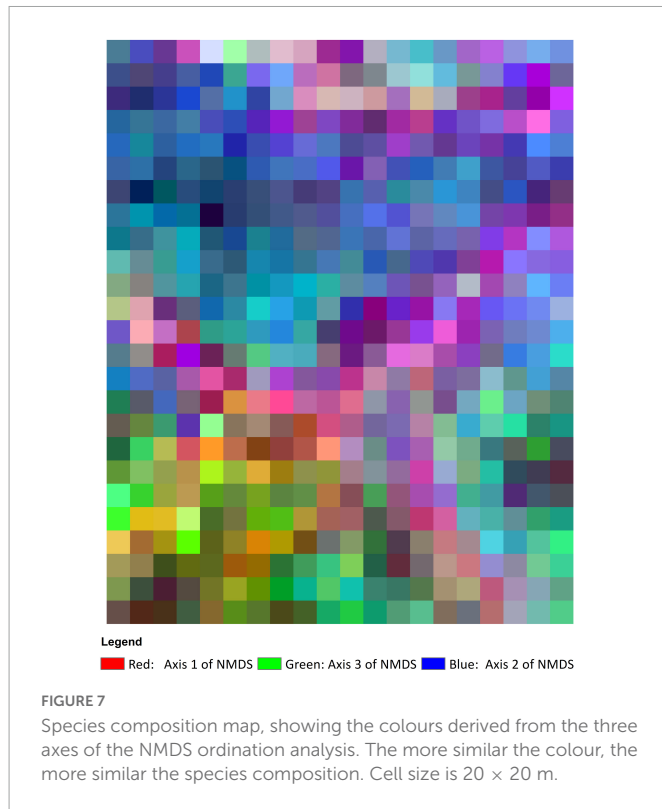
3.6. Species–VTT association using torus translation test

Of the 108 species tested in the torus translation test, 70 (64.8%) were significantly associated with at least one VTT (Supplementary Table 2). Twenty-seven species (25.0%) were negatively associated with GP (Table 2), which was the highest number of species among all VTTs, and 17 species (15.7%) were negatively associated with SF. Equally, different VTTs were significantly associated with certain species. FF had the highest number of positively associated species (31) (Table 3), which was significantly greater than that for all other

VTTs, whereas FF, GS, and SS had relatively few negatively associated species (Table 2).

4. Discussion

In this study, we explored the impact of historical vegetation type changes, as characterised by a series of empirically defined VTTs, on stem density, AGB, species diversity, and species composition in a secondary lowland forest in South China. We quantified the relative contribution of VTT and topographic variables on the fine-scale distribution of tree species. We report that, at the landscape scale, the distribution of trees today is still heavily constrained by historical VTTs, even after 60 years of combined passive and active recovery. Our findings clearly demonstrate that, although stem density and



AGB may recover in a few decades, species diversity and composition do not recover that rapidly.

4.1. Generalists dominate the entire plot

Species colonising during early succession are usually regarded as generalists or “winner” species (McKinney and Lockwood, 1999; Zhao et al., 2015) owing to their ability to tolerate, and attain dominance under harsh conditions. This appears to be the case at our study site. The common understorey shrub *Psychotria asiatica* alone accounted for 33% of all stems, and the fast-growing trees

Aporosa dioica, *Diospyros morrisiana*, and *Machilus chekiangensis* were among the most abundant species throughout the entire plot (Supplementary Table 1). These species exhibit several ecological traits characteristic of generalists, including fruits that are attractive to common wildlife and which are consequently widely dispersed, and high drought-tolerance during the early growth phase, allowing them to compete with grasses and so colonise grassland (Tabarelli et al., 2012; Zhao et al., 2015). The seed source of these winner species may have been nearby patches of old-growth forest or shrubland during the initial degraded phase, or they could have dispersed into the plot from further afield.

Classical models of forest succession predict that once the canopy has closed, mid- or late-seral species arrive and establish, thereby facilitating community enrichment (Ashton et al., 2001; Poorter et al., 2021). Our results show that this may be unlikely to happen rapidly, given that late-seral species are often rare and overwhelmingly restricted to small patches of old-growth forest (FF), and that seed dispersers are locally extinct, hence limiting opportunities for recovery.

4.2. Forest structure and diversity of different VTTs

Whilst initial vegetation type was found to have a significant impact on present-day abundance-based diversity indices, impact in terms of stem density, AGB and incidence-based diversity indices, which relate to spatial distribution, was limited. In terms of forest age, the different VTTs identified in the TPK plot decline in the order FF > (SE, SS) > (GP, GS). In old-growth forest, individual tree girth is usually greater and stem density is lower as compared with younger secondary forest (but see Augusto et al., 2000). Indeed, our results confirm that, at TPK, younger forest (i.e., SE, SS, GP, and GS) tends to have a higher stem density than does older forest (FF). This difference appears to be primarily caused by the presence of very large numbers of small saplings and shrubs (1 cm < DBH ≤ 5 cm) in shrubland and young forest.

Higher stem densities in these younger forest communities could indicate that competition among individuals is intense (Picard, 2019) and that natural stem-thinning is therefore likely to ensue (Field et al., 2020; Wu et al., 2020). However, stem density peaks in SE, despite this representing a comparatively advanced state of secondary succession in the sequence observed at TPK, suggesting that self-thinning has failed along this successional pathway. We note that an over-dominance of generalist shrubs (e.g., *Psychotria asiatica*) and faster growing, early seral trees (e.g., *Machilus chekiangensis*) in the SF VTT is linked to lower species diversity, higher stem density, and crucially, an absence of late-seral species, as compared with old-growth FF. This appears to limit tree girth increment and prevent species turnover, two features consistent with arrested succession (Kennard, 2002; Whitfield et al., 2014). The markedly different species composition observed between the SF and FF VTTs reinforces this inference and suggests that the successional pathway taken by post-disturbance secondary vegetation at TPK does not lead to reinstatement of authentic late-seral communities.

Poorter et al. (2016) found that AGB can recover by up to 90% of old-growth values after more than 60 years of succession, and that the impact of land-use history on present-day forest composition and structure may be limited in the neotropics. In contrast, our

TABLE 2 Species negatively associated with each vegetation transition type (VTT).

| Vegetation transition type | No. of species | Species |
|----------------------------|----------------|--|
| FF | 7 | <i>Aporosa dioica</i> , <i>Daphniphyllum calycinum</i> , <i>Ilex asprella</i> , <i>Glochidion wrightii</i> , <i>Cratoxylum cochinchinense</i> , <i>Cinnamomum parthenoxylon</i> , <i>Castanopsis lamontii</i> |
| GP | 27 | <i>Ardisia quinquegona</i> , <i>Ilex pubescens</i> , <i>Sterculia lanceolata</i> , <i>Ilex viridis</i> , <i>Casearia velutina</i> , <i>Ficus fistulosa</i> , <i>Dichroa febrifuga</i> , <i>Turpinia arguta</i> , <i>Adina pilulifera</i> , <i>Vitex quinata</i> , <i>Archidendron clypearia</i> , <i>Carallia brachiata</i> , <i>Glochidion eriocarpum</i> , <i>Saurauia tristyla</i> , <i>Macaranga sampsonii</i> , <i>Zanthoxylum avicennae</i> , <i>Eurya distichophylla</i> , <i>Cleistocalyx nervosus</i> , <i>Alleizettella leucocarpa</i> , <i>Antidesma venosum</i> , <i>Ardisia hanceana</i> , <i>Huodendron biaristatum</i> var. <i>parviflorum</i> , <i>Mallotus hookerianus</i> , <i>Ficus pyriformis</i> , <i>Antidesma japonicum</i> , <i>Cunninghamia lanceolata</i> , <i>Elaeocarpus nitentifolius</i> |
| GS | 4 | <i>Machilus chekiangensis</i> , <i>Castanopsis carlesii</i> , <i>Syzygium championii</i> , <i>Mallotus hookerianus</i> |
| SF | 17 | <i>Schefflera heptaphylla</i> , <i>Dichroa febrifuga</i> , <i>Lithocarpus elizabethiae</i> , <i>Macaranga sampsonii</i> , <i>Sloanea sinensis</i> , <i>Eurya distichophylla</i> , <i>Breynia fruticosa</i> , <i>Homalium cochinchinense</i> , <i>Maesa perlaria</i> , <i>Huodendron biaristatum</i> var. <i>parviflorum</i> , <i>Sapium discolor</i> , <i>Antidesma fordii</i> , <i>Mallotus hookerianus</i> , <i>Myrica rubra</i> , <i>Ficus pyriformis</i> , <i>Acacia confusa</i> , <i>Antidesma japonicum</i> |
| SS | 5 | <i>Castanopsis fabri</i> , <i>Macaranga sampsonii</i> , <i>Castanopsis carlesii</i> , <i>Huodendron biaristatum</i> var. <i>parviflorum</i> , <i>Antidesma japonicum</i> |

TABLE 3 Species positively associated with each vegetation transition type (VTT).

| Vegetation transition type | No. of species | Species |
|----------------------------|----------------|---|
| FF | 31 | <i>Ardisia quinquegona</i> , <i>Euonymus</i> sp., <i>Ilex pubescens</i> , <i>Sterculia lanceolata</i> , <i>Ilex viridis</i> , <i>Blastus cochinchinensis</i> , <i>Syzygium rehderianum</i> , <i>Wikstroemia nutans</i> , <i>Turpinia arguta</i> , <i>Archidendron clypearia</i> , <i>Ilex kwangtungensis</i> , <i>Carallia brachiata</i> , <i>Macaranga sampsonii</i> , <i>Sloanea sinensis</i> , <i>Callicarpa brevipes</i> , <i>Aidia canthioides</i> , <i>Aquilaria sinensis</i> , <i>Lithocarpus glaber</i> , <i>Eurya distichophylla</i> , <i>Gardenia jasminoides</i> , <i>Sinosideroxylon wightianum</i> , <i>Ixonanthes reticulata</i> , <i>Antidesma venosum</i> , <i>Huodendron biaristatum</i> var. <i>parviflorum</i> , <i>Artocarpus styracifolius</i> , <i>Ehretia longiflora</i> , <i>Mallotus hookerianus</i> , <i>Ficus pyriformis</i> , <i>Acacia confusa</i> , <i>Antidesma japonicum</i> , <i>Elaeocarpus nitentifolius</i> |
| GP | 8 | <i>Machilus chekiangensis</i> , <i>Aporosa dioica</i> , <i>Ilex asprella</i> , <i>Litsea rotundifolia</i> var. <i>oblongifolia</i> , <i>Castanopsis lamontii</i> , <i>Castanopsis fabri</i> , <i>Castanopsis carlesii</i> , <i>Myrica rubra</i> |
| GS | 9 | <i>Machilus pauhoi</i> , <i>Machilus velutina</i> , <i>Machilus breviflora</i> , <i>Adina pilulifera</i> , <i>Cratoxylum cochinchinense</i> , <i>Zanthoxylum avicennae</i> , <i>Maesa perlaria</i> , <i>Sapium discolor</i> , <i>Viburnum odoratissimum</i> |
| SF | 4 | <i>Itea chinensis</i> , <i>Reevesia thyrsoidea</i> , <i>Ixonanthes reticulata</i> , <i>Artocarpus styracifolius</i> |
| SS | 4 | <i>Garcinia oblongifolia</i> , <i>Ardisia quinquegona</i> , <i>Vitex quinata</i> , <i>Carallia brachiata</i> |

findings demonstrate that land-use history as reflected by historical VTTs can have a significant impact on the recovery of AGB, even after six decades of post-disturbance recovery, which is more in line with predictions made by [Jakovac et al. \(2021\)](#). Previous studies have shown that AGB is mainly accounted for by large-diameter stems ([Stephenson et al., 2014](#); [Lutz et al., 2018](#)) and that large trees are expected to occur more in old-growth forest than in younger associations ([Brown et al., 1997](#)). Our results show that in tropical Asia, where old-growth forest has been extensively converted into agricultural lands, this may not be entirely correct. We find that comparatively young secondary communities, represented by GS, GP, and SF in our study, have higher AGB than FF, the oldest forest community in our analysis. This appears to be because the number of small stems is significantly greater in the younger communities and the number of larger trees is low in FF. Indeed, tree size in South China's remnant old-growth patches are limited owing to several factors. Firstly, although the remnant patches may contain late-seral species, they too have usually been subject to intensive disturbance histories, including fire ([Chau and Corlett, 1994](#)), firewood collection ([Corlett, 1999](#)), and selective logging ([Zhuang and Corlett, 1997](#)) over a period of centuries. Secondly, because these patches are generally restricted to steep ravines, tree size may have been limited by rocky conditions and a lack of top soil due to seasonal flooding, which can lead to stunted tree growth ([Lopez and Kursar, 2003](#)). Thirdly, once the canopy of immediately adjacent secondary forest has been able to

close through regeneration, the environment along the streams could be too dark and therefore less suitable for remaining late-seral species to recruit and spread ([Lebrija-Trejos et al., 2011](#)).

In comparison, GS, GP, and SF appear to have higher AGB because winner, generalist species ([McKinney and Lockwood, 1999](#); [Tabarelli et al., 2012](#); [Filgueiras et al., 2021](#)) can successfully establish and grow to a larger size or attain a higher stem density on nearby slopes ([Zhao et al., 2015](#)). Indeed, significant increases in AGB are mainly generated by the presence of larger stems (DBH > 20 cm) throughout all VTTs, but because high stem density is associated with higher AGB, it does not necessarily reflect a recovery in species composition ([Rozendaal et al., 2019](#)). The exceptionally high number of stems in the young secondary forest communities studied here is primarily made up of generalist and winner species, indicative of arrested succession ([Goldsmith et al., 2011](#)).

4.3. Factors affecting species accumulation and seedling establishment

In analysing forest succession, it is common to substitute space for time to represent a chronosequence ([Abbas et al., 2016, 2019](#); [Poorter et al., 2021](#)). In the present study, however, we used historic aerial photographs to identify past vegetation types and reconstruct successional pathways, allowing us to estimate the impact of historic

land use more accurately. Although species composition was not documented in each subplot at the time the photographs were taken, we were able to retrospectively determine vegetation type using a statistical approach. By overlaying vegetation type distributions as inferred from the resulting time sequence, the specific disturbance history of each subplot could be inferred. This approach reduces ambiguity and highlights subtle but important differences between diverging successional pathways (Norden et al., 2011; Arroyo-Rodríguez et al., 2017; Jakovac et al., 2021).

Vegetation transition types alone was found to explain 4.4% of variation in present-day species distribution, as compared to 9.7% contributed by topography. A further 2.9% of variation was explained by both factors combined. It is not surprising that the effects of VTT are confounded with those caused by topography, given that both factors tend to act synergistically in constraining ecological tolerance (Guo et al., 2017; Schmitt et al., 2021). For example, it is conceivable that in ravines that are too steep or too rocky for conversion to agriculture, pre-existing forest cover was deliberately retained to maintain water supply (Luke et al., 2017).

Previous studies have shown that, although species richness can recover within a few decades in the tropics (Abbas et al., 2019), species composition may only partially recover (Xu et al., 2015). Similarly, our data reveal that, whereas species richness in the various VTTs was able to recover within six decades, species composition has not converged with that observed in old-growth patches (FF) over the same period, indicating that passive forest succession in these VTTs is slow. Potential underlying reasons for this include dispersal limitation (Palma et al., 2021), reduced species pool (Zobel et al., 1998), priority effects (Fukami, 2015; Fukami et al., 2016), competition (Connell and Slatyer, 1977; Chen et al., 2019), and environmental filtering (Jakovac et al., 2016, 2021), all of which are known to affect both tree seedlings and saplings.

4.4. Why are late-seral species restricted to small old-growth patches?

Multiple studies have found that differences in species composition can be explained by dispersal limitation (Condit et al., 2002; Shen et al., 2009; Palma et al., 2021), environmental gradients (Graco-Roza et al., 2022), and stochasticity (Asefa et al., 2020). However, the term “dispersal limitation” may be too general, encompassing numerous inter-related factors. In fact, there may be several inter-dependent reasons for the failure of establishment of late-successional species (Uhl, 1987), such as those which were found to be restricted to FF in the present study.

Firstly, the number of seeds that allow these species to establish in neighbouring areas may be far below the minimum threshold required for successful expansion (Palma et al., 2020) due, for example, to high rates of seed predation (Chung and Corlett, 2006) or because mother trees are confined to less than optimal conditions and are thus suppressed by over-dominant surrounding trees (Ding and Zang, 2021).

Secondly, a species' ability to germinate and persist will be affected by seed quality, which is itself influenced by genetic factors (Leimu et al., 2010). Trees occurring in old-growth patches within secondary forest are often isolated from other conspecific populations, and hence subject to reduced gene flow (Zeng et al., 2012). Consequently, these species typically exhibit the effects of inbreeding (Leimu et al., 2010; Young et al., 1996) and so

exhibit reduced seed viability and depressed seed-set (Kuussaari et al., 2009; Dullinger et al., 2012). Since this is often indicative of extinction debt (Kuussaari et al., 2009), conservation attention is important.

Thirdly, even if the species were able to produce a sufficient number of viable seeds, an absence of suitable dispersal agents may prevent them from recolonising surrounding vegetation types (Corlett, 2017; Silva et al., 2020). Brancalion et al. (2018) have shown that late-seral species tend to have larger fruits or seeds that are dispersed by animals or birds. In our study, a number of species within the FF VTT have larger fruits or seeds that are attractive to animals, for example, *Lithocarpus elizabethae*, *Sloanea sinensis*, *Artocarpus styracifolius*, and *Elaeocarpus nitentifolius* (Corlett, 2011). Successful dispersal of these species into adjacent areas is dependent on a range of dispersal agents, including hornbills, large squirrels, gibbons and other birds and mammals which are no longer present in Hong Kong (Corlett, 2011). One solution for overcoming this ecological barrier and associated extinction debt would be to reintroduce these locally extinct animal species back into Hong Kong's secondary forests (Svenning and Faurby, 2017; Carver et al., 2021). However, it is questionable whether today's secondary vegetation could support the survival of these large dispersal agents: Hong Kong's secondary forests are mostly too homogenised to provide year-round food supply (van Schaik et al., 1993; Lichstein et al., 2004; Keith et al., 2009; Corlett, 2011).

4.5. Low-diversity forest plantations can impede natural recovery

Pine trees have been widely used for afforestation in Hong Kong (Corlett, 1999). However, the pine trees previously planted in TPK (*P. massoniana*) were mostly eradicated by wilt disease during the 1970s, resulting in reversion to grassland and shrubland (Zhuang, 1997). The impact of this can be seen in our results: species diversity was significantly greater in GS than in GP, and it approximated more closely to that found in FF, indicating that natural regeneration was more effective than low diversity active restoration in terms of overall ecological recovery. Indeed, species composition in areas previously under pine plantation differed markedly from that in other VTTs, even after decades of recovery and natural succession. The number of negatively associated species within the pine plantation area was much greater than that in other VTTs, particularly with respect to species indicative of old-growth primary forest, such as *Turpinia arguta*, *Mallotus hookerianus*, and *Ficus pyriformis*. Previous research suggests that *Pinus* species impose an intense priority effect on natural regeneration (Tomimura et al., 2012) through niche pre-emption and modification (Fukami, 2015). In addition, monocultural plantations are known to negatively affect soil properties, including cation exchange capacity and availability of phosphorous and potassium (Caravaca et al., 2002; Maestre and Cortina, 2004), plus they can adversely affect the composition and diversity of the seedling layer (Comita et al., 2010). It thus seems important to recognise that any short- to medium-term benefits associated with monocultural plantations in terms of soil stabilisation and reduced fire risk (Corlett, 1999) could be counteracted by these kinds of long-term detrimental impacts, which can in turn lead to arrested succession (Goldsmith et al., 2011). Indeed, planting low diversity species mixes can be risky (Holl et al., 2022), strongly influencing the successional pathway and available species pool in a way that can mean complete canopy coverage is not attained.

4.6. Management and conservation implications

Although biotic homogenisation is often prevalent in secondary forests (McKinney and Lockwood, 1999; Holl et al., 2022), secondary forests themselves are not necessarily homogeneous. In particular, patches of old-growth forest that harbour a diverse set of late-seral species may be scattered within a secondary forest matrix in a non-random manner (Liu et al., 2019; Liu and Slik, 2014). Such patches are likely to retain higher species diversity and thus be of greater conservation value (Cardoso et al., 2022), and our results underscore the importance of ensuring that they serve as reservoirs of regenerative potential by identifying and removing key barriers to spread.

Indeed, we reveal that the effects of historical VTTs can persist for 60 years or longer, demonstrating that past disturbance regimes should be taken into account in studies of community assembly and forest succession in degraded tropical landscapes. Our data indicate that many species are unable to colonise monocultural plantations, reinforcing their artificially low diversity, and secondarily making them more vulnerable to pests and diseases, thereby retarding succession (Siemann and Rogers, 2006; Liu et al., 2018; Wu et al., 2021). Conversely, multispecies forest plantations are likely to offer preferable outcomes in terms of ecosystem services (Feng et al., 2022).

Conservation intervention is clearly necessary to secure the long-term persistence of rare, late-seral species, and overcome the bottlenecks discussed here, by, for instance, selectively thinning the understorey to improve fine-scale conditions that support dispersal, establishment and turnover (Deng et al., 2020; Ding and Zang, 2021). Enhancement planting should also be considered to increase overall biodiversity after thinning (Corlett, 2011; Abbas et al., 2020), and such interventions may not only be critical for trees and shrubs, but also herbaceous elements, too.

Data availability statement

Publicly available datasets were analyzed in this study. This data can be found here: <https://forestgeo.si.edu/sites/asia/hong-kong>.

Author contributions

HZ: data curation, formal analysis, investigation, methodology, visualization, writing original draft, and review and editing. JZ: conceptualization, data curation, methodology, software,

validation, writing original draft, and review and editing. MLC: formal analysis, methodology, visualization, and review and editing. BCHH: investigation, methodology, project administration, and review and editing. GAF: conceptualization, investigation, methodology, project administration, and review and editing. SWG: conceptualization, investigation, project administration, and review and editing. All authors contributed to the article and approved the submitted version.

Acknowledgments

We acknowledge the constructive comments received from mentors present at the 2019 ForestGEO Annual Analytical Workshop funded by the Smithsonian Institution, especially Stuart J. Davies and Sabrina E. Russo for their suggestions on data analysis. We thank Chengjin Chu's lab for providing wood density data for several species. We also thank Prof. Anne Chao for providing comments and suggestions on rarefaction and extrapolation with Hill's numbers. We greatly thank the people who conducted the field survey and data entry for the Tai Po Kau Plot. The survey would not have been possible without financial support from HSBC.

Conflict of interest

The authors declare that the research was conducted in the absence of any commercial or financial relationships that could be construed as a potential conflict of interest.

Publisher's note

All claims expressed in this article are solely those of the authors and do not necessarily represent those of their affiliated organizations, or those of the publisher, the editors and the reviewers. Any product that may be evaluated in this article, or claim that may be made by its manufacturer, is not guaranteed or endorsed by the publisher.

Supplementary material

The Supplementary Material for this article can be found online at: <https://www.frontiersin.org/articles/10.3389/ffgc.2023.1098666/full#supplementary-material>

References

- Abbas, S. (2017). *Remote sensing of forest succession in Hong Kong's country parks*. Available online at: <https://theses.lib.polyu.edu.hk/handle/200/8886> (accessed July 13, 2022).
- Abbas, S., Nichol, J. E., and Fischer, G. A. (2016). A 70-year perspective on tropical forest regeneration. *Sci. Total Environ.* 544, 544–552. doi: 10.1016/j.scitotenv.2015.11.171
- Abbas, S., Nichol, J. E., Fischer, G. A., Wong, M. S., and Irteza, S. M. (2020). Impact assessment of a super-typhoon on Hong Kong's secondary vegetation and recommendations for restoration of resilience in the forest succession. *Agric. For. Meteorol.* 280:107784. doi: 10.1016/j.agrformet.2019.107784
- Abbas, S., Nichol, J. E., Zhang, J., and Fischer, G. A. (2019). The accumulation of species and recovery of species composition along a 70 year succession in a tropical secondary forest. *Ecol. Indic.* 106:105524. doi: 10.1016/j.ecolind.2019.105524
- Anderson-Teixeira, K. J., Davies, S. J., Bennett, A. C., Gonzalez-Akre, E. B., Muller-Landau, H. C., Joseph Wright, S., et al. (2015). CTFs-ForestGEO: A worldwide network

- monitoring forests in an era of global change. *Glob. Change Biol.* 21, 528–549. doi: 10.1111/gcb.12712
- Arroyo-Rodríguez, V., Melo, F. P. L., Martínez-Ramos, M., Bongers, F., Chazdon, R. L., Meave, J. A., et al. (2017). Multiple successional pathways in human-modified tropical landscapes: New insights from forest succession, forest fragmentation and landscape ecology research: Multiple successional pathways. *Biol. Rev.* 92, 326–340. doi: 10.1111/brv.12231
- Asefa, M., Wen, H., Brown, C., Cao, M., Xu, K., and Hu, Y. (2020). Ecological drivers of tree assemblage in tropical, subtropical and subalpine forests. *J. Veg. Sci.* 31, 107–117. doi: 10.1111/jvs.12819
- Ashton, M. S., Gunatilleke, C. V. S., Singhakumara, B. M. P., and Gunatilleke, I. A. U. N. (2001). Restoration pathways for rain forest in southwest Sri Lanka: A review of concepts and models. *For. Ecol. Manag.* 154, 409–430. doi: 10.1016/S0378-1127(01)00512-6
- Atkinson, J., and Bonser, S. P. (2020). “Active” and “passive” ecological restoration strategies in meta-analysis. *Restor. Ecol.* 28, 1032–1035. doi: 10.1111/rec.13229
- Augusto, A., Tabanez, J., and Viana, V. M. (2000). Patch structure within Brazilian Atlantic forest fragments and implications for conservation. *Biotropica* 32, 925–933. doi: 10.1111/j.1744-7429.2000.tb00630.x
- Bin, Y., Spence, J., Wu, L., Li, B., Hao, Z., Ye, W., et al. (2016). Species-habitat associations and demographic rates of forest trees. *Ecography* 39, 9–16. doi: 10.1111/ecog.00787
- Borcard, D., Legendre, P., and Drapeau, P. (1992). Partialling out the spatial component of ecological variation. *Ecology* 73, 1045–1055. doi: 10.2307/1940179
- Brancalion, P. H. S., Bello, C., Chazdon, R. L., Galetti, M., Jordano, P., Lima, R. A. F., et al. (2018). Maximizing biodiversity conservation and carbon stocking in restored tropical forests. *Conserv. Lett.* 11:e12454. doi: 10.1111/conl.12454
- Brancalion, P. H. S., Niamir, A., Broadbent, E., Crouzeilles, R., Barros, F. S. M., Almeyda Zambrano, A. M., et al. (2019). Global restoration opportunities in tropical rainforest landscapes. *Sci. Adv.* 5:eav3223. doi: 10.1126/sciadv.aav3223
- Bray, J. R., and Curtis, J. T. (1957). An ordination of the upland forest communities of Southern Wisconsin. *Ecol. Monogr.* 27, 325–349. doi: 10.2307/1942268
- Brown, C. D., and Boutin, C. (2009). Linking past land use, recent disturbance, and dispersal mechanism to forest composition. *Biol. Conserv.* 142, 1647–1656. doi: 10.1016/j.bioccon.2009.02.035
- Brown, S., and Lugo, A. E. (1990). Tropical secondary forests. *J. Trop. Ecol.* 6, 1–32. doi: 10.1017/S0266467400003989
- Brown, S., Schroeder, P., and Birdsey, R. (1997). Aboveground biomass distribution of US eastern hardwood forests and the use of large trees as an indicator of forest development. *For. Ecol. Manag.* 96, 37–47. doi: 10.1016/S0378-1127(97)00044-3
- Caravaca, F., Garcia, C., Hernández, M. T., and Roldán, A. (2002). Aggregate stability changes after organic amendment and mycorrhizal inoculation in the afforestation of a semi-arid site with *Pinus halepensis*. *Appl. Soil Ecol.* 19, 199–208. doi: 10.1016/S0929-1393(01)00189-5
- Cardoso, F. C. G., Capellessio, E. S., de Brites, R. M., Inague, G., and Marques, M. C. M. (2022). Landscape conservation as a strategy for recovering biodiversity: Lessons from a long-term program of pasture restoration in the southern Atlantic Forest. *J. Appl. Ecol.* 59, 2309–2321. doi: 10.1111/1365-2664.14240
- Carver, S., Convery, I., Hawkins, S., Beyers, R., Eagle, A., Kun, Z., et al. (2021). Guiding principles for rewilding. *Conserv. Biol.* 35, 1882–1893. doi: 10.1111/cobi.13730
- Chao, A., and Jost, L. (2012). Coverage-based rarefaction and extrapolation: Standardizing samples by completeness rather than size. *Ecology* 93, 2533–2547. doi: 10.1890/11-1952.1
- Chao, A., Gotelli, N. J., Hsieh, T. C., Sander, E. L., Ma, K. H., Colwell, R. K., et al. (2014). Rarefaction and extrapolation with Hill numbers: A framework for sampling and estimation in species diversity studies. *Ecol. Monogr.* 84, 45–67. doi: 10.1890/13-0133.1
- Chase, J. M. (2003). Community assembly: When should history matter? *Oecologia* 136, 489–498. doi: 10.1007/s00442-003-1311-7
- Chau, L. K. C., and Corlett, R. T. (1994). “Fire and weather in Hong Kong,” in *Proceedings of the 12th conference on fire and forest meteorology*, Jekyll Island, GA, 442–452.
- Chave, J., Andalo, C., Brown, S., Cairns, M. A., Chambers, J. Q., Eamus, D., et al. (2005). Tree allometry and improved estimation of carbon stocks and balance in tropical forests. *Oecologia* 145, 87–99. doi: 10.1007/s00442-005-0100-x
- Chazdon, R. L. (2003). Tropical forest recovery: Legacies of human impact and natural disturbances. *Perspect. Plant Ecol. Evol. Syst.* 6, 51–71. doi: 10.1078/1433-8319-00042
- Chen, Y., Uriarte, M., Wright, S. J., and Yu, S. (2019). Effects of neighborhood trait composition on tree survival differ between drought and postdrought periods. *Ecology* 100:e02766. doi: 10.1002/ecy.2766
- Chung, K. P. S., and Corlett, R. T. (2006). Rodent diversity in a highly degraded tropical landscape: Hong Kong, South China. *Biodivers. Conserv.* 15, 4521–4532. doi: 10.1007/s10531-005-5102-9
- Comaniciu, D., and Meer, P. (1999). “Mean shift analysis and applications,” in *Proceedings of the 7th IEEE international conference on computer vision*, (Kerkyra: IEEE), 1197–1203. doi: 10.1109/ICCV.1999.790416
- Comita, L. S., Condit, R., and Hubbell, S. P. (2007). Developmental changes in habitat associations of tropical trees. *J. Ecol.* 95, 482–492.
- Comita, L. S., Thompson, J., Uriarte, M., Jonckheere, I., Canham, C. D., and Zimmerman, J. K. (2010). Interactive effects of land use history and natural disturbance on seedling dynamics in a subtropical forest. *Ecol. Appl.* 20, 1270–1284. doi: 10.1890/09-1350.1
- Condit, R. (1998). *Tropical forest census plots*. Berlin: Springer. doi: 10.1007/978-3-662-03664-8
- Condit, R., Pitman, N., Leigh, E. G., Chave, J., Terborgh, J., Foster, R. B., et al. (2002). Beta-diversity in tropical forest trees. *Science* 295, 666–669. doi: 10.1126/science.1066854
- Connell, J. H., and Slatyer, R. O. (1977). Mechanisms of succession in natural communities and their role in community stability and organization. *Am. Nat.* 111, 1119–1144. doi: 10.1086/283241
- Corlett, R. T. (1994). What is secondary forest? *J. Trop. Ecol.* 10, 445–447. doi: 10.1017/S0266467400008129
- Corlett, R. T. (1999). Environmental forestry in Hong Kong: 1871–1997. *For. Ecol. Manag.* 116, 93–105. doi: 10.1016/S0378-1127(98)00443-5
- Corlett, R. T. (2011). Seed dispersal in Hong Kong, China: Past, present and possible futures. *Integr. Zool.* 6, 97–109. doi: 10.1111/j.1749-4877.2011.00235.x
- Corlett, R. T. (2017). Frugivory and seed dispersal by vertebrates in tropical and subtropical Asia: An update. *Glob. Ecol. Conserv.* 11, 1–22. doi: 10.1016/j.gecco.2017.04.007
- Crouzeilles, R., Ferreira, M. S., Chazdon, R. L., Lindenmayer, D. B., Sansevero, J. B. B., Monteiro, L., et al. (2017). Ecological restoration success is higher for natural regeneration than for active restoration in tropical forests. *Sci. Adv.* 3:e1701345. doi: 10.1126/sciadv.1701345
- Davies, S. J., Abiem, I., Abu Salim, K., Aguilar, S., Allen, D., Alonso, A., et al. (2021). ForestGEO: Understanding forest diversity and dynamics through a global observatory network. *Biol. Conserv.* 253:108907. doi: 10.1016/j.bioccon.2020.108907
- de Medeiros-Sarmiento, P. S., Ferreira, L. V., and Gastauer, M. (2021). Natural regeneration triggers compositional and functional shifts in soil seed banks. *Sci. Total Environ.* 753:141934. doi: 10.1016/j.scitotenv.2020.141934
- Deng, C., Zhang, S., Lu, Y., Froese, R. E., Xu, X., Zeng, J., et al. (2020). Thinning effects on forest evolution in Masson pine (*Pinus massoniana* Lamb.) conversion from pure plantations into mixed forests. *For. Ecol. Manag.* 477:118503. doi: 10.1016/j.foreco.2020.118503
- Dent, D. H., and Wright, J. S. (2009). The future of tropical species in secondary forests: A quantitative review. *Biol. Conserv.* 142, 2833–2843. doi: 10.1016/j.bioccon.2009.05.035
- Ding, Y., and Zang, R. (2021). Effects of thinning on the demography and functional community structure of a secondary tropical lowland rain forest. *J. Environ. Manage.* 279:111805. doi: 10.1016/j.jenvman.2020.111805
- Dullinger, S., Gattringer, A., Thuiller, W., Moser, D., Zimmermann, N. E., Guisan, A., et al. (2012). Extinction debt of high-mountain plants under twenty-first-century climate change. *Nat. Clim. Change* 2, 619–622. doi: 10.1038/nclimate1514
- Egler, F. E. (1954). Vegetation science concepts I. Initial floristic composition, a factor in old-field vegetation development with 2 figs. *Veg. Acta Geobot.* 4, 412–417. doi: 10.1007/BF00275587
- ESRI (2019). *ArcGIS*. Redlands, CA: ESRI.
- Feng, Y., Schmid, B., Loreau, M., Forrester, D. I., Fei, S., Zhu, J., et al. (2022). Multispecies forest plantations outyield monocultures across a broad range of conditions. *Science* 376, 865–868. doi: 10.1126/science.abm6363
- Field, J. P., Breshears, D. D., Bradford, J. B., Law, D. J., Feng, X., and Allen, C. D. (2020). Forest management under megadrought: Urgent needs at finer scale and higher intensity. *Front. For. Glob. Change* 3:502669. doi: 10.3389/ffgc.2020.502669
- Filgueiras, B. K. C., Peres, C. A., Melo, F. P. L., Leal, I. R., and Tabarelli, M. (2021). Winner-loser species replacements in human-modified landscapes. *Trends Ecol. Evol.* 36, 545–555. doi: 10.1016/j.tree.2021.02.006
- Food and Agriculture Organization of the United Nations (2018). *Global forest resources assessment FRA 2020, terms and definitions, i8661en*. Rome: Food and Agriculture Organization of the United Nations.
- Fukami, T. (2015). Historical contingency in community assembly: Integrating niches, species pools, and priority effects. *Annu. Rev. Ecol. Evol. Syst.* 46, 1–23. doi: 10.1146/annurev-ecolsys-110411-160340
- Fukami, T., Mordecai, E. A., and Ostling, A. (2016). A framework for priority effects. *J. Veg. Sci.* 27, 655–657. doi: 10.1111/jvs.12434
- Goldsmith, G. R., Comita, L. S., and Chua, S. C. (2011). Evidence for arrested succession within a tropical forest fragment in Singapore. *J. Trop. Ecol.* 27, 323–326. doi: 10.1017/S0266467411000010
- Goldsmith, G. R., Comita, L. S., Morefield, L. L., Condit, R., and Hubbell, S. P. (2006). Long-term research impacts on seedling community structure and composition in a permanent forest plot. *For. Ecol. Manag.* 234, 34–39. doi: 10.1016/j.foreco.2006.06.011
- Graco-Roza, C., Aarnio, S., Abrego, N., Acosta, A. T. R., Alahuhta, J., Altman, J., et al. (2022). Distance decay 2.0—A global synthesis of taxonomic and functional turnover in ecological communities. *Glob. Ecol. Biogeogr.* 31, 1399–1421. doi: 10.1111/geb.13513

- Gunatilleke, C. V. S., Gunatilleke, I. A. U. N., Esufali, S., Harms, K. E., Ashton, P. M. S., Burslem, D. F. R. P., et al. (2006). Species-habitat associations in a Sri Lankan dipterocarp forest. *J. Trop. Ecol.* 22, 371–384. doi: 10.1017/S0266467406003282
- Guo, Y., Wang, B., Li, D., Mallik, A. U., Xiang, W., Ding, T., et al. (2017). Effects of topography and spatial processes on structuring tree species composition in a diverse heterogeneous tropical karst seasonal rainforest. *Flora* 231, 21–28. doi: 10.1016/j.flora.2017.04.002
- Guo, Y., Wang, B., Mallik, A. U., Huang, F., Xiang, W., Ding, T., et al. (2016). Topographic species-habitat associations of tree species in a heterogeneous tropical karst seasonal rain forest, China. *J. Plant Ecol.* 10, 450–460. doi: 10.1093/jpe/rtw057
- Harms, K. E., Condit, R., Hubbell, S. P., and Foster, R. B. (2001). Habitat associations of trees and shrubs in a 50-ha neotropical forest plot: Habitat associations of trees and shrubs. *J. Ecol.* 89, 947–959. doi: 10.1111/j.1365-2745.2001.00615.x
- Hermly, M., and Verheyen, K. (2007). Legacies of the past in the present-day forest biodiversity: A review of past land-use effects on forest plant species composition and diversity. *Ecol. Res.* 22, 361–371. doi: 10.1007/s11284-007-0354-3
- Hill, M. O. (1973). Diversity and evenness: A unifying notation and its consequences. *Ecology* 54, 427–432. doi: 10.2307/1934352
- Hogan, J. A., Zimmerman, J. K., Uriarte, M., Turner, B. L., and Thompson, J. (2016). Land-use history augments environment-plant community relationship strength in a Puerto Rican wet forest. *J. Ecol.* 104, 1466–1477. doi: 10.1111/1365-2745.12608
- Holl, K. D., Luong, J. C., and Brancalion, P. H. S. (2022). Overcoming biotic homogenization in ecological restoration. *Trends Ecol. Evol.* 37, 777–788. doi: 10.1016/j.tree.2022.05.002
- Holl, K. D., Stout, V. M., Reid, J. L., and Zahawi, R. A. (2013). Testing heterogeneity-diversity relationships in tropical forest restoration. *Oecologia* 173, 569–578. doi: 10.1007/s00442-013-2632-9
- Hsieh, T. C., Ma, K. H., and Chao, A. (2016). iNEXT: An R package for rarefaction and extrapolation of species diversity (Hill numbers). *Methods Ecol. Evol.* 7, 1451–1456. doi: 10.1111/2041-210X.12613
- Jakovac, C. C., Bongers, F., Kuyper, T. W., Mesquita, R. C. G., and Peña-Claros, M. (2016). Land use as a filter for species composition in Amazonian secondary forests. *J. Veg. Sci.* 27, 1104–1116. doi: 10.1111/jvs.12457
- Jakovac, C. C., Junqueira, A. B., Crouzeilles, R., Peña-Claros, M., Mesquita, R. C. G., and Bongers, F. (2021). The role of land-use history in driving successional pathways and its implications for the restoration of tropical forests. *Biol. Rev.* 96, 1114–1134. doi: 10.1111/brv.12694
- Johnstone, J. F., Allen, C. D., Franklin, J. F., Frelich, L. E., Harvey, B. J., Higuera, P. E., et al. (2016). Changing disturbance regimes, ecological memory, and forest resilience. *Front. Ecol. Environ.* 14:369–378. doi: 10.1002/fee.1311
- Jost, L. (2007). Partitioning diversity into independent alpha and beta components. *Ecology* 88, 2427–2439. doi: 10.1890/06-1736.1
- Karger, D. N., Tuomisto, H., Amoroso, V. B., Darnaedi, D., Hidayat, A., Abrahamczyk, S., et al. (2015). The importance of species pool size for community composition. *Ecography* 38, 1243–1253. doi: 10.1111/ecog.01322
- Keith, S. A., Newton, A. C., Morecroft, M. D., Bealey, C. E., and Bullock, J. M. (2009). Taxonomic homogenization of woodland plant communities over 70 years. *Proc. R. Soc. B Biol. Sci.* 276, 3539–3544. doi: 10.1098/rspb.2009.0938
- Kennard, D. K. (2002). Secondary forest succession in a tropical dry forest: Patterns of development across a 50-year chronosequence in lowland Bolivia. *J. Trop. Ecol.* 18, 53–66. doi: 10.1017/S0266467402002031
- Koleff, P., Gaston, K. J., and Lennon, J. J. (2003). Measuring beta diversity for presence-absence data. *J. Anim. Ecol.* 72, 367–382. doi: 10.1046/j.1365-2656.2003.00710.x
- Kuussaari, M., Bommarco, R., Heikkinen, R. K., Helm, A., Krauss, J., Lindborg, R., et al. (2009). Extinction debt: A challenge for biodiversity conservation. *Trends Ecol. Evol.* 24, 564–571. doi: 10.1016/j.tree.2009.04.011
- Lai, J., Mi, X., Ren, H., and Ma, K. (2009). Species-habitat associations change in a subtropical forest of China. *J. Veg. Sci.* 20, 415–423. doi: 10.1111/j.1654-1103.2009.01065.x
- Lamb, D., Erskine, P. D., and Parrotta, J. A. (2005). Restoration of degraded tropical forest landscapes. *Science* 310, 1628–1632. doi: 10.1126/science.111773
- Lebrija-Trejos, E., Pérez-García, E. A., Meave, J. A., Poorter, L., and Bongers, F. (2011). Environmental changes during secondary succession in a tropical dry forest in Mexico. *J. Trop. Ecol.* 27, 477–489. doi: 10.1017/S0266467411000253
- Legendre, P. (2008). Studying beta diversity: Ecological variation partitioning by multiple regression and canonical analysis. *J. Plant Ecol.* 1, 3–8. doi: 10.1093/jpe/rtm001
- Legendre, P., and Legendre, L. (2012). *Numerical ecology*, 3rd Edn. Amsterdam: Elsevier.
- Leimu, R., Vergeer, P., Angeloni, F., and Ouborg, N. J. (2010). Habitat fragmentation, climate change, and inbreeding in plants: Habitat fragmentation, climate change and inbreeding in plants. *Ann. N. Y. Acad. Sci.* 1195, 84–98. doi: 10.1111/j.1749-6632.2010.05450.x
- Lepore, M. (2018). *fgeo.habitat: Analyze soils and tree-habitat data*. Available online at: <https://github.com/helixcn/fgeo.habitat> (accessed June 20, 2022).
- Lichstein, J. W., Grau, H. R., and Aragón, R. (2004). Recruitment limitation in secondary forests dominated by an exotic tree. *J. Veg. Sci.* 15, 721–728. doi: 10.1111/j.1654-1103.2004.tb02314.x
- Liu, C. L. C., Kuchma, O., and Krutovsky, K. V. (2018). Mixed-species versus monocultures in plantation forestry: Development, benefits, ecosystem services and perspectives for the future. *Glob. Ecol. Conserv.* 15:e00419. doi: 10.1016/j.gecco.2018.e00419
- Liu, J.-J., and Slik, J. W. F. (2014). Forest fragment spatial distribution matters for tropical tree conservation. *Biol. Conserv.* 171, 99–106. doi: 10.1016/j.biocon.2014.01.004
- Liu, J.-J., Coomes, D. A., Gibson, L., Hu, G., Liu, J., Luo, Y., et al. (2019). Forest fragmentation in China and its effect on biodiversity. *Biol. Rev.* 94, 1636–1657. doi: 10.1111/brv.12519
- Lopez, O. R., and Kursar, T. A. (2003). Does flood tolerance explain tree species distribution in tropical seasonally flooded habitats? *Oecologia* 136, 193–204. doi: 10.1007/s00442-003-1259-7
- Lugo, A. E. (1992). “Tree plantations for rehabilitating damaged forest lands in the tropics,” in *Ecosystem rehabilitation: Ecosystem analysis and synthesis*, ed. K. Mohan (Hague: SPB Academic Publishing), 247–255.
- Luke, S. H., Barclay, H., Bidin, K., Chey, V. K., Ewers, R. M., Foster, W. A., et al. (2017). The effects of catchment and riparian forest quality on stream environmental conditions across a tropical rainforest and oil palm landscape in Malaysian Borneo. *Ecology* 10, e1827. doi: 10.1002/eco.1827
- Lutz, J. A., Furniss, T. J., Johnson, D. J., Davies, S. J., Allen, D., Alonso, A., et al. (2018). Global importance of large-diameter trees. *Glob. Ecol. Biogeogr.* 27, 849–864. doi: 10.1111/geb.12747
- Maestre, F. T., and Cortina, J. (2004). Are *Pinus halepensis* plantations useful as a restoration tool in semiarid Mediterranean areas? *For. Ecol. Manag.* 198, 303–317. doi: 10.1016/j.foreco.2004.05.040
- McKinney, M. L., and Lockwood, J. L. (1999). Biotic homogenization: A few winners replacing many losers in the next mass extinction. *Trends Ecol. Evol.* 14, 450–453. doi: 10.1016/S0169-5347(99)01679-1
- Meli, P., Holl, K. D., Rey Benayas, J. M., Jones, H. P., Jones, P. C., Montoya, D., et al. (2017). A global review of past land use, climate, and active vs. passive restoration effects on forest recovery. *PLoS One* 12:e0171368. doi: 10.1371/journal.pone.0171368
- Nicholson, B. (1996). Tai Po Kau nature reserve, new territories, Hong Kong: A reafforestation history. *Asian J. Environ. Manag.* 4, 103–120.
- Norden, N., Mesquita, R. C. G., Bentos, T. V., Chazdon, R. L., and Williamson, G. B. (2011). Contrasting community compensatory trends in alternative successional pathways in central Amazonia. *Oikos* 120, 143–151. doi: 10.1111/j.1600-0706.2010.18335.x
- Oksanen, J., Simpson, G. L., Blanchet, F. G., Kindt, R., Legendre, P., Minchin, P. R., et al. (2022). *vegan: Community ecology package Version 2.6-4*. Available online at: <https://CRAN.R-project.org/package=vegan> (accessed October 12, 2022).
- Osazuwa-Peters, O. L., Jiménez, I., Oberle, B., Chapman, C. A., and Zanne, A. E. (2015). Selective logging: Do rates of forest turnover in stems, species composition and functional traits decrease with time since disturbance?—A 45 year perspective. *For. Ecol. Manag.* 357, 10–21. doi: 10.1016/j.foreco.2015.08.002
- Palma, A. C., Goosem, M., Fensham, R. J., Goosem, S., Preece, N. D., Stevenson, P. R., et al. (2021). Dispersal and recruitment limitations in secondary forests. *J. Veg. Sci.* 32:e12975. doi: 10.1111/jvs.12975
- Palma, A. C., Goosem, M., Stevenson, P. R., and Laurance, S. G. W. (2020). Enhancing plant diversity in secondary forests. *Front. For. Glob. Change* 3:571352. doi: 10.3389/ffgc.2020.571352
- Paul, J. R., Randle, A. M., Chapman, C. A., and Chapman, L. J. (2004). Arrested succession in logging gaps: Is tree seedling growth and survival limiting? *Afr. J. Ecol.* 42, 245–251. doi: 10.1111/j.1365-2028.2004.00435.x
- Peres-Neto, P. R., Legendre, P., Dray, S., and Borcard, D. (2006). Variation partitioning of species data matrices: Estimation and comparison of fractions. *Ecology* 87, 2614–2625. doi: 10.1890/0012-9658(2006)87[2614:vposdm]2.0.co;2
- Picard, N. (2019). Asymmetric competition can shape the size distribution of trees in a natural tropical forest. *For. Sci.* 65, 562–569. doi: 10.1093/forcsci/fxz018
- Poorter, L., Bongers, F., Aide, T. M., Almeyda Zambrano, A. M., Balvanera, P., Becknell, J. M., et al. (2016). Biomass resilience of neotropical secondary forests. *Nature* 530, 211–214. doi: 10.1038/nature16512
- Poorter, L., Craven, D., Jakovac, C. C., van der Sande, M. T., Amisshah, L., Bongers, F., et al. (2021). Multidimensional tropical forest recovery. *Science* 374, 1370–1376. doi: 10.1126/science.abh3629
- Reid, J. L., Fagan, M. E., Lucas, J., Slaughter, J., and Zahawi, R. A. (2019). The ephemerality of secondary forests in southern Costa Rica. *Conserv. Lett.* 12:e12607. doi: 10.1111/conl.12607
- Réjou-Méchain, M., Tanguy, A., Piponiot, C., Chave, J., and Hérault, B. (2017). biomass: An R package for estimating above-ground biomass and its uncertainty in tropical forests. *Methods Ecol. Evol.* 8, 1163–1167. doi: 10.1111/2041-210X.12753
- Rozendaal, D. M. A., Bongers, F., Aide, T. M., Alvarez-Dávila, E., Ascarrunz, N., Balvanera, P., et al. (2019). Biodiversity recovery of Neotropical secondary forests. *Sci. Adv.* 5:eau3114. doi: 10.1126/sciadv.aau3114

- Schmitt, S., Tyskland, N., Derroire, G., Heuertz, M., and Hérault, B. (2021). Topography shapes the local coexistence of tree species within species complexes of Neotropical forests. *Oecologia* 196, 389–398. doi: 10.1007/s00442-021-04939-2
- Shen, G., Yu, M., Hu, X.-S., Mi, X., Ren, H., Sun, I.-F., et al. (2009). Species–area relationships explained by the joint effects of dispersal limitation and habitat heterogeneity. *Ecology* 90, 3033–3041. doi: 10.1890/08-1646.1
- Siemann, E., and Rogers, W. E. (2006). Recruitment limitation, seedling performance and persistence of exotic tree monocultures. *Biol. Invasions* 8, 979–991.
- Silva, W. R., Zaniratto, C. P., Ferreira, J. O. V., Rigacci, E. D. B., Oliveira, J. F., Morandi, M. E. F., et al. (2020). Inducing seed dispersal by generalist frugivores: A new technique to overcome dispersal limitation in restoration. *J. Appl. Ecol.* 57, 2340–2348. doi: 10.1111/1365-2664.13731
- Stephenson, N. L., Das, A. J., Condit, R., Russo, S. E., Baker, P. J., Beckman, N. G., et al. (2014). Rate of tree carbon accumulation increases continuously with tree size. *Nature* 507, 90–93. doi: 10.1038/nature12914
- Svenning, J.-C., and Faurby, S. (2017). Prehistoric and historic baselines for trophic rewilding in the Neotropics. *Perspect. Ecol. Conserv.* 15, 282–291. doi: 10.1016/j.pecon.2017.09.006
- Tabarelli, M., Peres, C. A., and Melo, F. P. L. (2012). The ‘few winners and many losers’ paradigm revisited: Emerging prospects for tropical forest biodiversity. *Biol. Conserv.* 155, 136–140. doi: 10.1016/j.biocon.2012.06.020
- Thessler, S., Ruokolainen, K., Tuomisto, H., and Tomppo, E. (2005). Mapping gradual landscape-scale floristic changes in Amazonian primary rain forests by combining ordination and remote sensing: Mapping floristic changes in Amazonian rain forests. *Glob. Ecol. Biogeogr.* 14, 315–325. doi: 10.1111/j.1466-822X.2005.00158.x
- Thompson, J., Lugo, A. E., and Thomlinson, J. (2007). Land use history, hurricane disturbance, and the fate of introduced species in a subtropical wet forest in Puerto Rico. *Plant Ecol.* 192, 289–301. doi: 10.1007/s11258-007-9318-5
- Tomimura, C., Singhakumara, B. M. P., and Ashton, P. M. S. (2012). Pattern and Composition of secondary succession beneath Caribbean pine plantations of Southwest Sri Lanka. *J. Sustain. For.* 31, 818–834. doi: 10.1080/10549811.2011.640076
- Turner, I. M., and Corlett, R. T. (1996). The conservation value of small, isolated fragments of lowland tropical rain forest. *Trends Ecol. Evol.* 11, 330–333. doi: 10.1016/0169-5347(96)10046-X
- Uhl, C. (1987). Factors controlling succession following slash-and-burn agriculture in Amazonia. *J. Ecol.* 75:377. doi: 10.2307/2260425
- Uriarte, M., Canham, C. D., Thompson, J., and Zimmerman, J. K. (2004). A neighborhood analysis of tree growth and survival in a hurricane-driven tropical forest. *Ecol. Monogr.* 74, 591–614. doi: 10.1890/03-4031
- van Schaik, C. P., Terborgh, J. W., and Wright, S. J. (1993). The phenology of tropical forests: Adaptive significance and consequences for primary consumers. *Annu. Rev. Ecol. Syst.* 24, 353–377. doi: 10.1146/annurev.es.24.110193.002033
- Weidlich, E. W. A., Nelson, C. R., Maron, J. L., Callaway, R. M., Delory, B. M., and Temperton, V. M. (2021). Priority effects and ecological restoration. *Restor. Ecol.* 29:e13317. doi: 10.1111/rec.13317
- Whitfield, T. J. S., Lasky, J. R., Damas, K., Sosanika, G., Molem, K., and Montgomery, R. A. (2014). Species richness, forest structure, and functional diversity during succession in the New Guinea lowlands. *Biotropica* 46, 538–548. doi: 10.1111/btp.12136
- Wilson, M. V., and Shmida, A. (1984). Measuring beta diversity with presence-absence data. *J. Ecol.* 72:1055. doi: 10.2307/2259551
- Wright, S. J. (2005). Tropical forests in a changing environment. *Trends Ecol. Evol.* 20, 553–560. doi: 10.1016/j.tree.2005.07.009
- Wu, C., Jiang, B., Yuan, W., Shen, A., Yang, S., Yao, S., et al. (2020). On the management of large-diameter trees in China's forests. *Forests* 11:111. doi: 10.3390/f11010111
- Wu, W., Kuang, L., Li, Y., He, L., Mou, Z., Wang, F., et al. (2021). Faster recovery of soil biodiversity in native species mixture than in Eucalyptus monoculture after 60 years afforestation in tropical degraded coastal terraces. *Glob. Change Biol.* 27, 5329–5340. doi: 10.1111/gcb.15774
- Xu, H., Li, Y., Liu, S., Zang, R., He, F., and Spence, J. R. (2015). Partial recovery of a tropical rain forest a half-century after clear-cut and selective logging. *J. Appl. Ecol.* 52, 1044–1052. doi: 10.1111/1365-2664.12448
- Yadav, J., and Sharma, M. (2013). A review of k-mean algorithm. *Int. J. Eng. Trends Technol.* 4, 2972–2976.
- Yin, D., Liu, Y., Ye, Q., Cadotte, M. W., and He, F. (2021). Trait hierarchies are stronger than trait dissimilarities in structuring spatial co-occurrence patterns of common tree species in a subtropical forest. *Ecol. Evol.* 11, 7366–7377. doi: 10.1002/ece3.7567
- Young, A., Boyle, T., and Brown, T. (1996). The population genetic consequences of habitat fragmentation for plants. *Trends Ecol. Evol.* 11, 413–418. doi: 10.1016/0169-5347(96)10045-8
- Young, T. P., and Peffer, E. (2010). “Recalcitrant understory layers” revisited: Arrested succession and the long life-spans of clonal mid-successional species. *Can. J. For. Res.* 40, 1184–1188. doi: 10.1139/X10-066
- Zeng, X., Michalski, S. G., Fischer, M., and Durka, W. (2012). Species diversity and population density affect genetic structure and gene dispersal in a subtropical understory shrub. *J. Plant Ecol.* 5, 270–278. doi: 10.1093/jpe/rtr029
- Zhang, H., Chen, H. Y. H., Lian, J., John, R., Li Ronghua, Liu, H., et al. (2018). Using functional trait diversity patterns to disentangle the scale-dependent ecological processes in a subtropical forest. *Funct. Ecol.* 32, 1379–1389. doi: 10.1111/1365-2435.13079
- Zhao, M., Pan, B., Tan, Y., and Corlett, R. T. (2015). Winners and losers among tree species in Xishuangbanna: Which traits are most important? *Sci. Bull.* 60, 916–924. doi: 10.1007/s11434-015-0799-7
- Zhuang, X.-Y. (1997). Rehabilitation and development of forest on degraded hills of Hong Kong. *For. Ecol. Manag.* 99, 197–201. doi: 10.1016/S0378-1127(97)00205-3
- Zhuang, X.-Y., and Corlett, R. T. (1997). Forest and forest succession in Hong Kong. *China. J. Trop. Ecol.* 13, 857–866. doi: 10.1017/S0266467400011032
- Zobel, M., van der Maarel, E., and Dupré, C. (1998). Species pool: The concept, its determination and significance for community restoration. *Appl. Veg. Sci.* 1, 55–66. doi: 10.2307/1479085
- Zuleta, D., Russo, S. E., Barona, A., Barreto-Silva, J. S., Cardenas, D., Castaño, N., et al. (2020). Importance of topography for tree species habitat distributions in a terra firme forest in the Colombian Amazon. *Plant Soil* 450, 133–149. doi: 10.1007/s11104-018-3878-0



OPEN ACCESS

EDITED BY

Nophea Sasaki,
Asian Institute of Technology, Thailand

REVIEWED BY

Richard T. Corlett,
Xishuangbanna Tropical Botanical Garden
(CAS), China
Nilanchal Patel,
Birla Institute of Technology, Mesra, India
Chiwei Xiao,
Institute of Geographic Sciences and Natural
Resources Research (CAS), China

*CORRESPONDENCE

Nagai Shin
✉ nagais@jamstec.go.jp

†These authors have contributed equally to this work

SPECIALTY SECTION

This article was submitted to
Tropical Forests,
a section of the journal
Frontiers in Forests and Global Change

RECEIVED 24 November 2022

ACCEPTED 08 February 2023

PUBLISHED 22 February 2023








CITATION

Shin N, Katsumata C, Miura T, Tsutsumida N, Ichie T, Kotani A, Nakagawa M, Khoon KL, Kobayashi H, Kumagai T, Tei S, Pungga RaS, Yamada T, Kameda A, Yanagisawa M, Nasahara KN, Muraoka H, Ichii K and Tokumoto Y (2023) Perspective: Improving the accuracy of plant phenology observations and land-cover and land-use detection by optical satellite remote-sensing in the Asian tropics.
Front. For. Glob. Change 6:1106723.
doi: 10.3389/ffgc.2023.1106723

COPYRIGHT

© 2023 Shin, Katsumata, Miura, Tsutsumida, Ichie, Kotani, Nakagawa, Khoon, Kobayashi, Kumagai, Tei, Pungga, Yamada, Kameda, Yanagisawa, Nasahara, Muraoka, Ichii and Tokumoto. This is an open-access article distributed under the terms of the [Creative Commons Attribution License \(CC BY\)](https://creativecommons.org/licenses/by/4.0/). The use, distribution or reproduction in other forums is permitted, provided the original author(s) and the copyright owner(s) are credited and that the original publication in this journal is cited, in accordance with accepted academic practice. No use, distribution or reproduction is permitted which does not comply with these terms.

Perspective: Improving the accuracy of plant phenology observations and land-cover and land-use detection by optical satellite remote-sensing in the Asian tropics

Nagai Shin^{1*†}, Chifuyu Katsumata^{1†}, Tomoaki Miura^{1,2†}, Narumasa Tsutsumida ³, Tomoaki Ichie⁴, Ayumi Kotani⁵, Michiko Nakagawa⁵, Kho Lip Khoon⁶, Hideki Kobayashi¹, Tomo'omi Kumagai ⁷, Shunsuke Tei⁸, Runi anak Sylvester Pungga ⁹, Taizo Yamada ¹⁰, Akihiro Kameda ¹¹, Masayuki Yanagisawa¹², Kenlo Nishida Nasahara ¹³, Hiroyuki Muraoka^{14,15}, Kazuhito Ichii¹⁶ and Yuji Tokumoto ¹⁷

¹Research Institute for Global Change, Japan Agency for Marine-Earth Science and Technology, Yokohama, Japan, ²Department of Natural Resources and Environmental Management, University of Hawai'i at Mānoa, Honolulu, HI, United States, ³Graduate School of Science and Engineering, Saitama University, Saitama, Japan, ⁴Faculty of Agriculture and Marine Science, Kochi University, Nankoku, Japan, ⁵Graduate School of Bioagricultural Sciences, Nagoya University, Nagoya, Japan, ⁶Economic Planning Unit Sarawak, Chief Minister's Department Sarawak, Kuching, Malaysia, ⁷Graduate School of Agricultural and Life Sciences, The University of Tokyo, Tokyo, Japan, ⁸Forestry and Forest Products Research Institute, Tsukuba, Japan, ⁹Research, Development and Innovation Division, International Affairs Division, Forest Department Sarawak, Kuching, Malaysia, ¹⁰Historiographical Institute of the University of Tokyo, The University of Tokyo, Tokyo, Japan, ¹¹National Museum of Japanese History, Chiba, Japan, ¹²Center for Southeast Asian Studies, Kyoto University, Kyoto, Japan, ¹³Faculty of Life and Environmental Sciences, University of Tsukuba, Tsukuba, Japan, ¹⁴River Basin Research Centre, Gifu University, Gifu, Japan, ¹⁵Division of Biodiversity, National Institute for Environmental Studies, Tsukuba, Japan, ¹⁶Center for Environmental Remote Sensing, Chiba University, Chiba, Japan, ¹⁷Tenure Track Promotion Office, University of Miyazaki, Miyazaki, Japan

Recent advances in satellite-borne optical sensors led to important developments in the monitoring of tropical ecosystems in Asia, which have been strongly affected by recent anthropogenic activities and climate change. Based on our feasibility analyses conducted in Indonesia in Sumatra and Sarawak, Malaysia in Borneo, we discuss the current situation, problems, recent improvements, and future tasks regarding plant phenology observations and land-cover and land-use detection. We found that the Multispectral Instrument (MSI) on board the Sentinel-2A/2B satellites with a 10-m spatial resolution and 5-day observational intervals could be used to monitor phenology among tree species. For the Advanced Himawari Imager (AHI) on board the Himawari-8 geostationary satellite with a 1,000-m spatial resolution and 10-min observational intervals, we found that the time-series in vegetation indices without gaps due to cloud contamination may be used to accurately detect the timing and patterns of phenology among tree species, although the spatial resolution of the sensor requires further improvement. We also found and validated that text and pictures with geolocation information published on the Internet, and historical field notes

could be used for ground-truthing land cover and land use in the past and present time. The future development of both high frequency (≤ 10 min) and high spatial resolution (≤ 10 m) optical sensors aboard satellites is expected to dramatically improve our understanding of ecosystems in the tropical Asia.

KEYWORDS

deforestation, general flowering event, geostationary satellite (GEO), optical sensor, cloud contamination, Sarawak (Malaysia), Sumatra

1. Introduction

In the tropics, where biodiversity is the highest (FAO, and UNEP, 2020; Secretariat of the Convention on Biological Diversity, 2020), there is an urgent need to accurately evaluate the spatiotemporal variation of ecosystem functions, ecosystem services which have recently been called “nature’s contributions to people” (Díaz et al., 2018),¹ and biodiversity under the rapid anthropogenic impacts and climate change occurring there (Estoque et al., 2019). Toward this aim, we require accurate and continuous observations of plant phenology (e.g., flowering, leaf flush, leaf coloring, and leaf fall), which serve as proxies of the responses of organisms and ecosystems to the environment (Tang et al., 2016; Piao et al., 2019), and of land-cover and land-use change. Data on plant phenology, and land-cover and land-use change help to explain the spatiotemporal variability of ecosystem properties (e.g., photosynthesis and evapotranspiration, carbon stocks and flows, the land surface’s albedo, and energy balances; Penñuelas et al., 2009; Kumagai et al., 2013; Richardson et al., 2013; Wu et al., 2016), emission of biogenic volatile organic compounds (BVOCs; Penñuelas et al., 2009; Richardson et al., 2013; IPCC, 2021), cultural ecosystem services (e.g., festivals and recreation opportunities; Sakurai et al., 2011; Sparks, 2014; Nagai et al., 2019), regulating ecosystem services (e.g., pollinator abundances and pollination; Lautenbach et al., 2012; Rohde and Pilliod, 2021), environmental changes in various habitats (Muraoka et al., 2012; Gray and Ewers, 2021), and biodiversity conservation (Morissette et al., 2009; Secades et al., 2014; Morellato et al., 2016). Phenological mismatch between plants and their animal pollinators and consumers caused by the changes of the timing of each phenology due to climate change, reduces the biodiversity (Visser and Gienapp, 2019; Secretariat of the Convention on Biological Diversity, 2020). The evaluation of spatial-temporal variability of the interaction between landscape, which is mainly explained by land cover and land use, and anthropogenic activities, also provides fundamental knowledge to deeply understand the spatial-temporal variability of ecosystem functions, ecosystem services and biodiversity under climate and societal changes.

Satellite remote-sensing by optical sensors is useful for evaluating the spatiotemporal variation of plant phenology, land cover, and land use over a broad scale (Muraoka et al., 2012;

Nagai et al., 2020a; Shin et al., 2023). Since 1972 when Landsat-1 was launched,² satellite optical sensors that observe visible and near-infrared regions of the electro-magnetic spectrum have continuously monitored the state of the ground surface from plot to global scales (Table 1 shows a summary of the specification of optical sensors on board satellites shown in this perspective paper). However, these optical sensors are affected by atmospheric noise and cloud contamination, which is the biggest disadvantage of optical sensors. The opportunity for observation under clear sky conditions in the tropics is much rarer than in other regions (Nagai et al., 2011, 2014a).

In contrast, synthetic aperture radar (SAR) on board satellites is not affected by atmospheric noise and cloud contamination and allows for nighttime observation (e.g., Phased-Array type L-band Synthetic Aperture Radar 2 on board the Advanced Land Observing Satellite [ALOS]-2) and measurement of the spatiotemporal variation of ecosystem structures. SAR transmits microwaves and then actively receives the returned microwave off the ground surface, allowing the detection of forest/non-forest domains, land use and land cover, and aboveground biomass of forests (Miettinen and Liew, 2011; Avtar et al., 2014; Shimada et al., 2014; Kou et al., 2015; Li L. et al., 2015; Stelmaszczuk-Górska et al., 2018). However, SAR cannot observe plant phenology, which is mainly shown as a characteristic of color change of canopy surface on satellite remote-sensing in optical signals. Thus, advancement in SAR technology and/or the integration of SAR and optical sensors will be needed for the accurate detection of land cover and land use (Najib et al., 2020).

To improve the accuracy of phenology observations (e.g., detection of accurate timing of flowering, leaf-flush, and leaf-fall in each ecosystem and/or tree species) and land-cover and land-use detection (e.g., categorization of various land use type and immediate detection of land cover change with a high spatial resolution), we ideally require an optical sensor with high spatial (e.g., 10 m), temporal (e.g., daily interval), and wavelength (many narrow spectral bands) resolutions. However, these three properties have not yet been attained simultaneously with a single sensor due to trade-offs especially between spatial and temporal resolutions (Nagai et al., 2020a). This limitation has made it difficult to accurately monitor the ground surface in the tropics, where the plant phenology and its synchrony among tree species are much less clear than in temperate and boreal vegetation (Harrison, 2001; Nakaji et al., 2014; Nagai et al., 2016a; Osada, 2018; Nakagawa et al.,

1 <https://ipbes.net/news/natures-contributions-people-ncp-article-ipbes-experts-science>

2 <https://landsat.gsfc.nasa.gov/>

2019). Higher diversity and heterogeneity of tree species in the Asian tropics (Lee et al., 2002) make satellite-based phenological observations difficult. Marked land-cover and land-use changes have accelerated in the tropics due to anthropogenic activities (e.g., deforestation) and climate change (e.g., forest fires triggered by the El Niño–Southern Oscillation; Ichikawa, 2007; Segah et al., 2010; Wooster et al., 2012; Hansen et al., 2013; Nagai et al., 2014a; Marlier et al., 2015; Spessa et al., 2015).

For phenology observations and detection of the interannual variation of land cover and land use, researchers have frequently used data observed by optical sensors on board public satellites with high frequency but a coarse spatial resolution, such as the Advanced Very High Resolution Radiometer (AVHRR) on board the National Oceanic and Atmospheric Administration satellite (NOAA; 1100-m spatial resolution at a daily interval; e.g., Erasmí et al., 2014; Garonna et al., 2014; Buitenwerf et al., 2015; Gao et al., 2019), the Moderate Resolution Imaging Spectroradiometer (MODIS) on board the Terra and Aqua satellites (250- to 500-m spatial resolution at a daily interval; e.g., Zhang et al., 2003; Miettinen et al., 2011; Pennec et al., 2011; Jin et al., 2019), and the VEGETATION optical sensor on board the Satellite Pour l'Observation de la Terre (SPOT; 1000-m spatial resolution at a daily interval, ³e.g., Delbart et al., 2006, 2015; Segah et al., 2010; Kobayashi et al., 2016). Also for this purpose, researchers have frequently used data observed by optical sensors on board public satellites with low frequency (16-day intervals) but a moderately high spatial resolution (30 m) such as the Landsat series of satellites (Segah et al., 2010; Kou et al., 2015; Li P. et al., 2015; Ishihara and Tadano, 2017; Morozumi et al., 2019). In contrast, for the detection of land cover and land use with a fine-scale, they have frequently used data observed by optical sensors on board commercial satellites (e.g., the RapidEye: Imukova et al., 2015; Pfeifer et al., 2016; the WorldView series satellites: ⁴Nomura and Mitchard, 2018; Rahmandhana et al., 2022) with a high spatial resolution (e.g., 50 cm) but quite low frequency (e.g., 46-day intervals).

Some advantages of optical sensors on board public satellites are the uniformity of observed data coverage, stable long-term continuous observations from the long-term missions (e.g., the Landsat series of satellites: See text footnote 2), and free usage on the Internet. In contrast, the data observed by optical sensors on board commercial satellites tend to be low-frequency data distributed in urban areas, meaning that we cannot easily access satellite data in remote regions. Although researchers could request satellite image acquisitions of remote regions to these companies, it is an impractical idea to request periodic broad-scale satellite observations in remote regions over a long period due to the cost of obtaining such commercial data.

In the latter half of the 2010s, the spatiotemporal resolution of optical sensors on board public satellites remarkably progressed with the launch of the Multispectral Instrument (MSI) on board the Sentinel-2A/2B satellites, with a 10-m spatial resolution at 5-day intervals (e.g., Nomura and Mitchard, 2018; Persson et al., 2018; Vrieling et al., 2018; Chang et al., 2021), ⁵and the Advanced Himawari Imager (AHI) on board the Himawari-8 geostationary

satellite, with a 1,000-m spatial resolution at 10-min intervals (at 2.5-min intervals around Japan; Miura et al., 2019; Yan et al., 2019; Miura and Nagai, 2020). ⁶Although these optical sensors do not satisfy the need for simultaneous high spatial, temporal, and wavelength resolutions, these optical sensors will be expected to provide much more accurate and precise satellite observations, along with a reduction of uncertainties and systematic noise in land-cover and land-use detection and phenology observations (Shin et al., 2023). Continuous and extensive satellite observations by these optical sensors will be also expected to develop spatiotemporally interpolating and extrapolating *in situ* observed data on ecosystem functions and biodiversity in each tropical observation field.

In this perspective paper, based on this recent progress in the optical sensors on board satellites and the development of observation systems in the latter half of the 2010s, we focus on satellite optical sensors and discuss the current situation, problems, and recent improvements, as well as future tasks regarding phenology observations and land-cover and land-use detection in the Asian tropics. Here, we focus on island or maritime Southeast Asia. In order to discuss concretely, we review our feasibility analyses in Sarawak, Malaysia in Borneo, where our research group has conducted field studies to validate satellite remote-sensing since the 2010s, and Indonesia in Sumatra by using data from the Sentinel-2A/2B–MSI and the Himawari-8–AHI satellites. In Section 2, we describe how the accuracy of satellite phenology observations can be improved from the viewpoints of advanced resolution sensors and frequency of satellite observations. Next, in Section 3, we describe how to improve the accuracy of land-cover and land-use detection from the viewpoints of detection of year-to-year variability and collection of past and present ground-truth information. Then, in Section 4, we discuss the future tasks to help improve our understanding of Asian tropical ecosystems. Finally, in Section 5, we conclude our discussions in this perspective paper.

2. Improvements in the accuracy of satellite phenology observations

2.1. Monitoring of plant phenology by using advanced resolution sensors

Figure 1 shows the time-series of vegetation indices of Lambir Hills National Park (primary tropical rain forest; 4°12'04"N, 114°02'21"E; Nakagawa et al., 2019) and the Lambir oil palm plantation (4°09'07"N, 113°57'58"E) in Sarawak, Malaysia in Borneo observed by the Sentinel-2A/2B–MSI (atmosphere corrected data) and Himawari-8–AHI satellites. Primary tropical rain forests, oil palm plantation forests, and secondary forests are typical landscape features in this area (Ichikawa, 2007). In addition, typical canopy surface images of Lambir Hills National Park are shown in **Figure 2**. We show only NDVI values for the Himawari-8–AHI satellite because we used the reflectance data at the top of the atmosphere (i.e., atmosphere uncorrected data). For the Sentinel-2A/2B–MSI satellites, we selected observation scenes

³ <https://spot-vegetation.com/en>

⁴ <https://earth.esa.int/eogateway/missions/worldview>

⁵ <https://sentinel.esa.int/web/sentinel/missions/sentinel-2>

⁶ <https://www.data.jma.go.jp/mscweb/en/index.html>

TABLE 1 Summary of the optical sensors on board public satellite.

| Sensor | Satellite | Spatial resolution | Temporal resolution | Spectral bands | Swath | Period | URL of specification |
|--|---|---|---------------------------------|--|--|-----------------------------------|--|
| Multispectral Scanner (MSS), Thematic Mapper (TM), Enhanced Thematic Mapper Plus (ETM +), Operational Land Imager (OLI), and OLI-2 | Landsat series | 68 × 83 m (MSS); 30, 120 m (TM); 15, 30, 60 m (ETM +, OLI); 15, 30, 100 m (OLI-2) | 18-days (MSS); 16-days | 0.5–1.1 μm (4 or 5 bands; MSS), 0.45–12.5 μm (7 bands, TM); 0.45–12.5 μm (8 bands, ETM +); 0.435–12.51 μm (11 bands, ETM +); 0.433–12.5 μm (11 bands, OLI-2) | 185 km (MSS, TM, OLI, OLI-2); 183 km (ETM +) | Since 1972 | https://landsat.gsfc.nasa.gov/ |
| Advanced Very High Resolution Radiometer (AVHRR) | NOAA Polar Orbiting Environmental Satellites (POES), Meteorological Operational Satellite (MetOp) | 1,100 m | daily | 0.58–12.5 μm (4 or 5 bands) | 2399 km | Since 1981 | https://www.avl.class.noaa.gov/release/data_available/avhrr/index.htm ; https://www.eumetsat.int/oursatellites/metop-series |
| Moderate Resolution Imaging Spectroradiometer (MODIS) | Terra and Aqua | 250, 500, 1,000 m | daily | 0.405–14.385 μm (36 bands) | 2330 km | Since 1999 and 2002, respectively | https://modis.gsfc.nasa.gov/ |
| Vegetation-1/2 | Satellite Pour l'Observation de la Terre (SPOT)-4/5 | 1,000 m | daily | 0.43–1.75 μm (4 bands) | 2200 km | Since 1998 | https://earth.esa.int/eogateway/missions/spot |
| Advanced Visible and Near Infrared Radiometer type 2 (AVNIR-2) | Advanced Land Observing Satellite (ALOS) | 10 m | 46-days | 0.42–0.89 μm (4 bands) | 70 km | 2006–2011 | https://www.eorc.jaxa.jp/ALOS/en/index_e.htm |
| MultiSpectral Instrument (MSI) | Sentinel-2A/2B | 10, 20, 60 m | 5-days | 0.4924–21.857 μm (13 bands) | 290 km | Since 2015 and 2017, respectively | https://sentinel.esa.int/web/sentinel/missions/sentinel-2 |
| Advanced Himawari Imager (AHI) | Himawari-8 | 1000 m | 10 min. (2.5 min. around Japan) | 0.47–13.3 μm (16 bands) | Geostationary position: 140.7°E | Since 2015 | https://www.data.jma.go.jp/mscweb/en/index.html |

Revised in this table in Shin et al. (2023).

with cloud cover $\leq 10\%$, but we plotted all values observed by the Himawari-8–AHI satellites. For the Himawari-8–AHI satellite, we plotted values observed at 3 h around the culmination time because there was no property in the data regarding the cloud contamination. Despite the occurrence of general flowering in Lambir Hills National Park in May 2019, which occurs every 1–4 years, and the color of the canopy surface changing from dark green to whitish green (Sakai et al., 2006; Azmy et al., 2016; Chechina and Hamann, 2019; Ushio et al., 2020), every vegetation index showed no clear seasonal change (low values may be affected by cloud contamination). During the general flowering period, no data were observed by the Sentinel-2A/2B–MSI satellites under clear sky conditions (Figure 1). MSI Green-Red Vegetation Index (GRVI; Motohka et al., 2010) values observed at Lambir Hills National Park were about 0.05 smaller than those at the Lambir oil palm plantation, reflecting the difference in color of the canopy surface between tropical rain forest (dark green) and the oil palm plantation (light green). Nagai et al. (2016a) reported that NDVI and GRVI values observed by the photodiode sensors installed at the top of a crane tower in Lambir Hills National Park were almost constant throughout the year. In contrast, the time-series of the ratio of R, G, and B digital numbers to the total RGB digital numbers extracted from daily canopy surface images taken at

Lambir Hills National Park showed characteristics of leaf flush and flowering among individual trees (Nagai et al., 2016a). These results indicate the possibility that long-term continuous observations by future advanced optical sensors on board satellites with a high spatial resolution and high temporal resolution (high frequent) may detect characteristics of phenology for each tree species in a tropical rain forest. In fact, the RGB composite images observed by the PlanetScope constellation of satellites, which consist of approximately 180 microsatsellites (as of 16 November 2022; a commercial endeavor),^{7,8} with an approximately 3-m spatial resolution at a daily interval could detect the characteristics of flowering phenology among tree species in Lambir Hills National Park during the general flowering event in May 2019 (Miura et al., 2023). The swath range that can be observed at one time by each PlanetScope microsatsellite is narrow (25 km), but the entire observation system of approximately 180 microsatsellites resolved the trade-off between spatial and temporal resolutions. Some previous studies indicated this advantage of PlanetScope constellation of satellites observations in alpine, temperate, and

⁷ <https://earth.esa.int/eogateway/missions/planetscope>

⁸ <https://www.planet.com/products/planet-imagery/>

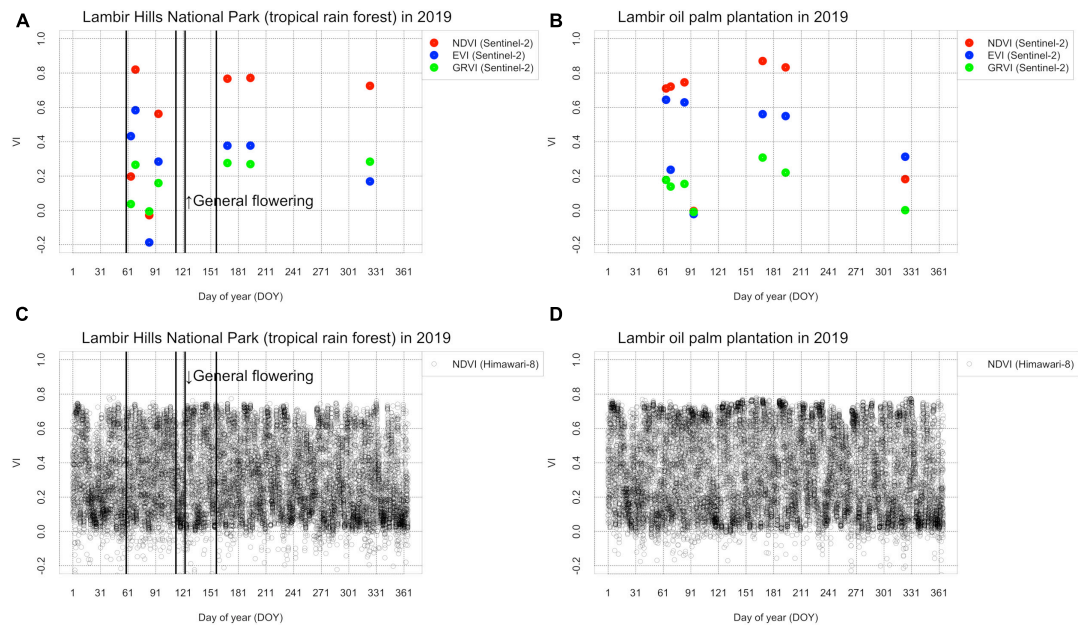


FIGURE 1

Time-series of vegetation indices observed by (A,B) the Sentinel-2A/2B–MSI and (C,D) the Himawari-8–AHI satellites in Lambir Hills National Park (primitive tropical rain forests; 4°12′04″N, 114°02′21″E) and the Lambir oil palm plantation (4°09′07″N, 113°57′58″E) in northwestern Borneo. The thick vertical solid lines in (A,C) indicate the dates of canopy surface images in Figure 2. Cloud contamination appeared in Lambir Hills National Park and the Lambir oil palm plantation images on 5 March, 10 March (only in the Lambir oil palm plantation), 25 March, 4 April, and 20 November (only in the Lambir oil palm plantation). A cloud shadow appeared in Lambir Hills National Park image on 20 November.

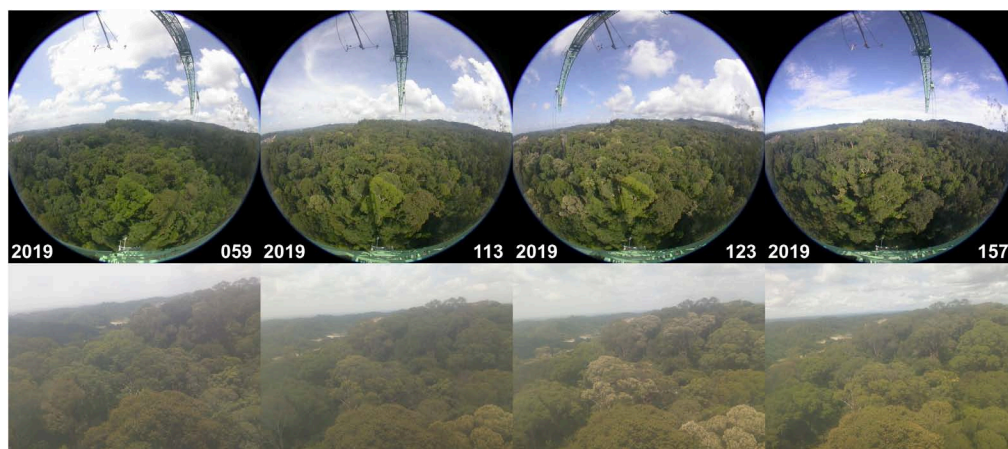


FIGURE 2

Typical canopy surface images taken at the top of a crane tower in Lambir Hills National Park (<http://www.pheno-eye.org/>). The day of year (DOY) is shown in the bottom-right corners of each image. General flowering was shown on DOY 123.

tropical regions (Leach et al., 2019; John et al., 2020; Wang et al., 2020, 2023; Moon et al., 2021; Wu et al., 2021).

How can we detect the characteristics of phenology in tropical rain forests consisting of evergreen broad-leaved trees, with seasonality much less clear than that of deciduous trees, with optical sensors on board satellites? Previous studies reported that the RGB composite images observed by the Sentinel-2A/2B–MSI satellites, with the highest spatial resolution among the optical sensors on board public satellites, detected the color change on the canopy surface of *Castanopsis sieboldii*, *Castanopsis cuspidate*, and *Lithocarpus edulis* (evergreen oak tree species) caused by leaf

flush (light green) and successive flowering (cream) in Japan (Nagai et al., 2020b; Shinohara and Nasahara, 2022; Shin et al., 2023). These plants are insect-pollinated flowers of Fagaceae and their flowers bloom across the whole canopy surface. The timing of flowering is different among these tree species (*L. edulis* is approximately one month later than *C. sieboldii* and *C. cuspidate*). In a tropical rainforest in Borneo (Lambir Hills National Park), Miura et al. (2023) reported that the spectral reflectance observed by the PlanetScope constellation satellites detected the characteristic of color change on the canopy surface of *Dryobalanops aromatica*, *Shorea ochracea*, *Swintonia foxworthyi*, and *Pentace borneensis*

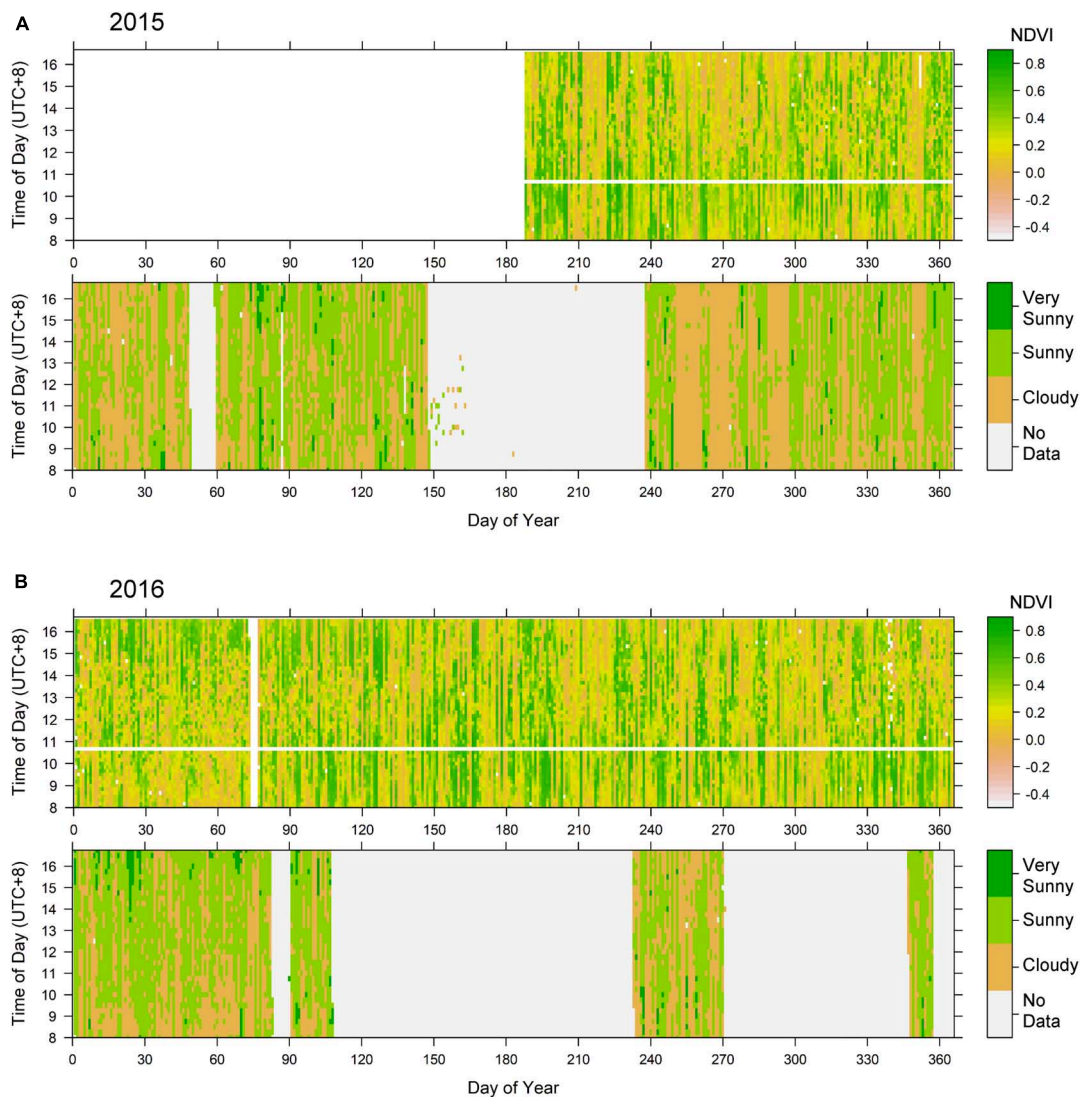


FIGURE 3

Relationship between NDVI values observed by the Himawari-8-AHI satellite and state of cloud cover based on *in situ* observed sky images in Lambir Hills National Park during 8:05 and 16:45 LST (UTC + 8) from (A) 2015 and (B) 2016 (sky images from Nagai et al., 2018).

during a general flowering in 2019. These results indicate the possibility that satellite-based observations may be used to track the phenological timing and patterns of various tree species in tropical rain forests in tandem with ground-truth information.

Remote-sensing can detect the color of the canopy surface of various tree species, which indicate the characteristics of leaf traits (leaf size, leaf biomass, leaf thickness, amount of pigments in a leaf, and angle of leaves) and structures (tree structure and height) (Sims and Gamon, 2002; Luke et al., 2013; Noda et al., 2014; Asner et al., 2015; Noda et al., 2021; Rahmandhana et al., 2022). The characteristics of leaf longevity, which is explained by leaf-flush and leaf-fall phenology, were correlated with the type of photosynthesis, leaf traits and structures, and climate (Wright et al., 2004; Kikuzawa, 2005; Onoda et al., 2011; Kikuzawa et al., 2013). These facts indicate the importance of discriminating each tree species by referring to the characteristics of phenology and canopy structures and mapping the geographic distributions for each tree species at a broad scale. In Lambir Hills National Park, however, the

geographic distribution of each tree species is heterogeneous due to microtopography (Lee et al., 2002). The collection of ground-truth information for various tree species, thus, is both an important and challenging task. Integrating *in situ* and satellite-based phenological observations should also result in the tree discrimination of forests in the Asian tropics.

2.2. Improvement of the frequency of satellite observations

As mentioned above, the Sentinel-2A/2B-MSI satellites have the potential to remarkably improve phenology observations in the tropics. The MSI observations occur at 5-day intervals, however, and in 2019, we only obtained seven scenes with cloud cover $\leq 10\%$ (Figure 1). In addition, we confirmed that cloud contamination appeared in Lambir Hills National Park and the Lambir oil palm plantation images on 5 March, 10 March (only in the Lambir oil

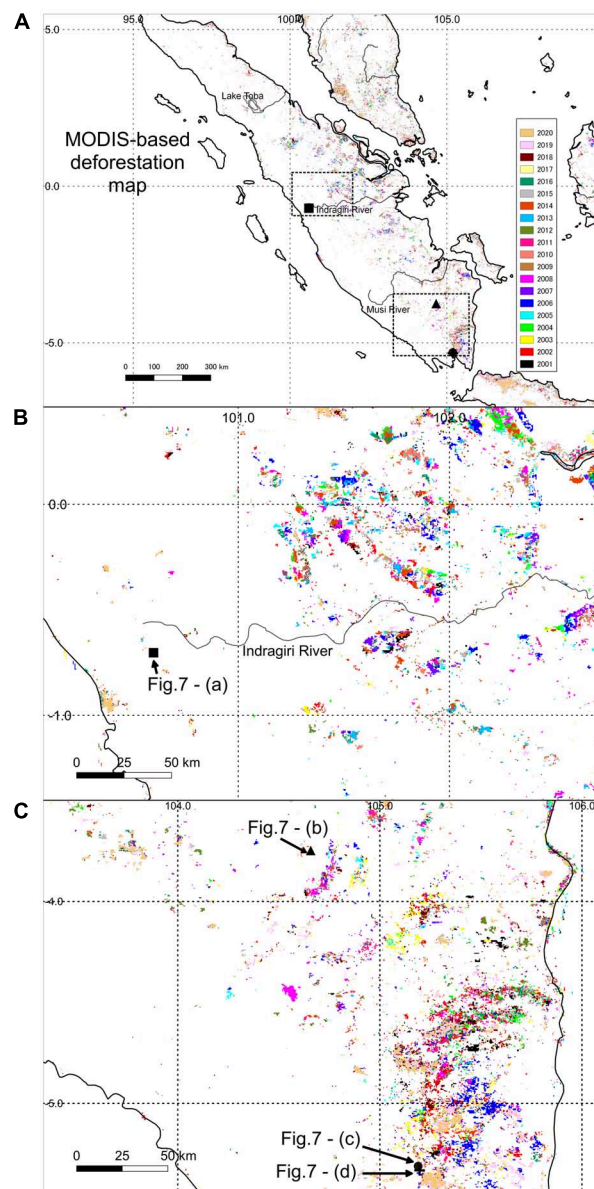
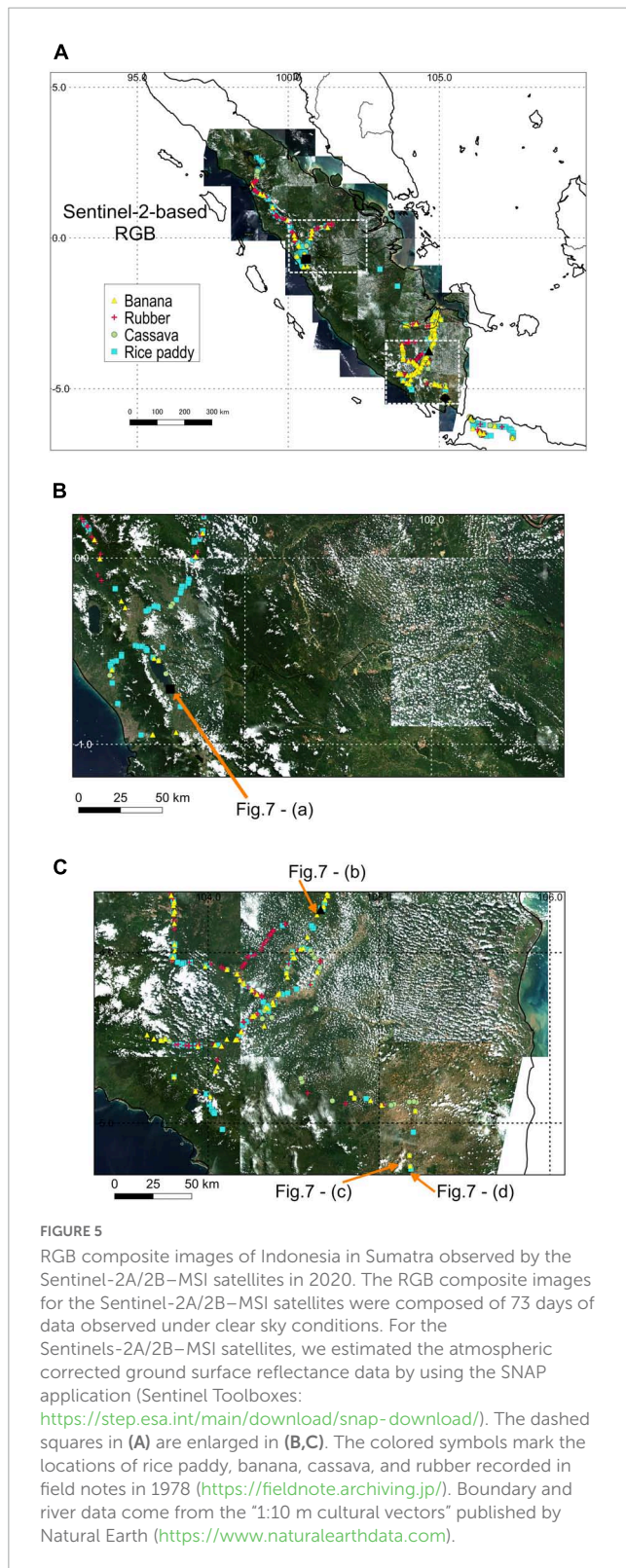


FIGURE 4

Spatiotemporal variation of deforestation in Indonesia in Sumatra from 2001 to 2020 detected by analyzing the time-series of daily GRVI observed by the Terra/Aqua–MODIS satellites (adapted from Nagai et al., 2014b). Each color indicates the latest deforested year. The dashed squares in (A) are enlarged in (B) and (C). Boundary and river data come from the “1:10 m cultural vectors” published by Natural Earth (<https://www.naturalearthdata.com>).

palm plantation), 25 March, 4 April, and 20 November (only in the Lambir oil palm plantation) by visually checking the RGB composite images. In addition, we confirmed that a cloud shadow appeared in Lambir Hills National Park image on 20 November. Therefore, it appears that the Sentinel-2A/2B–MSI satellites cannot observe the characteristics of phenology for each tree species in the suitable period under clear sky conditions. In contrast, the observation frequency of the Himawari-8–AHI satellite under clear sky conditions is much higher than that of the Sentinel-2A/2B–MSI (Figure 1). In fact, even though the sky image taken at 10:30 (LST) in Lambir Hills National Park, which was the time of the Sentinel-2A/2B–MSI satellites passage, showed cloudy skies, many other images showed clear skies at other times (Nagai et al., 2018).

In previous phenology studies that analyzed time-series of satellite-observed vegetation indices, the researchers used the 8-day, 10-day, and bimonthly composite data in order to eliminate noise and missing data caused by atmospheric noise and cloud contamination and smoothed the composite time-series data by applying some fitting functions (Zhang et al., 2003; Delbart et al., 2006, 2015; Erasmi et al., 2009, 2014; Pennec et al., 2011; Wu et al., 2014; Garonna et al., 2014; Buitenwerf et al., 2015; Kobayashi et al., 2016; Park et al., 2016; Gao et al., 2019; Jin et al., 2019). These analyses were based on the hypothesis that vegetation indices observed under clear sky conditions, which might show the most accurate value, were higher than those under cloudy and rainy conditions. Therefore, the smoothed values are estimated values



but not true values. The values smoothed by applying the fitting functions may include two types of systematic errors: (1) an actual value was eventually eliminated, or (2) an actual missing value was eventually misread as a true value. For instance, in the case of an abrupt decrease of vegetation caused by a landslide, vegetation indices after the landslide may be eliminated as noise by applying

some fitting functions. In addition, in the case of successive cloudy and rainy conditions in a certain period, smoothed vegetation indices may be misinterpreted as a decrease of vegetation. Thus, from a statistical viewpoint, we should avoid smoothing as much as possible.

The frequency of the observations of vegetation indices in East Asia by the Himawari-8-AHI satellite is 10-min intervals. If we only select the vegetation indices observed during the daytime that were little affected by the solar elevation angle (e.g., 3 h around noon), we can obtain many data observed under clear sky conditions (Miura et al., 2019). Figure 3 shows the relationship between NDVI values observed by the Himawari-8-AHI satellite and state of cloud cover based on *in situ* observed sky images in Lambir Hills National Park during 8:05 and 16:45 LST (UTC + 8) from 2015 to 2016. The occurrences of higher NDVI values (> 0.8) coincided well with the timings of *in situ* “very sunny” or “sunny” sky conditions, despite including missing data of sky images. The analysis of Figure 3 indicated that the number of days with clear sky conditions ranged from 57 to 96, which was much more than vegetation index observed by the Terra/Aqua-MODIS satellites (1–5 days per month in the southwest monsoon period [May–October] and 0–2 days per month in the northeast monsoon period [November–April] in Borneo; at a daily interval; Nagai et al., 2014a). In addition, the confidence in the change in vegetation indices, which was detected by the actual change of vegetation or not (i.e., systematic noise caused by atmospheric noise and cloud contamination), may also increase by checking high-frequency continuously observed data under clear sky conditions. So, if we can extract data observed only under clear sky conditions, we scarcely need to smooth by applying fitting functions. Despite a coarse spatial resolution (1,000 m), the vegetation indices observed by the Himawari-8-AHI satellite may indicate fairly accurate values.

At present, however, the Himawari-8-AHI satellite is still not suitable with regard to spatial resolution for phenology observations in tropical rain forests. In fact, despite the high frequency of observations under clear sky conditions, no characteristic change in the time-series of NDVI was shown in May 2019, when the general flowering occurred in Lambir Hills National Park (Figures 1, 2). The time-series in GRVI, which can detect the change of color of the canopy surface (Motohka et al., 2010; Nagai et al., 2014b), might capture some characteristic of temporal change. In Lambir Hills National Park, the time-series in the ratio of RGB digital numbers for each individual tree extracted from daily canopy surface images showed differences among tree species around the general flowering period (Nagai et al., 2016a). In contrast, those for the whole canopy showed almost constant values throughout the year (Nagai et al., 2016a), perhaps because not all individuals and tree species flowered at the same time. In this case, the target region of canopy surface images was within at most 100 m (Nagai et al., 2016a), but in the Lambir Hills National Park, which consists of over 1000 tree species (Lee et al., 2002), vegetation indices observed by the Himawari-8-AHI satellite can detect the average phenology of various tree species within a 1,000-m-by-1,000-m area. Therefore, for accurate phenology observations in tropical rain forests, we require an onboard optical sensor with a high spatial resolution to discriminate each tree individual (≤ 10 m) at high temporal frequencies (on the order of 10-min interval) to eliminate cloud contaminations in satellite data.

Despite the uncertainty caused by the heterogeneity of tree species and microtopography, previous studies indicated that the time-series of vegetation indices could be used to accurately detect the spatiotemporal variation of leaf flush and leaf fall in deciduous forests in Japan by validating the indices against long-term continuous *in situ* observed data (Miura et al., 2019; Yan et al., 2019). Despite the effect of microtopography (elevation) on phenology and the differences in timing and patterns of leaf flush and leaf fall among tree species (Inoue et al., 2014; Nagai et al., 2014b; Shin et al., 2021a), leaf flush and leaf fall within a narrow region (e.g., 1,000-m square) occur rapidly and nearly simultaneously. The Japanese government is planning to launch a geostationary satellite with an optical sensor with a 3- to 4-m spatial resolution. Such future developments in optical sensors on board satellites with high observation frequency and high spatial resolution will remarkably improve the accuracy of phenology observations in tropical rain forests, where the phenological timing and patterns differ among the numerous and highly diverse tree species (Osada, 2018; Reich et al., 2004).

3. Improvements in the accuracy of land-cover and land-use detection

3.1. Detection of year-to-year variability of land-cover and land-use change

Figure 4 shows that the interannual variation of deforestation from 2001 to 2020 could be detected by analyzing the time-series of the daily GRVI observed by the Terra/Aqua–MODIS satellites [500-m spatial resolution; adapted from Nagai et al. (2014b)] in Indonesia in Sumatra, where marked land-cover and land-use change has occurred due to deforestation and expansion of oil palm plantations (Ichikawa, 2007; Fitzherbert et al., 2008; GEAS, 2011; Koh et al., 2011; Miettinen et al., 2011; Hansen et al., 2013; Carlson et al., 2014; Nagai et al., 2014a; Estoque et al., 2019; Najib et al., 2020). Here, we defined deforestation as having occurred at points where the ratio of number of days observed GRVI < 0 under clear sky conditions to total observed GRVI under clear sky conditions was above 80% (Nagai et al., 2014a). This hypothesis was based on the fact that GRVI < 0 after leaf fall or when there was no vegetation (Motohka et al., 2010; Nagai et al., 2014b). In the deforested area detected by the Terra/Aqua–MODIS satellites (Figure 4), we also identify that vegetation is sparse by visually inspecting the RGB composite images observed by the Sentinel-2A/2B–MSI satellites with a 10-m spatial resolution (shown in brown; Figure 5). In addition, we identify that GRVI observed by the Sentinel-2A/2B–MSI satellites showed under 0 (Figure 6). From 2001 to 2020, the deforested areas continuously expanded in Riau (central Sumatra; Figure 4C) and Lampung (southern Sumatra; Figure 4B). In Indonesia, the loss rate of primary forests has declined since 2016 according to the Secretariat of the Convention on Biological Diversity (2020); however, our analysis suggests that the deforestation is still ongoing.

9 <https://www8.cao.go.jp/space/comitee/27-anpo/anpo-dai32/siryou1-1.pdf>

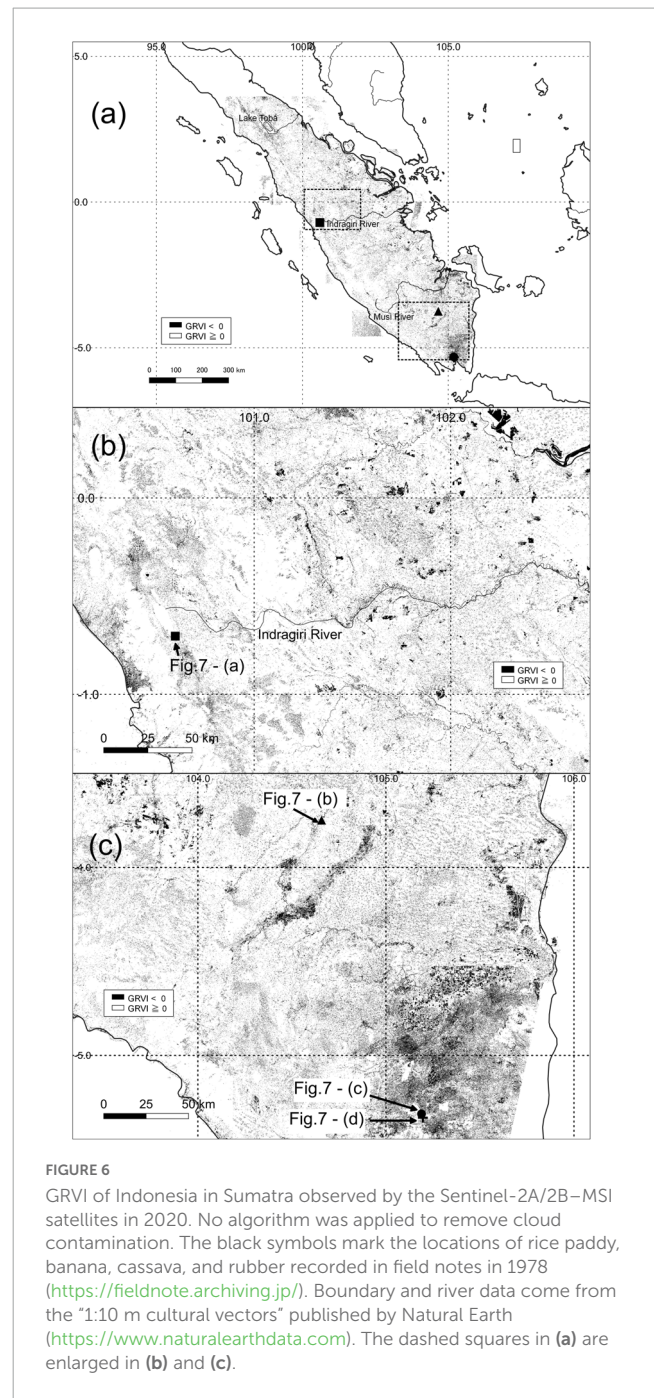


FIGURE 6

GRVI of Indonesia in Sumatra observed by the Sentinel-2A/2B–MSI satellites in 2020. No algorithm was applied to remove cloud contamination. The black symbols mark the locations of rice paddy, banana, cassava, and rubber recorded in field notes in 1978 (<https://fieldnote.archiving.jp/>). Boundary and river data come from the “1:10 m cultural vectors” published by Natural Earth (<https://www.naturalearthdata.com>). The dashed squares in (a) are enlarged in (b) and (c).

Interannual variation of deforestation in the tropics has been detected by analyzing the time-series of vegetation indices observed by the Landsat series (30-m spatial resolution at 16-day intervals; Hansen et al., 2013). However, for those satellites capturing data at 16-day intervals, it is possible that no data are observed under clear sky conditions throughout an entire year especially in the Asian tropics, which is one of regions with active atmospheric water circulation. In addition, in the case of the ETM + sensor on board the Landsat-7 satellite, each observation scene always included partial missing data due to a systematic error in the sensor (malfunction of the scan line corrector; Wang et al., 2021). For the Terra/Aqua–MODIS satellite observations with a 500-m spatial resolution, we could detect large-scale land-cover and land-use



change in the tropics, including the establishment of oil palm and acacia plantations after deforestation (Nagai et al., 2014a), but we could not accurately detect local-scale changes such as the loss of vegetation caused by a landslide, which typically occurs at an area smaller than a footprint of satellite data (1 pixel size of satellite data) with a coarse spatial resolution (500-m or 1,000-m; Miura and Nagai, 2020). In contrast, high-frequency observations by the Sentinel-2A/2B-MSI satellites with a 10-m spatial resolution at 5-day intervals may improve the accuracy of detecting interannual variation of land cover and land use in the tropics. Using the time-series of the vegetation index observed by the Sentinel-2A/2B-MSI satellites, whose data will be accumulated over a long period, should help us to more accurately detect the interannual variation of the geographic distribution of deforestation by applying the same analysis as was applied to the Terra/Aqua-MODIS satellites data.

3.2. Collection of past and present ground-truth information

To improve and validate the accuracy of satellite-based land-cover and land-use maps, we must collect ground-truth information at multiple points (Tsutsumida et al., 2019). One way to achieve this is by using digital camera images with the geolocation information, time, and date shot at multiple points that have been

uploaded on the Mapillary website,¹⁰ which is a crowdsourcing project. For some reported points, we can use images taken on different dates, thus allowing us to obtain evidence of land-cover and land-use change over a short period. Funada and Tsutsumida (2022) also indicated the usability of the street-level photographs published on the Mapillary to map the geographical distribution of cherry flowering in Fukushima in Japan. The text and images uploaded to the Degree Conference Project (DCP) website¹¹ are also useful ground-truth information regarding land cover and land use. Previous studies reported the suitability of information on the DCP for use in validating satellite-based land-cover and land-use maps (Iwao et al., 2011; Soyama et al., 2017).

Figure 7 shows Mapillary images at four locations that were typical landscapes in Indonesia in Sumatra, according to field notes recorded in 1978 (full details are mentioned later). Mapillary also contains many images taken at intervals along the route of a participant's trip by using a car-mounted camera. Such uploaded data may have a geographic bias and be concentrated in areas that are strongly affected by anthropogenic activities (e.g., on streets). Compared with Mapillary, there is less systematic bias in the geographic distribution of target points published on the DCP website, which allows users to choose the intersection of

¹⁰ <https://www.mapillary.com/>

¹¹ <https://confluence.org/>

latitude and longitude integer values in remote regions that have been little affected by human activities. However, the data volume of Mapillary (more than 1.8 billion street-level images as of 16 November 2022; See text footnote 10) is much larger than that of the DCP (about 1.32 million photographs as of 16 November 2022; See text footnote 11), making the usability of Mapillary superior. By actively uploading captured images with geolocation information on Mapillary, especially in the points and areas where images have not yet been uploaded, field scientists can help to reduce the missing areas of *in situ* observations.

Another important issue is how to obtain ground-truth information regarding land cover and land use in the past. This solution deepens our understanding of the conversion processes of deforestation and agricultural expansion. We may estimate the historical land cover and land use by examining the present conditions. For instance, we can assume that areas now covered by oil palm and acacia plantations in Sarawak, Malaysia in Borneo were once covered by tropical rain forests (Nagai et al., 2014a). Without ground-truthing, however, those values will always remain as estimates. To solve this issue, landscape descriptions in research field notes may provide useful ground-truth information regarding past land cover and land use. A group of Japanese scientists at Kyoto University launched the “Inheriting field notes” project (Takata et al., 2014; Yamada, 2015)¹² and have published 46,281 sets of digitalized field notes on their website.¹³ Those field notes include field trips in the Middle East, the Mediterranean, Africa, South Asia, East Asia, Southeast Asia, and Oceania from 1967 to 2016 (mainly the 1980s and 1990s). At the time of the field trips, researchers could not use the tools to capture geolocation information, such as a Global Positioning System (GPS) receiver or a digital camera with this function. However, by thoroughly examining the time-series of objective descriptions in the field notes, we can roughly identify the landscape at a certain point.

For instance, by applying a text mining approach to field notes recorded in Indonesia in Sumatra in 1978 (1802 items) we analyzed the frequency of the words used (Yamamoto et al., 2015). The field notes included typical words regarding landscapes, such as rice paddy (total of 283 cases), banana (164 cases), cassava (136 cases), and rubber (185 cases), which allowed us to identify the landscape at that time. These words are also useful ground-truth information regarding the land cover and land use in Indonesia in Sumatra in 1978. We plotted the locations of rice paddy, banana, cassava, and rubber extracted from the field notes in Figure 5. In addition, by using the Mapillary images (Figure 7), we compared the land cover and land use in 1978 published on field notes with those at the present time. Despite the difficulty in checking precise geolocations, we could validate that there was no land-cover and land-use change at two points, where rice paddy and banana were recorded in the field notes. However, like the Mapillary images, many points recorded on the field notes may be located in areas that were strongly affected by anthropogenic activities. The retirement and decease of owners will accelerate the loss of personal analog data such as field notes. Rescuing and archiving of these analog data and information is an urgent issue (Shin et al., 2020).

4. Future tasks to help improve our understanding of Asian tropical ecosystems

To improve our understanding of Asian tropical ecosystems, we propose five issues that need to be addressed: (1) further collecting ground-truth information from multiple locations and various periods; (2) improving the classification of plant functional types (PFTs) on land-cover and land-use maps and detecting the interannual variation of PFTs; (3) studying the interactions between terrestrial and marine ecosystems; (4) investigating the interaction between land-cover and land-use change and anthropogenic activities; and (5) developing integrative analysis and evaluation of *in situ* and satellite-observed data.

4.1. Further collection of ground-truth information from multiple locations and various periods

In conjunction with the development of optical sensors on board satellites, researchers also need to gather ground-truth information obtained at multiple locations in various periods. The quality of satellite data depends on the accuracy and precision of atmospheric and geometric corrections of those data. Previous studies used locally collected data such as daily phenology images and spectrum data observed from towers (Nagai et al., 2014a, 2020a,b; Nakaji et al., 2014; Lopes et al., 2016). Such ground-truth information provides accurate and precise data collected over a long period. However, the number of locations in the tropics where phenology images and spectrum data are being collected is still limited (Nakaji et al., 2014; Nasahara and Nagai, 2015; Lopes et al., 2016; Alberton et al., 2017; Nagai et al., 2018, 2020a).

Another way to obtain detailed ground-truth information from multiple locations for a broad-scale picture of historical changes in land cover and land use is to examine “social sensing data,” a type of big data. These include videos posted to YouTube and old television programs (De Frenne et al., 2018; Shin et al., 2022b), and text and photographs with geotag information posted to social networking services (e.g., Twitter, Instagram, and Flickr; Fernández-Bellon and Kane, 2020; Silva et al., 2018; Song et al., 2020; Yoshimura and Hiura, 2017). The interests and movement of people at various locations can also be tracked by analyzing the access statistics of Google (Google Trends: Takada, 2012; Proulx et al., 2013),¹⁴ number of visitors at Wikipedia (Fernández-Bellon and Kane, 2020), and geolocation information of mobile phones (Chang et al., 2021; Pintér and Felde, 2021). For instance, the analysis of Twitter posts was useful for evaluating the spatiotemporal variation of the timing of leaf coloring in Japan (Shin et al., 2021b). Kotani et al. (2021) and Shin et al. (2022a) analyzed the time-series of Google Trends and/or Yandex statistics (a major search engine in Russia)¹⁵ to assess the spatiotemporal characteristics of people’s interest in the use of berries in Arctic and the Russian Far East regions,

12 https://newsletter.cseas.kyoto-u.ac.jp/jp/02/02_02_yanagisawa.html

13 <https://fieldnote.archiving.jp/>

14 <https://trends.google.com/trends/>

15 <https://wordstat.yandex.com>

which the authors used as proxy data of ripening phenology. Likewise, people's interests in oil extracted from illipe nuts (Borneo tallow nut), which are seeds of Dipterocarpaceae species (Blicher-Mathiesen, 1994), may be useful as ground-truth information for ripening phenology in Sarawak, Malaysia Borneo.

4.2. Improving classification of PFTs on land-cover and land-use maps and detecting interannual variation of PFTs

As an example of a detailed land-cover and land-use map in Asia with a high spatial resolution, the Japan Aerospace Exploration Agency has published the land-cover and land-use maps of Japan and Vietnam with 10-m or 30-m spatial resolutions by integrative analysis of data from multi-satellites such as the Sentinel-2A/2B-MSI, the ALOS-AVNIR2 (Advanced Visible and Near Infrared Radiometer type 2), the Landsat series satellites, and the ALOS2-PALSAR2 (Hirayama et al., 2022; Hoang et al., 2020).¹⁶ However, these maps of Japan did not account for the interannual variation in land cover and land use. In addition, PFTs were classified into broad categories, such as deciduous broad-leaved forest and evergreen coniferous forest. To accurately evaluate the spatiotemporal variation of the heat, water, and carbon cycles and biodiversity in the tropics, and to understand the sensitivity of vegetation to environmental change and succession, accurate classification of PFTs and detection of their interannual variation are needed. For instance, traits of photosynthesis and evapotranspiration differ among ecosystems and tree species in the tropics (Ishida et al., 2005; Kenzo et al., 2004, 2006, 2011, 2015). The improved classification of PFTs and discrimination of tree species based on photosynthesis, leaf traits, and leaf and canopy structures are important tasks because these traits help to account for the sensitivity of the flowering, leaf-flush, and leaf-fall phenology and leaf longevity to environmental changes and succession.

4.3. Studying the interactions between terrestrial and marine ecosystems

The soil in the tropics is oligotrophic (Fujii et al., 2018), and land-cover and land-use change due to deforestation has strongly affected not only the heat, water, and carbon cycles (Carlson et al., 2014; Kumagai et al., 2013; Takahashi et al., 2017), but also coastal ecosystems due to the outflow of nutrients from the soil surface to rivers (Tanaka et al., 2021). To accurately evaluate the spatiotemporal variation of ecosystem functions, ecosystem services, and biodiversity triggered by anthropogenic activities and climate change, we need to improve our understanding of the interactions between terrestrial and marine ecosystems. The SeaWiFS (1.13-km at a daily interval)¹⁷ and Aqua-MODIS satellites, which were launched around 2000, observe ocean color and allow for estimation of chlorophyll concentration (O'Reilly et al., 1998; Schollaert et al., 2003; Gregg and Casey, 2004;

Siswanto and Tanaka, 2014; Groom et al., 2019). In addition, the Second Generation Global Imager (SGLI) on board the Global Change Observation Mission-Climate (GCOM-C) satellite (250-m at 2-day intervals)¹⁸ improved the accuracy and precision of ocean color observations (Murakami, 2016; Matsuoka et al., 2021). Further research should examine, for instance, the relationship between the interannual variation of deforestation and the spatiotemporal variation of the chlorophyll concentrations in the coastal areas of some river basins.

4.4. Investigating the interaction between land-cover and land-use change and anthropogenic activities

To understand the spatiotemporal variation of ecosystem services and biodiversity, we must evaluate the spatiotemporal variation of the interaction between land-cover and land-use change and anthropogenic activities. For this, the nighttime light data observed by the Visible Infrared Imaging Radiometer Suite (VIIRS) on board the Suomi NPP satellite (Day/Night Band [DNB]; 750-m at a daily interval; Elvidge et al., 2017, 2021)¹⁹ may be useful, as land-cover and land-use change has caused the spatiotemporal variation of nighttime light. In a study of 46 cities with more than 50,000 inhabitants, Ivan et al. (2020) reported the suitability of the Suomi NPP-VIIRS satellite-observed nighttime light to evaluate the geographic variation of income. Studies of tropical regions could use these satellite data to examine the relationship between the interannual variation of deforestation and spatiotemporal expansion of the nighttime light.

4.5. Developing integrative analysis and evaluation of in situ and satellite-observed data

Despite the language barrier (Amano et al., 2016), the collection of *in situ* observed data and ecophysiological information in each country and region (especially non-English data and information; Nagai et al., 2016b; Takeuchi et al., 2021) will accelerate the development of integrative analysis and evaluation of *in situ* and satellite-observed data. As noted by Farley et al. (2018), researchers should aim to conduct more big data analyses by integrating citizen science, which has superior veracity; real-time sensor networks, which have superior velocity; *in situ* observed data collected by scientists, which have superior variety; and remote-sensing, which has a superior volume. The support of international scientific networking communities such as the Asia-Pacific Biodiversity Observation Network (Takeuchi et al., 2021)²⁰, the Asia-Oceania GEO,²¹ and the East Asia and Pacific International Long-Term Ecological Research Network (Kim et al., 2018)²² is indispensable for the development of these integrated

¹⁶ https://www.eorc.jaxa.jp/ALOS/jp/dataset/tulc_j.htm

¹⁷ <https://oceancolor.gsfc.nasa.gov/SeaWiFS/>

¹⁸ https://suzaku.eorc.jaxa.jp/GCOM_C/index.html

¹⁹ <https://ncc.nesdis.noaa.gov/VIIRS/>

²⁰ <http://www.esabii.biodic.go.jp/ap-bon/japanese/index.html>

²¹ <https://aogeo.net/en/>

²² <https://www.ilter.network/>

studies. Takeuchi et al. (2021) emphasized the necessity of satellite observations that provide the academic perspectives and evidence needed to implement natural ecosystem conservation policies. We further encourage the use of *in situ* observed data to improve the accuracy and precision of analyses of satellite observations and reinforcing the networking of research communities working with *in situ* and satellite observations in the Asian tropics (Dronova and Taddeo, 2022; Shin et al., 2023).

5. Conclusion

Our discussions in this perspective paper can be summarized that future advances in the optical sensors on board satellites with high frequency (≤ 10 min) and high spatial resolution (≤ 10 m) are expected to deepen our understanding of ecosystems in the Asian tropics, thus improving our knowledge of phenological changes as well as land-cover and land-use changes due to anthropogenic activities and climate change. Consequently, we could deeply understand the temporal change of the friction between people and ecosystems in the Asian tropics (i.e., degree of the unsustainable circumstances) under societal and climate changes. Despite unclear phenology with a high biodiversity as well as high heterogeneity of land cover and land use, the day is undoubtedly coming when we can monitor tropical ecosystems in Asia even at the individual tree scale. Now, we are in the beginning of a new era of satellite remote-sensing.

Author contributions

NS designed the study. NS, CK, TM, and KI collected and analyzed the data. NS, TM, and YT wrote the manuscript. All authors contributed to critical manuscript revision and read and approved the submitted version.

References

- Alberton, B., Torres, R. S., Cancian, L. F., Borges, B. D., Almeida, J., Mariano, G. C., et al. (2017). Introducing digital cameras to monitor plant phenology in the tropics: Applications for conservation. *Perspect. Ecol. Conserv.* 15, 82–90.
- Amano, T., González-Varo, J. P., and Sutherland, W. J. (2016). Languages are still a major barrier to global science. *PLoS Biol.* 14:e2000933. doi: 10.1371/journal.pbio.2000933
- Asner, G. P., Martin, R. E., Anderson, C. B., and Knapp, D. E. (2015). Quantifying forest canopy traits: Imaging spectroscopy versus field survey. *Remote Sens. Environ.* 158, 15–27.
- Avtar, R., Suzuki, R., and Sawada, H. (2014). Natural forest biomass estimation based on plantation information using PALSAR data. *PLoS One* 9:e86121. doi: 10.1371/journal.pone.0086121
- Azmy, M. M., Hashim, M., Numata, S., Hosaka, T., Noor, N. S. M., and Fletcher, C. (2016). Satellite-based characterization of climatic conditions before large-scale general flowering events in Peninsular Malaysia. *Sci. Rep.* 6:32329. doi: 10.1038/srep32329
- Blicher-Mathiesen, U. (1994). Borneo Illipe, a fat product from different *Shorea* spp. (Dipterocarpaceae). *Econ. Bot.* 48, 231–242. doi: 10.1007/BF02862321
- Buitenwerf, R., Rose, L., and Higgins, S. I. (2015). Three decades of multi-dimensional change in global leaf phenology. *Nat. Clim. Change* 5, 364–368. doi: 10.1038/NCLIMATE2533
- Carlson, K. M., Curran, L. M., Ponette-González, A. G., Ratnasari, D., Ruspita, Lisnawati, N., et al. (2014). Influence of watershed-climate interactions on stream temperature, sediment yield, and metabolism along a land use intensity gradient in Indonesian Borneo. *J. Geophys. Res. Biogeosci.* 119, 1110–1128. doi: 10.1002/2013JG002516
- Chang, S., Wang, Z., Mao, D., Liu, F., Lai, L., and Yu, H. (2021). Identifying urban functional areas in China's Changchun city from Sentinel-2 images and social sensing data. *Remote Sens.* 13:4512. doi: 10.3390/rs13224512
- Chechina, M., and Hamann, A. (2019). Climatic drivers of dipterocarp mass-flowering in South-East Asia. *J. Trop. Ecol.* 35, 108–117.
- De Frenne, P., Van Langenhove, L., Van Driessche, A., Bertrand, C., Verheyen, K., and Vangansbeke, P. (2018). Using archived television video footage to quantify phenology responses to climate change. *Methods Ecol. Evol.* 9, 1874–1882. doi: 10.1111/2041-210X.13024
- Delbart, N., Beaubien, E., Kergoat, L., and Le Toan, T. (2015). Comparing land surface phenology with leafing and flowering observations from the PlantWatch citizen network. *Remote Sens. Environ.* 160, 273–280. doi: 10.1016/j.rse.2015.01.012
- Delbart, N., Le Toan, T., Kergoat, L., and Fedotova, V. (2006). Remote sensing of spring phenology in boreal regions: A free of snow-effect method using NOAA-AVHRR and SPOT-VGT data (1982–2004). *Remote Sens. Environ.* 101, 52–62.
- Díaz, S., Pascual, U., Stenseke, M., Martín-López, B., Watson, R. T., Molnár, Z., et al. (2018). Assessing nature's contributions to people. *Science* 359, 270–272.
- Dronova, I., and Taddeo, S. (2022). Remote sensing of phenology: Towards the comprehensive indicators of plant community dynamics from species to regional scales. *J. Ecol.* 110, 1460–1484. doi: 10.1111/1365-2745.138

Funding

This research was supported by the Global Change Observation Mission (ER2GCF104) of the Japan Aerospace Exploration Agency and KAKENHI grant (21H02229, 21H05178, and 22K12352) from the Japan Society for the Promotion of Science.

Acknowledgments

We thank Dr. Eko Siswanto (JAMSTEC) for providing useful information. We thank Ms. Mika Takeuchi (JAMSTEC) for assistance of analysis. We also thank the editor and reviewers for their constructive comments.

Conflict of interest

The authors declare that the research was conducted in the absence of any commercial or financial relationships that could be construed as a potential conflict of interest.

Publisher's note

All claims expressed in this article are solely those of the authors and do not necessarily represent those of their affiliated organizations, or those of the publisher, the editors and the reviewers. Any product that may be evaluated in this article, or claim that may be made by its manufacturer, is not guaranteed or endorsed by the publisher.

- Elvidge, C. D., Baugh, K., Zhizhin, M., Hsu, F. C., and Ghosh, T. (2017). VIIRS night-time lights. *Int. J. Remote Sens.* 38, 5860–5879. doi: 10.1080/01431161.2017.1342050
- Elvidge, C. D., Zhizhin, M., Ghosh, T., Hsu, F.-C., and Taneja, J. (2021). Annual time series of global VIIRS nighttime lights derived from monthly averages: 2012 to 2019. *Remote Sens.* 13:922. doi: 10.3390/rs13050922
- Erasmí, S., Propastin, P., Kappas, M., and Panferov, O. (2009). Spatial patterns of NDVI variation over Indonesia and their relationship to ENSO warm events during the period 1982–2006. *J. Clim.* 22, 6612–6623.
- Erasmí, S., Schucknecht, A., Barbosa, M. P., and Matschullat, J. (2014). Vegetation greenness in Northeastern Brazil and its relation to ENSO warm events. *Remote Sens.* 6, 3041–3058. doi: 10.3390/rs6043041
- Estoque, R. C., Ooba, M., Avitabile, V., Hijioka, Y., DasGupta, R., Togawa, T., et al. (2019). The future of Southeast Asia's forests. *Nat. Commun.* 10:1829. doi: 10.1038/s41467-019-09646-4
- FAO, and UNEP (2020). *The state of the world's forests 2020. Forests, biodiversity and people*. Rome: FAO. doi: 10.4060/ca8642en
- Farley, S. S., Dawson, A., Goring, S. J., and Williams, J. W. (2018). Situating ecology as a big-data science: Current advances, challenges, and solutions. *BioScience* 68, 563–576. doi: 10.1093/biosci/biy068
- Fernández-Bellón, D., and Kane, A. (2020). Natural history films raise species awareness—a big data approach. *Conserv. Lett.* 13:e12678. doi: 10.1111/conl.12678
- Fitzherbert, E. B., Struebig, M. J., Morel, A., Danielsen, F., Brühl, C. A., Donald, P. F., et al. (2008). How will oil palm expansion affect biodiversity? *Trends Ecol. Evol.* 23, 538–545.
- Fujii, K., Shibata, M., Kitajima, K., Ichie, T., Kitayama, K., and Turner, B. L. (2018). Plant–soil interactions maintain biodiversity and functions of tropical forest ecosystems. *Ecol. Res.* 33, 149–160. doi: 10.1007/s11284-017-1511-y
- Funada, S., and Tsutsumida, N. (2022). Mapping cherry blossoms from geotagged street-level photos. *bioRxiv* [Preprint]. doi: 10.1101/2022.01.18.476550
- Gao, M., Piao, S., Chen, A., Yang, H., Liu, Q., Fu, Y. H., et al. (2019). Divergent changes in the elevational gradient of vegetation activities over the last 30 years. *Nat. Commun.* 10:2970. doi: 10.1038/s41467-019-11035-w
- Garonna, I., De Jong, R., De Wit, A. J. W., Múcher, C. A., Schmid, B., and Schaepman, M. E. (2014). Strong contribution of autumn phenology to changes in satellite-derived growing season length estimates across Europe (1982–2011). *Glob. Change Biol.* 20, 3457–3470. doi: 10.1111/gcb.12625
- GEAS (2011). *Oil palm plantations: Threats and opportunities for tropical ecosystems*. Nairobi: UNEP Global Environmental Alter Service, 8.
- Gray, R. E. J., and Ewers, R. M. (2021). Monitoring forest phenology in a changing world. *Forests* 12:297. doi: 10.3390/f12030297
- Gregg, W. W., and Casey, N. M. (2004). Global and regional evaluation of the SeaWiFS chlorophyll data set. *Remote Sens. Environ.* 93, 463–479. doi: 10.1016/j.rse.2003.12.012
- Groom, S., Sathyendranath, S., Ban, Y., Bernard, S., Brewin, R., Brotas, V., et al. (2019). Satellite ocean colour: Current status and future perspective. *Front. Mar. Sci.* 6:485. doi: 10.3389/fmars.2019.00485
- Hansen, M. C., Potapov, P. V., Moore, R., Hancher, M., Turubanova, S. A., Tyukavina, A., et al. (2013). High-resolution global maps of 21st-century forest cover change. *Science* 342, 850–853.
- Harrison, R. D. (2001). Drought and the consequences of El Niño in Borneo: A case study of figs. *Popul. Ecol.* 43, 63–75.
- Hirayama, S., Tadono, T., Ohki, M., Mizukami, Y., Nasahara, K. N., Imamura, K., et al. (2022). Generation of high-resolution land use and land cover maps in JAPAN Version 21.11. *J. Remote Sens. Soc. Jpn.* 42, 199–216. doi: 10.11440/rssj.42.199
- Hoang, T. T., Truong, V. T., Hayashi, M., Tadono, T., and Nasahara, K. N. (2020). New JAXA high-resolution land use/land cover map for Vietnam aiming for natural forest and plantation forest monitoring. *Remote Sens.* 12:2707.
- Ichikawa, M. (2007). Degradation and loss of forest land and land-use changes in Sarawak, East Malaysia: A study of native land use by the Iban. *Ecol. Res.* 22, 403–413. doi: 10.1007/s11284-007-0365-0
- Imukova, K., Ingwersen, J., and Streck, T. (2015). Determining the spatial and temporal dynamics of the green vegetation fraction of croplands using high-resolution RapidEye satellite images. *Agric. For. Meteorol.* 206, 113–123. doi: 10.1016/j.agrformet.2015.03.003
- Inoue, T., Nagai, S., Saitoh, T. M., Muraoka, H., Nasahara, K. N., and Koizumi, H. (2014). Detection of the different characteristics of year-to-year variation in foliage phenology among deciduous broad-leaved tree species by using daily continuous canopy surface images. *Ecol. Inform.* 22, 58–68.
- IPCC (2021). “Summary for policymakers,” in *Climate change 2021: The physical science basis. Contribution of working group I to the sixth assessment report of the intergovernmental panel on climate change*, eds V. Masson-Delmotte, P. Zhai, A. Pirani, S. L. Connors, C. Péan, S. Berger, et al. (Cambridge: Cambridge University Press). doi: 10.1017/9781009157896
- Ishida, A., Toma, T., and Marjenah. (2005). A comparison of in situ leaf photosynthesis and chlorophyll fluorescence at the top canopies in rainforest mature trees. *JARQ* 39, 57–67. doi: 10.6090/jarq.39.57
- Ishihara, M., and Tadano, T. (2017). Land cover changes induced by the great east Japan earthquake in 2011. *Sci. Rep.* 7:45769. doi: 10.1038/srep45769
- Ivan, K., Holobáčá, I.-H., Benedek, J., and Török, I. (2020). VIIRS nighttime light data for income estimation at local level. *Remote Sens.* 12:2950. doi: 10.3390/rs12182950
- Iwao, K., Nasahara, K. N., Kinoshita, T., Yamagata, Y., Patton, D., and Tsuchida, S. (2011). Creation of new global land cover map with map integration. *J. Geogr. Inf. Syst.* 3, 160–165.
- Jin, H., Jönsson, A. M., Olsson, C., Lindström, J., Jönsson, P., and Eklundh, L. (2019). New satellite-based estimates show significant trends in spring phenology and complex sensitivities to temperature and precipitation at northern European latitudes. *Int. J. Biometeorol.* 63, 763–775. doi: 10.1007/s00484-019-01690-5
- John, A., Ong, J., Theobald, E. J., Olden, J. D., Tan, A., and HilleRisLambers, J. (2020). Detecting montane flowering phenology with CubeSat imagery. *Remote Sens.* 12:2894. doi: 10.3390/rs12182894
- Kenzo, T., Ichie, T., Watanabe, Y., Yoneda, R., Ninomiya, I., and Koike, T. (2006). Changes in photosynthesis and leaf characteristics with tree height in five dipterocarp species in a tropical rain forest. *Tree Physiol.* 26, 865–873. doi: 10.1093/treephys/26.7.865
- Kenzo, T., Ichie, T., Yoneda, R., Kitahashi, Y., Watanabe, Y., Ninomiya, I., et al. (2004). Interspecific variation of photosynthesis and leaf characteristics in five canopy trees of Dipterocarpaceae in tropical rain forest. *Tree Physiol.* 24, 1187–1192. doi: 10.1093/treephys/24.10.1187
- Kenzo, T., Inoue, Y., Yoshimura, M., Yamashita, M., Tanaka-Oda, A., and Ichie, T. (2015). Height-related changes in leaf photosynthetic traits in diverse Bornean tropical rain forest trees. *Oecologia* 177, 191–202. doi: 10.1007/s00442-014-3126-0
- Kenzo, T., Yoneda, R., Matsumoto, Y., Alias, M. A., and Muhamad, N. M. (2011). Growth and photosynthetic response of four Malaysian indigenous tree species under different light conditions. *J. Trop. For. Sci.* 23, 271–281.
- Kikuzawa, K. (2005). *Ecology of leaf longevity: From individual leaves to ecosystems*. Tokyo: Kyoritsu Shuppan Co., Ltd, 212.
- Kikuzawa, K., Onoda, Y., Wright, I. J., and Reich, P. B. (2013). Mechanisms underlying global temperature-related patterns in leaf longevity. *Glob. Ecol. Biogeogr.* 22, 982–993.
- Kim, E. S., Trisurat, Y., Muraoka, H., Shibata, H., Amoroso, V., Boldgiv, B., et al. (2018). International long-term ecological research east asia-pacific regional network (ILTER-EAP): History, development and perspectives. *Ecol. Res.* 33, 19–34. doi: 10.1007/s11284-017-1523-7
- Kobayashi, H., Yunus, A. P., Nagai, S., Sugiura, K., Kim, Y., Dam, B. V., et al. (2016). Latitudinal gradient of spruce forest understory and tundra phenology in Alaska as observed from satellite and ground-based data. *Remote Sens. Environ.* 177, 160–170. doi: 10.1016/j.rse.2016.02.020
- Koh, L. P., Miettinen, J., Liew, S. C., and Ghazoul, J. (2011). Remotely sensed evidence of tropical peatland conversion to oil palm. *PNAS* 108, 5127–5132. doi: 10.1073/pnas.1018776108
- Kotani, A., Shin, N., Tei, S., Makarov, A., and Gavrilyeva, T. (2021). Seasonality in human interest in berry plants detection by google trends. *Front. For. Glob. Change* 4:688835. doi: 10.3389/ffgc.2021.688835
- Kou, W., Xiao, X., Dong, J., Gan, S., Zhai, D., Zhang, G., et al. (2015). Mapping deciduous rubber plantation areas and stand ages with PALSAR and Landsat images. *Remote Sens.* 7, 1048–1073. doi: 10.3390/rs70101048
- Kumagai, T., Kanamori, H., and Yasunari, T. (2013). Deforestation-induced reduction in rainfall. *Hydrol. Process* 27, 3811–3814. doi: 10.1002/hyp.10060
- Lautenbach, S., Seppelt, R., Liebscher, J., and Dormann, C. F. (2012). Spatial and temporal trends of global pollination benefit. *PLoS One* 7:e35954. doi: 10.1371/journal.pone.0035954
- Leach, N., Coops, N. C., and Obrknezev, N. (2019). Normalization method for multi-sensor high spatial and temporal resolution satellite imagery with radiometric inconsistencies. *Comput. Electron. Agric.* 164:104893. doi: 10.1016/j.compag.2019.104893
- Lee, H. S., Ashton, P. S., Yamakura, T., Tan, S., Davies, S. J., Itoh, A., et al. (2002). *The 52-hectare forest research plot at Lambir Hills, Sarawak, Malaysia: Tree distribution maps, diameter tables and species documentation. Forest Department Sarawak and the Arnold arboretum-CTFS Asia program*. Kuching: Forest Department Sarawak.
- Li, L., Dong, J., Tenku, S. N., and Xiao, X. (2015). Mapping oil palm plantations in Cameroon using PALSAR 50-m orthorectified mosaic images. *Remote Sens.* 7, 1206–1224. doi: 10.3390/rs70201206
- Li, P., Zhang, J., and Feng, Z. (2015). Mapping rubber tree plantations using a Landsat-based phenological algorithm in Xishuangbanna, southwest China. *Remote Sens. Lett.* 6, 49–58. doi: 10.1080/2150704X.2014.996678

- Lopes, A. P., Nelson, B. W., Wu, J., Graça, P. M. L. A., Tavares, J. V., Prohaska, N., et al. (2016). Leaf flush drives dry season green-up of the Central Amazon. *Remote Sens. Environ.* 182, 90–98. doi: 10.1016/j.rse.2016.05.009
- Luke, P., Stenberg, P., Rautiainen, M., Mttus, M., and Vanhatalo, K. M. (2013). Optical properties of leaves and needles for boreal tree species in Europe. *Remote Sens. Lett.* 4, 667–676. doi: 10.1080/2150704X.2013.782112
- Marlier, M. E., DeFries, R. S., Kim, P. S., Gaveau, D. L. A., Koplitz, S. N., Jacob, D. J., et al. (2015). Regional air quality impacts of future fire emissions in Sumatra and Kalimantan. *Environ. Res. Lett.* 10:054010. doi: 10.1046/j.1440-1843.2000.00248.x
- Matsuoka, A., Campbell, J. W., Hooker, S. B., Steinmetz, F., Ogata, K., Hirata, T., et al. (2021). Performance of JAXA's SGLI standard ocean color products for oceanic to coastal waters: Chlorophyll a concentration and light absorption coefficients of colored dissolved organic matter. *J. Oceanogr.* 93, 187–208. doi: 10.1007/s10872-021-00617-2
- Miettinen, J., and Liew, S. C. (2011). Separability of insular Southeast Asian woody plantation species in the 50 m resolution ALOS PALSAR mosaic product. *Remote Sens. Lett.* 2, 299–307.
- Miettinen, J., Shi, C., and Liew, S. C. (2011). Deforestation rates in insular Southeast Asia between 2000 and 2010. *Glob. Change Biol.* 17, 2261–2270.
- Miura, T., and Nagai, S. (2020). Landslide detection with Himawari-8 geostationary satellite data: A case study of a torrential rain event in Kyushu, Japan. *Remote Sens.* 12:1734. doi: 10.3390/rs12111734
- Miura, T., Nagai, S., Takeuchi, M., Ichii, K., and Yoshioka, H. (2019). Improved characterisation of vegetation and land surface seasonal dynamics in central Japan with Himawari-8 hypertemporal data. *Sci. Rep.* 9:15692. doi: 10.1038/s41598-019-52076-x
- Miura, T., Tokumoto, Y., Shin, N., Shimizu, K. K., Pungga, R. A. S., and Ichie, T. (2023). Utility of commercial high-resolution satellite imagery for monitoring general flowering in Sarawak, Borneo. *Ecol. Res.* doi: 10.1111/1440-1703.12382
- Moon, M., Richardson, A. D., and Friedl, M. A. (2021). Multiscale assessment of land surface phenology from harmonized landsat 8 and sentinel-2, PlanetScope, and PhenoCam imagery. *Remote Sens. Environ.* 266:112716. doi: 10.1016/j.rse.2021.112716
- Morellato, L. P. C., Alberton, B., Alvarado, S. T., Borges, B., Buisson, E., Camargo, M. G. G., et al. (2016). Linking plant phenology to conservation biology. *Biol. Conserv.* 195, 60–72.
- Morissette, J. T., Richardson, A. D., Knapp, A. K., Fisher, J. I., Graham, E. A., Abatzoglou, J., et al. (2009). Tracking the rhythm of the seasons in the face of global change: Phenological research in the 21st century. *Front. Ecol. Environ.* 7:253–260. doi: 10.1890/070217
- Morozumi, T., Shingubara, R., Murase, J., Nagai, S., Kobayashi, H., Takano, S., et al. (2019). Usability of water surface reflectance for the determination of riverine dissolved methane during extreme flooding in northeastern Siberia. *Polar Sci.* 21, 186–194. doi: 10.1016/j.polar.2019.01.005
- Motohka, T., Nasahara, K. N., Oguma, H., and Tsuchida, S. (2010). Applicability of green-red vegetation index for remote sensing of vegetation phenology. *Remote Sens.* 2, 2369–2387.
- Murakami, H. (2016). Ocean color sensor (GCOM-C/SGLI). *Bull. Coast. Oceanogr.* 54, 3–9.
- Muraoka, H., Ishii, R., Nagai, S., Suzuki, R., Motohka, T., Noda, H., et al. (2012). "Linking remote sensing and in situ ecosystem/biodiversity observations by "satellite ecology," in *Biodiversity observation network in Asia-Pacific region*, eds S. Nakano, T. Nakashizuka, and T. Yahara (Tokyo: Springer Verlag), 277–308.
- Nagai, S., Akitsu, T., Saitoh, T. M., Busey, R. C., Fukuzawa, K., Honda, Y., et al. (2018). 8 million phenological and sky images from 29 ecosystems from the Arctic to the tropics: The phenological eyes network. *Ecol. Res.* 33, 1091–1092. doi: 10.1007/s1284-018-1633-x
- Nagai, S., Nasahara, K. N., Akitsu, T. K., Saitoh, T. M., and Muraoka, H. (2020a). "Importance of the collection of abundant ground-truth data for accurate detection of spatial and temporal variability of vegetation by satellite remote sensing," in *Biogeochemical cycles: Ecological drivers and environmental impact. Geophysical monograph*, Vol. 251, eds K. Dontsova, Z. Balogh-Brunstad, and G. Le Roux (New York, NY: John Wiley and Sons, Inc). doi: 10.1002/9781119413332.ch11
- Nagai, S., Endo, T., and Nasahara, K. N. (2020b). Phenology observations in Institute for Nature Study by fine spatio-temporal resolution satellite: SENTINEL-2A/B. *Miscell. Rep. Inst. Nat. Stud.* 52, 19–24.
- Nagai, S., Ichie, T., Yoneyama, A., Kobayashi, H., Inoue, T., Ishii, R., et al. (2016a). Usability of time-lapse digital camera images to detect characteristics of tree phenology in a tropical rainforest. *Ecol. Inform.* 32, 91–106.
- Nagai, S., Nasahara, K. N., Inoue, T., Saitoh, T. M., and Suzuki, R. (2016b). Review: Advances in in situ and satellite phenological observations in Japan. *Int. J. Biometeorol.* 60, 615–627. doi: 10.1007/s00484-015-1053-3
- Nagai, S., Ishii, R., Suhaili, A., Kobayashi, H., Matsuoka, M., Ichie, T., et al. (2014a). Usability of noise-free daily satellite-observed green-red vegetation index values for monitoring ecosystem changes in Borneo. *Int. J. Biometeorol.* 35, 7910–7926.
- Nagai, S., Inoue, T., Ohtsuka, T., Kobayashi, H., Kurumado, K., Muraoka, H., et al. (2014b). Relationship between spatio-temporal characteristics of leaf-fall phenology and seasonal variations in near surface- and satellite-observed vegetation indices in a cool-temperate deciduous broad-leaved forest in Japan. *Int. J. Remote Sens.* 35, 3520–3536.
- Nagai, S., Saitoh, T. M., and Yoshitake, S. (2019). Cultural ecosystem services provided by flowering of cherry trees under climate change: A case study of the relationship between the periods of flowering and festivals. *Int. J. Biometeorol.* 63, 1051–1058. doi: 10.1007/s00484-019-01719-9
- Nagai, S., Saitoh, T. M., Suzuki, R., Nasahara, K. N., Lee, W.-K., Son, Y., et al. (2011). The necessity and availability of noise-free daily satellite-observed NDVI during rapid phenological changes in terrestrial ecosystems in East Asia. *For. Sci. Tech.* 7, 174–183.
- Najib, N. E. M., Kanniah, K. D., Cracknell, A. P., and Yu, L. (2020). Synergy of active and passive remote sensing data for effective mapping of oil palm plantation in Malaysia. *Forests* 11:858. doi: 10.3390/f11080858
- Nakagawa, M., Ushio, M., Kume, T., and Nakashizuka, T. (2019). Seasonal and long-term patterns in litterfall in a Bornean tropical rainforest. *Ecol. Res.* 34, 31–39. doi: 10.1111/1440-1703.1003
- Nakaji, T., Kosugi, Y., Takanashi, S., Niiyama, K., Noguchi, S., Tani, M., et al. (2014). Estimation of light-use efficiency through a combinational use of the photochemical reflectance index and vapor pressure deficit in an evergreen tropical rainforest at Pasoh, Peninsular Malaysia. *Remote Sens. Environ.* 150, 82–92.
- Nasahara, K. N., and Nagai, S. (2015). Review: Development of an in situ observation network for terrestrial ecological remote sensing—the phenological eyes network (PEN). *Ecol. Res.* 30, 211–223.
- Noda, H. M., Motohka, T., Murakami, K., Muraoka, H., and Nasahara, K. N. (2014). Reflectance and transmittance spectra of leaves and shoots of 22 vascular plant species and reflectance spectra of trunks and branches of 12 tree species in Japan. *Ecol. Res.* 29:111. doi: 10.1007/s1284-013-1096-z
- Noda, H. M., Muraoka, H., and Nasahara, K. N. (2021). Plant ecophysiological processes in spectral profiles: Perspective from a deciduous broadleaf forest. *J. Plant Res.* 134, 737–751. doi: 10.1007/s10265-021-01302-7
- Nomura, K., and Mitchard, E. T. A. (2018). More than meets the eye: Using sentinel-2 to map small plantations in complex forest landscapes. *Remote Sens.* 10:1693. doi: 10.3390/rs10111693
- O'Reilly, J. E., Maritorena, S., Mitchell, B. G., Siegel, D. A., Carder, K. L., Garver, S. A., et al. (1998). Ocean color chlorophyll algorithms for SeaWiFS. *J. Geophys. Res.* 103, 24937–24953. doi: 10.1029/98JC02160
- Onoda, Y., Westoby, M., Adler, P. B., Choong, A. M. F., Clissold, F. J., Cornelissen, J. H. C., et al. (2011). Global patterns of leaf mechanical properties. *Ecol. Lett.* 14, 301–312.
- Osada, N. (2018). Diversity in leaf phenology of tree species in a tropical rain forest in Malaysia. *Sci. Rep. Facul. Agricul. Meijo Univ.* 54, 29–35.
- Park, T., Ganguly, S., Tømmervik, H., Euskirchen, E. S., Høgda, K.-A., Karlens, S. R., et al. (2016). Changes in growing season duration and productivity of northern vegetation inferred from long-term remote sensing data. *Environ. Res. Lett.* 11:084001.
- Penneac, A., Gond, V., and Sabatier, D. (2011). Tropical forest phenology in French Guiana from MODIS time series. *Remote Sens. Lett.* 2, 337–345. doi: 10.1080/01431161.2010.507610
- Penñuelas, J., Rutishauser, T., and Filella, I. (2009). Phenology feedbacks on climate change. *Science* 324, 887–888.
- Persson, M., Lindberg, E., and Reese, H. (2018). Tree species classification with multi-temporal Sentinel-2 data. *Remote Sens.* 10:1794. doi: 10.3390/rs10111794
- Pfeifer, M., Kor, L., Nilus, R., Turner, E., Cusack, J., Lysenko, I., et al. (2016). Mapping the structure of Borneo's tropical forests across a degradation gradient. *Remote Sens. Environ.* 176, 84–97. doi: 10.1016/j.rse.2016.01.014
- Piao, S., Liu, Q., Chen, A., Janssens, I. A., Fu, Y., Dai, J., et al. (2019). Plant phenology and global climate change: Current progresses and challenges. *Glob. Change Biol.* 25, 1922–1940. doi: 10.1111/gcb.14619
- Pintér, G., and Felde, I. (2021). Analyzing the behavior and financial status of soccer fans from a mobile phone network perspective: Euro 2016, a case study. *Information* 12:468. doi: 10.3390/info12110468
- Proulx, R., Massicotte, P., and Pélino, M. (2013). Googling trends in conservation biology. *Conserv. Biol.* 28, 44–51. doi: 10.1111/cobi.12131
- Rahmandhana, A. D., Kamal, M., and Wicaksono, P. (2022). Spectral reflectance-based mangrove species mapping from WorldView-2 imagery of Karimunjawa and Kemujan Island, central Java province, Indonesia. *Remote Sens.* 14:183. doi: 10.3390/rs14010183
- Reich, P. B., Uhl, C., Walters, M. B., Prugh, L., and Ellsworth, D. S. (2004). Leaf demography and phenology in Amazonian rain forest: A census of 40000 leaves of 23 tree species. *Ecol. Monogr.* 74, 3–23.
- Richardson, A. D., Keenan, T. F., Migliavacca, M., Ryu, Y., Sonnentag, O., and Toomey, M. (2013). Climate change, phenology, and phenological control of vegetation feedbacks to the climate system. *Agri. For. Meteorol.* 169, 156–173.
- Rohde, A. T., and Pilliod, D. S. (2021). Spatiotemporal dynamics of insect pollinator communities in sagebrush steppe associated with weather and vegetation. *Glob. Ecol. Conserv.* 29:e01691. doi: 10.1016/j.gecco.2021.e01691

- Sakai, S., Harrison, R. D., Momose, K., Kuraji, K., Nagamasu, H., Yasunari, T., et al. (2006). Irregular droughts trigger mass flowering in aseasonal tropical forests in Asia. *Amer. J. Bot.* 93, 1134–1139. doi: 10.3732/ajb.93.8.1134
- Sakurai, R., Jacobson, S. K., Kobori, H., Primack, R., Oka, K., Komatsu, N., et al. (2011). Culture and climate change: Japanese cherry blossom festivals and stakeholders' knowledge and attitudes about global climate change. *Biol. Conserv.* 144, 654–658.
- Schollaert, S. E., Yoder, J. A., O'Reilly, J. E., and Westphal, D. L. (2003). Influence of dust and sulfate aerosols on ocean color spectra and chlorophyll a concentrations derived from SeaWiFS off the U.S. east coast. *J. Geophys. Res.* 108:3191. doi: 10.1029/2000JC000555
- Secades, C., O'Connor, B., Brown, C., and Walpole, M. (2014). *Earth observation for biodiversity monitoring: A review of current approaches and future opportunities for tracking progress towards the Aichi biodiversity targets*. Technical Series No. 72. Montréal, QC: Secretariat of the Convention on Biological Diversity, 183.
- Secretariat of the Convention on Biological Diversity (2020). *Global biodiversity outlook 5*. Montréal, QC: Secretariat of the Convention on Biological Diversity, 208.
- Segah, H., Tani, H., and Hirano, T. (2010). Detection of fire impact and vegetation recovery over tropical peat swamp forest by satellite data and ground-based NDVI instrument. *Int. J. Remote Sens.* 31, 5297–5314.
- Shimada, M., Itoh, T., Motohka, T., Watanabe, M., Tomohiro, S., Thapa, R., et al. (2014). New global forest/non-forest maps from ALOS PALSAR data (2007–2010). *Remote Sens. Environ.* 155, 13–31.
- Shin, N., Kotani, A., Maruya, Y., and Oishi, Y. (2022b). Data mining by watching old documentary TV programs to learn about the relationships between people's lives and the landscape in Sakha in the perestroika era at the end of the 1980s. *EarthArXiv* [Preprint]. doi: 10.31223/X5KW79
- Shin, N., Kotani, A., Maruya, Y., and Gavrielyeva, T. (2022a). Can Yandex statistics and google trends be used to detect people's interests in berries in the Russian far east? *Polar Sci.* 33:100871. doi: 10.1016/j.polar.2022.100871
- Shin, N., Saitoh, T. M., and Nasahara, K. N. (2021a). How did the characteristics of the growing season change during the past 100 years at a steep river basin in Japan? *PLoS One* 16:e0255078. doi: 10.1371/journal.pone.0255078
- Shin, N., Maruya, Y., Saitoh, T. M., and Tsutsumida, N. (2021b). Usefulness of social sensing using text mining of tweets for detection of autumn phenology. *Front. For. Glob. Change* 4:659910. doi: 10.3389/ffgc.2021.659910
- Shin, N., Saitoh, T. M., Takeuchi, Y., Miura, T., Aiba, M., Kurokawa, H., et al. (2023). Review: Monitoring of land cover changes and plant phenology by remote-sensing in East Asia. *Ecol. Res.* 38, 111–133. doi: 10.1111/1440-1703.12371
- Shin, N., Shibata, H., Osawa, T., Yamakita, T., Nakamura, M., and Kenta, T. (2020). Toward more data publication of long-term ecological observations. *Ecol. Res.* 35, 700–707. doi: 10.1111/gcb.15123
- Shinohara, M., and Nasahara, K. N. (2022). Utility of flowering signals in the detection of evergreen tree species with a mid-resolution optical satellite sensor. *J. Remote Sens. Soc. Jpn.* 42, 129–134.
- Silva, S. J., Barbieri, L. K., and Thomer, A. K. (2018). Observing vegetation phenology through social media. *PLoS One* 13:e0197325. doi: 10.1371/journal.pone.0197325
- Sims, D. A., and Gamon, J. A. (2002). Relationship between leaf pigment content and spectral reflectance across a wide range of species, leaf structures and developmental stages. *Remote Sens. Environ.* 81, 337–354.
- Siswanto, E., and Tanaka, K. (2014). Phytoplankton biomass dynamics in the strait of Malacca within the period of the SeaWiFS full mission: Seasonal cycles, interannual variations and decadal-scale trends. *Remote Sens.* 6, 2718–2742. doi: 10.3390/rs6042718
- Song, X. P., Richards, D. R., He, P., and Tan, P. Y. (2020). Does geo-located social media reflect the visit frequency of urban parks? A city-wide analysis using the count and content of photographs. *Landscape Urban Plan.* 203:103908. doi: 10.1016/j.landurbplan.2020.103908
- Soyama, N., Akitsu, T., and Temulun, T. (2017). Reference dataset production manual for the accuracy assessment of global land cover products using information from the degree confluence project. *Overall Educa. Res. Center Bull. Tenri Univ.* 15, 31–39.
- Sparks, T. H. (2014). Local-scale adaptation to climate change: The village flower festival. *Clim. Res.* 60, 87–89.
- Spessa, A. C., Field, R. D., Pappenberger, F., Langner, A., Enghart, S., Weber, U., et al. (2015). Seasonal forecasting of fire over Kalimantan, Indonesia. *Nat. Hazards Earth Syst. Sci.* 15, 429–442.
- Stelmaszczyk-Górska, M. A., Urbazaev, M., Schmulius, C., and Thiel, C. (2018). Estimation of above-ground biomass over boreal forests on Siberia using updated in situ, ALOS-2 PALSAR-2, and RADARSAT-2 data. *Remote Sens.* 10:1550. doi: 10.3390/rs10101550
- Takada, K. (2012). Japanese interest in “Hotaru” (Fireflies) and “Kabuto-Mushi” (Japanese rhinoceros beetles) corresponds with seasonality in visible abundance. *Insects* 3, 424–431. doi: 10.3390/insects3020424
- Takahashi, A., Kumagai, T., Kanamori, H., Fujinami, H., and Hiyama, T. (2017). Impact of tropical deforestation and forest degradation on precipitation over Borneo Island. *J. Hydrometeorol.* 18, 2907–2922. doi: 10.1175/JHM-D-17-0008.1
- Takata, Y., Watanabe, H., Yanagisawa, M., and Yamada, T. (2014). *A visualization method of field notes based on locations and topic models. Jimmonkon 2014 ronbunshu*. Tokyo: Information Processing Society of Japan, 57–62.
- Takeuchi, Y., Muraoka, H., Yamakita, T., Kano, Y., Nagai, S., Bunthang, T., et al. (2021). The Asia-Pacific biodiversity observation network: 10-year achievements and new strategies to 2030. *Ecol. Res.* 36, 232–257. doi: 10.1111/1440-1703.12212
- Tanaka, Y., Minggat, E., and Roseli, W. (2021). The impact of tropical land-use change on downstream riverine and estuarine water properties and biogeochemical cycles: A review. *Ecol. Process* 10:40. doi: 10.1186/s13717-021-00315-3
- Tang, J., Korner, C., Muraoka, H., Piao, S., Shen, M., Thackeray, S., et al. (2016). Emerging opportunities and challenges in phenology: A review. *Ecosphere* 7:e01436. doi: 10.1002/ecs2.1436
- Tsutsumida, N., Nagai, S., Rodríguez-Veiga, P., Katagi, J., Nasahara, K., and Tadono, T. (2019). Mapping spatial accuracy of forest type classification in JAXA's high-resolution land use and land cover map. *ISPRS Ann. Photogr. Remote Sens. Spatial Inf. Sci.* IV-3/W1, 57–63. doi: 10.5194/isprs-annals-IV-3-W1-57-2019
- Ushio, M., Osada, Y., Kumagai, T., Kume, T., Pungga, R. S., Nakashizuka, T., et al. (2020). Dynamic and synergistic influences of air temperature and rainfall on general flowering in a Bornean lowland tropical forest. *Ecol. Res.* 35, 17–29. doi: 10.1111/1440-1703.12057
- Visser, M. E., and Gienapp, P. (2019). Evolutionary and demographic consequences of phenological mismatches. *Nat. Ecol. Evol.* 3, 879–885. doi: 10.1038/s41559-019-0880-8
- Vrieling, A., Meroni, M., Darvishzadeh, R., Skidmore, A. K., Wang, T., Zurita-Milla, R., et al. (2018). Vegetation phenology from Sentinel-2 and field cameras for a Dutch barrier island. *Remote Sens. Environ.* 215, 517–529.
- Wang, J., Song, G., Liddell, M., Morellato, P., Lee, C. K. F., Yang, D., et al. (2023). An ecologically-constrained deep learning model for tropical leaf phenology monitoring using PlanetScope satellites. *Remote Sens. Environ.* 286:113429. doi: 10.1016/j.rse.2022.113429
- Wang, J., Yang, D., Detto, M., Nelson, B. W., Chen, M., Guan, K., et al. (2020). Multi-scale integration of satellite remote sensing improves characterization of dry-season green-up in an Amazon tropical evergreen forest. *Remote Sens. Environ.* 246:111865. doi: 10.1016/j.rse.2020.111865
- Wang, Q., Wang, L., Li, Z., Tong, X., and Atkinson, P. M. (2021). Spatial-spectral radial basis function-based interpolation for Landsat ETM+ SLC-off image gap filling. *IEEE Trans. Geosci. Remote Sens.* 59, 7901–7917.
- Wooster, M. J., Perry, G. L. W., and Zoumas, A. (2012). Fire, drought and El Niño relationships on Borneo (Southeast Asia) in the pre-MODIS era (1980–2000). *Biogeosciences* 9, 317–340.
- Wright, I. J., Reich, P. B., Westoby, M., Ackerly, D. D., Baruch, Z., Bongers, F., et al. (2004). The worldwide leaf economics spectrum. *Nature* 428, 821–827.
- Wu, C., Gonsamo, A., Gough, C. M., Chen, J. M., and Xu, S. (2014). Modeling growing season phenology in North American forests using seasonal mean vegetation indices from MODIS. *Remote Sens. Environ.* 147, 79–88. doi: 10.1016/j.rse.2014.03.001
- Wu, J., Albert, L. P., Lopes, A. P., Restrepo-Coupe, N., Hayek, M., Wiedemann, K. T., et al. (2016). Leaf development and demography explain photosynthetic seasonality in Amazon evergreen forests. *Science* 351:972. doi: 10.1126/science.aad5068
- Wu, S., Wang, J., Yan, Z., Song, G., Chen, Y., Ma, Q., et al. (2021). Monitoring tree-crown scale autumn leaf phenology in a temperate forest with an integration of PlanetScope and drone remote sensing observations. *ISPRS J. Photogr. Remote Sens.* 171, 36–48. doi: 10.1016/j.isprsjprs.2020.10.017
- Yamada, T. (2015). Characterizing scenes in field note: Knowledge processing using vocabulary. *Joho Chishiki Gakkaishi* 25, 315–324.
- Yamamoto, Y., Fujino, T., and Kubota, T. (2015). *First book in data mining using R*. Tokyo: Ohmsha, 230.
- Yan, D., Zhang, X., Nagai, S., Yu, Y., Akitsu, T., Nasahara, K. N., et al. (2019). Evaluating land surface phenology from the advanced Himawari imager using observations from MODIS and the phenological eyes network. *Int. J. Appl. Earth Observ. Geoinf.* 79, 71–83.
- Yoshimura, N., and Hiura, T. (2017). Demand and supply of cultural ecosystem services: Use of geotagged photos to map the aesthetic value of landscapes in Hokkaido. *Ecosyst. Serv.* 24, 68–78. doi: 10.1016/j.ecoser.2017.02.009
- Zhang, X. Y., Friedl, M. A., Schaaf, C. B., Strahler, A. H., Hodges, J. C. F., Gao, F., et al. (2003). Monitoring vegetation phenology using MODIS. *Remote Sens. Environ.* 84, 471–475.



OPEN ACCESS

EDITED BY

Ling Zhang,
Jiangxi Agricultural University, China

REVIEWED BY

Bangliang Deng,
Nanchang Institute of Technology, China
Knut Asbjørn Solhaug,
Norwegian University of Life Sciences, Norway

*CORRESPONDENCE

Zhili Liu
✉ liuzl2093@126.com

SPECIALTY SECTION

This article was submitted to
Temperate and Boreal Forests,
a section of the journal
Frontiers in Forests and Global Change

RECEIVED 23 December 2022

ACCEPTED 20 February 2023

PUBLISHED 06 March 2023

CITATION

Wang K, Jin G and Liu Z (2023) Dynamic
variation of non-structural carbohydrates
in branches and leaves of temperate
broad-leaved tree species over a complete life
history.

Front. For. Glob. Change 6:1130604.
doi: 10.3389/ffgc.2023.1130604

COPYRIGHT

© 2023 Wang, Jin and Liu. This is an
open-access article distributed under the terms
of the [Creative Commons Attribution License
\(CC BY\)](https://creativecommons.org/licenses/by/4.0/). The use, distribution or reproduction
in other forums is permitted, provided the
original author(s) and the copyright owner(s)
are credited and that the original publication in
this journal is cited, in accordance with
accepted academic practice. No use,
distribution or reproduction is permitted which
does not comply with these terms.

Dynamic variation of non-structural carbohydrates in branches and leaves of temperate broad-leaved tree species over a complete life history

Kaibo Wang^{1,2,3}, Guangze Jin^{1,2,3} and Zhili Liu^{1,2,3*}

¹Center for Ecological Research, Northeast Forestry University, Harbin, China, ²Key Laboratory of Sustainable Forest Ecosystem Management-Ministry of Education, Northeast Forestry University, Harbin, China, ³Northeast Asia Biodiversity Research Center, Northeast Forestry University, Harbin, China

The composition of non-structural carbohydrates (NSC), one of the photosynthetic products of plants, reflects the survival strategy of a plant. Although several studies have investigated variation of NSC content in woody plants over a set time scale, few studies have considered the dynamic variation of NSC over a continuous life history. In this study, the leaves, new twigs, and old branches of seven temperate broad-leaved tree species (diffuse-porous species: *Betula platyphylla*, *Betula costata*, *Tilia amurensis*, *Acer pictum* subsp. *mono*; ring-porous species: *Ulmus davidiana* var. *japonica*, *Ulmus laciniata*, *Fraxinus mandshurica*) were observed at three life history stages (seedling, sapling, and mature tree) to measure the dynamic changes of NSC and its influencing factors throughout the entire life cycles of these species. The results showed that life history, wood type, and environmental factors (soil nitrogen and phosphorus content, soil pH) significantly affected the NSC content in leaves and branches (including both new twigs and old branches). As plants grew, the NSC content in the leaves and branches generally showed an upward trend, meaning the total non-structural carbohydrate (TNC) content and soluble sugar (SS) content increased significantly, and the starch (ST) content was relatively stable. Lastly, there was no significant difference in NSC content between the canopy layers of mature trees. This indicates that the influence of life stage on NSC content in leaves and branches of plants may be dominated by genetics instead of being regulated by light factors.

KEYWORDS

broad-leaved tree species, leaves and branches, non-structural carbohydrates, survival strategies, life history

1. Introduction

Forest vegetation, due to its role as a vital carbon sink in the global ecosystem (Yadav et al., 2022), is essential for the regulation of climate and carbon balance. To be a sink instead of a source, the net photosynthesis of forest vegetation must be positive (Beer et al., 2010), and thus photosynthetic products play a role in regulating forest productivity (Bonan, 2008). Non-structural carbohydrate (NSC), comprised of one of the photosynthetic products of

plants (Zhang et al., 2013), is a mobile carbon pool (Wang and Wang, 2019). It participates in multiple physiological activities of plants, such as respiratory processes, metabolic activities, signal transduction, etc., and is of great significance for maintaining plant life activities. NSC mainly exists in the forms of soluble sugar (SS) and starch (ST) (Furze et al., 2021). SS, which includes oligosaccharides (sucrose, raffinose, and stachyose) and monosaccharides (glucose and fructose), provides direct energy materials for respiration, defense, plant stress signaling, phloem transport, and osmoregulation, while ST exists as a temporary or long-term energy store that plants can convert into SS when carbon demand exceeds supply (Piper and Paula, 2020; Signori-Müller et al., 2021a). The absorption and utilization of plant carbon can be judged based on variations in plant NSC content (Hoch et al., 2003), which reflect the adaptation strategies of plants when experiencing changes in the external environment (Myers and Kitajima, 2007). When the NSC content in plant tissues continues to decline, it means that the carbon demand is higher than the supply, and the carbon reserve is inadequate. When the NSC content is elevated or relatively stable, it means that the supply of carbon is greater than the demand, so carbon does not limit growth at all (Hoch et al., 2002). Thus, the growth status of forest vegetation can be characterized by the variation in a plant's NSC content.

Studies on NSC in tree organs have mainly focused on the differences in intra- or interspecific concentration over various spatiotemporal scales, mostly in saplings and mature trees. However, there are few studies investigating the dynamic changes in NSC content over a continuous life history at the temporal scale. Some studies have shown that deciduous plants have evident seasonal fluctuations in the content of NSC and its components, with the lowest SS content in early summer and the highest content during dormancy, which is related to the germination and apoptosis of plant leaves (Piispanen and Saranpää, 2001; Regier et al., 2010). Similarly, at each developmental stage, woody plants differ in branch and leaf physiological and morphological characteristics (Mediavilla et al., 2013), and they vary in their adaptation strategies in response to a changing environment. This in turn leads to differences in carbon fixation, metabolism, allocation, and storage *in vivo* (Grulke and Retzlaff, 2001). In general, specific leaf weight, leaf nitrogen content, water use efficiency, stomatal conductance, and carbon assimilation all increase as diameter at breast height (DBH) increases (Thomas and Winner, 2002; Song et al., 2019). For example, in *Pinus ponderosa*, the concentration of mobile carbon pools increased significantly in the upper canopy tissues as tree height increased (Sala and Hoch, 2009); in *Pinus koraiensis*, the NSC content of current-year needles increased significantly at the leaf unfolding period as age increased, and the NSC content of current-year and perennial needles generally decreased significantly at the leaf fall period as age increased (Yan et al., 2022). Plants within the same community at different life history stages are subject to similar climatic and soil conditions (Zhang et al., 2018), but seedlings and saplings have relatively weaker light resources compared to mature trees (Liu et al., 2019). Further, plants at the seedling stage are more sensitive and vulnerable to changes in the external environment. In addition, organ age is one of the driving forces behind the shift in plant ecological strategies (Liu et al., 2021). It has been shown that tree size has a stronger effect on leaf traits than do environmental factors (Liu et al., 2020). Therefore, the patterns of change in NSC and the regulatory factors still need to be studied

in depth at different life history stages (e.g., seedlings, saplings, and mature trees) (Hartmann et al., 2018; Signori-Müller et al., 2021b).

Non-structural carbohydrates (NSC) is distributed in most tree organs, such as the leaves, branches, trunks, and roots. Furze et al. (2019) showed that branches were the largest reservoir of total NSC and fluctuated seasonally, while total NSC in roots remained stable throughout the year. This is because the NSC content in branches were used to support springtime growth, and roots need relatively stable NSC content to cope with catastrophic situations. NSC is used for different purposes in different organs, and as a result, its distribution varies across organs. Similarly, species differ in their NSC distributions, which are one reason why NSC distributions are commonly associated with different biological characteristics of tree species (Hoch et al., 2003). Because most of the water absorbed by plant roots from the soil is dissipated by transpiration, and a small portion is transported to the leaves for photosynthesis, one wonders whether differences in water transport among plants lead to differences in NSC levels among species. Angiosperms can be divided into diffuse-porous species (relatively small diameter of the inner lumen of the duct) and ring-porous species (relatively large diameter of the inner lumen of the duct) (Taneda and Sperry, 2008). Studies have shown that the NSC storage of the entire tree overall is higher in ring-porous than in diffuse-porous species (Barbaroux and Bréda, 2002; Furze et al., 2019). In one example, the ST content of the whole tree was also higher in *Quercus petraea*, a ring-porous species, than in *Fagus sylvatica*, a diffuse-porous species (Barbaroux et al., 2003).

Numerous studies have confirmed that physiological ecological factors related to plant photosynthesis may affect the synthesis and distribution of NSC in plants to some extent, such as Nitrogen (N) and phosphorus (P) (Farrar and Jones, 2000; Millard et al., 2007). It has been shown that the response of TNC to soil N content varies. For example, TNC in plants increases with soil N content, but the increase is inhibited when the N content exceeds a certain threshold (Thomas et al., 2005). TNC content has a positive or insignificant response to the increase of environmental P content (Wang et al., 2014). However, few studies have explored the impact of multiple environmental factors along with plant size on NSC, simultaneously. Light intensity is another dominant factor in plant photosynthesis. Even in a single individual, different canopy positions can cause differences in plant light intensity and water availability (Yan et al., 2012). Therefore, canopy differences may lead to different NSC contents in different plants, even though several studies have found that canopy position had no significant effect on NSC (Yan et al., 2012, 2022; Li et al., 2017).

In this study, four diffuse-porous species (*Betula platyphylla*, *Betula costata*, *Tilia amurensis*, *Acer pictum* subsp. *mono*) and three ring-porous species (*Ulmus davidiana* var. *japonica*, *Ulmus laciniata*, *Fraxinus mandshurica*) in a broad-leaved Korean pine forest in Northeast China were selected as the research subjects. The NSC content was determined in leaves, new twigs, and old branches in different life history stages (seedling, sapling, and mature trees) to explore whether life history, wood type, and soil factors (soil water content, soil N and P content, soil pH) would affect the NSC content in branches (new twigs, old branches) and leaves, and to analyze the dynamics of NSC in leaves, new twigs, and old branches throughout the duration of a continuous life history. In this regard, the following hypotheses were made: (1) life history, wood type, and soil factors all affect the NSC

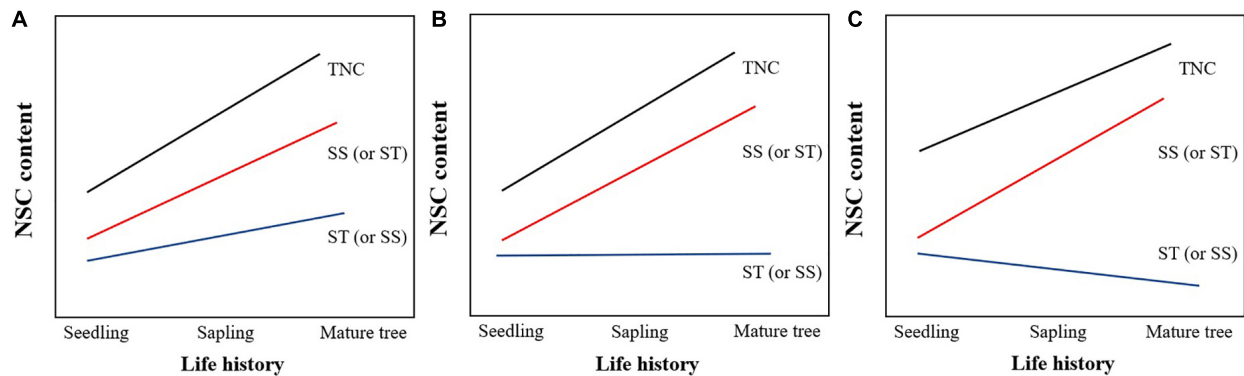


FIGURE 1

Hypothetical diagram of the changing trend of non-structural carbohydrates (NSC) content with life history. (A) SS and ST both tend to increase; (B) one of SS and ST tends to increase and the other is in a stable state; (C) one of SS and ST shows an increasing trend and the other shows a decreasing trend, but the increase will be greater than the decrease.

TABLE 1 Statistical information of diameter at breast height (DBH) (cm).

| Species | Life history | Mean \pm SD | Minimum | Maximum | CV (%) |
|---|--------------|----------------|---------|---------|--------|
| <i>Betula platyphylla</i> | Seedling | 5.1 \pm 0.3 | 4.8 | 5.5 | 4.9 |
| | Sapling | 18.8 \pm 1.4 | 15.3 | 20.0 | 7.3 |
| | Mature tree | 41.0 \pm 2.2 | 37.6 | 44.4 | 5.3 |
| <i>Betula costata</i> | Seedling | 4.9 \pm 0.9 | 3.2 | 6.3 | 18.4 |
| | Sapling | 17.3 \pm 0.6 | 16.2 | 18.1 | 3.7 |
| | Mature tree | 41.8 \pm 1.8 | 39.5 | 44.2 | 4.3 |
| <i>Tilia amurensis</i> | Seedling | 4.4 \pm 0.6 | 3.5 | 5.3 | 14.0 |
| | Sapling | 17.7 \pm 1.5 | 15.3 | 19.8 | 8.4 |
| | Mature tree | 43.0 \pm 2.8 | 39.8 | 49.5 | 6.5 |
| <i>Acer pictum</i> subsp. <i>mono</i> | Seedling | 3.8 \pm 0.6 | 2.7 | 4.8 | 16.5 |
| | Sapling | 17.2 \pm 1.8 | 15.0 | 19.1 | 10.7 |
| | Mature tree | 41.3 \pm 2.2 | 38.3 | 44.7 | 5.3 |
| <i>Ulmus davidiana</i> var. <i>japonica</i> | Seedling | 4.0 \pm 0.7 | 2.8 | 5.0 | 17.0 |
| | Sapling | 17.8 \pm 1.7 | 15.2 | 20.0 | 9.3 |
| | Mature tree | 42.2 \pm 2.0 | 38.3 | 45.0 | 4.7 |
| <i>Ulmus laciniata</i> | Seedling | 3.8 \pm 0.6 | 2.8 | 5.0 | 16.1 |
| | Sapling | 18.3 \pm 1.1 | 16.7 | 20.0 | 6.2 |
| | Mature tree | 41.3 \pm 0.9 | 39.5 | 42.5 | 2.2 |
| <i>Fraxinus mandshurica</i> | Seedling | 4.8 \pm 0.7 | 3.7 | 6.0 | 13.7 |
| | Sapling | 17.8 \pm 1.1 | 16.0 | 19.1 | 6.3 |
| | Mature tree | 42.1 \pm 1.4 | 40.0 | 44.3 | 3.4 |

content of leaves, new twigs, and old branches; (2) the total non-structural carbohydrate (TNC) content in leaves, new twigs, and old branches tends to increase with tree growth, according to one of the following three conjectures (Figure 1): SS and ST both tend to increase; one of SS and ST tends to increase and the other is in a stable state; one of SS and ST shows an increasing trend and the other shows a decreasing trend, but the increase will be greater than the decrease; (3) The NSC content in leaves, new twigs, and old branches will not differ significantly among canopy layers.

2. Materials and methods

2.1. Study region

The field survey was conducted in August 2020 in the Heilongjiang Liangshui National Nature Reserve (47°10'50"N, 128°53'20"E), located on the southern slope of the Xiao Hinggan Mountains. The reserve has an altitude range of 300–780 m and an average slope of 10°–15°, which classifies the region as having a

temperate continental monsoon climate with four distinct seasons. The winter is lengthy and cold, and the summer is short and warm, with an average annual precipitation of about 676 mm. The average annual maximum temperature is 7.5° and minimum temperature is -6.6°, with a large annual temperature difference. The reserve is the most typical and intact coniferous and broad-leaved mixed forest in the northern temperate zone of China. *P. koraiensis* is the main established species, but other broad-leaved species are also abundant.

2.2. Experimental design

Seven broad-leaved tree species, which include *B. platyphylla*, *B. albosinensis*, *T. amurensis*, *A. pictum* subsp. *mono*, *U. davidiana* var. *japonica*, *U. laciniata*, and *F. mandshurica* were selected for study and classified into two major wood types, the first four of which were diffuse-porous species and the latter three of which were ring-porous species. To reduce the effect of light conditions on tree NSC, 30 individuals of each tree species were selected under full light conditions as far away from each other as possible and classified into different life history stages, according to the difference in DBH (Thomas, 2010; Masaki et al., 2021). And each of the three life stages, 10 individuals growing on the approximate south slope and well into their life history stage were selected. The categories were seedlings (DBH = 0~3 cm), saplings (DBH = 18~23 cm), and mature trees (DBH = 35~40 cm) (Table 1). Leaves (morphologically intact and in great growth), new twigs (current year), and old branches (perennial) were sampled within each life history stage. To distinguish between new twigs and old branches, the nodal rings, which are formed by bud scale scars on the branches, were checked. Subsequently, the collected branches and leaves were marked and placed in a cryogenic foam box. After being brought back to the laboratory, they were placed in the oven at 105°C for 20 min and then dried at 65°C to a constant weight. Finally, the sample was crushed for the NSC determination.

Seedlings and saplings were measured twice. Mature trees were divided into three canopy layers—upper, middle, and lower, and measurements on each canopy layer were also repeated twice. In order to avoid the influence of spatial autocorrelation among the sample trees on the experimental results, the distance between any two sample trees had to be greater than 5 m.

2.3. NSC measurements

In this paper, NSC is defined as the free, low molecular weight sugars SS and ST, the sum of which is denoted as TNC (Liu et al., 2019; Signori-Müller et al., 2021a). NSC incorporates TNC, SS, and ST. These contents were measured using an improved phenol-sulfuric acid method (Buisse and Merckx, 1993), and their concentrations are expressed here as percentage dry weight (%DM).

First, 40 mg of the ground dry sample was inserted into a 10 mL centrifuge tube and soaked overnight in 10 mL of 80% ethanol. The soaked sample was centrifuged twice at 4,000 rpm in a DT5-4B low-speed benchtop centrifuge (Beijing Era Beili Centrifuge Co., Ltd., Beijing, China), and the supernatant was poured into a volumetric flask for constant volume, which was used to determine the SS.

TABLE 2 The influence of wood type, life history [diameter at breast height (DBH)], and environmental factors (soil water content, soil nitrogen content, soil phosphorus content, soil pH) on non-structural carbohydrates (NSC) content.

| Organ | NSC components | DBH (cm) | Wood type | Soil water content (g/g) | Soil nitrogen content (mg/g) | Soil phosphorus content (mg/g) | Soil pH | Intercept |
|------------|----------------|----------|-----------|--------------------------|------------------------------|--------------------------------|----------|-----------|
| Leaf | SS | 0.70*** | -0.37* | 0.51** | -0.50** | 0.37* | 0.57*** | 5.08*** |
| | ST | -0.01 | -0.19** | 0.02 | -0.11 | -0.04 | -0.13 | 4.75*** |
| New twig | TNC | 0.69*** | -0.56** | 0.53* | -0.61** | 0.34 | -0.70*** | 9.83*** |
| | SS | 1.00*** | 0.48** | 0.26 | -0.49* | 0.30 | 0.83 | 6.34*** |
| | ST | 0.26 | 0.48** | 0.05 | -0.36* | 0.32* | -0.10 | 5.19*** |
| Old branch | TNC | 1.26*** | 0.96*** | 0.30 | -0.85** | 0.61* | -0.93*** | 11.53*** |
| | SS | 1.01*** | 0.36** | 0.06 | -0.12 | 0.11 | -0.79*** | 6.38*** |
| | ST | 0.33*** | 0.25* | -0.01 | -0.30* | 0.18 | -0.32** | 4.46*** |
| | TNC | 1.35*** | 0.61** | 0.06 | -0.41 | 0.29 | -1.12*** | 10.84*** |

p* < 0.05, *p* < 0.01, ****p* < 0.001.

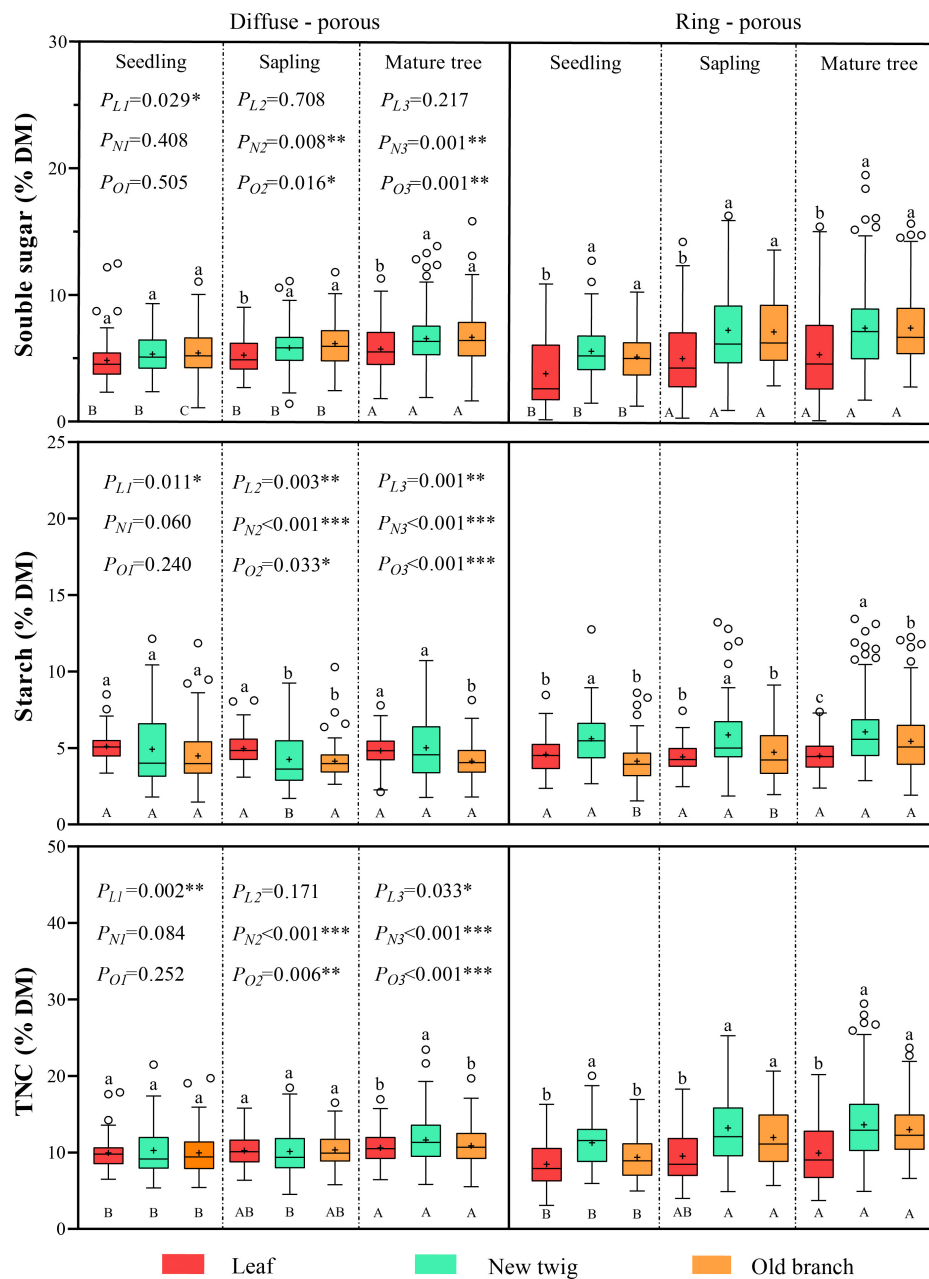


FIGURE 2 Non-structural carbohydrates (NSC) content in different organs of diffuse-porous and ring-porous species at each life history stage. Capital and lowercase letters indicate the differences between life history stages and organs under same wood types, respectively; *P*-values represent the comparison of leaves, new twigs and old branches in two species of wood types at the same life history stage, in which L, N, and O represent leaves, new twigs and old branches respectively; 1, 2, and 3 represent seedlings, sapling, and mature trees, respectively. Dots indicate outliers and “+” indicates mean values. **p* < 0.05, ***p* < 0.01, ****p* < 0.001.

Then, the residue remaining after ethanol extraction was dried. Next 10 mL of deionized water was added, and the solution was mixed well. After gelatinization in a boiling water bath, the solution was cooled to below 60°C. One mL of 0.5% α-amylase solution was added, and the water bath was kept at 60°C for 1 h. The enzymatic solution was centrifuged at 2,000 rpm and filtered to maintain a constant volume with the deionized water for the determination of the ST content. Finally, SS and ST were determined. One mL of the sugar solution was taken into the glass tube, and then one mL of 28% phenol solution (dissolved in 80% ethanol) was added. Next,

concentrated sulfuric acid was added immediately, and the glass tube was shaken for 1 min. The absorption value was measured by a spectrophotometer (722 N, Shanghai Yidi Analytical Instrument Co., Ltd., Shanghai, China) at 490 nm after 15 min.

2.4. Soil water and nutrient availability

Around the sample tree, a soil corer was used to collect about 10 cm of soil at the base of the trunk at three sampling

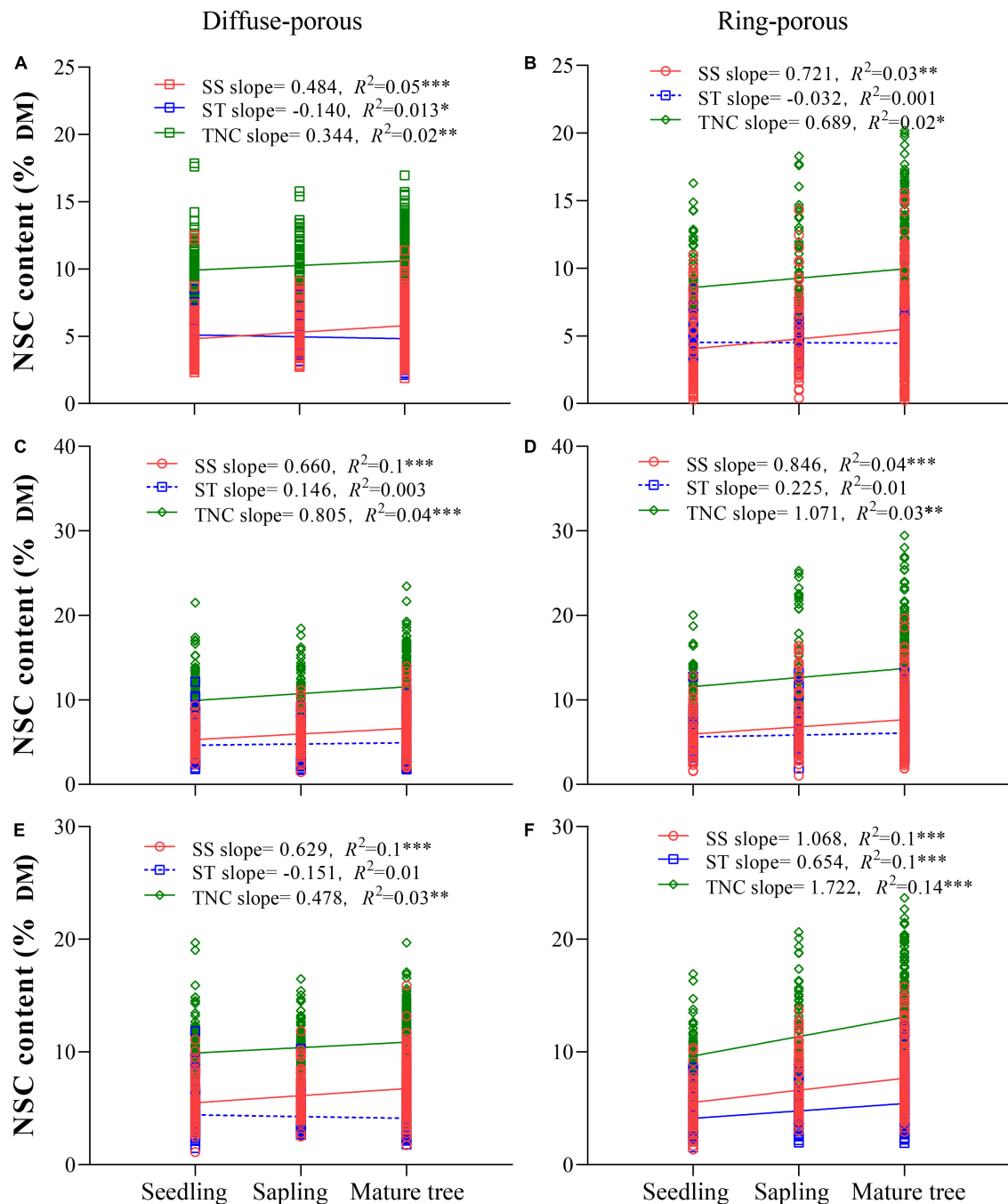


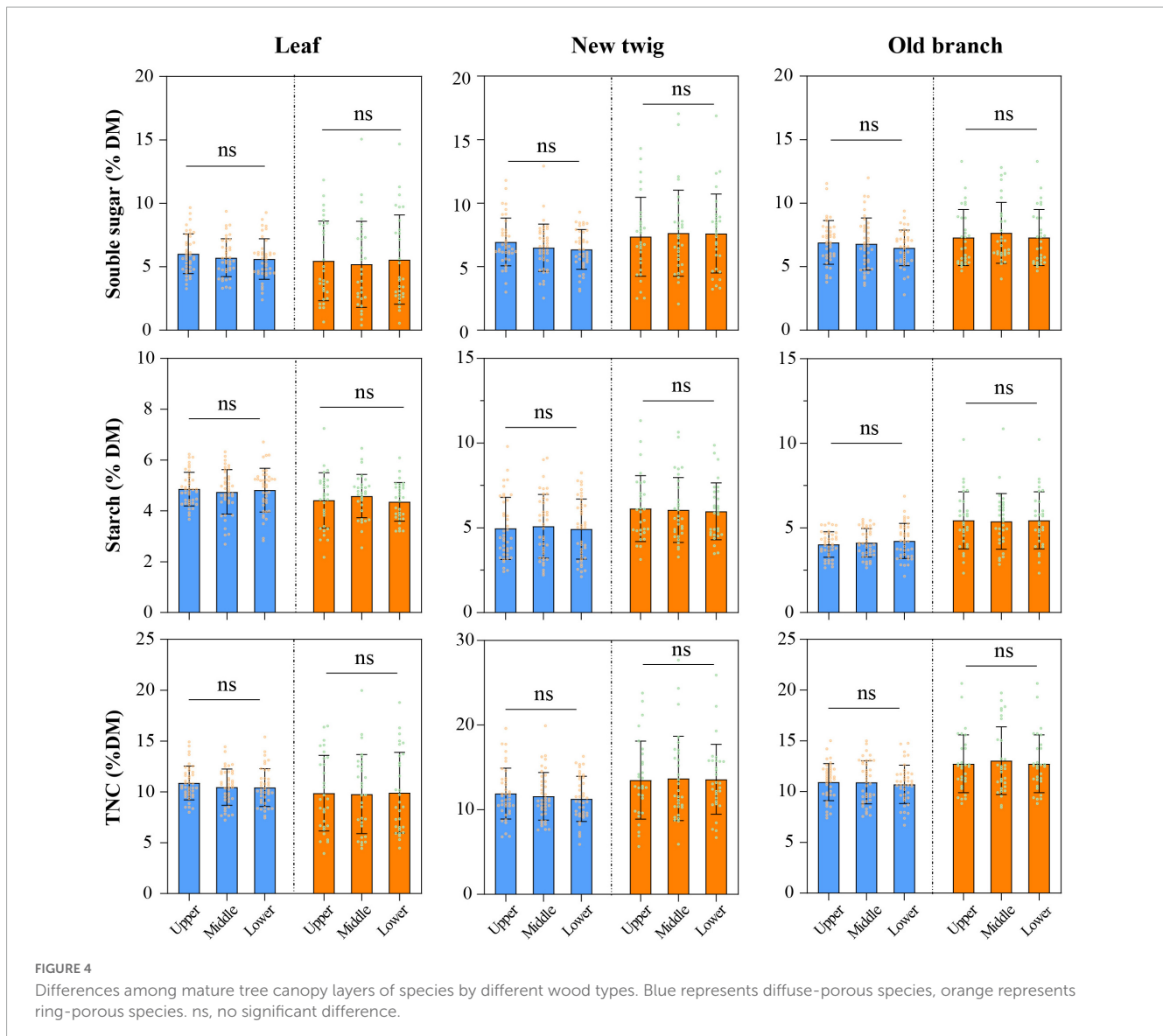
FIGURE 3

Variations of non-structural carbohydrates (NSC) components with life history in different organs of diffuse-porous and ring-porous species. (A,B) Shows leaf composition; (C,D) shows new twig composition; (E,F) shows old branch composition. The dashed lines indicate non-significant variation. * $p < 0.05$, ** $p < 0.01$, *** $p < 0.001$.

points (the angle between any two sampling points was about 120°). The three soil samples were mixed evenly after removing obvious impurities, and then the soil water content (g/g) was determined by the oven-drying method (Liu et al., 2020). Soil total N content (mg/g) and total P content (mg/g) were measured using the AQ 400 automatic intermittent chemical analyzer (SEAL Analytical, Mequon, WI, USA) (Jing et al., 2017). Soil pH was measured by pH meter (HANNA pH211, Italy).

2.5. Data analysis

In this study, data was statistically analyzed in SPSS 22.0 and R-4.1.0 (R Core Team, 2021) and plotted in GraphPad Prism 8.0. Generalized linear models of DBH, wood type and environmental factors (soil water content, soil N and P content, soil pH) with NSC components were constructed using the “glm” function in R. One-way analysis of variance (ANOVA) and the least significant difference (LSD) was used to compare the differences in organ



and life history of tree species under different wood types. The same method was used to test for differences between the different canopy layers of mature tree's branches and leaves. To compare organs at different stages of life history in the two wood types, an independent sample *T*-test was performed. A linear regression was also run with NSC components against life history stages. All tests were performed at a significance level of $\alpha = 0.05$.

3. Result

3.1. Factors influencing NSC concentration

Life history (DBH) had a significant effect on SS and TNC in leaves, new twigs, and old branches ($p < 0.05$), but only on ST in old branches ($p < 0.05$). The effect of wood type on TNC was significant in leaves, new twigs, and old branches ($p < 0.05$) (Table 2). The effects of environmental factors on NSC varied by organ (Table 2):

soil water content only had a significant effect on SS and TNC content in leaves; soil N content had significant effects on TNC of leaves and new twigs, soil P content only had significant effects on TNC of new twigs, and soil pH had significant effects on TNC of leaves, new twigs, and old branches. Compared with soil P content, the effect of soil N content on leaves and branches (new twigs and old branches) was more significant and tended to be negatively correlated (Table 2).

3.2. Variations in NSC concentration with life history and organ

For the seven tree species, there was an overall increasing trend in the NSC content of leaves, new twigs, and old branches as the plant grew. For the diffuse-porous species, the SS content of leaves, new twigs, and old branches was significantly higher in the mature tree stage than in the other two life history stages, and the TNC content was significantly higher than in the seedling stage, while

the ST content was stable in all life history stages of leaves and old branches, without significant differences (Figure 2). For the ring-porous species, the SS and TNC contents of leaves, new twigs, and old branches were significantly lower in the seedling stage than in the other two life history stages, while ST contents in leaves and new twigs did not differ significantly among the life history stages (Figure 2).

For diffuse-porous species, at the sapling stage, SS content was significantly lower in leaves than in branches, while ST content was significantly higher. At the mature tree stage, SS content was also significantly lower in leaves than in branches, while ST content was significantly lower in old branches than in leaves and new twigs, and TNC content was significantly higher in new twigs than in leaves and old branches (Figure 2). However, there was no significant difference in NSC content between leaves and branches at the seedling stage, and the fluctuation was slight among the three organs (Supplementary Table 1). For the ring-porous species, the differences in NSC content in leaves and branches were similar among the three life history stages, with the overall performance being higher in SS and TNC content for branches than for leaves, and significantly higher in ST content for new twigs than for leaves and old branches (Figure 2).

Diffuse-porous species had a higher NSC content in their leaves and a lower content in their new twigs than ring-porous species. The NSC content of the old branches was higher than that of the ring-porous species at the seedling stage only. In contrast, NSC content was lower than that of the ring-porous species at the other two life history stages (Figure 2). Comparing the two wood types, leaves were the only organ in which NSC content differed significantly at the seedling stage, but at the sapling and mature tree stages, the ST content in leaves differed significantly, and the NSC content in branches showed significant differences too (Figure 2).

Across both wood types, SS and TNC contents in leaves and branches increased significantly as life history stages progressed (Figure 3). For the diffuse-porous species, ST content decreased significantly only in leaves at a later life history stage (Figure 3A), while ST content in branches did not vary significantly with life history (Figures 3C, E). For the ring-porous species, ST content varied significantly only in old branches, and ST content in leaves and new twigs did not vary significantly with life history (Figures 3B, D, F).

3.3. Variation in NSC concentration with canopy

Among species of the same wood type, there was no significant difference in NSC content between different canopy layers in leaves and branches of the mature trees (Figure 4). The CV of NSC content in all three canopy layers of diffuse-porous species were: leaf TNC, 0.152~0.178; new twig TNC, 0.236~0.253; old branch TNC, 0.166~0.194 (Supplementary Table 3). The CV of NSC content in leaves and branches of ring-porous species, in all three canopy layers, were: leaf TNC, 0.375~0.425; new twig TNC, 0.332~0.381; old branch TNC, 0.262~0.299 (Supplementary Table 3). The CV of NSC content was similar among the three canopy layers of all species, regardless of wood type. The CV of NSC

content in the canopy layers were smaller in the diffuse-porous than in the ring-porous species (Supplementary Table 3).

4. Discussion

4.1. Factors influencing NSC concentration

The functional traits of plants vary throughout the life cycle, from the time it is a seed, to when it becomes a full-grown individual, and so do the trade-offs between different stages of branches and leaves (Wright et al., 2010; Liu et al., 2019, 2021). Compared to mature trees, seedlings experience poor light conditions, have large, thin leaves (Augspurger and Bartlett, 2003; He and Yan, 2018), and have a relatively weak ability to intercept light and synthesize carbon (Niklas et al., 2007). Thus seedlings tend to compensate for the harsh environment with a relatively high specific leaf area (He and Yan, 2018). As trees grow, the plant exerts more energy into the branches to enhance their functions of mechanical support and water supply capacity so as to accommodate the increased leaf area and transpiration rate (Niinemets et al., 2004; Fan et al., 2017). Seedlings experience a stronger trade-off between growth rate and mortality compared to mature trees (Wright et al., 2010), and thus at the seedling stage, plants are resource acquisition-oriented. This means that seedlings prioritize nutrients for growth and development. In contrast, mature trees are relatively conservative in their resource use, and they only use increased resources when resisting adverse environments (He and Yan, 2018). From this, it has been inferred that carbohydrates, as essential energy substances for the growth and development processes of plants, are equally affected by the stages of life and the environmental factors in their distribution. This inference was verified in this study—life history has a significant effect on NSC (Table 2).

It was confirmed that the diffuse- and ring-porous species differ in their TNC content (Barbaroux and Bréda, 2002; Barbaroux et al., 2003). Our results also showed that wood type had a significant effect on TNC content in leaves and branches ($p < 0.05$) (Table 2), which was consistent with previous studies. The synthesis of TNC is inseparable from the operation of the hydraulic system of various plant organs, and the water conductivity of the hydraulic system is also different due to the differences in xylem vessels in the two wood types (Taneda and Sperry, 2008; McCulloh et al., 2010). This may be one of the reasons for the significant effect of materiality on NSC.

Soil water content only had a significant effect on leaf TNC content (Table 2), which opposed Hypothesis 1. However, it is consistent with the findings of Lintunen et al. (2016). Soil N content had significant effects on the TNC of leaves and branches, and it was negatively correlated with NSC (Table 2). The N element is related to the synthesis of plant photosynthetic pigments, which in a certain range can promote the photosynthesis of plants (Nakaji et al., 2001). That a high N content inhibits photosynthetic pigment synthesis may be the reason for the negative correlation between soil N content and NSC. On the other hand, it is possible that plants need to absorb large amounts of N from the soil during their growing season, and this leads to higher carbon input for their

morphogenesis (Eissenstat and Yanai, 1997; Wang et al., 2017). Soil pH affects the photosynthetic and osmoregulatory systems of plants (Yang et al., 2022), so it is significantly correlated with leaf and branch NSC components (Table 2).

4.2. Variation of NSC concentration with life history and organ

The differences in NSC across different life histories and organs characterize the differences in physiological regulation and adaptive strategies to the external environment (Augsburger and Bartlett, 2003). Overall, the NSC content in leaves and branches increased with maturing life stages, which is consistent with hypothesis 2. Sala and Hoch (2009) and Zhang et al. (2018) also showed that TNC storage in trees increases from the seedling to the mature tree stage. During these three growth stages, the photosynthetic capacity and water use efficiency of the plant gradually increases (Cavender-Bares and Bazzaz, 2000; Thomas, 2010), and hence the TNC synthesis content also showed an increasing trend. With the growth of trees, the tension of the xylem increases, and cavitation and embolism are more likely to occur (Sala and Hoch, 2009). The repair process may require a large amount of SS. The ST content of mature trees is higher than in saplings and seedlings, which is related to the survival strategy where big trees tend to reserve more energy in the event they must resist various environmental stresses. The results of this study further showed that the SS and TNC contents in leaves and branches of species of both wood types increased significantly with life history, and the ST content did not change significantly throughout the life history stages in either leaves or branches (Figure 3). This result confirmed conjecture 2 in hypothesis 2, that the variation in TNC was mainly caused by SS. This is consistent with the results of Zhang et al. (2013), where the changes in TNC were caused by NSC components in branches. Zhang et al. (2013) and Yan et al. (2022) also found that the increase of TNC in needles was more closely related to the increase of SS during the leaf unfolding period for *P. koraiensis*. This may be related to the season of the plant. Plants consume a large amount of ST in winter in response to cold stress and germination in spring (Piispanen and Saranpää, 2001; Lintunen et al., 2016), so a part of SS produced in the growing season was converted into ST to make up for the consumption, which may result in the change of TNC in summer more closely related to SS. However, Hoch et al. (2003) and Schadel et al. (2009) showed that the changes in branch TNC were more closely related to ST. It may be due to differences in sampling seasons and tree species.

By comparing the NSC contents in leaves, new twigs, and old branches of species of the two wood types in each life history stage, it was found that the SS content was higher in branches than in leaves, and the ST content was higher in leaves than in branches (Figure 2). However, TNC content did not change consistently in the life stages of the diffuse-porous species, and for the ring-porous species, the contents were higher in the branches than in the leaves (Figure 2). Furze et al. (2019) suggested that high SS concentrations in branches helps trees resist low temperatures in the canopy. The carbon limitation hypothesis indicates that the stress of low temperatures weakens the photosynthetic capacity of

plants and reduces their carbon assimilation capacity, which results in insufficient carbon supply, reduced NSC content, and reduced growth rate (Wardle, 1993; Wang and Wang, 2019). Therefore, increasing SS content in branches may be a conservative survival strategy for plants that need to resist external low-temperature environments. Ring-porous species are not only less resistant to low temperatures and drought (Yuan et al., 2021), but they also tend to have a higher risk of embolism and cavitation (Hack et al., 2006; Taneda and Sperry, 2008), which may result in higher SS content than in diffuse-porous species (Figure 2). Signori-Müller et al. (2021b) studied two types of plants with different growth rates in the Amazon forest. The results showed that the NSC content was higher in branches than in leaves for fast-growing species under sufficient light conditions, while the opposite was true for slow-growing species. Thus, the difference in NSC content in leaves and branches of woody plants is the embodiment of different survival strategies. Further discussion on the dynamic changes of NSC content in new twigs and old branches showed that the NSC content was higher in new twigs than in old branches, at all three life history stages (Figure 2). The results were similar to those of Zhang et al. (2013), regarding the NSC of new twigs and old branches of 12 tree species in temperate zones. According to the principle of near distribution of carbon sources, branches are the closest organ to the carbon source of leaves, and thus they have priority for claiming photosynthetic products. Further, because of their proximity to buds, old branches may be the most vital carbon source for tree germination and growth in the spring (Wong et al., 2003; Spann et al., 2008). The new twigs in the current growing season are old relative to the sprouting branches of the coming year, thus it is inferred that new twigs store more NSC than old branches during the growing season. This is both to maintain the growth and development of the current year, and to provide a source of carbon for the sprouting of leaves and branches in the coming year.

4.3. Variation of NSC concentration with canopy

To test hypothesis 3, this study analyzed the NSC content of mature tree canopies, and the results were consistent with our hypothesis (Figure 4). Zhang et al. (2015) studied the NSC concentration in temperate canopy branches and leaves and found that the canopy had no significant effect on the NSC concentration in leaves and twigs, but had a significant effect on coarse branches, which was relatively consistent with the results of this study. In the study on the effect of the canopy on the NSC of fast-growing and slow-growing trees in the Amazon forest, no significant difference was found in NSC concentration between different canopy branches and leaves (Signori-Müller et al., 2021b). The result suggests that variability in plant NSC may be more so determined by genetic characteristics than by variations in the vertical gradient of light environmental factors. However, Woodruff and Meinzer (2011) showed that the NSC content of branches above the canopy differed significantly among Douglas-fir (*Pseudotsuga menziesii* Mirb. Franco) individuals of different tree heights. Heights can indicate life history stages to a certain extent (Liu et al., 2020; Masaki et al., 2021), so the source of this

difference may not only be attributed to changes in light gradients. Studies on evergreen conifer species have shown that the canopy layer influences needle NSC concentrations (Gholz and Cropper, 1991; Niinemets, 1997), which may be related to the selection of tree species types, their different habitats and phenological periods.

5. Conclusion

According to the dynamic NSC contents in leaves and branches of seven broad-leaved tree species in different life history stages, it was found that the NSC content of woody plants was not only affected by external environmental factors (soil N and P content, soil pH), but also correlated with their genetic characteristics (life history, wood type, etc.). As the trees aged and grew, the NSC content in leaves and branches also increased, while the ST content was relatively stable throughout the life history stages. Therefore, the increase of NSC content in plants during the growing season was likely caused by SS. The NSC content differed between the species of different wood types. Overall, the NSC content was higher in the leaves of the diffuse-porous than of the ring-porous species, while the NSC content was lower in the branches. However, this study found no significant difference in NSC content between the canopy layers of mature trees. Although the light environment was associated with NSC content in plants, the dynamic changes of NSC throughout the continuous life history of these seven broad-leaved species were not driven mainly by light factors, and the content fluctuations may be more closely related to their genetic characteristics.

Data availability statement

The raw data supporting the conclusions of this article will be made available by the authors, without undue reservation.

Author contributions

ZL and KW planned and designed the research. KW performed experiments, analyzed the data, and wrote the manuscript with substantial contributions from ZL and GJ. ZL provided helpful comments in the draft. All authors contributed to the article and approved the submitted version.

References

- Augspurger, C. K., and Bartlett, E. A. (2003). Differences in leaf phenology between juvenile and adult trees in a temperate deciduous forest. *Tree Physiol.* 23, 517–525. doi: 10.1093/treephys/23.8.517
- Barbaroux, C., and Bréda, N. (2002). Contrasting distribution and seasonal dynamics of carbohydrate reserves in stem wood of adult ring-porous sessile oak and diffuse-porous beech trees. *Tree Physiol.* 22, 1201–1210. doi: 10.1093/treephys/22.17.1201
- Barbaroux, C., Bréda, N., and Dufrière, E. (2003). Distribution of above-ground and below-ground carbohydrate reserves in adult trees of two contrasting broad-leaved species (*Quercus petraea* and *Fagus sylvatica*). *New Phytol.* 157, 605–615. doi: 10.1046/j.1469-8137.2003.00681.x
- Beer, C., Reichstein, M., Tomelleri, E., Ciais, P., Jung, M., Carvalhais, N., et al. (2010). Terrestrial gross carbon dioxide uptake: Global distribution and covariation with climate. *Science* 329, 834–838.
- Bonan, G. B. (2008). Forests and climate change: Forcings, feedbacks, and the climate benefits of forests. *Science* 320, 1444–1449. doi: 10.1126/science.1155121
- Buyse, J., and Merckx, R. (1993). An improved colorimetric method to quantify sugar content of plant tissue. *J. Exp. Bot.* 44, 1627–1629.
- Cavender-Bares, J., and Bazzaz, F. A. (2000). Changes in drought response strategies with ontogeny in *Quercus mibra*: Implications for scaling from seedlings to mature trees. *Oecologia* 124, 8–18. doi: 10.1007/PL00008865

Funding

This work was supported by the National Key R&D Program of China (2022YFD2201100), the National Natural Science Foundation of China (31971636), and the Fundamental Research Funds for the Central Universities (2572022DS13).

Acknowledgments

We thank Dr. Annalise Elliot at the University of Kansas for her assistance with English language and grammatical editing of the manuscript. We also thank the responsible editor and two reviewers for their constructive and helpful comments that helped to improve the manuscript.

Conflict of interest

The authors declare that the research was conducted in the absence of any commercial or financial relationships that could be construed as a potential conflict of interest.

Publisher's note

All claims expressed in this article are solely those of the authors and do not necessarily represent those of their affiliated organizations, or those of the publisher, the editors and the reviewers. Any product that may be evaluated in this article, or claim that may be made by its manufacturer, is not guaranteed or endorsed by the publisher.

Supplementary material

The Supplementary Material for this article can be found online at: <https://www.frontiersin.org/articles/10.3389/ffgc.2023.1130604/full#supplementary-material>

- Eissenstat, D. M., and Yanai, R. D. (1997). The ecology of root lifespan. *Adv. Ecol. Res.* 27, 1–60.
- Fan, Z. X., Sterck, F., Zhang, S. B., Fu, P. L., and Hao, G. Y. (2017). Tradeoff between stem hydraulic efficiency and mechanical strength affects leaf-stem allometry in 28 *Ficus* tree species. *Front. Plant Sci.* 8:1619. doi: 10.3389/fpls.2017.01619
- Farrar, J. F., and Jones, D. L. (2000). The control of carbon acquisition by roots. *New Phytol.* 147, 43–53.
- Furze, M. E., Huggett, B. A., Aubrecht, D. M., Stolz, C. D., Carbone, M. S., and Richardson, A. D. (2019). Whole-tree nonstructural carbohydrate storage and seasonal dynamics in five temperate species. *New Phytol.* 221, 1466–1477. doi: 10.1111/nph.15462
- Furze, M. E., Wainwright, D. K., Huggett, B. A., Knipfer, T., McElrone, A. J., and Brodersen, C. R. (2021). Ecologically driven selection of nonstructural carbohydrate storage in oak trees. *New Phytol.* 232, 567–578. doi: 10.1111/nph.17605
- Gholz, H. L., and Cropper, W. P. Jr. (1991). Carbohydrate dynamics in mature *Pinus elliottii* var. *elliottii* trees. *Can. J. For. Res.* 21, 1742–1747.
- Grulke, N. E., and Retzlaff, W. A. (2001). Changes in physiological attributes of ponderosa pine from seedling to mature tree. *Tree Physiol.* 21, 275–286. doi: 10.1093/treephys/21.5.275
- Hack, U. G., Sperry, J. S., Wheeler, J. K., and Castro, L. (2006). Scaling of angiosperm xylem structure with safety and efficiency. *Tree Physiol.* 26, 689–701.
- Hartmann, H., Adams, H. D., Hammond, W. M., Hoch, G., Landhäusser, S. M., Wiley, E., et al. (2018). Identifying differences in carbohydrate dynamics of seedlings and mature trees to improve carbon allocation in models for trees and forests. *Environ. Exp. Bot.* 152, 7–18.
- He, D., and Yan, E. R. (2018). Size-dependent variations in individual traits and trait scaling relationships within a shade-tolerant evergreen tree species. *Am. J. Bot.* 105, 1165–1174. doi: 10.1002/ajb2.1132
- Hoch, G., Marianne, P., and Christian, K. (2002). Altitudinal increase of mobile carbon pools in *Pinus cembra* suggests sink limitation of growth at the Swiss treeline. *Oikos* 98, 361–374.
- Hoch, G., Richter, A., and Körner, C. (2003). Non-structural carbon compounds in temperate forest trees. *Plant Cell Environ.* 26, 1067–1081.
- Jing, H., Zhou, H. X., Wang, G. L., Xue, S., Liu, G. B., and Duan, M. C. (2017). Nitrogen addition changes the stoichiometry and growth rate of different organs in *Pinus tabulaeformis* seedlings. *Front. Plant Sci.* 8:1922. doi: 10.3389/fpls.2017.01922
- Li, M. C., Kong, G. Q., and Zhu, J. J. (2017). Vertical and leaf-age-related variations of nonstructural carbohydrates in two alpine timberline species, southeastern Tibetan Plateau. *J. For. Res.* 14, 229–235.
- Lintunen, A., Paljakka, T., Jyske, T., Peltoniemi, M., Sterck, F., von Arx, G., et al. (2016). Osmolality and non-structural carbohydrate composition in the secondary phloem of trees across a latitudinal gradient in Europe. *Front. Plant Sci.* 7:726. doi: 10.3389/fpls.2016.00726
- Liu, C., Jin, G. Z., and Liu, Z. Z. (2021). Importance of organ age in driving intraspecific trait variation and coordination for three evergreen coniferous species. *Ecol. Indic.* 121:107099.
- Liu, H. Y., Shangguan, H. L., Zhou, M., Airebule, P., Zhao, P. W., He, W. Q., et al. (2019). Differentiated responses of nonstructural carbohydrate allocation to climatic dryness and drought events in the Inner Asian arid timberline. *Agric. For. Meteorol.* 271, 355–361.
- Liu, Z. L., Hikosaka, K., Li, F. R., and Jin, G. Z. (2020). Variations in leaf economics spectrum traits for an evergreen coniferous species: Tree size dominates over environment factors. *Funct. Ecol.* 34, 458–467.
- Liu, Z. L., Jiang, F., Li, F. R., and Jin, G. Z. (2019). Coordination of intra and inter-species leaf traits according to leaf phenology and plant age for three temperate broadleaf species with different shade tolerances. *For. Ecol. Manag.* 434, 63–75.
- Masaki, T., Kitagawa, R., Nakashizuka, T., Shibata, M., and Tanaka, H. (2021). Interspecific variation in mortality and growth and changes in their relationship with size class in an old-growth temperate forest. *Ecol. Evol.* 11, 8869–8881. doi: 10.1002/ece3.7720
- McCulloh, K., Sperry, J. S., Lachenbruch, B., Meinzer, F. C., Reich, P. B., and Voelker, S. (2010). Moving water well: Comparing hydraulic efficiency in twigs and trunks of coniferous, ring-porous, and diffuse-porous saplings from temperate and tropical forests. *New Phytol.* 186, 439–450. doi: 10.1111/j.1469-8137.2010.03181.x
- Mediavilla, S., Herranz, M., Gonzalez-Zurdo, P., and Escudero, A. (2013). Ontogenetic transition in leaf traits: A new cost associated with the increase in leaf longevity. *J. Plant Ecol.* 7, 567–575.
- Millard, P., Sommerkorn, M., and Grete, G.-A. (2007). Environmental change and carbon limitation in trees: A biochemical, ecophysiological and ecosystem appraisal. *New Phytol.* 175, 11–28. doi: 10.1111/j.1469-8137.2007.02079.x
- Myers, J. A., and Kitajima, K. (2007). Carbohydrate storage enhances seedling shade and stress tolerance in a neotropical forest. *J. Ecol.* 95, 383–395.
- Nakaji, T., Fukami, M., Dokiya, Y., and Izuta, T. (2001). Effects of high nitrogen load on growth, photosynthesis and nutrient status of *Cryptomeria japonica* and *Pinus densiflora* seedlings. *Trees* 15, 453–461.
- Niinemets, Ü. (1997). Distribution patterns of foliar carbon and nitrogen as affected by tree dimensions and relative light conditions in the canopy of *Picea abies*. *Trees* 11, 144–154. doi: 10.1007/PL00009663
- Niinemets, Ü., Sparrow, A., and Cescatti, A. (2004). Light capture efficiency decreases with increasing tree age and size in the southern hemisphere gymnosperm *Agathis australis*. *Trees* 19, 177–190. doi: 10.1007/s00468-004-0379-y
- Niklas, K. J., Cobb, E. D., Niinemets, Ü., Reich, P. B., Sellin, A., Shipley, B., et al. (2007). “Diminishing returns” in the scaling of functional leaf traits across and within species groups. *Proc. Natl. Acad. Sci. U.S.A.* 104, 8891–8896. doi: 10.1073/pnas.0701135104
- Piispänen, R., and Saranpää, P. (2001). Variation of non-structural carbohydrates in silver birch (*Betula pendula* Roth) wood. *Trees* 15, 444–451. doi: 10.1007/s004680100125
- Piper, F. I., and Paula, S. (2020). The role of nonstructural carbohydrates storage in forest resilience under climate change. *Curr. For. Rep.* 6, 1–13.
- R Core Team (2021). *R: A language and environment for statistical computing*. Vienna: R Foundation for Statistical Computing.
- Regier, N., Streb, S., Zeeman, S. C., and Frey, B. (2010). Seasonal changes in starch and sugar content of poplar (*Populus deltoides* x *nigra* cv. Dorskamp) and the impact of stem girdling on carbohydrate allocation to roots. *Tree Physiol.* 30, 979–987.
- Sala, A., and Hoch, G. (2009). Height-related growth declines in ponderosa pine are not due to carbon limitation. *Plant Cell Environ.* 32, 22–30. doi: 10.1111/j.1365-3040.2008.01896.x
- Schadel, C., Blochl, A., Richter, A., and Hoch, G. (2009). Short-term dynamics of nonstructural carbohydrates and hemicelluloses in young branches of temperate forest trees during bud break. *Tree Physiol.* 29, 901–911. doi: 10.1093/treephys/tp034
- Signori-Müller, C., Oliveira, R. S., Barros, F., Tavares, J. V., and Galbraith, D. (2021a). Non-structural carbohydrates mediate seasonal water stress across Amazon forests. *Nat. Commun.* 12:2310. doi: 10.1038/s41467-021-22378-8
- Signori-Müller, C., Oliveira, R. S., Valentim Tavares, J., Carvalho Diniz, F., Gilpin, M., Barros, V. F., et al. (2021b). Variation of non-structural carbohydrates across the fast-slow continuum in Amazon forest canopy trees. *Funct. Ecol.* 36, 341–355.
- Song, Z. P., Liu, Y. H., Su, H. X., and Hou, J. H. (2019). N-P utilization of *Acer mono* leaves at different life history stages across altitudinal gradients. *Ecol. Evol.* 10, 851–862. doi: 10.1002/ece3.5945
- Spann, T. M., Beede, R. H., and DeJong, T. M. (2008). Seasonal carbohydrate storage and mobilization in bearing and non-bearing pistachio (*Pistacia vera*) trees. *Tree Physiol.* 28, 207–213.
- Taneda, H., and Sperry, J. S. (2008). A case-study of water transport in co-occurring ring- versus diffuse-porous trees: Contrasts in water-status, conducting capacity, cavitation and vessel refilling. *Tree Physiol.* 28, 1641–1651. doi: 10.1093/treephys/28.11.1641
- Thomas, S. C. (2010). Photosynthetic capacity peaks at intermediate size in temperate deciduous trees. *Tree Physiol.* 30, 555–573. doi: 10.1093/treephys/tpq005
- Thomas, S. C., and Winner, W. E. (2002). Photosynthetic differences between saplings and adult trees: An integration of field results by meta-analysis. *Tree Physiol.* 22, 117–127. doi: 10.1093/treephys/22.2-3.117
- Thomas, V. F. D., Braun, S., and Flückiger, W. (2005). Effects of simultaneous ozone exposure and nitrogen loads on carbohydrate concentrations, biomass, and growth of young spruce trees (*Picea abies*). *Environ. Pollut.* 137, 507–516. doi: 10.1016/j.envpol.2005.02.002
- Wang, K., Lei, H., Xia, Y., and Yu, G. Q. (2017). Responses of non-structural carbohydrates of poplar seedlings to increased precipitation and nitrogen addition. *Chin. J. Appl. Ecol.* 28, 399–407. doi: 10.13287/j.1001-9332.201702.012
- Wang, X., Luo, W. T., Yu, Q., Yan, C. F., Xu, Z. W., Li, M. H., et al. (2014). Effects of nutrient addition on nitrogen, phosphorus and non-structural carbohydrates concentrations in leaves of dominant plant species in a semiarid steppe. *Chin. J. Ecol.* 33, 1795–1802.
- Wang, Z. G., and Wang, C. K. (2019). Mechanisms of carbon source-sink limitations to tree growth. *Chin. J. Plant Ecol.* 43, 1036–1047. doi: 10.17521/cjpe.2019.0104
- Wardle, P. (1993). “Causes of alpine timberline: A review of the hypotheses,” in *Forest development in cold climates*, eds J. N. Alden, J. L. Mastrandano, and S. Ødum (Berlin: Springer), 89–103. doi: 10.1007/s004420050540
- Wong, B. L., Baggett, K. L., and Rye, A. H. (2003). Seasonal patterns of reserve and soluble carbohydrates in mature sugar maple (*Acer saccharum*). *Can. J. Bot.* 81, 780–788. doi: 10.1139/b03-079
- Woodruff, D. R., and Meinzer, F. C. (2011). Water stress, shoot growth and storage of non-structural carbohydrates along a tree height gradient in a tall conifer. *Plant Cell Environ.* 34, 1920–1930. doi: 10.1111/j.1365-3040.2011.02388.x
- Wright, S. J., Kitajima, K., Kraft, N. J. B., Reich, P. B., Wright, I. J., Bunker, D. E., et al. (2010). Functional traits and the growth-mortality trade-off in tropical trees. *Ecology* 91, 3664–3674.
- Yadav, V. S., Yadav, S. S., Gupta, S. R., Meena, R. S., Lal, R., Sheoran, N. S., et al. (2022). Carbon sequestration potential and CO₂ fluxes in a tropical forest ecosystem. *Ecol. Eng.* 176:106541. doi: 10.1016/j.ecoleng.2022.106541

- Yan, C. F., Han, S. J., Zhou, Y. M., Wang, C. G., Dai, G. H., Xiao, W. F., et al. (2012). Needle-age related variability in nitrogen, mobile carbohydrates, and $\delta^{13}\text{C}$ within *Pinus koraiensis* tree crowns. *PLoS One* 7:e35076. doi: 10.1371/journal.pone.0035076
- Yan, L. N., Zhang, Z. Y., Jin, G. Z., and Liu, Z. L. (2022). Variations of leaf nonstructural carbohydrates in an evergreen coniferous species: Needle age and phenology dominate over life history. *Ecol. Indic.* 136:108685. doi: 10.1016/j.ecolind.2022.108685
- Yang, H., Wu, Y., Zhang, C., Wu, W., Lyu, L., and Li, W. (2022). Comprehensive resistance evaluation of 15 blueberry cultivars under high soil pH stress based on growth phenotype and physiological traits. *Front. Plant Sci.* 13:1072621. doi: 10.3389/fpls.2022.1072621
- Yuan, D. Y., Zhu, L. J., Cherubini, P., Li, Z. S., Zhang, Y. D., and Wang, X. C. (2021). Species-specific indication of 13 tree species growth on climate warming in temperate forest community of northeast China. *Ecol. Indic.* 133:108389.
- Zhang, H. Y., Wang, C. K., and Wang, X. C. (2013). Comparison of concentrations of non-structural carbohydrates between new twigs and old branches for 12 temperate species. *Acta Ecol. Sin.* 33, 5675–5685.
- Zhang, H. Y., Wang, C. K., and Wang, X. C. (2015). Within-crown variation in concentrations of non-structural carbohydrates of five temperate tree species. *Acta Ecol. Sin.* 35, 6496–6506.
- Zhang, Q. Y., Jia, X. X., Shao, M. A., and Ma, C. K. (2018). Unfolding non-structural carbohydrates from sapling to dying black locust on China's loess plateau. *J. Plant Growth Regul.* 37, 794–802.



OPEN ACCESS

EDITED BY

Ling Zhang,
Jiangxi Agricultural University, China

REVIEWED BY

Xintong Xu,
Nanjing Agricultural University, China
Xiaojun Liu,
Ningxia University, China

*CORRESPONDENCE

Shaoming Ye
✉ yshaoming@163.com

†These authors have contributed equally to this work and share first authorship

SPECIALTY SECTION

This article was submitted to
Forest Disturbance,
a section of the journal
Frontiers in Forests and Global Change

RECEIVED 11 January 2023

ACCEPTED 23 February 2023

PUBLISHED 09 March 2023

CITATION

He Y, Zhang Q, Jiang C, Lan Y, Zhang H and Ye S (2023) Mixed planting improves soil aggregate stability and aggregate-associated C-N-P accumulation in subtropical China. *Front. For. Glob. Change* 6:1141953. doi: 10.3389/ffgc.2023.1141953

COPYRIGHT

© 2023 He, Zhang, Jiang, Lan, Zhang and Ye. This is an open-access article distributed under the terms of the [Creative Commons Attribution License \(CC BY\)](https://creativecommons.org/licenses/by/4.0/). The use, distribution or reproduction in other forums is permitted, provided the original author(s) and the copyright owner(s) are credited and that the original publication in this journal is cited, in accordance with accepted academic practice. No use, distribution or reproduction is permitted which does not comply with these terms.

Mixed planting improves soil aggregate stability and aggregate-associated C-N-P accumulation in subtropical China

Yaqin He^{1†}, Qianchun Zhang^{1†}, Chenyang Jiang¹, Yahui Lan¹, Han Zhang¹ and Shaoming Ye^{1,2*}

¹College of Forestry, Guangxi University, Nanning, China, ²Guangxi Key Laboratory of Forest Ecology and Conservation, Nanning, China

Research on the variations in soil aggregate stability and ecological stoichiometry at aggregate scales by stand type is of great significance in investigating the distribution, limitation, balance, and cycling of organic carbon, nitrogen, and phosphorus (C-N-P). However, the effect of pure and mixed Chinese fir plantations on soil aggregate stability, organic carbon (OC), total nitrogen (TN), and total phosphorus (TP) stoichiometry characteristics at aggregate scales is still unclear. In this research, we explored the variations in soil aggregate mean weight diameter (MWD) and geometric mean diameter (GMD); soil OC, TN, and TP contents and stocks and the C:N:P ratios as affected by different stand types (mixed stands of Chinese fir and *Mytilaria laosensis*, mixed stands of Chinese fir and *Michelia macclurei*, and pure stand of Chinese fir); and aggregate size (<0.25, 0.25–1, 1–2, and >2 mm) at 0–20 and 20–40 cm depths in subtropical China. The soil OC and TN contents, as well as C:N:P ratios declined as aggregate size increased, whereas the C-N-P stocks showed the opposite tendencies, which were more distributed in >2 mm aggregates. Mixed stands of Chinese fir and *M. laosensis* with Chinese fir and *M. macclurei* displayed significantly higher soil aggregate stability, aggregate-associated TP content, OC and TN contents and stocks, and C:N and C:P ratios than did pure stands of Chinese fir. Soil aggregate stability was significantly positively correlated with the C-N-P contents and stocks as well as the C:N and C:P ratios, especially the C:N ratio and TN content. Overall, this work offers further information for scientific management and sustainable development of Chinese fir plantations, soil OC and nutrient cycling with ecological stoichiometry in the global terrestrial ecosystem.

KEYWORDS

Chinese fir plantations, stand type, soil aggregate, ecological stoichiometry, soil organic carbon and nutrient

1. Introduction

Plantations are considered one of the most widely distributed forest types worldwide, mitigating land degradation and facilitating material cycles and energy fluxes in ecosystems (Yang et al., 2021). China has the greatest plantation area (Zhou L. et al., 2020). Among different plantations, Chinese fir, also called *Cunninghamia lanceolata*, is a vital afforestation species in China, due to its rapid growth, superior material, and high economic value, with plantations comprising approximately 19% of the country's plantation area (Zhou L. et al., 2020; Tong et al., 2021). Guangxi has one of the most major Chinese fir plantations (CFPs) in widely cultivated provinces in China, and this is due to its unique climate and geographical location. However, the decreased productivity of CFPs has long been a major impediment in Guangxi. To pursue rapid tree growth and timber productivity, long-term succession cropping of CFPs has resulted in homogeneous stand structures and decreased soil fertility and productivity (Wang et al., 2020). Mixed forests of Chinese fir can also contribute to soil productivity, quality and health (Huang K. X. et al., 2020). Thus, the establishment of mixed forests is an effective approach for stabilizing soil structure and enhancing the soil nutrient status and sustainability of CFPs. This research has important theoretical guidance and practical significance for improving the quality and sustainable development of CFPs and the sustainable utilization of soil resources in CFPs.

Aggregates widely constitute the basic unit of soil structure, and they can affect soil structural stability and fertility maintenance (Six and Paustian, 2014). Soil aggregate stability is a vital index that is closely associated with soil organic carbon (OC) mitigation and nutrient restitution (Guo et al., 2020; Ma et al., 2022). It is generally evaluated by using the changes in the mean weight diameter (MWD, mm) and geometric mean diameter (GMD, mm) (Zhang Y. et al., 2021). Soil aggregate stability is impacted by soil physical-chemical properties, tree litter, root exudates, and surface runoff (Rivera and Bonilla, 2020; Feng et al., 2021). In addition, the stability of soil aggregates is strongly closely related to soil C and nitrogen (N) stability (Lu et al., 2019). Substantial studies have focused on exploring the relationship between soil aggregate stability and organic carbon (OC) content (Shen et al., 2021; Ma et al., 2022; Yao et al., 2022), indicating that OC content is a key factor affecting soil aggregate stability. During Chinese fir planting, soil OC and total nitrogen (TN) contents have a significant positive correlation with soil aggregate stability (Mao et al., 2021). Forest conversion can impact soil aggregate stability (Li et al., 2022). Additionally, introducing broadleaved tree species into CFPs can improve soil aggregate stability (Gao et al., 2022; Tang et al., 2023). However, most studies have not determined the key factors affecting variation in soil aggregate stability under different stand types of CFPs. Therefore, it is vital to reveal the soil aggregate stability of CFPs with different stand types to evaluate the soil structure and storage stability of soil nutrients.

Ecological chemometrics is an excellent way to determine covariation patterns and coupling relations of chemical elements (such as major elements: C, N, P), and this method has received more attention in exploring soil nutrient cycling and limiting effects (Zhang J. H. et al., 2021). Soil aggregates with different particle sizes have specific roles in nutrient supply, storage, and

limiting elements. In addition, the composition of aggregates can significantly affect the distribution of C–N–P contents, and the changes in their content distribution significantly impact the regulation of soil aggregate stability (Xu et al., 2019). A common agreement among studies is that mixed stands of Chinese fir increase the contents of OC and TN within different sizes of aggregates (Wang et al., 2020; Xu et al., 2020). Moreover, compared to pure stands, mixed stands have shown a significant increase in soil C:N:P ratios (Xu et al., 2020). Soil C–N–P contents and stocks are significantly influenced by various sizes of aggregates, but these studies display different results (Six et al., 2004). According to certain research, soil C, N, and P contents decrease as aggregate size increases (Tang and Wang, 2022), although the soil C, N, and P stocks show the opposite trend (Wang et al., 2020). Thus, further studies should investigate the variations in aggregate-associated C–N–P stoichiometry in relation to multiple stand types of CFPs to provide a new strategy for evaluating the correlations between soil aggregate stability and soil nutrient stoichiometry in plantation ecosystems.

Our previous research showed that soil depth can affect aggregate-associated C–N–P stoichiometry in a chronosequence of CFPs (Tang and Wang, 2022). However, how soil aggregate size and stand type in CFPs affect soil aggregate stability and C, N, and P stoichiometric properties is still unknown. Therefore, this study aimed to comprehensively quantify the responses of soil aggregate stability, the C–N–P contents and stocks, and the ratio of C:N:P to aggregate sizes (>2, 1–2, 0.25–1, and <0.25 mm) and stand types (mixed Chinese fir with *Mytilaria laosensis* Lecomte plantations, mixed Chinese fir with *Michelia macclurei* Dandy plantations, and pure CFPs) at 0–20 and 20–40 cm. This research assumed that (i) soil C–N–P stocks are more distributed in >2 mm aggregates; (ii) mixed CFPs have higher soil aggregate stability, aggregate-related C–N–P contents and stocks than pure CFPs; and (iii) soil TN content is the key parameter related to the changes in soil aggregate stability.

2. Materials and methods

2.1. Experimental site

We conducted this study in November 2020 at the Qingshan Experimental Field, which is in Longzhou County, Chongzuo city, Guangxi Zhuang Autonomous Region, China (22°08'–22°44' N, 106°33'–107°12' E) (Figure 1). The Qingshan Experimental Field has a subtropical monsoon environment and is in the concentrated production region of Chinese fir in Guangxi. The annual mean temperature and precipitation are 21°C and 1400 mm, respectively. The primary types of terrains include low mountains and hills. The native rock is dominated by limestone. The soil type is mainly latosol (pH 4.8–5.5), and the soil depth is over 80 cm. Due to long-term and intense human disturbance, the native vegetation in the region has been almost completely destroyed, and large-scale CFPs have rapidly expanded. Experimental and demonstration forests of valuable and high-quality Chinese fir mixed with broadleaved tree species are mainly plantations of mixed Chinese fir and *M. laosensis* as well as mixed Chinese fir and *M. macclurei* in this study region. Meanwhile, *Maesa japonica*, *Brassaia actinophylla*,

Rubus alceaefolius, *Litsea variabilis*, *Blechnum orientale*, *Mussaenda pubescens*, *Pteris semipinnata*, and *Evodia lepta* comprise most of the understory vegetation.

2.2. Experimental design

In this research, we collected soil samples from three stand types of CFPs, which were established in 1992 (Table 1). To reduce soil spatial variations, the three stand types were placed in similar geomorphologic units with similar altitude, slope gradient and aspect, soil parent material, and fertilization practices. The spacing between the three stand types was 2 m × 3 m. Mixed stands had a 3:1 mixed proportion. For each stand type, we performed a complete random design and duplicated in quintuplicate to produce in fifteen CFPs (3 stand types × 5 replicates) (Figure 1). Every two CFPs were separated by more than 800 m to avoid pseudo-replication and reduce spatial self-correlation. A plot (20 m × 20 m) was randomly selected at more than 50 m across the plantation edge for each CFP.

2.3. Litter and soil sampling

The mixed litterfall samples were acquired from the soil surface by five randomized 1 m × 1 m subplots. The 15 mixed litterfall samples (3 stand types × 5 replicates) were then desiccated in an oven at 80°C until they reached a constant weight (Table 1). In addition, soil specimens in the research were acquired from places similar to the litterfall samples and were collected through spades from 0 to 20 and 20 to 40 cm, separately. Afterward, 5 soil samples were combined. Then, 30 mixed soil specimens (3 stand types × 5 replicates × 2 soil depths) were separated into natural aggregates, and macrofauna, coarse roots, and stones were removed. To measure the bulk density (BD), total porosity (Pt), pH, OC, TN, and TP contents in bulk soil, cutting rings were used to randomly collect from every soil layer for the other 5 soil samples for each plot (Table 2).

2.4. Soil aggregate separation

Different sized sieves (continuous diameters: 2, 1, 0.25 mm) were used for soil aggregate isolation by a dry-sieving approach (Six and Paustian, 2014). Eventually, the aggregate sizes were categorized as >2, 1–2, 0.25–1, and <0.25 mm.

2.5. Soil property analyses

Before examining the physical-chemical characteristics of the soil, air drying at room temperature was applied to soil samples, including aggregates and bulk soil. Soil BD and Pt were detected using a cutting ring (Lu, 1999). A glass electrode was used to measure soil pH (Lu, 1999). The micro-Kjeldahl approach was performed to measure soil TN (Bremner, 1996), while the Olsen approach was used to detect soil TP (Bray and Kurtz, 1945). The acid dichromate wet oxidation approach by Nelson and Sommers (1996) was used to detect soil OC.

2.6. Data statistics

Soil MWD and GMD are the key indicators used to evaluate the stability of soil aggregates (Kong et al., 2022). Larger values of MWD and GMD indicate stronger soil aggregate stability (Zhou L. et al., 2020). The formula calculations for MWD and GMD are as follows (Zhang Y. et al., 2021):

$$\text{MWD} = \sum_{i=1}^4 (X_i \times W_i) \quad (1)$$

$$\text{GMD} = \exp \left[\frac{\sum_{i=1}^4 (W_i \times \ln(X_i))}{\sum_{i=1}^4 (W_i)} \right] \quad (2)$$

where X_i (mm) is the mean diameter of the i th-sized aggregates, and W_i (% in weight) is the proportion of the i th-sized aggregates in bulk soil.

The formula used to calculate soil OC stocks (OCS, g m^{-2}) is as follows (Eynard et al., 2005):

$$\text{OCS} = \sum_{i=1}^4 (X_i \times W_i) \times B \times H \times 10 \quad (3)$$

where B (g cm^{-3}), H (cm), and X_i (g kg^{-1}) denote the bulk density, soil depth, and OC content within i th size aggregates, respectively. The number 10 is the unit conversion factor. Similarly, soil TN and TP stocks (TNS and TPS, g m^{-2}) were also calculated.

Since stand type and aggregate size were the two main factors, statistical analyses were performed according to soil depth. SPSS 26.0 was used to conduct statistical analysis (Table 3). All datasets were tested for homogeneity of variances and the normal distribution of residuals prior to performing analysis of variance (ANOVA) to ensure that the assumptions of statistical analysis were met. We performed one-way and two-way ANOVAs to explore the effects of stand type on litter and bulk soil properties and the influences of aggregate size and stand type on soil aggregate properties, respectively. Then, to compare various stand types and aggregate sizes, the post-hoc Tukey HSD test was used, with $P < 0.05$ denoting statistical significance. The effect of different soil depths on aggregates in the same stand type was evaluated using a two-tailed independent sample t test, with $P < 0.05$ considered statistically significant. Furthermore, a generalized linear model was utilized to analyze the correlation between aggregate-related OC and nutrients in different stand types. Redundancy analysis (RDA) was utilized by CANOCO 5.0 to determine the influences of environmental parameters on soil aggregate stability. The association of soil aggregate stability with ecological stoichiometric characteristics in bulk soil was analyzed by Pearson's correlation analysis.

3. Results

3.1. Bulk soil properties under different stand types

The soil Pt, OC, TN, TP, OCS, TNS, TPS, C/N, and C/P in mixed stands had significantly higher levels than those in pure

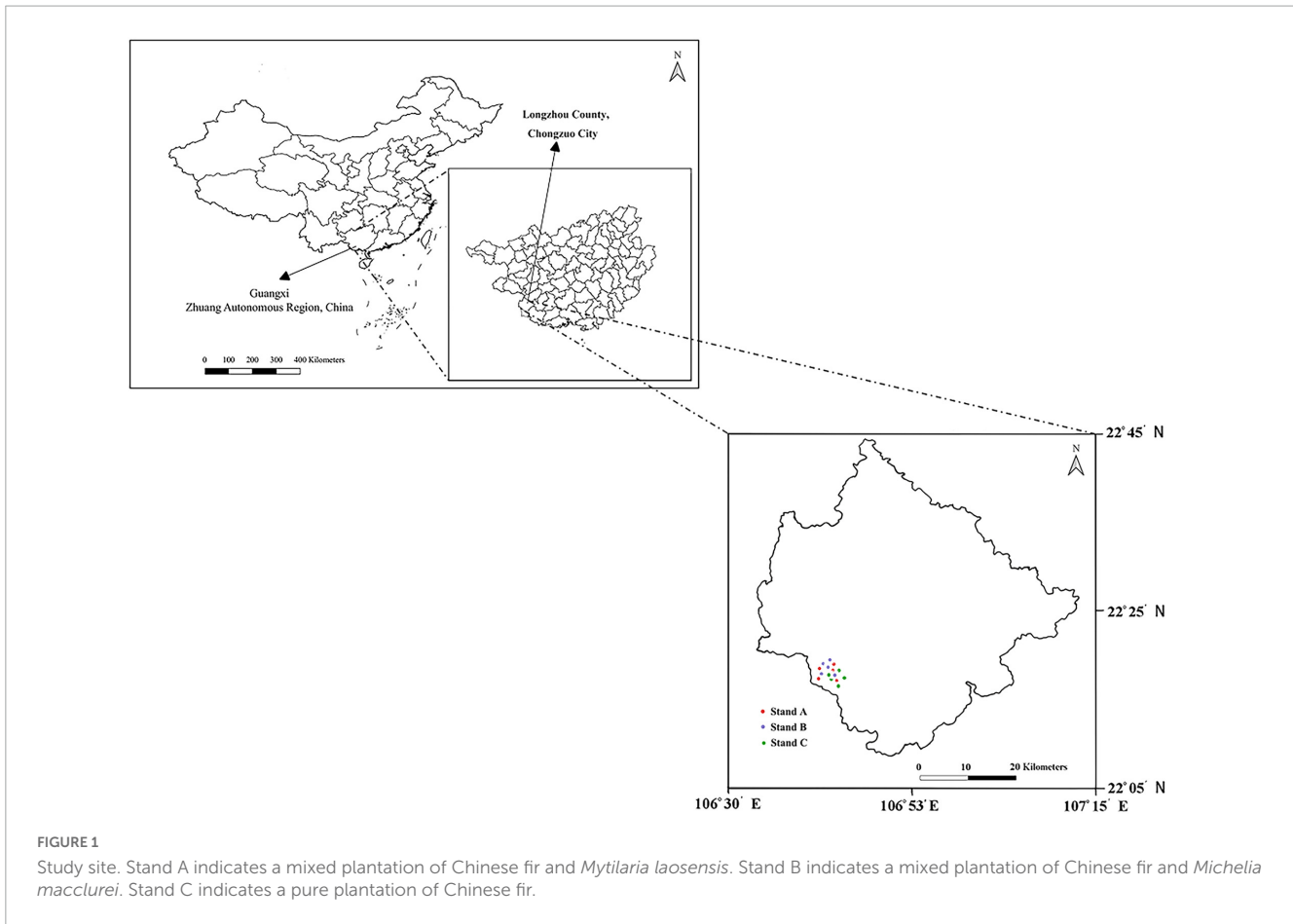


FIGURE 1 Study site. Stand A indicates a mixed plantation of Chinese fir and *Mytilaria laosensis*. Stand B indicates a mixed plantation of Chinese fir and *Michelia macclurei*. Stand C indicates a pure plantation of Chinese fir.

TABLE 1 Basic information of sample plots in Chinese fir plantations with different stand types.

| Stand type | Altitude (m) | Slope (°) | Aspect (°) | Mean height (m) | Mean diameter (cm) | Crown density | Litterfall amount (gm ⁻²) |
|------------|--------------|-----------|------------|-----------------|--------------------|---------------|---------------------------------------|
| Stand A | 730 | 27 | 185 | 16.29 ± 0.21 a | 21.03 ± 0.63 a | 0.85 ± 0.01 a | 455 ± 23 b |
| Stand B | 725 | 25 | 178 | 16.47 ± 0.33 a | 21.30 ± 0.49 a | 0.85 ± 0.01 a | 504 ± 27 a |
| Stand C | 728 | 30 | 183 | 13.64 ± 0.12 b | 16.92 ± 0.37 b | 0.85 ± 0.01 a | 324 ± 12 c |

Data indicate the average of five replicates ± standard deviations. Stand A indicates a mixed plantation of Chinese fir and *Mytilaria laosensis*. Stand B indicates a mixed plantation of Chinese fir and *Michelia macclurei*. Stand C indicates pure plantation of Chinese fir. Various lowercase letters indicate significant differences among the different stand types at $P < 0.05$.

stands among both layers (0–40 cm), whereas the soil BD and pH showed opposite trends (Table 2). In the three stands, soil OC and nutrients significantly decreased with increasing, whereas soil BD presented the opposite trend.

3.2. Aggregate distribution and stability among diverse stand types and aggregate sizes

Most fractions, regardless of the stand type, were composed of >2 mm aggregates, with average proportions of 43.33% (0–20 cm) and 39.26% (20–40 cm) (Figure 2). Mixed stands had considerably greater distributions of >2 mm and <0.25 mm aggregates at both depths compared to pure stands, but this tendency was reversed for the 1–2 mm and 0.25–1 mm aggregates. Additionally, for every soil profile, mixed stands

had much higher MWD (Figure 3A) and GMD (Figure 3B) values than did pure stands. The MWD and GMD values increased significantly among the three stands as the soil depth decreased.

3.3. Aggregate-associated OC, TN, and TP contents and stoichiometric characteristics

The soil OC and TN contents among the three stands displayed significant increases with decreasing aggregate size at both depths, but the TP content showed no significant variations in aggregates (Table 4). Moreover, the OC, TN, and TP contents in aggregates among mixed stands were higher than those among pure stands at both depths, especially in mixed stand B. Besides, soil aggregate-associated OC, TN, and TP contents

TABLE 2 Bulk soil properties in Chinese fir plantations with different stand types.

| Variable | 0–20 cm soil depth | | | 20–40 cm soil depth | | |
|--------------------------|--------------------|----------------------------|--------------------|---------------------|-----------------------------|--------------------|
| | Stand A | Stand B | Stand C | Stand A | Stand B | Stand C |
| BD (g cm ⁻³) | 1.26 ± 0.01 b* | 1.24 ± 0.01 b* | 1.31 ± 0.02 a** | 1.27 ± 0.01 b* | 1.26 ± 0.01 b* | 1.33 ± 0.01 a** |
| Pt (%) | 52.38 ± 0.38 a** | 53.13 ± 0.22 a** | 50.42 ± 0.28 b** | 52.92 ± 0.19 a** | 52.60 ± 0.19 a** | 49.96 ± 0.83 b** |
| pH | 4.33 ± 0.01 b** | 4.31 ± 0.01 c** | 4.37 ± 0.00 a** | 4.30 ± 0.01 b** | 4.27 ± 0.01 b** | 4.41 ± 0.02 a** |
| OC (g kg ⁻¹) | 24.80 ± 0.84 b** | 33.34 ± 1.16 a** | 20.96 ± 0.42 c** | 10.17 ± 0.73 b** | 17.16 ± 0.82 a** | 7.25 ± 0.47 c** |
| TN (g kg ⁻¹) | 1.25 ± 0.03 b** | 1.46 ± 0.01 a** | 1.26 ± 0.01 b** | 0.75 ± 0.01 b** | 1.21 ± 0.03 a** | 0.68 ± 0.02 c** |
| TP (g kg ⁻¹) | 0.27 ± 0.00 a** | 0.28 ± 0.00 a* | 0.24 ± 0.01 b** | 0.25 ± 0.00 a** | 0.25 ± 0.01 a* | 0.20 ± 0.01 b** |
| C/N | 19.92 ± 0.53 b** | 22.9 ± 0.88 a** | 16.67 ± 0.33 c** | 13.38 ± 0.86 a** | 14.14 ± 0.61 a** | 10.67 ± 0.40 b** |
| C/P | 95.75 ± 4.61 b** | 124.52 ± 5.71 a** | 90.15 ± 2.70 b** | 42.43 ± 3.46 b** | 71.14 ± 5.40 a** | 37.56 ± 2.02 b** |
| N/P | 4.82 ± 0.13 b** | 5.43 ± 0.07 a** | 5.38 ± 0.19 a** | 3.13 ± 0.07 b** | 4.95 ± 0.30 a** | 3.52 ± 0.17 b** |
| OCS (g m ⁻²) | 624.93 ± 47.31 b** | 826.83 ± 64.48 a** | 549.05 ± 24.62 c** | 258.42 ± 41.48 b** | 426.1 ± 44.88 a** | 192.81 ± 27.87 c** |
| TNS (g m ⁻²) | 31.39 ± 1.52 b** | 36.24 ± 0.51 a** | 32.96 ± 0.39 b** | 19.17 ± 0.43 b** | 30.45 ± 1.61 a** | 18.01 ± 1.26 b** |
| TPS (g m ⁻²) | 6.72 ± 0.26 a** | 6.83 ± 0.2 a ^{ns} | 6.32 ± 0.38 b** | 6.23 ± 0.21b** | 6.33 ± 0.51 a ^{ns} | 5.23 ± 0.55 c** |

Pt stands for total porosity. BD stands for bulk density. OC, TN and TP represent the organic carbon, total nitrogen and total phosphorus contents in bulk soil, respectively. C/N, C/P and N/P represent the organic carbon, total nitrogen and total phosphorus ratios in bulk soil, respectively. OCS, TNS and TPS represent the stocks of organic carbon, total nitrogen, and total phosphorus in bulk soil, respectively. Various lowercase letters indicate significant differences among the different stand types at $P < 0.05$. ** and * stand for significant differences among the different soil depths at $P < 0.01$ and $P < 0.05$, respectively. ^{ns}Stands for no significant differences among the different soil depths.

TABLE 3 Litterfall and soil properties as influenced by aggregate size and stand type in Chinese fir plantations.

| Variable | Litterfall | 0–20 cm soil depth | | | 20–40 cm soil depth | | |
|--|------------|--------------------|----|-------|---------------------|----|-------|
| | S | S | A | S × A | S | A | S × A |
| Litterfall amount (g m ⁻²) | ** | | | | | | |
| BD (g cm ⁻³) | | ** | | | ** | | |
| Pt (%) | | ** | | | ** | | |
| Soil pH | | ** | | | ** | | |
| Soil aggregate proportion | | Ns | ** | ** | Ns | ** | ** |
| MWD | | ** | ** | ** | ** | ** | ** |
| GMD | | ** | ** | ** | ** | ** | ** |
| OC (g kg ⁻¹) | | ** | ** | Ns | ** | ** | ** |
| TN (g kg ⁻¹) | | ** | ** | ** | ** | ** | Ns |
| TP (g kg ⁻¹) | | ** | Ns | ** | ** | Ns | Ns |
| C/N ratio | | ** | ** | Ns | ** | ** | * |
| C/P ratio | | ** | ** | ** | ** | ** | ** |
| N/P ratio | | Ns | ** | ** | ** | ** | Ns |
| OCS (g m ⁻²) | | ** | ** | ** | ** | ** | ** |
| TNS (g m ⁻²) | | ** | ** | ** | ** | ** | ** |
| TPS (g m ⁻²) | | Ns | ** | ** | ** | ** | ** |
| Percentage contribution of OCS (%) | | Ns | ** | ** | Ns | ** | ** |
| Percentage contribution of TNS (%) | | Ns | ** | ** | Ns | ** | ** |
| Percentage contribution of TPS (%) | | Ns | ** | ** | Ns | ** | ** |

S stands for stand type. A stands for aggregate size. Ns stands for no significant differences. MWD and GMD stand for mean weight diameter and geometric mean diameter, respectively. OC, TN and TP stand for organic carbon, total nitrogen and total phosphorus contents, respectively. OCS, TNS with TPS stand for the stock of organic carbon, total nitrogen, and total phosphorus, respectively. C/N, C/P and N/P stand for organic carbon, total nitrogen and total phosphorus ratios, respectively.

* $P < 0.05$; ** $P < 0.01$.

among the three stands increased as the soil depth decreased. There was a significant positive correlation ($P < 0.05$) between the OC, TN and TP contents for different soil aggregate sizes in the three stand types (Figure 4). The linear relationship

between the OC and TN contents is shown in Figure 4A ($R^2 = 0.86$, $P < 0.01$). However, the linear fits between OC and TP contents (Figure 4B) as well as the TN and TP contents (Figure 4C) were low. In addition, the change in TP

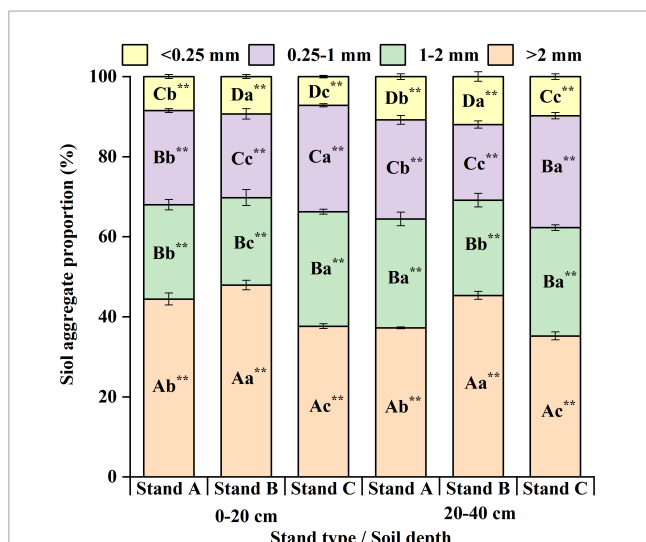


FIGURE 2 Soil aggregate distribution in Chinese fir plantations with different stand types. Data indicate the average of 5 replicates \pm standard deviations. Various capital letters stand for significant differences among the different aggregate sizes at $P < 0.05$. Various lowercase letters stand for significant differences among the different stand types at $P < 0.05$. ** and * stand for significant differences among the different soil depths at $P < 0.01$ and $P < 0.05$, respectively. ^{ns}Stands for no significant differences among the different soil depths.

3.4. Aggregate-associated OCS, TNS, and TPS under different stand types

Regardless of the stand type, OCS (Figure 5A), TNS (Figure 5B), and TPS (Figure 5C) and their contribution percentages had a dominant distribution in >2 mm aggregates at both depths. For example, among the three stands, the OCS associated with the >2 mm aggregates was $196.92\text{--}381.01$ g m⁻² (0–20 cm) and $60.36\text{--}164.93$ g m⁻² (20–40 cm), accounting for 35.59–45.75% (0–20 cm) and 31.40–38.02% (20–40 cm) of the OCS in bulk soil (Supplementary Figure 1A), respectively, but the OCS associated with the <0.25 mm aggregates was only $46.12\text{--}66.54$ g m⁻² (0–20 cm) and $22.69\text{--}68.86$ g m⁻² (20–40 cm) (Figure 5A), contributing to 8.34–10.74% (0–20 cm) and 11.81–15.84% (20–40 cm) of the OCS in bulk soil (Supplementary Figure 1A), respectively. The TNS (Figure 5B) and TPS (Figure 5C) associated with soil aggregates showed similar trends. Regardless of the soil depth, the aggregate-associated OCS, TNS, and TPS showed the higher levels in mixed stand than those in pure stand. Notably, mixed stands had greater percentage contributions of OCS, TNS, and TPS within the >2 and <0.25 mm aggregates than did pure stands, while other aggregates showed the opposite pattern.

3.5. Soil aggregate stability as influenced by soil ecological stoichiometric characteristics

The influences of soil ecological stoichiometric characteristics (such as OC, TN, TP, C/N, C/P, N/P, OCS, TNS, and TPS) on soil aggregate stability (such as MWD and GMD) across the three stands of Chinese fir were determined by RDA. The influence order was C/N $>$ TP $>$ TPS $>$ N/P $>$ C/P $>$ OCS $>$ OC $>$ TN $>$ TNS at the 0–20 cm depth (Figure 6A). Specifically, the C/N and TP represented the key factors that explained 77.4 and 11.3% of

content lagged behind TN and OC contents based on the slope (Figures 4B, C).

Irrespective of the stand type, the C:N:P ratio (Table 4) significantly increased as aggregate size decreased at both depths. In the 0–40 cm layer, the mixed stands aggregate-associated C/N (12.02–23.66) and C/P ratios (36.19–136.3) were greater than those in pure stands (C/N: 10.39–19.46; C/P: 31.79–116.57). Additionally, the aggregate-associated N/P ratio in stand B was notably higher than that of stands A and C at the 20–40 cm depth.

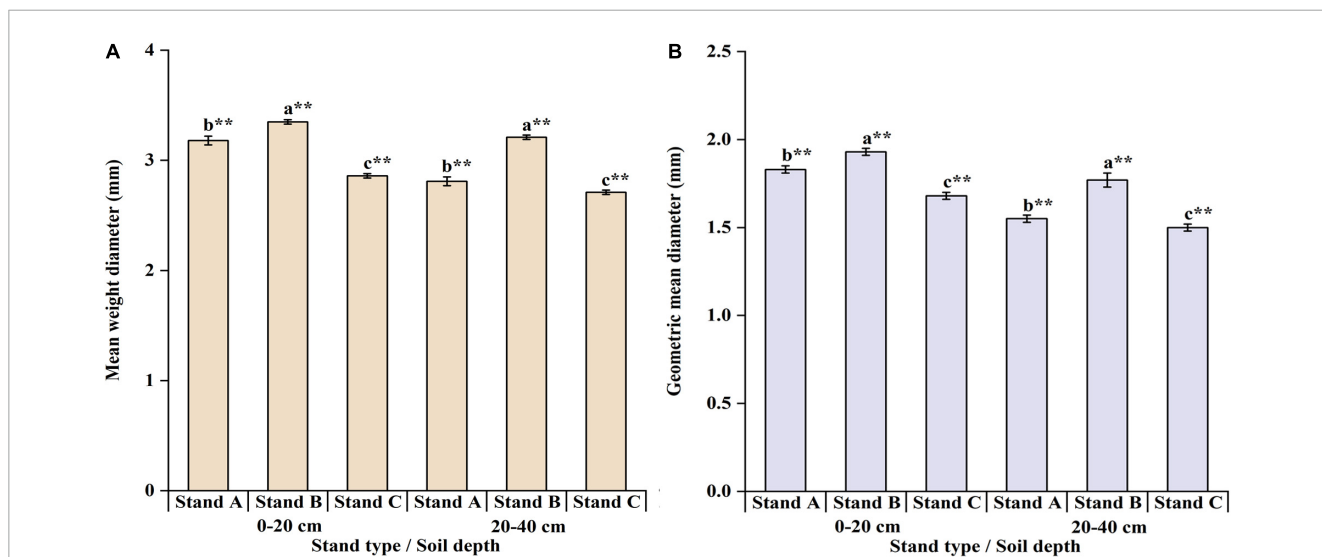


FIGURE 3 Distribution of mean weight diameter (A) and geometric mean diameter (B) in Chinese fir plantations with different stand types.

TABLE 4 Aggregate-associated OC, TN and TP contents and stoichiometric characteristics.

| Variable | Soil depth (cm) | Stand type | Aggregate size (mm) | | | |
|--------------------------|-----------------|------------|-------------------------------|-------------------------------|------------------------------|-------------------------------|
| | | | >2 | 1–2 | 0.25–1 | <0.25 |
| OC (g kg ⁻¹) | 0–20 | Stand A | 21.42 ± 2.13 Bb** | 24.77 ± 2.76 Bb** | 29.02 ± 3.7 Ab** | 30.88 ± 2.81 Ab** |
| | | Stand B | 31.82 ± 3.14 Ba** | 32.85 ± 3.73 Ba** | 35.07 ± 2.45 ABa** | 38.37 ± 2.3 Aa** |
| | | Stand C | 19.81 ± 0.86 Bb** | 20.11 ± 1.63 Bc** | 22.58 ± 1.89 Ac** | 24.33 ± 2.16 Ac** |
| | 20–40 | Stand A | 8.57 ± 1.87 Bb** | 9.22 ± 1.76 Bb** | 12.28 ± 1.54 Ab** | 13.25 ± 2.2 Ab** |
| | | Stand B | 14.38 ± 2.9 Ba** | 15.49 ± 2.49 Ba** | 22.41 ± 3.29 Aa** | 22.75 ± 3.02 Aa** |
| | | Stand C | 6.46 ± 0.55 Bb** | 7.25 ± 1.69 ABb** | 7.71 ± 1.53 ABc** | 8.76 ± 1.05 Ac** |
| TN (g kg ⁻¹) | 0–20 | Stand A | 1.1 ± 0.12 Cc** | 1.33 ± 0.03 Bb** | 1.34 ± 0.11 Bb** | 1.5 ± 0.03 Ab** |
| | | Stand B | 1.36 ± 0.06 Da** | 1.57 ± 0.04 Ba** | 1.48 ± 0.04 Ca* | 1.68 ± 0.05 Aa** |
| | | Stand C | 1.25 ± 0.04 Ab** | 1.27 ± 0.06 Ab** | 1.26 ± 0.02 Ac** | 1.25 ± 0.06 Ac** |
| | 20–40 | Stand A | 0.68 ± 0.04 Bb** | 0.72 ± 0.04 Bb** | 0.85 ± 0.02 Ab** | 0.88 ± 0.07 Ab** |
| | | Stand B | 1.19 ± 0.04 Aa** | 1.17 ± 0.09 Aa** | 1.26 ± 0.14 Aa* | 1.26 ± 0.09 Aa** |
| | | Stand C | 0.63 ± 0.08 Bb** | 0.68 ± 0.08 ABb** | 0.71 ± 0.05 ABc** | 0.76 ± 0.03 Ac** |
| TP (g kg ⁻¹) | 0–20 | Stand A | 0.29 ± 0.02 Aa ^{ns} | 0.21 ± 0.04 Bb ^{ns} | 0.27 ± 0.01 Aa ^{ns} | 0.27 ± 0.03 Aa ^{ns} |
| | | Stand B | 0.23 ± 0.01 Bc* | 0.33 ± 0.02 Aa** | 0.32 ± 0.04 Aa** | 0.25 ± 0.03 Ba** |
| | | Stand C | 0.26 ± 0.02 Ab** | 0.24 ± 0.05 Ab ^{ns} | 0.22 ± 0.05 Ab ^{ns} | 0.21 ± 0.01 Ab ^{ns} |
| | 20–40 | Stand A | 0.25 ± 0.04 Aab ^{ns} | 0.24 ± 0.03 Aa ^{ns} | 0.25 ± 0.04 Aa ^{ns} | 0.23 ± 0.01 Aab ^{ns} |
| | | Stand B | 0.27 ± 0.03 Aa* | 0.24 ± 0.03 ABa** | 0.22 ± 0.05 Bab** | 0.25 ± 0.01 ABa** |
| | | Stand C | 0.21 ± 0.02 Ab** | 0.19 ± 0.03 Ab ^{ns} | 0.18 ± 0.03 Ab ^{ns} | 0.21 ± 0.04 Ab ^{ns} |
| C/N | 0–20 | Stand A | 19.60 ± 1.28 Ab** | 18.63 ± 0.95 Aa** | 21.60 ± 0.64 Aa** | 20.60 ± 0.74 Ab** |
| | | Stand B | 23.49 ± 1.33 Aa** | 20.87 ± 0.99 Aa** | 23.66 ± 0.92 Aa** | 22.90 ± 0.49 Aa** |
| | | Stand C | 15.88 ± 0.36 Bc** | 15.80 ± 0.55 Bb** | 17.96 ± 0.73 Ab** | 19.46 ± 0.74 Ab** |
| | 20–40 | Stand A | 12.52 ± 1.05 Aa** | 12.89 ± 1.04 Aa** | 14.47 ± 0.96 Ab** | 15.02 ± 0.90 Ab** |
| | | Stand B | 12.02 ± 0.98 Ba** | 13.32 ± 0.90 Ba** | 17.82 ± 1.26 Aa** | 17.96 ± 0.70 Aa** |
| | | Stand C | 10.39 ± 0.46 Aa** | 10.55 ± 0.79 Aa** | 10.80 ± 0.71 Ac** | 11.60 ± 0.52 Ac** |
| C/P | 0–20 | Stand A | 73.58 ± 3.77 Bb** | 119.05 ± 11.89 Aa** | 107.54 ± 5.78 Aa** | 114.96 ± 6.85 Ab** |
| | | Stand B | 136.3 ± 8.35 Aa** | 99.63 ± 6.49 Bab** | 111.36 ± 8.25 Ba** | 151.59 ± 5.94 Aa** |
| | | Stand C | 76.27 ± 3.75 Cb** | 84.93 ± 7.04 Bcb** | 108.24 ± 12.31 ABa** | 116.57 ± 7.91 Ab** |
| | 20–40 | Stand A | 36.19 ± 5.17 Bb** | 38.81 ± 4.65 Bb** | 49.19 ± 3.85 ABb** | 57.48 ± 5.46 Ab** |
| | | Stand B | 53.20 ± 5.20 Ba** | 65.62 ± 5.67 Ba** | 108.43 ± 13.68 Aa** | 90.98 ± 4.13 Aa** |
| | | Stand C | 31.79 ± 2.13 Ab** | 38.50 ± 4.62 Ab** | 42.38 ± 3.80 Ab** | 41.89 ± 1.71 Ac** |
| N/P | 0–20 | Stand A | 3.78 ± 0.15 Cc* | 6.38 ± 0.48 Aa** | 4.97 ± 0.16 Bab** | 5.59 ± 0.30 ABb** |
| | | Stand B | 5.81 ± 0.16 Ba** | 4.77 ± 0.14 Cb ^{ns} | 4.71 ± 0.30 Cb ^{ns} | 6.62 ± 0.25 Aa** |
| | | Stand C | 4.80 ± 0.16 Ab** | 5.43 ± 0.59 Aab* | 5.98 ± 0.51 Aa** | 5.97 ± 0.24 Aab** |
| | 20–40 | Stand A | 2.85 ± 0.27 Bb* | 2.99 ± 0.18 Bb** | 3.41 ± 0.19 ABb** | 3.82 ± 0.21 Ab** |
| | | Stand B | 4.43 ± 0.25 Ba** | 4.97 ± 0.40 ABa ^{ns} | 6.13 ± 0.77 Aa ^{ns} | 5.06 ± 0.05 ABa** |
| | | Stand C | 3.07 ± 0.18 Ab** | 3.65 ± 0.39 Ab* | 3.93 ± 0.25 Ab** | 3.65 ± 0.23 Ab** |

Various capital letters stand for significant differences among the different aggregate sizes at $P < 0.05$. Various lowercase letters stand for significant differences among the different stand types at $P < 0.05$. ** and * stand for significant differences among the different soil depths at $P < 0.01$ and $P < 0.05$, respectively. ^{ns}Stands for no significant differences among the different soil depths.

the stand type variations in soil aggregate stability, respectively. However, it is worth noting that the influence order was TN > TPS > N/P > TNS > TP > C/P > OC > C/N > OCS at the 20–40 cm depth (Figure 6B). Specifically, TN and TPS explained 96.4 and 1.1% of the stand type variations in soil

aggregate stability, respectively. In addition, there was consensus between the Pearson’s correlation analysis results (Supplementary Figure 2) and the RDA results. We also found that MWD and GMD had significant and positive correlations with C/N, C/P, OC, TN, TP, OCS, TNS, and TPS.

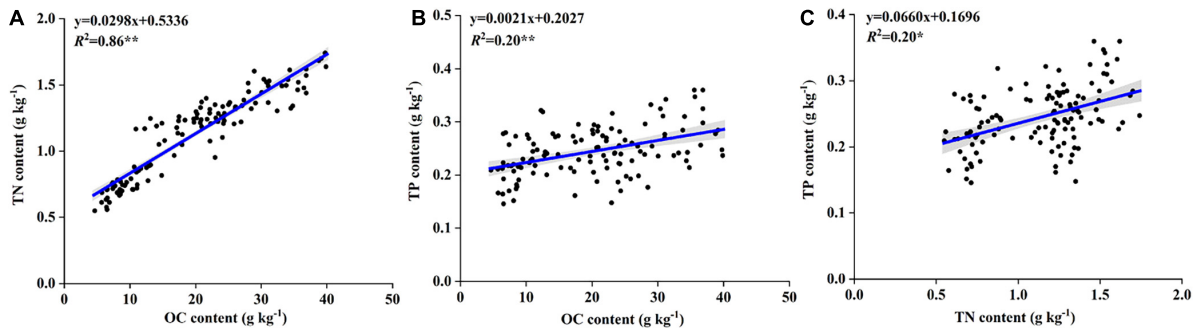


FIGURE 4

Relationships of aggregate-associated OC (A), TN (B), and TP (C) contents in Chinese fir plantations with different stand types. OC, TN, and TP stand for the contents of organic carbon, total nitrogen and total phosphorus in different aggregate sizes, respectively. ** and * stand for significant correlations at $P < 0.01$ and $P < 0.05$, respectively.

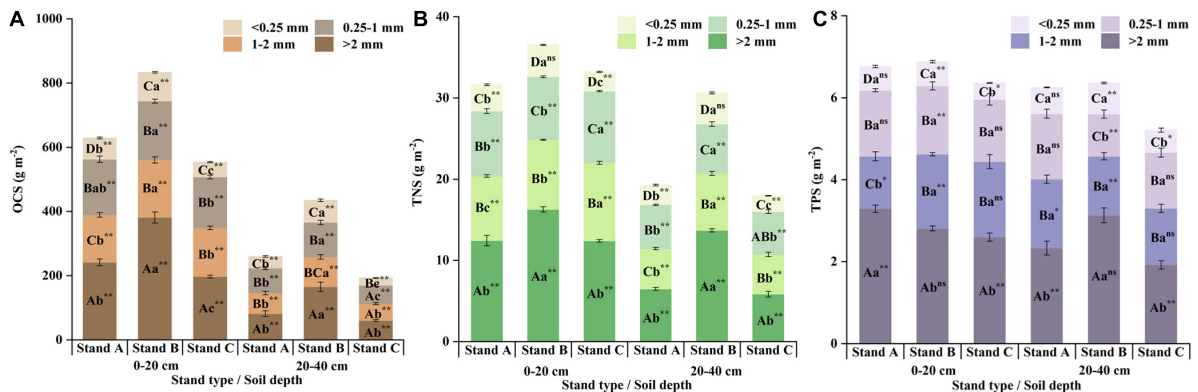


FIGURE 5

Aggregate-associated OCS (A), TNS (B), and TPS (C) in Chinese fir plantations with different stand types. OCS, TNS and TPS stand for the stocks of organic carbon, total nitrogen, and total phosphorus in different aggregate sizes, respectively. ** and * stand for significant differences among the different soil depths at $P < 0.01$ and $P < 0.05$, respectively. ^{ns}Stand for no significant differences among the different soil depths.

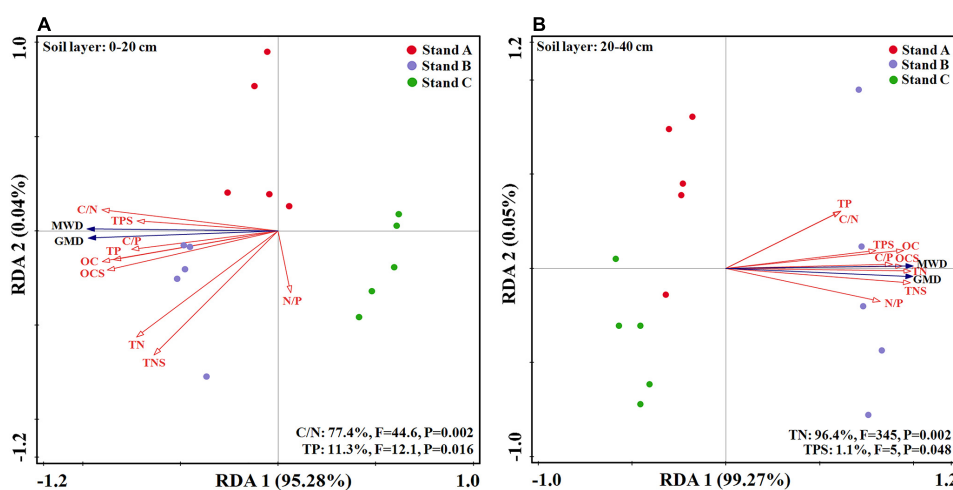


FIGURE 6

Redundancy analysis of soil aggregate stability and soil ecological stoichiometric characteristics across the three stand types at 0–20 cm (A) and 20–40 cm (B). MWD and GMD stand for mean weight diameter and geometric mean diameter, respectively. OC, TN, and TP stand for the contents of organic carbon, total nitrogen and total phosphorus in bulk soil, respectively. OCS, TNS, and TPS stand for the stocks of organic carbon, total nitrogen, and total phosphorus in bulk soil, respectively. C/N, C/P, and N/P stand for the ratios of organic carbon, total nitrogen and total phosphorus in bulk soil, respectively. The red and blue arrows stand for explanatory variable and response variable, respectively.

4. Discussion

4.1. Aggregate distribution and stability

Variation in the proportion of soil aggregates confirms the distribution of soil porosity and its morphological characteristics (Six et al., 2004). Moreover, soil aggregate stability can represent the ability of soil to supply and store soil nutrients (Gelaw et al., 2015). Therefore, exploring soil aggregate distribution and stability is vital for evaluating soil structure. In this study, mixed stands favored the formation of >2 mm aggregates, confirming earlier studies that aggregate distribution is significantly affected by stand type (Wang S. Q. et al., 2021). According to the hierarchical concept of soil aggregates, plant litterfall quality can be used to identify soil aggregate distribution, thereby influencing the composition of soil aggregates (Six and Paustian, 2014; Tang and Wang, 2022). In this study, the litter amount (Table 1) in the mixed stands was significantly higher than that in the pure stands. Likewise, the increased amount of plant litterfall and coverage area in the mixed stands decreased rainfall leaching, thus resulting in the protection of >2 mm aggregates from dispersion with water. To encourage the creation of cementing agents and the development of >2 mm aggregates, mixed forests have a better capacity to contain a significant amount of organic matter derived from plant residue inputs (Picariello et al., 2021; Zhao et al., 2021). Moreover, organic matter can stimulate the formation of soil aggregates and regulate soil aggregation (Feng et al., 2020).

The conversion of forest can significantly impact soil aggregate stability (Meng et al., 2022). Forest conversion affects the decomposition of litter to change organic colloids, thereby modifying soil aggregation and stability (Kerdran et al., 2020; Li et al., 2022). Likewise, based on Table 3, the MWD and GMD were influenced by stand type. Due to the greater stability index (MWD, GMD) values (Figure 3) in mixed stands, the mixed stands in this study had had stronger soil aggregate stability than pure stands, which is consistent with the findings from Tang et al. (2023). This result might be due to the greater litterfall residue (Table 1) and the proportion of >2 mm aggregates proportions (Figure 2) in the mixed stands. The >2 mm aggregates can provide a physical protection for organic matter, resulting in a significant increase in soil aggregate stability (Xie et al., 2018). In addition, a highly significant correlation between soil aggregate stability and organic matter has been reported (Li et al., 2022). Soil aggregate stability has a negative relationship with BD and a positive relationship with Pt (Liu et al., 2021). In contrast to pure stands, where the soil BD was much higher, mixed stands had significantly lower soil BD (Table 3), while soil Pt showed the reverse pattern, which suggested the mixed stands had higher soil aggregate stability. The reduced soil organic matter may be driven by increased soil densification, causing lower soil aggregate stability in pure stands (Faustino et al., 2020). Notably, this study discovered that there were more >2 mm aggregates in the 0–20 cm layer than in the 20–40 cm layer (Figure 2). Similarly, a large amount of organic matter from litter is mostly distributed in the soil surface (You et al., 2020). Organic matter is one of the most important persistent binding agents for facilitating soil aggregate formation (Smith et al., 2014). Organic matter is beneficial for the soil aggregation process because it binds different chemical bonds in the form of micelles (Sarker

et al., 2018). Moreover, some studies have demonstrated that the interaction between organic matter and metal oxides is a key factor promoting soil aggregate formation and affecting aggregate stability (Li et al., 2023). These factors might explain the higher stability of soil aggregates in the 0–20 cm layer.

4.2. Aggregate-associated OC, TN, and TP contents under different stand types

In this research, OC and TN (Table 4) contents were mainly distributed in <0.25 mm aggregates. Because <0.25 mm aggregates have larger specific surface areas than other aggregates, they have a higher adsorption capacity for nutrients derived from litter residues and root exudates (Egan et al., 2018). Therefore, OC and TN contents showed significant decreases as aggregate size increased. However, Xu et al. (2020) reported the opposite result, probably because plantation management measures and site conditions can influence the OC and TN contents in the various-sized aggregates. Similarly, in the present study, there was a covariation pattern between the contents of OC and TN within different-sized aggregates. Since C and N act on the structural elements of organic matter, the aggregate-associated OC and TN contents within aggregates can affect variations in the content of soil organic matter (Cooper et al., 2020). However, TP has different responses to aggregate size. Some studies have demonstrated that aggregate size has no significant effects on TP, which showed a random distribution in different-sized aggregates (Huang K. X. et al., 2020; Wang S. Q. et al., 2021). Notably, consistent with other studies, the soil TP contents of the three stands were spread uniformly throughout the aggregates (Zhang et al., 2022). P is a sedimentary mineral that readily mixes in soil with iron (Fe) and aluminum (Al) but is not utilized by plants (Dong et al., 2020). In this study, the change in soil TP content lagged behind the soil OC and TN contents at aggregate scale, indicating that soil TP content is a limiting nutrient. In addition, the soil TP content was relatively low (Table 2) due to the relatively fixed P sources, which is a common phenomenon in subtropical China (Tong et al., 2021). Meanwhile, the soil in southern China is typically acidic, and the utilization of soil TP for plant growth is commonly low in these subtropical regions (Hou et al., 2020; Zhang et al., 2022).

Stand conversion could affect soil physicochemical properties and soil nutrient inputs due to variations in forest structure and tree species composition by changing litterfall quality and tree root exudates (Koutika et al., 2020). Our findings demonstrated that mixed stands, particularly mixed Chinese fir with *M. macclurei* plantations, significantly enhanced the accumulation of aggregate-related OC and nutrients compared to pure stands. The promotion of mixed stands was mainly driven by the higher soil aggregate stability and increased litter volumes, which are key factors for improving soil structure and organic matter content accumulation by regulating microbial communities, thereby increasing the soil OC and TN contents in aggregates (Huang K. X. et al., 2020; Gao et al., 2022). Moreover, the litter quality and root distribution of *M. macclurei* were better than those of *M. laosensis* and Chinese fir; therefore, *M. macclurei* has a stronger capacity for nutrient return and availability to plant residue decomposition and stimulates

organic matter production for soil aggregation (Xu et al., 2020; Wang S. Q. et al., 2021).

4.3. Aggregate-associated stoichiometric ratios under different stand types

Generally, stoichiometric ratios, as key parameters of soil fertility and quality, are important for determining the cycling and limitation of chemical elements (Wang et al., 2022). The C/N rate impacts organic matter degradation according to the study by Six and Paustian (2014). In this current research, C/N was higher in <0.25 mm aggregates across various stands, suggesting that the organic matter in the <0.25 mm aggregates was more stable and older than that in other sized aggregates, confirming the results of the study from Six et al. (2004). Our research found that the contents of OC and TN were also higher in the aggregate of <0.25 mm across various stand types, but the TP content was even in diverse-sized aggregates. This result is because P has selective adsorption properties on aggregates of different particle sizes (Huang Y. Z. et al., 2020). A coordinated trend was visible in the OC and TN components that were related to aggregates (Figure 4A). Thus, the present study indicated that the responses of C/P and N/P to different aggregate sizes mainly determined the responses of OC and TN to the different-sized aggregates. Despite the results being consistent with those of the studies from Cui et al. (2021), previous studies have reported that the aggregate distribution can influence the key biogeochemical cycling of N and P. The high ratio of C/N improves OC as well as nutrient retention in the short term (Six and Paustian, 2014). Moreover, C/P and N/P can be widely used to represent the vegetation constraints by nutrient demand and soil nutrient supply. The aggregate-related C/N and C/P were considerably higher in the mixed stands than in the pure stand at both depths, favoring OC and nutrient accumulation. Our most recent findings relate to the mechanisms described in the paragraphs below. This result may have occurred as a result of the higher soil aggregate stability in mixed stands, which offered physical protection for soil organic matter and nutrients (Six et al., 2004). More importantly, our study suggested that the contents of OC, TN, and TP in mixed stands had significantly greater distributions than those in pure stands, increasing the inputs of organic matter in the mixed stands (Wang Z. C. et al., 2021). The introduction of broadleaf trees into monoculture coniferous stands (Chinese fir) can improve plant species composition and diversity to increase quantity and quality of litterfall and soil nutrient return (Tan et al., 2022). Additionally, *M. laosensis* and *M. macclurei* produce litterfall residues of greater quality than Chinese fir, promoting the growth and reproduction of soil microorganisms or increasing enzyme activity (Wang S. Q. et al., 2021). Previous studies confirmed that the C:N:P ratio in the >2 mm aggregates among mixed stands notably increased (Xu et al., 2020), resulting in a lower consumption of soil OC and nutrients and a greater nutrient availability in mixed stands.

Among the three CFPs, the mean ratio of the soil C/N ratio (16.28) was higher than the mean soil in China (14.3) and the mean soil globally (11.9), while the mean ratios of C/P (76.93) and N/P (4.54) were lower than the average soil in China (136.93 and 186.13, respectively) and the average soil globally (Tian et al., 2010;

Tang and Wang, 2022). This result indicated that the organic matter decomposition rates were relatively low and that soil specimens in the study site were possibly limited by the OC or TN contents. This result may be due to the fast growth of Chinese fir, and many soil nutrients are supplied, generally leading to soil nutrient limitations. Moreover, these results were mainly related to the low levels of OC and nutrients. The average soil OC, TN, and TP contents across all stand types in this study were 18.95, 1.10, and 0.25 g kg⁻¹, respectively. These values were lower than the average soil OC, TN, and TP contents in China, which were 30.40, 2.21, and 0.20–1.10 g kg⁻¹, respectively (Tian et al., 2010). Early studies have indicated that N is regarded as a common nutrient limitation in the CFPs of Guangxi (Tong et al., 2020; Tang and Wang, 2022), while China has one of the highest N levels reported worldwide, especially in subtropical forests (Wang et al., 2018). This study site with long-term high temperatures and heavy rainfall has experienced surface weathering and erosion, which accelerated significant losses in the contents of OC and TN, thus resulting in lower C/P and N/P with the limitations of OC and TN.

4.4. Aggregate-associated OCS, TNS, and TPS under different stand types

In this study, the OCS, TNS, and TPS in the >2 mm aggregates were the highest, indicating that the >2 mm aggregates mainly carried soil OC and nutrients. Thus, this finding supports our first hypothesis. Generally, the OCS, TNS, and TPS distributions were closely related to their contents with aggregate size (Egan et al., 2018). The >2 mm aggregates had the lowest contents of C–N–P (Figure 5) but made the largest contributions to the OCS, TNS, and TPS (Supplementary Figure 1). The turnover time of the OC content in the >2 mm aggregates was shorter than that in the <0.25 mm aggregates, thus promoting the higher OCS in >2 mm aggregates (Lu et al., 2019; Wang et al., 2023). In addition, it is considered that the litter residues are easily combined with >2 mm aggregates (Six et al., 2004). According to this research, aggregate-associated OCS, TNS, and TPS would be influenced by aggregate size, not the aggregate-associated OC, TN, and TP contents. Thus, >2 mm aggregates were the greatest contributors to the OCS, TNS, and TPS, as evidenced by the highest composition of >2 mm aggregates compared with the other fractions (Figure 2). Our result was confirmed in previous study findings (Wu et al., 2022).

In comparison to pure stands, mixed stands showed greater levels of OCS (Figure 5A), TNS (Figure 5B), and TPS (Figure 5C) among the different-sized aggregates, suggesting that mixed stands were better able to store OC and nutrients. Due to the stability of the soil aggregates, mixed stands in this study had much higher tree height and diameter with litter quantities than did pure stands, which increased the ability of the plantations to intercept rainwater and lessened the effects of leaching. Moreover, stable soil aggregates can store more organic matter and nutrients, thereby achieving soil fertilizer retention (Gelaw et al., 2015). The successive cropping of CFPs resulted in excessive accumulation of alleles and relatively low accumulation rates of soil organic matter, which caused the occurrence of self-toxicity, influenced soil enzyme activity and decreased soil fertility (Huang et al., 2000), thus returning fewer nutrients to the soil. Overall, the above explanation

of the mechanism supports our second hypothesis. Notably, OCS, TNS and TPS within 0.25–1 mm and 1–2 mm aggregates in mixed stands were greater than those in pure stand (Figure 5), but the percentage contribution of OCS, TNS and TPS in 0.25–1 mm and 1–2 mm aggregates to bulk soil in pure stand were greater than that in mixed stands (Supplementary Figure 1). This may be owing to the significant higher proportion of 0.25–1 mm and 1–2 mm aggregates in pure stand. Consequently, based on our results, the effect of stand type on the OCS, TNS and TPS within soil aggregates seem to be mostly depended on the composition of different soil sized aggregates.

4.5. Soil aggregate stability as influenced by soil ecological stoichiometric characteristics

In this study, the stability of soil aggregates in mixed stands was dramatically greater than that in pure stands, which positively affected OC and nutrient accumulation. Thus, the stability of aggregates may be influenced by forest management, mixed plantation structure and tree species. This is likely because mixed stands have improved stand structural heterogeneity, species richness and litter amount. Moreover, mixed stands improve soil structure to reduce nutrient loss from the soil. Similarly, our results were confirmed by RDA (Figure 6) and Pearson's correlation analysis (Supplementary Figure 2). Likewise, there is a notably positive correlation between soil aggregate stability and the contents of TN with TP, TPS, in addition to the C/N ratio. The results of this study differed from those of Mao et al. (2021), who found that the contents of OC and TN can have a significant impact on soil aggregate stability across different stand ages of CFPs. Rather, this study found that the C/N ratio and TN content in 0–20 cm (Figure 6A) and 20–40 cm (Figure 6B), respectively, were the main key factors of variation in soil aggregate stability across various stands. The soil C/N ratio is considered the best predictor of soil aggregate stability, and the impacts of the soil C/N ratio on soil aggregate stability have been reported (Liu et al., 2020). The higher soil C/N ratio could reduce the degree of humification to increase the retention of organic matter. Similarly, higher contents of OC and nutrients were found in mixed stands, while this result can be explained by the greater organic matter input in mixed stands. Generally, soil aggregate stability is strongly associated with organic matter. Organic matter plays a critical role in the cementing agents of soil aggregation, and it has an impact on soil aggregation stabilization. Moreover, C and N are structural elements of organic matter, which can provide material for soil aggregation (Cooper et al., 2020). Our results showed that the accumulation and decomposition of the OC and TN in soil were relatively consistent and probably limiting elements of plant growth, especially TN. In addition, soil TN has a significant positive correlation with soil aggregate stability (Zhu et al., 2021). In particular, the study site has been affected by strong weathering due to extreme heat and rainfall, resulting in the P limitation of the regional soils, which affects plant growth and causes a decrease in organic matter inputs; thus, soil aggregate stability declines (Wu et al., 2018; Zhang et al., 2022). As a result, the four parameters, including the C/N ratio, the TN and TP concentrations, and the TPS, had a substantial impact on

soil aggregate stability with stand type in CFPs. Specifically, the TN content and C/N ratio were key contributors affecting soil aggregate stability in the three stands, which supports our third hypothesis.

5. Conclusion

Irrespective of the diverse stand types of CFPs, the soil OC and TN contents together with the C/N, C/P, and N/P ratios significantly increased as the aggregate size decreased in all soil profiles, but the OCS, TNS, and TPS showed clearly opposite trends. At the aggregate scale, mixed CFPs with *M. laosensis* and mixed CFPs with *M. macclurei* had better soil aggregate stability and nutrient conditions than did pure CFPs at both soil depths. The soil C/N ratio in this research region was higher than that in other CFP planted regions in China and around the world, while the C/P and N/P ratios were much lower, indicating lower OC and TN contents, especially TN content. In addition, soil aggregate stability was dominantly influenced by the C/N ratio, TN, TP, and TPS. Therefore, the present research is conducive to providing supplementary information for our understanding of promoting degraded soil restoration and sustainable forest management in global forest ecosystems.

Data availability statement

The raw data supporting the conclusions of this article will be made available by the authors, without undue reservation.

Author contributions

YH: investigation, data curation, experimental results analysis, and writing—original draft. QZ: conceptualization, investigation, methodology, and experimental results analysis. CJ: investigation, methodology, data processing, and visualization. YL: conceptualization, data curation, and writing—reviewing and editing. HZ: investigation, validation, and writing—reviewing and editing. SY: conceptualization, supervision, and writing—reviewing and editing. All authors contributed to the article and approved the submitted version.

Funding

This research was supported by the National Natural Science Foundation of China (Grant Numbers: 31460196 and 32260382).

Acknowledgments

We greatly appreciate American Journal Experts (www.aje.cn) for their language editing assistance during the preparation of this manuscript. This manuscript has previously been preprinted (He et al., 2022).

Conflict of interest

The authors declare that the research was conducted in the absence of any commercial or financial relationships that could be construed as a potential conflict of interest.

Publisher's note

All claims expressed in this article are solely those of the authors and do not necessarily represent those of their affiliated

organizations, or those of the publisher, the editors and the reviewers. Any product that may be evaluated in this article, or claim that may be made by its manufacturer, is not guaranteed or endorsed by the publisher.

Supplementary material

The Supplementary Material for this article can be found online at: <https://www.frontiersin.org/articles/10.3389/ffgc.2023.1141953/full#supplementary-material>

References

- Bray, R. H., and Kurtz, L. T. (1945). Determination of total, organic, and available forms of phosphorus in soils. *Soil Sci.* 59, 39–46. doi: 10.1097/00010694-194501000-00006
- Bremner, J. M. (1996). "Nitrogen-total," in *Methods of soils analysis: Chemical methods*, Part 3, ed. D. L. Sparks (Madison, WI: American Society of Agronomy), 1085–1121.
- Cooper, J., Greenberg, I., Ludwig, B., Hippich, L., Fischer, D., Glaser, B., et al. (2020). Effect of biochar and compost on soil properties and organic matter in aggregate size fractions under field conditions. *Agr. Ecosyst. Environ.* 295:106882. doi: 10.1016/j.agee.2020.106882
- Cui, H., Ou, Y., Wang, L. X., Liang, A. Z., Yan, B. X., and Li, Y. X. (2021). Dynamic changes in microbial communities and nutrient stoichiometry associated with soil aggregate structure in restored wetlands. *Catena* 197:104984. doi: 10.1016/j.catena.2020.104984
- Dong, Z. W., Li, C. J., Li, S. Y., Lei, J. Q., Zhao, Y., and Umut, H. (2020). Stoichiometric features of C, N, and P in soil and litter of Tamarix cones and their relationship with environmental factors in the Taklimakan Desert, China. *J. Soil Sediments* 20, 690–704. doi: 10.1007/s11368-019-02481-6
- Egan, G., Crawley, M. J., and Fornara, D. A. (2018). Effects of long-term grassland management on the carbon and nitrogen pools of different soil aggregate fractions. *Sci. Total Environ.* 614, 810–819. doi: 10.1016/j.scitotenv.2017.09.165
- Eynard, A., Schumacher, T. E., Lindstrom, M. J., and Malo, D. D. (2005). Effects of agricultural management systems on soil organic carbon in aggregates of Ustolls and Usterts. *Soil Tillage Res.* 81, 253–263. doi: 10.1016/j.still.2004.09.012
- Faustino, L. L., Marciano, C. R., and Alves, M. C. (2020). Morphometry and size distribution of aggregates from a Typic Hapludult soil under natural secondary forest, implanted leguminous trees and degraded pasture in the Atlantic coast of Brazil. *Geoderma Reg.* 23:e00350. doi: 10.1016/j.geodrs.2020.e00350
- Feng, H. J., Wang, S. Y., Gao, Z. D., Pan, H., Zhuge, Y. P., Ren, X. Q., et al. (2021). Aggregate stability and organic carbon stock under different land uses integrally regulated by binding agents and chemical properties in saline-sodic soils. *Land Degrad. Dev.* 32, 4151–4161. doi: 10.1002/ldr.4019
- Feng, Y., Han, S. J., Wei, Y. Q., Xiao, J. Z., Geng, S. C., Gu, Y., et al. (2020). Comparative study of lignin stabilizing mechanisms in soil aggregates at virgin mixed broadleaf-pine forest and secondary broadleaf forest at Changbai Mountain Nature Reserve, Northeast China. *Ecol. Indic.* 117:106665. doi: 10.1016/j.ecolind.2020.106665
- Gao, G. N., Huang, X. M., Xu, H. C., Wang, Y., Shen, W. J., Zhang, W., et al. (2022). Conversion of pure Chinese fir plantation to multi-layered mixed plantation enhances the soil aggregate stability by regulating microbial communities in subtropical China. *For. Ecosyst.* 9:100078. doi: 10.1016/j.fecs.2022.100078
- Gelaw, A. M., Singh, B. R., and Lal, R. (2015). Organic carbon and nitrogen associated with soil aggregates and particle sizes under different land uses in Tigray, Northern Ethiopia. *Land Degrad. Dev.* 26, 690–700. doi: 10.1002/ldr.2261
- Guo, Y. F., Fan, R. Q., Zhang, X. P., Zhang, Y., and Liang, A. Z. (2020). Tillage-induced effects on SOC through changes in aggregate stability and soil pore structure. *Sci. Total Environ.* 703:134617.
- He, Y. Q., Zhang, Q. C., Jiang, C. Y., Lan, Y. H., Zhang, H., and Ye, S. M. (2022). Variations in soil aggregate stability and aggregate-associated C-N-P stoichiometry by stand type in Chinese fir. *Authorea*. [preprint]. doi: 10.22541/au.166091773.32293720/v1
- Hou, E. Q., Luo, Y. Q., Kuang, Y. W., Chen, C. G., Lu, X. K., Jiang, L. F., et al. (2020). Global meta-analysis shows pervasive phosphorus limitation of aboveground plant production in natural terrestrial ecosystems. *Nat. Commun.* 11:637. doi: 10.1038/s41467-020-14492-w
- Huang, K. X., Tang, X. Y., Qin, H., He, S. C., Ye, S. M., and Huang, D. W. (2020). Effect of close-to-nature management on carbon and nitrogen accumulation of ground cover and soil in *Cunninghamia lanceolata* plantations. *Ecol. Environ. Sci.* 29, 1556–1565. doi: 10.16258/j.cnki.1674-5906.2020.08.007
- Huang, Y. Z., Wang, S. Q., and Ye, S. M. (2020). Effects of *Cunninghamia lanceolata* stand types on the changes of aggregate-related organic carbon and nutrients in surface soil. *Chin. J. Appl. Ecol.* 31, 2857–2865. doi: 10.13287/j.1001-9332.202009.003
- Huang, Z. Q., Liao, L. P., and Wang, S. L. (2000). Allelopathy of phenolics from decomposing stump roots in replant Chinese fir woodland. *J. Chem. Ecol.* 26, 2211–2219. doi: 10.1023/A:1005580718765
- Kerdran, D., Drewer, J., Chung, A. Y. C., Majalap, N., Slade, E. M., Brechet, L., et al. (2020). Litter inputs, but not litter diversity, maintain soil processes in degraded tropical forests-across-continental comparison. *Front. For. Glob. Change* 2:90. doi: 10.3389/ffgc.2019.00090
- Kong, T. W., Liu, B., Mark, H., Zhou, W. Y., Su, Y. H., Wang, S., et al. (2022). Effects of shelterbelt transformation on soil aggregates characterization and erodibility in China black soil farmland. *Agriculture* 12:1917. doi: 10.3390/agriculture12111917
- Koutika, L. S., Cafiero, L., Bevivino, A., and Merino, A. (2020). Organic matter quality of forest floor as a driver of C and P dynamics in acacia and eucalypt plantations established on a Ferralic Arenosols, Congo. *For. Ecosyst.* 7, 511–525. doi: 10.1186/s40663-020-00249-w
- Li, C., Yu, Z. Z., Lin, J., Meng, M. J., Zhao, Y. P., Jia, Z. H., et al. (2022). Forest conversion and soil depth can modify the contributions of organic and inorganic colloids to the stability of soil aggregates. *Forests* 13:546. doi: 10.3390/f13040546
- Li, Q., Hu, W. F., Li, L. F., and Li, Y. C. (2023). Interactions between organic matter and Fe oxides at soil micro-interfaces: Quantification, associations, and influencing factors. *Sci. Total Environ.* 855:158710. doi: 10.1016/j.scitotenv.2022.158710
- Liu, D. D., Ju, W. L., Jin, X. L., Li, M. D., Shen, G. T., Duan, C. J., et al. (2021). Associated soil aggregate nutrients and controlling factors on aggregate stability in semiarid grassland under different grazing prohibition timeframes. *Sci. Total Environ.* 777:146104. doi: 10.1016/j.scitotenv.2021.146104
- Liu, Y. J., Peng, S. G., Xiao, Y. S., Xiang, P. H., Tang, C. G., Zhou, Q. M., et al. (2020). Stability of soil aggregate and its relationship with carbon nitrogen ratio in rice-tobacco rotation areas in Hunan province. *Acta Tabacaria Sin.* 26, 75–83. doi: 10.16472/j.chinatobacco.2019.272
- Lu, M. Z., Yang, M. Y., Yang, Y. R., Wang, D. L., and Sheng, L. X. (2019). Soil carbon and nutrient sequestration linking to soil aggregate in a temperate fen in Northeast China. *Ecol. Indic.* 98, 869–878. doi: 10.1016/j.ecolind.2018.11.054
- Lu, R. K. (1999). *Analytical methods of soil agrochemistry*. Beijing: China Agricultural Science and Technology Publishing House, 18–99.
- Ma, Y., Cheng, X. Q., Kang, F. F., and Han, H. R. (2022). Effects of thinning on soil aggregation, organic carbon and labile carbon component distribution in Larix principis-rupprechtii plantations in North China. *Ecol. Indic.* 139:108873. doi: 10.1016/j.ecolind.2022.108873
- Mao, L., Tang, L. L., Ye, S. M., and Wang, S. Q. (2021). Soil organic C and total N as well as microbial biomass C and N affect aggregate stability in a chronosequence of Chinese fir plantations. *Eur. J. Soil Biol.* 106:103347. doi: 10.1016/j.ejsobi.2021.103347
- Meng, M. J., Li, C., Zhao, Y. P., Lin, J., Liu, X., Jia, Z. H., et al. (2022). Long-term forest conversion affects soil stability and humic substances in aggregate fractions in subtropical China. *Forests* 13:339. doi: 10.3390/f13020339
- Nelson, D. W., and Sommers, L. E. (1996). "Total carbon, organic carbon and organic matter," in *Methods of soil analysis*, Part 3, ed. D. L. Sparks (Ankeny: American Society of Agronomy), 961–1010.

- Picariello, E., Baldantoni, D., Izzo, F., Langella, A., and Nicola, F. D. (2021). Soil organic matter stability and microbial community in relation to different plant cover: A focus on forests characterizing Mediterranean area. *Appl. Soil Ecol.* 162:103897. doi: 10.1016/j.apsoil.2021.103897
- Rivera, J. I., and Bonilla, C. A. (2020). Predicting soil aggregate stability using readily available soil properties and machine learning techniques. *Catena* 187:104408. doi: 10.1016/j.catena.2019.104408
- Sarker, T. C., Incerti, G., Spaccini, R., Piccolo, A., Mazzoleni, S., and Bonanomi, G. (2018). Linking organic matter chemistry with soil aggregate stability: Insight from ^{13}C NMR spectroscopy. *Soil Biol. Biochem.* 117, 175–184. doi: 10.1016/j.soilbio.2017.11.011
- Shen, Y. F., Cheng, R. M., Xiao, W. F., and Yang, S. (2021). Effects of understory removal and thinning on soil aggregation, and organic carbon distribution in *Pinus massoniana* plantations in the three Gorges Reservoir area. *Ecol. Indic.* 123:107323. doi: 10.1016/j.ecolind.2020.107323
- Six, J., and Paustian, K. (2014). Aggregate-associated soil organic matter as an ecosystem property and a measurement tool. *Soil Biol. Biochem.* 68, A4–A9. doi: 10.1016/j.soilbio.2013.06.014
- Six, J., Bossuyt, H., Degryze, S., and Deneff, K. (2004). A history of research on the link between (micro) aggregates, soil biota, and soil organic matter dynamics. *Soil Tillage Res.* 79, 7–31.
- Smith, A. P., Marín-Spiotta, E., Graaff, M. A., and Balsler, T. C. (2014). Microbial community structure varies across soil organic matter aggregate pools during tropical land cover change. *Soil Biol. Biochem.* 77, 292–303. doi: 10.1016/j.soilbio.2014.05.030
- Tan, X. M., Zhang, W., Xiao, N., Mo, X. Q., Gao, G. N., You, Y. M., et al. (2022). Effects of understory plant species composition and diversity under transforming Chinese fir into precious indigenous broadleaf plantations. *Acta Ecol. Sin.* 42, 2931–2942. doi: 10.5846/stxb202102060383
- Tang, L. L., and Wang, S. Q. (2022). Dynamics of soil aggregate-related C-N-P stoichiometric characteristics with stand age and soil depth in Chinese fir plantations. *Land Degrad. Dev.* 33, 1290–1306. doi: 10.1002/ldr.4217
- Tang, L. L., Mao, L., Wang, Z. Y., Ye, S. M., and Wang, S. Q. (2023). Mixed with broadleaf tree species improved soil aggregate stability in Chinese Fir (*Cunninghamia lanceolata*) plantations: Based on the Le Bissonnais method. *J. Soil Sci. Plant Nutr.* doi: 10.1007/s42729-023-01166-x
- Tian, H. Q., Chen, G. S., Zhang, C., Melillo, J. M., and Hall, C. A. S. (2010). Pattern and variation of C:N:P ratios in China's soils: A synthesis of observational data. *Biogeochemistry* 98, 139–151. doi: 10.1007/s10533-009-9382-0
- Tong, R., Wu, T. G., Jiang, B., Wang, Z. G., Xie, B. L., and Zhou, B. Z. (2021). Soil carbon, nitrogen, and phosphorus stoichiometry and its influencing factors in Chinese fir plantations across subtropical China. *Front. For. Glob. Change* 27:1086328. doi: 10.3389/ffgc.2022.1086328
- Tong, R., Zhou, B. Z., Jiang, L., Ge, X. G., and Cao, Y. H. (2020). The growth of Chinese fir is limited by nitrogen: Evidences from N:P ratio, N or P variability and NuRE based on a regional investigation. *For. Ecol. Manage.* 460:117905. doi: 10.1016/j.foreco.2020.117905
- Wang, J. X., Lan, J. C., Long, Q. X., Wang, S. S., Qi, X., and Huang, M. Z. (2023). Soil organic carbon transfer in aggregates subjected to afforestation in karst region as indicated by ^{13}C natural abundance. *For. Ecol. Manage.* 531:120798. doi: 10.1016/j.foreco.2023.120798
- Wang, L. J., Wang, P., Sheng, M. Y., and Tian, J. (2018). Ecological stoichiometry and environmental influencing factors of soil nutrients in the karst rocky desertification ecosystem, southwest China. *Glob. Ecol. Conserv.* 16:e00449. doi: 10.1016/j.gecco.2018.e00449
- Wang, S. Q., Huang, Y. Z., and Ye, S. M. (2021). Distribution of organic carbon and nutrients in soil aggregates under different stand types of *Cunninghamia lanceolata* in southern Guangxi of China. *Soil Sci. Plant Nutr.* 67, 427–438. doi: 10.1080/00380768.2021.1932585
- Wang, S. Q., Yao, X. Y., and Ye, S. M. (2020). Soil aggregate-related organic carbon and relevant enzyme activities as affected by tea (*Camellia sinensis* L.) planting age in hilly region of southern Guangxi, China. *Appl. Soil Ecol.* 150:103444.
- Wang, Y., Zheng, Y., Liu, Y., Huang, J., and Mantimin, A. (2022). Spatial prediction models for soil stoichiometry in complex terrains: A case study of Schrenk's spruce forest in the Tianshan mountains. *Forests* 13:1407. doi: 10.3390/f13091407
- Wang, Z. C., He, G. X., Hou, Z. H., Luo, Z., Chen, S. X., Lu, J., et al. (2021). Soil C:N:P stoichiometry of typical coniferous (*Cunninghamia lanceolata*) and/or evergreen broadleaved (*Phoebe bournei*) plantations in south China. *For. Ecol. Manage.* 486:118974. doi: 10.1016/j.foreco.2021.118974
- Wu, W., Zheng, Z. C., Li, T. X., He, S. Q., Zhang, X. Z., Wang, Y. D., et al. (2018). Distribution of inorganic phosphorus fractions in water-stable aggregates of soil from tea plantations converted from Farmland in the Hilly region of western Sichuan, China. *J. Soils Sediments* 18, 906–916. doi: 10.1007/s11368-017-1834-x
- Wu, Y., Wang, Q., Wang, H. M., Wang, W. J., Zhong, Z. L., and Di, G. L. (2022). Effects of poplar shelterbelt plantations on soil aggregate distribution and organic carbon in northeastern China. *Forests* 13:1546. doi: 10.3390/f13101546
- Xie, J., Peng, B., Wang, R., Batbayar, J., Hoogmoed, M., Yang, Y., et al. (2018). Responses of crop productivity and physical protection of organic carbon by macroaggregates to long-term fertilization of an Anthroisol. *Eur. J. Soil Sci.* 69, 555–567. doi: 10.1111/ejss.12546
- Xu, C. Y., Pu, L. J., Li, J. G., and Ming, Z. (2019). Effect of reclamation on C, N, and P stoichiometry in soil and soil aggregates of a coastal wetland in eastern China. *J. Soils Sediments* 19, 1215–1225. doi: 10.1007/s11368-018-2131-z
- Xu, H. D., Yuan, H. J., Yu, M. K., and Cheng, X. G. (2020). Large macroaggregate properties are sensitive to the conversion of pure plantation to uneven-aged mixed plantations. *Catena* 194:104724. doi: 10.1016/j.catena.2020.104724
- Yang, H. B., Vina, A., Winkler, J. A., Chung, M. G., Huang, Q. Y., Dou, Y., et al. (2021). A global assessment of the impact of individual protected areas on preventing forest loss. *Sci. Total Environ.* 777:145995. doi: 10.1016/j.scitotenv.2021.145995
- Yao, Y., Chen, J. D., Li, F., Sun, M. W., Yang, X. C., Wang, G., et al. (2022). Exchangeable Ca^{2+} content and soil aggregate stability control the soil organic carbon content in degraded Horqin grassland. *Ecol. Indic.* 134:108507. doi: 10.1016/j.ecolind.2021.108507
- You, Y. M., Xu, H. C., Wu, X. P., Zhou, X. G., Tan, X. M., Li, M., et al. (2020). Native broadleaf tree species stimulate topsoil nutrient transformation by changing microbial community composition and physiological function, but not biomass in subtropical plantations with low P status-ScienceDirect. *For. Ecol. Manage.* 477:118491. doi: 10.1016/j.foreco.2020.118491
- Zhang, J. H., Li, M. X., Xu, L., Zhu, J. X., Dai, G. H., and He, N. P. (2021). C:N:P stoichiometry in terrestrial ecosystems in China. *Sci. Total Environ.* 795:148849. doi: 10.1016/j.scitotenv.2021.148849
- Zhang, Y., Shengzhe, E., Wang, Y. N., Su, S. M., Bai, L. Y., Wu, C. X., et al. (2021). Long-term manure application enhances the stability of aggregates and aggregate-associated carbon by regulating soil physicochemical characteristics. *Catena* 203:105342. doi: 10.1016/j.catena.2021.105342
- Zhang, Z., Huang, Y. Z., He, X. X., Ye, S. M., and Wang, S. Q. (2022). Dynamics of soil inorganic phosphorus fractions at aggregate scales in a chronosequence of Chinese fir plantations. *J. Moun. Sci.* 19, 136–150. doi: 10.1007/s11629-021-6813-4
- Zhao, Z. H., Gao, S. F., Lu, C. Y., Li, X. Y., Li, F., and Wang, T. Y. (2021). Effects of different tillage and fertilization management practices on soil organic carbon and aggregates under the rice-wheat rotation system. *Soil Till. Res.* 212:105071. doi: 10.1016/j.still.2021.105071
- Zhou, L., Sun, Y. J., Saeed, S., Zhang, B., and Luo, M. (2020). The difference of soil properties between pure and mixed Chinese fir (*Cunninghamia lanceolata*) plantations depends on tree species. *Glob. Ecol. Conserv.* 22:e01009. doi: 10.1016/j.gecco.2020.e01009
- Zhou, M., Liu, C. Z., Wang, J., Meng, Q. F., Yuan, Y., Ma, X. F., et al. (2020). Soil aggregates stability and storage of soil organic carbon respond to cropping systems on Black Soils of Northeast China. *Sci. Rep.* 10:265. doi: 10.1038/s41598-019-57193-1
- Zhu, G.-y., Shangguan, Z.-p., and Deng, L. (2021). Variations in soil aggregate stability due to land use changes from agricultural land on the Loess Plateau, China. *Catena* 200:105181. doi: 10.1016/j.catena.2021.105181



OPEN ACCESS

EDITED BY

Jess K. Zimmerman,
University of Puerto Rico, Puerto Rico

REVIEWED BY

Przemyslaw Zelazowski,
University of Warsaw, Poland
Sebastian Martinuzzi,
University of Wisconsin-Madison, United States

*CORRESPONDENCE

Shaoqiang Wang
✉ sqwang@igsnr.ac.cn
Hao Shi
✉ haoshi@rcees.ac.cn

SPECIALTY SECTION

This article was submitted to
Forest Disturbance,
a section of the journal
Frontiers in Forests and Global Change

RECEIVED 15 February 2023

ACCEPTED 30 March 2023

PUBLISHED 17 April 2023

CITATION

Chen J, Wang S, Shi H, Chen B, Wang J,
Zheng C and Zhu K (2023) Radiation and
temperature dominate the spatiotemporal
variability in resilience of subtropical
evergreen forests in China.
Front. For. Glob. Change 6:1166481.
doi: 10.3389/ffgc.2023.1166481

COPYRIGHT

© 2023 Chen, Wang, Shi, Chen, Wang, Zheng
and Zhu. This is an open-access article
distributed under the terms of the [Creative
Commons Attribution License \(CC BY\)](#). The
use, distribution or reproduction in other
forums is permitted, provided the original
author(s) and the copyright owner(s) are
credited and that the original publication in this
journal is cited, in accordance with accepted
academic practice. No use, distribution or
reproduction is permitted which does not
comply with these terms.

Radiation and temperature dominate the spatiotemporal variability in resilience of subtropical evergreen forests in China

Jinghua Chen¹, Shaoqiang Wang^{1,2,3*}, Hao Shi^{4*}, Bin Chen^{1,2},
Junbang Wang^{1,2}, Chen Zheng^{1,2} and Kai Zhu^{1,2}

¹Key Laboratory of Ecosystem Network Observation and Modeling, Institute of Geographic Sciences and Natural Resources Research, Chinese Academy of Sciences, Beijing, China, ²College of Resources and Environment, University of Chinese Academy of Sciences, Beijing, China, ³Key Laboratory of Regional Ecological Process and Environment Evolution, School of Geography and Information Engineering, China University of Geosciences, Wuhan, China, ⁴State Key Laboratory of Urban and Regional Ecology, Research Center for Eco-Environmental Sciences, Chinese Academy of Sciences, Beijing, China

Forest resilience is crucial to the mitigation of climate change, due to the enormous potential of forests to reduce atmospheric carbon dioxide concentrations and the possible conversion of forests from net carbon sinks into carbon sources following external disturbances. Subtropical forests are suffering the highest rates of forest change, but how they are evolving in response to climate change is little known. In this study, we estimated the spatial pattern and temporal trend of the resilience of subtropical evergreen forests in China by applying the lag-one autocorrelation (AC1) method to satellite kernel normalized difference vegetation index (kNDVI) data over the past two decades and identified the influential environmental factors that affect the ecosystem resilience by developing random forest (RF) regression models. The computed long-term AC1 based on kNDVI for the 2001–2020 period depicts considerable spatial variability in the resilience of the subtropical evergreen forests in China, with lower resilience at lower latitudes. The RF regression analysis suggests that the spatial variability in the forest resilience can be re-established by forest and climatic variables, and is largely affected by climate, with the three most influential variables being solar radiation (SR, %incMSE = 20.7 ± 1.8%), vapor pressure deficit (VPD, %incMSE = 13.8 ± 0.2%) and minimum temperature (T_{min} , %incMSE = 13.3 ± 1.2%). Higher forest resilience is more likely to be located in areas with less radiation stress, adequate water availability, and less warming. Trend analysis shows a declining trend for the resilience of subtropical evergreen forests in China since the 2000s but an increasing forest resilience in the last decade, which is mainly dominated by temperature changes, including average and minimum temperatures. Considering the expected warming-dominated period in times of rapid climatic change, we suggest potential critical responses for subtropical forest productivity to the disturbances should be of greater concern in the future.

KEYWORDS

resilience, evergreen forests, kNDVI, spatiotemporal variability, random forest analysis

1. Introduction

Forests cover nearly 30% of the global land surface, or approximately 41 million km². Forest ecosystems play an essential role in global carbon cycle, offsetting one-third of the anthropogenic carbon emissions (Pan et al., 2011; Friedlingstein et al., 2022). They are regarded as a core component of mitigating future climate change. However, forest ecosystems are severely threatened by more frequent and severe disturbances due to climate change. The persistence and functionality of forests are highly dependent on their ability to withstand and recover from environmental disturbances, that is, their resilience (Ibáñez et al., 2019; Forzieri et al., 2022). Resilience is the ability of a system to absorb change and disturbance and recover to pre-disturbance structure and function (Holling, 1973; Bai et al., 2019; Yi and Jackson, 2021). Forest resilience may not withstand an increase in disturbances caused by climate change, resulting in permanent alterations of ecosystems or transitions to non-forest ecosystems when tipping points are reached (Seidl et al., 2017). There is a possibility of the transition of tropical rainforests to savanna due to the trigger of external disturbances (Verbesselt et al., 2016; Lovejoy and Nobre, 2018; Hubau et al., 2020). Moreover, the risk of transitions to alternative ecosystem states becomes a global feature, and extends to higher latitudes (Abis and Brovkin, 2017). Forests hold enormous potential for reducing atmospheric carbon dioxide concentrations (Lewis et al., 2019), but ecosystem transitions could convert net carbon sinks into sources (Hubau et al., 2020), so the resilience of forests is essential to the mitigation of climate change.

Resilience can be characterized by the rate of an ecosystem recovering to equilibrium from disturbances (Scheffer et al., 2009). Theoretically, the recovery rate of an ecosystem after external disturbances can be detected by its internal natural fluctuations. The state fluctuations of the ecosystem resulting from disturbances can reflect the declines in recovery rates through an increase in temporal autocorrelation, i.e., the ecosystem state becomes more correlated in subsequent time (Verbesselt et al., 2016). Thus, the lag-one autocorrelation (AC1), which measures the degree to which adjacent time spans of a given time series are correlated, has been proposed as a gauge of vegetation resilience in several studies (Dakos et al., 2012; Verbesselt et al., 2016; Liu et al., 2019). Higher AC1 represents lower resilience, and the increase in AC1 has been termed as an early-warning signal for critical transition. Empirically, recovery rate can be estimated by fitting the time series of vegetation structure or function to an exponential function, as it recovers toward its previous state after each abrupt negative transition (Smith et al., 2022). Studies on the empirical recovery rate (r) have demonstrated that the theoretical resilience AC1 is related to the empirical resilience r through an exponential relationship, that is, $AC1 = e^{r\Delta t}$, which corroborates the effectiveness of AC1 by the empirical recovery rate from external disturbances (Scheffer et al., 2009; Smith et al., 2022).

Recent studies reveal that global forests have experienced a significant decline in resilience since the early 2000s, but the trends were spatially heterogeneous (Forzieri et al., 2022; Smith et al., 2022). It's shown that (1) tropical, temperate, and arid forests have experienced the significant decreases in resilience,

presumably blamed on increased water scarcity and climate variability, and (2) boreal forests are differently characterized with an overall upward trend in resilience, perhaps benefiting from warming and CO₂ fertilization (Forzieri et al., 2022). Moreover, previous research has explored the possible factors contributing to the regional variations in forest resilience. Boulton et al. (2022) stated that the resilience of the Amazon rainforest was deteriorating faster in areas with less rainfall and closer to human activity. Fang and Zhang (2019) illustrated that tree resilience to drought in the Tibetan Plateau was linked to moisture availability, diurnal temperature range, and growth consistency. Higher moisture has great effects on recovery as regional humidity increases in arid boreal forests (Ibáñez et al., 2019).

Numerous studies focus on the resilience of tropical rainforests due to their importance in providing ecosystem services and complexity in responding to climate change (Cole et al., 2014; Verbesselt et al., 2016). In contrast, subtropical forests are suffering the highest rates of disturbance globally due to the practice of intensive forestry (Hansen et al., 2013), whereas how they are evolving in response to climate change is little known. The knowledge gap regarding the lack of spatial patterns and its mechanism in promoting resilience in subtropical forests remains to be filled.

China has 208 million hectares of forest, of which the southern forests account for about 44.7% (Zhao et al., 2015). The vast hills and mountains of southern China have a warm and humid climate, providing superior natural conditions for forest growth. The subtropical forests in southern China are a crucial component of the carbon sink in the East Asian monsoon region (Yu et al., 2014). Unfortunately, with the intensification of global warming, the forests in southern China are increasingly endangered by numerous disturbances. Since the 21st century, the southern region of China has suffered several consecutive climatic extremes, including the 2008 winter storm, the 2010 spring drought, the 2013 heat waves (Zhang et al., 2012; Huang et al., 2013; Pei et al., 2013), and the recent 2022 heat waves. Experimental evidence of increased extreme weather is raising concerns about variability in the resilience of the evergreen forests in southern China; further assessment of the resilience of these forests is still required to fully comprehend the response of ecosystems in China to climate change.

Here, we estimate the resilience from a time series of satellite-based vegetation index data to investigate the spatial pattern of subtropical evergreen forest resilience over the past two decades in southern China. The objectives of this study are to (1) quantify the resilience and its trend in subtropical evergreen forests, and (2) reveal the key drivers of forest resilience. The kernel normalized difference vegetation index (kNDVI), which has recently been suggested as a reliable substitute for ecosystem productivity (Camps-Valls et al., 2021), is used here as an appropriate metric to represent ecosystem function. Specifically, we computed the AC1 as a resilience indicator from satellite-based kNDVI data for the 2001–2020 period at 0.05° spatial resolution, and developed random forest regression models to identify the interplay of environmental drivers that affect the ability of ecosystems to recover from disturbances.

2. Materials and methods

2.1. Study area

Southern China (97°31′–122°57′E, 18°10′–34°14′N) includes the enormous region bordered by the Qinling–Huaihe Line to the north and the Qinghai–Tibet Plateau to the west (Figure 1). The topography of the region varies greatly from east to west, with plateau and basins dominating in the west and plains and hills widespread in the east. The major climate type in the region is subtropical monsoon climate, which is warm and humid. The average annual temperature here is 17.3°C and the average annual precipitation is 1,480 mm during the years 2001–2020. Southern China has a large vegetation cover of around 2.3 million km², 46.1% of which is evergreen forests, including evergreen needleleaf forest (ENF, 26.5%), evergreen broadleaf forest (EBF, 15.8%), and mixed forest (MF, 3.9%) (Wu et al., 2014). The study area is usually accompanied by sufficient rainfall and high temperatures, but seasonal and even extreme drought conditions can occur occasionally.

2.2. Datasets

We collected satellite kNDVI, forest age, and meteorological data from various sources. All input data were resampled to 0.05° of spatial resolution and a monthly time scale, and masked by the evergreen forest cover extracted from the land cover map of China.

2.2.1. kNDVI data

The kNDVI is a newly developed nonlinear generalization of the well-known normalized difference vegetation index (NDVI) by using the kernel method, which exhibits consistently strong correlations with ecosystem productivity (Camps-Valls et al., 2021). kNDVI can be calculated using the following computational equation:

$$kNDVI = \tanh(NDVI^2) \quad (1)$$

Here, kNDVI was used as a functional indicator to detect state changes in forest ecosystems (Hu et al., 2022). The monthly MODIS NDVI product (MOD13C2; Collection 6) at 0.05° spatial resolution from 2001 to 2020 was obtained from the online Data Pool at the USGS Land Processes Distributed Active Archive Centre (LPDAAC).¹ The data quality assessment product (QA-data) of the MOD13C2 product provides pixel-by-pixel information on the cloud conditions and overall data usefulness. We retained cloud-free pixels with good and marginal overall quality.

2.2.2. Forest age

The forest stand age data used in this study was obtained from a map of China's forest stand age with a spatial resolution of 1 km, which was estimated from the remotely sensed forest height in 2005 using the relationship between tree height and forest age from forest inventory data (Zhang C. et al., 2014). The map illustrates that the mean forest age across China was 43 years in 2005. Young and

middle-aged forests occupy the majority of forests in current China. The map also demonstrates a great spatial heterogeneity in China's forest age, with young forests in south and east and old forests in southwest, northwest, and northeast. The forest age across our study area is 36.9 ± 24.8 years. The forest age map was resampled to a 0.5° × 0.5° spatial resolution to match the satellite data.

2.2.3. Meteorological data

The gridded meteorological data, including air temperature, precipitation, solar radiation, and vapor pressure deficit during 2001–2020, were retrieved from the interpolation using the ANUSPLIN software (Hutchinson, 1995) based on 836 meteorological station data from the National Meteorological Information Centre of the China Meteorological Administration (Wang et al., 2017). The gridded meteorological data has 1 km of spatial resolution and an 8-day time step. The station observation data include daily average, maximum, and minimum air temperatures (T_a , T_{min} , and T_{max} in °C), daily total precipitation (Pre in mm), relative humidity (RH in %), and sunshine hour (SH in h). The daily total solar radiation (SR in $W\ m^{-2}$) was acquired from the interpolated sunshine hour data through the use of the solar radiation model developed by Bonan (1989). Vapor pressure deficit (VPD, kPa) was quantified as a function of temperature and relative humidity (Murray, 1966). All meteorological data were interpolated to daily scales using the spline method, and then aggregated into monthly averages or totals (Pre), and spatially resampled to the 0.5° × 0.5° resolution.

2.2.4. Land cover

The land cover data were derived from ChinaCover2010,² a land cover map of China in 2010. The ChinaCover2010 dataset was produced on the basis of Chinese domestic HJ 1A/1B satellite and *in situ* data, and classified by an object-oriented method (Wu et al., 2014). The spatial resolution of ChinaCover2010 is 30 m, and the classification accuracy reaches 85% (Zhang L. et al., 2014). The dataset classifies Chinese land surface into 38 types, including evergreen needleleaf forests (ENF), evergreen broadleaf forests (EBF), and mixed forests (MF). The evergreen forest cover was extracted from the land cover map, which was also resampled to 0.05° spatial resolution using the majority method.

2.3. Resilience indicator of forest ecosystems

We estimated the resilience of forest ecosystems using lag-one autocorrelation (AC1) (Dakos et al., 2015; Verbesselt et al., 2016). The AC1 was computed on the detrended and deseasoned kNDVI time series for each forest pixel. The kNDVI data were detrended and deseasoned through seasonal trend decomposition by loess (STL) (Cleveland et al., 1990; Smith et al., 2022). We used a period of 12 (1 year on monthly scale) and an adaptive loess filter to decompose the full-year signal. Following the rules of thumb originally proposed by Cleveland et al. (1990), we set 23 (1 month less than 2 years) and 13 (1 month more than 1 year) as the values

¹ <http://lpdaac.usgs.gov>

² <http://www.geodata.cn>

for the trend smoother and the low-pass filter, respectively. Thus, the residual time-series term was detrended and deseasoned from the original kNDVI data, and used for the further AC1 calculation. The AC1 computation on the whole kNDVI residual time series (2001–2020) was referred to as long-term AC1. To detect the temporal dynamics of the forest resilience, we also computed AC1 on a monthly scale over 5-year rolling windows over the 2001–2020 period, which was referred to as AC1 time series.

To support the resilience revealed by the kNDVI-based AC1, we applied an empirical method proposed by Smith et al. (2022) to estimate the recovery rate and compared it with the theoretical AC1. Firstly, we applied a 9-month moving window over the residual time series of kNDVI data and calculated the mean difference between the preceding and rest halves of the moving window. We then used a Savitzky–Golay filter (Savitzky and Golay, 1964) to smooth the aforementioned time series for the purpose of eliminating high-frequency noise. Next, values above the 99th percentile were distinguished and the subsequent time spans were labeled as disturbance periods. For each detected disturbance period, we used a 4-month constraint to locate local minima of the residual time series as the starting point of recovery. Finally, we fitted an exponential function to the 5-year time series after the starting point to compute the exponent r , which is regarded as the empirical recovery rate. Subsequently, we performed a comparative analysis between the empirical r and the theoretical one computed via $r_{AC1} = \log(AC1)$.

2.4. Trends analysis of the forest resilience

Mann–Kendall (MK) trend test with Sen's slope estimator was used in this study to analyze the temporal trend of evergreen forest resilience in China over the last two decades. The MK test is a non-parametric model on the basis of the rank system proposed by Mann (1945) and Kendall (1975). For the time series X_1, X_2, \dots, X_n , the MK statistic (S) can be computed as:

$$S = \sum_{i=1}^{n-1} \sum_{j=i+1}^n \text{sgn}(X_j - X_i) \quad (2)$$

where n represents the number of observations, X_i and X_j are the successive information estimation on occasion i and j . sgn represents the sign function given by:

$$\text{sgn}(X_j - X_i) = \begin{cases} 1 & (X_j - X_i) > 0 \\ 0 & (X_j - X_i) = 0 \\ -1 & (X_j - X_i) < 0 \end{cases} \quad (3)$$

Thus, standardized test statistic (Z) can be computed with variance $\text{var}(S)$ by utilizing the following equations:

$$Z = \begin{cases} \frac{S-1}{\sqrt{\text{var}(S)}} & S > 0 \\ 0 & S = 0 \\ \frac{S+1}{\sqrt{\text{var}(S)}} & S < 0 \end{cases} \quad (4)$$

The determined Z values follow the normal distribution and is utilized as a measure of trend significance. Given a significance level of α , the null hypothesis of no trend was rejected when

$|Z| \geq Z_{1-\alpha/2}$, indicating a significant trend of the series. Otherwise, the null hypothesis was accepted at the significance level of α . We here set the significant level $\alpha = 0.05$ and thus $Z_{1-\alpha/2} = 1.96$.

The magnitude of the trend in the data time series was determined using Sen's estimator (Sen, 1968). The Sen's estimator is simple to compute, robust to outliers, and requires limited *priori* information about measurement errors (Fernandes and Leblanc, 2005). The slope of data can be calculated as follows:

$$\beta = \text{Median} \left(\frac{X_j - X_i}{j - i} \right) \quad (5)$$

where β denotes the trend degree, which is used to determine the rise (positive β values) and fall (negative β values) of the time series trend.

To verify the rationality and robustness of the trend analysis, we also applied the univariate stationary first-order Gaussian autoregressive (AR) method, which could avoid the issue that the MK method may not fully account for the temporal autocorrelation (Ives et al., 2021). We fit the time series using the model:

$$X_i(t) = a_i + c_i t + \varepsilon_i(t) \quad (6)$$

where $\varepsilon_i(t)$ is a univariate stationary first-order Gaussian autoregressive process with mean zero for each separate time series, and the vector of $\varepsilon_i(t)$ ($t = 1, 2, \dots, T$) has a multivariate Gaussian distribution [details in Ives et al. (2021)]. This regression model with lag-1 autoregressive error terms for every time series is fitted by Restricted Maximum Likelihood (REML). The AR method was conducted using the remotePARTS package in RStudio.

2.5. Random forest regression analysis of forest resilience

In order to quantify the environmental factors modulating the forest resilience, we applied random forest (RF) regression analysis to explore the relationship between AC1 and explanatory variables. The RF analysis was applied not only for the spatial pattern of the entire long-term AC1, but also for the time series data in each grid cell. The environmental explanatory variables contain forest properties (forest age and annual averaged kNDVI) and climatic variables (temperature, precipitation, solar radiation, and VPD). The climatic variables were expressed as averages and extremes shown in Table 1. All climatic variables were computed annually and then averaged over time as background climate. Maximum and minimum temperatures were collected on a daily scale and integrated for the study period. Maximum precipitation was calculated from the monthly total precipitation, while maximum VPD was the maximum value for the period. These four factors were regarded as extreme climate. Thus, a set of 10 predictor variables representing the forest attribute, background climate, and extreme climate were considered here (Table 1). All environmental variables were calculated for the same period as the long-term AC1 and AC1 time series, respectively, for subsequent spatial and time series analysis.

The existence of multicollinearity among environmental variables produces inconsistent model outputs and reduces the prediction accuracy of the models (Midi and Bagheri, 2010). Therefore, we used variance inflation factor (VIF) in this study

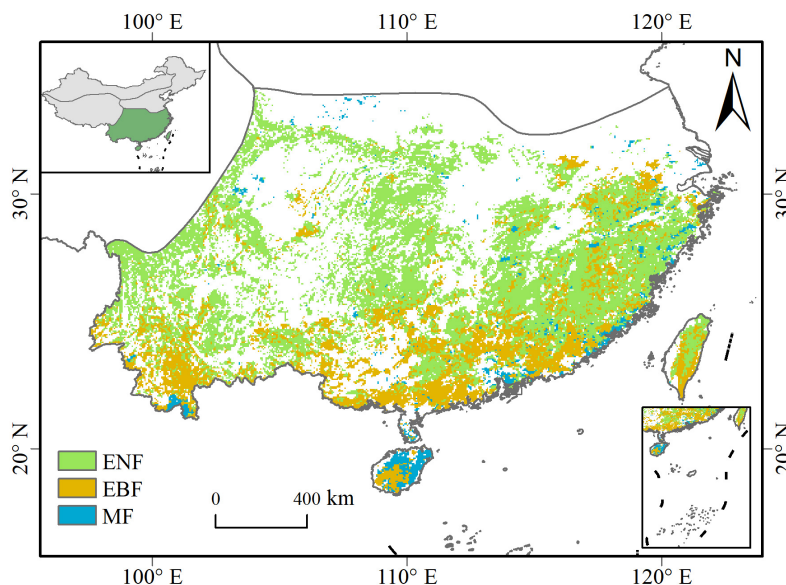


FIGURE 1 Distribution of evergreen forests in Southern China. ENF, evergreen needleleaf forests; EBF, evergreen broadleaf forests; MF, mixed forests.

to detect the multicollinearity among the ten environmental variables and select the least correlated variables before building the regression models. The VIF analysis was conducted, respectively, for the spatial pattern of the environmental variables and the time series of the variables in each grid cell. Several VIF thresholds, i.e., 10, 5, or 3.3, are recommended for selection of variables (Hair et al., 2009; Kock and Lynn, 2012). Given the magnitude of the sample sizes, we fixed the VIF threshold at 3.3 for the spatial grid analysis and at 10 for the time series analysis. We iteratively eliminated the variable with the largest VIF, until the VIFs of all remaining variables were less than the threshold values.

The RF regression models were then developed to identify the emergent relationships between AC1 and the selected forest and climate metrics. We divided the dataset randomly into two subsets to develop the RF model: one training subset with 75% of records used for model calibration, and one test subset with the remaining 25% of records used for model validation. The key

parameters used in the RF model implemented here, including the number of regression trees in the forest, the maximum depth of the tree, the number of features considered at each split and so on, were identified using the method of RandomizedSearchCV algorithm (details in Supplementary Table 1) from Python Scikit-learn package (Pedregosa et al., 2011). The model performances were assessed on the basis of coefficient of determination (R^2), root mean squared error (rMSE), and percentage bias (PBIAS).

Variable importance ranking was synchronously calculated in the RF regression model and used to quantify how individual environmental factors influence the forest resilience (i.e., AC1). The variable importance was quantified by the increase in mean square error of predictions (%IncMSE) caused by scrambling the values of a variable. Larger error before and after permutation indicates that the variable is more important in the forest and contributes more to predictive accuracy than the others (Breiman, 2001). And we explored the AC1 across gradients of influential vegetation and climate features using partial dependence plots, which show the dependence between the response variable and a set of explanatory variables. Partial dependency plots evaluate the impact of each individual driver by holding the impacts of all the other potential drivers constant (Geng et al., 2021). Furthermore, we also used partial correlation analysis to confirm the robustness of the analysis.

TABLE 1 Environmental explanatory variables used in the forest resilience model.

| Variable name | Category | Abbreviation |
|--------------------------------|--------------------|--------------------|
| Forest age | Forest attribute | Age |
| Average annual kNDVI | Forest attribute | kNDVI |
| Average annual temperature | Background climate | T _a |
| Average annual precipitation | Background climate | Pre |
| Average annual solar radiation | Background climate | SR |
| Average annual VPD | Background climate | VPD |
| Minimum temperature | Extreme climate | T _{min} |
| Maximum temperature | Extreme climate | T _{max} |
| Maximum precipitation | Extreme climate | P _{max} |
| Maximum VPD | Extreme climate | VPD _{max} |

3. Results

3.1. Spatial variation of forest resilience in southern China

We explored the long-term lag-one autocorrelation (AC1) at pixel level from the kNDVI time series (2001–2020) for the subtropical evergreen forests in China. Results demonstrate that the evergreen forests exhibit considerable spatial variability in

long-term AC1 (Figure 2A). The long-term AC1 increases with decreasing latitude (Figure 2B), indicating that the resilience of the subtropical evergreen forest may be reduced at lower latitudes. Low-resilience forests are mainly located in the Yunnan-Guizhou plateau, Hainan Island, and the coastal hilly regions. AC1 increases with mean annual temperature under a given precipitation while decreasing with total annual precipitation under a given temperature (Figure 2C). Low resilience (high values in AC1) is observed for temperatures above 18°C and precipitation levels below 1,600 mm. Moreover, higher temperatures (above 24°C) lead to low resilience despite adequate precipitation.

We tested the indication of the kNDVI-based AC1 for the subtropical evergreen forests in China based on an empirical method of detecting disturbances and estimating recovery rates proposed by Smith et al. (2022). The comparison of theoretical and empirical estimates of the recovery rate reveals broad spatial consistency between the theoretical r_{AC1} and the empirical r for areas where the recovery rate can be estimated empirically (Figures 3A, C). The theoretical AC1 and the empirical recovery rate support the theoretically expected exponential relationships (Figure 3B, $R^2 = 0.91$ for the exponential fit). Moreover, the correspondence between theoretical and empirical estimates remains good even if different R^2 thresholds for the exponential fit to the recovering time series after external disturbances are considered (Figure 3D, $R^2 \geq 0.84$ for the exponential fit).

3.2. Driving forces of the spatial variability in forest resilience

A random forest (RF) regression model was developed to identify the relationships between long-term AC1 and the selected forest and climatic metrics. Age, kNDVI, SR, VPD, T_{min} , T_{max} , P_{max} , and VPD_{max} were selected as predictor variables, while T_a and Pre were eliminated due to exceeding the VIF threshold (Supplementary Table 2). The variations in AC1 were well reproduced by the RF model with the predictor variables as input (Supplementary Figure 1). Results of RF analysis show that the spatial variability in long-term AC1 of the evergreen forests in southern China is largely explained by local environmental conditions ($R^2 = 0.70$, $rMSE = 0.0004$, $PBIAS = 0.034$, Figure 4A). The RF regression analysis shows that the most influential predictor of the spatial variability in the evergreen forest resilience is solar radiation (SR), with $\%incMSE = 20.7 \pm 1.8\%$. Vapor pressure deficit (VPD, $\%incMSE = 13.8 \pm 0.2\%$) and minimum temperature (T_{min} , $\%incMSE = 13.3 \pm 1.2\%$) are also important to the forest resilience. SR, VPD, and T_{min} are the major driving forces behind the resilience of subtropical evergreen forests in China among the climatic and biotic factors, accounting for roughly half of the variability in the forest resilience (Figure 4B). The remaining variables are of secondary importance to the forest resilience. The findings of the partial correlation analysis similarly show that SR has the highest partial correlation with the long-term AC1, followed by T_a and T_{min} (Supplementary Figure 2). T_a was excluded from the VIF variable selection due to its high correlation with VPD (Pearson $r = 0.79$, $p < 0.001$, Supplementary Figure 3).

The partial dependence plots (Figure 5) show that the long-term AC1 increased with SR, VPD, and T_{min} , indicating that the forest resilience decreased with the increases in these variables. Low

SR ($< 150 \text{ W m}^{-2}$) leads to high resilience (low AC1) of evergreen forests, while the value of AC1 remains high (low resilience) when $SR > 180 \text{ W m}^{-2}$ (Figure 5A). AC1 increases (resilience decreases) as the VPD value rises, and the rate of increase is gradually accelerated (Figure 5B). The forest resilience remains constantly low with T_{min} less than -15°C , then sharply increases until T_{min} reaches -10°C , and finally stays high (Figure 5C). Overall, areas with less radiation stress, adequate water availability, and less warming are more likely to have higher forest resilience when taking the magnitude of the effects of these dominant drivers into account.

3.3. Temporal trends of forest resilience and their dominant factors

Figure 6 depicts the temporal trend of the forest resilience for the entire subtropical evergreen forests and in each grid cell using the MK trend test. For the entire study period, the AC1 significantly increased ($\beta > 0$, $|Z| > Z_{1-\alpha/2}$) when considering the subtropical evergreen forests as a whole, indicating a declining trend in its forest resilience (Figure 6A). Besides, the trend distribution of all forest grid cells also shows that the increasing trend of AC1 dominates (Figure 6A). The AR method shows the spatial consistency of the trend in the majority of grid cells with the results of the MK method (Supplementary Figure 4), revealing a decreasing resilience in subtropical evergreen forests in China since the 2000s through the upward trend of AC1. But the trends of AC1 differ across plant functional types (PFT) and time periods (Figures 6A, C–E; Table 2). Over the last two decades, there was a significant decreasing trend in forest resilience for ENF, but an insignificant increasing trend for EBF, and even a significant increasing trend for MF. As for different time periods, all three forest types showed a significant increase in resilience in 2005–2010 and 2015–2020, but a decrease in resilience in 2010–2014 (significant in all but MF). Thus, although the resilience of subtropical evergreen forests in China has shown an overall decreasing trend in the past 20 years, the resilience has been gradually rising in recent years.

We then assessed the dominant driving forces for the temporal variability in forest resilience by applying the VIF analysis and RF regression analysis with the AC1 time series in each grid cell. We found that the temporal variation of AC1 in these evergreen forest grid cells was not driven by one or two uniform variables. However, the most dominant driving variables are temperatures, including average and minimum temperatures (T_a and T_{min}) (Figure 7A). The grid cells with T_a as the most important variable occupy 15.8% of all forest grid cells, and the grid cells with T_{min} occupy 13.2% of all grid cells. VPD and Pre followed with a cover percentage of 11.5 and 10.8%, respectively. The cover percentages of the other variables are all less than 10%. We also assessed the cover percentages of the most influential variables for different PFTs (Figure 7B). T_a is still the most important variable with the highest percentages for ENF, EBF, and MF. T_{min} is the second important variable for ENF and EBF, while forest age influences the trends of resilience in MF more than T_{min} (Figure 7B).

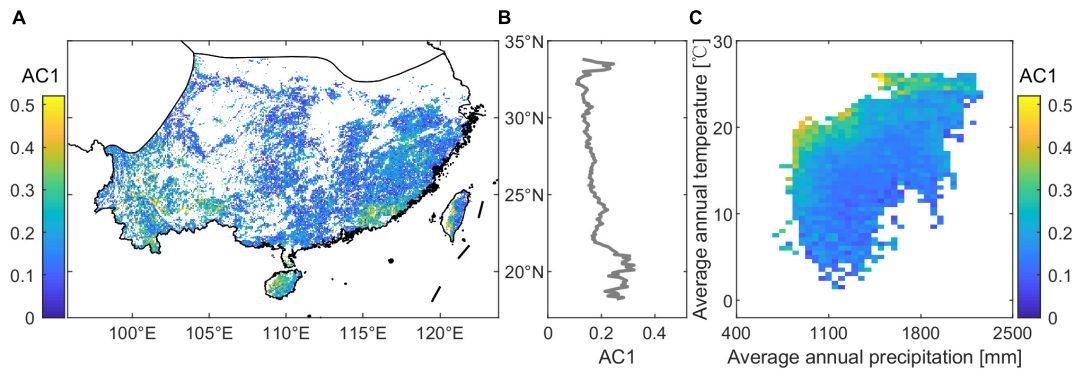


FIGURE 2 Spatial variation in the resilience of subtropical evergreen forests in China. **(A)** Spatial map of long-term lag-one autocorrelation (AC1) computed from kNDVI data for the whole 2001–2020 period. **(B)** Long-term AC1 with latitude. **(C)** Long-term AC1 binned as a function of precipitation and temperature.

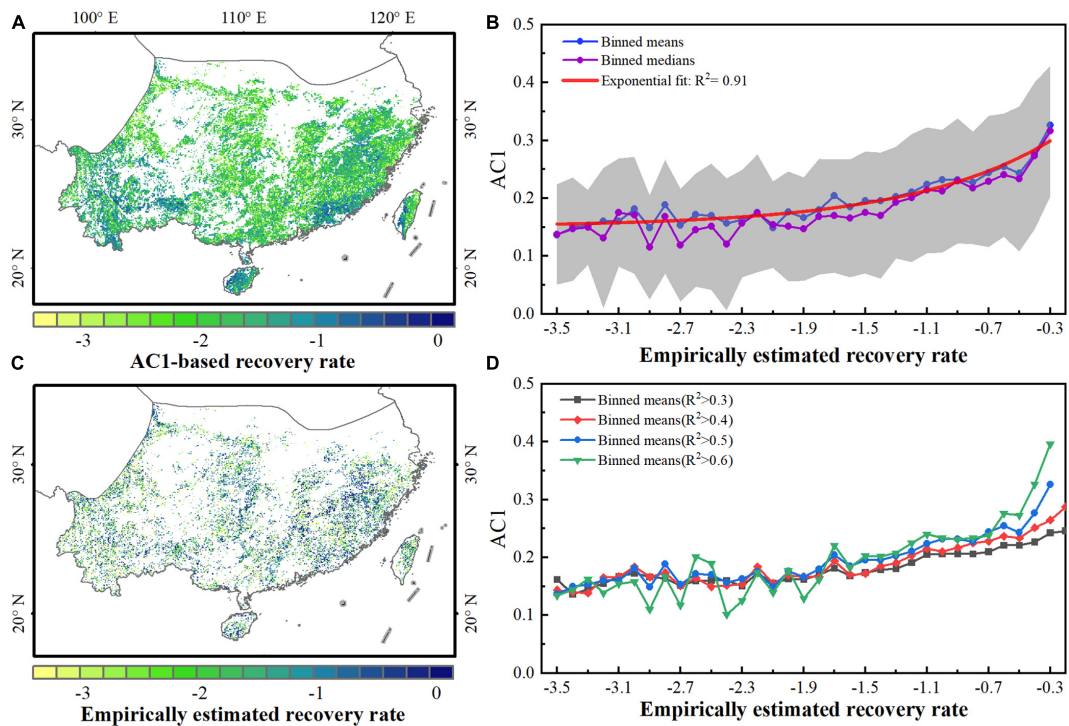


FIGURE 3 Comparison between theoretical resilience (AC1) metrics and empirical recovery rates based on satellite kNDVI data. **(A)** Theoretical estimate of the recovery rate computed from the AC1 at each grid. **(B)** Empirical estimate of the recovery rate (for well-determined exponential fits, $R^2 > 0.2$). **(C)** Relationship between AC1 and empirical recovery rates from exponential fits with $R^2 > 0.5$. **(D)** Binned means of AC1 as a function of the empirically estimated recovery rate under different R^2 thresholds.

4. Discussion

4.1. Indication of AC1 to forest resilience

The previous studies on ecosystem resilience mostly quantified the recovery time or the extent of ecosystem loss after a single special disturbance, such as drought (Longo et al., 2018; Huang and Xia, 2019), heat wave (Tatarinov et al., 2016; Guha et al., 2018), and wildfire (Stevens-Rumann et al., 2018; Hart et al.,

2019). For example, Huang and Xia (2019) define resilience to drought as the rate of EVI recovering to its pre-drought level; Hart et al. (2019) defines resilience to wildfire as the probability of the forest state recovering to its original state after a stand-replacing wildfire. But this definition is only applicable if strong external disturbances occur to natural vegetation systems (Smith et al., 2022). The resilience of natural ecosystems is hardly quantified in the above ways due to the scarcity of strong external disturbances. The temporal autocorrelation from long-term satellite vegetation datasets, namely the kNDVI-based AC1 in this study, breaks

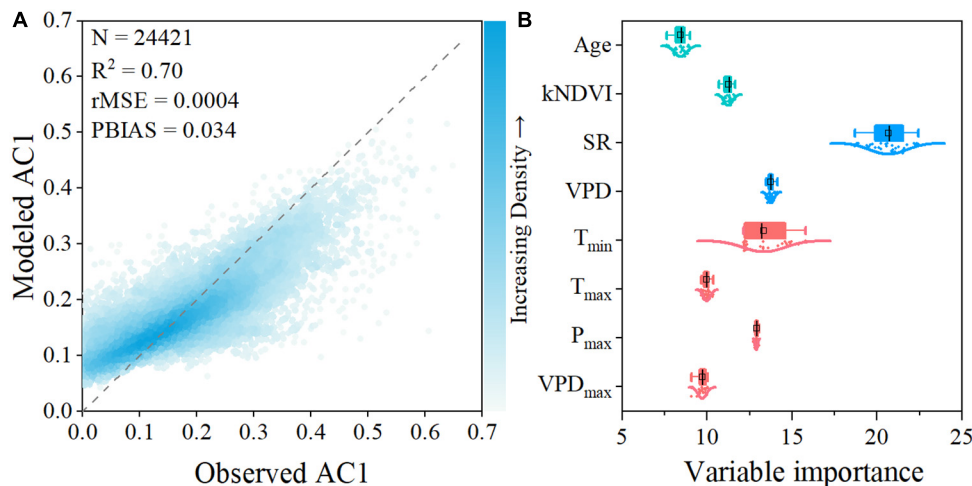


FIGURE 4 Model performance and variable importance of the selected variables for explaining the spatial long-term AC1 using a random forest regression model. **(A)** Comparison between measured AC1 and modeled AC1. **(B)** Variable importance of the predictor variables within the RF regression model. Variable importance is quantified by the increase in mean square error (%IncMSE).

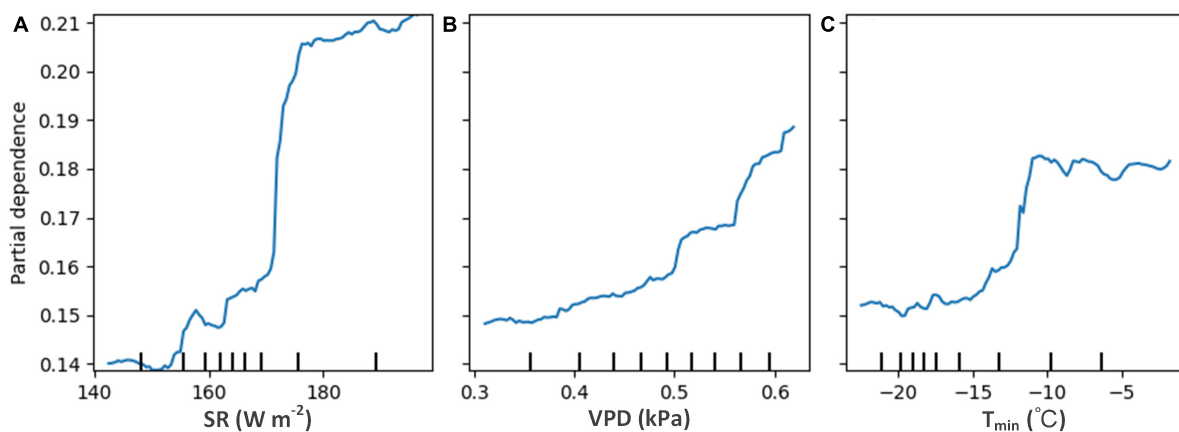


FIGURE 5 Partial dependence plots for the three most influential variables in the model for long-term AC1. **(A)** For solar radiation (SR), **(B)** for vapor pressure deficit (VPD), and **(C)** for minimum temperature (T_{min}).

TABLE 2 Temporal trends of forest resilience for different time periods and plant functional types.

| | 2005–2020 | | 2005–2009 | | 2010–2014 | | 2015–2020 | |
|-----|------------------------------|--------|------------------------------|-------|------------------------------|------|------------------------------|-------|
| | β ($\times 10^{-4}$) | Z | β ($\times 10^{-4}$) | Z | β ($\times 10^{-4}$) | Z | β ($\times 10^{-4}$) | Z |
| ALL | 0.56 | 2.58 | -3.49 | -4.96 | 4.77 | 9.69 | -3.53 | -9.00 |
| ENF | 1.13 | 5.18 | -2.69 | -4.92 | 5.46 | 9.84 | -3.80 | -8.74 |
| EBF | -0.34 | -1.43 | -5.11 | -5.68 | 4.21 | 9.10 | -2.73 | -7.51 |
| MF | -2.35 | -12.60 | -5.34 | -5.66 | 1.12 | 1.72 | -5.12 | -7.85 |

“ALL” means the entire subtropical evergreen forests; “ENF” means evergreen needleleaf forests; “EBF” means evergreen broadleaf forests; “MF” means mixed forests. “ β ” is the trend degree, with positive ones representing declining resilience and negative ones representing increasing resilience. “Z” is utilized as a measure of trend significance, with $|Z| \geq 1.96$ indicating a significant trend.

the limitation of the absence of strong disturbances and can be leveraged to evaluate broader spatial patterns of forest resilience.

Besides, ecosystem resilience metrics are typically computed by ecosystem state variables (such as biomass and species abundance), which are difficult to directly connect to ecosystem processes

described by rates (Hu et al., 2022). Spectral indices are convenient proxies for canopy structure and leaf biochemical features, and consequently to track the dynamics of vegetation photosynthetic activity [i.e., gross primary production (GPP)]. But the celebrated NDVI has well-known issues with nonlinearities and saturation

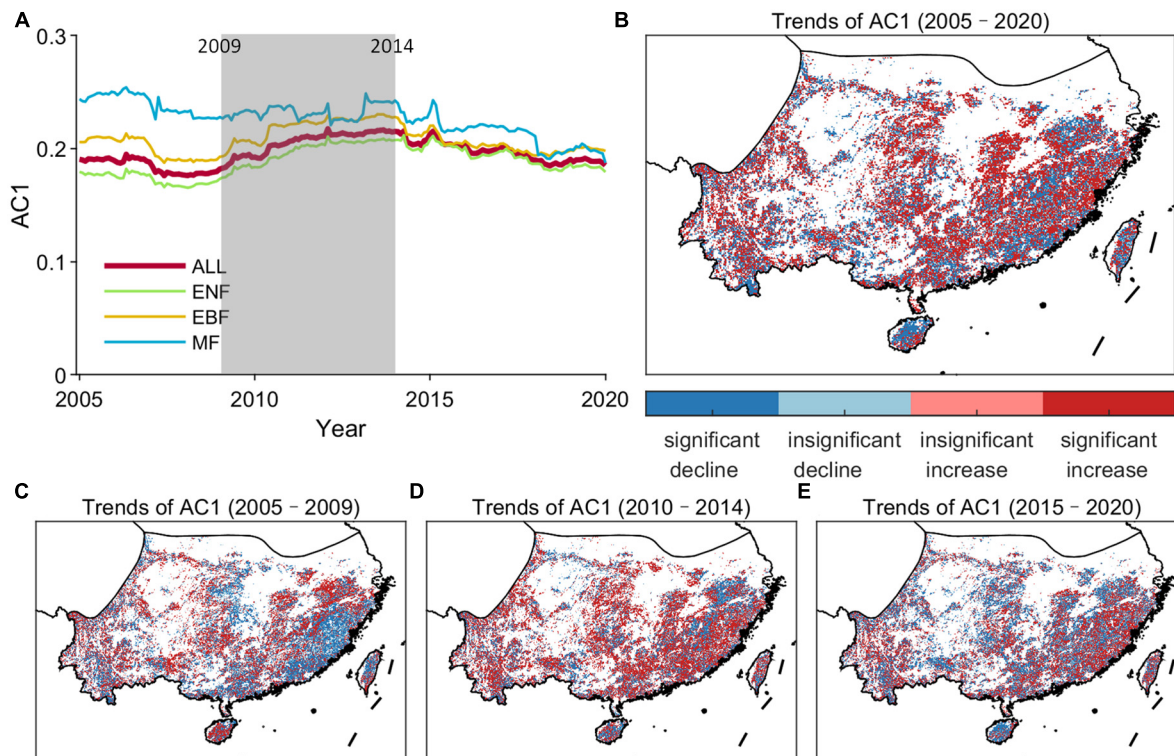


FIGURE 6 Temporal trends of the resilience of subtropical evergreen forests in China. (A) Temporal changes in AC1 computed in a 5-year moving window over 2001–2020 kNDVI time series for the subtropical evergreen forests. (B) Spatial map of the temporal trends in AC1 time series during 2005–2020. (C) Spatial map of the temporal trends in AC1 time series during 2005–2009. (D) Spatial map of the temporal trends in AC1 time series during 2010–2014. (E) Spatial map of the temporal trends in AC1 time series during 2015–2020. “ALL” means the entire subtropical evergreen forests.

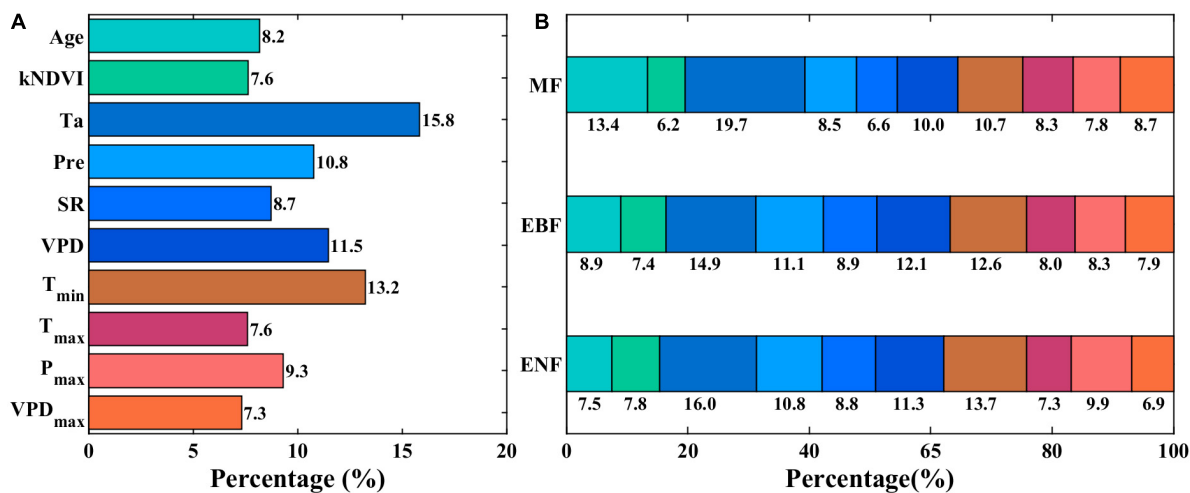


FIGURE 7 Variable importance of selected environmental variables for explaining the AC1 time series in each grid of subtropical evergreen forests in China. (A) Cover percentages of different most influential environmental variables. (B) Cover percentages of the most influential variables across the plant functional types.

effects at high vegetation productivity (Huete et al., 1997). A new index called NIR_v, calculated by multiplying NDVI with NIR, is not a dimensionless quantity (or actual index) despite its good performance in relation to GPP (Wang et al., 2023). kNDVI shows good characteristics like boundedness, low error propagation, and

less sensitivity to orbital drifts (Wang et al., 2021, 2023), and is therefore a more appropriate proxy for GPP than NDVI and NIR_v. Thus, we used kNDVI as an indicator of ecosystem function to compute the lag-one autocorrelation (AC1) from its time series as a measure of forest resilience.

The indication of kNDVI-based AC1 to the evergreen forest resilience has been supported by the empirical recovery rate proposed by Smith et al. (2022) in an intuitive way and on a per-point basis (Figure 3). The empirical recovery rate was computed by delineating the large disturbances using the 99th percentile method and then curve-fitting the subsequent time series of recovering ecosystem state. It might be more realistic because it clearly detected disturbances. We found that the empirical recovery rate from external disturbances was more sparsely distributed than the AC1-based recovery rate (Figures 3A, C). Not all forest areas have undergone rapid and drastic changes during the period; thus, vegetation resilience in these areas is impossible to be directly quantified through recovery from an external disturbance (Smith et al., 2022). In contrast, AC1-based recovery rate can be obtained under a broader range of conditions. In areas where the recovery rate can be estimated empirically from large disturbances, the empirical recovery rate shows broad spatial consistency with the theoretically computed r_{AC1} and binned means or medians of AC1 can be well-fitted as a function of the empirical recovery rate. Thus, the AC1 from the kNDVI data reveals the forest resilience of the subtropical evergreen forests.

4.2. Drivers of the evergreen forest resilience

Some hypotheses on abiotic and biotic factors that can influence resilience have been tested with numerous spatial and temporal datasets. Consistent with our study, climate is a key abiotic factor hypothesized to affect ecosystem resilience (Willis et al., 2018). We found that solar radiation is the dominant driver influencing the spatial pattern of forest resilience in the subtropical evergreen forests of China (Figures 4B, 5A), which is in line with the results in Forzieri et al. (2022). Higher solar radiation leads to less resilient forests, which explains the decreasing forest resilience with decreasing latitude (Figure 2B). It's well-founded that elevated temperatures and water limitations are systematically associated with worldwide cases of massive tree mortality (Ibáñez et al., 2019). Our analysis shows that temperature rather than precipitation has a clear influence on both the spatial variability and temporal trend in the resilience of subtropical evergreen forests in China (Figures 4B, 7B). The findings here imply that resilience of the subtropical evergreen forest may be declined at higher daily minimum temperature (T_{min}), which may be explained by the decelerating growth rates with higher T_{min} in forest trees (Feeley et al., 2007). We also found that water limitation (high VPD) slows down the forests' capacity to recover after disturbances (Figure 5B). Poorter et al. (2016) also reported that the recovery of above-ground biomass increased with water availability (higher precipitation and lower water deficit) in neotropical dry forests. Under water-deficit conditions, trees close their stomata, reduce photosynthesis, and consume stored carbohydrates to maintain metabolism, hindering growth and recovery of trees. Besides, rising temperatures may amplify the impacts of water deficit on tree mortality, then on forest resilience (Adams et al., 2009).

In addition, a suite of biotic factors needs to be considered. In this study, we assumed forest age and the average annual forest photosynthetic activity as possible biotic factors influencing

forest resilience. Although they are of secondary importance in the spatiotemporal variations in forest resilience, high values of AC1 (low resilience) typically occur at locations characterized by high long-term average kNDVI and forest age (Supplementary Figure 2). This suggests that high productivity does not mean high resilience, but rather the opposite. Nonproductive forests may be more resilient to disturbances, because their previous states are more easily attained. Older forests may provide more various stem diameter sizes and thus, more complex structure than younger forests (Jeffries et al., 2006), making it more difficult to recover to the previous states. It's also reported that increases in plant flammability and wind damage vulnerability with forest age promote reduced resilience to climate variability (Oliver and Larson, 1996; Kitzberger et al., 2012).

Other abiotic factors such as soil attributes and number of disturbances are also proven to be influential to the forest resilience. High soil fertility has a positive influence on biomass recovery, and soils with low clay content have higher resilience (Oliveras and Malhi, 2016; Poorter et al., 2016). A system experiences more disturbances recovers faster, perhaps because the vegetation is gradually dominated by species with fast response and adaptation abilities to disturbance (Cole et al., 2014; Willis et al., 2018). Another biotic factor that has been widely considered but not in this study is biodiversity (Hodgson et al., 2015). Ecosystems with greater biodiversity will be more resilient to disturbances, but this is not always the case. African regions with the highest plant species richness exhibit the greatest sensitivity to environmental disturbances (Liu et al., 2022). Our study focuses more on the characteristics of vegetation and meteorology, which reproduce the spatial and temporal variation of resilience well despite ignoring the above factors. In the future, these factors need to be studied for better identifying the underlying mechanisms of the tempo-spatial variations in resilience of subtropical evergreen forests in China.

5. Conclusion

In this study, we estimated the temporal autocorrelation (AC1) from a time series of the satellite kNDVI dataset to investigate the spatial pattern and temporal variability of evergreen forest resilience over the past two decades in southern China. The major conclusions are drawn as follows:

- (1) The computed long-term AC1 depicts considerable spatial variability in the resilience of the subtropical evergreen forests in China, with low resilience occurring in low-latitude areas such as the Yunnan-Guizhou plateau, Hainan Island, and the coastal hilly regions.
- (2) The spatial variability in the forest resilience can be re-established with RF model by forest and climatic variables, and is largely affected by SR, VPD, and T_{min} . Higher forest resilience is more likely to be found in locations with less radiation stress, adequate water availability, and less warming.
- (3) The forest resilience has shown a declining trend over the past two decades but has increased in the recent decade. Temperature changes, including average and minimum temperatures, dominate the temporal trends in the resilience of subtropical evergreen forests in China.

From the findings of this study, we suggest more attention should be paid to the subtropical evergreen forests to deal with the warming climate in times of rapid global change.

Data availability statement

The original contributions presented in this study are included in the article/**Supplementary material**, further inquiries can be directed to the corresponding authors.

Author contributions

JC, SW, and HS contributed to the conception and design of the study. JC and BC performed the statistical analysis. JW collected and processed the data. JC and SW wrote the first draft of the manuscript. CZ and KZ wrote sections of the manuscript. All authors discussed the results, contributed to the revisions, and approved the submitted version.

Funding

This work was financially supported by the National Natural Science Foundation of China (grant numbers: 41871342 and 42101479), the Strategic Priority Research Program of the Chinese

References

- Abis, B., and Brovkin, V. (2017). Environmental conditions for alternative tree-cover states in high latitudes. *Biogeosciences* 14, 511–527. doi: 10.5194/bg-14-511-2017
- Adams, H. D., Guardiola-Claramonte, M., Barron-Gafford, G. A., Villegas, J. C., Breshers, D. D., Zou, C. B., et al. (2009). Temperature sensitivity of drought-induced tree mortality portends increased regional die-off under global-change-type drought. *Proc. Natl. Acad. Sci. U.S.A.* 106, 7063–7066. doi: 10.1073/pnas.0901438106
- Bai, J., Shi, H., Yu, Q., Xie, Z., Li, L., Luo, G., et al. (2019). Satellite-observed vegetation stability in response to changes in climate and total water storage in Central Asia. *Sci. Total Environ.* 659, 862–871. doi: 10.1016/j.scitotenv.2018.12.418
- Bonan, G. B. (1989). A computer model of the solar radiation, soil moisture, and soil thermal regimes in boreal forests. *Ecol. Modell.* 45, 275–306. doi: 10.1016/0304-3800(89)90076-8
- Boulton, C. A., Lenton, T. M., and Boers, N. (2022). Pronounced loss of Amazon rainforest resilience since the early 2000s. *Nat. Clim. Change* 12, 271–278. doi: 10.1038/s41558-022-01287-8
- Breiman, L. (2001). Random forests. *Mach. Learn.* 45, 5–32. doi: 10.1023/A:1010933404324
- Camps-Valls, G., Campos-Taberner, M., Moreno-Martinez, Á., Walther, S., Duveiller, G., Cescatti, A., et al. (2021). A unified vegetation index for quantifying the terrestrial biosphere. *Sci. Adv.* 7:eabc7447. doi: 10.1126/sciadv.abc7447
- Cleveland, R. B., Cleveland, W. S., McRae, J. E., and Terpenning, I. (1990). STL: A seasonal-trend decomposition. *J. Off. Stat.* 6, 3–73.
- Cole, L. E., Bhagwat, S. A., and Willis, K. J. (2014). Recovery and resilience of tropical forests after disturbance. *Nat. Commun.* 5, 1–7. doi: 10.1038/ncomms4906
- Dakos, V., Carpenter, S. R., van Nes, E. H., and Scheffer, M. (2015). Resilience indicators: Prospects and limitations for early warnings of regime shifts. *Philos. Trans. R. Soc. B Biol. Sci.* 370:20130263. doi: 10.1098/rstb.2013.0263
- Dakos, V., Van Nes, E. H., d'Odorico, P., and Scheffer, M. (2012). Robustness of variance and autocorrelation as indicators of critical slowing down. *Ecology* 93, 264–271. doi: 10.1890/11-0889.1
- Fang, O., and Zhang, Q. B. (2019). Tree resilience to drought increases in the Tibetan Plateau. *Glob. Change Biol.* 25, 245–253. doi: 10.1111/gcb.14470
- Feeley, K. J., Joseph Wright, S., Nur Supardi, M., Kassim, A. R., and Davies, S. J. (2007). Decelerating growth in tropical forest trees. *Ecol. Lett.* 10, 461–469. doi: 10.1111/j.1461-0248.2007.01033.x
- Fernandes, R., and Leblanc, S. G. (2005). Parametric (modified least squares) and non-parametric (Theil-Sen) linear regressions for predicting biophysical parameters in the presence of measurement errors. *Remote Sens. Environ.* 95, 303–316. doi: 10.1016/j.rse.2005.01.005
- Forzieri, G., Dakos, V., McDowell, N. G., Ramdane, A., and Cescatti, A. (2022). Emerging signals of declining forest resilience under climate change. *Nature* 608, 534–539. doi: 10.1038/s41586-022-04959-9
- Friedlingstein, P., Jones, M. W., O'Sullivan, M., Andrew, R. M., Bakker, D. C., Hauck, J., et al. (2022). Global carbon budget 2021. *Earth Syst. Sci. Data* 14, 1917–2005. doi: 10.5194/essd-14-1917-2022
- Geng, S., Yang, L., Sun, Z., Wang, Z., Qian, J., Jiang, C., et al. (2021). Spatiotemporal patterns and driving forces of remotely sensed urban agglomeration heat islands in South China. *Sci. Total Environ.* 800:149499. doi: 10.1016/j.scitotenv.2021.149499
- Guha, A., Han, J., Cummings, C., McLennan, D. A., and Warren, J. M. (2018). Differential ecophysiological responses and resilience to heat wave events in four co-occurring temperate tree species. *Environ. Res. Lett.* 13:065008. doi: 10.1088/1748-9326/aabcd8
- Hair, J. F., Black, W. C., Babin, B. J., and Anderson, R. E. (2009). *Multivariate data analysis*, Vol. 24. Upper Saddle River, NJ: Macmillan, 899.
- Hansen, M. C., Potapov, P. V., Moore, R., Hancher, M., Turubanova, S. A., Tyukavina, A., et al. (2013). High-resolution global maps of 21st-century forest cover change. *Science* 342, 850–853. doi: 10.1126/science.1244693
- Hart, S. J., Henkelman, J., McLoughlin, P. D., Nielsen, S. E., Truchon-Savard, A., and Johnstone, J. F. (2019). Examining forest resilience to changing fire frequency in a fire-prone region of boreal forest. *Glob. Change Biol.* 25, 869–884. doi: 10.1111/gcb.14550
- Hodgson, D., McDonald, J. L., and Hosken, D. J. (2015). What do you mean, 'resilient'? *Trends Ecol. Evol.* 30, 503–506. doi: 10.1016/j.tree.2015.06.010

Academy of Sciences (grant number: XDA23100202), and the China Postdoctoral Science Foundation (grant number: 2020M680654).

Conflict of interest

The authors declare that the research was conducted in the absence of any commercial or financial relationships that could be construed as a potential conflict of interest.

Publisher's note

All claims expressed in this article are solely those of the authors and do not necessarily represent those of their affiliated organizations, or those of the publisher, the editors and the reviewers. Any product that may be evaluated in this article, or claim that may be made by its manufacturer, is not guaranteed or endorsed by the publisher.

Supplementary material

The Supplementary Material for this article can be found online at: <https://www.frontiersin.org/articles/10.3389/ffgc.2023.1166481/full#supplementary-material>

- Holling, C. S. (1973). Resilience and stability of ecological systems. *Annu. Rev. Ecol. Syst.* 4, 1–23. doi: 10.1146/annurev.es.04.110173.000245
- Hu, Z., Dakos, V., and Rietkerk, M. (2022). Using functional indicators to detect state changes in terrestrial ecosystems. *Trends Ecol. Evol.* 37, 1036–1045. doi: 10.1016/j.tree.2022.07.011
- Huang, K., and Xia, J. (2019). High ecosystem stability of evergreen broadleaf forests under severe droughts. *Glob. Change Biol.* 25, 3494–3503. doi: 10.1111/gcb.14748
- Huang, K., Wang, S., Zhou, L., Wang, H., Liu, Y., and Yang, F. (2013). Effects of drought and ice rain on potential productivity of a subtropical coniferous plantation from 2003 to 2010 based on eddy covariance flux observation. *Environ. Res. Lett.* 8:035021. doi: 10.1088/1748-9326/8/3/035021
- Hubau, W., Lewis, S. L., Phillips, O. L., Affum-Baffoe, K., Bectman, H., Cuní-Sánchez, A., et al. (2020). Asynchronous carbon sink saturation in African and Amazonian tropical forests. *Nature* 579, 80–87. doi: 10.1038/s41586-020-2035-0
- Huete, A. R., Liu, H., and van Leeuwen, W. J. (1997). “The use of vegetation indices in forested regions: Issues of linearity and saturation,” in *Proceedings of the IGARSS’97. 1997 IEEE International Geoscience and Remote Sensing Symposium Proceedings. Remote Sensing—a scientific vision for sustainable development*, Vol. 4 (Piscataway, NJ: IEEE), 1966–1968.
- Hutchinson, M. F. (1995). Interpolating mean rainfall using thin plate smoothing splines. *Int. J. Geogr. Inf. Sci.* 9, 385–403. doi: 10.1080/02693799508902045
- Ibáñez, I., Acharya, K., Juno, E., Karounos, C., Lee, B. R., McCollum, C., et al. (2019). Forest resilience under global environmental change: Do we have the information we need? A systematic review. *PLoS One* 14:e0222207. doi: 10.1371/journal.pone.0222207
- Ives, A. R., Zhu, L., Wang, F., Zhu, J., Morrow, C. J., and Radeloff, V. C. (2021). Statistical inference for trends in spatiotemporal data. *Remote Sens. Environ.* 266:112678. doi: 10.1016/j.rse.2021.112678
- Jeffries, J. M., Marquis, R. J., and Forkner, R. E. (2006). Forest age influences oak insect herbivore community structure, richness, and density. *Ecol. Appl.* 16, 901–912. doi: 10.1890/1051-0761(2006)016[0901:FAIOIH]2.0.CO;2
- Kendall, M. G. (1975). *Rank correlation measures*. London: Charles Griffin.
- Kitzberger, T., Aráoz, E., Gowda, J. H., Mermoz, M., and Morales, J. M. (2012). Decreases in fire spread probability with forest age promotes alternative community states, reduced resilience to climate variability and large fire regime shifts. *Ecosystems* 15, 97–112. doi: 10.1007/s10021-011-9494-y
- Kock, N., and Lynn, G. (2012). Lateral collinearity and misleading results in variance-based SEM: An illustration and recommendations. *J. Assoc. Inf. Sci. Technol.* 13, 546–580. doi: 10.17705/1jais.00302
- Lewis, S. L., Wheeler, C. E., Mitchard, E. T., and Koch, A. (2019). Restoring natural forests is the best way to remove atmospheric carbon. *Nature* 568, 25–28. doi: 10.1038/d41586-019-01026-8
- Liu, D., Wang, T., Peñuelas, J., and Piao, S. (2022). Drought resistance enhanced by tree species diversity in global forests. *Nat. Geosci.* 15, 800–804. doi: 10.1038/s41561-022-01026-w
- Liu, Y., Kumar, M., Katul, G. G., and Porporato, A. (2019). Reduced resilience as an early warning signal of forest mortality. *Nat. Clim. Change* 9, 880–885. doi: 10.1038/s41558-019-0583-9
- Longo, M., Knox, R. G., Levine, N. M., Alves, L. F., Bonal, D., Camargo, P. B., et al. (2018). Ecosystem heterogeneity and diversity mitigate Amazon forest resilience to frequent extreme droughts. *New Phytol.* 219, 914–931. doi: 10.1111/nph.15185
- Lovejoy, T. E., and Nobre, C. (2018). Amazon tipping point. *Sci. Adv.* 4:eaat2340. doi: 10.1126/sciadv.aat2340
- Mann, H. B. (1945). Nonparametric tests against trend. *Econometrica* 13, 245–259. doi: 10.2307/1907187
- Midi, H., and Bagheri, A. (2010). “Robust multicollinearity diagnostic measure in collinear data set,” in *Proceedings of the 4th international conference on applied mathematics, simulation, modeling* (Stevens Point, WI: World Scientific and Engineering Academy and Society (WSEAS)), 138–142.
- Murray, F. W. (1966). *On the computation of saturation vapor pressure*. Santa Monica, CA: Rand Corp.
- Oliver, C. D., and Larson, B. C. (1996). *Forest stand dynamics: Updated edition*. Hoboken, NJ: John Wiley and sons.
- Oliveras, I., and Malhi, Y. (2016). Many shades of green: The dynamic tropical forest–savannah transition zones. *Philos. Trans. R. Soc. B Biol. Sci.* 371:20150308. doi: 10.1098/rstb.2015.0308
- Pan, Y., Birdsey, R. A., Fang, J., Houghton, R., Kauppi, P. E., Kurz, W. A., et al. (2011). A large and persistent carbon sink in the world’s forests. *Science* 333, 988–993. doi: 10.1126/science.1201609
- Pedregosa, F., Varoquaux, G., Gramfort, A., Michel, V., Thirion, B., Grisel, O., et al. (2011). Scikit-learn: Machine learning in Python. *J. Mach. Learn. Technol.* 12, 2825–2830.
- Pei, F., Li, X., Liu, X., and Lao, C. (2013). Assessing the impacts of droughts on net primary productivity in China. *J. Environ. Manage.* 114, 362–371. doi: 10.1016/j.jenvman.2012.10.031
- Poorter, L., Bongers, F., Aide, T. M., Almeyda Zambrano, A. M., Balvanera, P., Becknell, J. M., et al. (2016). Biomass resilience of Neotropical secondary forests. *Nature* 530, 211–214. doi: 10.1038/nature16512
- Savitzky, A., and Golay, M. J. (1964). Smoothing and differentiation of data by simplified least squares procedures. *Anal. Chem.* 36, 1627–1639. doi: 10.1021/ac60214a047
- Scheffer, M., Bascompte, J., Brock, W. A., Brovkin, V., Carpenter, S. R., Dakos, V., et al. (2009). Early-warning signals for critical transitions. *Nature* 461, 53–59. doi: 10.1038/nature08227
- Seidl, R., Thom, D., Kautz, M., Martin-Benito, D., Peltoniemi, M., Vacchiano, G., et al. (2017). Forest disturbances under climate change. *Nat. Clim. Change* 7, 395–402. doi: 10.1038/nclimate3303
- Sen, P. K. (1968). Estimates of the regression coefficient based on Kendall’s tau. *J. Am. Stat. Assoc.* 63, 1379–1389. doi: 10.1080/01621459.1968.10480934
- Smith, T., Traxl, D., and Boers, N. (2022). Empirical evidence for recent global shifts in vegetation resilience. *Nat. Clim. Change* 12, 477–484. doi: 10.1038/s41558-022-01352-2
- Stevens-Rumann, C. S., Kemp, K. B., Higuera, P. E., Harvey, B. J., Rother, M. T., Donato, D. C., et al. (2018). Evidence for declining forest resilience to wildfires under climate change. *Ecol. Lett.* 21, 243–252. doi: 10.1111/ele.12889
- Tatarinov, F., Rotenberg, E., Maseyk, K., Ogée, J., Klein, T., and Yakir, D. (2016). Resilience to seasonal heat wave episodes in a Mediterranean pine forest. *New Phytol.* 210, 485–496. doi: 10.1111/nph.13791
- Verbesselt, J., Umlauf, N., Hirota, M., Holmgren, M., Van Nes, E. H., Herold, M., et al. (2016). Remotely sensed resilience of tropical forests. *Nat. Clim. Change* 6, 1028–1031. doi: 10.1038/nclimate3108
- Wang, J., Wang, J., Ye, H., Liu, Y., and He, H. (2017). An interpolated temperature and precipitation dataset at 1-km grid resolution in China (2000–2012). *China Sci. Data* 2, 88–95.
- Wang, Q., Moreno-Martínez, Á., Muñoz-Marí, J., Campos-Taberner, M., and Camps-Valls, G. (2023). Estimation of vegetation traits with kernel NDVI. *ISPRS J. Photogramm. Remote Sens.* 195, 408–417. doi: 10.1016/j.isprsjprs.2022.12.019
- Wang, S., Zhang, Y., Ju, W., Chen, J. M., Cescatti, A., Sardans, J., et al. (2021). Response to comments on “recent global decline of CO₂ fertilization effects on vegetation photosynthesis”. *Science* 373:eabg7484. doi: 10.1126/science.abg7484
- Willis, K. J., Jeffers, E. S., and Tovar, C. (2018). What makes a terrestrial ecosystem resilient? *Science* 359, 988–989. doi: 10.1126/science.aar5439
- Wu, B., Yuan, Q., Yan, C., Wang, Z., Yu, X., Li, A., et al. (2014). Land cover changes of china from 2000 to 2010. *Quat. Res.* 34, 723–731.
- Yi, C., and Jackson, N. (2021). A review of measuring ecosystem resilience to disturbance. *Environ. Res. Lett.* 16:053008. doi: 10.1088/1748-9326/abd0f9
- Yu, G., Chen, Z., Piao, S., Peng, C., Ciais, P., Wang, Q., et al. (2014). High carbon dioxide uptake by subtropical forest ecosystems in the East Asian monsoon region. *Proc. Natl. Acad. Sci. U.S.A.* 111, 4910–4915. doi: 10.1073/pnas.1317065111
- Zhang, C., Ju, W., Chen, J. M., Li, D., Wang, X., Fan, W., et al. (2014). Mapping forest stand age in China using remotely sensed forest height and observation data. *J. Geophys. Res. Biogeosci.* 119, 1163–1179. doi: 10.1002/2013JG002515
- Zhang, L., Li, X., Yuan, Q., and Liu, Y. (2014). Object-based approach to national land cover mapping using HJ satellite imagery. *J. Appl. Remote Sens.* 8:083686. doi: 10.1117/1.JRS.8.083686
- Zhang, L., Xiao, J., Li, J., Wang, K., Lei, L., and Guo, H. (2012). The 2010 spring drought reduced primary productivity in southwestern China. *Environ. Res. Lett.* 7:045706. doi: 10.1088/1748-9326/7/4/045706
- Zhao, Q., Huang, G., and Wang, L. (2015). Forest ecosystems in the south China: Functions, problems and countermeasures. *J. For. Environ.* 35, 289–296.



OPEN ACCESS

EDITED BY
Matthieu Chauvat,
Université de Rouen, France

REVIEWED BY
Qiang Yang,
Lanzhou University, China
Christina Biasi,
University of Eastern Finland, Finland

*CORRESPONDENCE
Ling Zhang
✉ lingzhang09@126.com

RECEIVED 10 March 2023
ACCEPTED 05 May 2023
PUBLISHED 24 May 2023

CITATION

Lai XQ, Luo LC, Fang HF, Zhang L, Shad N, Bai J, Li AX, Zhang X, Yu YD, Wang H and Siemann E (2023) Bacterial and fungal inhibitor interacted impacting growth of invasive *Triadica sebifera* and soil N₂O emissions.
Front. For. Glob. Change 6:1183336.
doi: 10.3389/ffgc.2023.1183336

COPYRIGHT

© 2023 Lai, Luo, Fang, Zhang, Shad, Bai, Li, Zhang, Yu, Wang and Siemann. This is an open-access article distributed under the terms of the [Creative Commons Attribution License \(CC BY\)](https://creativecommons.org/licenses/by/4.0/). The use, distribution or reproduction in other forums is permitted, provided the original author(s) and the copyright owner(s) are credited and that the original publication in this journal is cited, in accordance with accepted academic practice. No use, distribution or reproduction is permitted which does not comply with these terms.

Bacterial and fungal inhibitor interacted impacting growth of invasive *Triadica sebifera* and soil N₂O emissions

Xiaoqin Lai¹, Laicong Luo¹, Haifu Fang¹, Ling Zhang^{1*}, Nasir Shad¹, Jian Bai¹, Aixin Li¹, Xi Zhang¹, Yadi Yu¹, Hao Wang¹ and Evan Siemann²

¹Jiangxi Provincial Key Laboratory of Silviculture, College of Forestry, Jiangxi Agricultural University, Nanchang, China, ²Department of Biosciences, Rice University, Houston, TX, United States

Plant invasions affect biodiversity and seriously endanger the stability of ecosystems. Invasive plants show strong adaptability and growth advantages but are influenced by various factors. Soil bacteria and fungi are critical to plant growth and are important factors affecting plant invasions. Plant invasions also affect soil N₂O emissions, but the effects of invasive plants from different population origins on N₂O emissions and their microbial mechanisms are not clear. In this experiment, we grew *Triadica sebifera* from native (China) and invasive (USA) populations with or without bacterial (streptomycin) and/or fungal (iprodione) inhibitors in a factorial experiment in which we measured plant growth and soil N₂O emissions of *T. sebifera*. Plants from invasive populations had higher leaf masses than those from native populations when soil bacteria were not inhibited (with or without fungal inhibition) which might reflect that they are more dependent on soil bacteria. Cumulative N₂O emissions were higher for soils with invasive *T. sebifera* than those with a plant from a native population. Bacterial inhibitor application reduced cumulative N₂O emissions but reductions were larger with application of the fungal inhibitor either alone or in combination with the bacterial inhibitor. This suggests that fungi play a strong role in plant performance and soil N₂O emissions. Therefore, it is important to further understand the effects of soil microorganisms on the growth of *T. sebifera* and soil N₂O emissions to provide a more comprehensive scientific basis for understanding the causes and consequences of plant invasions.

KEYWORDS

bacterial inhibitor, fungal inhibitor, soil microorganisms, plant growth, soil N₂O emissions, invasive plant

1. Introduction

With rapid industrialization, the concentration of greenhouse gases in the atmosphere has increased significantly, and global climate change is becoming increasingly problematic. The Paris Agreement proposed the goal of keeping the global average temperature less than 2°C above pre-industrial warming by 2100. However, it is difficult to control warming below 1.5°C at present (Rogelj et al., 2016), and it is necessary to reduce total GHG emissions.

Nitrous oxide (N₂O) is an important greenhouse gas (Walling and Vaneckhaute, 2020) that persists in the atmosphere for 121 years with a warming potential 265 times higher than that of CO₂ on a 100-year scale (IPCC, 2014). N₂O is also extremely damaging to the ozone layer (Ravishankara et al., 2009). While a variety of CO₂ reduction measures are emerging, non-CO₂ greenhouse gas reduction such as N₂O should also receive attention.

Nitrous oxide is produced by complex nitrification and denitrification processes carried out by various microbial communities, including bacteria, fungi and archaea (Zhong et al., 2022). Soil N₂O emissions are largely derived from these two processes (Hu et al., 2015), accounting for 70% of total global emissions (Fowler et al., 2013). Bacteria have been the main contributors to N₂O release from soils (Johnson et al., 1996). However, in desert and semi-arid grassland soils, fungi are the main contributors (>70%) to N₂O release (Marusenko et al., 2013). In order to reduce N₂O emissions from agroforestry systems, studies have been conducted on the effects of bacterial and fungal inhibitors on N₂O emissions. Herold et al. (2012) studied the effect of tilled soil on fungal and bacterial denitrification and biomass by adding cycloheximide (fungal inhibitor) and streptomycin (bacterial inhibitor). Castaldi and Smith (1998) found that the addition of peptone to forest soils significantly stimulated the release of N₂O, while low concentrations of cycloheximide rapidly reduced N₂O release, indicating that fungi are the main contributors to N₂O release in forest soils. Biological inhibitors can be used to inhibit the activity of bacteria and fungi involved in nitrification and denitrification processes, and further studies are needed to investigate the effect of biological inhibitors on soil N₂O emissions.

In the context of global climate change, plant invasion can affect biodiversity and jeopardize the stability of forest ecosystems (Bradley et al., 2010; Ehrenfeld, 2010). Soil microbes are an important component of forest ecosystems (Fritze et al., 1994), and bacteria and fungi are major components of soil microbial communities (Rousk et al., 2009). Soil biology is an important factor affecting plant performance and invasion potential (Reinhart and Callaway, 2006). Soil microorganisms (e.g., mycorrhizal fungi, rhizobia, etc.) can efficiently assist invasive plants to utilize nutrients such as nitrogen (Huang et al., 2016) and phosphorus (Zhang et al., 2013) to facilitate plant invasion. Invasive plants show strong adaptability and growth advantages but are influenced by various factors (Zou et al., 2006; Ehrenfeld, 2010; De Marco et al., 2022). For example, nitrogen deposition enhances the biomass and leaf area of invasive *Triadica sebifera* (Deng et al., 2019b) and increases the invasive potential of *Mikania micrantha* and *Chromolaena odorata* (Zhang et al., 2016). Higher temperatures, increased CO₂, and nitrogen deposition can exacerbate plant invasion, and conversely, plant invasion can affect greenhouse gas emissions (Lei et al., 2010). Although there have been numerous studies on the impact of invasive exotic plants on ecosystem carbon and nitrogen cycles (Liao et al., 2007, 2008) knowledge of the mechanisms of N₂O emissions is limited.

The growth and activity of soil microorganisms can be stimulated due to greater root biomass of invasive plants, production of more secretions, easier access to soil

microorganisms, and increased rate of N uptake (Zou et al., 2006). Nijjer et al. (2008) found that exotic tree species benefited more from soil arbuscular mycorrhizal compared to native species in a pot experiment. This suggests that soil organisms play an important role in the invasion of alien species. There is also variation among populations of exotic plants in their interactions with soil organisms (Yang et al., 2015). For instance, *T. sebifera* plants from invasive populations have stronger soil microbial utilization capacity compared to those from native populations, confirming the role of soil microbes in promoting the growth of invasive *T. sebifera* (Zhang et al., 2012). However, the effects of invasive plants with different populations origins on N₂O emissions and their microbial mechanisms are not clear.

Triadica sebifera (Euphorbiaceae; synonym *Sapium sebiferum*) is an economic tree endemic to China with a long history of cultivation and is an important industrial oilseed tree in China, combining economic and ornamental values. It was introduced to the United States as an oil species and ornamental tree in the late 18th century and has become invasive and impacted ecosystems in the southeastern United States in part because of increased competitive ability of invasive populations (Huang et al., 2012; Zhang et al., 2012, 2013, 2020). The effects of biotic and abiotic factors on plants of different species origins are complex (Reinhart and Callaway, 2006; Bradley et al., 2010). Invasive *T. sebifera* has higher plant height, stem and total biomass, higher nitrogen uptake rate and relative growth rate than native *T. sebifera* (Zou et al., 2007; Zhang et al., 2013; Deng et al., 2017), and lower root to shoot ratio (Zhang et al., 2017). Zou et al. (2006) found soil CO₂ and N₂O emissions were higher for soils associated with *T. sebifera* from invasive vs. native populations. But, the contributions of soil fungi and bacteria to growth of *T. sebifera* plants from different population origins and associated soil N₂O emissions are unclear.

In this experiment, we grew *T. sebifera* from native (China) and invasive (USA) populations with or without bacterial (streptomycin) and/or fungal (iprodione) inhibitors in a factorial experiment in which we measured plant growth and soil N₂O emissions of *T. sebifera*. We hypothesized that: (1) *T. sebifera* plants from invasive populations will be impacted more negatively by suppression of soil microbes than ones from native populations. (2) Suppression of soil microbes will have a larger impact on soil N₂O emissions with *T. sebifera* plants from invasive populations.

2. Materials and methods

2.1. Seed and soil collection

In November 2018, we collected seeds from three populations of *T. sebifera* in both China (where it is native) and the United States (where it is introduced and now invasive) (Table 1). In April 2019, we collected *T. sebifera* non-rhizosphere soil (depth 0–20 cm after removing surface litter) from under three trees (>300 m apart) in Nanchang Jiangxi, China. We removed visible stones, plant root fragments and other intrusive materials from the soil, sieved the soil with a 2 cm sieve and mixed it thoroughly (Yang et al., 2013; Deng et al., 2019b).

TABLE 1 Locations of native and invasive *Triadica sebifera* populations used in the study.

| Source population | Longitude | Latitude |
|-------------------|-----------|----------|
| China | | |
| Jiangxi | 117.12°E | 28.45°N |
| Jiangsu | 118.37°E | 31.23°N |
| Zhejiang | 118.20°E | 27.12°N |
| USA | | |
| Georgia | 81.01°W | 32.01°N |
| Texas | 95.03°W | 29.78°N |
| Louisiana | 93.15°W | 30.23°N |

2.2. Experimental design

This study site is located at Jiangxi Agricultural University, Nanchang, China (115°50'10" E, 28°45'53" N). It has a subtropical humid monsoon climate. The average annual temperature is 18°C, the maximum temperature in midsummer can reach above 40°C, and the minimum temperature in winter can reach below -10°C; the average annual rainfall is 1,600–1,700 mm, the rainfall is uneven in the year, the rainfall is concentrated in April–June, the soil type is typical red soil.

We conducted a factorial experiment in pots in a greenhouse. The experimental factors were bacterial inhibitor (control vs. streptomycin), fungal inhibitor (control vs. iprodione) and plant population origin (native vs. invasive). We applied 5ml of streptomycin solution (3 g kg⁻¹) to bacterial inhibitor pots and 5ml of iprodione solution (1 g kg⁻¹) to fungal inhibitor pots (Nijjer et al., 2008; Fang et al., 2021). We applied 5 ml of deionized water to control soils. We included three *T. sebifera* populations for each range. In total, there were 72 pots (two bacterial inhibitor × two fungal inhibitor × two origins × three populations × three replications).

Soil characteristics were: organic carbon 14.41 ± 2.19 g kg⁻¹, total N 1.33 g kg⁻¹, NH₄⁺-N 1.12 mg kg⁻¹, NO₃⁻-N 1.24 ± 0.42 mg kg⁻¹, total phosphorus 0.32 ± 0.03 g kg⁻¹ and soil pH 5.26 ± 0.01 (Fang et al., 2021). In April 2019, we planted seeds into trays filled with potting soil. After seed germination, we selected similar-sized seedlings and individually transplanted them into 1.5 L plastic pots, which were filled with 1.5 kg of the treated *T. sebifera* non-rhizosphere soil. Each pot had a ring for mounting a gas collection chamber.

We measured N₂O fluxes by gas chromatography of air samples collected in static opaque chambers. We placed the plexiglass, foil-wrapped chamber (60 cm tall, 18 cm diameter) into the water filled ring (between 2:30 and 5:30 p.m.). We collected 40 ml of gas with a plastic 60 ml syringe 0, 10, 20, and 30 min after chamber installation which we brought back to the laboratory for analysis. We took gas samples from July to October in 2019, at days 1, 6, 9, 12, 18, 28, 35, 38, 41, 48, 56, 65, and 80, starting 1 week after transplantation. Soil temperature (Supplementary Figures 1A, B), and moisture (5 cm depth) (Supplementary Figures 2A, B) were monitored simultaneously when N₂O emission rates (Supplementary Figures 3A, B) were measured.

We measured plant height and leaf number then harvested leaves, stems, and roots separately. We dried them at 60°C for 72 h then weighed them and calculated root to shoot ratio and total mass.

2.3. Soil N₂O emission determination

We estimated soil N₂O emission rates as:

$$F = P \times V \times \frac{\Delta c}{\Delta t} \times \frac{1}{RT} \times M \times \frac{1}{S}$$

where F indicates soil N₂O emission rate (μg m⁻²h⁻¹), P stands for standard atmospheric pressure (Pa) (which should be adjusted if partial pressure of water vapor of chamber air taken into consideration) (Carter and Gregorich, 2007; Deng et al., 2019a), V refers to the volume of chamber headspace (m³), Δc/Δt means the rate of N₂O (ppb) concentration change with time based on linear regressions (Domeignoz-Horta et al., 2018; Pärn et al., 2018), R stands for universal gas constant (m³ mol⁻¹ k⁻¹), T is the absolute air temperature (k), M means the molecular mass N₂O (g mol⁻¹), and S indicates the collar area (m²).

We estimated cumulative soil N₂O emissions as:

$$E = \sum_{i=1}^n \frac{(F_i + F_{i+1})}{2} \times (t_{i+1} - t_i) \times 24$$

where E indicates cumulative soil N₂O emissions (μg m⁻²) (Deng et al., 2019a; He et al., 2019), F indicates soil N₂O emission rate (μg m⁻² h⁻¹), i means the ith measurement, (t_{i+1}-t_i) refers to the time span (days) between two measurements, and n means the total number of the measurements.

2.4. Data analyses

We used ANOVAs to test the fixed effects of bacterial inhibitor, fungal inhibitor, *T. sebifera* origin and the their interactions on plant height, root mass, stem mass, leaf mass, total mass, root to shoot ratio, soil N₂O emission rate and cumulative N₂O emissions. We included population nested within origin as a random effect. We used least significant difference (LSD) tests to distinguish among means for significant factors with more than two levels (α = 0.05). We performed all statistical analyses using JMP 9.0 Software (Gary, NC, USA).

3. Results

3.1. Soil temperature and soil moisture

Soil temperatures and moisture were similar among treatments for both invasive and native *T. sebifera* population pots (Supplementary Figures 1, 2). Soil temperature and moisture reached their minimum and maximums, respectively, in October at the end of the experiment (Supplementary Figures 1, 2).

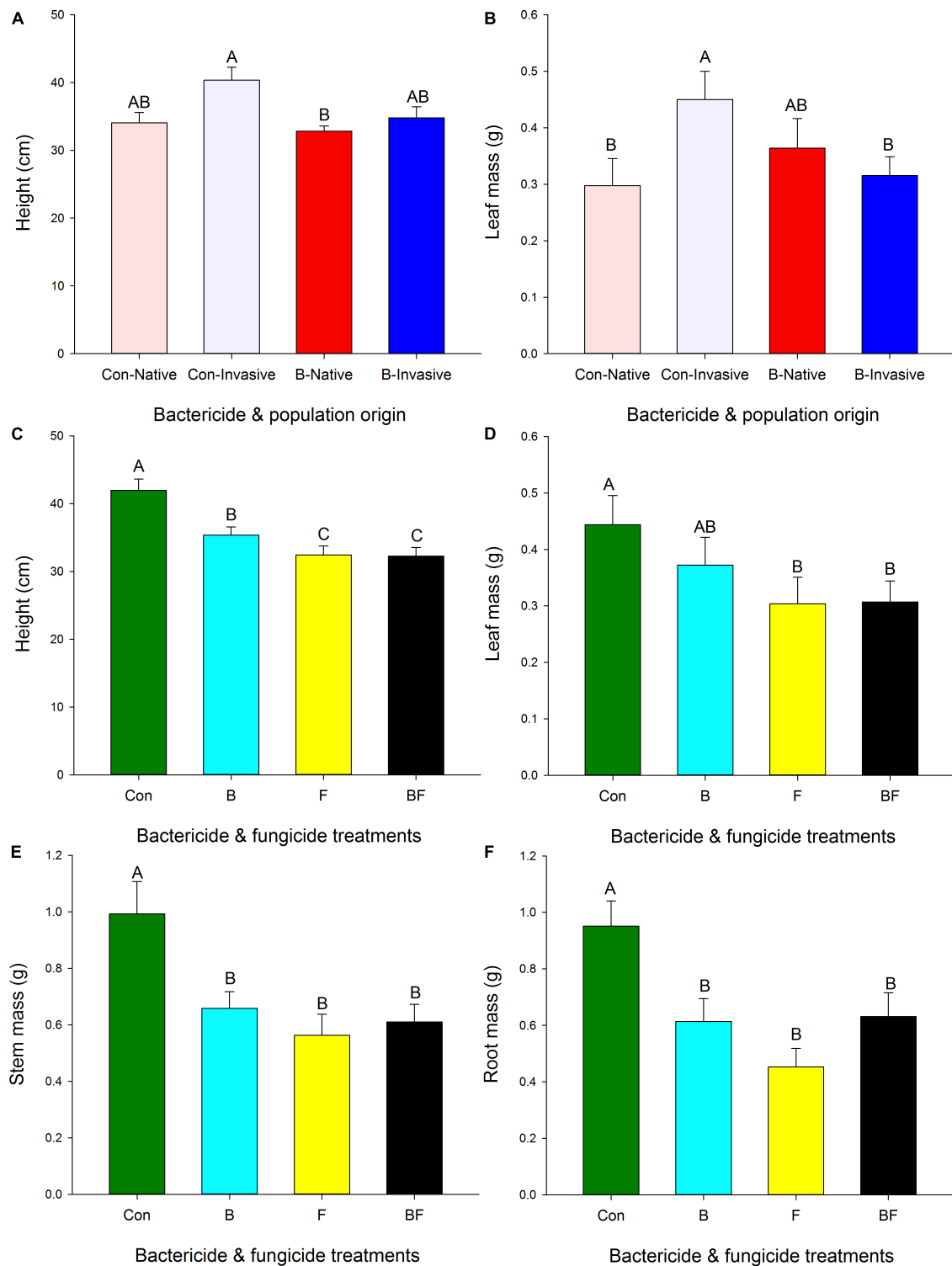


FIGURE 1

Effect of origin, bacterial and fungal inhibitor on height (A), leaf mass (B), height (C), leaf mass (D), stem mass (E), root mass (F) of *Triadica sebifera* (mean \pm se). Con, control; B, bacteria inhibitor; F, fungal inhibitor; BF, bacteria inhibitor and fungal inhibitor. Means with the same letters did not differ in *post-hoc* tests ($p < 0.05$).

3.2. Plant growth

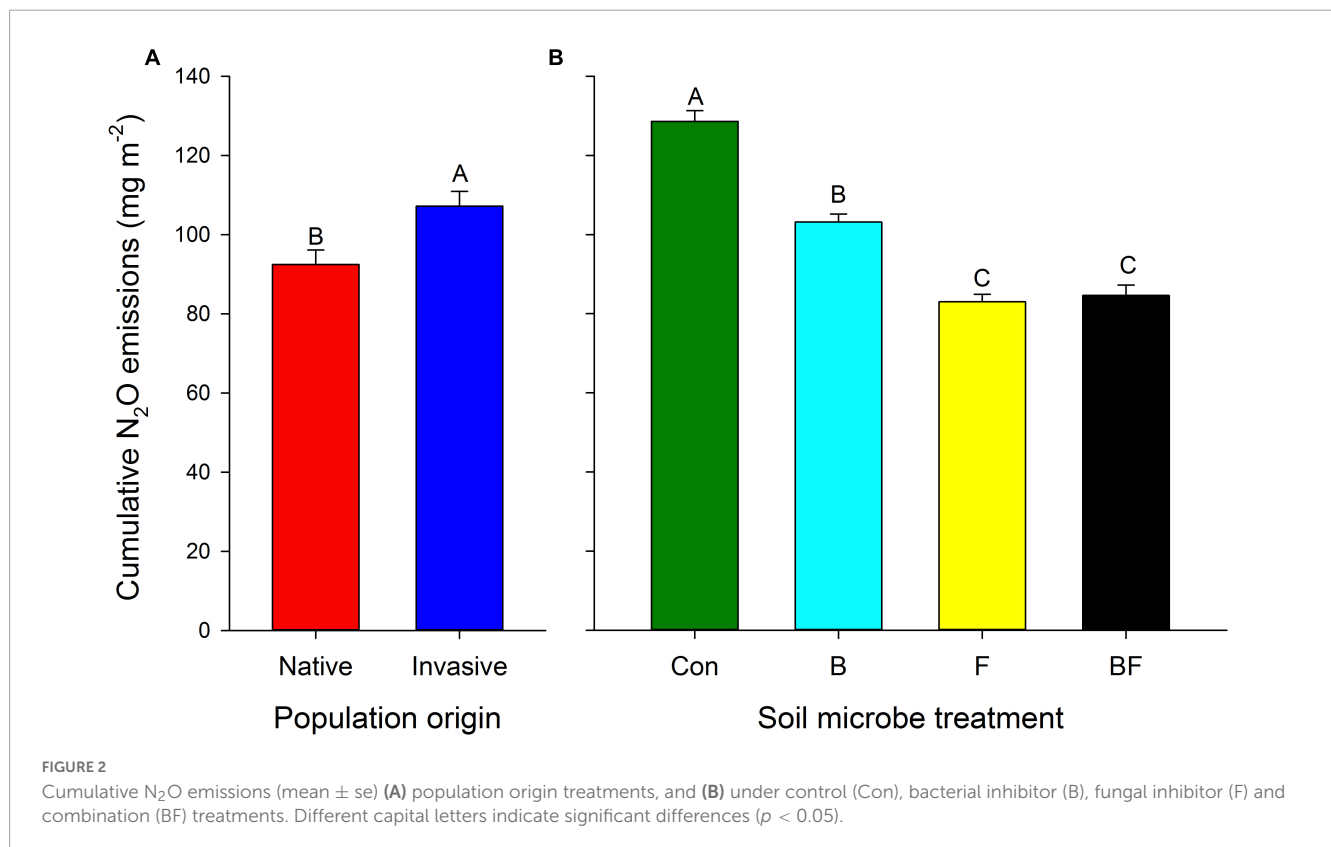
Plant height depended on the interaction of bacterial inhibitor with fungal inhibitor and with population origin (Figure 1 and

Table 2). Plants from invasive populations in control soils were taller than those from native populations with bacterial inhibitor (Figure 1A). Plants were shorter with bacterial inhibitor than in control soils but plants were even shorter with fungal inhibitor

TABLE 2 The dependence of growth on *Triadica sebifera* with different populations, origin (O), bacteria inhibitor (B), fungal inhibitor (F), and their interaction in ANOVAs.

| Fixed effects | df | Height | | Root mass | | Stem mass | | Leaf mass | | Total mass | | R:S | |
|---------------|------|--------------|-------------------|--------------|---------------|--------------|---------------|-------------|---------------|--------------|---------------|-------------|---------------|
| | | F | P | F | P | F | P | F | P | F | P | F | P |
| O | 1.4 | 1.24 | 0.3278 | 1.20 | 0.3350 | 1.30 | 0.3183 | 0.77 | 0.4306 | 1.40 | 0.3028 | <0.01 | 0.9501 |
| B | 1.60 | 14.07 | 0.0004 | 1.13 | 0.2930 | 4.55 | 0.0370 | 0.59 | 0.4441 | 4.71 | 0.0339 | 0.06 | 0.8075 |
| F | 1.60 | 48.94 | <0.0001 | 10.32 | 0.0021 | 12.56 | 0.0008 | 5.41 | 0.0235 | 13.21 | 0.0006 | 0.73 | 0.3975 |
| B × F | 1.60 | 12.63 | 0.0007 | 11.90 | 0.0010 | 8.03 | 0.0062 | 0.72 | 0.3993 | 13.00 | 0.0006 | 8.58 | 0.0048 |
| O × B | 1.60 | 5.68 | 0.0203 | 2.50 | 0.1194 | 1.31 | 0.2576 | 5.16 | 0.0266 | 1.64 | 0.2050 | 0.01 | 0.9364 |
| O × F | 1.60 | 2.01 | 0.1618 | 0.89 | 0.3499 | 0.35 | 0.5574 | 1.38 | 0.2447 | 0.13 | 0.7168 | 1.37 | 0.2457 |
| O × B × F | 1.60 | 0.05 | 0.8301 | 1.25 | 0.2671 | 0.18 | 0.6724 | 0.24 | 0.6256 | 0.07 | 0.7863 | 1.56 | 0.2172 |
| Random effect | | z | P | z | P | z | P | z | P | z | P | z | P |
| Populations | | 1.33 | 0.0917 | 0.83 | 0.2027 | 1.21 | 0.1135 | 0.62 | 0.2675 | 1.06 | 0.1436 | 0.98 | 0.1636 |

Significant results are shown in bold.



applied alone or with both the fungal and bacterial inhibitor (Figure 1C). A similar pattern was found for root, stem and total mass (Figures 1E, F and Table 2).

Leaf mass was lower with fungal inhibitor (Figure 1D and Table 2). The interaction between the bacterial inhibitor and *T. sebifera* population origin had a significant effect on the leaf mass of *T. sebifera* (Table 2). Under the control, the leaf mass of *T. sebifera* was significantly higher than that of the native *T. sebifera*, while the leaf mass of *T. sebifera* of the invasive population origin was significantly lower after the application of bacterial inhibitors (Figure 1B). Root:shoot depended on the interaction of bacterial and fungal inhibitors with lower root:shoot with either inhibitor

applied alone ($B = 0.60$, $F = 0.52$) than when neither (0.66) or both (0.69) were applied (Table 2). Population did not significantly affect any variable (Table 2).

3.3. Soil N₂O emission rate and cumulative N₂O emission

Both N₂O emission rate (+13.73%) and cumulative N₂O emissions were higher with soils associated with plants from invasive vs. native populations (Figure 2A, Table 3, and Supplementary Figure 3A). The strength of this effect on soil

TABLE 3 The dependence of N₂O emission on *Triadica sebifera* with different populations, origin (O), bacteria inhibitor (B), fungal inhibitor (F), and their inhibitor as a fixed factor and measurement time (day) as a random factor in ANOVAs.

| Fixed effects | N ₂ O emission rate | | | Cumulative N ₂ O emissions | | |
|---------------|--------------------------------|----------------|-------------------|---------------------------------------|---------------|-------------------|
| | df | F | P | df | F | P |
| O | 1.64 | 44.46 | <0.0001 | 1,4 | 79.46 | 0.0009 |
| B | 1.64 | 283.07 | <0.0001 | 1,60 | 16.75 | 0.0001 |
| F | 1.64 | 2163.59 | <0.0001 | 1,60 | 121.61 | <0.0001 |
| B × F | 1.64 | 189.35 | <0.0001 | 1,60 | 21.57 | <0.0001 |
| O × B | 1.64 | 1.09 | 0.3004 | 1,60 | 0.34 | 0.5620 |
| O × F | 1.64 | 0.04 | 0.8508 | 1,60 | 0.46 | 0.5024 |
| O × B × F | 1.64 | 0.03 | 0.8679 | 1,60 | 0.28 | 0.5974 |
| Days | 12.768 | 194.73 | <0.0001 | | | |
| × O | 12.768 | 10.71 | <0.0001 | | | |
| × B | 12.768 | 6.02 | <0.0001 | | | |
| × F | 12.768 | 38.62 | <0.0001 | | | |
| × B × F | 12.768 | 3.45 | <0.0001 | | | |
| × O × B | 12.768 | 0.80 | 0.6550 | | | |
| × O × F | 12.768 | 0.72 | 0.7374 | | | |
| × O × B × F | 12.768 | 0.52 | 0.9051 | | | |
| Random effect | | z | P | | z | p |
| Populations | | 1.29 | 0.3050 | | 2.32 | 0.0204 |

Significant results are shown in bold.

N₂O emissions was stronger later in the experiment (Figure 3A and Table 3). Application of bacterial inhibitors, fungal inhibitors and both had significant negative effects on N₂O emission rates compared to untreated control soils (decreased by −22.23, −43.81, and −46.04%, respectively) (Supplementary Figure 3B and Table 3). These effects were stronger at times of higher N₂O emissions (Figure 3B). Cumulative N₂O emissions showed a similar dependence on inhibitors with smaller reductions with bacterial inhibitor alone than with the application of fungal inhibitor alone or with the bacterial inhibitor (Figure 2B and Table 3).

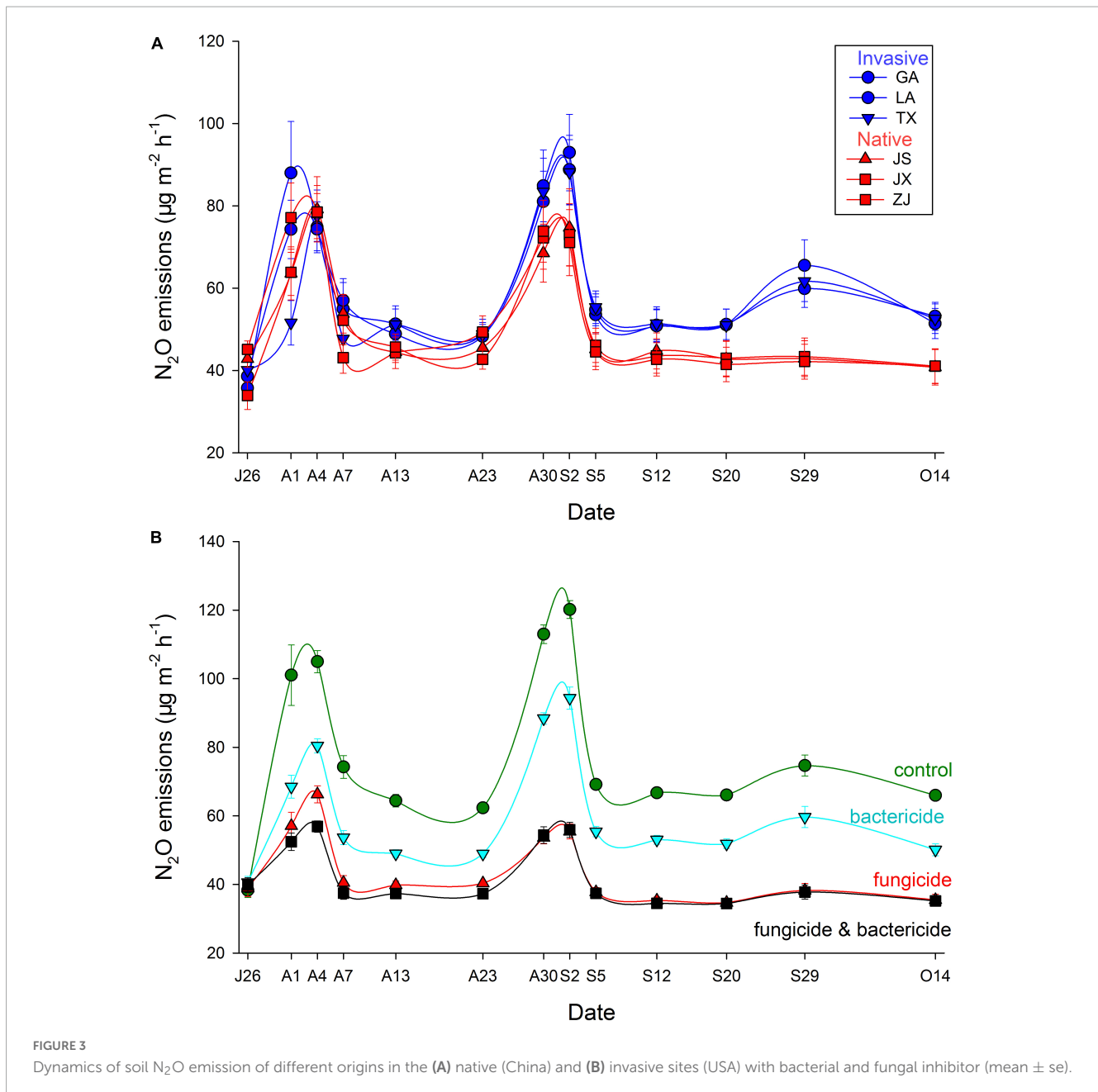
4. Discussion

4.1. Effect of population origin and inhibitors on growth of *T. sebifera*

The bacterial inhibitor had a larger negative impact on the height and leaf mass of *T. sebifera* plants from invasive populations more than ones from native populations (Figures 1A, B). Other studies have found that the interactions of *T. sebifera* from invasive populations with soil microbes differ from those of plants from native populations (e.g., Zou et al., 2007; Yang et al., 2015; Shad et al., 2022). For instance, soil microorganisms can promote the rapid mineralization and uptake of soil organic N by *T. sebifera*, and it has been found that invasive *T. sebifera* promotes soil N mineralization more than native *T. sebifera* (Zhang et al., 2012, 2017). Increased rates of N uptake by invasive *T. sebifera* will likely

also stimulate the growth and activity of soil microorganisms (Zou et al., 2006, 2007; Zhang et al., 2013). Soil microbial communities play a critical role in the successful invasion of plants (Reinhart and Callaway, 2006; Callaway et al., 2011; Zhang et al., 2012) so this finding that invasive and native populations differ in their responses to inhibition of soil bacteria suggests that there may be important differences in the interactions of *T. sebifera* with soil bacteria in the invasive vs. native ranges.

The bacterial and fungal inhibitors had widespread effects on *T. sebifera* performance that did not depend on plant population origin. Across a number of response variables, the bacterial inhibitor decreased *T. sebifera* performance but these decreases were generally much smaller than the negative impacts of application of the fungal inhibitor alone or in combination with the bacterial inhibitor. Soil beneficial microorganisms (e.g., mycorrhizal fungi, rhizobia, etc.) can promote plant invasions by increasing uptake of nitrogen, water and phosphorus from the soil (Reinhart and Callaway, 2006; Callaway et al., 2011; Huang et al., 2016). Because *T. sebifera* receives significant benefits from mycorrhizal associations, it is likely suppression of mycorrhizae contributed to the large negative effect of the fungal inhibitor on plant performance (Nijjer et al., 2007, 2008; Yang et al., 2015; Deng et al., 2017). The relatively lower impact of suppression of soil bacteria on *T. sebifera* performance may reflect the fact that it does not have a close symbiotic relationship with bacteria such as hosting nitrogen fixing bacteria (Pile et al., 2017). However, a larger impact of bacterial inhibition vs. fungal inhibition might occur for a plant that hosts rhizobia but is not mycorrhizal.



4.2. Effect of population origin and inhibitors on soil N₂O emissions of *T. sebifera*

Soil N₂O emissions are mainly produced by microbially mediated nitrification and denitrification (Hu et al., 2015), and microbial community structure and abundance affect soil N₂O emissions (Banerjee et al., 2016). Zhang et al. (2018) found that perennial invasive plants affect soil GHG emissions, and invasive sites increased soil N₂O emissions compared to the native sites. *Triadica sebifera* plants from invasive populations had a higher N₂O emission rate (Supplementary Figure 3A) and cumulative N₂O emission (Figure 2A) than those from native populations, which is consistent with the findings of Zou et al. (2006) and Zhang et al. (2018). One likely explanation for this stimulation of N₂O

emissions is the higher root activity found for *T. sebifera* from invasive populations reviewed by Pile et al. (2017).

Fang et al. (2022) found that nitrification and denitrification rates and subsequent soil N₂O emissions were inhibited when bacterial and fungal inhibitors were applied, and that streptomycin and iprodione applied alone or simultaneously had an inhibitory effect on N₂O emission rates. This is consistent with our experimental results, where both bacterial and fungal inhibitors and their interactions had a significant inhibitory effect on cumulative N₂O emission compared to the control (Figure 2B). Not only are bacteria the main contributors to N₂O release from soil (Johnson et al., 1996), but fungi also play an important role. Fungal nitrification occurs mainly in acidic forest soils, and denitrification occurs mainly in forest soils, grassland soils, and semi-arid areas, where it plays a major role in N₂O release

(Huang and Long, 2014). Cumulative N₂O emissions with fungal inhibitors were significantly lower than those from bacterial inhibitors (Figure 2B). It showed that both fungi and bacteria played an important role in soil N₂O emissions, but fungi contributed more to promote *T. sebifera* soil N₂O emissions. It is important to note, however, that there could be non-target effects of the bacterial and/or fungal inhibitors that we did not explicitly test in this experiment.

Climate change can lead to changes in soil temperature and humidity, which can affect the rate of nitrogen mineralization (Guntiñas et al., 2012), and it is important to include soil temperature and humidity when studying soil greenhouse gas emissions. It has been shown that CO₂ emissions from different land uses are significantly and positively correlated with soil temperature, and that N₂O emission fluxes from different land use types increase and then decrease with increasing soil moisture, reaching a maximum at 25% gravity water content (Sang et al., 2021). Although soil temperature and moisture were not confounded with our treatments here, the insights from this research area would be strengthened by having a variety of environmental treatments.

Exotic plant invasion and global climate change interact to shape greenhouse gas emissions with climate change promoting plant invasion and plant invasion affecting greenhouse gas emissions such as N₂O by influencing ecosystem carbon and nitrogen cycles (Yuan et al., 2015). Plant invasion can have an impact on GHG emissions, such as increasing soil N₂O emissions (Zou et al., 2006; Zhang et al., 2018). Increased nitrogen deposition, increased greenhouse gas emissions, and higher temperatures affect ecosystem stability and lead to increased plant invasiveness (Lei et al., 2010; Bradley et al., 2012; Deng et al., 2019b). Studies have been conducted to combine global climate change and plant invasion (Fennell et al., 2013; Huang et al., 2013; Sorte et al., 2013), but scientific studies on how non-CO₂ greenhouse gases such as N₂O interact with plant invasion are still lacking, and research in this area should continue to be strengthened to understand the causes and consequences of plant invasions, especially in the context of greenhouse gas emissions.

5. Conclusion

We found that soil microorganisms play an important role in the performance of *T. sebifera* with fungal inhibition causing large decreases in plant performance and bacterial inhibition causing smaller decreases in plant performance, especially for plants from native populations that were less sensitive to bacterial suppression. The application of bacterial and fungal inhibitors was effective in mitigating soil N₂O emissions, with fungal inhibitors being more effective. Application of fungal inhibitors alone had lower cumulative N₂O emission than bacterial inhibitors alone, indicating that fungi played an important role in contributing to soil N₂O emissions. More long-term, comprehensive studies are needed to more fully understand the effects of this potential microbial mechanism on invasive plant growth and soil N₂O emissions.

Data availability statement

The original contributions presented in this study are included in the article/Supplementary material, further inquiries can be directed to the corresponding author.

Author contributions

XL was responsible for writing this manuscript, analyzed and processed the data, and made figures and tables. LZ designed the experiment and reviewed and edited the manuscript. LL and HF helped with the experiment. NS, JB, XZ, YY, and HW reviewed and edited the manuscript. ES reviewed and edited the manuscript, and revised the tables and figures. All authors contributed to the article and agreed to the final version of the manuscript.

Funding

This study was supported by the National Natural Science Foundation of China (31770749) and Jiangxi “Double Thousand Plan” Science and Technology Innovation High-end Talent Project (jxsq2019201078).

Acknowledgments

We thank Prof. Jianqing Ding and Dr. Baoliang Tian of Henan University for providing seeds of different populations of *Triadica sebifera*.

Conflict of interest

The authors declare that the research was conducted in the absence of any commercial or financial relationships that could be construed as a potential conflict of interest.

Publisher's note

All claims expressed in this article are solely those of the authors and do not necessarily represent those of their affiliated organizations, or those of the publisher, the editors and the reviewers. Any product that may be evaluated in this article, or claim that may be made by its manufacturer, is not guaranteed or endorsed by the publisher.

Supplementary material

The Supplementary Material for this article can be found online at: <https://www.frontiersin.org/articles/10.3389/ffgc.2023.1183336/full#supplementary-material>

References

- Banerjee, S., Helgason, B., Wang, L., Winsley, T., Ferrari, B. C., and Siciliano, S. D. (2016). Legacy effects of soil moisture on microbial community structure and N₂O emissions. *Soil Biol. Biochem.* 95, 40–50. doi: 10.1016/j.soilbio.2015.12.004
- Bradley, B. A., Blumenthal, D. M., Wilcove, D. S., and Ziska, L. H. (2010). Predicting plant invasions in an era of global change. *Trends Ecol. Evol.* 25, 310–318. doi: 10.1016/j.tree.2009.12.003
- Bradley, B. A., Blumenthal, D. M., Early, R., Grosholz, E. D., Lawler, J. J., Mille, L. P., et al. (2012). Global change, global trade, and the next wave of plant invasions. *Front. Ecol. Environ.* 10:20–28. doi: 10.1890/110145
- Callaway, R. M., Bedmar, E. J., Reinhart, K. O., Silvan, C. G., and Klironomos, J. (2011). Differences in soil carbon and nitrogen pools between afforested pine forests and natural shrublands in a Mediterranean area. *Appl. Soil Ecol.* 170:104262. doi: 10.1016/j.apsoil.2021.104262
- Deng, B. L., Liu, Q., Liu, X. S., Zheng, L. Y., Jiang, L. B., Guo, X. M., et al. (2017). Effects of enhanced UV-B radiation and nitrogen deposition on the growth of invasive plant *Triadica sebifera*. *Chin. J. Plant Ecol.* 41, 471–479. doi: 10.17521/cjpe.2016.0292
- Deng, B., Liu, X., Zheng, L., Liu, Q., Guo, X., and Zhang, L. (2019b). Effects of nitrogen deposition and UV-B radiation on seedling performance of Chinese tallow tree (*Triadica sebifera*): A photosynthesis perspective. *For. Ecol. Manage.* 433, 453–458. doi: 10.1016/j.foreco.2018.11.038
- Deng, B., Fang, H., Jiang, N., Feng, W., Luo, L., Wang, J., et al. (2019a). Biochar is comparable to dicyandiamide in the mitigation of nitrous oxide emissions from *Camellia oleifera* Abel. fields. *Forests* 10:12:1076. doi: 10.3390/f10121076
- Domeignoz-Horta, L. A., Philippot, L., Peyrard, C., Bru, D., Breuil, M. C., Bizouard, F., et al. (2018). Peaks of in situ N₂O emissions are influenced by N₂O-producing and reducing microbial communities across arable soils. *Glob. Chang. Biol.* 24, 360–370. doi: 10.1111/gcb.13853
- Ehrenfeld, J. G. (2010). Ecosystem consequences of biological invasions. *Annu. Rev. Ecol. Syst.* 41, 59–80. doi: 10.1146/annurev-ecolsys-102209-144650
- Fang, H. F., Feng, W. X., Luo, L. C., Gao, Y., Wang, B. H., Nasir, S., et al. (2021). Effects of soil microorganisms on chlorophyll fluorescence characteristics of invasive *Triadica sebifera* with nitrogen deposition. *Acta Ecol. Sin.* 41, 9377–9387. doi: 10.5846/stxb202004080828
- Fang, H., Gao, Y., Zhang, Q., Ma, L., Wang, B., Shad, N., et al. (2022). Moso bamboo and Japanese cedar seedlings differently affected soil N₂O emissions. *J. Plant Ecol.* 15, 277–285. doi: 10.1093/jpe/rtab091
- Fennell, M., Murphy, J. E., Gallagher, T., and Osborne, B. (2013). Simulating the effects of climate change on the distribution of an invasive plant, using a high resolution, local scale, mechanistic approach: challenges and insights. *Glob. Chang. Biol.* 19, 1262–1274. doi: 10.1111/gcb.12102
- Fowler, D., Coyle, M., Skiba, U., Sutton, M. A., Cape, J. N., Reis, S., et al. (2013). The global nitrogen cycle in the twenty-first century. *Philos. T. R. Soc. B* 368:20130164. doi: 10.1098/rstb.2013.0164
- Fritze, H., Smolander, A., Levula, T., Kitunen, V., and Mälkönen, E. (1994). Wood-ash fertilization and fire treatments in a Scots pine forest stand: Effects on the organic layer, microbial biomass, and microbial activity. *Biol. Fertil. Soils.* 17, 57–63.
- Guntiñas, M. E., Leirós, M. C., Trasar-Cepeda, C., and Gil-Sotres, F. (2012). Effects of moisture and temperature on net soil nitrogen mineralization: A laboratory study. *Eur. J. Soil Biol.* 48, 73–80. doi: 10.1016/j.ejsobi.2011.07.015
- Herold, M. B., Baggs, E. M., and Daniell, T. J. (2012). Fungal and bacterial denitrification are differently affected by long-term pH amendment and cultivation of arable soil. *Soil Biol. Biochem.* 54, 25–35. doi: 10.1016/j.soilbio.2012.04.031
- He, T., Yuan, J., Luo, J., Wang, W., Fan, J., Liu, D., et al. (2019). Organic fertilizers have divergent effects on soil N₂O emissions. *Biol. Fertil. Soils* 55, 685–699. doi: 10.1007/s00374-019-01385-4
- Huang, J., Xu, X., Wang, M., Nie, M., Qiu, S., Wang, Q., et al. (2016). Responses of soil nitrogen fixation to *Spartina alterniflora* invasion and nitrogen addition in a Chinese salt marsh. *Sci. Rep.* 6:20384. doi: 10.1038/srep20384
- Huang, W., Carrillo, J., Ding, J., and Siemann, E. (2012). Interactive effects of herbivory and competition intensity determine invasive plant performance. *Oecologia* 170, 373–382. doi: 10.1007/s00442-012-2328-6
- Huang, W., Wang, Y., and Ding, J. Q. (2013). A review of adaptive evolution of defense strategies in an invasive plant species, Chinese tallow (*Triadica sebifera*). *Chin. J. Plant Ecol.* 37, 889–900. doi: 10.3724/SP.J.1258.2013.00092
- Huang, Y., and Long, X. E. (2014). Contribution of fungi to soil nitrous oxide emission and their research methods: A review. *Chin. J. Appl. Ecol.* 25, 1213–1220.
- Hu, H. W., Chen, D., and He, J. Z. (2015). Microbial regulation of terrestrial nitrous oxide formation: Understanding the biological pathways for prediction of emission rates. *FEMS Microbiol. Rev.* 39, 729–749. doi: 10.1093/femsre/fuv021
- IPCC (2014). *Synthesis Report, Climate Change. Geneva, Switzerland: Contribution of working groups I, II, III to the fifth assessment report of the Intergovernmental Panel on Climate Change.* Geneva: IPCC, 1–164.
- Johnson, C. K., Vigil, M. F., Doxtader, K. G., and Beard, W. E. (1996). Measuring bacterial and fungal substrate-induced respiration in dry soils. *Soil Biol. Biochem.* 28, 427–432. doi: 10.1016/0038-0717(96)00004-1
- Lei, Y., Xiao, H., and Feng, Y. (2010). Impacts of alien plant invasions on biodiversity and evolutionary responses of native species. *Biodiv. Sci.* 18:622. doi: 10.3724/SP.J.1003.2010.622
- Liao, C., Luo, Y., Jiang, L., Zhou, X., Wu, X., Chen, J., et al. (2007). Invasion of *Spartina alterniflora* enhanced ecosystem carbon and nitrogen stocks in the Yangtze estuary, China. *Ecosystems* 10, 1351–1361. doi: 10.1007/s10021-007-9103-2
- Liao, C., Peng, R., Luo, Y., Zhou, X., Wu, X., Chen, J., et al. (2008). Altered ecosystem carbon and nitrogen cycles by plant invasion: A meta-analysis. *New Phytol.* 177, 706–714. doi: 10.1111/j.1469-8137.2007.02290.x
- Marusenko, Y., Huber, D. P., and Hall, S. J. (2013). Fungi mediate nitrous oxide production but not ammonia oxidation in aridland soils of the southwestern US. *Soil Biol. Biochem.* 63, 24–36. doi: 10.1016/j.soilbio.2013.03.018
- Nijjer, S., Rogers, W. E., Lee, C. T. A., and Siemann, E. (2008). The effects of soil biota and fertilization on the success of *Sapium sebiferum*. *Appl. Soil Ecol.* 38, 1–11. doi: 10.1016/j.apsoil.2007.08.002
- Nijjer, S., Rogers, W. E., and Siemann, E. (2007). Negative plant-soil feedbacks may limit persistence of an invasive tree due to rapid accumulation of soil pathogens. *Proc. R. Soc. B: Biol. Sci.* 274, 2621–2627.
- Pärn, J., Verhoeven, J. T., Butterbach-Bahl, K., Dise, N. B., Ullah, S., Aasa, A., et al. (2018). Nitrogen-rich organic soils under warm well-drained conditions are global nitrous oxide emission hotspots. *Nat. Commun.* 9:1135. doi: 10.1038/s41467-018-03540-1
- Pile, L. S., Wang, G. G., Stovall, J. P., Siemann, E., Wheeler, G. S., and Gabler, C. A. (2017). Mechanisms of Chinese tallow (*Triadica sebifera*) invasion and their management implications - A review. *For. Ecol. Manage.* 404, 1–13. doi: 10.1016/j.foreco.2017.08.023
- Ravishankara, A. R., Daniel, J. S., and Portmann, R. W. (2009). Nitrous oxide (N₂O): The dominant ozone-depleting substance emitted in the 21st century. *Science* 326, 123–125. doi: 10.1126/science.1176985
- Reinhart, K. O., and Callaway, R. M. (2006). Soil biota and invasive plants. *New Phytol.* 170, 445–457. doi: 10.1111/j.1469-8137.2006.01715.x
- Rogelj, J., Den Elzen, M., Höhne, N., Fransen, T., Fekete, H., and Winkler, H. (2016). Paris Agreement climate proposals need a boost to keep warming well below 2°C. *Nature* 534, 631–639. doi: 10.1038/nature18307
- Rousk, J., Brookes, P. C., and Bååth, E. (2009). Contrasting soil pH effects on fungal and bacterial growth suggest functional redundancy in carbon mineralization. *Appl. Environ. Microbiol.* 75, 1589–1596. doi: 10.1128/AEM.02775-08
- Sang, W. X., Yang, H. L., and Tang, J. W. (2021). Response of soil greenhouse gas emissions to temperature and moisture across different land-use types. *J. East Chin. Norm. Univ (Nat Sci)*. 2021, 109–120.
- Shad, N., Liu, Q., Fang, H., Wang, B., Gao, Y., Liu, X., et al. (2022). Soil sterilization and fertility impacts on urease and belowground mass specific phosphatase activity vary among Chinese tallow tree (*Triadica sebifera*) populations. *Plant Ecol.* 223, 397–406. doi: 10.1007/s11258-021-01215-4
- Sorte, C. J., Ibáñez, I., Blumenthal, D. M., Molinari, N. A., Miller, L. P., Grosholz, E. D., et al. (2013). Poised to prosper? A cross-system comparison of climate change effects on native and non-native species performance. *Ecol. Lett.* 16, 261–270. doi: 10.1111/ele.12017
- Walling, E., and Vaneekhaute, C. (2020). Greenhouse gas emissions from inorganic and organic fertilizer production and use: A review of emission factors and their variability. *J. Environ. Manage.* 276:112121. doi: 10.1016/j.jenvman.2020.112121
- Yang, Q., Carrillo, J., Jin, H., Shang, L., Hovick, S. M., Nijjer, S., et al. (2013). Plant-soil biota interactions of an invasive species in its native and introduced ranges: Implications for invasion success. *Soil Biol. Biochem.* 65, 78–85. doi: 10.1016/j.soilbio.2013.05.004
- Yang, Q., Li, B., and Siemann, E. (2015). The effects of fertilization on plant-soil interactions and salinity tolerance of invasive *Triadica sebifera*. *Plant Soil* 394, 99–107. doi: 10.1007/s11104-015-2520-7

- Yuan, J., Ding, W., Liu, D., Kang, H., Freeman, C., Xiang, J., et al. (2015). Exotic *Spartina alterniflora* invasion alters ecosystem-atmosphere exchange of CH₄ and N₂O and carbon sequestration in a coastal salt marsh in China. *Glob. Chang. Biol.* 21, 1567–1580. doi: 10.1111/gcb.12797
- Zhang, J., Siemann, E., Tian, B., Huang, W., and Ding, J. (2020). Differences in seed properties and germination between native and introduced populations of *Triadica sebifera*. *J. Plant Ecol.* 13, 70–77. doi: 10.1093/jpe/rtz048
- Zhang, L., Chen, X., and Wen, D. (2016). Interactive effects of rising CO₂ and elevated nitrogen and phosphorus on nitrogen allocation in invasive weeds *Mikania micrantha* and *Chromolaena odorata*. *Biol. Invasions* 18, 1391–1407. doi: 10.1007/s10530-016-1089-2
- Zhang, L., Wang, H., Chen, N. N., and Zou, J. W. (2012). Effects of soil biotic communities on the seedling performance of native and invasive provenances of *Triadica sebifera*. *J. Biosafety* 21, 41–45.
- Zhang, L., Wang, S., Liu, S., Liu, X., Zou, J., and Siemann, E. (2018). Perennial forb invasions alter greenhouse gas balance between ecosystem and atmosphere in an annual grassland in China. *Sci. Total Environ.* 642, 781–788. doi: 10.1016/j.scitotenv.2018.06.111
- Zhang, L., Zhang, Y., Wang, H., Zou, J., and Siemann, E. (2013). Chinese tallow trees (*Triadica sebifera*) from the invasive range outperform those from the native range with an active soil community or phosphorus fertilization. *PLoS One* 8:e74233. doi: 10.1371/journal.pone.0074233
- Zhang, L., Zou, J., and Siemann, E. (2017). Interactive effects of elevated CO₂ and nitrogen deposition accelerate litter decomposition cycles of invasive tree (*Triadica sebifera*). *For. Ecol. Manage.* 385, 189–197. doi: 10.1016/j.foreco.2016.11.045
- Zhong, L., Qing, J., Liu, M., Cai, X., Li, G., Chen, G., et al. (2022). Fungi and archaea control soil N₂O production potential in Chinese grasslands rather than bacteria. *Front. Microbiol.* 13:1494. doi: 10.3389/fmicb.2022.844663
- Zou, J., Rogers, W. E., DeWalt, S. J., and Siemann, E. (2006). The effect of Chinese tallow tree (*Sapium sebiferum*) ecotype on soil-plant system carbon and nitrogen processes. *Oecologia* 150, 272–281. doi: 10.1007/s00442-006-0512-2
- Zou, J. W., Rogers, W. E., and Siemann, E. (2007). Differences in morphological and physiological traits between native and invasive populations of *Sapium sebiferum*. *Funct. Ecol.* 21, 721–730. doi: 10.1111/j.1365-2435.2007.01298.x



OPEN ACCESS

EDITED BY

Mengyang Hou,
Hebei University, China

REVIEWED BY

Jie Zheng,
Peking University, China
Fengting Wang,
Zhejiang Agriculture and Forestry
University, China

*CORRESPONDENCE

Shaowen Zhang
✉ zsw1100@163.com

†These authors have contributed equally to this work and share first authorship

RECEIVED 23 March 2023

ACCEPTED 28 April 2023

PUBLISHED 02 June 2023

CITATION

Ding N, Li D, Zhang S, Shi K and Chen W (2023) Research on subsidy standards for public welfare forests based on a dynamic game model—Analysis of a case in Jiangxi, China. *Front. For. Glob. Change* 6:1192140. doi: 10.3389/ffgc.2023.1192140

COPYRIGHT

© 2023 Ding, Li, Zhang, Shi and Chen. This is an open-access article distributed under the terms of the [Creative Commons Attribution License \(CC BY\)](https://creativecommons.org/licenses/by/4.0/). The use, distribution or reproduction in other forums is permitted, provided the original author(s) and the copyright owner(s) are credited and that the original publication in this journal is cited, in accordance with accepted academic practice. No use, distribution or reproduction is permitted which does not comply with these terms.

Research on subsidy standards for public welfare forests based on a dynamic game model—Analysis of a case in Jiangxi, China

Na Ding^{1,2†}, Da Li^{3†}, Shaowen Zhang^{1*}, Kankan Shi² and Wei Chen²

¹School of Economics & Management, Beijing Forestry University, Beijing, China, ²National Academy of Forestry and Grassland Administration, Beijing, China, ³Urbanization Research Institute, Beijing City University, Beijing, China

To understand the behavior of the main participants in public welfare forest projects, this article constructs a “forest farmers–local government–central government” dynamic game model by setting the game scope and game principles. The game payment matrix and game equilibrium solutions show that (1) expanding the value of ecological products in the forest to improve operating income will increase the participation of forest farmers; (2) the local government’s enthusiasm for leading public welfare forest projects is mainly influenced by the positive effects of planting and management costs, which provides the theoretical basis for central government to intervene in regional ecological governance; (3) when the central government leads public welfare forest projects, the enthusiasm of the local government for afforestation is positively influenced by the central government’s subsidies. Finally, based on the game equilibrium solution, the expected results of forest farmers’ operational income are calculated using the case of Jiangxi, which confirms the importance of increasing forest farmers’ operational income.

KEYWORDS

public welfare forests, subsidy standard, major players, game model, Jiangxi

1. Introduction

Since the turn of the 21st century, the contradiction between the environment and the development of China has become increasingly prominent. Ecological problems, such as haze and sandstorms, are frequent. On this basis, the government has decided to develop a forestry plan. In recent years, the number of public welfare forestry projects has been increasing rapidly, and the amount of investment has also gradually increased, especially in construction to maintain the original ecological environment. The government has promoted several key forestry projects in succession, for example, natural forest protection projects, forestation engineering, and the “Jing-Jin-Ji” sandstorm control project. In public welfare forestry projects, the distribution of interests and responsibilities among the major players has become increasingly obvious and important. This article focuses on the application of fund allocation, economic benefits, responsibility, and reciprocity in a game, which involves the main participants of a public welfare forestry project.

Forestry projects have both material and ecological implications for public welfare. A public welfare forestry project needs the participation of farmers, village collectives, the government, and various social organizations. After the forestry project forms at a certain scale, it shows the externality of forestry. Therefore, it is necessary to identify and deepen the analysis of many key players in public welfare forestry projects to clarify the role

and influence of the main participants in reform to facilitate the implementation of public welfare forestry projects and to ensure the distribution of ultimate ecological, economic, and social benefits.

1.1. Public welfare forestry project

The government's investment project is a fixed asset investment project constructed through financial investment, issuance of treasury bonds or local fiscal bonds, foreign government grants, financial guarantees of domestic and foreign financial organizations, loans, and administrative income (Shen et al., 2014). Governmental investment project funds mainly come from public funds, which ultimately come from all taxpayers. This defines the public nature of government investment projects, meaning these projects impact broad masses of people (Zhang and Feng, 2014).

A public welfare forestry project is a project in which investment by the government is the main activity. Forestry has a complex ecological, economic, and social function. It cannot be a substitute for the construction of diverse ecological environments and is a powerful guarantee of the development of an ecological civilization. A public welfare forestry project defines forestry's economic externalities, which include carbon sinks, sand fixation, and water conservation (Milton and Gregory, 2008). Therefore, in the obvious contradiction between the ecological environment and economic development, the problem faced in Chinese contemporary forestry is how to promote a favorable relationship between the two. It also means that the government's dominant position in China's forestry construction cannot be shaken in the short term. The special nature of public welfare forestry projects is that the short-term/long-term benefits of forestry projects show strong ecological and social benefits but have few economic benefits. Thus, public welfare forestry projects should emphasize economic externalities when defining the main players' motivation.

1.2. Major players in public welfare forestry projects

Project participants belong to a biological system, and their purpose and various activities are to achieve the functions such as carbon sequestration, water conservation, biodiversity, etc. (Wu et al., 2021). In organizations, people's behavior is influenced by factors related to measurement standards and remuneration in their thought (Wang, 2011). The most important stakeholders in a construction project are the project owners, construction supervision companies, and construction contractors; thus, project participants mainly refer to the owners, contractors, and supervisors participating in the construction project and who should be regarded as equal in terms of their interests and positions (Peng et al., 2007).

Based on the above definition of the major players, the major players' definition of a public welfare forestry project in this article is as follows: it defines people who have "Put a certain 'specific investment' into the individual or organization of the public welfare

forestry project, and therefore, they need to take some form of risk in this course of the project, for they can influence the expectations and implementation of the project".

This definition reflects the fact that the major players in a public welfare forestry project must carry out "specific investments" for this reform (Liu and Li, 2016). The government's "specialized investment" includes financial investment, human capital investment, and monopoly resources (Xu, 2016), while the forest farmers' "specialized investment" includes skill investment and labor investment (Wu and Zhang, 2015). In addition, the main participants in a public forestry project should bear the risks faced in the public welfare forestry projects (Ji, 2015). Finally, the main participants in a public forestry project must be affected by the objectives of the implementation project, which may have either negative or positive effect (Fei, 2015). According to research, the main determinant participants in the reform of the collective forest tenure system include the central government, local government, and forest farmers, which have high legitimacy, high influence, and high urgency and have the closest relationship with the project (Wu, 2014).

1.3. Analysis of rights of the major players

The article defines foresters as "social beings" because they seek to maximize their interests and also measure the social impact of their behavior, which is the basis of all behavioral strategies (Lin, 2013; Qian, 2015; Wang, 2015).

As a member of society, foresters do not have long-term income from afforestation or public welfare forest projects. Their compensation includes government funding, subsidies, salary income, and income from the undergrowth economy. Therefore, whether foresters participate in afforestation projects depends on the government's labor compensation for them and also on the individual forester's sense of social responsibility (Zhang, 2012; Han and Fei, 2013; Zhou, 2014). According to externality theory, the standard of forestry subsidies should reach an ecological value that it can achieve; that is, the subsidy of forestry production should reach the marginal external benefit level of the optimal production level (Zhang et al., 2000). Local governments serve as intermediaries between the central government and foresters. To foresters, local governments are the promoters of afforestation and public welfare forest projects, while for the central government, local governments are the implementers of these projects (Zhou, 2021). In addition, the central government is the implementer of afforestation projects. Local governments also display some "seeking profit" behaviors as they need to measure how to use land or areas of forest to improve economic performance, but they must also consider ecological benefits at the local level, showing its complex "social" nature of these initiatives (Liu, 2012).

The central government in China develops specific policies that represent the common interests of the masses. The "social nature" of the central government is strengthened as the public nature of these policies becomes more prominent. That is, the central government is not limited by immediate interests and also considers long-term targets to develop policy options compared to

the other two major players (Wu, 2011; Xu et al., 2011; Yuan and Ma, 2012).

The central government, therefore, considers whether the long-term benefits of public welfare forest projects are consistent with the overall national interest to determine whether to implement them.

2. Methods

The definitions and analysis of the key players provide us with three major players in public welfare forestry projects, including the central government, local governments, and foresters. In this section, we discuss the tripartite relationship within the game in detail and build a dynamic game model of the major players in a public welfare forestry project.

According to incomplete information dynamic game theory, in a dynamic game, actions have a prioritized sequence. Under the conditions of incomplete information, each game participant knows the relationships of the other player types involved in the game, as well as the probabilities of corresponding choices likely to be made by the “economic” persons involved. However, participants do not know which specific type belongs to the other people involved (Li et al., 2019). Moreover, because there is an action sequence, later actors can observe the behavior of the first players and obtain information concerning the players first, thus confirming or correcting their actions toward the first players (Wu and Zhang, 2014).

2.1. Related concepts

The article clarifies the basic concepts (ecological loss and ecological benefit), and policy-related concepts such as establishment and maintenance cost, sunk cost, and management expenses. The explanations of these concepts are as follows:

1. Ecological loss

The destruction of ecological resources and the resultant economic losses are called ecological losses. The versatility of ecological resources determines their multiple values, therefore, measuring economic loss due to the destruction of ecological resources should be based on the measurement of the various values of the ecological functions. For example, economic losses due to the destruction of ecological resources should be the sum of the value of the ecological loss of resources (Zi, 2004).

2. Ecological benefit

Ecological benefit and loss are equal. The economic benefits of general ecological resources are calculated by the method of calculating ecological losses.

3. Establishment and maintenance cost

The establishment and maintenance cost consists of afforestation costs and nurturing costs. Afforestation costs

refer to the expenses incurred before the forest closure, including investigation and design, land preparation, planting, and replanting. Nurturing costs refer to the expenses incurred after afforestation until the forest is accepted as qualified, including loosening soil, weeding, drought prevention, frost protection, and fertilization.

4. Management expenses

Management expenses refer to expenses incurred after the forest has been accepted as qualified until harvesting (or achieving the predetermined production and management objectives) to prevent and eliminate various damages and disasters to forests, ensure the healthy growth of trees, and avoid or reduce the loss of forest resources. Specific components include forest protection fees, nurturing thinning fees, afforestation facility fees, fine seed testing fees, investigation and design fees, and other management fees.

5. Government subsidies

Government subsidies contain the management and maintenance subsidies provided by the government to encourage farmers to participate in public welfare forest projects.

6. Management expenses

Management expenses depend on the public management expenses and regulatory expenditures of government departments.

2.2. Dynamic game framework

According to the characteristics, relationships, and related concepts of public welfare forestry projects, a dynamic game framework of the major players is given as follows:

2.2.1. Game subjects

The central government, local government, and foresters.

2.2.2. Game subject action order

The central government is the sponsor of a public welfare forestry project, and it develops the plan first; then, the local government implements it, and the foresters ultimately manage and protect it.

2.2.3. Game principle

First, an ecological loss is equal to an ecological benefit. It shows that the profit (loss) coefficients are consistent, and the central government's and the local government's revenue (loss) are proportional to the distribution (Wang and Deng, 2009). As shown below, the coefficient of the local ecological profit (loss) is $(1-\theta)$, and the coefficient of the central government's ecological profit (loss) is θ . Second, the stakeholder who has dominant power pays for the establishment and maintenance costs. Lastly, the level of enthusiasm of local governments in

constructing public welfare forest projects is judged by the proportion of management expenses paid. We believe that the payment proportion of local governments is consistent with the ecological benefit (loss) coefficient, which is $(1-\theta)$.

2.2.4. Foresters

1. The probability of foresters participating in the public welfare forestry project: η ; the probability of not participating in the public welfare forestry project: $1-\eta$. ($0 \leq \eta \leq 1$)
2. The foresters' government subsidies received by participating in the public welfare forestry project: I ; the opportunity cost of not participating in public service forest projects: A .
3. The cost of afforestation and nurturing in the absence of access to government subsidies: M_0 .
4. The foresters' operating income obtained when participating in public welfare forest projects, which is income obtained from a variety of business activities conducted outside forestry, such as catering, tourism, and undergrowth economy activities: U .

2.2.5. Local government

1. The probability of the local government actively promoting the public welfare forestry project: ζ ; the probability of not promoting the project: $1-\zeta$. ($0 \leq \zeta \leq 1$).
2. The cost of afforestation and nurturing: M_0 ; the management expenses of public welfare forest projects: $(1-\theta)M_1$.
3. The local government's revenue (profit) after the foresters participate in the public welfare forestry project: $(1-\theta)P$.
4. The local government's loss (loss) if the foresters do not participate in the public welfare forestry project: $(1-\theta)L$.
5. The central government's punishment of the local government's failure to implement the public welfare forestry project (money): B .
6. The central government reward for the local government actively implementing the public welfare forestry project (money): R .

2.2.6. Central government

1. The probability that the central government actively promotes the public welfare forestry project: ε ; the probability of negative promotion: $1-\varepsilon$, ($0 \leq \varepsilon \leq 1$).
2. The pure cost of the afforestation for the central government: M_0 ; the cost of afforestation and nurturing: M_2 .
3. The central government's revenue (profit) after the foresters participate in the public welfare forestry project: θP .
4. The central government's loss (loss) if the foresters do not participate in the public welfare forestry project: θL .
5. Dominated by the central government, punishment (funding or rights) for passively promoting public welfare forest projects by local government: B .

6. Reward (funding) from the central government for actively constructing public welfare forest projects by local governments: R .

A game tree of the major players is obtained in the public welfare forestry project according to the game sequence and game relationships. The end node of the game tree is marked by the numbers 1–8, which represents the information set of the eight different game situations. The game tree is given in [Figure 1](#).

The nodes (1–8) in the game tree are each a state of the dynamic game. For example, node 5 represents that the central government positively promotes the public welfare forestry project, the local government actively promotes the public welfare forestry project, and the foresters participate in the public welfare forestry project. The payoff matrix (foresters, local government, and central government) order is as follows:

$$[I - A + U, -M_0 - M_1 + (1 - \theta)P - I, \theta P].$$

3. Results

The following part departs from this model step by step, from shallower to deeper. In increasing order, they are Forester's "self-game" model, the "local government–foresters game" model, and the "central government–local government–foresters game" model. The model should be interpreted progressively.

3.1. Foresters self-game model

The foresters, as social persons, will consider whether to participate in the public welfare forestry project and start the interests of the game in the absence of central government or local government financial subsidies ([Lu et al., 2021](#)).

The final node in the game tree is marked by numbers 7–8, which represent the information set of two different game situations. The forester's self-game tree is shown in [Figure 2](#).

Thus, the foresters' payment matrix is obtained, as shown in [Table 1](#).

When the income for participating is equal to foresters not participating in public welfare forest projects, the game reaches equilibrium. Thus,

$$\eta(-A - M_0 - M_1 + U) = (1 - \eta)(A - U),$$

$$\eta = \frac{U - A}{M_0 + M_1}.$$

It can be inferred that the enthusiasm of forest farmers to participate in public welfare forest projects increases with the improvement of public welfare forest operating income and decreases with the increase of establishment and maintenance costs, management expenses, and opportunity costs.

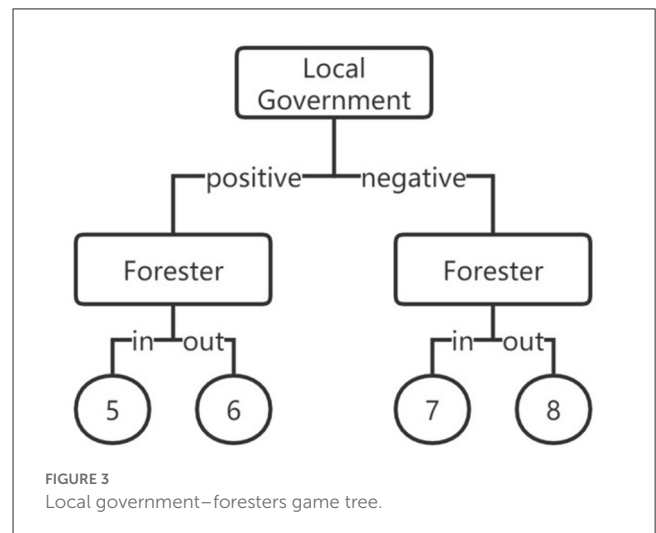
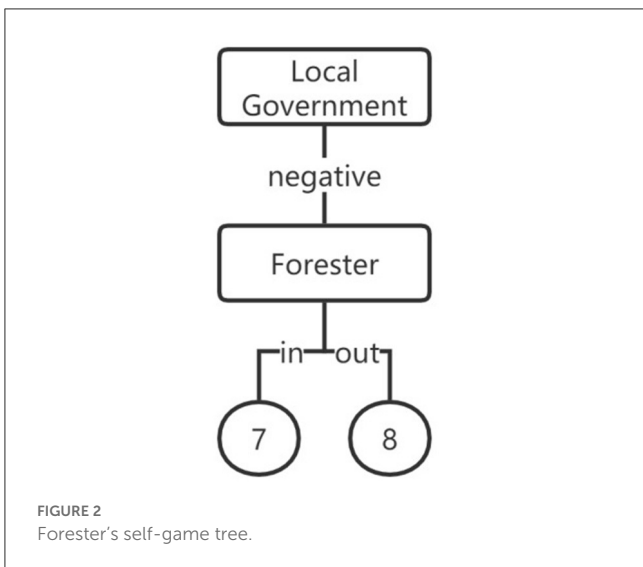
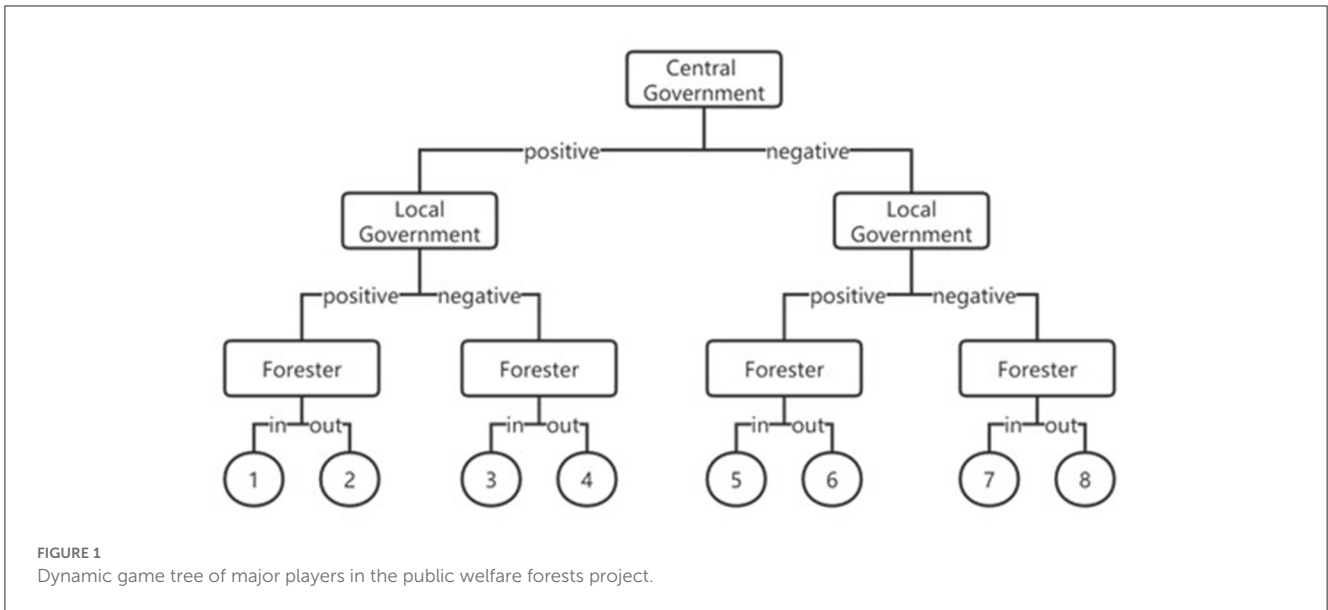


TABLE 1 Foresters payment matrix.

| Node | Foresters payment matrix |
|------|--------------------------|
| 7 | $[-A - M_0 - M_1 + U]$ |
| 8 | $[A - U]$ |

TABLE 2 Local government-foresters payment matrix.

| Node | Local government-foresters payment matrix |
|------|--|
| 5 | $[I - A + U, -M_0 - M_1 - I + (1 - \theta) P]$ |
| 6 | $[A - I - U, -(1 - \theta) L]$ |
| 7 | $[-A - M_0 - M_1 + U, (1 - \theta) P]$ |
| 8 | $[A - U, -(1 - \theta) L]$ |

3.2. Local government-foresters game model

In the absence of the central government's involvement in the public welfare forestry project, local governments and foresters, as participants in the game, will consider whether to construct public welfare forestry project, and then start the interesting game.

We can obtain the game tree according to the order and relationships of the game. The final node of the game tree is marked

by the numbers 5–8, which represents four kinds of information sets of different game situations.

The local government-foresters game tree is shown in [Figure 3](#).

Thus, we can obtain the local government-foresters' payment matrix, as shown in [Table 2](#).

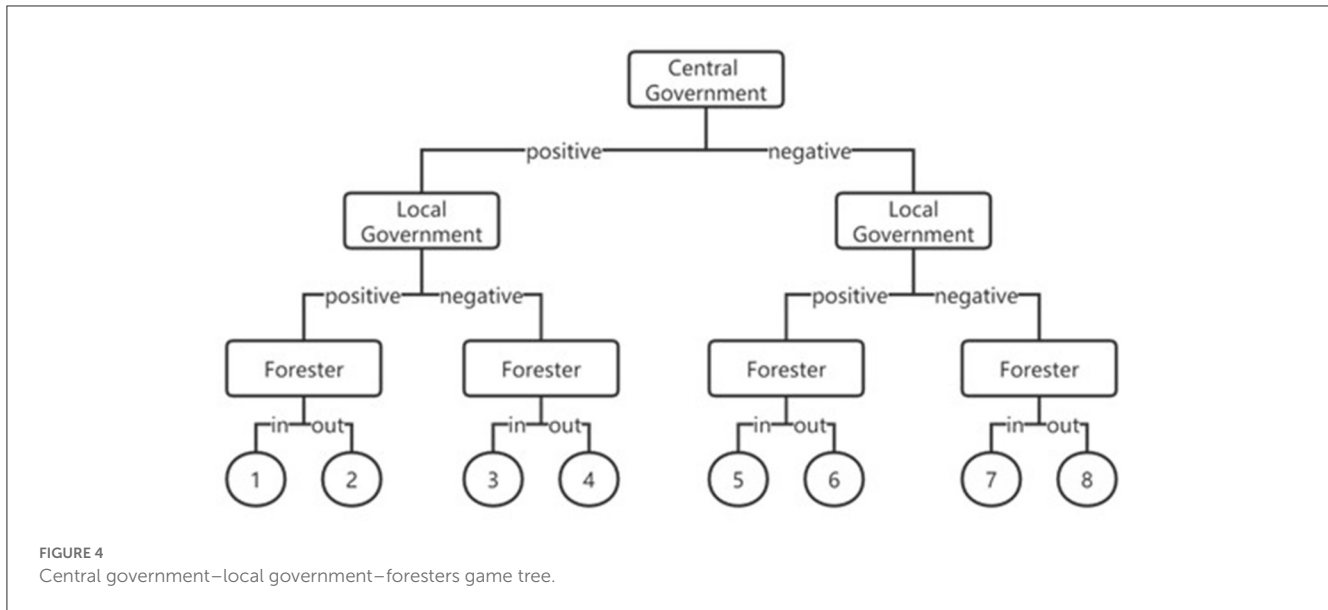


FIGURE 4 Central government–local government–foresters game tree.

According to the payment matrix, it can be inferred that the profit function of forest farmers is as follows:

$$F_1 = \eta \zeta (I - A + U) + (1 - \eta) \zeta (A - I - U) + (1 - \zeta) \eta (-A - M_0 - M_1 + U) + (1 - \zeta) (1 - \eta) (A - U).$$

When $\frac{\partial F_1}{\partial \eta} = 0$, to maximize the payment function of forest farmers, the formula is as follows:

$$\zeta^* = 1 - \frac{2I + 3U - 3A}{2I - A + U + M_0 + M_1}.$$

The profit function of local governments is as follows:

$$F_2 = \eta \zeta [-M_0 - M_1 + (1 - \theta) P - I] + (1 - \eta) \zeta [-(1 - \theta) L] + \eta (1 - \zeta) (1 - \theta) P + (1 - \eta) (1 - \zeta) [-(1 - \theta) L].$$

The partial derivative of the payment function of local governments with respect to ζ is $\frac{\partial F_2}{\partial \zeta} = \zeta (M_0 + M_1 + I)$. It can be inferred that when $\eta = 1$, the payment function of local governments reaches its maximum value of $[-\zeta (M_0 + M_1 + I)]$, and local governments will choose to make $\zeta = 0$ to achieve this maximum value. At this time, $U = A + \frac{M_0 + M_1}{2}$. This means that forest farmers will only have the initiative to participate in afforestation independently if $U \geq A + \frac{M_0 + M_1}{2}$. That is, even if the operating income of public welfare forest projects is greater than the opportunity cost, it is still not enough to motivate forest farmers to participate unless it is added with half of the sum of establishment and maintenance costs and management expenses.

3.3. Central government–local government–foresters game model

In the case of the central government, local governments, and forest farmers, all of whom are participating in the public welfare forestry project as game participants will consider whether to carry out the public welfare forestry project and the interests of the game.

TABLE 3 Central government–local government–foresters payment matrix.

| Node | Central government–local government–foresters payment matrix. |
|------|--|
| 1 | $[U+I-A, -(1-\theta)M_1+(1-\theta)P+R, \theta P-M_0-\theta M_1-R-I]$ |
| 2 | $[A-I-U, -(1-\theta)L+R, -\theta L-R]$ |
| 3 | $[U+I-A, -B+(1-\theta)P, -M_0-M_1+B+\theta P-I]$ |
| 4 | $[A-I-U, -B-(1-\theta)L, B-\theta L]$ |
| 5 | $[I-A+U, -M_0-M_1-I+(1-\theta)P, \theta P]$ |
| 6 | $[A-I-U, -(1-\theta)L, -\theta L]$ |
| 7 | $[-A-M_0-M_1+U, (1-\theta)P, \theta P]$ |
| 8 | $[A-U, -(1-\theta)L, -\theta L]$ |

According to the game order and the game relationships, the game tree of the main participants in the public welfare forestry project is obtained. The final node of the game tree is denoted by the numbers 1–8, which represent the information sets of eight different game situations. The central government–local government–forest farmer’s game tree is given in Figure 4.

Thus, we can get the central government–local government–foresters payment matrix, as given in Table 3.

According to the payment matrix, the profit function of the three stakeholders can be known. The profit function of forest farmers is as follows:

$$F_1 = \eta \zeta \varepsilon (U + I - A) + (1 - \eta) \zeta \varepsilon (A - I - U) + \eta (1 - \zeta) \varepsilon (U + I - A) + (1 - \eta) (1 - \zeta) \varepsilon (A - I - U) + \eta \zeta (1 - \varepsilon) (U + I - A) + (1 - \eta) \zeta (1 - \varepsilon) (A - I - U) + \eta (1 - \zeta) (1 - \varepsilon) (-A - M_0 - M_1 + U) + (1 - \eta) (1 - \zeta) (1 - \varepsilon) (A - U)$$

Therefore, to maximize the payment function of forest farmers, $\frac{\partial F_1}{\partial \eta} = 0$,

$$\zeta^* = 1 - \frac{U + I - A}{I + \frac{1}{2(M_0 + M_1)}}.$$

Similarly, the profit function of local governments is as follows:

$$\begin{aligned} F_2 = & \eta \zeta \varepsilon [-(1 - \theta) M_1 + (1 - \theta) P + R] \\ & + (1 - \eta) \zeta \varepsilon [-(1 - \theta) L + R] \\ & + \eta (1 - \zeta) \varepsilon [-B + (1 - \theta) P] \\ & + (1 - \eta) (1 - \zeta) \varepsilon [-B - (1 - \theta) L] \\ & + \eta \zeta (1 - \varepsilon) [-M_0 + M_1 - I + (1 - \theta) P] \\ & + (1 - \eta) \zeta (1 - \varepsilon) [-(1 - \theta) L] \\ & \quad \eta (1 - \zeta) (1 - \varepsilon) [(1 - \theta) P] \\ & + (1 - \eta) (1 - \zeta) (1 - \varepsilon) [-(1 - \theta) L]. \end{aligned}$$

Therefore, to maximize the payment function of local governments, $\frac{\partial F_2}{\partial \zeta} = 0$,

$$\eta^* = \frac{\varepsilon (R + B)}{(M_0 + M_1 + I) - \varepsilon (M_0 + \theta M_1 + I)}.$$

The profit function of the central government is as follows:

$$\begin{aligned} F_3 = & \eta \zeta \varepsilon [\theta P - M_0 - \theta M_1 - R - I] + (1 - \eta) \zeta \varepsilon (-\theta L - R) \\ & + \eta (1 - \zeta) \varepsilon (-M_0 - M_1 + B + \theta P - I) \\ & + (1 - \eta) (1 - \zeta) \varepsilon (B - \theta L) \\ & + \eta \zeta (1 - \varepsilon) \theta P - (1 - \eta) \zeta (1 - \varepsilon) \theta L \\ & + \eta (1 - \zeta) (1 - \varepsilon) \theta P - (1 - \eta) (1 - \zeta) (1 - \varepsilon) \theta L. \end{aligned}$$

According to the results, the initiative of local governments to promote public welfare forest projects is not determined by the initiative of the central government or forest farmers. The value of ζ^* shows that the initiative of local governments to promote public welfare forest projects mainly includes two aspects: (1) market factors, including the operating income U of forest farmers participating in public welfare forest projects, opportunity cost A , establishment and maintenance costs M_0 , and management expenses M_1 , and (2) government factors, including the subsidies paid by the government I . It is particularly important to note that the central government's funding reward and punishment mechanism has no effect on the initiative of local governments, and other incentive measures are needed. Consistent with the results of the "game model of local government and forest farmers", when $\zeta = 0$, $U = A + \frac{M_0 + M_1}{2}$. In contrast, when $\zeta = 1$, $A = I - U$, which indicates that, when the opportunity cost is high, the government must establish a public welfare forest construction mechanism and implement public welfare forest projects by increasing subsidies.

The result of η^* shows that the initiative of the central government and forest farmers to participate in public welfare forest projects mutually influence each other. Considering that the decision-making of the central government is dominant, two cases are considered when $\varepsilon^* = 0$ and 1, respectively.

When $\varepsilon^* = 0$, $\eta = 0$, indicating that if the central government does not lead public welfare forest projects, the central

government's revenue will be $-\theta L$. When $\varepsilon^* = 1$, $\eta = \frac{R+B}{(1-\theta)M_1}$, it can be observed that, if the central government leads public welfare forest projects, the enthusiasm of forest farmers to participate in such projects mainly includes two aspects: (1) market factors, mainly referring to the management fees M_1 that forest farmers need to pay for participating in public welfare forest projects, and (2) governmental factors, including the punishment B and reward R that local governments bear from the central government, as well as the responsibility-sharing ratio θ between the central and local governments. As the proportion θ of responsibility-sharing by the central government increases, the enthusiasm of forest farmers also increases. Of course, this also means that the ecological importance of public welfare forest projects becomes higher and must be led by the central government. Such projects generally refer to regional and watershed projects.

3.4. Case study in Jiangxi province

In 2021, the total area of public forest in Jiangxi Province was 3.4248 million hm^2 , of which the area of national public forests was 2.1857 million hm^2 , accounting for 63.82%, and the area of local public forests was 1.2392 million hm^2 , accounting for 36.18%.

The total value of the public welfare forest ecosystem services reached RMB¥ 527.846 billion. In 2020, the average compensation standard for ecological public welfare forests was RMB¥ 322.5/ hm^2 , including the management and protection subsidy, which was RMB¥ 315/ hm^2 , and the average public management and protection subsidy was RMB¥ 7.5/ hm^2 .

In 2020, the compensation funds for ecological public welfare forests were arranged and used (Liu et al., 2013), and the requirements of the Management Measures for Ecological Public Welfare Forests in Jiangxi Province (No. 4, 2019) were implemented (Lou et al., 2008). Among the labor subsidies for the collective and individual management and protection of public welfare forests, the supervision expenditure for township governments, grassroots forestry stations, and administrative law enforcement should not be higher than RMB¥ 7.5/ hm^2 (count as RMB¥ 7.5/ hm^2).

Therefore, it can be observed that the management cost $M_1 = \text{RMB¥ } 322.5/\text{hm}^2$.

The total ecological benefits of public welfare forests are RMB¥ 5,278.46 billion, among which the national public welfare forest ecological benefits are RMB¥ 3,368.71 billion, and the local public welfare forest ecological benefits are RMB¥ 1,909.75 billion.

According to the relevant forest land transfer website, the transfer price of some forest land is approximately RMB¥ 4,500/($\text{hm}^2 \cdot \text{year}$). Then, the opportunity costs for the forest farmers are RMB¥ 4,500/ hm^2 (A).

In Jiangxi Province, the main problem is the forest division, suppose the cost of afforestation M_0 is 0.

According to the equilibrium result of the game model, when neither the central nor the local government participates in public welfare forest projects, the operating income value of forest farmers is $U = M_1 + M_0 + A$, which is RMB¥ 4,822.5/ hm^2 , and an operating income of

RMB¥ 165.16 billion needs to be guaranteed each year to independently construct 3.4248 million hm² of public welfare forests. Currently, it is necessary to expand market channels, especially when there are costs for establishing and tending the public welfare forest projects, which require more investment.

4. Conclusion

This article presents a three-stage dynamic game model to theoretically deduce the game equilibrium solution among the main participants of public welfare forest projects (foresters, local governments, and the central government), providing theoretical guidance for the subsequent construction of public welfare forest projects. The main conclusions are as follows:

1. Forest farmers will only actively engage in afforestation if their operating income is high. In recent years, the transformations created through different potential approaches to public welfare forest projects, especially collective public welfare forests, have been explored. The conclusion of this article suggests that the undergrowth economy, carbon sinks, ecotourism, and value realization of ecological products could increase operating income and improve the enthusiasm of forest farmers to participate. The main difficulties faced by forest farmers are afforestation costs, the temptation to secure income through other work, and the main limitation is the lack of deserved government subsidies.
2. When the local government leads public welfare forest projects, its enthusiasm for participation is mainly affected by afforestation costs and management fees. The greater the two factors, the lower the enthusiasm. This provides a theoretical basis for the central government to intervene in regional ecological governance.
3. When the central government leads public welfare forest projects, the afforestation enthusiasm of the local government is not related to the central government's reward and punishment measures (R and B). That is, as long as the central

government releases a public welfare forest plan, the local government will implement it according to the plan. However, the enthusiasm of the local government is still affected by the central government's subsidies. The higher the subsidies, the more public management subsidies the local government can obtain, and the higher the participation enthusiasm. This shows that management subsidies are an effective means of motivating participation at the local level.

Data availability statement

The original contributions presented in the study are included in the article/supplementary material, further inquiries can be directed to the corresponding author.

Author contributions

ND: writing—original draft. DL: writing—reviewing and editing. SZ: supervision and revising. KS: empirical analysis. WC: research design and data collection. All authors contributed to the manuscript and approved the submitted version.

Conflict of interest

The authors declare that the research was conducted in the absence of any commercial or financial relationships that could be construed as a potential conflict of interest.

Publisher's note

All claims expressed in this article are solely those of the authors and do not necessarily represent those of their affiliated organizations, or those of the publisher, the editors and the reviewers. Any product that may be evaluated in this article, or claim that may be made by its manufacturer, is not guaranteed or endorsed by the publisher.

References

- Fei, W. (2015). Search on game behavior of interested parties in ecotourism development of famous towns and villages with historical and cultural background. *Ecol. Econ.* 31, 143–146.
- Han, L., and Fei, M. M. (2013). Analysis of land use decision-making game relationship based on interested parties theory. *Resource. Ind.* 15, 149–154.
- Ji, S. (2015). *Research on Equilibrium Mechanism of Interested Parties in Marine Space Planning*. [dissertation]. [Qingdao]: Ocean University of China.
- Li, D., Zhang, S. H., Huang, J. L., Zhang, B. J., and Feng, Q. (2019). Research on the standards of state-owned public welfare forests management and protection subsidy based on game theory. *J. Arid Land Resource Environ.* 33, 66–73. doi: 10.1080/15324982.2018.1563241
- Lin, Y. (2013). Analysis of interested parties game behavior in grassland ecological compensation. *Tibet Sci.* 11, 19–21.
- Liu, C. Y., and Li, X. M. (2016). Economic cycle, stakeholder game and accounting information quality. *Macroeconomics.* 4, 115–123.
- Liu, H., Zheng, L., Wu, J., Liao, Y., and H. (2013). Past and future ecosystem service trade-offs in Poyang Lake Basin under different land use policy scenarios. *Arabian J. Geosci.* 13, 1–16. doi: 10.1007/s12517-019-5004-x
- Liu, K. H. (2012). *Game study on collective forest right system reform based on interested parties—taking manas county as an example*. [dissertation/master's thesis]. [Urumqi]: Xinjiang Agricultural University.
- Lou, C., Liu, A. X., and Zhu, G. M. (2008). Management pattern of ecological public welfare forests in South China. *Front. Forest. China.* 3, 58–63. doi: 10.1007/s11461-008-0011-1
- Lu, X. H., Zhang, Y. W., and Zou, Y. C. (2021). Evolutionary game and numerical simulation of cultivated land protection policies implementation in China. *Discr. Dyn. Nat. Soc.* 2021, 1–14. doi: 10.1155/2021/5600298
- Milton, D. R., and Gregory, D. J. (2008). *Project management: best practice case analysis*. Beijing, China: Publishing house of electronics industry. 3, 98–127.
- Peng, H., Cheng, G., Xu, Z., Yin, Y., and Xu, W. (2007). Social, economic, and ecological impacts of the "Grain for Green" project in China: A

- Preliminary case in Zhangye, Northwest China. *J. Environ. Manag.* 85, 774–784. doi: 10.1016/j.jenvman.2006.09.015
- Qian, L. (2015). *Research on compensation mechanism of county-level public hospitals based on interested parties game*. Master's Thesis, Ningxia Medical University, Yinchuan, China.
- Shen, L., Ye, K., and Mao, C. (2014). *Proceedings of the 17th International Symposium on Advancement of Construction Management and Real Estate*. Berlin: Springer. Electronic: ISBN: 978-3-642-35548-6.
- Wang, C. (2015). Interpreting the Urbanization of Migrant Population from the Perspective of Interested Parties Theory. *Comp. Econ. Soc. Syst.* 3, 81–91.
- Wang, W., and Deng, D. Q. (2009). "On a game model of forestry investment between the central government and the local government in China," in *Chinese Control and Decision Conference* (Guilin) 4521–4524. doi: 10.1109/CCDC.2009.5191962
- Wang, W. D. (2011). "The study on the early warning mechanism of network structure risk of industrial clusters," in *International Conference on E-Business and E-Government (ICEE)*. doi: 10.1109/ICEBEG.2011.5882507
- Wu, S. H., Hou, X. R., Peng, M. X., Cheng, M., Xue, J. B., and Bao, H. J. (2021). Evaluation of Suitability and Model Partitioning for Realizing the Value of Ecological Regulation Service Products—Taking Lishui City, Zhejiang Province as an Example. *China Land Sci.* 35, 81–89.
- Wu, S. N. (2014). *Research on construction and application of game model of interested parties in reform of collective forest tenure system*. [dissertation/doctoral thesis]. [Beijing]: Beijing Forestry University.
- Wu, S. N., and Zhang, S. W. (2014). Game analysis of Chinese stakeholders in collective forest rights system reform. *Chin. J. Popul. Resour. Environ.* 4, 330–337. doi: 10.1080/10042857.2014.953777
- Wu, X. L. (2011). *Research on interest coordination mechanism of interested parties in BOT project based on game model*. [dissertation/doctoral thesis]. [Nanjing]: Nanjing University.
- Wu, Z. C., and Zhang, J. M. (2015). Evolutionary game analysis of interested parties in grain production. *Stat. Decis.* 22, 61–64.
- Xu, J. X., Xie, Z. Z., and Su, S. P. (2011). Game analysis of the stakeholders in the process of poverty alleviation through science and technology. *J. Cent. South Univ. For. Technol. Soc. Sci.* 5, 68–70.
- Xu, L. M. (2016). *Research on government behavior, interest game and institutional innovation of agricultural insurance in China*. [dissertation/doctoral thesis]. [Wuhan]: Central China Normal University.
- Yuan, H. C., and Ma, H. (2012). Game analysis in the construction claim negotiations. *Proc. Eng.* 28, 586–593. doi: 10.1016/j.proeng.2012.01.773
- Zhang, C. M. (2012). *Research on benefit distribution of EPC project based on cooperative game*. [dissertation/master's thesis]. [Tianjin]: Tianjin University.
- Zhang, P. C., Shao, G. F., Zhao, G., Denis, C. L., Master, G. R., Parker, J. B., et al. (2000). China's forest policy for the 21st Century. *Science*. 288, 2135–2136. doi: 10.1126/science.288.5474.2135
- Zhang, R. J., and Feng, H. (2014). The quantitative analysis methods and application of environmental impact on railway location. *Appl. Mech. Mater.* 522, 778–782. doi: 10.4028/www.scientific.net/AMM.522-524.778
- Zhou, C. H. (2021). Game theory-based analysis of local governments' behavioral dissimulation in the third party soil pollution control under chinese-style fiscal decentralization. *Land* 10, 389. doi: 10.3390/land10040389
- Zhou, D. (2014). *Research on management model of nature reserve based on interested parties*. Doctoral Thesis. [dissertation/master's thesis]. Dalian: Dalian University of Technology.
- Zi, C. (2004). *An analysis on the ecological loss of expressway construction and case study*. [dissertation/master's thesis]. [Chongqing]: Chong Qing University.



OPEN ACCESS

EDITED BY

Hubert Hasenauer,
University of Natural Resources and Life
Sciences, Austria

REVIEWED BY

Romà Ogaya,
Ecological and Forestry Applications Research
Center (CREAF), Spain
María Leticia Monge-González,
Instituto de Ecología (INECOL), Mexico

*CORRESPONDENCE

Zhongqian Cheng
✉ zhongqian@stu.pku.edu.cn
Markku Larjavaara
✉ markku.larjavaara@helsinki.fi

RECEIVED 16 March 2023

ACCEPTED 19 May 2023

PUBLISHED 14 June 2023

CITATION

Cheng Z, Aakala T and Larjavaara M (2023)
Elevation, aspect, and slope influence woody
vegetation structure and composition but not
species richness in a human-influenced
landscape in northwestern Yunnan, China.
Front. For. Glob. Change 6:1187724.
doi: 10.3389/ffgc.2023.1187724

COPYRIGHT

© 2023 Cheng, Aakala and Larjavaara. This is an
open-access article distributed under the terms
of the [Creative Commons Attribution License
\(CC BY\)](https://creativecommons.org/licenses/by/4.0/). The use, distribution or reproduction
in other forums is permitted, provided the
original author(s) and the copyright owner(s)
are credited and that the original publication in
this journal is cited, in accordance with
accepted academic practice. No use,
distribution or reproduction is permitted which
does not comply with these terms.

Elevation, aspect, and slope influence woody vegetation structure and composition but not species richness in a human-influenced landscape in northwestern Yunnan, China

Zhongqian Cheng^{1,2,3*}, Tuomas Aakala³ and Markku Larjavaara^{4*}

¹Key Laboratory for Earth Surface Processes of the Ministry of Education, Peking University, Beijing, China, ²Institute of Ecology, College of Urban and Environmental Sciences, Peking University, Beijing, China, ³Faculty of Science and Forestry, School of Forest Sciences, University of Eastern Finland, Joensuu, Finland, ⁴Department of Forest Sciences, Faculty of Agriculture and Forestry, University of Helsinki, Helsinki, Finland

Elevation-for-latitude substitution offers a tool for studying the influence of temperature and precipitation variability on vegetation structure and composition. Understanding how elevation, aspect, and slope influence vegetation patterns may help in predicting how climate change influences human forest usage and in developing strategies for ensuring the sustained provision of ecosystem services. However, most ecological studies have been carried out in protected areas, leaving forest areas used by humans to lesser attention. Therefore, we asked how elevation, aspect, and slope impact the vegetation on a human-influenced mountain. We measured woody vegetation size, richness, and composition on a mountain with plots set systematically in four cardinal directions at 100-m elevational intervals from the peak, from 1900 to 4200 m above sea level, in the Hengduan Mountains in eastern Himalaya, southwestern China. We quantified how tree maximum height, basal area, aboveground biomass (AGB), tree and shrub species richness, and woody species composition changed with elevation, aspect, and slope. Based on generalized linear models, the maximum tree height, tree basal area, and woody species AGB followed a unimodal trend along elevational gradients, with tree height and basal area peaking at 3100 m, while AGB was highest at 3300 m and somewhat higher on the southern slope. Basal area increased with slope degree. Neither tree nor shrub species richness was influenced by elevation, aspect, or slope. According to canonical correspondence analysis and TWINSpan classification, elevation and north-south orientation of the slope were major factors influencing woody species compositions, and vegetation was classified into five types of communities. Our results indicated that the influences of elevation, aspect, and slope on woody vegetation structure were similar in a human-influenced forested mountain area as in protected mountain landscapes based on the literature. However, as forests in this area are used more intensively at low and middle

elevations of the southern and western slopes, where aridity restricts tree size and AGB, climate change is likely to challenge traditional harvesting practices and place pressure on moving forest usage to higher altitudes.

KEYWORDS

elevational gradients, aspect, slope degree, vegetation structure, vegetation composition

1. Introduction

Understanding how vegetation structure and dynamics depend on climate is a fundamental basis for predicting their phenotypes among various environmental conditions (Moritz and Agudo, 2013), and their fate under a changing climate (Bonan, 2008; Xu et al., 2019). Such predictions are important for understanding species range shifts and biodiversity more generally (Elsen and Tingley, 2015). These changes can have detrimental consequences, such as decreasing forest productivity and increasing risk of natural disturbances, for human communities that rely on forest ecosystems.

Studying how climate impacts vegetation by field sampling large areas using standardized field techniques is arduous and is often hampered by variation in confounding environmental factors (Sanders and Rahbek, 2012). An alternative is to set such studies in smaller areas with elevational variation, i.e., substituting elevation for latitude (Jump et al., 2009). As an example, a 5.2–6.5°C decrease in mean annual temperature every 1000 km toward a higher latitudinal in the temperate region corresponds to a mere 1000 m upslope elevation shift (Colwell et al., 2008). As this elevation-for-latitude substitution allows covering climate gradients over short distances (Sanders and Rahbek, 2012; Rahbek et al., 2019a), many confounding factors, such as biogeographical history, time since glaciation, and soil formation, which covary along latitudinal gradients may change less along elevational gradients (Körner, 2007). Mountains could consequently be treated as relatively uniform and continuous entities at a regional scale (Moeslund et al., 2013). Mountain topography can thus serve as an excellent substitution of a global environment for studying vegetation distributions and functions in the context of climate change (Sanders and Rahbek, 2012).

Topography, specifically elevation, slope, and aspect, influence vegetation structures and dynamics (Grytnes, 2003; Sanders and Rahbek, 2012). Of these, the effect of elevation on vegetation is the most studied topographic factor. Atmospheric pressure and air temperature consistently decrease while radiation under a cloudless sky and the fraction of ultraviolet-B uniformly increase with elevation, whereas other factors, such as precipitation, hours of sunshine, growing season length, geology, and human land use, are mountain-specific variables (Körner, 2007).

A combination of environmental factors at each elevational belt shapes the vegetation structure and composition by controlling the temperature, soil moisture, and light available (Sanders and Rahbek, 2012; Moeslund et al., 2013). A low temperature at high elevations limits tree growth (Fan et al., 2009; Wang et al., 2014, 2021; Gaire et al., 2020), height (Kunwar et al., 2021), basal area

(Acharya et al., 2011), and living biomass (Lin et al., 2012; Wang et al., 2014).

Species richness at the community level may vary with elevation in four ways: a monotonic decrease, a plateau before descent, and hump-shaped and inverse hump-shaped curves. These patterns commonly result from a combination of decreasing temperature and mountain-specific precipitation patterns along elevational gradients (Tang and Fang, 2004; Tang et al., 2012; Yang et al., 2016a).

In addition to the effect of elevation, the slope degree controls vegetation size, composition, and distribution by influencing wind speed, soil water and nutrient content, solar radiation intensity, and seed dispersal distance (Moeslund et al., 2013) and more indirectly by influencing fire severities and frequencies (Rogean and Armstrong, 2017; Gowda et al., 2019). On steeper slopes, higher wind speeds lead to shorter trees (Gardiner et al., 2016). Deep-rooted species are potentially better adapted to steeper slopes because of wind conditions but also due to soil stability issues (Moore et al., 2018). Litter depth changes with slope degree due to sliding caused by wind and gravity, leading to spatial variations in soil moisture, nutrient status, and soil temperature (Dulamsuren and Hauck, 2008), which again indirectly influence fire regimes (Luo et al., 2021).

Aspect influences solar radiation, precipitation, and wind, which in turn impact vegetation composition, structure, and growth (Burnett et al., 2008; Moeslund et al., 2013; Qin et al., 2021). In the temperate region of the Northern Hemisphere, equator-facing aspects between the south and southwest experience a remarkably warmer microclimate than other slopes (Perring, 1959). This temperature difference has been demonstrated to influence species composition and diversity at various scales in several mountain ranges (Yang et al., 2016b; Heydari et al., 2021; Qin et al., 2021). The dryness of equator-facing slopes increases fire severity, consequently influencing vegetation (Beatty and Taylor, 2001). These could either change the vegetation structure and species richness (Gowda et al., 2019) or alter fire return intervals (Rogean and Armstrong, 2017).

Studies on vegetation patterns show that less-human-impacted study sites are typically preferred to avoid the confounding factors caused by human influence. However, completely intact forest landscapes only covered 22% of forested land globally in 2000 (Potapov et al., 2017). Although many researchers have already emphasized the importance of understanding human impacts on forest ecosystems at local (Monge-González et al., 2019), regional (Qu et al., 2020; Ge et al., 2021), and global scales (Isbell et al., 2017), most ecological studies were nonetheless conducted in protected areas (Martin et al., 2012). Because of this systematic bias, studies in unprotected landscapes are especially valuable for understanding the current state of forested ecosystems of the world. More

importantly, the management of managed landscapes benefits from evidence-based guidelines that can ensure the sustained provision of ecosystem services in the changing world.

To set up our research, we chose Wujing county, a sparsely populated (population density 12.2 people km⁻²) region in northwestern Yunnan, China. As in most of the world, most vegetation ecological research in northwestern Yunnan has been carried out in protected areas, but we selected a mountain where local people still utilize wood from the forests. We arranged the sample plots systematically and objectively along cardinal compass directions and contours, thereby avoiding a potential bias from restricting the sampling close to roads or trails. Specifically, we studied how three topographic factors, i.e., elevation, aspect, and slope, influence (1) vegetation structure, represented by maximum height, basal area, and aboveground biomass (AGB); (2) woody species richness; and (3) woody species composition in this human-impacted landscape. For each of these, we hypothesized that (1) vegetation structure and richness would follow a hump-shaped pattern along elevational gradients due to more frequent disturbances and a more xeric climate at lowest elevations, and cold temperatures at highest elevations that constrain vegetation growth; (2) these vegetation attributes would show a linear increase from cooler to warmer aspects along both north-south and east-west orientations; and (3) these attributes would also show an increase with slope steepness due to less human activity at steeper slopes; (4) Vegetation composition would be driven by elevation, aspect, and slope degree.

2. Materials and methods

2.1. Location and geography

We chose Shangri-La, Diqing Tibetan Autonomous Prefecture, in the northwestern corner of Yunnan Province in China as our study area. It is part of the eastern Himalaya-Hengduan Mountain region, which is characterized by dramatic topographical differences. This area is a globally recognized hotspot for biodiversity conservation (Myers et al., 2000; Sloan et al., 2014; Rahbek et al., 2019b) and a high-priority area for restoration efforts (Strassburg et al., 2020). For example, the area has the highest number of gymnosperm species in the world (Barthlott et al., 2007). The climate is controlled by the Indian southwest monsoon in the southwest and the southeast Pacific monsoon in the southeast (Li et al., 2011; Shen, 2016). Three parallel rivers, Jinsha River, Nu River, and Lancang River, running from north to south, are separated by the Hengduan Mountains. The area has distinct dry and wet seasons, with rainy summers and dry winters. The dramatic topography results in broad climatic gradients ranging from subtropical to polar along elevational gradients (Liu et al., 2016).

We narrowed down our study area to Wujing County in Shangri-La by balancing accessibility and remoteness, and by utilizing the digital elevation model (DEM) to locate the greatest elevational difference. To explore the area, we interviewed local people and conducted field visits to various mountains in Wujing. We tried to avoid recent major construction projects in the mountains and protected areas, ensuring that the selected

mountain represented the region. Ultimately, we selected a mountain (27.66–27.73°N, 99.45–99.54°E) peaking at 4231 m. Its base reaches the Jinsha River, a tributary of the Yangtze River, at 1920 m above sea level to the west, while Wujing town is located nearby. The majority of settled villages are situated at approximately 3000 m on the western and southern slopes of the mountain. Although the land is owned by the state, the local community can use the forest with permission.

Before the Natural Forest Protection Program was launched in 1998 (Hua et al., 2018), large-scale logging operations were carried out in the region including the studied landscape. Significant tree harvesting has probably been carried out, and in the decades before this project, logs have been floating in the Yangtze river for transportation to eastern China (Isbell et al., 2017). Unfortunately, at the time of interviewing the local people and discussing the history of the mountain and residents' livelihoods, we lacked scientific data on this harvesting history and on other impacts by people on these forests. Nowadays, villagers can apply for cutting permits from the local state-owned forest farm to log timber for building houses or to use as firewood. Meanwhile, when funding is available, the local forest farm calls on villagers to afforest the open land areas and along the roads, by seeding or planting seedlings. Villagers also used to grow crops at some distance from the village among the forests, but this practice was abandoned after the Grain for Green Project launched in 1999 (Hua et al., 2016). Three ethnic minorities live in the area. Naxi and Lisu peoples mainly cultivate lower-elevation land, while Tibetans additionally raise yaks and cattle at elevations above 3500 m.

During 1958–2021, the mean annual air temperature (MAT) of the closest meteorological station (28.02° N; 99.73°E) at 3290 m was 5.2°C and the mean annual precipitation (MAP) was 702 mm, with >90% of the precipitation falling from April to October according to climatic data derived from the National Meteorological Information Center of China.¹ Soils at altitudes between 2000 and 4000 m can be classified as yellow cinnamon soil, mountain dark brown soil, mountain brown coniferous forest soil, or alpine meadow soil (Huang et al., 2020). In terms of IUCN Global Ecosystem Typology (Keith et al., 2020), the study area is tropical or subtropical lowland rainforests, boreal and temperate high montane forests and woodlands, deciduous temperate forests, and pastures.

2.2. Study design

To determine the sampling plots, we utilized the Advanced Land Observing Satellite (ALOS) DEM with 30-m resolution to locate the contours. The mountain's highest point was identified as the primary reference point (Peak in Figure 1). Four transects were drawn at the cardinal north, east, south, and west of the peak, which continued until they intersected with a river or a significant incline where the subsequent plot would be higher than the previous plot. Circular plots were placed at the intersections of the contours and transects, except in the presence of a village, cropland, or road. In total, we established 50 plots: eight plots at 3500–4200 m in the north transect, four plots at 3900–4200 m in the east transect,

¹ <http://data.cma.cn/>

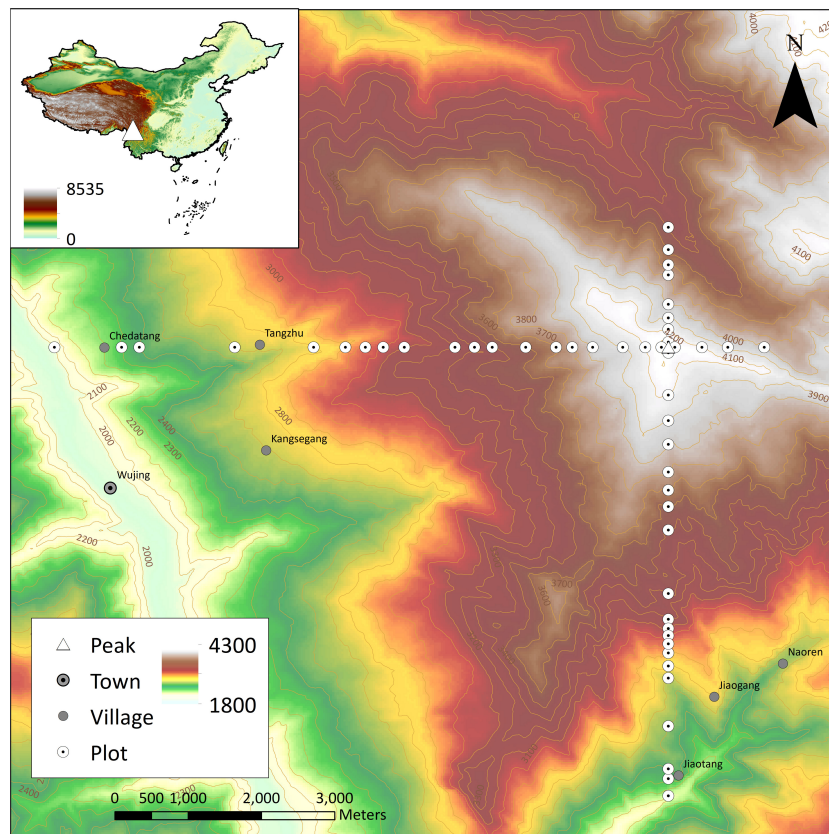


FIGURE 1
Research area location and plot arrangement.

twenty plots at 2200–4200 m in the south transect (excluding 2300 m due to a cliff), and eighteen plots at 2000–4200 m in the west transect (excluding 2100, 2200, 2300, 2600, and 2700 m due to the presence of villages). North and east transects were shorter because the mountain is asymmetric with longer slopes to deep valleys in the south and west. We derived plot information on elevation, aspect in azimuth degree, and slope degree from the DEM. All the procedures were carried out using ArcGIS 10.6 software (ESRI, USA).

2.3. Field sampling

To maintain a relatively consistent number of trees across all plots, we calculated the radius of each circular plot based on the number of trees with a diameter at breast height (DBH) greater than 3 cm found within a 5-m radius plot centered around the plot's midpoint. If more than 25 trees were counted, the plot radius was set at 5 m. If the plot contained between 11 and 25 trees, a 10-m radius was used. If the plot contained between 6 and 11 trees, a 15-m radius was used. If the plot contained less than 6 trees, a 20-m radius was used.

The plots were named based on a combination of the compass direction of each transect and the elevation of the plot. However, for three of the 50 plots, the standard radius could not be used. Plot S2200, located at the southernmost point of the transect, was

situated on the edge of a riverbank that we wished to exclude. Therefore, we reduced the plot radius to 6 m. Plot S2600 was located on abandoned cropland that was surrounded by planted trees. To exclude the trees, we set the plot radius to 2.5 m, extending to the border of the planted area. Plot S3200 was located at a cliff edge, and we reduced the plot radius to 2.5 m to accommodate the terrain.

Starting from the north direction, trees with diameter at 1.3 m height (DBH) of more than 3 cm were counted clockwise, mapped, and measured. Trees that were forked below 1.3 m were counted as separate individuals. Each tree was numbered with an aluminum tag. Tree mapping was performed by recording the azimuth (measured by Garmin GPSMAP 66i) and distance (measured by Haglöf Vertex Laser Geo, Haglöf Ltd., Sweden) of the tree from the plot center. The DBH of all trees were measured with a DBH tape. To reduce the amount of fieldwork, the heights of the first five trees (measured with a Vertex Laser Geo or a 20-m fishing rod) were measured for each species in the plots, and subsequently the height was measured whenever the DBH of a tree was either larger or smaller than the first five trees. Heights for the remaining trees were estimated based on plot- and species-specific height–DBH relationships. Dead standing trees with DBH > 10 cm were recorded if they were in the early stage of decay, their heights were measured only if the remaining stem was more than half of their final height. Cut stumps were mostly shorter than 1.3 m, and they are not considered. The species, height, diameter, coverage of the plot in percentage, number, and distribution was recorded for shrubs with more than one main stem growing from

the ground in the 2.5-m radius subplot with the same center. For herbaceous vascular plants, their species, height, cover, and number were recorded in the 1-m radius subplot with the same center. Species identification and their scientific name were checked using the *Flora of China online edition* (Institute of Botany, Chinese Academy of Sciences).

2.4. Statistical analysis

All statistical data analyses were computed in R language using R Studio (Crawley, 2013).

Non-linear regression analysis was carried out to estimate the heights of unmeasured trees. The relationship between height and DBH was expressed as the function (Zhang et al., 2020) (Eq. 1):

$$\log(y) = a + b \log(x) \quad (1)$$

where x is DBH, y is height, respectively; a , b are the estimated parameters.

To obtain comparable values for plots of varying sizes for species richness and maximum height, we used the area from 5-m radius plots, namely 78.5 m², as the basis for these two attributes. We used the actual measured value when plot radius was 5 m. Otherwise, we used the relationship between richness and area as the basic model, which also followed the same form as Eq. 1, where x was area computed based on the distance of the tree to the plot center and y was either the tree species richness or the maximum height, respectively (Scheiner, 2003; Lyman and Ames, 2007). All non-linear parameter analyses were carried out with the *nls* function in the *dplyr* package (Hadley et al., 2023). However, this function in R requires more than three observations. Thus, if a plot had two tree species, we recorded the number of species within a 5-m radius. For plots that had only one species, the estimated number was one.

For calculating the AGB of tree species (Mg ha⁻¹), we first searched for species- and genus-specific allometric equations. However, for *Quercus* and *Juglans* these were parameterized with much smaller trees than what were growing on our plots. Therefore, instead of extrapolating, which could potentially have led to severe biases, we used a pantropical AGB model from Equation 4 in Chave et al. (2014):

$$\text{AGB} = 0.0673 \times (\rho D^2 H)^{0.976}, \quad (2)$$

where ρ is wood-specific gravity in g cm⁻³ derived from a wood density dataset in the *BIOMASS* package; D is DBH of a tree in cm; H is height in m. This calculation was carried out with the *BIOMASS* package (Rejou-Mechain et al., 2017).

We used species-, genus-, or community-specific allometric equations for calculating the AGB of shrub species (Zhang and Liu, 2010; Wang J. et al., 2012; Xie et al., 2018). We first investigated species-specific allometric equations, and if no matching ones were found, we used equations from the same genus. If no such equations were available, we used general equations from the vegetation community located in a region close by that contained similar species. The allometric equations for shrubs are in Supplementary Table 1.

In addition to estimating the maximum height of tree species, AGB, and tree species richness, BA per hectare was calculated based

on individual DBH, plot area, and the number of trees. These values were then converted to hectares. Shrub species richness was determined by analyzing the data collected from a subplot with a 2.5-m radius.

Plot aspects in azimuth degrees were sine transformed to provide information of each plot's east–west orientation (aspect EW), from west (sine = -1), north or south (sine = 0), to east (sine = 1). Similarly, they were cosine transformed to represent north–south orientation (aspect NS), from south (cosine = -1), east or west (cosine = 0), to north (cosine = 1) (Joly and Gillet, 2017).

Canonical correspondence analysis (CCA) was used to identify relationships with species and elevation, aspect EW, aspect NS, and slope. The proportions of each species out of the total AGB were used to estimate the importance of each species and was log (1 + x) transformed. ANOVA and Monte Carlo significance tests were used to check whether CCA ordination for both axes and for all environmental factors were significant. Multicollinearity between environmental factors was evaluated with variance inflation factors (VIFs). We used variation partitioning to distinguish the contribution proportion of these four environmental factors to the vegetation distribution pattern. TWINSpan classification was implemented for grouping plots. Jaccard similarity index was used to classify vegetation community groups. A height 1.5 m was used where the hierarchical cluster of woody species shall be cut. Ordination was carried out with the *vegan* package (Oksanen et al., 2022), and classification was performed with packages *vegan* (Oksanen et al., 2022) and *twinspanR* (Zeleny, 2021).

Generalized linear models (GLM) were used to detect the responses of AGB per ha, the estimated maximum tree height in the 5-m radius, basal area per hectare, estimated tree species richness in the 5-m radius, and shrub species richness in the 2.5-m radius to elevation, aspect EW, aspect NS, and slope. Considering that the response variable to elevation could either be monotone or a second-order polynomial (Rowe and Lidgard, 2009), the testing environmental independent variables were second-order polynomial elevation, elevation, aspect EW, aspect NS, slope, interaction of elevation and aspect EW, interaction of elevation and aspect NS, interaction of elevation and slope, interaction of aspect EW and slope, and interaction of aspect NS and slope. We used a log-transformed value with Gaussian distribution for AGB, maximum tree height in the 5-m radius, and basal area per hectare, while we log transformed the number of species and used the Poisson distribution for tree and shrub species richness. Akaike information criterion (AIC) (Akaike, 1973) was used to select the best model. χ^2 was defined as null deviance minus the residual deviance of the best model. The models were validated by checking whether the assumptions are met. The residuals plot for regression models were presented in Supplementary Figure 1. GLM was carried out using the *lme4* package (Bates et al., 2015), and AIC evaluation was calculated with the *MuMIn* package (Bartoń, 2022).

3. Results

There were 42 plots with trees, including young forests, secondary forests after disturbance, and mature forests. The eight treeless plots were all located at least 3900 m above sea level in

the west and south transects, except plot S2600, which was on abandoned cropland. We tagged 1225 trees, 34 of which were standing dead trees. The mean tree density of all plots was 1548 trees ha⁻¹. Stand density was greatest in a pure *Pinus yunnanensis* forest in W2400 (6875 trees ha⁻¹), followed by 5603 trees ha⁻¹ in S3200, where *Quercus aquifolioides* and *Pinus yunnanensis* were the dominant tree species. The third highest density was found in N4200, 4170 trees ha⁻¹, with *Rhododendron beesianum* the only species. Tree density was very low in W3600 and W3700, only 64 and 96 trees ha⁻¹. We recorded 76 woody species, including 59 tree species, 22 shrub species, and 5 species that were either trees or shrubs. The five species were: *Camellia yunnanensis*, *Juniperus squamata*, *Quercus aquifolioides*, *Rhododendron anthosphaerum*, and *Rhododendron beesianum*. Their shrub form is defined as lacking a clear main stem.

In the 42 tree plots, the estimated maximum height in the 5-m radius plot ranged from a 3.5-m *Rhododendron beesianum* in N4200 to a 27.8 m *Quercus aquifolioides* in S3300 (Figures 2A1–A4). The tallest tree for which height was measured was an *Abies georgei*, 31.8 m in N3900. Elevation strongly influenced the estimated maximum height in the 5-m radius with a hump-shaped trend along the elevational gradient (Table 1 and Figure 2A1).

The BA for all 42 tree plots ranged from 1.5 to 85.4 m² ha⁻¹ (Figures 2B1–B4). The smallest BA occurred in W2000, which was just above the main road and the Yangtze River, dominated by *Pistacia weinmanniifolia*. The largest BA was recorded in S3200, with *Quercus aquifolioides* as the dominant species. Both elevation and slope had significant effects on BA (Table 1). BA was higher at medium elevations than at low and high elevations (Figure 2B1). According to the AIC score of the GLM model selection, slope showed one of the lowest AIC scores despite being insignificant in the full model ($p = 0.122$; Table 1), and BA increased with slope degree (Figure 2B4).

The AGB of woody species for all plots ranged from <0.1 to 656.3 Mg ha⁻¹, with a mean value of 128.8 Mg ha⁻¹ (Figures 2C1–C4). For the eight treeless plots, the total woody species AGBs were <1.0 Mg ha⁻¹. The lowest AGB in the tree plots was W2000 (3.1 Mg ha⁻¹). The highest AGBs were found in S3200, S3300, and W3400 (480.3, 602.9, and 656.3 Mg ha⁻¹, respectively), which were all dominated by *Quercus aquifolioides*. The AGBs of the two deadwood-dominated plots, W3600 and W3700, were 34.4 and 23.1 Mg ha⁻¹, respectively. AGB was significantly influenced by elevation (Table 1). The trend of AGB along elevational gradients followed a hump-shaped curve, which peaked at 3300 m (Figure 2C1). Even though the residuals of AGB against aspect NS showed heteroscedasticity, AGB decreased slightly from the south to the north aspect (Figure 2C3). Furthermore, AGB was significantly influenced by their interaction (Table 1 and Supplementary Figure 2).

W3000 had the highest estimated tree species richness with 12 tree species. S2700, S2800, and W3200 had 12, 10, and 11 tree species within the 10-m radius, which resulted in estimated 5-m radius plot values of 4.3, 6.0, and 6.6 species, respectively (Figures 2D1–D4). There were only 0.24 tree species in the 5-m radius in W3300, yet the plot's actual tree species richness is 7 due to the plot radius being 20 m. Similarly, the estimated tree richness in the 5-m radius was 0.36 species in W3700, while the measured number in the 20-m radius plot was 5. We observed no clear pattern of tree species richness in the 5-m radius along

environmental gradients, except for a potential unimodal trend of tree species richness along elevational gradients ($p = 0.0529$; Figure 2 and Table 1).

Thirty-nine of the 50 plots contained shrubs. The number of species per plot ranged from one to three (Figures 2D1–D4). Tree plot E4200 had three shrub species: *Rhododendron beesianum*, *Rhododendron rupicola* var. *chryseum*, and *Berberis yunnanensis*. *Fargesia spathacea*, *Rhododendron beesianum*, and *Asparagus miscanthus* were found in S3000, and *Fargesia spathacea*, *Rhododendron beesianum*, and *Cotoneaster franchetii* grew in S3300. Three shrub species found in treeless plot S4100 were *Rhododendron rupicola* var. *chryseum*, *Berberis yunnanensis*, and *Juniperus squamata*. Like tree species richness, shrub species richness did not show any clear trends along environmental gradients (Figure 2 and Table 1).

Elevation, aspect EW, aspect NS, and slope showed significant effects on woody vegetation community composition in the study area, explaining 51.9% of the variation in vegetation composition data ($F = 2.0669$, $p = 0.001$). Elevation explained 27.9% of the variation, while aspect EW, aspect NS, and slope explained 11.2%, 19.3%, and 10.0% of the variation, respectively. The interactions between these topographic factors have less significant impacts than their individual effects (see Supplementary Figure 3).

The eigenvalue and proportion of explanatory variables in the selected CCA1 and CCA2 were 0.870 and 6.40% ($F = 3.408$, $p = 0.001$), and 0.563 and 4.14 ($F = 2.205$, $p = 0.002$), respectively. The first two axes of CCA accumulate explained 67.9% of the relationship between environmental factors and vegetation composition. Elevation and aspect EW were negatively correlated, and aspect NS and slope were positively correlated to CCA1. Elevation, aspect EW, and aspect NS were positively connected, and slope was negatively connected to CCA2 (Table 2). CCA1 was mainly constituted by elevation and slope, CCA2 was composed by aspect NS and aspect EW. Elevation and aspect NS were the most relevant variables in predicting vegetation community compositions, accounting for 9.88 and 7.14% of the variation, respectively.

The ordination of 50 sample plots indicated that all studied plots can be divided into five groups based on their woody species biomass proportion (Figure 3). Both W2000 (green color in Figure 3), located close to the Yangtze River, and S2600 (sky blue color in Figure 3), which was on abandoned cropland, were isolated plots, as they did not correlate with the other plots. S2200–2500, S2700–3300, W2400–2800, and W3000–3100 (red color in Figure 3) were positively correlated, and they were mainly tree plots at medium to low elevation in the west and south transects. W2900, W3300–3900, S3400–3800, E3900–4100, and N3500–4200 (black color in Figure 3) illustrated positive correlations among each other and were in the medium to high elevation. S3900, S4000, S4100, S4200, W4000, W4100, W4200, and E4200 (navy blue in Figure 3) were positively correlated, representing alpine shrub and grassland in the south and west transects. Specifically, W2900, W3300–3600, and S3400 were placed in between two communities (red and black ones), meaning they shared some similar woody species compositions. Similarly, E4200 was located close to the tree plots at a high elevation in the north and east transects because it is in forested part of the tree and alpine grassland ecotone.

The ordination of 76 sample species illustrated five vegetation community types (Supplementary Figure 4, same below) with four

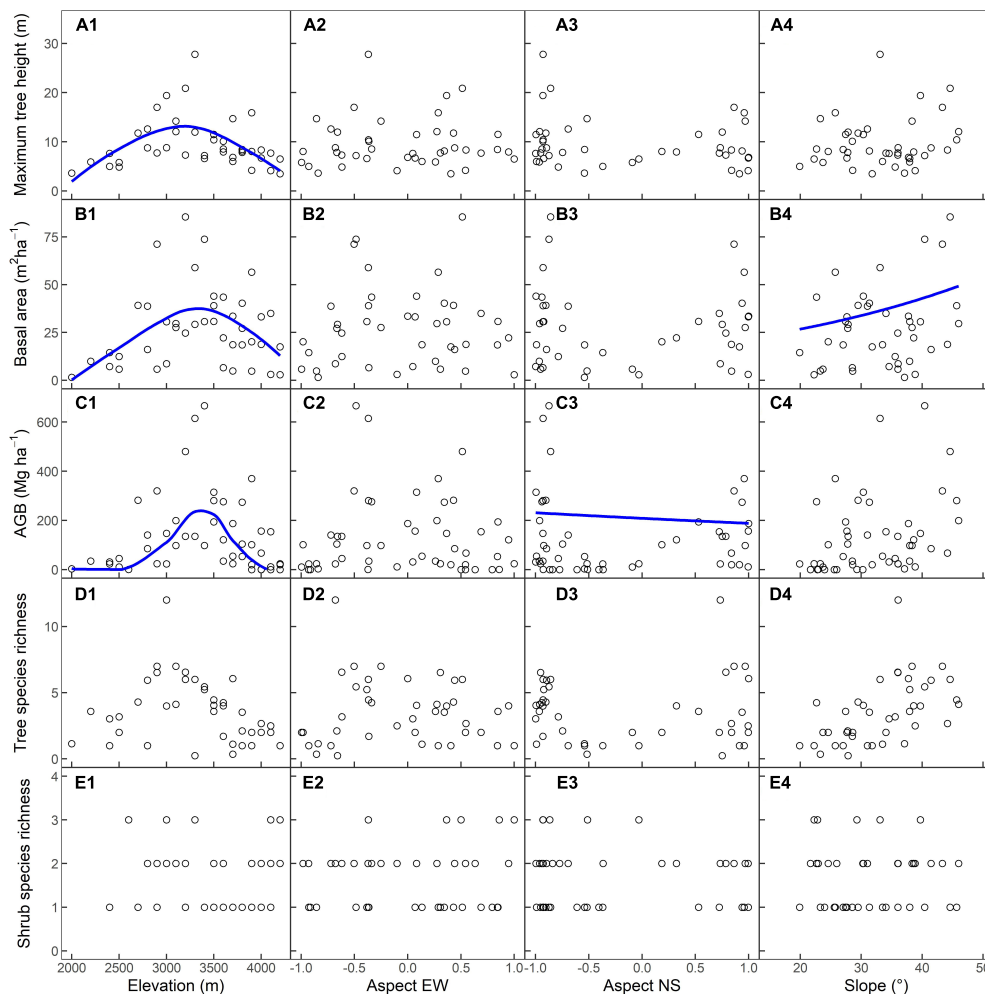


FIGURE 2 Relationship between elevation, aspect east–west orientation (EW), aspect north-south orientation (NS), slope, and (A1–A4) estimated maximum tree heights in the 5-m radius (m), (B1–B4) basal area (BA, m²·ha⁻¹), (C1–C4) aboveground biomass (AGB; Mg·ha⁻¹), (D1–D4) estimated tree species richness in the 5-m radius, and (E1–E4) shrub richness in the 2.5-m radius. Smoothing lines for one given environmental variable to the response variables were fitted by GLMs ($p < 0.05$), and median values of other variables were used.

TABLE 1 Summary of GLM regression.

| Response variables | Estimated regression parameters | Coefficients | T-value | P of parameters | χ^2 | P-value of model* | R ² * |
|--|---------------------------------|--------------|---------|-----------------|----------|-------------------|------------------|
| Estimated maximum height in the 5-m radius (m) | Intercept | -8.400 | -2.699 | 0.011* | 333.7 | <0.001*** | 0.330 |
| | Elevation ² | < - 0.001 | -3.618 | 0.001*** | | | |
| | Elevation | 0.007 | 3.537 | 0.001** | | | |
| BA (m ² ·ha ⁻¹) | Intercept | -12.200 | -1.999 | 0.053 | 5164 | <0.001*** | 0.307 |
| | Elevation ² | < - 0.001 | -2.430 | 0.020* | | | |
| | Elevation | 0.009 | 2.426 | 0.020* | | | |
| | Slope | 0.023 | 1.580 | 0.122 | | | |
| AGB Mg·ha ⁻¹ | Intercept | -23.248 | -0.244 | 0.808 | 589888 | <0.001*** | 0.555 |
| | Elevation ² | -485.138 | -3.517 | 0.902 | | | |
| | Elevation | 17.252 | 0.123 | 0.001*** | | | |
| | AspectNS | -10.252 | -3.111 | 0.003** | | | |
| | AspectNS: Elevation | 0.004 | 3.129 | 0.003** | | | |

*Coefficient of determination calculated based on the likelihood-ratio test (R_{LR}²). ***P < 0.001, **P < 0.01, *P < 0.01. BA denotes basal area, AGB denotes aboveground biomass.

TABLE 2 Conditional effects table from canonical correspondence analysis (CCA) ordination showing the partial effect of each environmental factor, representing the F -value (and its significance) on woody vegetation community composition, its variance inflation factor (VIF), and its correlations with two CCA axes.

| Environmental variables | Variance (%) | F | P | VIF | CCA1 | CCA2 |
|-------------------------|--------------|-------|----------|-------|--------|--------|
| Elevation | 10.83 | 3.348 | 0.001*** | 1.374 | -0.985 | 0.057 |
| Aspect EW | 1.16 | 1.514 | 0.026* | 1.099 | -0.233 | 0.121 |
| Aspect NS | 8.57 | 2.164 | 0.001*** | 1.126 | 0.217 | 0.953 |
| Slope | 3.28 | 1.242 | 0.170 | 1.192 | 0.487 | -0.051 |

EW, east-west orientation; NS, north-south orientation. *** $P < 0.001$, * $P < 0.01$.

distinct vegetation communities. *Pseudotsuga*, *Padus*, *Camellia*, *Pinus*, and *Cinnamomum* occurrences (green in **Supplementary Figure 4**) correlated positively with each other at medium elevation on a moderate slope. *Castanopsis*, *Sophora*, and *Malus* (navy blue in **Supplementary Figure 4**) had positive associations and were located at lower altitudes than the previous community, with a more southern or western aspect. The physical environment of *Cornus*, *Acer*, *Machilus*, *Toxicodendron*, etc. (red in **Supplementary Figure 4**) was quite similar to *Castanopsis*, *Sophora*, and *Malus*, but could still be divided into two distinct communities. *Tilia*, *Tsuga*, *Rhododendron*, *Crataegus*, *Taxus*, etc. (light blue in **Supplementary Figure 4**) were located at medium elevation on the southern or western aspect on a medium slope. The remaining species were positively connected to each other regardless of variations in their environmental factors, which could possibly be explained by their wide distributions in the study area.

4. Discussions

Our study demonstrated the influence of elevation, aspect, and slope on the woody vegetation in a human-impacted landscape. Consistent with previous research (Wang et al., 2014; Ullah et al., 2021), we found that elevation is a significant predictor of vegetation size. Specifically, the estimated maximum height, BA, and AGB followed a unimodal trend along the elevational gradient, peaking at 3100 m for maximum tree height and BA, and at 3300 m for AGB, before decreasing at higher elevations. However, we did not observe a clear relationship between species richness and any topographical attributes. Additionally, BA increased with slope steepness, while AGB decreased with a south to north aspect. We also generated separate visualizations of the five vegetation attributes along elevation for each of the four transects (see **Supplementary Figure 5**). The compositions and distributions of vegetation communities were primarily determined by elevation and north-south orientation.

Vegetation size and biomass largely influenced by climatic factors, e.g., mean annual temperature, total annual precipitation, and annual solar radiation that determine vegetation patterns along environmental gradients (Šímová et al., 2018; O'Brien et al., 2000). We found maximum tree height, BA, and AGB to each follow a unimodal pattern along the elevational gradients. The climate in our research area is reportedly dry at lower elevations of the valley in the west transect facing the Yangtze River (Shen, 2016; Yang et al., 2016a), making aridity one of the constraint factors limiting tree size (Munne-Bosch, 2018) and biomass accumulation (Muller-Landau et al., 2021) at lower elevations. If precipitation does not

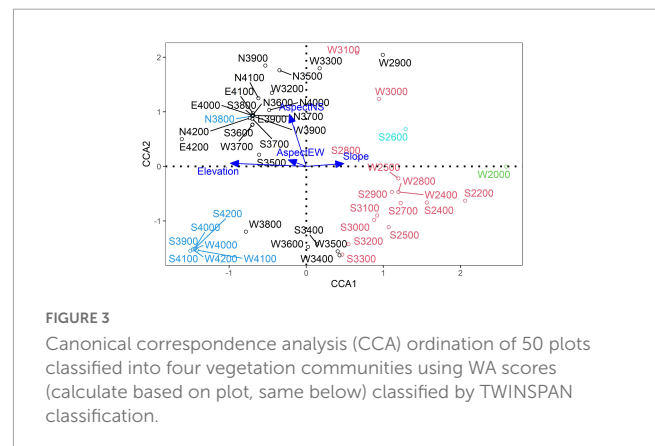


FIGURE 3 Canonical correspondence analysis (CCA) ordination of 50 plots classified into four vegetation communities using WA scores (calculate based on plot, same below) classified by TWINSpan classification.

vary greatly, temperature becomes the most limiting climate factor in AGB. In northern Pakistan, for instance, forest AGB presented a monotonous decline from 850 to 8600 m, where mean annual precipitation is consistently lower than at 200 m while the mean annual temperature ranges from 40 to -10°C (Ullah et al., 2021).

Both natural and anthropogenic disturbances influence vegetation patterns in unprotected mountain landscapes. Villages are mainly located below 3000 m and activities such as wood harvesting, grazing, and igniting fires, both intentional and unintentional, have likely decreased tree size and AGB in lower elevations where human presence is more frequent, making it occasionally difficult to distinguish the climatic effects of elevation from human use of the forest. As an example, Acharya et al. (2011) found a unimodal pattern of BA from 300 m to 4700 m in the eastern Himalayas to be due to human disturbances from surrounding lower elevation villages. Occasionally ancient human-use of the forest can be inferred from vegetation structure and composition (Foster et al., 1992). In our study area, the shrub growth form of *Quercus aquifolioides* at low elevations was potentially one such indicator.

The range of elevation sampled may have influenced observed patterns of vegetation structure along elevational gradients. Our findings differ from those of Alves et al. (2010), who found AGB to increase with elevation up to 1100 m in a coastal Atlantic forest, and from those of Wang Y. et al. (2012) and Wang et al. (2014), who found that maximum tree height and AGB of *Abies georgei* decreased along elevational gradients, peaked at 3800 m and 3100 m, respectively, in the Tibetan Plateau. Our study covered an elevation range of 2000–4200 m above sea level, with structural attributes peaking around 3000 m and declining as elevation increased. This emphasizes the importance of sampling the entire

elevational gradient to accurately describe the relationship between vegetation and the environment.

We observed a slightly higher AGB at the southern aspect than the northern aspect, which was consistent with a result focusing on the effects of elevation on vegetation, where a warmer climate in the southern aspect is conducive to AGB accumulation (Pepin et al., 2017).

The influence of elevation on aboveground biomass (AGB) can vary depending on the north-south orientation of aspect, and vice versa. In our study, we observed that AGB tends to be higher at mid-elevation on south-facing slopes.

In addition, BA increased slightly with slope degree, which is less straightforward to explain. However, one possible explanation is that steep slopes may reduce fire occurrence and spread due to a lack of fuel, allowing trees to grow taller and have larger basal area compared to areas with more frequent fires (Morandini et al., 2002; Gowda et al., 2019).

Although woody species richness appears to reach its highest values at mid-elevations, none of the trends of woody species richness along environmental gradients encompassed in the topographic variables were statistically significant. This is inconsistent with many studies conducted in protected forests located close to our research area (Wang et al., 2007; Xu et al., 2016; Yang et al., 2016a). However, this finding is consistent with earlier findings concerning the absence of β -diversity trends for tree and shrub species along elevational gradients in 46 mountains of China (Tang et al., 2012) that were well protected only from 1997 to 2008.

Topographic heterogeneity is strongly connected with species diversity (Stein et al., 2014). Other researchers have concluded from nearby protected areas that vascular plant richness along elevational gradients, ranging from either 3100–4300 m or from 2000 to 4300 m in the Hengduan Mountain presented a unimodal shape, with highest richness in the mid-elevational range (Wang et al., 2007; Yang et al., 2016b). We did not find a clear trend of woody species richness changes along EW or NS orientations. Yang et al. (2016b) found 300 vascular plant species on the western aspect compared with 501 vascular plant species on the eastern aspect of Baima Snow Mountain Reserves, very close to our study area. Our results demonstrated that tree species richness tended to increase with slope degree, although this was not statistically significant.

Elevation and NS aspect were the two dominant topographical factors determining woody species distributions in our study area. Slope had a relatively minor effect on these factors. The impact of the NS aspect was much greater than that of the EW aspect. Woody vegetation in the 50 sample plots could be grouped into five types: hot-dry valley shrub-like forests, abandoned cropland, mid-low warm aspect forests, high elevation forests, and alpine shrub and grassland. When considering the indicator woody species in the area, all woody species classified into five vegetation communities, four of which placed in their distinct environmental conditions. *Pseudotsuga*, *Pinus*, and *Cinnamomum* communities were placed at medium elevation, both the *Acer* community and *Castanopsis* community were at the medium-to-low elevation on a steeper slope, *Tilia*, *Tsuga*, *Taxus*, and *Picea* communities were in the medium elevation at a warm aspect. The remaining species, though grouped into one, presented little information of their environmental preferences.

Previous studies have indicated that topographic factors are major drivers of vascular plant distribution patterns

(Moeslund et al., 2013). We found elevation and aspect to be the two most relevant variables defining vegetation composition, with slope degree playing a smaller role. Similarly, Fadl et al. (2021) reported the distribution of vascular plant species to be strongly affected by elevation and NS aspect at an elevation range from 1060 to 1240 m in Sarawat Mountain, Saudi Arabia. Bai et al. (2021) demonstrated elevation to be the primary driving factor of vascular plant distribution in a *Larix gmelinii* forest in northeast China, while aspect was the second most important factor and slope had only minor importance.

Our study had limitations that either constrained the external use of the results or called for further research. Firstly, our sampling design, based on contours, led to a slight overrepresentation of steep slopes. Secondly, our research was based on landscape-scale sampling, and the results should not be assumed to hold in other regions. Thirdly, earlier studies have shown that forests in southwestern China are commonly disturbed by fire (Han et al., 2015) and potentially other major natural disturbances, which should optimally be included in forest structure studies. Future research on disturbance history would therefore be valuable. Topographic attributes indirectly affected vegetation via different climatic variables at each site. Detecting climatic factors at each plot to link with the topographic attributes would be helpful for understanding the influence of the local climate on vegetation in mountainous regions. Despite these problems, our results are valuable for understanding vegetation structure changes along environmental gradients, but the picture would improve further with more information on these listed problems.

Our study highlights that differences in vegetation structure, richness, and composition were correlated with elevation, aspect, and slope degree, which can be used as a baseline for predicting AGB shifting under climate change. At higher elevations, close to the peak of our research area, AGB decreased with increasing elevation, suggesting an increase under a warming climate. While at elevations of 2000–3300 m in this study, warmer temperatures are likely to reduce AGB via increased disturbances, assuming that precipitation is not changing.

Our results on tree size and biomass could be used to provide recommendations for designing forest management plans including carbon sequestration objectives. As most settlements in this area are below 3000 m and harvesting *Pinus* and *Quercus* trunks currently occurs mainly at this range of elevation, increasing aridity caused by climate change is likely to cause challenges, eventually leading to a pressure to move human activities upward.

Data availability statement

The original contributions presented in this study are included in the article/**Supplementary material**, further inquiries can be directed to the corresponding authors.

Author contributions

ZC participated in the collection of field data, performed the statistical analyses, prepared the figures, and wrote the original

manuscript. TA provided insight into the data used and the mathematical aspects of the methods. ML conceived the idea of the manuscript, applied for funding, planned the experiments, and participated in the collection of field data. All authors discussed the results, thoroughly revised the manuscript, contributed critically to the drafts, and gave final approval for publication.

Funding

This research was supported by the National Natural Science Foundation of China (No. 32171539).

Conflict of interest

The authors declare that the research was conducted in the absence of any commercial or financial relationships that could be construed as a potential conflict of interest.

References

- Acharya, B. K., Chettri, B., and Vijayan, L. (2011). Distribution pattern of trees along an elevation gradient of Eastern Himalaya, India. *Acta Oecol.* 37, 329–336. doi: 10.1016/j.actao.2011.03.005
- Akaike, H. (1973). "Information theory and an extension of the maximum likelihood principle," in *International symposium on information theory*, eds B. N. Petrov and F. Csaki (Budapest: Akademiai Kiado), 267–281.
- Alves, L. F., Vieira, S. A., Scaranello, M. A., Camargo, P. B., Santos, F. A. M., Joly, C. A., et al. (2010). Forest structure and live aboveground biomass variation along an elevational gradient of tropical Atlantic moist forest (Brazil). *For. Ecol. Manag.* 260, 679–691. doi: 10.1016/j.foreco.2010.05.023
- Bai, X., Sadia, S., and Yu, J. (2021). Community composition and structure along environmental gradients of Larix gmelinii forest in northeast China. *Pakistan J. Bot.* 53, 1845–1850. doi: 10.30848/PJB2021-5(24)
- Barthlott, W., Hostert, A., Kier, G., Küper, W., Kreft, H., Mutke, J., et al. (2007). Geographic patterns of vascular plant diversity at continental to global scales. *Erdkunde* 61, 305–315. doi: 10.3112/erdkunde.2007.04.01
- Bartoń, K. (2022). *MuMIn: multi-model inference. R package version 1.46.0*. Available online at: <https://CRAN.R-project.org/package=MUMIn> (accessed January 20, 2022).
- Bates, D., Maechler, M., Bolker, B., and Walker, S. (2015). Fitting linear mixed-effects models using lme4. *J. Stat. Softw.* 67, 1–48. doi: 10.18637/jss.v067.i01
- Beaty, R. M., and Taylor, A. H. (2001). Spatial and temporal variation of fire regimes in a mixed conifer forest landscape, Southern Cascades, California, USA. *J. Biogeogr.* 28, 955–966. doi: 10.1046/j.1365-2699.2001.00591.x
- Bonan, G. B. (2008). Forests and climate change: Forcings, feedbacks, and the climate benefits of forests. *Science* 320, 1444–1449. doi: 10.1126/science.1155121
- Burnett, B. N., Meyer, G. A., and McFadden, L. D. (2008). Aspect-related microclimatic influences on slope forms and processes, northeastern Arizona. *J. Geophys. Res.* 113:F03002. doi: 10.1029/2007JF000789
- Chave, J., Rejou-Mechain, M., Burquez, A., Chidumayo, E., Colgan, M. S., Delitti, W. B., et al. (2014). Improved allometric models to estimate the aboveground biomass of tropical trees. *Glob. Change Biol.* 20, 3177–3190. doi: 10.1111/gcb.12629
- Colwell, R. K., Brehm, G., Cardelus, C. L., Gilman, A. C., and Longino, J. T. (2008). Global warming, elevational range shifts, and lowland biotic attrition in the wet tropics. *Science* 322, 258–261. doi: 10.1126/science.1162547
- Crawley, M. J. (2013). *The R Book*, 2nd Edn. Chichester: John Wiley & Sons Ltd.
- Dulamsuren, C., and Hauck, M. (2008). Spatial and seasonal variation of climate on steppe slopes of the northern Mongolian mountain taiga. *Grassl. Sci.* 54, 217–230. doi: 10.1111/j.1744-697X.2008.00128.x
- Elsen, P. R., and Tingley, M. W. (2015). Global mountain topography and the fate of montane species under climate change. *Nat. Clim. Change* 5, 772–776. doi: 10.1038/nclimate2656
- Fadl, M. A., Al-Yasi, H. M., and Alsharif, E. A. (2021). Impact of elevation and slope aspect on floristic composition in wadi Elkor, Sarawat Mountain, Saudi Arabia. *Sci. Rep.* 11:16160. doi: 10.1038/s41598-021-95450-4
- Fan, Z.-X., Bräuning, A., Cao, K.-F., and Zhu, S.-D. (2009). Growth-climate responses of high-elevation conifers in the central Hengduan Mountains, southwestern China. *For. Ecol. Manag.* 258, 306–313. doi: 10.1016/j.foreco.2009.04.017
- Foster, D. R., Zebryk, T., Schoonmaker, P., and Lezberg, A. (1992). Post-settlement history of human land-use and vegetation dynamics of a *Tsuga canadensis* (Hemlock) woodlot in central New England. *J. Ecol.* 80, 773–786. doi: 10.2307/2260865
- Gaire, N. P., Fan, Z.-X., Bräuning, A., Panthi, S., Rana, P., Shrestha, A., et al. (2020). *Abies spectabilis* shows stable growth relations to temperature, but changing response to moisture conditions along an elevation gradient in the central Himalaya. *Dendrochronologia* 60:125675. doi: 10.1016/j.dendro.2020.125675
- Gardiner, B., Berry, P., and Moulia, B. (2016). Review: wind impacts on plant growth, mechanics and damage. *Plant Sci.* 245, 94–118. doi: 10.1016/j.plantsci.2016.01.006
- Ge, W., Deng, L., Wang, F., and Han, J. (2021). Quantifying the contributions of human activities and climate change to vegetation net primary productivity dynamics in China from 2001 to 2016. *Sci. Total Environ.* 773:145648. doi: 10.1016/j.scitotenv.2021.145648
- Gowda, J. H., Tiribelli, F., Mermoz, M., Kitzberger, T., and Morales, J. M. (2019). Fragmentation modulates the response of dichotomous landscapes to fire and seed dispersal. *Ecol. Modell.* 392, 22–30. doi: 10.1016/j.ecolmodel.2018.10.014
- Grytnes, J. A. (2003). Species-richness patterns of vascular plants along seven altitudinal transects in Norway. *Ecography* 26, 291–300. doi: 10.1034/j.1600-0587.2003.03358.x
- Hadley, W., Romain, F., Lionel, H., Kirill, M., and Davis, V. (2023). *dplyr: a grammar of data manipulation. R package version 1.1.0*. Available online at: <https://CRAN.R-project.org/package=dplyr> (accessed January 20, 2022).
- Han, J., Shen, Z., Ying, L., Li, G., and Chen, A. (2015). Early post-fire regeneration of a fire-prone subtropical mixed Yunnan pine forest in Southwest China: effects of pre-fire vegetation, fire severity and topographic factors. *For. Ecol. Manag.* 356, 31–40. doi: 10.1016/j.foreco.2015.06.016
- Heydari, M., Cheraghi, J., Omidipour, R., Mirab-balou, M., and Pothier, D. (2021). Beta diversity of plant community and soil mesofauna along an elevational gradient in a mountainous semi-arid oak forest. *Commun. Ecol.* 22, 165–176. doi: 10.1007/s42974-021-00046-7
- Hua, F., Wang, X., Zheng, X., Fisher, B., Wang, L., Zhu, J., et al. (2016). Opportunities for biodiversity gains under the world's largest reforestation programme. *Nat. Commun.* 7:12717. doi: 10.1038/ncomms12717
- Hua, F., Xu, J., and Wilcove, D. S. (2018). A new opportunity to recover native forests in China. *Conserv. Lett.* 11:e12396. doi: 10.1111/conl.12396

Publisher's note

All claims expressed in this article are solely those of the authors and do not necessarily represent those of their affiliated organizations, or those of the publisher, the editors and the reviewers. Any product that may be evaluated in this article, or claim that may be made by its manufacturer, is not guaranteed or endorsed by the publisher.

Supplementary material

The Supplementary Material for this article can be found online at: <https://www.frontiersin.org/articles/10.3389/ffgc.2023.1187724/full#supplementary-material>

- Huang, B., Lu, S., and Zhang, G. (2020). *Soil series of China: central and western regions vol., Yunnan vol.* Beijing: Science press.
- Isbell, F., Gonzalez, A., Loreau, M., Cowles, J., Diaz, S., Hector, A., et al. (2017). Linking the influence and dependence of people on biodiversity across scales. *Nature* 546, 65–72. doi: 10.1038/nature22899
- Joly, D., and Gillet, F. (2017). Interpolation of temperatures under forest cover on a regional scale in the French Jura Mountains. *Int. J. Climatol.* 37, 659–670. doi: 10.1002/joc.5029
- Jump, A. S., Matyas, C., and Penuelas, J. (2009). The altitude-for-latitude disparity in the range retractions of woody species. *Trends Ecol. Evol.* 24, 694–701. doi: 10.1016/j.tree.2009.06.007
- Keith, D. A., Ferrer-Paris, J. R., Nicholson, E., and Kingsford, R. T. (2020). *The IUCN global ecosystem typology 2.0: descriptive profiles for biomes and ecosystem functional groups*. Gland: IUCN. doi: 10.2305/IUCN.CH.2020.13.en
- Körner, C. (2007). The use of 'altitude' in ecological research. *Trends Ecol. Evol.* 22, 569–574. doi: 10.1016/j.tree.2007.09.006
- Kunwar, S., Wang, L. Q., Chaudhary, R., Joshi, P. R., Ali, A., and Ward, D. (2021). Stand density of co-existing species regulates above-ground biomass along a local-scale elevational gradient in tropical forests. *Appl. Veg. Sci.* 24:e12577. doi: 10.1111/avsc.12577
- Li, Z., He, Y., Wang, C., Wang, X., Xin, H., Zhang, W., et al. (2011). Spatial and temporal trends of temperature and precipitation during 1960–2008 at the Hengduan Mountains, China. *Quat. Int.* 236, 127–142. doi: 10.1016/j.quaint.2010.05.017
- Lin, D., Lai, J., Muller-Landau, H. C., Mi, X., and Ma, K. (2012). Topographic variation in aboveground biomass in a subtropical evergreen broad-leaved forest in China. *PLoS One* 7:e48244. doi: 10.1371/journal.pone.0048244
- Liu, Y., Li, P., Xu, Y., Shi, S., Ying, L., Zhang, W., et al. (2016). Quantitative classification and ordination for plant communities in dry valleys of Southwest China. *Biodivers. Sci.* 24, 378–388. doi: 10.17520/biods.2015241
- Luo, Y., Zhao, X., Li, Y., Liu, X., Wang, L., Wang, X., et al. (2021). Wind disturbance on litter production affects soil carbon accumulation in degraded sandy grasslands in semi-arid sandy grassland. *Ecol. Eng.* 171:106373. doi: 10.1016/j.ecoleng.2021.106373
- Lyman, R. L., and Ames, K. M. (2007). On the use of species-area curves to detect the effects of sample size. *J. Archaeol. Sci.* 34, 1985–1990. doi: 10.1016/j.jas.2007.01.011
- Martin, L. J., Blossey, B., and Ellis, E. (2012). Mapping where ecologists work: biases in the global distribution of terrestrial ecological observations. *Front. Ecol. Environ.* 10:195–201. doi: 10.1890/110154
- Moeslund, J. E., Arge, L., Bocher, P. K., Dalgaard, T., and Svenning, J.-C. (2013). Topography as a driver of local terrestrial vascular plant diversity patterns. *Nordic J. Bot.* 31, 129–144. doi: 10.1111/nj.1756-1051.2013.00082.x
- Monge-González, M. L., Craven, D., Krömer, T., Castillo-Campos, G., Hernández-Sánchez, A., Guzmán-Jacob, V., et al. (2019). Response of tree diversity and community composition to forest use intensity along a tropical elevational gradient. *Appl. Veg. Sci.* 23, 69–79. doi: 10.1111/avsc.12465
- Moore, J., Gardiner, B., and Sellier, D. (2018). "Tree mechanics and wind loading," in *Plant biomechanics*, eds A. Geitmann and J. Gril (Berlin: Springer), 79–106. doi: 10.1007/978-3-319-79099-2_4
- Morandini, F., Santoni, P. A., Balbi, J. H., Ventura, J. M., and Mendes-Lopes, J. M. (2002). A two-dimensional model of fire spread across a fuel bed including wind combined with slope conditions. *Int. J. Wildland Fire* 11, 53–63. doi: 10.1071/WF01043
- Moritz, C., and Agudo, R. (2013). The future of species under climate change: resilience or decline? *Science* 341, 504–508. doi: 10.1126/science.1237190
- Muller-Landau, H. C., Cushman, K. C., Arroyo, E. E., Martinez Cano, I., Anderson-Teixeira, K. J., and Backiel, B. (2021). Patterns and mechanisms of spatial variation in tropical forest productivity, woody residence time, and biomass. *New Phytol.* 229, 3065–3087. doi: 10.1111/nph.17084
- Munne-Bosch, S. (2018). Limits to tree growth and longevity. *Trends Plant Sci.* 23, 985–993. doi: 10.1016/j.tplants.2018.08.001
- Myers, N., Mittermeier, R. A., Mittermeier, C. G., da Fonseca, G. A., and Kent, J. (2000). Biodiversity hotspots for conservation priorities. *Nature* 403, 853–858. doi: 10.1038/35002501
- O'Brien, E. M., Field, R., and Whittaker, R. J. (2000). Climatic gradients in woody plant (tree and shrub) diversity: water-energy dynamics, residual variation, and topography. *Oikos* 89, 588–600. doi: 10.1034/j.1600-0706.2000.89319.x
- Oksanen, J., Simpson, G. L., Blanchet, F. G., Kindt, R., Legendre, P., Minchin, P. R., et al. (2022). *vegan: Community Ecology Package. R package version 2.6-4*. Available online at: <https://CRAN.R-project.org/package=vegan> (accessed December 20, 2021).
- Pepin, N. C., Pike, G., Schaefer, M., Boston, C. M., and Lovell, H. (2017). A comparison of simultaneous temperature and humidity observations from the SW and NE slopes of Kilimanjaro: the role of slope aspect and differential land-cover in controlling mountain climate. *Glob. Planet. Change* 157, 244–258. doi: 10.1016/j.gloplacha.2017.08.006
- Perring, F. (1959). Topographical gradients of chalk grassland. *J. Ecol.* 47, 447–481. doi: 10.2307/2257376
- Potapov, P., Hansen, M. C., Laestadius, L., Turubanova, S., Yaroshenko, A., Thies, C., et al. (2017). The last frontiers of wilderness: tracking loss of intact forest landscapes from 2000 to 2013. *Sci. Adv.* 3:e1600821. doi: 10.1126/sciadv.1600821
- Qin, Y., Feng, Q., Adamowski, J. F., Zhu, M., and Zhang, X. (2021). Community level response of leaf stoichiometry to slope aspect in a montane environment: a case study from the Central Qilian Mountains, China. *Glob. Ecol. Conserv.* 28:e01703. doi: 10.1016/j.gecco.2021.e01703
- Qu, S., Wang, L., Lin, A., Yu, D., Yuan, M., and Li, C. A. (2020). Distinguishing the impacts of climate change and anthropogenic factors on vegetation dynamics in the Yangtze River Basin, China. *Ecol. Indic.* 108:105724. doi: 10.1016/j.ecolind.2019.105724
- Rahbek, C., Borregaard, M. K., Antonelli, A., Colwell, R. K., Holt, B. G., Nogues-Bravo, D., et al. (2019a). Building mountain biodiversity: geological and evolutionary processes. *Science* 365, 1114–1119. doi: 10.1126/science.aax0151
- Rahbek, C., Borregaard, M. K., Colwell, R. K., Dalsgaard, B., Holt, B. G., Morueta-Holme, N., et al. (2019b). Humboldt's enigma: what causes global patterns of mountain biodiversity? *Science* 365, 1108–1113. doi: 10.1126/science.aax0149
- Rejou-Mechain, M., Tanguy, A., Piponiot, C., Chave, J., and Herault, B. (2017). BIOMASS: an R package for estimating above-ground biomass and its uncertainty in tropical forests. *Methods Ecol. Evol.* 8, 1163–1167. doi: 10.1111/2041-210X.12753
- Rogeanu, M.-P., and Armstrong, G. W. (2017). Quantifying the effect of elevation and aspect on fire return intervals in the Canadian rocky mountains. *For. Ecol. Manag.* 384, 248–261. doi: 10.1016/j.foreco.2016.10.035
- Rowe, R. J., and Lidgard, S. (2009). Elevational gradients and species richness: do methods change pattern perception? *Glob. Ecol. Biogeogr.* 18, 163–177. doi: 10.1111/j.1466-8238.2008.00438.x
- Sanders, N. J., and Rahbek, C. (2012). The patterns and causes of elevational diversity gradients. *Ecography* 35, 1–3. doi: 10.1111/j.1600-0587.2011.07338.x
- Scheiner, S. M. (2003). Six types of species-area curves. *Glob. Ecol. Biogeogr.* 12, 441–447. doi: 10.1046/j.1466-822X.2003.00061.x
- Shen, Z. (2016). Plant diversity in the dry valleys of Southwest China: spatial deviation and determinants for flora and plant communities. *Biodivers. Sci.* 24, 363–366. doi: 10.17520/biods.2016049
- Šimová, I., Violle, C., Svenning, J. C., Kattge, J., Engemann, K., Sandel, B., et al. (2018). Spatial patterns and climate relationships of major plant traits in the New World differ between woody and herbaceous species. *J. Biogeogr.* 45, 895–916. doi: 10.1111/jbi.13171
- Sloan, S., Jenkins, C. N., Joppa, L. N., Gaveau, D. L. A., and Laurance, W. F. (2014). Remaining natural vegetation in the global biodiversity hotspots. *Biol. Conserv.* 177, 12–24. doi: 10.1016/j.biocon.2014.05.027
- Stein, A., Gerstner, K., Kreft, H., and Arita, H. (2014). Environmental heterogeneity as a universal driver of species richness across taxa, biomes and spatial scales. *Ecol. Lett.* 17, 866–880. doi: 10.1111/ele.12277
- Strassburg, B. B. N., Iribarrem, A., Beyer, H. L., Cordeiro, C. L., Crouzeilles, R., Jakovac, C. C., et al. (2020). Global priority areas for ecosystem restoration. *Nature* 586, 724–729. doi: 10.1038/s41586-020-2784-9
- Tang, Z., and Fang, J. (2004). A review on the elevational patterns of plant species diversity. *Biodivers. Sci.* 20, 20–28. doi: 10.17520/biods.2004004
- Tang, Z., Fang, J., Chi, X., Feng, J., Liu, Y., Shen, Z., et al. (2012). Patterns of plant beta-diversity along elevational and latitudinal gradients in mountain forests of China. *Ecography* 35, 1083–1091. doi: 10.1111/j.1600-0587.2012.06882.x
- Ullah, F., Gilani, H., Sanaei, A., Hussain, K., and Ali, A. (2021). Stand structure determines aboveground biomass across temperate forest types and species mixture along a local-scale elevational gradient. *For. Ecol. Manag.* 486:118984. doi: 10.1016/j.foreco.2021.118984
- Wang, G., Ran, F., Chang, R., Yang, Y., Luo, J., and Jianrong, F. (2014). Variations in the live biomass and carbon pools of *Abies georgei* along an elevation gradient on the Tibetan Plateau, China. *For. Ecol. Manag.* 329, 255–263. doi: 10.1016/j.foreco.2014.06.023
- Wang, J., Ou, G., Tang, J., Zhenlong, L., Li, H., and Hui, X. (2012). Biomass estimation model of shrub community at *Jatropha curcas* growing area in Lincang of Yunnan. *J. West China For. Sci.* 41:167.
- Wang, Y., Cufar, K., Eckstein, D., and Liang, E. (2012). Variation of maximum tree height and annual shoot growth of Smith fir at various elevations in the Sygera Mountains, southeastern Tibetan Plateau. *PLoS One* 7:e31725. doi: 10.1371/journal.pone.0031725
- Wang, Z., Liu, X., Wang, H., Zheng, K., Li, H., Wang, G., et al. (2021). Monitoring vegetation greenness in response to climate variation along the elevation gradient in the three-river source region of China. *ISPRS Int. J. Geo Inform.* 10:193. doi: 10.3390/ijgi10030193

- Wang, Z., Tang, Z., and Fang, J. (2007). Altitudinal patterns of seed plant richness in the Gaoligong Mountains, south-east Tibet, China. *Divers. Distribut.* 13, 845–854. doi: 10.1111/j.1472-4642.2007.00335.x
- Xie, Z., Wang, Y., Tang, Z., and Xu, W. (2018). *Handbook of biomass allometric models of shrubs in China*. Beijing: Science press.
- Xu, Y., Li, P., Liu, Y., Zhang, W., and Qin, S. (2016). Spatial patterns and determinants of species richness of alien and native plants in the Nujiang River valley. *Biodivers. Sci.* 24, 389–398. doi: 10.17520/biods.2015243
- Xu, Y., Shen, Z., Ying, L., Zang, R., and Jiang, Y. (2019). Effects of current climate, paleo-climate, and habitat heterogeneity in determining biogeographical patterns of evergreen broad-leaved woody plants in China. *J. Geogr. Sci.* 29, 1142–1158. doi: 10.1007/s11442-019-1650-x
- Yang, Y., Han, J., Liu, Y., Zhongyong, C., Shi, S., Sina, C., et al. (2016a). A comparison of the altitudinal patterns in plant species diversity within the dry valleys of the three parallel rivers region, northwestern Yunnan. *Biodivers. Sci.* 24, 440–452. doi: 10.17520/biods.2015361
- Yang, Y., Shen, Z., Han, J., and Zhongyong, C. (2016b). Plant diversity along the eastern and western slopes of Baima Snow Mountain, China. *Forests* 7:89. doi: 10.3390/f7040089
- Zeleny, D. (2021). *twinspanR: TTwo-way INdicator SPecies ANalysis (and its modified version) in R. R package version 0.22*. Available online at: <https://github.com/zdealveindy/twinspanR> (accessed January 10, 2022).
- Zhang, W., Zhao, L., Larjavaara, M., Morris, E. C., Sterck, F. J., and Wang, G. (2020). Height-diameter allometric relationships for seedlings and trees across China. *Acta Oecol.* 108:103621. doi: 10.1016/j.actao.2020.103621
- Zhang, Y., and Liu, Y. (2010). *Datasets of China ecosystem research station. Forest Ecosystems Vol. Ailaoshan Station in Yunnan Province: 2003–2007*. Beijing: China agriculture press.



OPEN ACCESS

EDITED BY

Marcus Schaub,
Snow and Landscape Research
(WSL), Switzerland

REVIEWED BY

Astrid Moser-Reischl,
Technical University of Munich, Germany
Petre Waldner,
Swiss Federal Institute for Forest, Snow, and
Landscape Research (WSL), Switzerland

*CORRESPONDENCE

Yonghong Zhao
✉ zhaoyh0303@126.com
Weijun Zhao
✉ zhaoweijun1019@126.com

RECEIVED 24 March 2023

ACCEPTED 12 June 2023

PUBLISHED 10 July 2023

CITATION

Zhao Y, Zhao W and Fang H (2023) Influence of hydrothermal factors on a coniferous forest canopy in the semiarid alpine region of Northwest China.
Front. For. Glob. Change 6:1193221.
doi: 10.3389/ffgc.2023.1193221

COPYRIGHT

© 2023 Zhao, Zhao and Fang. This is an open-access article distributed under the terms of the [Creative Commons Attribution License \(CC BY\)](https://creativecommons.org/licenses/by/4.0/). The use, distribution or reproduction in other forums is permitted, provided the original author(s) and the copyright owner(s) are credited and that the original publication in this journal is cited, in accordance with accepted academic practice. No use, distribution or reproduction is permitted which does not comply with these terms.

Influence of hydrothermal factors on a coniferous forest canopy in the semiarid alpine region of Northwest China

Yonghong Zhao^{1,2*}, Weijun Zhao^{3*} and Huijun Fang¹

¹College of Geographical Science, Qinghai Normal University, Xining, China, ²Key Laboratory of Physical Geography and Environmental Processes, College of Geographical Science, Qinghai Normal University, Xining, Qinghai, China, ³Academy of Water Resources Conservation Forests in Qilian Mountain of Gansu Province, Zhangye, China

Analyzing the physiological response of trees to climate change in the Qilian Mountains region is key to studying the impact of global change on forest ecosystems in the semiarid alpine region of Northwest China. The leaf area index (*LAI*) of the canopy of a forest is an important input parameter for simulating carbon and water cycles in forest ecosystems. Studying the relationship between *LAI* and environmental factors can provide a scientific basis for accurately describing the structure, function, and ecohydrological processes of forest ecosystems and theoretically guide for sustainable management of water conservation in forests. Methods: In this study, the *LAI* of the *Picea crassifolia* canopy was monitored for 2 years (2015–2016) by field observations, and its dynamic changes were analyzed. The relations between *LAI* and air temperature (*AT*), precipitation (*P*), soil temperature (*ST*), and soil water content (*SWC*) were studied using Pearson's correlation and multiple regression analyses. The results were as follows: seasonal variations in *LAI* showed a single-peak curve, which first increased, reached a maximum, remained relatively stable, and then decreased. The maximum value was 4.02 and 4.18 relatively observed in mid-August 2015 and 2016. The *LAI* of the *P. crassifolia* canopy in different months was positively correlated with *AT* and *P*. It was correlated between the *LAI* of the canopy with *ST*_{40–60} in May and June ($p < 0.05$) and was also highly positively correlated between the *LAI* of the canopy with *ST*_{60–80}, *ST*_{mean}, and *SWC*_{60–80} in July and August ($p < 0.01$). There was a positive correlation between the *LAI* of the canopy with *SWC*_{0–60} and *SWC*_{mean} in July and *SWC*_{0–60} and *SWC*_{mean} in August ($p < 0.05$). The *LAI* of the canopy was affected by *AT* and *ST* in May and July, *AT* and *P* in June, *P* in August, and *P* and *ST* in September. Our study implied that the rapid increase period of the *LAI* of the canopy was from late May to early July. The *LAI* of the canopy was more influenced by temperature and water in July and August. In addition, the *LAI* of the canopy has significant seasonal variation although it is evergreen coniferous tree species.

KEYWORDS

leaf area index, air temperature, soil temperature, precipitation, soil water content, Qilian Mountains

1. Introduction

Leaf area index (*LAI*), the ratio of the surface area of a plant leaf to the surface area of land *LAI*, is used to quantitatively describe changes in leaf growth and density at the community level (Watson, 1958). *LAI* is an important input parameter for simulating the carbon and water cycles in forest ecosystems (Weiss et al., 2004; Wang et al., 2005);

(Bequet et al., 2011) and is the key factor in explaining the variation in the net primary productivity of aboveground vegetation (Leuschner et al., 2006; Kinane et al., 2022), which is an important factor in describing the structural characteristics of forest canopies. It controls many physiological and ecological processes within forest ecosystems, such as plant photosynthesis and transpiration, canopy interception of precipitation, and exchange of matter and energy between the atmosphere and canopy (Dermoddy et al., 2006; Liu et al., 2013). *LAI* is closely related to ecological processes in forests, and accurate determination of seasonal changes in *LAI* is conducive to simulating the response of vegetation to climate change and predicting forest growth status (Liu, 2015). *LAI* plays an important role in studying energy cycles of the ecosystem at the forest stand, landscape, and regional scales.

At present, the methods to measure forest *LAI* include the indirect measurement method and the direct measurement method (Bréda, 2003; Cerný et al., 2020). The former is simple and convenient; however, its accuracy of measurement must be calibrated. However, some optical instrument methods based on radiometric measurements need to assume uniform canopy, random leaf distribution, and elliptical leaf angle distribution, such as *LAI*-2000, while Tracing Radiation and Architecture of Canopies (TRAC) can effectively address the agglomeration effect by measuring the agglomeration index and without needing to assume a random leaf distribution in space (Chen, 1996; Zhao et al., 2009a; Behera et al., 2010; Cerný et al., 2020). The latter technology is mature and accurate, and its measured value is usually considered a real *LAI*; however, it is time-consuming, laborious, and destructive (Yan et al., 2019; Cerný et al., 2020; Fang, 2021). Optical instruments mainly include digital hemispherical photography, *LAI*-2000/2200 plant canopy analyzer, TRAC, CI-110 LICOR DEMON, and other equipment, among which digital hemispherical photography and *LAI*-2200 plant canopy analyzer are widely used to simultaneously observe the structural parameters of the canopy at different zenith angles (Behling et al., 2016; Fang et al., 2021). Direct measurement methods mainly include the destructive sampling method (Chason et al., 1991), the allometric growth equation method (Vyas et al., 2010), the oblique point sampling method (Wilson, 1960), and the litter method (Sprintsin et al., 2011).

The leaf area index is affected by several factors and exhibits varying degrees of temporal and spatial heterogeneity (Luo et al., 2011). The relationship between *LAI* and climatic factors (temperature, precipitation, and soil moisture) can efficiently reflect the interactions between vegetation and the environment and is suitable for studying the ecohydrological processes under climate change (Huang et al., 2016; Karimi et al., 2020; Kinane et al., 2022). Li et al. (2012) used a simple biological model, the SiB2 method, to calculate *LAI* and to study the annual and interannual variations in different vegetation cover types of *LAI* in the Poyang Lake Basin and their relation with precipitation and air temperature (AT). They highlighted that the responses of *LAI* to precipitation and air temperature have, respectively, a time lag of 3 months and 1 month in the annual variation, and the interannual variation of *LAI* is mainly affected by the precipitation between May and July (Li et al., 2012). Wang et al. (2008) analyzed the influence of hydrothermal conditions on vegetation *LAI* in the Qinghai-Tibet Plateau at temporal and spatial scales using remote sensing data

and showed that *LAI* is correlated with temperature, soil moisture, and precipitation. Shao and Zeng (2011) compared potential *LAI* simulated by the dynamic vegetation model (CLM3.0-DGVM) with *LAI* derived from moderate-resolution imaging spectroradiometer (MODIS) and analyzed the spatial and temporal relations between *LAI* of different plant functional types on the current different types and climatic factors on the interannual scale. In addition, studies on *Hippophae rhamnoides* Linn and *Caragana intermedia* on the Loess Plateau indicated that *LAI* increased rapidly when precipitation and the water supply were sufficient, leading to a significant increase in the total amount of transpiration (Guo et al., 2007). However, an analysis of the US East Texas *Pinus taeda* stand canopy showed no significant relation between *LAI* and actual evapotranspiration ($r^2 = 0.06$) (Hebert and Jack, 1998), and plants from different biomes tended to grow relatively small leaves in arid environments to reduce the total leaf area, thereby reducing transpiration (Meier and Leuschner, 2008). In general, the main factors affecting vegetation *LAI* are temperature, water, and species.

Several studies have been conducted on vegetation *LAI* measurement methods and dynamic spatial and temporal (seasonal and interannual dynamics) changes in *LAI*; however, the relation between vegetation *LAI* and hydrothermal factors is not well understood. In particular, the relations between *LAI* of *P. crassifolia*, soil temperature (*ST*), and soil water content (*SWC*) in the Qilian Mountains of Northwest China are largely unexplored. Therefore, this study investigated the influence of hydrothermal factors on coniferous forest canopies in the semiarid alpine region of Northwest China. We monitored air temperature (*AT*), precipitation, *ST*, and *SWC* in the study area from 2015 to 2016 in this study. The objectives of this study are as follows: (1) to observe accurate monthly *LAI* dynamics using an *LAI*-2200C in coniferous stands; (2) to estimate the maximum stand *LAI* within the growing season indirectly using an *LAI*-2200C; and (3) to study the relation between *LAI* and *AT*, *P*, *ST*, and *SWC* in the Qilian Mountains.

2. Materials and methods

2.1. Study area

The study area is located in the Xishui Forest Area of the Qilian Mountains Natural Reserve. The geographical coordinates are approximately between 38°32′–38°33′ N and 100°17′–100°18′ E. These areas have the climate of alpine mountain forest grassland, with an annual *P* of 290–468 mm. The rainy season is mainly distributed from May to September, accounting for ~85% of annual *P*. The climatic characteristics were an average annual evaporation capacity of 1,082.7 mm, an annual average temperature of -0.6 to 2.1°C , and an annual average sunshine of 1,895 h. The average daily solar radiation intensity in 2015 and 2016 was $79.2\text{ W}\cdot\text{m}^{-2}\cdot\text{d}^{-1}$.

P. crassifolia is distributed in patches on shady and semi-shady slopes at altitudes of 2,500–3,300 m. The sunny slope is dominated by grasslands with scattered *Sabina przewalskii* and shrubs. The herbs mainly include *Carex lancifolia*, *Stipa purpurea*, *Agropyron cristatum*, *Leontopodium longifolium*, *Taraxacum monogolicum*, *Potentilla bifurca*, and *Pedicularis*. The shrubs in the basin mainly include alpine shrubs such as *Caragana tangutica* and *Berberis diaphana* Maxim. Under the forest, moss is

more developed; however, a few species, mainly *Abietinella abietina*, are scattered with *Bryoerythrophyllum tecurvirestrum* and *Tortula longimcronata*.

2.2. Sample plots

Three pure forest sample plots with *P. crassifolia* (25 × 25 m) were selected to observe the *LAI* of *P. crassifolia* in the study area in the growing season from May to October in 2015 and 2016 at an altitude of 2,700 m (38°33′14.8″ N, 100°17′5.4″ E). The selected plots were pure forests containing *P. crassifolia*, which originated from a natural secondary forest belonging to semi-mature forests. The horizontal distance between the three sample plots was ~50 m. Height and diameter at the breast of all trees with a diameter at breast height > 5 cm were measured with a wooden ruler in the sample plots during the stable growth period in 2016. The surveyed parameters included tree height, diameter at breast height, crown width, canopy closure, and forest age.

2.3. LAI measurement

An *LAI-2200C* plant canopy analyzer (LICOR, Lincoln, Nebraska, USA) was used to measure the canopy *LAI* of *P. crassifolia* sample plots every 10 days from May to October in 2015 and 2016. The measurement frequency was appropriately increased because of the rapid growth and change in the new branches of *P. crassifolia* at the beginning of the growing season, which means, the *LAI* of *P. crassifolia* canopy was measured every 6 days in May. A total of 25 points were measured in each sample plot according to a fixed S-shaped route, and the average value was taken as the characteristic *LAI* of the canopy layer of the sample plot. To ensure that the canopy layer outside the sample plot was not detected, the distance from the observation point to the upper and lower edges of the sample plot was 3 m (slope length), and the left and right edges were 2.5 m each. Two *LAI-2200C* plant canopy analyzers were used for synchronous and accurate measurement; one was placed in an open space outside the forest to measure the *A* value, and the other was placed in the sample plot to measure the value under the canopy (*B* value). A camera (*D80*, Nikon) was used to obtain hemispherical images of the vegetation canopy and to calculate the *LAI* of the forest canopy (Chen, 1996; Zhao et al., 2009a).

2.4. AT and P measurement

We used an automatic weather station (Campbell Scientific, Inc., Logan, Utah, USA) above 15 m height in the third sample plot to continuously obtain the data of *P* (P/mm) with a rain gauge (TE525MM, Campbell Sci., Logan, USA), solar radiation intensity ($R_s/w \cdot m^{-2}$) with a solar radiation sensor (Li200X, LICOR, Lincoln, Nebraska, USA), *AT* (T/°C) with a temperature sensor (HMP115A, Campbell Sci., Logan, USA), and relative humidity of the air (RH/%) with a humidity sensor (HMP45A, Campbell Sci., Logan, USA). The interval of data collection was 10 min.

2.5. ST and SWC measurement

A HOBO U30 sensor (Campbell Scientific, Inc. Logan, Utah, USA) was installed in 0–10, 10–20, 20–40, 40–60, and 60–80 cm soil layers in each different sample plot to monitor *ST* (°C) and *SWC* ($m^3 \cdot m^{-3}$). The interval of data collection was 30 min.

2.6. Data processing

A correction coefficient was required to adjust the measured *LAI*, which was low owing to the clustering effect of the coniferous forest. The measured *LAI* value used to calculate the correction coefficient was 0.996 (L_e). The aggregation coefficient (Ω_E) of *P. crassifolia* forest was 0.93 measured by Tracing Radiation and Architecture of Canopies (TRAC, Canada Center For Remote Sensing, Ottawa, Canada) (Zhao et al., 2009a), and the adjustment coefficient was calculated according to formula (1):

$$L = \frac{(1 - \alpha) L_e \gamma_E}{\Omega_E}, \quad (1)$$

where L_e is the effective *LAI* (acquired by instrumental observation), γ_E is the ratio of the total area of coniferous leaves to the cluster area, the conifer species is 1.4, and α , the ratio of non-leaf factors, such as the trunk, to total leaf area, was 0.12 (Chen, 1996). The adjustment coefficient was calculated as 1.32, which was multiplied by *LAI* measured by the *LAI-2000C* canopy analyzer to adjust the canopy *LAI* value according to formula (1).

Data were plotted using R version 4.2.1 software (AT&T Bell Laboratories, New Jersey, USA) and WPS Office 2021 (Kingsoft, Beijing, PRC). The relations between *LAI* of *P. crassifolia* and *P*, *AT*, *ST*, and *SWC* were analyzed using SPSS v.21.0 (SPSS Inc., Chicago, IL, USA) with Pearson correlation. Multiple stepwise linear regressions were used to examine the relation of *LAI* with hydrothermal factors. The multiple linear regression model mainly studies the relationship between a dependent variable and multiple independent variables, and its general form can be expressed as formula (2):

$$y = \beta_0 + \beta_1 x_1 + \beta_2 x_2 + \dots + \beta_k x_k + \varepsilon, \quad (2)$$

where y is the dependent variable, x is the independent variable, β_1, \dots, β_k are model parameters, and ε is Stochastic error. In this study, *LAI* is used as the dependent variable, and *AT*, *P*, *ST*, and *SWC* are used as independent variables to explore the relationship between them through this model.

3. Results

3.1. Hydrothermal conditions of the study site

Figure 1 shows that the thermal and water of three sample plots in the study site were synchronization. *P* and high temperature were all concentrated in the growing season (May to September). The maximum monthly *P* was 97.4 and 103.3 mm, respectively, in July 2015 and September 2016. The maximum monthly average

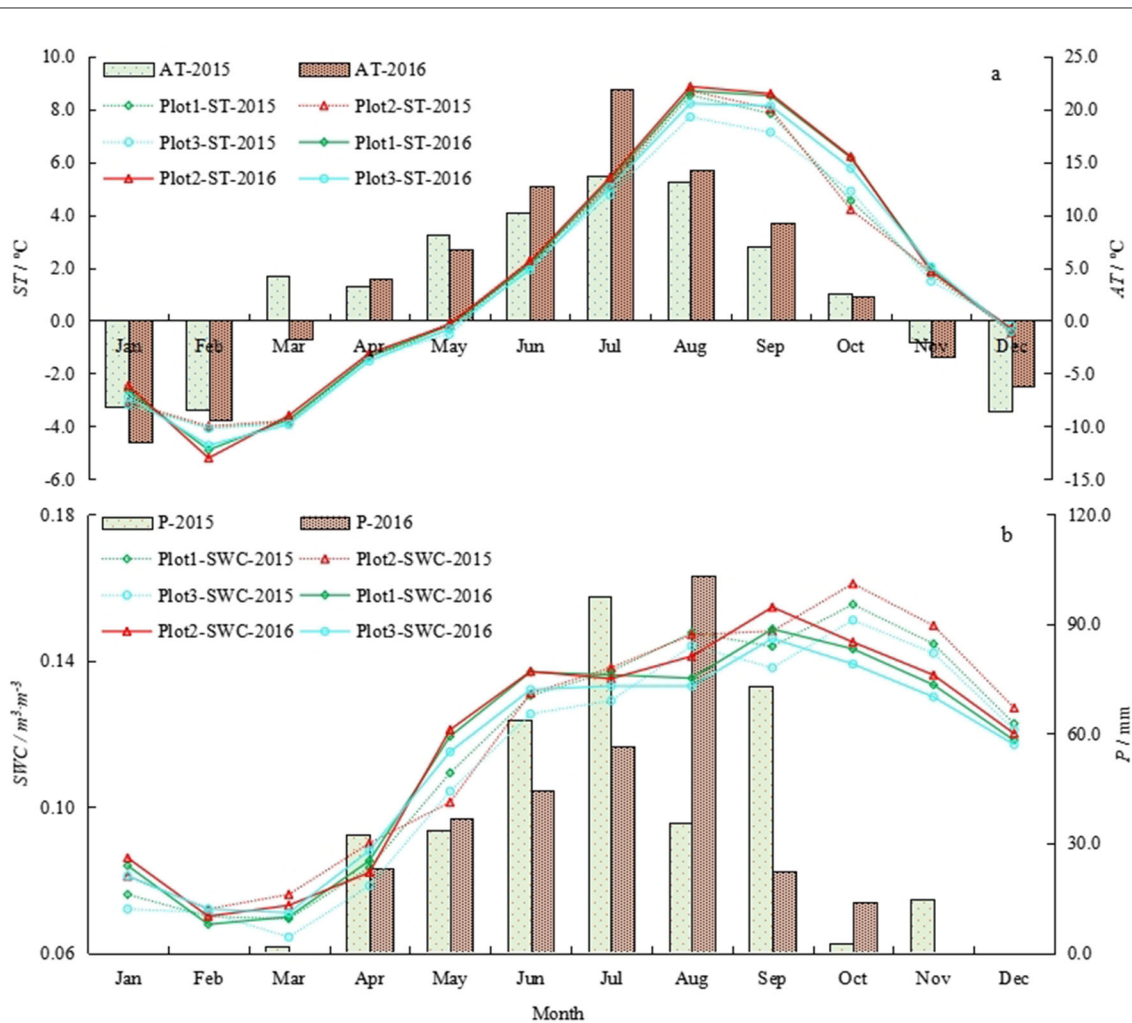


FIGURE 1 (a, b) Monthly average ST, AT, P, and SWC of three sample plots in 2015 and 2016.

AT was 13.7 and 21.8°C, respectively, in July 2015 and July 2016. The maximum monthly average ST was 8.5 and 8.6°C, respectively, in August 2015 and August 2016. The maximum monthly average SWC was 0.16 and 0.15, respectively, in October 2015 and October 2016.

and 4.10, respectively. The average, minimum, and maximum LAI values of the 3# sample plot were 3.17, 2.37, and 3.84, respectively. The LAI of the 1# and 2# sample plots was similar and higher than the LAI of the 3# sample plot. This result is consistent with the surveyed parameters summarized in Table 1.

3.2. Seasonal variation of LAI

As shown in Figure 2, the LAI of *P. crassifolia* in the three sample plots initially increased and then decreased during the two growth seasons (from May to September) in 2015 and 2016. The period from late May to early July was characterized by the rapid growth of LAI. Several withered and yellow coniferous leaves fell off in September, even though *P. crassifolia* is an evergreen coniferous forest, and LAI started decreasing. According to our field observations, over 2 consecutive years, these fallen leaves were old perennial or diseased withered leaves. In addition, the average, minimum, and maximum LAI values of the 1# sample plot were 3.39, 2.57, and 3.99, respectively. The average, minimum, and maximum LAI values of the 2# sample plot were 3.51, 2.73,

3.3. Relation between LAI and AT

Table 2 shows the results of the Pearson correlation analysis between the LAI of *P. crassifolia* and AT. LAI was positively correlated with AT, and a significant positive correlation ($p < 0.05$) was observed between LAI and AT during July–August 2015. LAI was positively correlated with AT in July and August of 2016 ($p < 0.05$).

3.4. Relation between LAI and ST

As shown in Figure 3, *P. crassifolia* LAI was positively correlated with ST in 2015 and 2016. In 2015, LAI was correlated

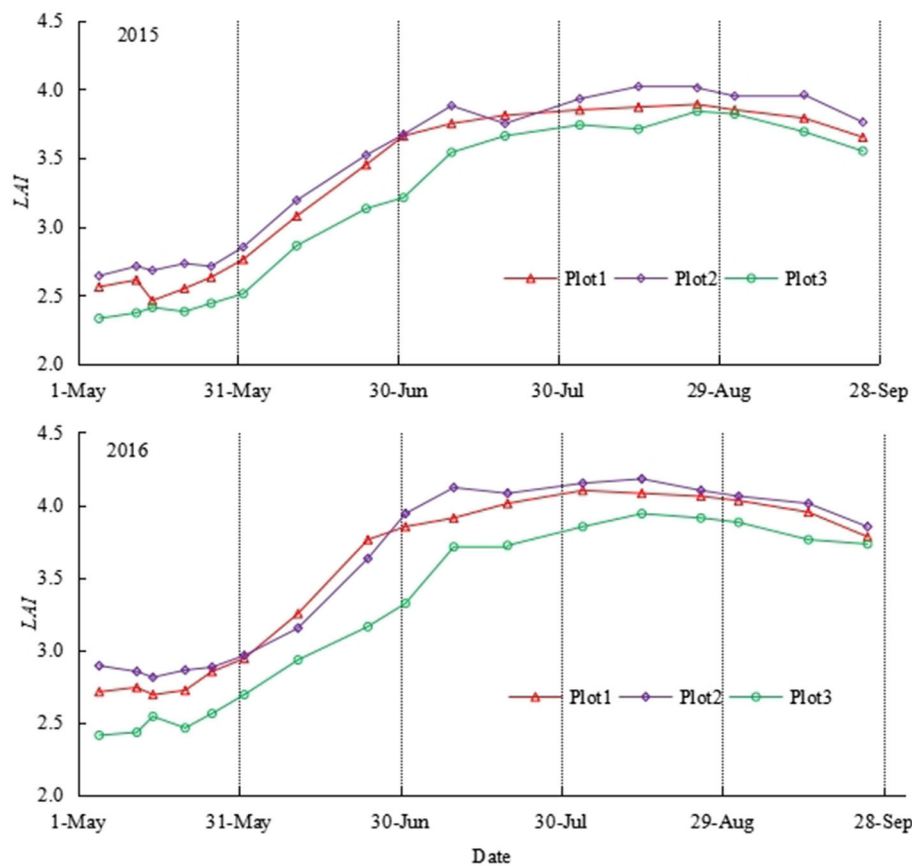


FIGURE 2 Seasonal variation of monthly average LAI in different sample plots in 2015 and 2016.

TABLE 1 Investigation of sample sites.

| Sample number | Canopy closure | Average forest age (a) | Stand density (strain · ha ⁻¹) | Average breast diameter (cm) | Average tree height (m) | Average crown (m) |
|---------------|----------------|------------------------|--|------------------------------|-------------------------|-------------------|
| 1 | 0.66 | 83 | 1,344 | 10.4 ± 4.2 | 7.9 ± 3.9 | 2.9 ± 0.9 |
| 2 | 0.68 | 84 | 1,328 | 11.9 ± 6.3 | 8.9 ± 4.0 | 3.0 ± 0.9 |
| 3 | 0.56 | 86 | 1,128 | 15.5 ± 9.1 | 10.7 ± 5.6 | 3.9 ± 1.1 |

TABLE 2 Pearson’s correlation coefficient between LAI and AT in 2015 and 2016.

| Year | Month | | | | |
|------|-------|-------|--------|--------|-----------|
| | May | June | July | August | September |
| 2015 | 0.402 | 0.334 | 0.533* | 0.878* | 0.335 |
| 2016 | 0.434 | 0.421 | 0.870* | 0.916* | 0.418 |

* $p < 0.05$; ** $p < 0.01$.

with ST_{0-40} and ST_{mean} in May, ST_{0-20} and ST_{mean} in June, and ST_{0-80} and ST_{mean} in September ($p > 0.05$). It was positively correlated with ST_{40-80} in May, ST_{20-80} in June, ST_{0-60} and ST_{mean} in July, and ST_{0-60} and ST_{mean} in August ($p < 0.05$). It was significantly positively correlated with ST_{60-80} in July and August ($p < 0.01$). In 2016, LAI was correlated with ST_{0-20} and

ST_{mean} in May and June, and ST_{0-80} and ST_{mean} in September ($p > 0.05$). It was positively correlated with ST_{20-80} in May and July and ST_{0-80} in July and August ($p < 0.05$). It was significantly positively correlated with ST_{mean} in July and August ($p < 0.01$).

3.5. Relation between LAI and P

The results in Table 3 show that the relation between the LAI of *P. crassifolia* and P in 2015 was consistent with that of 2016. *P. crassifolia* LAI was correlated ($p > 0.05$) with P in May 2015 and 2016. It was positively correlated ($p < 0.05$) with P in June, July, and August. It was negatively correlated ($p > 0.05$) with P in September. The rainfall distribution showed a large amount of P in July and August, during which the values of LAI were relatively larger. The maximum LAI was 4.02 and 4.18, respectively, which appeared in August 2015 and 2016.



FIGURE 3 Pearson's coefficient of correlation between the monthly average LAI and monthly average ST across the three plots calculated for each month of the years 2015 and 2016. *p < 0.05; **p < 0.01.

TABLE 3 Pearson's correlation coefficient between LAI and P in 2015 and 2016.

| Year | Month | | | | |
|------|-------|--------|--------|--------|-----------|
| | May | June | July | August | September |
| 2015 | 0.313 | 0.461* | 0.861* | 0.546* | -0.321 |
| 2016 | 0.298 | 0.553* | 0.649* | 0.713* | -0.247 |

*p < 0.05; **p < 0.01.

3.6. Relation between LAI and SWC

The results of a Pearson correlation analysis between the LAI of *P. crassifolia* and SWC in different soil layers are presented in Figure 4. The LAI of *P. crassifolia* was correlated with SWC, which was different between months. In 2015, it was correlated with SWC₀₋₁₀, SWC₂₀₋₈₀, and SWC_{mean} in May, SWC₀₋₈₀ and SWC_{mean} in June, and SWC₀₋₈₀ and SWC_{mean} in September ($p > 0.05$). It was positively correlated with SWC₀₋₈₀ and SWC_{mean} in July and August ($p < 0.05$). It was negatively correlated with SWC₁₀₋₂₀ in May ($p > 0.05$). In 2016, the LAI of *P. crassifolia* was correlated with SWC₀₋₂₀, SWC₄₀₋₈₀, and SWC_{mean} in May, SWC₀₋₈₀ and SWC_{mean} in June, and SWC₀₋₄₀, SWC₆₀₋₈₀, and SWC_{mean} in September ($p > 0.05$). It was positively correlated with SWC₀₋₆₀ and SWC_{mean} in July and SWC₀₋₆₀ and SWC_{mean} in August ($p < 0.05$). It was significantly positively correlated with SWC₆₀₋₈₀ in July and August ($p < 0.01$). It was negatively correlated with SWC₂₀₋₄₀ in May and SWC₄₀₋₆₀ in September ($p > 0.05$).

3.7. Multiple linear regression analysis between LAI and hydrothermal factors

Multiple linear regression analysis was performed between the LAI of *P. crassifolia* and AT, P, ST, and SWC during different months of the growing season in 2015 and 2016. The results of the multiple linear regression equations are presented in Table 4.

The multiple linear regression model fits the relations between LAI and AT, P, ST, and SWC. The model passed this test and was statistically significant.

The leaf area index was affected by AT and ST in May 2015 and 2016. AT and P mainly affected LAI in June 2015 and 2016. LAI was affected by AT, ST, and SWC in July 2015 but was affected by AT and ST in July 2016. LAI was affected by P and ST in August 2015 but was affected by AT, P, and SWC in August 2016. LAI was affected by P, ST, and SWC in September 2015 but was affected by P and ST in September 2016. On a monthly average, AT increased by 1°C and LAI changed by 2.30. P increased by 1 mm, and LAI changed by 5.39. ST increased by 1°C, and LAI changed by 3.18. SWC increased by 1, and LAI changed by 5.24. Overall, the main hydrothermal factors affecting the canopy LAI of *P. crassifolia* differed in July, August, and September.

4. Discussion

Canopy LAI often shows highly complex temporal and spatial variations (Zhao et al., 2009b; Liu et al., 2017), even in pure forests of the same age with a single stand structure (Bequet et al., 2012) because of many common environmental factors, such as forest structure, soil factors (moisture and physical and chemical properties), topographical factors (altitude, slope, and aspect) (Bequet et al., 2011; Kinane et al., 2022), and meteorological conditions (Luo et al., 2011; Li et al., 2012). Therefore, attention has been paid to temporal variations in the canopy LAI of different vegetation types in different regions.

4.1. Temporal and spatial variation of LAI

4.1.1. Temporal variation of LAI

Our study showed that LAI of *P. crassifolia* exhibited significant seasonal variation. LAI reached its maximum value in early August and slightly declined during late September. The large number of new shoots of *P. crassifolia* caused LAI to increase in the early growing season, and the fallen leaves led to a slight

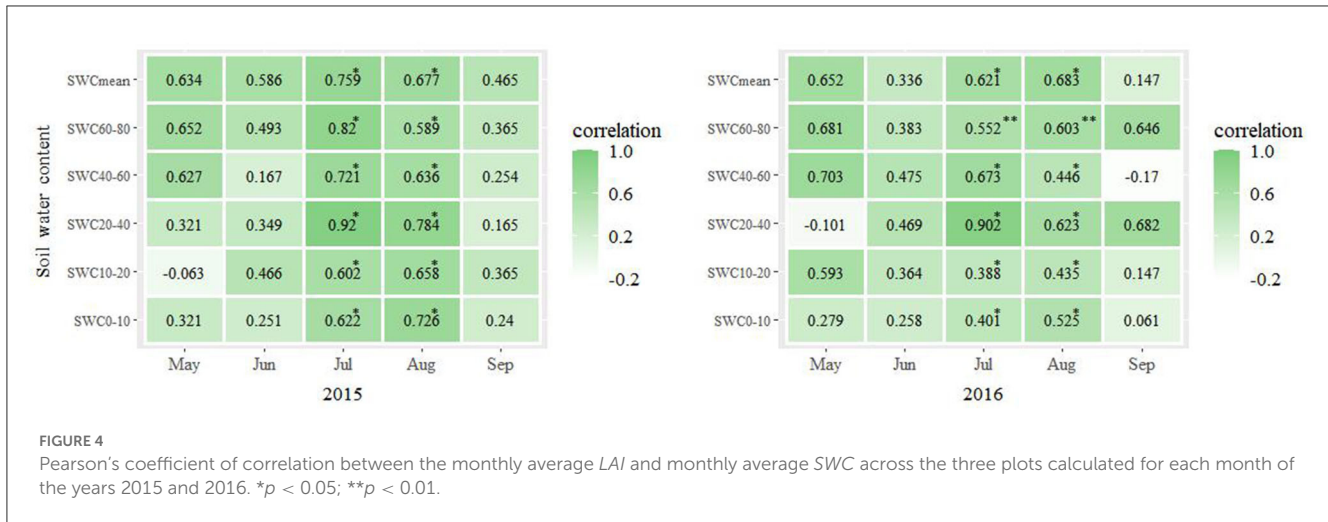


FIGURE 4 Pearson's coefficient of correlation between the monthly average LAI and monthly average SWC across the three plots calculated for each month of the years 2015 and 2016. * $p < 0.05$; ** $p < 0.01$.

TABLE 4 Multiple linear regression models of LAI with hydrothermal factors in 2015 and 2016.

| Years | Month | Stepwise regression equation | N | R ² | F | p |
|-------|-----------|--------------------------------------|----|----------------|--------|-------|
| 2015 | May | $y = 1.362x_1 + 0.287x_3$ | 15 | 0.754 | 13.065 | 0.084 |
| | June | $y = 3.295x_1 + 14.769x_2$ | 9 | 0.923 | 12.348 | 0.037 |
| | July | $y = 0.895x_1 + 0.205x_3 + 5.872x_4$ | 9 | 0.901 | 15.792 | 0.020 |
| | August | $y = 2.125x_2 + 5.365x_3$ | 9 | 0.815 | 10.631 | 0.135 |
| | September | $y = 1.09x_2 + 0.145x_3 - 0.029x_4$ | 9 | 0.982 | 16.304 | 0.036 |
| 2016 | May | $y = 6.954x_1 + 14.253x_3$ | 15 | 0.629 | 20.127 | 0.041 |
| | June | $y = 3.254x_1 + 7.158x_2$ | 9 | 0.775 | 13.396 | 0.039 |
| | July | $y = 0.042x_1 + 0.556x_3$ | 9 | 0.854 | 26.671 | 0.044 |
| | August | $y = 0.327x_1 + 2.836x_2 + 9.879x_4$ | 9 | 0.840 | 15.738 | 0.019 |
| | September | $y = 4.346x_2 + 1.442x_3$ | 9 | 0.967 | 29.595 | 0.153 |

where y , x_1 , x_2 , x_3 , and x_4 represent LAI, AT, P, ST (weighted average of soil temperature) in different soil layers, and SWC (weighted average soil water content in different soil layers), respectively. N represents the number of LAI observations.

decrease in LAI throughout the growing season. LAI in 2016 was slightly larger than that in 2015, which may be because the newly accumulated branches contributed to certain LAI based on our field observations. Our study suggests that the LAI of evergreen coniferous forests shows significant seasonal variation.

The annual and interannual variations in pure oak forest LAI were studied in the Champenoux forest in France. The results showed that oak LAI increased with the growth of new branches at the beginning of the annual growth season; however, the interannual changes were not significant (Bréda and Granier, 1996). The annual and interannual dynamics of vegetation LAI were also analyzed using the simple biosphere model (SiB2) method for the Poyang Lake Basin. The results showed that overall LAI of different vegetation cover types did not increase or decrease for 20 years but showed an alternating increasing or decreasing trend every 2–3 years, and the variation of evergreen coniferous forest LAI was significant (Li et al., 2012), which was consistent with our study. A seasonal dynamic study in the Liupan Mountains of North China showed that larch LAI increased linearly with an increase in canopy density, and the change in LAI in the growing season presented a single-peak curve (Han et al., 2015).

4.1.2. Spatial variation of LAI

As three sample plots were selected at the same altitude and slope, only the seasonal variation in the canopy LAI of *P. crassifolia* was studied. However, the spatial distribution of canopy LAI of *P. crassifolia* in the Qilian Mountains has been studied. The results showed that the LAI of *P. crassifolia* initially increased and then decreased with altitude in the Tianlaochi Basin of Sidalong Forestland in the Qilian Mountains because the limiting factors for the growth of *P. crassifolia* are mainly controlled by water at the low altitude and by the temperature at the high altitude (Zhao et al., 2009b). The spatial variability of canopy LAI in dark coniferous forests has also been studied in subalpine western Sichuan. The results indicated that altitude is an important factor affecting LAI. The difference in LAI between different altitude gradients is extremely significant, and the LAI of subalpine dark coniferous forests in western Sichuan increases with altitude (Lü et al., 2007). Analysis of the variogram of fir forest LAI in the Daxing'an Mountains showed that LAI depended on the spatial heterogeneity of months. The spatial heterogeneity of LAI in July and November was mainly induced by spatial autocorrelation and

accounted for 99.8% and 66.9% of the total spatial heterogeneity, respectively (Liu et al., 2013).

4.2. Effects of hydrothermal conditions on LAI

The response of vegetation to hydrothermal conditions is a key process in understanding the terrestrial carbon–water cycle, and attention has been paid to the relationship between vegetation LAI and environmental factors (Hebert and Jack, 1998; Meier and Leuschner, 2008; Luo et al., 2011; Shao and Zeng, 2011).

4.2.1. Effects of water on LAI

The leaf area index of the different vegetation types was highly correlated with P in the preceding 3 months and with an average temperature in the preceding 1 month in the Poyanghu Basin, and both of them were 95% significant. Interannual changes in LAI of different vegetation types were highly influenced by interannual changes in P in the Poyanghu Basin from May to July (Li et al., 2012). P mainly affected the seasonal variation in LAI, as was noticed by studying the relation between LAI and climatic factors in a *Quercus variabilis* plantation at the southern foot of Taihang Mountain between 2001 and 2019 (Huang et al., 2022). The LAI of beech has been found to be mainly controlled by physiological factors related to forest age, while the effects of chemical properties of soil and P are relatively low (Bequet et al., 2011). The CMIP5 model was used to study the response of LAI to drought, and LAI showed irregular increases and decreases with decreasing soil water content (Huang et al., 2016).

Our study implied that the LAI of *P. crassifolia* was positively correlated with P and highly positively correlated with SWC_{60-80} . This may be related to the root distribution of *P. crassifolia*. LAI was negatively correlated with P in September, probably because of the decrease in P in September in the alpine region.

4.2.2. Effects of temperature on LAI

Leaf area index data from remote sensing were used to study the response of global vegetation LAI to temperature, which indicated that the season and interannual changes in temperature on a global scale were significantly different in different ecosystems (Zhang et al., 2002). The effect of the slope scale on the LAI of *Larix principis-rupprechtii* was studied in the small basin of Liupan Mountain, which showed that the main influencing factors in May were solar radiation and air temperature (Wang et al., 2016; Liu et al., 2017). The monthly maximum temperature was found to be the most influential factor in the dynamics of LAI in loblolly pine plantations (Kinane et al., 2022). The correlation between LAI and hydrothermal conditions was positive on a time scale and a spatial scale in most regions on the Tibetan Plateau (Wang et al., 2008).

Our study implies that LAI is influenced more by temperature and water in July and August in alpine Northwest China. Therefore, an accurate understanding of the temporal and spatial variability of forest canopy LAI is highly significant for evaluating forest

productivity at multiple scales and for studying the energy and water balance from the basin to the region.

5. Conclusion

The rapidly increasing period of LAI of *P. crassifolia* canopy was from late May to early July. The maximum LAI of *P. crassifolia* occurred in mid-August. LAI of *P. crassifolia* forests also has significant seasonal variation although it is an evergreen coniferous tree species. The main hydrothermal factors affecting the canopy LAI of *P. crassifolia* differed in July, August, and September. The LAI of *P. crassifolia* was more influenced by temperature and water in July and August. The LAI-2200 and TRAC methods are valid for measuring the LAI of *P. crassifolia* canopy forests. This study may provide a scientific basis for studying the impact of global change on forest ecosystems.

Data availability statement

The raw data supporting the conclusions of this article will be made available by the authors, without undue reservation.

Author contributions

YZ and WZ contributed to the conception and design of the study. WZ wrote sections of the manuscript. YZ and HF organized the database and performed the statistical analysis. YZ wrote and revised the first draft of the manuscript. All authors approved the submitted version.

Funding

This study was financially supported by the National Natural Science Foundation of China (91425301 and 32060247) and the central government of Gansu province guides local science and Technology Development Fund projects (22ZY2QG001).

Acknowledgments

We thank Jian Ma, Shunli Wang, Liying Chen, Hui Zhang, and Kehai Zhang for supporting our field observations. Rongxin Wang for data acquisition and two independent reviewers' comments for improving our manuscript.

Conflict of interest

The authors declare that the research was conducted in the absence of any commercial or financial relationships that could be construed as a potential conflict of interest.

Publisher's note

All claims expressed in this article are solely those of the authors and do not necessarily represent those of their affiliated

organizations, or those of the publisher, the editors and the reviewers. Any product that may be evaluated in this article, or

claim that may be made by its manufacturer, is not guaranteed or endorsed by the publisher.

References

- Behera, S. K., Srivastava, P., Pathre, U. V., and Tuli, R. (2010). An indirect method of estimating leaf area index in *Jatropha curcas* L. using LAI-2000 Plant Canopy Analyzer. *Agric. For. Meteorol.* 150, 307–311. doi: 10.1016/j.agrformet.2009.11.009
- Behling, A., Sanquetta, C. R., Corte, A. D., Netto, S. P., Rodrigues, A. L., Caron, B. O., et al. (2016). Tracking leaf area index and coefficient of light extinction over the harvesting cycle of black wattle. *J. For. Res.* 27, 1–7. doi: 10.1007/s11676-016-0279-1
- Bequet, R., Campioli, M., Kint, V., Muys, V., Bogaert, J., and Ceulemans, R. (2012). Spatial variability of leaf area index in homogeneous forests relates to local variation in tree characteristics. *For. Sci.* 58, 633–640. doi: 10.5849/forsci.10-123
- Bequet, R., Campioli, M., Kint, V., Vansteenkiste, D., Muys, B., and Ceulemans, R. (2011). Leaf area index development in temperate oak and beech forests is driven by stand characteristics and weather conditions. *Trees Struct. Funct.* 25, 935–946. doi: 10.1007/s00468-011-0568-4
- Bréda, N. J. (2003). Ground-based measurements of leaf area index: a review of methods, instruments and current controversies. *J. Exp. Bot.* 54, 2403–2417. doi: 10.1093/jxb/erg263
- Bréda, N. J., and Granier, A. (1996). Intra- and interannual variations of transpiration, leaf area index and radial growth of a sessile oak stand (*Quercus petraea*). *Ann. For. Sci.* 53, 521–536. doi: 10.1051/forest:19960232
- Cerný, J., Haninec, P., and Pokorný, R. (2020). Leaf area index estimated by direct, semi-direct, and indirect methods in European beech and sycamore maple stands. *J. For. Res.* 31, 827–836. doi: 10.1007/s11676-018-0809-0
- Chason, J. W., Baldocchib, D. D., and Huston, M. A. (1991). A comparison of direct and indirect methods for estimating forest canopy leaf area. *Agric. For. Meteorol.* 57, 107–128. doi: 10.1016/0168-1923(91)90081-Z
- Chen, J. M. (1996). Optically-based methods for measuring seasonal variation of leaf area index in boreal conifer stands. *Agric. For. Meteorol.* 80, 135–163. doi: 10.1016/0168-1923(95)02291-0
- Dermodoy, O., Long, S. P., and Delucia, E. H. (2006). How does elevated CO₂ or ozone affect the leaf-area index of soybean when applied independently? *New Phytol.* 169, 145. doi: 10.1111/j.1469-8137.2005.01565.x
- Fang, H. L. (2021). Advances in measurement and remote sensing of forest vertical structure parameters: a case study of leaf area index and aggregation index. *Chin. Sci. Bull.* 66, 3141–3153. doi: 10.1360/TB-2020-1057
- Fang, H. L., Baret, F., Plummer, S., and Schaepman-Strub, G. (2021). An overview of global leaf area index (LAI): methods, products, validation, and applications. *Rev. Geophys.* 57, 739–799. doi: 10.1029/2018RG000608
- Guo, W. H., Li, B., Zhang, X. S., and Wang, R. Q. (2007). The impact of water stress on transpiration indices in *Hippophae rhamnoides* and *Caragana intermedia*. *Acta Ecol. Sin.* 27, 4132–4140. doi: 10.3321/j.issn:1000-0933.2007.10.021
- Han, X. S., Deng, L. L., Wang, Y. H., Xiong, W., Li, Z. H., Liu, Q., et al. (2015). Variation of aboveground biomass *Larix principis-rupprechtii* plantation along slopes in the Diedieougou basin of Liupan Mountains. *Scientia Silvae Sinicae.* 51:132–139. doi: 10.11707/j.1001-7488.20150317
- Hebert, M. T., and Jack, S. B. (1998). Leaf area index and site water balance of loblolly pine (*Pinus taeda* L.) across a precipitation gradient in East Texas. *For. Ecol. Manag.* 105, 273–282. doi: 10.1016/S0378-1127(97)00287-9
- Huang, H., Zheng, C. L., Meng, P., Zhang, J. S., Tong, X. J., and Cheng, X. F. (2022). Relationship between leaf area index and climate factors in a *Quercus variabilis* plantation at the southern foot of Taihang Mountain from 2001 to 2019. *Acta Ecol. Sin.* 43, 4. doi: 10.5846/stxb202112173576
- Huang, Y. Y., Gerber, S., Huang, T. Y., and Lichstein, J. W. (2016). Evaluating the drought response of CMIP5 models using global gross primary productivity, leaf area, precipitation, and soil moisture data. *Glob. Biogeochem. Cy.* 30, 1827–1846. doi: 10.1002/2016GB005480
- Karimi, S., Nazemi, A. H., Sadraddini, A. A., Xu, T. R., Bateni, S. M., and Fard, A. F. (2020). Estimation of forest leaf area index using meteorological data: assessment of heuristic models. *J. Environ. Inform.* 36, 119–132. doi: 10.3808/jei.202000430
- Kinane, S. M., Montes, C. R., Zapata, M., Bullock, B. P., Cook, R. L., and Mishra, D. R. (2022). Influence of environmental variables on leaf area index in loblolly pine plantations. *For. Ecol. Manag.* 523, 120445. doi: 10.1016/j.foreco.2022.120445
- Leuschner, C., Voß, S., Foetzi, A., and Clases, Y. (2006). Variation in leaf area index and stand leaf mass of European beech across gradients of soil acidity and precipitation. *Plant Ecol.* 186, 247–258. doi: 10.1007/s11258-006-9127-2
- Li, X. H., Zhang, Q., and Shao, M. (2012). Spatial and temporal variability of leaf area index in the Poyang lake basin and its relationship with climatic factors. *Resour. Environ. Yangtze Basin.* 21, 296–301.
- Liu, Y., Liu, R. G., Chen, J. N., Cheng, X., and Zheng, G. (2013). Current status and perspectives of leaf area index retrieval from optical remote sensing data. *J. Geo-Inf. Sci.* 15, 734–743. doi: 10.3724/SP.J.1047.2013.00734
- Liu, Z. (2015). *Spatia and temporal dynamics of leaf area index in typical forest in the northeast China*. Doctor's degree, Northeast Forestry University, Haerbin, Heilongjiang Province, China.
- Liu, Z. B., Wang, Y. H., Liu, Y., Tian, A., Wang, Y. R., and Zuo, H. J. (2017). Spatiotemporal variation and scale effect of canopy leaf area index of larch plantation on a slope of the semi-humid Liupan Mountains, Ningxia, China. *Chin. J. Plant Ecol.* 41, 749–760. doi: 10.17521/cjpe.2016.0288
- Lü Y. L., Liu, S. R., Sun, P. S., Zhang, G. B., and Zhang, R. P. (2007). Seasonal and spatial variation of leaf area index of sub-alpine dark coniferous forest during growing season in Western Sichuan. *Scientia Silvae Sinicae.* 43:1–7. doi: 10.11707/j.1001-7488.20070801
- Luo, Y. X., Xiang, H. Q., Zheng, X. B., Chen, J., and Zhou, C. X. (2011). The response of leaf area index of MODIS to mountainous meteorological conditions in Guizhou. *Ecol. Environ. Sci.* 20, 19–23. doi: 10.3969/j.issn.1674-5906.2011.01.004
- Meier, I. C., and Leuschner, C. (2008). Leaf size and leaf area index in *fagus sylvatica* forests: competing effects of precipitation, temperature, and nitrogen availability. *Ecosystems* 11, 655–669. doi: 10.1007/s10021-008-9135-2
- Shao, P., and Zeng, X. D. (2011). Spatiotemporal relationship of leaf area index simulated by CLM3.0-DGVM and climatic factors. *Acta Ecol. Sin.* 31, 4725–4731. doi: 10.1093/mp/ssq070
- Sprintsin, M., Cohen, S., Maseyk, K., Rotenberg, E., Grünzweig, J., Karnieli, A., et al. (2011). Long term and seasonal courses of leaf area index in a semi-arid forest plantation. *Agric. For. Meteorol.* 151, 565–574. doi: 10.1016/j.agrformet.2011.01.001
- Vyas, D., Mehta, N., Dinakaran, J., and Krishnaya, N. S. R. (2010). Allometric equations for estimating leaf area index (LAI) of two important tropical species (*Tectona grandis* and *Dendrocalamus strictus*). *J. For. Res.* 21, 197–200. doi: 10.1007/s11676-010-0032-0
- Wang, X. Q., Ma, L. Y., and Jia ZK Xu, C. Y. (2005). Research and application advances in leaf area index (LAI). *Chin. J. Ecol.* 24, 537–541. doi: 10.1360/biodiv.050022
- Wang, Y. N., Deng, X. X., Wang, Y. H., Cao, G. X., Yu, P. T., Xiong, W., et al. (2016). The slope scale effect of canopy LAI of *Larix principis-rupprechtii* plantation at the south side of Liupan Mountains. *Acta Ecol. Sin.* 36, 3564–3571. doi: 10.5846/stxb201409301940
- Wang, Y. Q., Shi, J. C., Jiang, I. M., Du, J. Y., Sun, R. J., and Tian, B. S. (2008). The application of remote sensing data to analyzing the influence of water thermal conditions on LAI of Qinghai-tibet plateau. *Rem. Sens. Land Resour.* 4, 81–86. doi: 10.6046/gtzyyq.2008.04.19
- Watson, D. J. (1958). The dependence of net assimilation rate on leaf-area index. *Ann. Bot.* 22, 37–54. doi: 10.1093/oxfordjournals.aob.a083596
- Weiss, M., Baret, F., Smith, G. J., Jonckheere, I., and Coppin, P. (2004). Review of methods for in situ leaf area index (LAI) determination Part II: estimation of LAI, errors and sampling. *Agric. For. Meteorol.* 121, 37–53. doi: 10.1016/j.agrformet.2003.08.001
- Wilson, J. W. (1960). Inclined point quadrats. *New Phytol.* 59, 1–7. doi: 10.1111/j.1469-8137.1960.tb06195.x
- Yan, G. J., Hu, R. H., Luo, J. H., Weiss, M., Jiang, H. L., Mu, X. H., et al. (2019). Review of indirect optical measurements of leaf area index: recent advances, challenges, and perspectives. *Agric. For. Meteorol.* 265, 390–411. doi: 10.1016/j.agrformet.2018.11.033
- Zhang, J. H., Fu, C. B., Yan, X. D., Seit, E., and Hiroshi, K. (2002). Global response analysis of LAI vs. surface air temperature and precipitation variations. *Chin. J. Geophys.* 45, 631–637. doi: 10.1002/cjg2.280
- Zhao, C. Y., Shen, W. H., and Peng, H. H. (2009a). Methods for determining canopy leaf area index of *Picea crassifolia* forest in Qilian Mountain, China. *Chin. J. Plant Ecol.* 33, 860–869. doi: 10.3773/j.issn.1005-264x.2009.05.004
- Zhao, C. Y., Shen, W. H., Peng, H. H., and Wang, C. (2009b). Simulation of spatial distribution of leaf area index of *Picea crassifolia* forest: with Pailugou basin of Qilian Mountain as an example. *J. Lanzhou. Univ. (Nat Sci)* 45, 68–72. doi: 10.13885/j.issn.0455-2059.2009.05.026



OPEN ACCESS

EDITED BY

Ling Zhang,
Jiangxi Agricultural University, China

REVIEWED BY

Shuai Ouyang,
Central South University of Forestry
and Technology, China
Qing-Wei Wang,
Chinese Academy of Sciences (CAS), China

*CORRESPONDENCE

Zhili Liu
✉ liuzl2093@126.com

RECEIVED 31 May 2023

ACCEPTED 04 July 2023

PUBLISHED 18 July 2023

CITATION

Jin MY, Jin GZ, Guo QX and Liu ZL (2023)
Responses of economic and anatomical leaf
traits to soil fertility factors in eight coexisting
broadleaf species in temperate forests.
Front. For. Glob. Change 6:1232333.
doi: 10.3389/ffgc.2023.1232333

COPYRIGHT

© 2023 Jin, Jin, Guo and Liu. This is an
open-access article distributed under the terms
of the [Creative Commons Attribution License
\(CC BY\)](#). The use, distribution or reproduction
in other forums is permitted, provided the
original author(s) and the copyright owner(s)
are credited and that the original publication in
this journal is cited, in accordance with
accepted academic practice. No use,
distribution or reproduction is permitted which
does not comply with these terms.

Responses of economic and anatomical leaf traits to soil fertility factors in eight coexisting broadleaf species in temperate forests

Mingyue Jin, Guangze Jin, Qingxi Guo and Zhili Liu*

Center for Ecological Research, Key Laboratory of Sustainable Forest, Ecosystem Management-Ministry of Education, Northeast Asia Biodiversity Research Center, Northeast Forestry University, Harbin, China

The multidimensionality of leaf traits allows plants to have diverse survival strategies to adapt to complex living environments. Whether the anatomical traits of leaves are associated with leaf economic traits and which group of traits are more strongly correlated with soil fertility factors remains unclear. We measured four leaf economic traits, four anatomical traits, and five soil fertility factors of eight coexisting broadleaf species distributed in mixed broadleaved-Korean pine (*Pinus koraiensis*) forests located in Northeast China. Results show a strong interdependence between economic and anatomical traits ($p < 0.05$). The range of variation between economic and anatomical traits were almost equal, but the causes of variation were different. Specific leaf area was positively correlated with the abaxial epidermis, negatively correlated with the ratio of spongy tissue to leaf thickness (ST/LT), and not correlated with adaxial epidermis. Leaf dry matter content was negatively correlated with the abaxial epidermis and adaxial epidermis, positively correlated with ST/LT. Specific leaf area, palisade tissue, and ST/LT showed stronger correlation with soil fertility factors than other traits. Soil fertility factors dominating trait variation were dependent upon the trait. Our results suggest anatomical traits can be considered in economic trait dimension. The coupled relationship between anatomical and economic traits is potentially a cost-effective adaptation strategy for species to improve efficiency in resource utilization. Our results provide evidence for the complex soil-trait relationship and suggest that future studies should emphasize the role of anatomic traits in predicting soil fertility changes.

KEYWORDS

leaf trait multidimensionality, economic traits, anatomical traits, soil fertility factors, plant adaptive strategy

1. Introduction

Plant leaf functional traits, specifically traits related to leaf persistence such as light capture and gas exchange, are important indicators in identifying plant life history strategies and predicting community assembly (Valladares and Niinemets, 2008; Terashima et al., 2011; Liu C. C. et al., 2020; Ni et al., 2022). Many studies have shown that traits vary along certain

dimensions (Wright et al., 2007; Li et al., 2015; Liu C. C. et al., 2019; Yang Y. Z. et al., 2019). For example, the leaf economics spectrum dimension, represented by the negative correlation between specific leaf area (SLA), leaf nitrogen content (LN) and leaf lifespan, is the balance between plant leaf resource acquisition (higher SLA, LN but shorter leaf lifespan) and conservation (lower SLA, LN but longer leaf lifespan) (Wright et al., 2004); In recent years, anatomical traits [e.g., adaxial and abaxial epidermis (AD; AB) and palisade tissue (PT)] attracted more attention from ecologists (Chen and Wang, 2009; Santos et al., 2015), because of the critical role in light absorption and gas exchange capacity of a leaf (Evans et al., 2009; Kröber et al., 2014; Ni et al., 2022). In this dimension, thinner epidermal thickness and thicker PT tend to allow deeper light penetration and faster gas diffusion rates (Verboven et al., 2015). However, the relationship between these two trait dimensions and their response to soil fertility remains unclear.

Relationships between leaf economic and anatomical traits have been examined at the species and community level. Coble and Cavaleri (2017) reported a positive correlation between PT and leaf mass per area (the reciprocal of the SLA) in sugar maple. Liu C. C. et al. (2019) found AB was negatively correlated with leaf dry matter content (LDMC) and reported a weak correlation between anatomical and economic traits in temperate and subtropical forests. Several of the relevant studies are limited when exploring the correlation between individual traits. The correlation between anatomical and economic traits has rarely been verified, especially for co-existing species in the same forest type at a regional scale.

The correlation between soil fertility factors and leaf traits reflects the trade-off between plant growth and nutrient conservation (Liu Z. L. et al., 2020). However, which groups of functional traits are strongly associated with soil fertility gradients remains unclear (Wright et al., 2005; Maire et al., 2015; Stark et al., 2017; Peng et al., 2018). Leaf economic traits, such as SLA, are considered good predictors of soil fertility. Hodgson et al. (2011) studied the correlation between economic traits and soil fertility and found SLA had a better response to soil fertility than other traits. Widely accepted is Westoby's (1998) conclusion that SLA is good indicator of soil fertility (Laughlin et al., 2010; De Frenne et al., 2011). Therefore, economic traits may have a stronger correlation with soil fertility factors. Anatomical traits are often reported as being closely related to the acquisition and utilization of light. PT can affect photosynthetic efficiency by regulating chloroplast content (Terashima et al., 2011; He et al., 2017) and sponge tissue can affect light density in leaves by regulating intercellular spaces (Kröber et al., 2014). Thus, anatomical traits may be more correlated with environmental factors significantly affecting the composition and structure of leaf cells and intercellular air space.

Soil fertility clearly influences the variation of leaf traits, but which soil fertility factors dominates the trait variation is unclear (Chartzoulakis et al., 2002; Ordoñez et al., 2009; Maire et al., 2015). Soil pH is closely related to soil mineralogical composition and can significantly affect the distribution of nutrients in soil (Uehara and Gilman, 1981; Quesada et al., 2010), and ultimately lead to changes in relative above-ground biomass (Zheng and Ma, 2018). Nutrient elements in the soil, which are important source of organic compounds for plants, significantly affect the variation in plant traits (Fan et al., 2015; Yang D. X. et al., 2019). Plants adapted to low soil fertility environments usually build leaves adapted to lower

respiratory carbon and water loss, e.g., higher LDMC but lower LN (Ordoñez et al., 2010; Jager et al., 2015; Lin et al., 2020). In addition, soil water content (SWC) affects the efficiency of plant nutrient and water uptake and utilization by affecting soil microbial viability and root development (Liu et al., 2010; Liu C. C. et al., 2019). The response of plants to soil gradient is related to the cause and extent of trait variation (Funk, 2008; Siefert and Ritchie, 2016; Zhou et al., 2018). A wider range of intraspecific traits variation is thought to provide plants with greater access to limiting resources (Lin et al., 2020). da Silveira Pontes et al. (2010) found trait plasticity regulates plant responses to nitrogen enrichment in grasslands. Ishii et al. (2018) found plants with higher intra-individual plasticity had greater acclimation potential to environmental perturbation. Therefore, intraspecific traits variation should be considered when predicting the response of plant to soil fertility gradients.

In this study, we selected eight coexisting broadleaf species as target species, as they are dominant and commonly associated with the distribution of mixed broadleaved-Korean pine (*Pinus koraiensis*) forests in Northeast China (Wang, 1994). Eight leaf traits (including four leaf economic traits and four anatomical traits) and five soil fertility factors were measured. The variation in soil fertility factors in the study area provide an ideal setting for testing soil fertility-trait relationships. We sought to answer the following questions: (1) what is the relationship between economic and anatomical traits? We hypothesize that there should be coupling relationship between economic traits and vein traits. (2) Which group of functional traits are more strongly associated with soil fertility gradients? We hypothesize that economic traits would show a stronger correlation with soil fertility than vein traits. (3) Which soil fertility factor dominates leaf trait variation? We hypothesize that soil nutrient may dominate traits variation.

2. Materials and methods

2.1. Sample design

Our study sites are distributed in the mixed broadleaved-Korean pine forests in Northeast China (Wang, 1994; **Supplementary Table 1**). Within each site, we selected eight coexisting broadleaf species in mid-July to August (**Supplementary Table 2**). Leaf sample collection for each species took place in south facing slopes with similar slope degrees. Three trees with similar tree height (measured by tree altimeter) and diameter at breast height were selected. Information for the sampled trees is shown in **Supplementary Table 2**. We cut 6 branches beginning at the first living branch to the top of the tree: upper south and north, middle south and north, lower south and north. In each sampling unit, 5 healthy and fully expanded leaves were selected to measure SLA and LDMC, and five leaves were selected to be fixed in a buffered formalin-acetic acid-alcohol fixation solution (70% ethanol: formalin: glacial acetic acid = 90: 5: 5) to measure anatomical traits, e.g., AB, AD, PT, and spongy tissue (ST). Totally, we collected 180 leaves to measure SLA, LDMC and anatomical traits for each tree species. Additionally, 10–20 leaves were used to measure LN and leaf phosphorus content (LP) (**Table 1**). Soil samples were collected for each sample tree. We removed the leaf litter and then collected soil samples at 0–10 cm depth, with three

TABLE 1 Information of eight leaf functional traits for all species.

| Leaf traits | Abbrev | Unit | Mean | SE | CV | Max | Min |
|------------------------------|--------|---------------------------------|--------|------|------|--------|-------|
| Specific leaf area | SLA | cm ² g ⁻¹ | 185.41 | 2.63 | 0.29 | 447.38 | 95.95 |
| Leaf dry matter content | LDMC | g g ⁻¹ | 0.34 | 0.00 | 0.15 | 0.47 | 0.22 |
| Leaf nitrogen content | LN | mg g ⁻¹ | 33.82 | 0.17 | 0.10 | 44.17 | 23.83 |
| Leaf phosphorus content | LP | mg g ⁻¹ | 1.60 | 0.02 | 0.31 | 3.57 | 0.67 |
| Abaxial epidermis thickness | AB | μm | 11.50 | 0.09 | 0.17 | 18.34 | 6.44 |
| Adaxial epidermis thickness | AD | μm | 15.69 | 0.16 | 0.22 | 25.55 | 10.20 |
| Palisade tissue | PT | μm | 15.44 | 0.19 | 0.25 | 30.20 | 6.60 |
| Spongy tissue/Leaf thickness | ST/LT | % | 65.60 | 0.92 | 0.29 | 123.17 | 25.65 |

replicates. The three subsamples were then mixed together, stored in vacuum plastic bags and transported to the lab.

2.2. Leaf trait measurements

For each sampled leaf, we used a micrometer to measure the non-main vein three times and then took the average value of the leaf thickness (precision: 0.01). We then measured fresh leaf mass (precision: 0.0001 g) and scanned leaf area (precision: 0.01 cm²; BenQ Corporation, Suzhou, China, 300 dpi resolution). After, we oven-dried the leaves to a constant weight (65°C, at least 72 h) and measured the mass (precision: 0.0001 g). SLA (cm² g⁻¹, SLA = leaf area/leaf dry mass) and LDMC (g g⁻¹, LDMC = leaf dry mass/fresh mass) were then calculated. We used a pulverizer to grind all the leaves into powder and oven-dried them. We then measured LN [mg g⁻¹, Hanon K9840 auto-Kjeldahl analyzer (Jinan Hanon Instruments Co. Ltd., Jinan, China)] and LP [mg g⁻¹, molybdenum blue colorimetric method, AQ2 automatic discontinuous chemical analyzer (SEAL Analytical, Inc., Mequon, WI, USA)] after digested with H₂SO₄-H₂O₂.

To measure anatomical traits, we first progressively dehydrated the leaves with ethanol series (70, 85, 95, and 100%) and then infiltrated them with warm paraffin. We obtained the leaf sections (7 μm) using a rotary microtome (KD-2258, Zhejiang, China). We then stained (Safranin and Fast Green), mounted and sealed (neutral glue) the leaves to take photographs. We used a light microscope (Olympus Electronics, Inc., Tsukuba, Japan) to measure AB, AD, PT, and ST [by using electronic image analysis equipment (cellSens Standard 1.11 software, Olympus Electronics Inc., Tsukuba, Japan)]. The ratio of spongy tissue to leaf thickness (ST/LT) was calculated by dividing the ST by the LT.

2.3. Soil factors measurements

After measuring soil samples for SWC [g g⁻¹, oven-drying method (Liu Z. L. et al., 2020)], we dried the soils and measured soil pH (HANNAPH211 pH meter), soil total carbon [mg g⁻¹, multiN/C3000 (Analytic Jena AG, Jena, Germany)], soil total nitrogen [mg g⁻¹, Hanon K9840 auto Kjeldahl analyzer (Jinan Hanon Instruments Co. Ltd., Jinan, China)] and soil total phosphorus (mg g⁻¹, molybdenum blue colorimetric method).

2.4. Statistical analysis

We used principal component analysis (PCAs) to determine the multivariate associations of leaf traits (PCAs) in R 3.4.2 (R Core Team, 2017). Eight leaf traits of eight species from three sites were input in the PCA. The first principal axis values of economic and anatomical traits were used to analyze the correlation between the two groups of traits (Li et al., 2015). For eight leaf traits, we used “lme” function in the “nlme” package to fit a linear mixed model (nested levels: leaf, direction, canopy, tree, and site). The “varcomp” function in the “ape” package was used to calculate the variance components associated with the nested level. The correlation between economic and anatomical traits, the correlation between the two sets of traits, and the correlation of soil fertility factors were analyzed using Pearson correlation analysis. General linear model was used to estimate responses of the eight leaf traits to soil fertility factors. We calculated the variance inflation factor (VIF) between every two bivariate independent variables in the model to prevent collinearity from affecting model accuracy (Supplementary Table 3). VIF was all less than 10, indicating no issues with collinearity (Dormann et al., 2013).

3. Results

The first two axis described 55.9% of the total variance (Figure 1A and Supplementary Figure 1). The first PCA axis (PC1) explained 33.5% of the variance and showed strong loadings from SLA and LDMC. The second PCA axis (PC2) explained an additional 22.4% of the variance and showed strong loadings from AD, AB, and ST/LT (Figure 1A and Table 2). Covariation occurred between the PC1 scores of leaf economics traits and anatomical traits ($p < 0.05$). The covariation further confirmed anatomical traits could be assigned to economic traits (Figure 1B).

The variation range of economic traits (17–30%) and anatomical traits (18–29%) was similar but the causes of trait variation were different. Intraspecific factors (tree + canopy + direction) explained most of the variation in economic traits (34–65%); while interspecific factors (species + site) explained most for most of the variation in anatomical traits (55–71%) (Figure 2). For economic traits, among the three intraspecific factors, direction explained the most trait changes in SLA, LN, and LP, followed by canopy. For LDMC, canopy explained the most trait variation followed by direction. For anatomical traits,

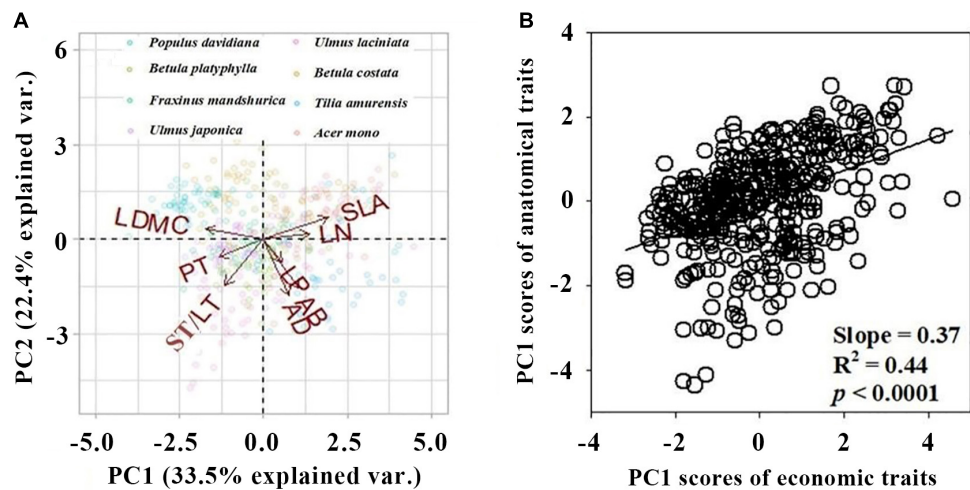


FIGURE 1 Principal component analysis (PCA) of eight leaf traits of eight species. **(A)** Biplot of the first two principal components loaded by trait variables. Arrows represent the principal component loadings associated with the leaf traits. The proportion of the total variation explained by the first two components is shown in parentheses next to the axis label. **(B)** The bivariate relationships between PC1 scores of economic trait and anatomical traits. All traits were log-transformed before analysis. Leaf trait abbreviations are provided in **Table 1**.

TABLE 2 Principal component analysis (PCA) results for the eight leaf traits.

| | PC1 | PC2 |
|-------------------------|-----------------|-------------------|
| Eigenvalue | 2.68 | 1.79 |
| Variation explained (%) | 33.50% | 22.40% |
| Interpretation of axis | Economic traits | Anatomical traits |
| SLA | 0.52 | 0.23 |
| LDMC | -0.46 | 0.11 |
| LN | 0.37 | 0.05 |
| LP | 0.15 | -0.24 |
| AB | 0.29 | -0.52 |
| AD | 0.21 | -0.59 |
| PT | -0.36 | -0.19 |
| ST/LT | -0.31 | -0.48 |

For each axis, the eigenvalues, proportion of variance explained and the loading scores of each trait on the first two components are provided. Trait abbreviations are provided in **Table 1**. |eigenvectors| > 0.4 are in bold.

tree species explained the most trait variation (**Figure 2**). We observed a significant correlation between economic traits and anatomical traits except for SLA vs. AD ($p < 0.05$; **Figure 3**). SLA was negatively correlated with AD and positively correlated with ST/LT. LDMC was positively correlated with AD and AB and negatively correlated with ST/LT (**Figure 3**).

Significant correlations occurred between most economic and anatomical traits and soil fertility factors ($p < 0.05$; **Figures 4, 5**). For economic traits, SLA was significantly correlated with five soil fertility factors. Other economic traits were not correlated with soil fertility factors, with the exception of LDMC vs. pH and STN, LN vs. pH and SWC, LP vs. STP and SWC (**Figure 4**). For anatomical traits, AB was significantly correlated with STN and pH, and AD

was significantly correlated with STN and SWC, PT and ST/LT were significantly correlated with soil fertility factors except PT vs. pH and ST/LT vs. SWC (**Figure 5**).

Soil fertility factors had stronger effects on anatomical traits compared to economic traits (**Table 3**). For economic traits, STN significantly affected SLA and LDMC. STP and SWC significantly affected SLA and LP. pH significantly affected SLA, LDMC, and LN (**Table 3**). For anatomical traits, STC significantly affected PT. STN affected all anatomical traits except AB. STP affected all anatomical traits except AD. pH significantly affected AB and PT, and SWC affected all anatomical traits (**Table 3**).

4. Discussion

4.1. Relationships between economic traits and anatomical traits

We found a strong interdependence between economic traits and anatomical traits in mixed broadleaved-Korean pine (*P. koraiensis*) forests (**Figure 1**). Our results support the first hypothesis. The coupled correlations are potentially a more cost-effective adaptation strategy for species to improve resource utilization efficiency (Yin et al., 2017; Liu C. C. et al., 2020). Our study is consistent with the findings of Liu C. C. et al. (2019). The leaf economic trait axis showed strong loadings from SLA and LDMC. This describes a shift from higher leaf dry-mass investment efficiency and lower moisture diffusion resistance to lower leaf dry-mass investment efficiency and higher moisture diffusion resistance (Wilson et al., 1999; Wright et al., 2004). Leaf anatomical trait axis showed strong loadings from AB, AD, and ST/LT. This describes the co-variation of leaf mechanical stability and gas exchange rate. Anatomical traits are often considered to be important indicators of photosynthesis (Terashima et al., 2011; Coble and Cavaleri, 2017). Leaf photosynthesis is constrained by economic traits because high

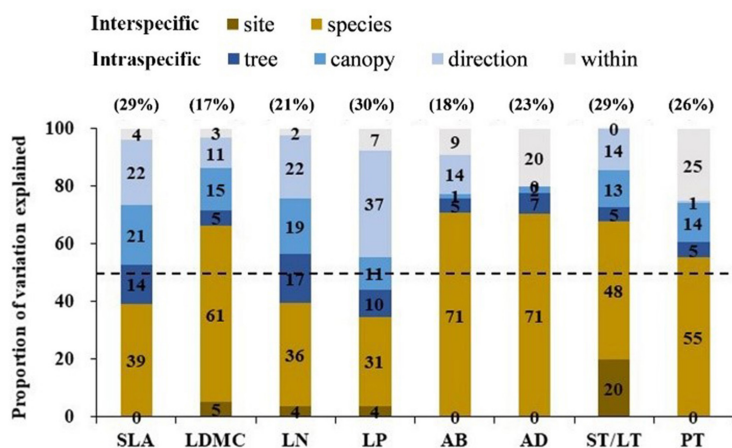


FIGURE 2
 Variance partitioning of the full nested linear models on four economic traits and four anatomical traits across five nested ecological scales. The number in brackets above the graph is the overall variation coefficient (%) of this trait. The 50% thresholds are given by a dashed line. Leaf trait abbreviations are provided in [Table 1](#).

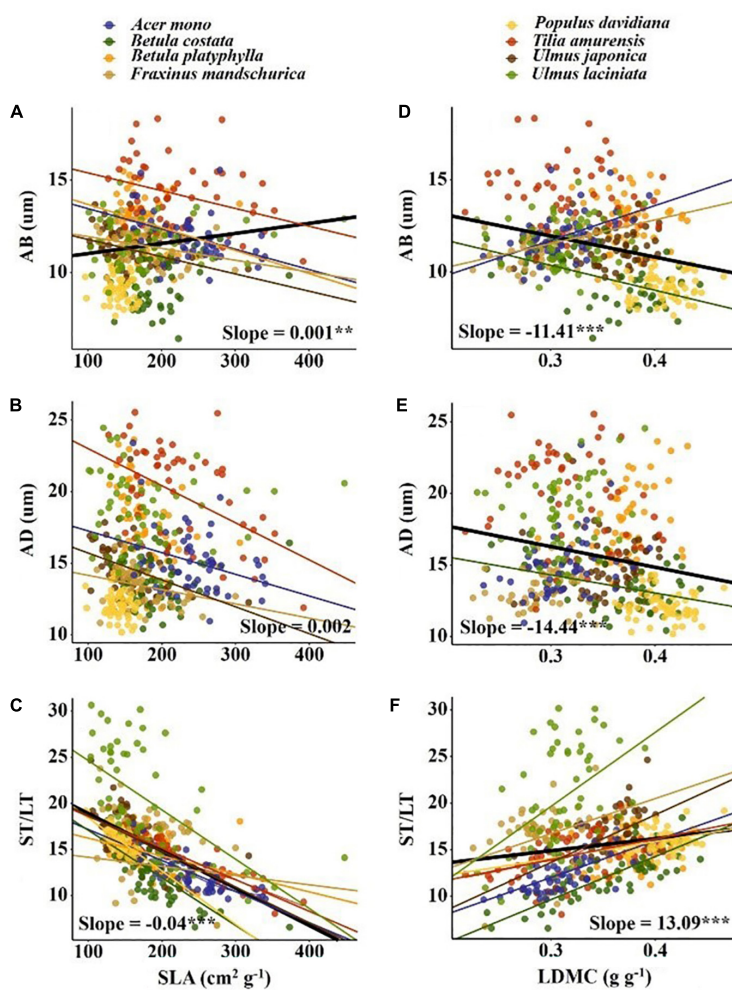


FIGURE 3
 Pearson's correlations between economic traits and anatomical traits. The solid line indicates that the correlation between leaf traits and soil fertility factor is significant at the 0.05 level. Slope and correlation significance in each figure were calculated at the interspecific level. (A–C) The relationship between SLA and AB, AD, ST/LT; (D–F) the relationship between LDMC and AB, AD, ST/LT.

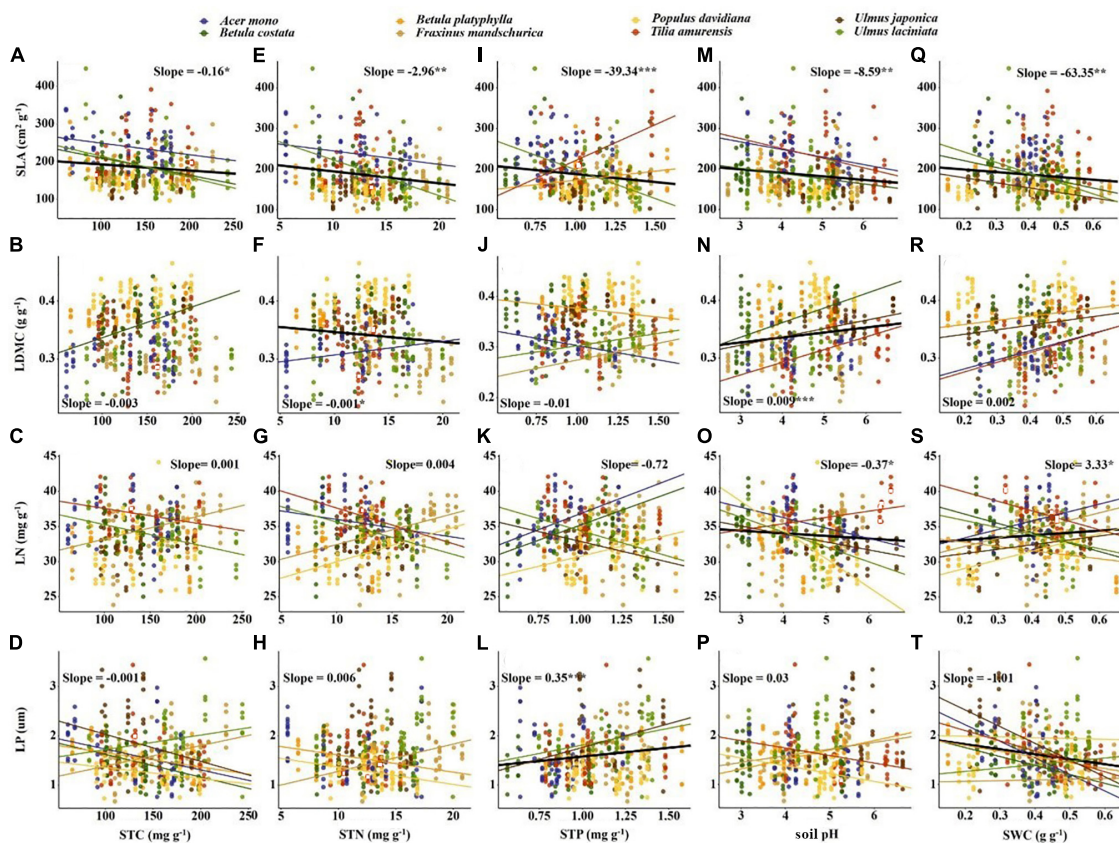


FIGURE 4

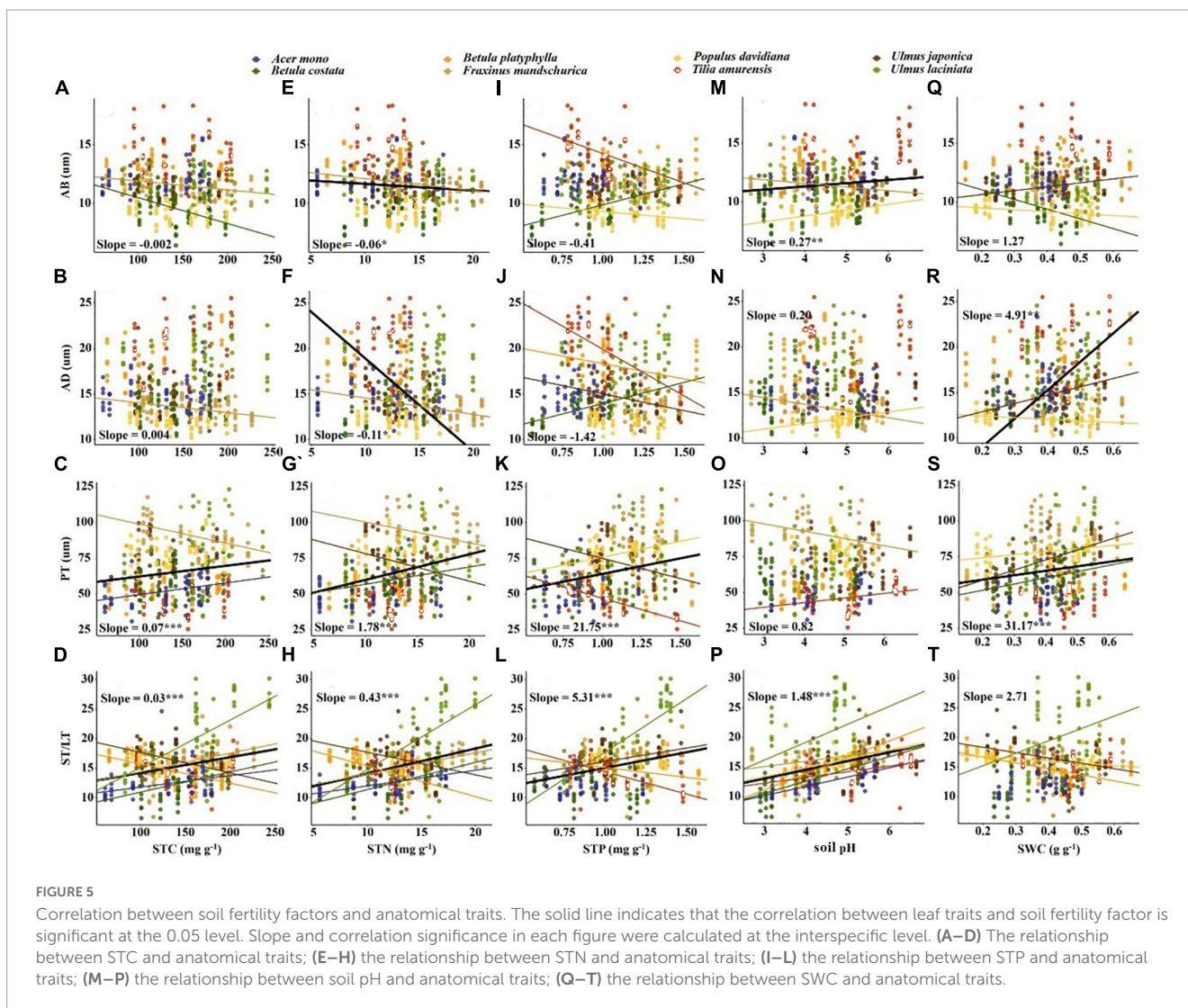
Correlation between soil fertility factors and economic traits. The solid line indicates that the correlation between leaf traits and soil fertility factor is significant at the 0.05 level. Slope and correlation significance in each figure were calculated at the interspecific level. (A–D) The relationship between STC and economic traits; (E–H) the relationship between STN and economic traits; (I–L) the relationship between STP and economic traits; (M–P) the relationship between soil pH and economic traits; (Q–T) the relationship between SWC and economic traits.

photosynthetic rates need efficient water supply and thus higher dry-mass investment (for example, to build a vein structure) (Sack and Scoffoni, 2013). Therefore, coupling between leaf construction costs and leaf photosynthesis might drive the coordination of plant economic and anatomical traits.

The range of intraspecific variation of economic traits and anatomical traits was almost equal, but the causes of intraspecific variation were different (Figure 2). For economic traits (except LDMC), intraspecific factors explain most of the trait variation. Among intraspecific factors, direction explained the most trait variation (22–37%, Figure 2), indicating these traits were highly responsive to light variation (Coble et al., 2017). For anatomical traits, interspecific factors explain most of the trait variation. Among interspecific factors, tree species explained most of the variation (48–71%, Figure 2), suggesting anatomical traits were less influenced by microclimate factors and more influenced by leaf construction traits or large-scale environmental factor variation. The target tree species selected for our study have a wide range of shade tolerance. The significant effect of shade tolerance on anatomical traits supports the results of Zhang et al. (2019). In addition, mycorrhizal differences between tree species may also be the cause of trait variation, because different mycorrhizal tree species may adapt to different soil nutrients (e.g., arbuscular mycorrhizal species tend to be adapted to areas with fertile soil;

while ectomycorrhizal species tend to be adapted to areas with infertile soil) (Phillips et al., 2013; Mao et al., 2019). Our results suggest when examining the effects of intraspecific variation on traits, the causes of intraspecific variation should be considered.

Significant correlations between economic and anatomical traits reflect trade-offs between plant leaf construction cost and photosynthetic capacity (Supplementary Figure 2). SLA was positively correlated with AB (Figure 3A). SLA reflects the light-capturing ability of the leaf (Wright et al., 2004) and AB reflects the ability to reduce the reflection of scattered light (Liu C. C. et al., 2019). Therefore, higher AB corresponds to a higher SLA and may signify the adaptation of plants to low light environment. SLA was negatively correlated with ST/LT (Figure 3C). This trade-off was also found at the intraspecific level in large-scale environments (Liu C. C. et al., 2019). For leaves, a higher ST/LT represents a higher proportion of ST and a higher ST is beneficial for leaves to better utilize scattered light (Terashima et al., 2011; Kröber et al., 2014). This may be the reason for the negative correlation between ST/LT and SLA. With the increase of LDMC, AB and AD decrease but ST/LT increases (Figures 3D–F). LDMC is an indicator of leaf moisture content. The increase in LDMC prompted a decrease in intercellular space and water content but increase in dry matter mass per volume (Wilson et al., 1999; Shipley and Vu, 2002). The thicker epidermis helps increase radiation



intensity inside the leaf and reduce mechanical damage from herbivores and wind (Thomas and Winner, 2002). The negative correlation between LDMC and the epidermis may be a trade-off between nutrient accumulation and protection. Higher LDMC corresponds to higher ST/LT, which may be an adaptive strategy for plants to maintain minimum water content and maximize light absorption.

4.2. Economic and anatomical traits show specific responses to soil fertility

The results showed that the response of economic and anatomical traits to soil fertility was different, and the main driving factors of trait variation depended on the trait, which may be related to the potential tradeoff between leaf light capture and water conduction. Our results do not support the second and third hypotheses.

For economic traits, SLA demonstrated a stronger correlation with soil fertility factors than other economic traits (e.g., LDMC, Table 3). This supports the findings from Laughlin et al. (2010) and De Frenne et al. (2011), who suggested SLA can better predict

soil fertility than other traits. The correlation between SLA and soil nutrients in our study (Figures 4A, E, I) were inconsistent with previous research results (Ordoñez et al., 2009; Maire et al., 2015). This may be attributed to the sampling site location in northeast China. The northeastern Chinese climate may affect the correlation between SLA and soil nutrients factors (Simpson et al., 2016). We also found a negative correlation between LDMC and STN, suggesting the preservation of more organic matter in leaves from infertile soil is of great significance for plant survival (Jager et al., 2015). In addition, past studies report soil nutrients usually correspond to leaf nutrient content, such as low LP was often found in low soil P environment (Ordoñez et al., 2009; Fan et al., 2015). The correlation between LP and STP in our study also fit into this framework (Figure 4L), however, no such relationship was found between other leaf nutrients and soil nutrient factors. The negative correlation between LP and SWC supports the results of Ordoñez et al. (2009) and Maire et al. (2015). The area with high soil moisture is also relatively high in soil P due to leaching, thus corresponding higher LP. We also found a positive correlation between LN and SWC (Wright et al., 2003), which may be because in arid areas, lower LN was beneficial to reduce photosynthetic water consumption and provide a conservative survival strategy

TABLE 3 The influence of five soil fertility factors on economic and anatomical traits by using a General linear model (GLM).

| | STC | | STN | | STP | | Soil pH | | SWC | | Intercept | | |
|-------------------|-------------|---------------|-----------|---------------|-----------|---------------|-----------|---------------|-----------|---------------|-----------|---------|-----------|
| | Leaf traits | Estimate Std. | p-value | Estimate Std. | p-value | Estimate Std. | p-value | Estimate Std. | p-value | Estimate Std. | p-value | p-value | |
| Economic traits | SLA | 0.182 | 0.132 | -2.546 | 0.048* | -25.771 | 0.027* | -7.824 | 0.007** | -62.19 | 0.045* | 281.857 | <0.001*** |
| | LDMC | 0 | 0.14 | -0.004 | <0.001*** | 0.003 | 0.805 | 0.011 | <0.001*** | 0.024 | 0.395 | 0.311 | <0.001*** |
| | LN | -0.007 | 0.384 | 0.078 | 0.354 | -1.383 | 0.071 | -0.426 | 0.024* | 3.583 | 0.078 | 35.753 | <0.001*** |
| | LP | 0.001 | 0.52 | 0.011 | 0.322 | 0.333 | 0.001** | 0.021 | 0.412 | -1.427 | <0.001*** | 1.495 | <0.001*** |
| Anatomical traits | AB | 0.001 | 0.52 | 0.011 | 0.322 | 0.333 | 0.001** | 0.021 | 0.412 | -1.427 | <0.001*** | 1.495 | <0.001*** |
| | AD | 0.012 | 0.105 | -0.339 | <0.001*** | -0.144 | 0.842 | 0.364 | 0.041* | 6.787 | <0.001*** | 14.057 | <0.001*** |
| | PT | -0.16 | <0.001*** | 2.571 | <0.001*** | 9.434 | 0.016* | -0.204 | 0.832 | 29.663 | 0.004** | 33.516 | <0.001*** |
| | ST/LT | 0.012 | 0.103 | 0.217 | 0.008** | 3.139 | <0.001*** | 1.312 | <0.001*** | -4.792 | 0.015* | 3.366 | 0.006** |

Estimated std. is the standardized regression coefficient. * $p < 0.05$, ** $p < 0.01$, *** $p < 0.001$. Leaf traits abbreviations are provided in Table 1. STC, soil total carbon; STN, soil total nitrogen; STP, soil total phosphorus; soil pH; SWC, soil water content.

for plants (Wright et al., 2005). Similar correlations were not found between SLA and SWC (Figure 4Q), which may be due to the large difference in shade tolerance of the selected tree species in our study. In addition, higher pH often implies higher nutrient utilization efficiency and usually corresponds to higher SLA, LN and lower LDMC. However, our results were contrary to this and may be due to the lower precipitation levels of our sampling area. Additionally, soil pH was more related to non-climatic factors, such as topography (Jenny, 1941), thus showing contrary results.

For anatomical traits, ST/LT and PT were positively correlated with STC, STN, and STP, while AB and AD were negatively correlated with STN. Soil nutrients, aboveground biomass, and canopy cover increase while the light density decreases (Hautier et al., 2009; Lin et al., 2020). Thicker PT and ST can contain more chloroplasts and have larger intercellular spaces (Mendes et al., 2001; Terashima et al., 2011; He et al., 2017). Thinner epidermis allows for facilitated CO₂ diffusion within a leaf (Verboven et al., 2015), thereby optimizing photosynthesis to adapt to low light environment. Plants tend to choose the quick-return strategy in lower pH soils. A thicker AB helps to reduce reflected light (Liu C. C. et al., 2019) and a larger ST/LT can improve the gas transport efficiency, both of which support rapid resource acquisition by plants (Verboven et al., 2015). Lower AD and PT correspond to soil with lower water content (Figures 5R, S). Leaves building smaller cells to maintain turgor may be a survival strategy against drought (Li et al., 2011), such results are also found in herbs and shrubs (He et al., 2017). Furthermore, we emphasize the importance of PT and ST/LT in predicting soil fertility due to the strong correlation between these two anatomical traits and soil fertility factors (Figure 5). This result may be related to the close relationship between these two traits and SLA, as SLA can be explained by the inverse of leaf thickness and leaf density (Poorter et al., 2009). Intercellular space size determines leaf thickness, while PT thickness determines leaf density (Sack et al., 2013; Onoda et al., 2017). Therefore, PT and ST/LT show a stronger response to soil fertility than epidermal thickness.

5. Conclusion

Our results clearly show a coupling relationship between economic and anatomical traits. We found difference in the causes of trait variation. Relative to economic traits, SLA had a stronger correlation with soil fertility than other traits. Relative to anatomical traits, PT and ST/LT had a stronger correlation with soil fertility than other traits and the main soil fertility factors driving the variation was dependent on traits. Our results provide a new perspective for understanding the correlation between leaf traits and soil fertility factors.

Data availability statement

The raw data supporting the conclusions of this article will be made available by the authors, without undue reservation.

Author contributions

ZL developed the idea. ZL and MJ carried out the experiment. MJ analyzed the dataset. GJ contributed to interpretation of data. MJ wrote the manuscript with substantial contributions from ZL, GJ, and QG. All authors contributed to the article and approved the submitted version.

Funding

This work was supported by the National Key R&D Program of China (2022YFD2201100), the National Natural Science Foundation of China (31971636), and the Fundamental Research Funds for the Central Universities (2572022DS13).

Acknowledgments

We would like to thank Dr. Joseph Elliot at the University of Kansas for his assistance with English language and grammatical editing of the manuscript.

References

- Chartzoulakis, K., Patskas, A., Kofidis, G., Bosabalidis, A. M., and Nastou, A. (2002). Water stress affects leaf anatomy, gas exchange, water relations and growth of two avocado cultivars. *Sci. Hortic.* 95, 39–50.
- Chen, L., and Wang, R. Z. (2009). Anatomical and physiological divergences and compensatory effects in two *Leymus chinensis* (Poaceae) ecotypes in Northeast China. *Agr. Ecosyst. Environ.* 134, 46–52.
- Coble, A. P., and Cavaleri, M. A. (2017). Vertical leaf mass per area gradient of mature sugar maple reflects both height-driven increases in vascular tissue and light-driven increases in palisade layer thickness. *Tree Physiol.* 37, 1337–1351. doi: 10.1093/treephys/tpx016
- Coble, A. P., Fogel, M. L., and Parker, G. G. (2017). Canopy gradients in leaf functional traits for species that differ in growth strategies and shade tolerance. *Tree Physiol.* 37, 1415–1425. doi: 10.1093/treephys/tpx048
- da Silveira Pontes, L., Louault, F., Carrere, P., Maire, V., Andueza, D., and Soussana, J. F. (2010). The role of plant traits and their plasticity in the response of pasture grasses to nutrients and cutting frequency. *Ann. Bot.* 105, 957–965. doi: 10.1093/aob/mcq066
- De Frenne, P., Graae, B. J., Kolb, A., Shevtsova, A., Baeten, L., Brunet, J., et al. (2011). An intraspecific application of the leaf-height-seed ecology strategy scheme to forest herbs along a latitudinal gradient. *Ecography* 34, 132–140.
- Dormann, C. F., Elith, J., Bacher, S., Buchmann, C., Carl, G., Carré, G., et al. (2013). Collinearity: A review of methods to deal with it and a simulation study evaluating their performance. *Ecography* 36, 27–46. doi: 10.1111/j.1600-0587.2012.07348.x
- Evans, J. R., Kaldenhoff, R., Genty, B., and Terashima, I. (2009). Resistances along the CO₂ diffusion pathway inside leaves. *J. Exp. Bot.* 60, 2235–2248. doi: 10.1093/jxb/erp117
- Fan, H., Wu, J., Liu, W., Yuan, Y., Hu, L., and Cai, Q. (2015). Linkages of plant and soil C:N:P stoichiometry and their relationships to forest growth in subtropical plantations. *Plant Soil* 392, 127–138. doi: 10.1007/s11103-015-0274-2
- Funk, J. L. (2008). Differences in plasticity between invasive and native plants from a low resource environment. *J. Ecol.* 96, 1162–1173.
- Hautier, Y., Pascal, A. N., and Andy, H. (2009). Competition for light causes plant biodiversity loss after eutrophication. *Science* 324, 636–638. doi: 10.1126/science.1169640
- He, N. P., Liu, C. C., Tian, M., Li, M. L., Yang, H., Yu, G. R., et al. (2017). Variation in leaf anatomical traits from tropical to cold-temperate forests and linkage to ecosystem functions. *Funct. Ecol.* 32, 10–19.
- Hodgson, J. G., Montserrat-Marti, G., Charles, M., Jones, G., Wilson, P., Shipley, B., et al. (2011). Is leaf dry matter content a better predictor of soil fertility than specific leaf area? *Ann. Bot.* 108, 1337–1345. doi: 10.1093/aob/mcr225
- Ishii, H. R., Horikawa, S., Noguchi, Y., and Azuma, W. (2018). Variation of intra-crown leaf plasticity of *Fagus crenata* across its geographical range in Japan. *For. Ecol. Manag.* 429, 437–448.
- Jager, M. M., Richardson, S. J., Bellingham, P. J., Clearwater, M. J., Laughlin, D. C., and De Deyn, G. (2015). Soil fertility induces coordinated responses of multiple independent functional traits. *J. Ecol.* 103, 374–385.
- Jenny, H. (1941). *Factors of soil formation: A system of quantitative pedology*. Dover, NY: McGraw-Hill Book Company, Inc.
- Kröber, W., Heklau, H., and Bruehlheide, H. (2014). Leaf morphology of 40 evergreen and deciduous broadleaved subtropical tree species and relationships to functional ecophysiological traits. *Plant Biol.* 17, 373–383. doi: 10.1111/plb.12250
- Laughlin, D. C., Leppert, J. J., Moore, M. M., and Sieg, C. H. (2010). A multi-trait test of the leaf-height-seed plant strategy scheme with 133 species from a pine forest flora. *Funct. Ecol.* 24, 493–501.
- Li, F. L., Bao, W. K., and Wu, N. (2011). Morphological, anatomical and physiological responses of *Campylotropis polyantha* (Franch.) Schindl. seedlings to progressive water stress. *Sci. Hortic.* 127, 436–443.
- Li, L., McCormack, M. L., Ma, C. G., Kong, D. L., Zhang, Q., Chen, X. Y., et al. (2015). Leaf economics and hydraulic traits are decoupled in five species-rich tropical-subtropical forests. *Ecol. Lett.* 18, 899–906. doi: 10.1111/ele.12466
- Lin, G. G., Zeng, D. H., and Mao, R. (2020). Traits and their plasticity determine responses of plant performance and community functional property to nitrogen enrichment in a boreal peatland. *Plant Soil* 1, 151–167.
- Liu, C. C., Li, Y., Xu, L., Chen, Z., and He, N. P. (2019). Variation in leaf morphological, stomatal, and anatomical traits and their relationships in temperate and subtropical forests. *Sci. Rep.* 9:5803. doi: 10.1038/s41598-019-42335-2
- Liu, C. C., Li, Y., Zhang, J., Baird, A. S., and He, N. P. (2020). Optimal community assembly related to leaf economic-hydraulic-anatomical traits. *Front. Plant Sci.* 11:341. doi: 10.3389/fpls.2020.00341
- Liu, C., Xiang, W. H., Zou, L. M., Lei, P. F., Zeng, Y. L., Ouyang, S., et al. (2019). Variation in the functional traits of fine roots is linked to phylogenetics in the common tree species of Chinese subtropical forests. *Plant Soil* 436, 347–364.
- Liu, G., Freschet, G. T., Pan, X., Cornelissen, J. H., Li, Y., and Dong, M. (2010). Coordinated variation in leaf and root traits across multiple spatial scales in Chinese

Conflict of interest

The authors declare that the research was conducted in the absence of any commercial or financial relationships that could be construed as a potential conflict of interest.

Publisher's note

All claims expressed in this article are solely those of the authors and do not necessarily represent those of their affiliated organizations, or those of the publisher, the editors and the reviewers. Any product that may be evaluated in this article, or claim that may be made by its manufacturer, is not guaranteed or endorsed by the publisher.

Supplementary material

The Supplementary Material for this article can be found online at: <https://www.frontiersin.org/articles/10.3389/ffgc.2023.1232333/full#supplementary-material>

- semi-arid and arid ecosystems. *New Phytol.* 188, 543–553. doi: 10.1111/j.1469-8137.2010.03388.x
- Liu, Z. L., Hikosaka, K., Li, F. R., and Jin, G. Z. (2020). Variations in leaf economics spectrum traits for an evergreen coniferous species: Tree size dominates over environment factors. *Funct. Ecol.* 34, 458–467.
- Maire, V., Wright, I. J., Prentice, I. C., Batjes, N. H., Bhaskar, R., van Bodegom, P. M., et al. (2015). Global effects of soil and climate on leaf photosynthetic traits and rates. *Global Ecol. Biogeogr.* 24, 706–717.
- Mao, Z. K., Corrales, A., Zhu, K., Yuan, Z. Q., Lin, F., Ye, J., et al. (2019). Tree mycorrhizal associations mediate soil fertility effects on forest community structure in a temperate forest. *New Phytol.* 223, 475–486. doi: 10.1111/nph.15742
- Mendes, M. M., Gazarini, L. C., and Rodrigues, M. L. (2001). Acclimation of *Myrtus communis* to contrasting Mediterranean light environments-effects on structure and chemical composition of foliage and plant water relations. *Environ. Exp. Bot.* 45, 165–178. doi: 10.1016/s0098-8472(01)00073-9
- Ni, X. F., Sun, L. J., Cai, Q., Ma, S. H., Feng, Y. H., Sun, Y. F., et al. (2022). Variation and determinants of leaf anatomical traits from boreal to tropical forests in eastern China. *Ecol. Indic.* 140:108992.
- Onoda, Y., Wright, I. J., Evans, J. R., Hikosaka, K., Kitajima, K., Niinemets, Ü, et al. (2017). Physiological and structural tradeoffs underlying the leaf economics spectrum. *New Phytol.* 214, 1447–1463.
- Ordoñez, J. C., Bodegom, P. M., Witte, J. P. M., Bartholomeus, R. P., Hal, J. R. V., and Aerts, R. (2010). Plant strategies in relation to resource supply in mesic to wet environments: Does theory mirror nature? *Am. Nat.* 175, 225–239. doi: 10.1086/649582
- Ordoñez, J. C., Bodegom, P. M., Witte, J. P. M., Wright, I. J., Reich, P. B., and Aerts, R. (2009). A global study of relationships between leaf traits, climate and soil measures of nutrient fertility. *Global Ecol. Biogeogr.* 18, 137–149. doi: 10.1002/ecy.4053
- Peng, C. Z., Chang, L. L., Yang, Q., Tong, Z., Wang, D., Tan, Y. H., et al. (2018). Comparative physiological and proteomic analyses of the chloroplasts in halophyte *Sesuvium portulacastrum* under differential salt conditions. *J. Plant Physiol.* 232, 141–150. doi: 10.1016/j.jplph.2018.10.028
- Phillips, R. P., Brzostek, E., and Midgley, M. G. (2013). The mycorrhizal-associated nutrient economy: A new framework for predicting carbon-nutrient couplings in temperate forests. *New Phytol.* 199, 41–51. doi: 10.1111/nph.12221
- Poorter, H., Niinemets, Ü, Poorter, L., Wright, I. J., and Villar, R. (2009). Causes and consequences of variation in leaf mass per area (LMA): A meta-analysis. *New Phytol.* 182, 565–588. doi: 10.1111/j.1469-8137.2009.02830.x
- Quesada, C. A., Lloyd, J., Schwarz, M., Patiño, S., Baker, T. R., Czimczik, C., et al. (2010). Variations in chemical and physical properties of Amazon forest soils in relation to their genesis. *Biogeosciences* 7, 1515–1541.
- R Core Team (2017). *R: A language and environment for statistical computing*. Vienna: R Foundation for Statistical Computing.
- Sack, L., and Scoffoni, C. (2013). Leaf venation: Structure, function, development, evolution, ecology and applications in the past, present and future. *New Phytol.* 198, 983–1000. doi: 10.1111/nph.12253
- Sack, L., Scoffoni, C., John, G. P., Poorter, H., Mason, C. M., Mendez-Alonzo, R., et al. (2013). How do leaf veins influence the worldwide leaf economic spectrum? Review and synthesis. *J. Exp. Bot.* 64, 4053–4080. doi: 10.1093/jxb/ert316
- Santos, K. R., Pereira, M. P., Ferreira, A. C. G., Rodrigues, L. C. D. A., Castro, E. M. D., Corrêa, F. F., et al. (2015). *Typha domingensis* Pers. growth responses to leaf anatomy and photosynthesis as influenced by phosphorus. *Aquat. Bot.* 122, 47–53.
- Shipley, B., and Vu, T. T. (2002). Dry matter content as a measure of dry matter concentration in plants and their parts. *New Phytol.* 153, 359–364.
- Siefert, A., and Ritchie, M. E. (2016). Intraspecific trait variation drives functional responses of old-field plant communities to nutrient enrichment. *Oecologia* 181, 245–255. doi: 10.1007/s00442-016-3563-z
- Simpson, A. H., Richardson, S. J., and Laughlin, D. C. (2016). Soil-climate interactions explain variation in foliar, stem, root and reproductive traits across temperate forests. *Glob. Ecol. Biogeogr.* 25, 964–978.
- Stark, J., Lehman, R., Crawford, L., Enquist, B. J., and Blonder, B. (2017). Does environmental heterogeneity drive functional trait variation? A test in montane and alpine meadows. *Oikos* 126, 1650–1659.
- Terashima, I., Hanba, Y. T., Tholen, D., and Niinemets, Ü (2011). Leaf functional anatomy in relation to photosynthesis. *Plant Physiol.* 155, 108–116.
- Thomas, S., and Winner, W. (2002). Photosynthetic differences between saplings and adult trees: An integration of field results by meta-analysis. *Tree Physiol.* 22, 117–127. doi: 10.1093/treephys/22.2-3.117
- Uehara, G., and Gilman, G. (1981). *The mineralogy, chemistry, and physics of tropical soils with variable charge clays*. Boulder, CO: Westview Press.
- Valladares, F., and Niinemets, Ü (2008). Shade tolerance, a key plant feature of complex nature and consequences. *Annu. Rev. Ecol. Evol.* 39, 237–257.
- Verboven, P., Herremans, E., Helfen, L., Ho, Q. T., Abera, M., Baumbach, T., et al. (2015). Synchrotron X-ray computed laminography of the three-dimensional anatomy of tomato leaves. *Plant J.* 81, 169–182. doi: 10.1111/tpj.12701
- Wang, Y. P. (1994). *Korean pine forest*. Harbin: Northeast Forestry University Press.
- Westoby, M. (1998). A leaf-height-seed (LHS) plant ecology strategy scheme. *Plant Soil* 199, 213–227.
- Wilson, P. J., Thompson, K., and Hodgson, J. G. (1999). Specific leaf area and leaf dry matter content as alternative predictors of plant strategies. *New Phytol.* 143, 155–162. doi: 10.1002/ecy.3986
- Wright, I. J., Ackerly, D. D., Frans, B., Harms, K. E., Guillermo, I. M., Miguel, M. R., et al. (2007). Relationships among ecologically important dimensions of plant trait variation in seven neotropical forests. *Ann. Bot.* 99, 1003–1015. doi: 10.1093/aob/mcl066
- Wright, I. J., Reich, P. B., and Westoby, M. (2003). Least-cost input mixtures of water and nitrogen for photosynthesis. *Am. Nat.* 161, 98–111. doi: 10.1086/344920
- Wright, I. J., Reich, P. B., Cornelissen, J. H., Falster, D. S., Garnier, E., Hikosaka, K., et al. (2005). Assessing the generality of global leaf trait relationships. *New Phytol.* 166, 485–496.
- Wright, I. J., Reich, P. B., Westoby, M., Ackerly, D. D., Baruch, Z., Bongers, F., et al. (2004). The worldwide leaf economics spectrum. *Nature* 428, 821–827.
- Yang, D. X., Song, L., and Jin, G. Z. (2019). The soil C:N:P stoichiometry is more sensitive than the leaf C:N:P stoichiometry to nitrogen addition: A four-year nitrogen addition experiment in a *Pinus koraiensis* plantation. *Plant Soil* 442, 183–198.
- Yang, Y. Z., Wang, H., Harrison, S. P., Prentice, I. C., Wright, I. J., Peng, C., et al. (2019). Quantifying leaf trait covariation and its controls across climates and biomes. *New Phytol.* 221, 155–168. doi: 10.1111/nph.15422
- Yin, Q., Wang, L., Lei, M. L., Dang, H., Quan, J. X., Tian, T. T., et al. (2017). The relationships between leaf economics and hydraulic traits of woody plants depend on water availability. *Sci. Total Environ.* 621, 245–252. doi: 10.1016/j.scitotenv.2017.11.171
- Zhang, X. S., Jin, G. Z., and Liu, Z. L. (2019). Contribution of leaf anatomical traits to leaf mass per area among canopy layers for five coexisting broadleaf species across shade tolerances at a regional scale. *Forest Ecol. Manag.* 452:117569.
- Zheng, Z., and Ma, P. F. (2018). Changes in above and belowground traits of a rhizome clonal plant explain its predominance under nitrogen addition. *Plant Soil* 432, 415–424.
- Zhou, X. L., Guo, Z., Zhang, P. F., and Du, G. Z. (2018). Shift in community functional composition following nitrogen fertilization in an alpine meadow through intraspecific trait variation and community composition change. *Plant Soil* 431, 289–302.



OPEN ACCESS

EDITED BY

Jeong-Wook Seo,
Chungbuk National University, Republic
of Korea

REVIEWED BY

David Ellison,
University of Bern, Switzerland
Thomas G. Huntington,
United States Geological Survey (USGS),
United States
Shutao Chen,
Nanjing University of Information Science
and Technology, China

*CORRESPONDENCE

Koichi Takahashi
✉ koichit@shinshu-u.ac.jp

RECEIVED 16 January 2023

ACCEPTED 05 July 2023

PUBLISHED 21 July 2023

CITATION

Takeda S, Majima R, Makita N and Takahashi K
(2023) Five-year measurement data along
a 1200 m elevational gradient reveals that
global warming increases soil respiration.
Front. For. Glob. Change 6:1145474.
doi: 10.3389/ffgc.2023.1145474

COPYRIGHT

© 2023 Takeda, Majima, Makita and Takahashi.
This is an open-access article distributed under
the terms of the [Creative Commons Attribution
License \(CC BY\)](https://creativecommons.org/licenses/by/4.0/). The use, distribution or
reproduction in other forums is permitted,
provided the original author(s) and the
copyright owner(s) are credited and that the
original publication in this journal is cited, in
accordance with accepted academic practice.
No use, distribution or reproduction is
permitted which does not comply with
these terms.

Five-year measurement data along a 1200 m elevational gradient reveals that global warming increases soil respiration

Soichiro Takeda¹, Ryota Majima², Naoki Makita^{2,3} and Koichi Takahashi^{2,3*}

¹Graduate School of Science and Technology, Shinshu University, Matsumoto, Japan, ²Faculty of Science, Shinshu University, Matsumoto, Japan, ³Institute of Mountain Science, Shinshu University, Matsumoto, Japan

Soil respiration is a major pathway for CO₂ emissions from ecosystems. Owing to its temperature dependency, the soil respiration rate is expected to increase due to global warming, particularly at high elevations. To clarify the effects of soil temperature and volumetric soil water content on soil respiration rates (R_S), we examined seasonal changes in R_S at five elevations of 1600–2800 m in subalpine coniferous forests in Japan for 5 years. The aboveground biomass of forest stands decreased from 282 to 29 Mg/ha as elevation increased. The monthly mean R_S was lower at higher elevations from July to October. While R_S was positively correlated with soil temperature at each elevation, the effect of soil water content on R_S varied among the five elevations. Seasonal changes in R_S could be reproduced from soil temperature and soil water content for each elevation in each year. R_S at any temperature was lower at higher elevations because R_S was also positively correlated with aboveground biomass. From 1600 to 2800 m, the annual R_S was estimated to decrease from 2.79 to 0.74 kg CO₂ year⁻¹ m⁻². The annual R_S along the elevational gradient was predicted to increase by 9–12% and 30–42% under low and high greenhouse gas emission scenarios (annual mean temperature 0.76°C and 3.3°C increases), respectively, during 2095–2100 compared to the current period 2015–2020. Increased soil respiration rate will accelerate global warming via the positive feedback. Overall, our findings suggest that soil respiration evaluation is important not only for calculating the carbon balance of forest stands due to global warming but also for predicting global warming owing to the feedback of CO₂ emission from soil to atmosphere.

KEYWORDS

CO₂ emission, elevation, Q₁₀, representative concentration pathways, soil respiration

1. Introduction

Soil respiration is a major pathway for CO₂ emissions from ecosystems (Bond-Lamberty and Thomson, 2010a). In forest ecosystems, soil contributes 60–80% of total ecosystem respiration (Law et al., 1999; Janssens et al., 2001). Soil respiration is the sum of the respiration of plant roots and microorganisms (Hanson et al., 2000). Notably, root

respiration accounts for an average of 46% of total soil respiration in forests (Hanson et al., 2000). The annual soil respiration rate, on a global scale, correlates positively with the mean annual temperature, annual precipitation, soil organic matter content, and productivity (Raich, 1998; Chen et al., 2014; Zhao et al., 2017). Owing to the suppression of plant's photosynthetic and organic matter decomposition rates in cold regions (Couteaux et al., 2002; Cornelissen et al., 2007; Takeda and Takahashi, 2020), global warming would increase the plants photosynthetic rate and consequently both root respiration rate and rate of plant detritus inputs to soil thereby increasing substrate availability or microbial decomposition/respiration. Notably, the soil respiration rate was shown to increase at a rate of 0.1 Pg C year⁻¹ during 1989–2008 on a global scale (Bond-Lamberty and Thomson, 2010b). Cold regions, such as those at high latitudes and elevations, are expected to shift from carbon sinks to carbon sources (Moore et al., 1999; McGuire et al., 2002) because the temperature sensitivities of organic matter decomposition and soil respiration rates are high in cold regions (Hendrickson, 2003; Janssens and Pilegaard, 2003; Xu et al., 2015; Klimek et al., 2016; Zhao et al., 2017). Therefore, soil respiration evaluation is important in considering the carbon balance in the ecosystems of cold regions (Rustad et al., 2001). However, no studies have predicted future soil respiration rates at high elevations in mountainous areas—a topic examined in this study.

Soil respiration is usually reported to be lower at higher elevations because of lower air temperature (or soil temperature) (Niklińska and Klimek, 2007; Badraghi et al., 2021), and lower aboveground and belowground biomass of plant communities (Shibistova et al., 2002; Epron et al., 2006; Jiang et al., 2013; Zhao et al., 2017; Zhang et al., 2021). In general, forest biomass decreases with increasing elevation (Takahashi, 2021). Therefore, the decreased soil respiration rate at high elevations is due to low temperatures and declined plant biomass.

Further, soil respiration changes seasonally and is usually highest in the summer (Kang et al., 2003; Soe and Buchmann, 2005; Caprez et al., 2012). As the high photosynthetic rate of plants in summer affects seasonal changes in the soil respiration rate via root respiration (Högberg et al., 2001; Curiel Yuste et al., 2004), temperature can be used to explain many variations in seasonal changes in soil respiration (Soe and Buchmann, 2005; Zhang et al., 2010; Chen et al., 2013). However, the effect of soil water content often varies with elevation. For example, while the soil respiration rate correlated positively with soil water content at low elevations, it correlated negatively with the same variable at high elevations (Huang et al., 2017).

Because central Japan has many high mountains, estimating carbon uptake at the landscape level requires investigating soil respiration along elevational gradients. Further, examining the change in the soil respiration rate along elevational gradients is necessary to clarify the impact of global warming on the carbon balance of forest stands. However, soil respiration measurements along elevational gradients have not yet been made in Japan. Therefore, the purpose of this study is to answer the following questions:

- (1) Does the soil respiration rate decrease with increasing elevation, and can the seasonal change in the soil

respiration rate at each elevation be explained by soil temperature and soil water content?

- (2) Can the mean annual temperature and stand biomass of trees explain the elevational variation in the annual soil respiration rate?
- (3) How much will global warming increase soil respiration rates along the elevational gradient by the year 2100?

2. Materials and methods

2.1. Study site

This study was conducted at five elevations (1600, 2000, 2300, 2500, and 2800 m) in a subalpine coniferous forest on the eastern slope of Mt. Norikura (36°06'N, 137°33'E, summit elevation 3026 m) in Chubu Sangaku National Park, Japan. Mt. Norikura is a volcano, but the last eruption was approximately 9000 years ago (Nakano and Uto, 1995). The soil substrate of the study site of 2800 m was scoria deposition with thin topsoil, while the study site of 1600 m was brown forest soil. An elevation of 1600 m is the lowest range limit of the subalpine zone. The treeline ecotone (*sensu* Körner, 2012) is located between 2500 and 2850 m (Takahashi and Yoshida, 2009; Takahashi et al., 2012). The mean annual temperatures of the study sites were estimated from the Nagawa Observatory (1068 m), which is the closest to the study sites, during the past 30 years (1981–2010) with the standard lapse rate (-0.6°C/100 m). The mean annual temperatures were 5.1°C at 1600 m, 2.7°C at 2000 m, 0.9°C at 2300 m, -0.3°C at 2500 m, and -2.1°C at 2800 m.

Four evergreen conifers (*Abies veitchii* Lindl., *A. mariesii* Mast., *Tsuga diversifolia* Mast., and *Picea jezoensis* var. *hondoensis* Rehder) were distributed between 1600 and 2500 m (Miyajima et al., 2007). However, the abundances of the four conifers were not uniform along the elevational gradient. *A. veitchii* dominates between 1600 m and 2200 m and *A. mariesii* dominates between 2000 m and 2500 m. The abundances of *T. diversifolia* and *P. jezoensis* var. *hondoensis* were lower than those of the two *Abies* species. Subordinate trees were all deciduous broad-leaved trees, such as *Betula ermanii* Cham. and *Sorbus commixta* Hedland. Dwarf pine *Pinus pumila* Regel dominated the treeline ecotone between 2500 and 2850 m (Miyajima et al., 2007), i.e., the study sites of 2500 and 2800 m were the lower and upper distribution limits of *P. pumila*, respectively. Dwarf bamboo *Sasa senanensis* Rehder is patchily distributed at 1600 m (Miyajima et al., 2007). The canopy height decreased with increasing elevation and was about 20 m at 1600 and 2000 m, about 10 m at 2300 m, 2 m at 2500 m, and 1 m at 2800 m (Miyajima and Takahashi, 2007; Takahashi and Yoshida, 2009).

2.2. Soil respiration measurements

Plots of 1.0, 0.6, 1.0, 0.05, and 0.004 ha were established at elevations of 1600, 2000, 2300, 2500, and 2800 m on the eastern slope of Mt. Norikura, respectively (Takeda and Takahashi, 2020). Soil respiration was measured at each plot in each elevation from July 2, 2015 to November 28, 2019. Measurements were performed

once a week on sunny or cloudy days at each elevation after snow melting (May–July) to the end of October each year. In addition, measurements were taken once a month during the snow cover period (December–April) at 1600 m from 2017 onward (i.e., two winter seasons). Soil respiration was measured on the snow surface. Measurements were conducted at three points in each elevation. No soil collar was installed at each elevation, but measurements were taken at the same three points at each elevation. Soil respiration rates were measured for 5 min at each point using a closed static chamber (a volume of 8.83 liter, base area of 0.05 m²), equipped with a portable CO₂ sensor (Vaisala, GMP343, Helsinki) and a data logger (Vaisala, MI70, Helsinki). The CO₂ concentration was recorded at 15-s intervals, and the soil respiration rate (R_s , g CO₂ h⁻¹ m⁻²) was calculated using Equation 1 (Bekku et al., 1995).

$$R_s = 60 \times 10^{-6} \alpha \rho V / S, \quad (1)$$

where α is the time rate of change in CO₂ concentration in the chamber (ppm/min), ρ is the density of CO₂ (mg/m³), V is the volume of the chamber (m³), and S is the basal area of the chamber (m²). Furthermore, the air temperature, volumetric soil water content, and soil temperature at a depth of 5 cm were measured along with the soil respiration measurement, except for the snow period at 1600 m. Air temperature was measured using a bar mercury thermometer. Soil water content and soil temperature were measured using a soil moisture sensor (EC-5, Meter Group, Inc., Pullman) and a digital thermometer (D619, Tateyama Kagaku Co., Ltd., Toyama), respectively. The soil temperature and soil water content at a depth of 5 cm were manually measured three times for each point of the soil respiration measurement, and the mean values of the three measurements were used for statistical analysis.

In addition to the manual measurements of soil temperature and soil water content at the time of the measurements of soil respiration rates, the soil water content and soil temperature at a depth of 5 cm were automatically recorded at hourly intervals during the 5 years from 2015 to 2019 near the soil respiration measurement site at each elevation, using five soil moisture sensors (EC-5, Meter Group, Inc., Pullman) equipped with a data logger (Em50, Meter Group, Inc., Pullman) and a thermometer (TR-52i, T & D Corporation, Matsumoto), respectively. The values of the five soil water contents of each elevation were averaged for each hour. Hourly automatic measurement data of the soil temperature and soil water content at a depth of 5 cm were used for the snow period at 1600 m because the soil temperature and soil water content could not be measured manually during the snow period.

2.3. Statistical analysis

A generalized linear model (GLM) was used to analyze the effects of the soil water content, soil temperature at a depth of 5 cm, and the observation year on the soil respiration rate for each elevation as follows:

$$\ln R_s = a_0 + a_1 T_s + a_2 W_S + a_3 W_S^2 + Y_i, \quad (2)$$

where \ln is the natural logarithm, R_s is the soil respiration rate (g CO₂ h⁻¹ m⁻²), T_s is the soil temperature (°C), W_S is the

volumetric soil water content (%), Y_i is the observation year i , a_0 is the constant, and a_1 – a_3 are regression coefficients. The squared value of W_S was included as an independent variable because the soil respiration rate may be at its peak at a certain W_S . The observation year was added as an explanatory variable because the soil respiration rate may be affected by unknown factors specific to the observation year (i.e., human error and interannual meteorological variation) other than the soil temperature and soil water content at the time of measurement. The observation year was used as a categorical variable. The effect of each observation year i between 2016 and 2019 on the soil respiration rate was expressed as the difference from that of 2015 (i.e., the constant value of Y_{2015} is zero).

Data of non-snow periods at the five elevations and those of the snow period at 1600 m after 2017 were also included in the dataset. The GLM analysis was performed for each elevation because the stand biomass of the trees differed along the elevational gradient. The number of measurements of soil respiration rates used for the statistical analysis were 376, 274, 239, 235, and 217 at 1600, 2000, 2300, 2500, and 2800 m, respectively. The selection of explanatory variables was performed by the Akaike Information Criteria (AIC) for Equation 2, and the model with the lowest AIC was selected as the best.

Sensitivity analysis was performed to examine the effects of soil temperature and soil water content on the soil respiration rate. The soil respiration rate was calculated using Equation 2 (the year was set as 2015) for the actual observed range of soil water content (about 10–60%) and for four soil temperature conditions (0–5.0, 5.1–10.0, 10.1–15.0, and 15.1–20.0°C).

Although soil temperature and soil water content at a depth of 5 cm were automatically measured at hourly intervals for 5 years at each elevation, the year-round measurements of soil temperature and soil water content at the five elevations could be performed for only 2 years (2018 and 2019) because of measurement challenges at certain elevations each year. Therefore, annual soil respiration rates at the five elevations were estimated using soil temperature and soil water content for the 2 years (2018 and 2019) only. Hourly soil respiration rates at each elevation were calculated by substituting hourly soil temperature and soil water content in 2018 and 2019 into Equation 2, and the annual soil respiration rate of each elevation in each year was obtained by summing the hourly soil respiration rates.

The temperature sensitivity (Q_{10}) of the soil respiration rate was calculated for each elevation in each year using Equations 3 and 4:

$$R_s = b_0 \times e^{b_1 T_s}, \quad (3)$$

$$Q_{10} = e^{10b_1}, \quad (4)$$

where R_s is the soil respiration rate (g CO₂ h⁻¹ m⁻²), T_s is the soil temperature, and b_0 and b_1 are the constant and exponent, respectively.

2.4. Future prediction of soil respiration rates

This study used the Agro-Meteorological Grid Square Data (AMGSD), the National Agriculture and Food Research

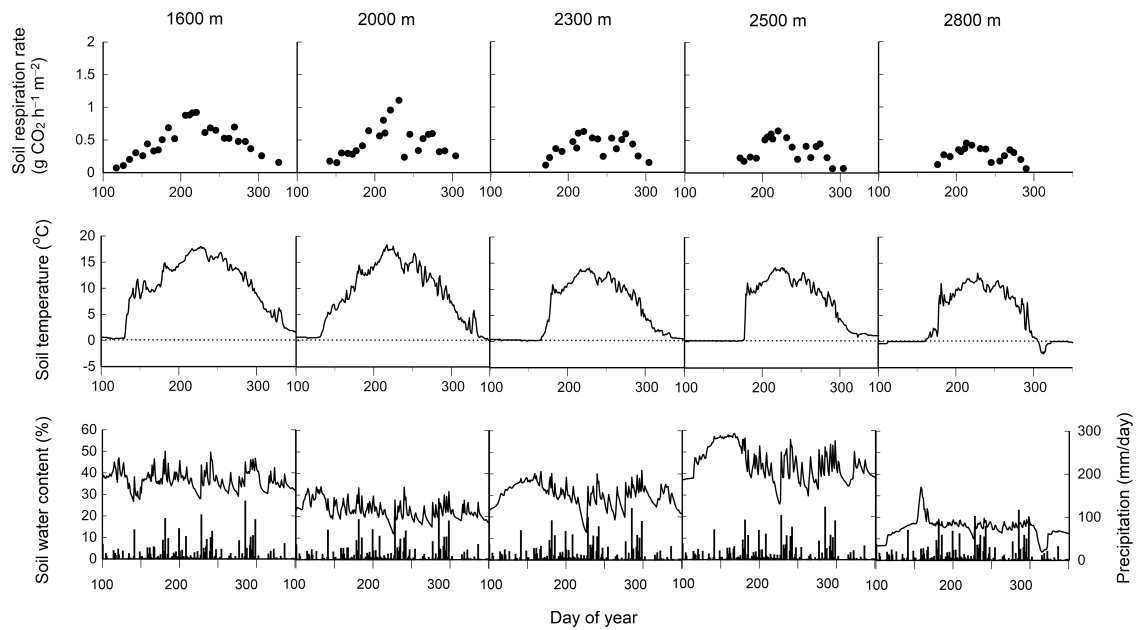


FIGURE 1
 Seasonal changes in soil respiration rates (**top row**), soil temperature (**middle row**), volumetric soil water content (**bottom row**, lines) at a depth of 5 cm, and daily precipitation (**bottom row**, bars) at five elevations in 2019 on Mt. Norikura, central Japan. The elevation is 1600, 2000, 2300, 2500, and 2800 m from the left to the right for each row of five panels. The day of the year (X axis) is depicted between 100 and 350 for each panel.

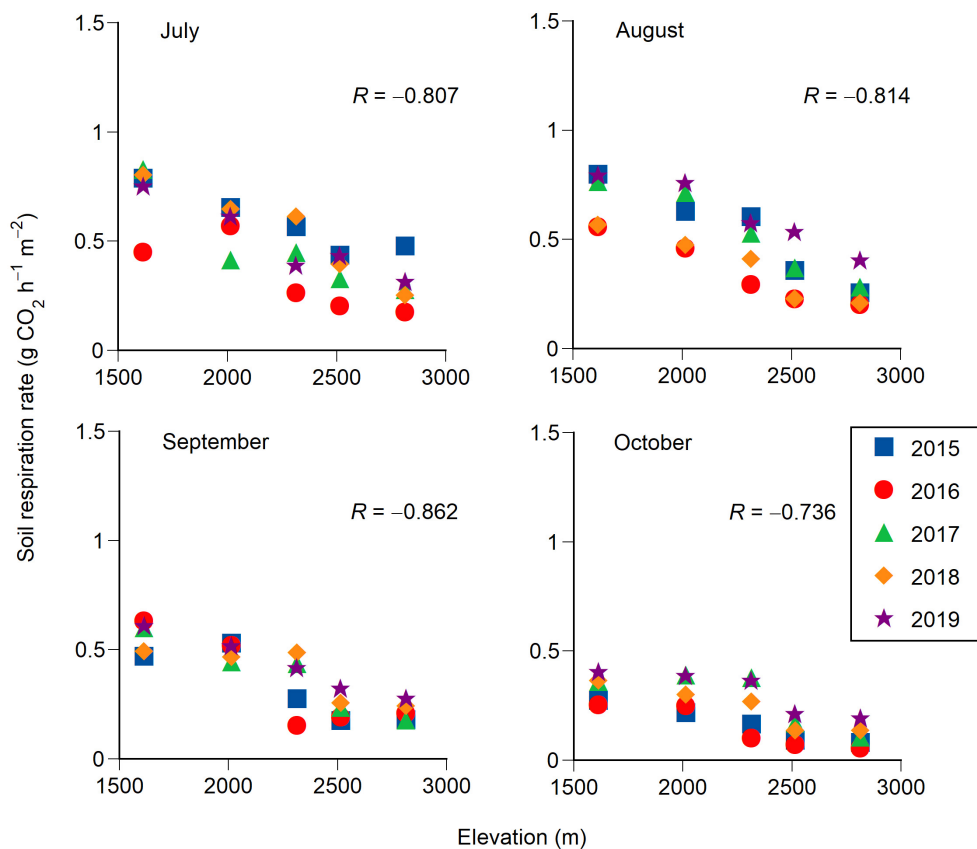


FIGURE 2
 Elevational changes in monthly mean soil respiration rates from July to October for 5 years (2015–2019). A Pearson correlation coefficient (R) is shown in each panel. Each correlation coefficient is significant ($P < 0.001$).

Organization (NARO) in Japan (Ohno et al., 2016; Kominami et al., 2019) to predict the change in the soil respiration rate at each elevation by climate change. Two climate change scenarios were used in this study: representative concentration pathways (RCP) 2.6 and 8.5 of the atmosphere–ocean general circulation model, the Model for Interdisciplinary Research on Climate (MIROC5). RCP 2.6 and RCP 8.5 are low- and high-future greenhouse gas emission scenarios, respectively. Under the RCP 2.6 scenario, the temperature will rise by 0.70°C during 2055–2060 and by 0.76°C during 2095–2100 compared to the current period 2015–2020. Under the RCP 8.5 scenario, the temperature will rise by 1.5°C during 2055–2060 and by 3.3°C during 2095–2100 compared to the current period 2015–2020. The third-order mesh data (1 × 1 km resolution) of AMGSD were obtained from NARO, and we used daily mean air temperatures of the two climate change scenarios.

Soil respiration rates at the five elevations were calculated for 2015–2020, 2055–2060, and 2095–2100. The soil respiration rate at each elevation was calculated using Equation 5, with only the soil temperature and stand biomass of trees as explanatory variables:

$$\ln R_s = c_0 + c_1 T_s + c_2 B, \quad (5)$$

where R_s is soil respiration rate (g CO₂ h⁻¹ m⁻²), T_s is soil temperature (°C), B is aboveground biomass (Mg/ha), c_0 is a constant, c_1 and c_2 are regression coefficients. The aboveground biomass values at 1600, 2000, 2300, 2500, and 2800 m were 282.4, 267.6, 195.3, 50.1, and 29.0 Mg/ha, respectively (Takeda and Takahashi, 2020). Soil water content was excluded from Equation 5 due to the difficulty of estimating it in the future, although it affects the soil respiration rate. Using the same dataset of the five elevations with which Equation 2 was analyzed, c_0 – c_2 of Equation 5 were estimated by GLM ($n = 1341$). The selection of explanatory variables was performed by AIC for Equation 5, and the model with the lowest AIC was selected as the best.

The daily mean soil temperature was estimated from the daily mean air temperature because soil temperature is omitted in AMGSD. Regression equations were made to estimate the soil temperature from the air temperature at the soil respiration measurement during the 5 years (2015–2019) for each elevation (Supplementary Table 1). Daily mean soil temperatures for 2015–2020, 2055–2060, and 2095–2100 were estimated by substituting the daily mean air temperature of AMGSD into the regression equation for each elevation. The soil temperature was almost 0°C in winter due to the insulation effect of snow cover from the results of year-round measurements of soil temperature. Therefore, this study assumed that soil temperature does not drop below 0°C even in winter. Furthermore, assuming that the aboveground biomass of each elevation is the same between the current period (2015–2020) and the two future periods (2055–2060, 2095–2100), this study calculated the soil respiration rates of the current and the two future periods from the aboveground biomass and the estimated daily mean soil temperature for each elevation. Because the soil respiration rate of Equation 5 is per hour, the daily soil respiration rate was calculated by multiplying this by 24. The annual soil respiration rate was estimated by summing the daily soil respiration rates for each year.

TABLE 1 Results of model selection for Equation 2, listed below, at five elevations.

| | Elevation (m) | | | | |
|-------|---------------|------------|------------|------------|------------|
| | 1600 | 2000 | 2300 | 2500 | 2800 |
| a_0 | −2.9093*** | −2.6558*** | −1.9745*** | −3.7264*** | −4.0979*** |
| a_1 | 0.1543*** | 0.1354*** | 0.1204*** | 0.1610*** | 0.1564*** |
| a_2 | 0.0069** | | | 0.0454 | 0.0940** |
| a_3 | | | −0.0002** | −0.0007* | −0.0019** |
| Y_i | | | | | |
| 2016 | −0.5566*** | | −0.8664*** | −0.5591*** | −0.8845*** |
| 2017 | −0.1343 | | 0.1309 | 0.0548 | −0.2511 |
| 2018 | −0.0285 | | −0.0801 | −0.2147 | −0.3197 |
| 2019 | −0.0716 | | −0.0815 | 0.1926 | 0.0885 |
| n | 342 | 274 | 239 | 235 | 217 |

* $P < 0.065$, ** $P < 0.01$, *** $P < 0.001$. $\ln R_s = a_0 + a_1 T_s + a_2 W_s + a_3 W_s^2 + Y_i$. The independent variables of Equation 2 are soil temperature (T_s), volumetric soil water content (W_s) and the square of W_s , and the observation year i (Y_i). The observation year was treated as a categorical variable, and is expressed as a difference from 2015 (i.e., the coefficient of 2015 is zero).

3. Results

Soil respiration rates at the five elevations in 2019 are shown as examples of elevational and seasonal changes in soil respiration rates (Figure 1). The soil water content tended to be lower throughout the year at 2800 m than at the other elevations because of the scoria substrate at 2800 m. The soil respiration rate was highest during early August (day of the year 210–220) at each elevation. This period also corresponded to the highest soil temperatures (Figure 1). The monthly mean soil respiration rate was lower at higher elevations for each month from July to October (Pearson correlation test, $P < 0.001$ for each month, Figure 2). The soil respiration rate in 2016 (especially July) tended to be lower than in the other years at each elevation, except for 2000 m (Figure 2 and Table 1).

Seasonal changes in soil respiration rates at the five elevations could be reproduced using Equation 2 for each year (Table 1 and Supplementary Figure 1). While the soil respiration rate correlated positively with the soil temperature for each elevation (Figure 3 and Table 1), it also correlated positively with the soil water content at 1600 m but was uncorrelated at 2000 m (Table 1). The soil respiration rate correlated negatively with the square of soil water content at 2300, 2500, and 2800 m (Table 1). The sensitivity analysis using Equation 2 revealed that the higher the soil temperature, the higher the soil respiration rate at any elevation (Figure 4). Under higher soil temperature conditions, the soil respiration rate at 1600 m tended to increase more with increasing soil water content, although the variation of the soil respiration was large at any soil water content (Figure 4). The effect of soil water content on the soil respiration rate was not recognized at 2000 m (Figure 4). The soil respiration rate at 2300 m tended to decrease with increasing soil water content at any soil temperature (Figure 4). The soil respiration rates increased with increasing soil water content until peaking at 30 and 25% at 2500 and 2800 m, respectively, and then soil respiration rates decreased with increasing soil water content (Figure 4).

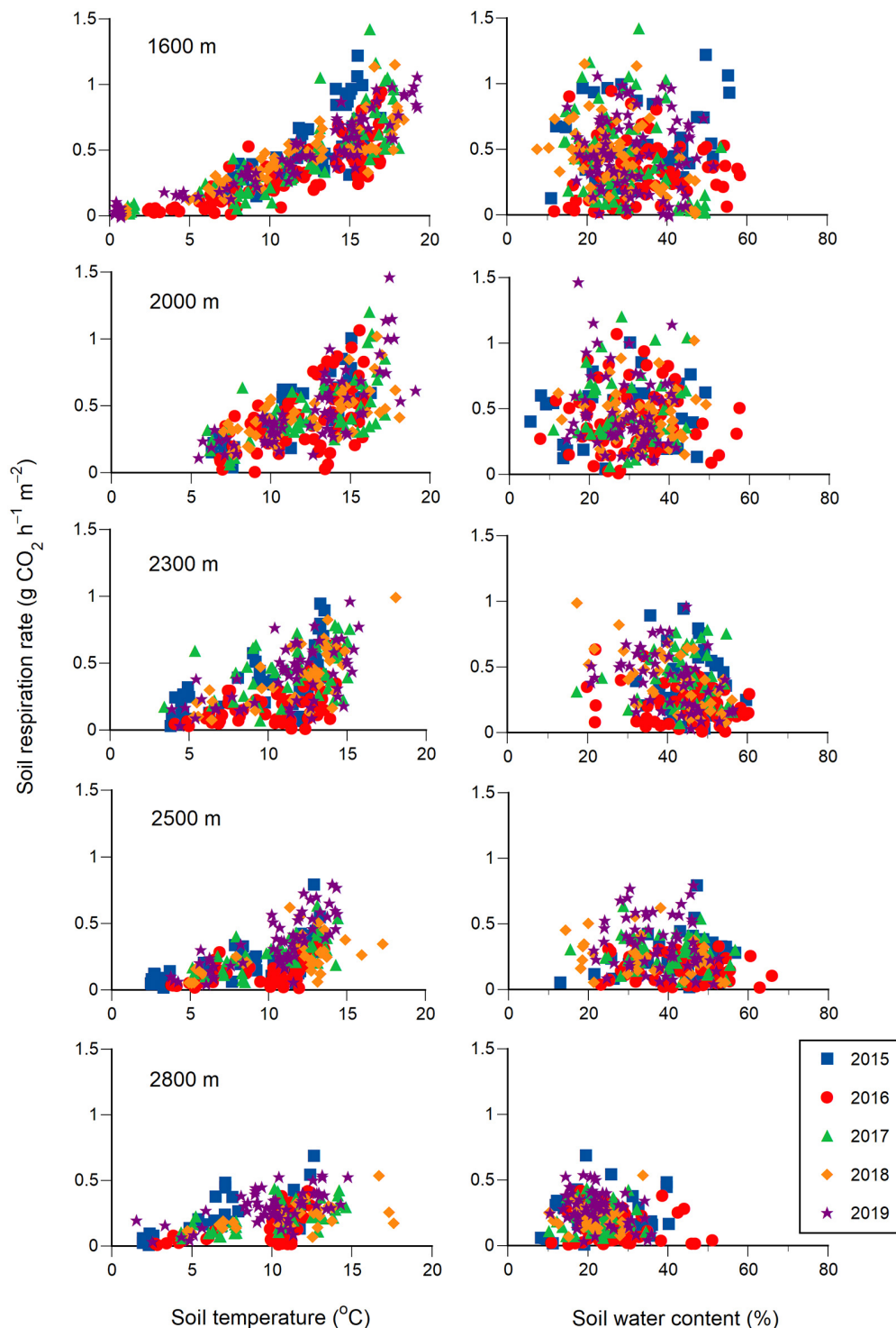


FIGURE 3

Relationships of soil respiration rates with soil temperature (left column) and soil water content (right column) at a depth of 5 cm at five elevations for 5 years (2015–2019). The elevations are 1600, 2000, 2300, 2500, and 2800 m from the top to the bottom for each column.

Annual soil respiration rates at the five elevations were calculated by substituting hourly measurement data for soil temperature and soil water content in 2018 and 2019 into Equation 2. Seasonal changes in the soil respiration rate at each elevation did not differ significantly between the 2 years (Supplementary Figure 2). Annual soil respiration rates were lower at higher

elevations, decreasing from 2.79 kg CO₂ year⁻¹ m⁻² at 1600 m to 0.74 kg CO₂ year⁻¹ m⁻² at 2800 m. The annual soil respiration rate correlated positively with the mean annual temperature (Pearson correlation test, $R = 0.92$, $P < 0.001$, $n = 10$) and the aboveground biomass ($R = 0.93$, $P < 0.001$, $n = 10$) (Figure 5).

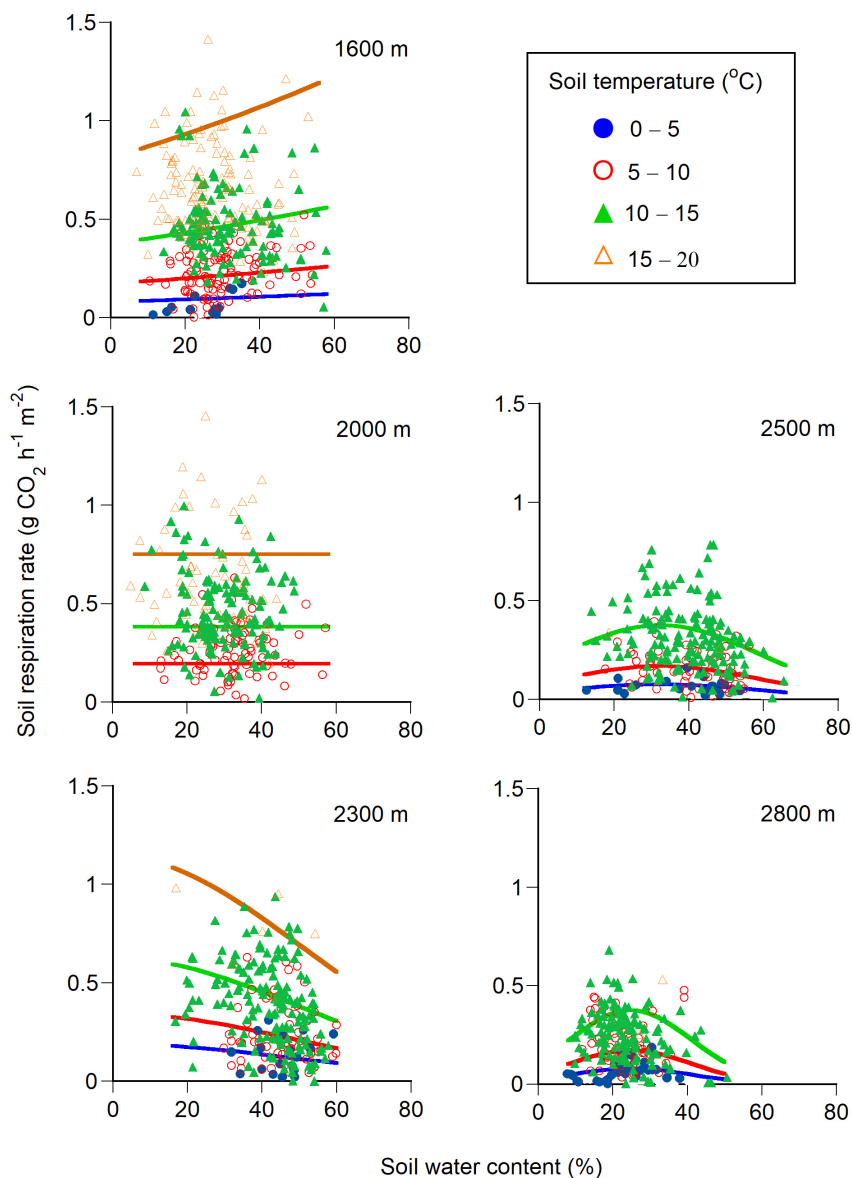


FIGURE 4

Changes in soil respiration rates with soil temperature and soil water content at a depth of 5 cm at five elevations (1600, 2000, 2300, 2500, and 2800 m). The soil respiration rate was calculated using Equation 2 in the main text for the three or four soil temperature conditions (0–5.0, 5.1–10.0, 10.1–15.0, and 15.1–20.0°C) at each elevation. See Table 1 for equation parameters (the measurement year was set as 2015). An average soil temperature was used to draw a regression line (Equation 2) for each soil temperature condition at each elevation (i.e., 3.6, 7.9, 12.5, 16.4°C at 1600 m, 8.0, 12.8, 16.2°C at 2000 m, 4.3, 7.7, 12.6°C at 2300 m, 3.5, 7.2, 11.7°C at 2500 m, and 3.5, 7.7, 11.6°C at 2800 m).

The temperature sensitivity (Q_{10}) of the soil respiration rate showed no elevational trend, with the mean value ranging from 2.7 to 5.1 across the five elevations (Supplementary Figure 3). The effects of soil temperature (T_s , °C) and aboveground biomass (B , Mg/ha) on the elevational change in the soil respiration rate (R_s , g CO₂ h⁻¹ m⁻²) was analyzed using Equation 5. The constant (c_0) and coefficients (c_1 , c_2) of Equation 5 were estimated by GLM as below ($P < 0.001$ for each of c_0 – c_2 , $n = 1341$).

$$\ln R_s = -3.437 + 0.168 T_s + 0.00127 B \quad (6)$$

The soil respiration rate was higher at lower elevations with greater biomass even at the same soil temperature because of the two positive coefficients of T_s and B (Figure 6).

Substituting the soil temperature estimated from the daily mean temperature of the climate change scenarios (RCP 2.6, RCP 8.5) into the soil temperature in Equation 6, the percent change in the annual soil respiration rate was estimated for the two future periods (2055–2060, 2095–2100) compared to the current period (2015–2020). The annual soil respiration rate along the elevational gradient was expected to increase by 9–12% and by 30–42% under the RCP 2.6 and RCP 8.5, respectively, during the future period (2095–2100) compared to the current period (2015–2020) (Figure 7). Under the two RCP scenarios, the percentage increase in the soil respiration rate was highest at 2000 m and slightly decreased with increasing elevation (Figure 7).

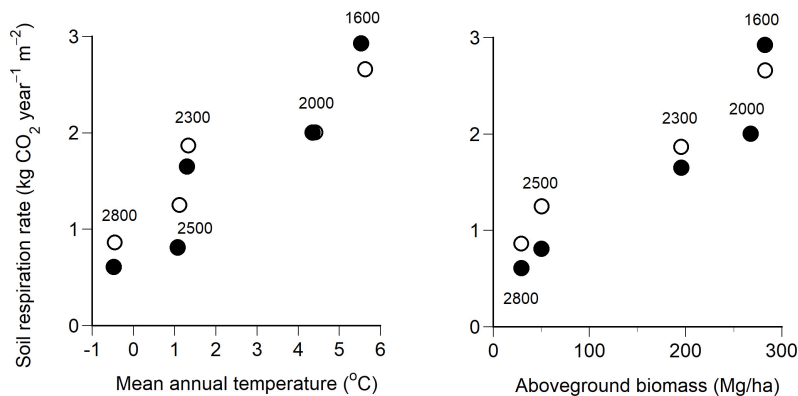


FIGURE 5

Relationships of annual soil respiration rates with mean annual temperature (left) and aboveground biomass (right) at the five elevations (1600, 2000, 2300, 2500, and 2800 m) for the 2 years, 2018 (●) and 2019 (○). The annual soil respiration rate was estimated by substituting hourly soil temperature and soil water content into Equation 2 in the main text. See Table 1 for the equation parameters. The unit of Mg/ha is equivalent to $\times 0.1 \text{ kg/m}^2$.

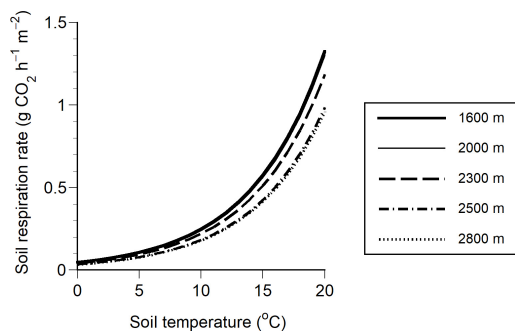


FIGURE 6

Relationship between soil respiration rate and soil temperature at a depth of 5 cm at five elevations (1600, 2000, 2300, 2500, and 2800 m). The regression lines of elevations of 1600 and 2000 m markedly overlapped, such that they are indistinguishable. The soil respiration rate at each elevation was calculated by substituting aboveground biomass into Equation 6. The aboveground biomass was 282.4, 267.6, 195.3, 50.1, and 29.0 Mg/ha at 1600, 2000, 2300, 2500, and 2800 m, respectively.

4. Discussion

4.1. Elevational and seasonal changes in soil respiration rates

This study showed that the soil respiration rate was lower at higher elevations with lower soil temperatures and stand biomass. Many studies on seasonal changes in the soil respiration rate have found positive correlations among the soil respiration rate, soil temperature, and biomass (Rustad et al., 2001; Wieser, 2004; Epron et al., 2006; Zhao et al., 2017; Zhang et al., 2021). Therefore, the soil respiration rate is often reported to be lower in higher elevations (Niklińska and Klimek, 2007; Badraghi et al., 2021). In addition, the photosynthetic rate of plants is temperature-dependent (DeLucia and Smith, 1987; Mellander et al., 2004; Zaka et al., 2016), and the root respiration rate is thought to increase when the photosynthetic rate is high due to high air and soil

temperatures (Sampson et al., 2007; Metcalfe et al., 2011). The photosynthetic rates of *Abies veitchii*, *A. mariesii*, and *Pinus pumila*, which are dominant in the sites of the present study, are decreased by low air and soil temperatures (Shimada and Takahashi, 2022; Suzuki and Takahashi, 2022). Therefore, lower soil respiration rates at higher elevations are undoubtedly caused by lower biomass and cooler temperatures.

Q_{10} has been shown to correlate negatively with temperature (Janssens and Pilegaard, 2003; Song et al., 2014; Xu et al., 2015) and is often reported to be greater at higher elevations and latitudes (Zhao et al., 2017; Badraghi et al., 2021). In addition, the Q_{10} value is usually approximately 2 at lowlands (Hashimoto, 2005; Meyer et al., 2018). Although no elevational trend in Q_{10} was found among the five elevations (1600–2800 m) studied, the average value of Q_{10} at each elevation ranged from 2.7 to 5.1. Therefore, Q_{10} was clearly higher at the five elevations in the subalpine zone than in the lowlands.

The effect of soil water content on the soil respiration rate differed among the five elevations. The soil respiration rate slightly increased with increasing soil water content at 1600 m when soil temperature was high but decreased at higher elevations when the soil water content exceeded the optimal soil water content, corroborating Huang et al.'s (2017) findings. This elevational change in the effects of soil water content on soil respiration rate is thought to correspond to the elevational change in meteorological conditions. In general, air temperature decreases while precipitation increases with increasing elevation in central Japan (Yamamura and Nakano, 1985; Yamada et al., 1995). Dendrochronological studies have often reported that climatic factors limiting tree growth change from less precipitation in summer at low elevations to low summer temperatures at high elevations (Adams and Kolb, 2005; Wang et al., 2005; Massaccesi et al., 2008; Peng et al., 2008). This is also true for the elevational gradient in the present study (Takahashi, 2003; Takahashi et al., 2003, 2005, 2011). Therefore, the positive correlation between the soil respiration rate and the soil water content in high soil temperature conditions at 1600 m indicates that the decrease in tree growth due to less precipitation (i.e., drought stress) reduces the root respiration rate and consequently the soil respiration rate.

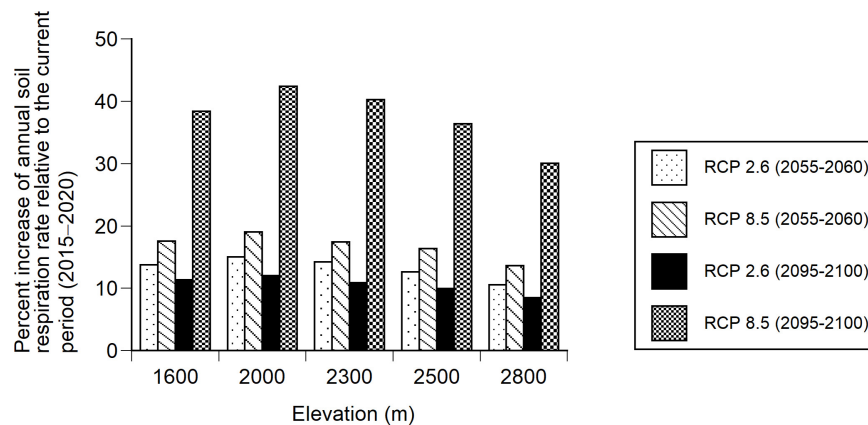


FIGURE 7

Percent increases in annual soil respiration rates for the two future periods, 2055–2060 and 2095–2100, relative to the current period (2015–2020) at the five elevations (1600, 2000, 2300, 2500, and 2800 m). Annual soil respiration rates were estimated using Equation 6 and two climate change scenarios (RCP 2.6 and RCP 8.5).

During the 5-year measurement, the soil respiration rate in 2016 (especially July) was lower than in the other measurement years even at the same elevation, except for 2000 m. Although the mean monthly temperature in July 2016 was almost the same as in the other measurement years, monthly precipitation was 48–68% lower than in the other measurement years (Supplementary Figure 4), resulting in longer drought stress compared to the other measurement years. The soil respiration rate decreases under drought stress (Davidson et al., 1998; Epron et al., 2004; Lellei-Kovács et al., 2011). Therefore, the soil respiration rate was considered to be low in July 2016.

4.2. Changes in soil respiration due to global warming

In this study, the annual soil respiration rate decreased from 2.79 to 0.74 kg CO₂ year⁻¹ m⁻² as elevation increased because the soil temperature and above ground biomass were lower at higher elevations. These annual respiration rates were within the range of reported values for the boreal ecosystem (Bond-Lamberty and Thomson, 2010a). The soil respiration rate at the five elevations (1600–2800 m) was expected to increase 9–12% (RCP 2.6) and 30–42% (RCP 8.5) by the year 2100 compared to the current period (2015–2020). The different results between the RCP 2.6 and RCP 8.5 scenarios were absolutely due to the difference in the temperature increase because concomitant changes in the soil water content and biomass were not taken into account. Compared to the current period (2015–2020), the global temperature will increase by 0.76°C and 3.3°C in 2095–2100 under the RCP 2.6 and RCP 8.5 scenarios, respectively. Therefore, global warming will increase the soil respiration rate, but the rate of the increase depends on how much temperature increases.

Unfortunately, there were no studies that estimated future soil respiration rates, so we cannot compare our estimates with previous studies. However, this study has some limitations in terms of predicting soil respiration rates by 2100. First, the soil respiration rate was predicted using soil temperature and

biomass without considering soil water content. The increase in temperature possibly reduces the soil water content by increasing the evapotranspiration rate. Although a rise in soil temperature increases the soil respiration rate, this effect can be offset by a decrease in soil water content (Schindlbacher et al., 2012). Second, the current relationship between soil temperature and soil respiration rate was assumed to remain the same in the future, but this may change. As soil temperature increases, the organic matter decomposition rate increases (Trofymow et al., 2002; Cornelissen et al., 2007; Takeda and Takahashi, 2020), resulting in an increased supply rate of soil nutrients, which may increase plant growth rate, root respiration rate, and stand biomass. Third, it is possible that stand biomass will increase due to global warming, although this study estimated the future soil respiration rate under the assumption that stand biomass does not change from the current biomass. Increase of stand biomass will increase the soil respiration rate. Forth, as vegetation shifts to faster-growing tree species due to global warming, the nutrient concentration of litter supplied to the forest floor increases, and the heterotrophic respiration rate may increase (Metcalfé et al., 2011). Given the preceding four points, investigating the future effects of global warming on soil respiration rates is necessary using a dynamic vegetation model (cf. Sato et al., 2007).

5. Conclusion

This study showed that (1) the soil respiration rate was lower at higher elevations for each month from July to October, and the seasonal change in the soil respiration rate at each elevation could be reproduced by the soil temperature and soil water content, (2) the annual soil respiration rate correlated positively with the mean annual temperature and the aboveground biomass, and (3) the annual soil respiration rate will increase 9–12% and 30–42% under the RCP 2.6 and RCP 8.5 scenarios, respectively, during the future period (2095–2100) compared to the current period (2015–2020). As a result, global warming is expected to increase soil respiration along the elevational gradient in the future.

In general, in high elevations with cool thermal conditions, tree growth is limited more by low summer temperatures (Buckley et al., 1997; Hopton and Pederson, 2005; Wang et al., 2005; Savva et al., 2006; Levanič et al., 2009; Takahashi and Okuhara, 2013). The higher the elevation, the lower the net primary production (NPP) along the elevational gradient of the present study (Takeda and Takahashi, 2020). Global warming increases NPP because of the positive correlation between mean annual temperature and NPP from a meta-analysis (Piao et al., 2006). However, both NPP and soil respiration rates influence the carbon balance at the ecosystem level (Randerson et al., 2002; Bond-Lamberty et al., 2004; Reichstein et al., 2005). Therefore, our findings suggest that soil respiration evaluation is important not only for calculating the carbon balance of forest stands due to global warming but also for predicting global warming owing to the feedback of CO₂ emission from soil to the atmosphere in mountain ecosystems.

Data availability statement

The raw data supporting the conclusions of this article will be made available by the authors, without undue reservation.

Author contributions

KT conceived the study and led the writing of the manuscript. KT, RM, and ST collected the data and analyzed the data. NM and KT revised the manuscript. All authors contributed to the article and approved the submitted version.

References

- Adams, H. D., and Kolb, T. E. (2005). Tree growth response to drought and temperature in a mountain landscape in northern Arizona, USA. *J. Biogeogr.* 32, 1629–1640. doi: 10.1111/j.1365-2699.2005.01292.x
- Badraghi, A., Ventura, M., Polo, A., Borruso, L., Giammarchi, F., and Montagnani, L. (2021). Soil respiration variation along an altitudinal gradient in the Italian Alps: Disentangling forest structure and temperature effects. *PLoS One* 16, e0247893. doi: 10.1371/journal.pone.0247893
- Bekku, Y., Koizumi, H., Nakadai, T., and Iwaki, H. (1995). Measurement of soil respiration using closed chamber method: An IRGA technique. *Ecol. Res.* 10, 369–373. doi: 10.1007/BF02347863
- Bond-Lamberty, B., and Thomson, A. (2010a). A global database of soil respiration data. *Biogeoscience* 7, 1915–1926. doi: 10.5194/bg-7-1915-2010
- Bond-Lamberty, B., and Thomson, A. (2010b). Temperature-associated increases in the global soil respiration record. *Nature* 464, 579–583. doi: 10.1038/nature08930
- Bond-Lamberty, B., Wang, C., and Gower, S. T. (2004). Net primary production and net ecosystem production of a boreal black spruce wildfire chronosequence. *Glob. Change Biol.* 10, 473–487. doi: 10.1111/j.1529-8817.2003.0742.x
- Buckley, B. M., Cook, E. R., Peterson, M. J., and Barbeti, M. (1997). A changing temperature response with elevation for *Lagarostrobos franklinii* in Tasmania, Australia. *Clim. Change* 36, 477–498. doi: 10.1023/A:1005322332230
- Caprez, R., Niklaus, P. A., and Körner, C. (2012). Forest soil respiration reflects plant productivity across a temperature gradient in the Alps. *Oecologia* 170, 1143–1154. doi: 10.1007/s00442-012-2371-3
- Chen, S., Zou, J., Hu, Z., Chen, H., and Lu, Y. (2014). Global annual soil respiration in relation to climate, soil properties and vegetation characteristics: Summary of available data. *Agr. For. Meteorol.* 19, 335–346. doi: 10.1016/j.agrformet.2014.08.020
- Chen, W., Jia, X., Zha, T., Wu, B., Zhang, Y., Li, C., et al. (2013). Soil respiration in a mixed urban forest in China in relation to soil temperature and water content. *Eur. J. Soil Biol.* 54, 63–68. doi: 10.1016/j.ejsobi.2012.10.001
- Cornelissen, J. H. C., van Bodegom, P. M., Aerts, R., Callaghan, T. V., van Logtestijn, R. S. P., Alatalo, J., et al. (2007). Global negative vegetation feedback to climate warming responses of leaf litter decomposition rates in cold biomes. *Ecol. Lett.* 10, 619–627. doi: 10.1111/j.1461-0248.2007.01051.x
- Couteaux, M. M., Sarmiento, L., Bottner, P., Acevedo, D., and Thiery, J. M. (2002). Decomposition of standard plant material along an altitudinal transect (65–3968 m) in the tropical Andes. *Soil Biol. Biochem.* 34, 69–78. doi: 10.1016/S0038-0717(01)00155-9
- Curiel Yuste, J., Janssens, I. A., Carrara, A., and Ceulemans, R. (2004). Annual Q₁₀ of soil respiration reflects plant phenological patterns as well as temperature sensitivity. *Glob. Change Biol.* 10, 161–169. doi: 10.1111/j.1529-8817.2003.00727.x
- Davidson, E. A., Belk, E., and Boone, R. D. (1998). Soil water content and temperature as independent or confounded factors controlling soil respiration in a temperature mixed hardwood forest. *Glob. Change Biol.* 4, 217–227. doi: 10.1046/j.1365-2486.1998.00128.x
- DeLucia, E. H., and Smith, W. K. (1987). Air and soil temperature limitations on photosynthesis in Engelmann spruce during summer. *Can. J. For. Res.* 17, 527–533. doi: 10.1139/x87-088
- Epron, D., Bosc, A., Bonal, D., and Freycon, V. (2006). Spatial variation of soil respiration across a topographic gradient in a tropical rain forest in French Guiana. *J. Trop. Ecol.* 22, 565–574. doi: 10.1017/S0266467406003415
- Epron, D., Nouvellon, Y., Roupsard, O., Mouvondy, W., Mabilia, A., Saint-André, L., et al. (2004). Spatial and temporal variations of soil respiration in a *Eucalyptus* plantation in Congo. *For. Ecol. Manage.* 202, 149–160. doi: 10.1016/j.foreco.2004.07.019

Funding

This study was partially supported by the Japan Society for the Promotion of Science (26292081 and 21K06331) and the joint research program of the Institute for Cosmic Ray Research, University of Tokyo.

Conflict of interest

The authors declare that the research was conducted in the absence of any commercial or financial relationships that could be construed as a potential conflict of interest.

Publisher's note

All claims expressed in this article are solely those of the authors and do not necessarily represent those of their affiliated organizations, or those of the publisher, the editors and the reviewers. Any product that may be evaluated in this article, or claim that may be made by its manufacturer, is not guaranteed or endorsed by the publisher.

Supplementary material

The Supplementary Material for this article can be found online at: <https://www.frontiersin.org/articles/10.3389/ffgc.2023.1145474/full#supplementary-material>

- Hanson, P. J., Edwards, N. T., Garten, C. T., and Andrews, J. A. (2000). Separating root and soil microbial contributions to soil respiration: A review of methods and observations. *Biogeochemistry* 48, 115–146. doi: 10.1023/A:1006244819642
- Hashimoto, S. (2005). Q_{10} values of soil respiration in Japanese forests. *J. For. Res.* 10, 409–413. doi: 10.1007/s10310-005-0164-9
- Hendrickson, O. (2003). Influences of global change on carbon sequestration by agricultural and forest soils. *Environ. Rev.* 11, 161–192. doi: 10.1139/a04-001
- Hopton, H. M., and Pederson, N. (2005). "Climate sensitivity of Atlantic white cedar at its northern range limit," in *Proceedings of the Arlington Echo Symposium, USDA Forest Service. Atlantic white cedar: ecology, restoration and management*, eds M. K. Burke and P. Sheridan (Sheville, NC: USDA Forest Service Southern Research Station), 22–30.
- Huang, Y. H., Hung, C. Y., Lin, I. R., Kume, T., Menyailo, O. V., and Cheng, C. H. (2017). Soil respiration patterns and rates at three Taiwanese forest plantations: Dependence on elevation, temperature, precipitation, and litterfall. *Bot. Stud.* 58:49. doi: 10.1186/s40529-017-0205-7
- Högberg, P., Nordgren, A., Buchmann, N., Taylor, A. F. S., Ekblad, A., Högger, M. N., et al. (2001). Large-scale forest girdling shows that current photosynthesis drives soil respiration. *Nature* 411, 789–792. doi: 10.1038/35081058
- Janssens, I. A., and Pilegaard, K. (2003). Large seasonal changes in Q_{10} of soil respiration in a beech forest. *Glob. Change Biol.* 9, 911–918. doi: 10.1046/j.1365-2486.2003.00636.x
- Janssens, I. A., Lankreijer, H., Matteucci, G., Kowalski, A. S., Buchmann, N., Epron, D., et al. (2001). Productivity overshadows temperature in determining soil and ecosystem respiration across European forests. *Glob. Change Biol.* 7, 269–278. doi: 10.1046/j.1365-2486.2001.00412.x
- Jiang, J., Zong, N., Song, M., Shi, P., Ma, W., Fu, G., et al. (2013). Responses of ecosystem respiration and its components to fertilization in an alpine meadow on the Tibetan Plateau. *Eur. J. Soil Biol.* 56, 101–106. doi: 10.1016/j.ejsobi.2013.03.001
- Kang, S., Doh, S., Lee, D., Lee, D., Jin, V. L., and Kimball, J. S. (2003). Topographic and climatic controls on soil respiration in six temperate mixed-hardwood forest slopes, Korea. *Glob. Change Biol.* 9, 1427–1437. doi: 10.1046/j.1365-2486.2003.00668.x
- Klimek, B., Jelonekiewicz, Ł., and Niklińska, M. (2016). Drivers of temperature sensitivity of decomposition of soil organic matter along a mountain altitudinal gradient in the Western Carpathians. *Ecol. Res.* 31, 609–615. doi: 10.1007/s11284-016-1369-4
- Kominami, Y., Sasaki, K., and Ohno, H. (2019). *User's manual for the agro-meteorological grid square data, Ver.4*. Tsukuba: NARO, 67pp (in Japanese).
- Körner, C. (2012). *Alpine treelines – functional ecology of the global high elevation tree limits*. Berlin: Springer. doi: 10.1007/978-3-0348-0396-0
- Law, B. E., Ryan, M. G., and Anthoni, P. M. (1999). Seasonal and annual respiration of a ponderosa pine ecosystem. *Glob. Change Biol.* 5, 169–182. doi: 10.1046/j.1365-2486.1999.00214.x
- Lellei-Kovács, E., Kovács-Láng, E., Botta-Dukát, Z., Kalapos, T., Emmett, B., and Beier, C. (2011). Thresholds and interactive effects of soil moisture on the temperature response of soil respiration. *Eur. J. Soil Biol.* 47, 247–255. doi: 10.1016/j.ejsobi.2011.05.004
- Levanič, T., Gričar, J., Gagen, M., Jalkanen, R., Loader, N. J., McCarroll, D., et al. (2009). The climate sensitivity of Norway spruce [*Picea abies* (L.) Karst.] in the southeastern European Alps. *Trees* 23, 169–180. doi: 10.1007/s00468-008-0265-0
- Massaccesi, G., Roig, F. A., Pastur, G. J. M., and Barrera, M. D. (2008). Growth patterns of *Nothofagus pumilio* trees along altitudinal gradients in Tierra del Fuego, Argentina. *Trees* 22, 245–255. doi: 10.1007/s00468-007-0181-8
- McGuire, A. D., Wirth, C., Apps, M., Beringer, J., Klein, J., Epstein, H., et al. (2002). Environmental variation, vegetation distribution, carbon dynamics and water/energy exchange at high latitudes. *J. Veg. Sci.* 13, 301–314. doi: 10.1111/j.1654-1103.2002.tb02055.x
- Mellander, P. E., Bishop, K., and Lundmark, T. (2004). The influence of soil temperature on transpiration: A plot scale manipulation in a young Scots pine stand. *For. Ecol. Manage.* 195, 15–28. doi: 10.1016/j.foreco.2004.02.051
- Metcalfe, D. B., Fisher, R. A., and Wardle, D. A. (2011). Plant communities as drivers of soil respiration: Pathways, mechanisms, and significance for global change. *Biogeosciences* 8, 2047–2061. doi: 10.5194/bg-8-2047-2011
- Meyer, N., Welp, G., and Amelung, W. (2018). The temperature sensitivity (Q_{10}) of soil respiration: Controlling factors and spatial prediction at regional scale based on environmental soil classes. *Glob. Biogeochem. Cycles* 32, 306–323. doi: 10.1002/2017GB005644
- Miyajima, Y., and Takahashi, K. (2007). Changes with altitude of the stand structure of temperate forests on Mount Norikura, central Japan. *J. For. Res.* 12, 187–192. doi: 10.1007/s10310-007-0002-3
- Miyajima, Y., Sato, T., and Takahashi, K. (2007). Altitudinal changes in vegetation of tree, herb and fern species on Mount Norikura, central Japan. *Veg. Sci.* 24, 29–40.
- Moore, D. J., Nowak, R. S., and Tausch, R. J. (1999). Gas exchange and carbon isotope discrimination of *Juniperus osteosperma* and *Juniperus occidentalis* across environmental gradients in the Great Basin of western North America. *Tree Physiol.* 19, 421–433. doi: 10.1093/treephys/19.7.421
- Nakano, S., and Uto, K. (1995). Volcanic history of Norikura Volcano based on K-Ar dating. *Program. Abst. Volcanol. Soc. Japan* 2, 91.
- Niklińska, M., and Klimek, B. (2007). Effect of temperature on the respiration rate of forest soil organic layer along an elevation gradient in the Polish Carpathians. *Biol. Fertil. Soils* 43, 511–518. doi: 10.1007/s00374-006-0129-y
- Ohno, H., Sasaki, K., Ohara, G., and Nakazono, K. O. U. (2016). Development of grid square air temperature and precipitation data compiled from observed, forecasted, and climatic normal data. *Clim. Biosphere* 16, 71–79. doi: 10.2480/cib.j-16-028
- Peng, J., Gou, X., Chen, F., Li, J., Liu, P., and Zhang, Y. (2008). Altitudinal variability of climate-tree growth relationships along a consistent slope of Anyemaqen Mountains, northeastern Tibetan Plateau. *Dendrochronologia* 26, 87–96. doi: 10.1016/j.dendro.2007.10.003
- Piao, S., Fang, J., and He, J. (2006). Variations in vegetation net primary production in the Qinghai-Xizang Plateau, China, from 1982 to 1999. *Clim. Change* 74, 253–267. doi: 10.1007/s10584-005-6339-8
- Raich, J. W. (1998). Aboveground productivity and soil respiration in three Hawaiian rain forests. *For. Ecol. Manage.* 107, 309–318. doi: 10.1016/S0378-1127(97)00347-2
- Randerson, J. T., Chapin, F. S. III, Harden, J. W., Neff, J. C., and Harmon, M. E. (2002). Net ecosystem production: A comprehensive measure of net carbon accumulation by ecosystems. *Ecol. Appl.* 12, 937–947. doi: 10.1890/1051-0761(2002)012[0937:NEPACM]2.0.CO;2
- Reichstein, M., Falge, E., Baldocchi, D., Papale, D., Aubinet, M., Berbigier, P., et al. (2005). On the separation of net ecosystem exchange into assimilation and ecosystem respiration: Review and improved algorithm. *Glob. Change Biol.* 11, 1424–1439. doi: 10.1111/j.1365-2486.2005.001002.x
- Rustad, L. E., Campbell, J. L., Marion, G. M., Norby, R. J., Mitchell, M. J., Hartley, A. E., et al. (2001). A meta-analysis of the response of soil respiration, net nitrogen mineralization, and aboveground plant growth to experimental ecosystem warming. *Oecologia* 126, 543–562. doi: 10.1007/s004420000544
- Sampson, D. A., Janssens, I. A., Curiel Yuste, J., and Ceulemans, R. (2007). Basal rates of soil respiration are correlated with photosynthesis in a mixed temperate forest. *Glob. Change Biol.* 13, 2008–2017. doi: 10.1111/j.1365-2486.2007.01414.x
- Sato, H., Itoh, A., and Kohyama, T. (2007). SEIB-DGVM: A new dynamic global vegetation model using a spatially explicit individual-based approach. *Ecol. Model.* 200, 279–307. doi: 10.1016/j.ecolmodel.2006.09.006
- Savva, Y., Oleksyn, J., Reich, P. B., Tjoelker, M. G., Vaganov, E. A., and Modrzyński, J. (2006). Interannual growth response of Norway spruce to climate along an altitudinal gradient in the Tatra Mountains, Poland. *Trees* 20, 735–746. doi: 10.1007/s00468-006-0088-9
- Schindlbacher, A., Wunderlich, S., Borken, W., Kitzler, B., Zechmeister-Boltenstern, S., and Jandl, R. (2012). Soil respiration under climate change: Prolonged summer drought offsets soil warming effects. *Glob. Change Biol.* 18, 2270–2279. doi: 10.1111/j.1365-2486.2012.02696.x
- Shibistova, O., Lloyd, J., Evgrafova, S., Savushkina, N., Zrazhevskaya, G., Arneth, A., et al. (2002). Seasonal and spatial variability in soil CO₂ efflux rates for a central Siberian *Pinus sylvestris* forest. *Tellus* 54B, 552–567. doi: 10.3402/tellus.v54i5.16687
- Shimada, R., and Takahashi, K. (2022). Diurnal and seasonal variations in photosynthetic rates of dwarf pine *Pinus pumila* at the treeline in central Japan. *Arc. Antarc. Alp. Res.* 54, 1–12. doi: 10.1080/15230430.2021.2022995
- Soe, A. R. B., and Buchmann, N. (2005). Spatial and temporal variations in soil respiration in relation to stand structure and soil parameters in an unmanaged beech forest. *Tree Physiol.* 25, 1427–1436. doi: 10.1093/treephys/25.11.1427
- Song, X., Peng, C., Zhao, Z., Zhang, Z., Guo, B., Wang, W., et al. (2014). Quantification of soil respiration in forest ecosystems across China. *Atmos. Environ.* 94, 546–551. doi: 10.1016/j.atmosenv.2014.05.071
- Suzuki, R., and Takahashi, K. (2022). Responses of photosynthetic rates to temperature in two conifers dominating at different elevations. *Landsc. Ecol. Eng.* 18, 389–395. doi: 10.1007/s11355-022-00500-2
- Takahashi, K. (2003). Effects of climatic conditions on shoot elongation of alpine dwarf pine (*Pinus pumila*) at its upper and lower altitudinal limits in central Japan. *Arc. Antarc. Alp. Res.* 35, 1–7. doi: 10.1657/1523-0430(2003)035[0001:EOCCOS]2.0.CO;2
- Takahashi, K. (2021). Productivity does not decrease at the climate extremes of tree ranges in the Japanese archipelago. *Oecologia* 197, 259–269. doi: 10.1007/s00442-021-05015-5
- Takahashi, K., and Okuhara, I. (2013). Forecasting the effects of global warming on radial growth of subalpine trees at the upper and lower distribution limits in central Japan. *Clim. Change* 117, 273–287. doi: 10.1007/s10584-012-0547-9
- Takahashi, K., and Yoshida, S. (2009). How the scrub height of *Pinus pumila* decreases at the treeline. *Ecol. Res.* 24, 847–854. doi: 10.1007/s11284-008-0558-1

- Takahashi, K., Azuma, H., and Yasue, K. (2003). Effects of climate on the radial growth of tree species in the upper and lower distribution limits of an altitudinal ecotone on Mt. Norikura, central Japan. *Ecol. Res.* 18, 549–558. doi: 10.1046/j.1440-1703.2003.00577.x
- Takahashi, K., Hirosawa, T., and Morishima, R. (2012). How the timberline formed: Altitudinal changes in stand structure and dynamics around the timberline in central Japan. *Ann. Bot.* 109, 1165–1174. doi: 10.1093/aob/mcs043
- Takahashi, K., Okuhara, I., Tokumitsu, Y., and Yasue, K. (2011). Responses to climate by tree-ring widths and maximum latewood densities of two *Abies* species at upper and lower altitudinal distribution limits in central Japan. *Trees* 25, 745–753. doi: 10.1007/s00468-011-0552-z
- Takahashi, K., Tokumitsu, Y., and Yasue, K. (2005). Climatic factors affecting the tree-ring width of *Betula ermanii* at the timberline on Mount Norikura, central Japan. *Ecol. Res.* 20, 445–451. doi: 10.1007/s11284-005-0060-y
- Takeda, S., and Takahashi, K. (2020). Elevational variation in abundance of coarse woody debris in subalpine forests, central Japan. *For. Ecol. Manage.* 473, 118295. doi: 10.1016/j.foreco.2020.118295
- Trofymow, J. A., Moore, T. R., Titus, B., Prescott, C., Morrison, I., Siltanen, M., et al. (2002). Rates of litter decomposition over 6 years in Canadian forests: Influence of litter quality and climate. *Can. J. For. Res.* 32, 789–804. doi: 10.1139/x01-117
- Wang, T., Ren, H., and Ma, K. (2005). Climatic signals in tree ring of *Picea schrenkiana* along an altitudinal gradient in the central Tianshan Mountains, northwestern China. *Trees* 19, 735–741. doi: 10.1007/s00468-005-0003-9
- Wieser, G. (2004). Seasonal variation of soil respiration in a *Pinus cembra* forest at the upper timberline in the Central Austrian Alps. *Tree Physiol.* 24, 475–480. doi: 10.1093/treephys/24.4.475
- Xu, Z., Tang, S., Xiong, L., Yang, W., Yin, H., Tu, L., et al. (2015). Temperature sensitivity of soil respiration in China's forest ecosystems: Patterns and controls. *Appl. Soil Ecol.* 93, 105–110. doi: 10.1016/j.apsoil.2015.04.008
- Yamada, T., Hibino, T., Araki, T., and Nakatsugawa, M. (1995). Statistical characteristics of rainfall in mountainous basins. *Proc. Japan Soc. Civil. Eng. II* 33, 1–13. doi: 10.2208/jjscej.1995.527_1
- Yamamura, R., and Nakano, H. (1985). Relationships between annual water losses and annual precipitation and altitude in forested watershed. *Bull. Fac. Agr. Shinshu Univ.* 22, 139–147.
- Zaka, S., Frak, E., Julier, B., Gastal, F., and Louarn, G. (2016). Intraspecific variation in thermal acclimation of photosynthesis across a range of temperatures in a perennial crop. *AoB Plants* 8:lw035. doi: 10.1093/aobpla/plw035
- Zhang, J., Liu, S., Liu, C., Wang, H., Luan, J., Liu, X., et al. (2021). Different mechanisms underlying divergent responses of autotrophic and heterotrophic respiration to long-term throughfall reduction in a warm-temperate oak forest. *For. Ecosyst.* 8:41. doi: 10.1186/s40663-021-00321-z
- Zhang, L. H., Chen, Y. N., Zhao, R. F., and Li, W. H. (2010). Significance of temperature and soil water content on soil respiration in three desert ecosystems in Northwest China. *J. Arid Environ.* 74, 1200–1211. doi: 10.1016/j.jaridenv.2010.05.031
- Zhao, J., Li, R., Li, X., and Tian, L. (2017). Environmental controls on soil respiration in alpine meadow along a large altitudinal gradient on the central Tibetan Plateau. *Catena* 159, 84–92. doi: 10.1016/j.catena.2017.08.007



OPEN ACCESS

EDITED BY

Taku Tsusaka,
Ostrom, Thailand

REVIEWED BY

Kikuko Shoyama,
National Research Institute for Earth Science
and Disaster Resilience (NIED), Japan
Ting Hua,
Beijing Normal University, China

*CORRESPONDENCE

Hui Fu
✉ iflying@126.com

RECEIVED 18 June 2023

ACCEPTED 28 July 2023

PUBLISHED 10 August 2023

CITATION

Lin X and Fu H (2023) Optimization of tropical rainforest ecosystem management: implications from the responses of ecosystem service values to landscape pattern changes in Hainan Tropical Rainforest National Park, China, over the past 40 years. *Front. For. Glob. Change* 6:1242068. doi: 10.3389/ffgc.2023.1242068

COPYRIGHT

© 2023 Lin and Fu. This is an open-access article distributed under the terms of the [Creative Commons Attribution License \(CC BY\)](https://creativecommons.org/licenses/by/4.0/). The use, distribution or reproduction in other forums is permitted, provided the original author(s) and the copyright owner(s) are credited and that the original publication in this journal is cited, in accordance with accepted academic practice. No use, distribution or reproduction is permitted which does not comply with these terms.

Optimization of tropical rainforest ecosystem management: implications from the responses of ecosystem service values to landscape pattern changes in Hainan Tropical Rainforest National Park, China, over the past 40 years

Xiaofu Lin and Hui Fu*

School of Tropical Agriculture and Forestry, Hainan University, Haikou, China

Exploring the comprehensive impact of landscape pattern changes on regional ecosystem service values (ESVs) over a long time series is significant for optimizing ecosystem management. This study took Hainan Tropical Rainforest National Park (HTRNP) as a case and first assessed its five vital ecosystem services (ESs): water supply (WS), water purification (WP), carbon storage (CS), soil retention (SR), and habitat quality (HQ). Based on the ESs assessment results, we further calculated their ESVs and quantified the responses of ESVs to landscape pattern changes during 1980–2020. The results revealed that: (1) Forestland is the basal landscape type of HTRNP. Landscape patterns changed significantly after 2000; the proportion of both cultivated land and grassland decreased, while the proportion of forestland, water, and construction land increased; with the areas and landscape dominance of both forestland and water increased, the agglomeration and connectivity of the overall landscape increased and its homogenization decreased. (2) WS, WP, CS, and SR services tended to weaken, and HQ service tended to strengthen. The spatial heterogeneities of WS and SR changed significantly over time. WS, HQ, SR, and CS are the main contributors to the total ESV. During 1980–2020, the four ESVs of WS, WP, SR, and CS showed a decreasing trend; HQ's ESV tended to increase, and the total ESV tended to decrease. (3) The increase of areas and dominance in forestland and water was the main reason that HQ's ESV tended to increase, and WP's ESV and CS's ESV tended to decrease. The construction land scale was relatively small, so its impacts on ESVs were limited. The responses of both WS's ESV and SR's ESV to landscape pattern changes were insignificant due to the impacts of topographic and climatic factors. The study results provide a reference for managing and optimizing HTRNP's ecosystem to improve its integrated benefits of crucial ESs.

KEYWORDS

landscape pattern, ecosystem service, spatial-temporal change, ecosystem service value, tropical rainforest, national park

1. Introduction

The concept of ecosystem service (ES) was first introduced in the report “Man’s Impact on the Global Environment,” published by the United Nations University (UNU) in the early 1970s. The introduction of this concept built a bridge between ecosystems and humans, emphasizing the importance of ecosystems to human welfare (Schröter et al., 2019). The welfare of humans depends on tangible services (such as food, medicines, and raw materials) and intangible services (such as ecotourism, aesthetic beauty, cultural landscapes, climate regulation, and flooding resistance) provided by forests, wetlands, and other ecological systems to maintain and guarantee (Ayensu et al., 1999; Kemkes et al., 2010; Hernández-Morcillo et al., 2013). The Millennium Ecosystem Assessment (MA) (Millennium Ecosystem Assessment, 2005) defined the ESs as the benefits humans derive from ecosystems and classified them into four categories: provisioning services, regulating services, supporting services, and cultural services. For human societies to fully recognize these ESs, the ecosystem service values (ESVs) accounting is gradually becoming an effective way to understand ecosystems’ multiple benefits (Guo et al., 2001). Costanza et al. (1997) have also pointed out that ESs monetization can help increase policymakers’ attention to ESs. While this approach to assigning economic values to ESs has raised questions and concerns among some scholars (Fairhead et al., 2012), it is undeniable that the approach of quantifying ESs in the form of a common currency has allowed people to weigh the relative importance of ESs against other services, and the importance of ESs was enhanced (Tallis and Kareiva, 2005; De Groot et al., 2012; Guswa et al., 2014). With the gradual development of relevant studies on ESVs (Kroeger and Casey, 2007; Campbell and Tilley, 2014; Salzman et al., 2018), the concept of ES has also been further improved and promoted.

The landscape pattern is a mixture of natural and human-managed patches (Turner, 1987). Landscape pattern changes have been widely identified as one of the essential driving factors of ES changes, and they affect the ESs supply by changing ecological processes (such as material cycles and energy distributions of regional ecosystems), thereby affecting ESVs (Lawler et al., 2014; Wang et al., 2015; Li et al., 2021). In recent years, research about the impacts of landscape types changes on ESs has progressed, and the research scales cover global and national (Arowolo et al., 2018; Kubiszewski et al., 2020), urban (Wang et al., 2018), watershed (Loomisa et al., 2018; Kertész et al., 2019), and agro-ecosystem (Baude et al., 2019). Research on the correlation mechanism between ESVs and landscape pattern changes has also made some progress: Yushanjiang et al. (2018) analyzed the spatial correlation among ESVs and landscape patterns in the Ebinur Lake watershed, Xinjiang; Hou et al. (2020) explored the correlation between ESVs and landscape pattern changes in Xi’an.

According to Aryal et al. (2022), most of the study regions are located in temperate regions, but there is still a lack of studies on the ESs in tropical regions, especially in developing countries. Although tropical regions only cover 40% of the Earth’s surface, they have the wealthiest species resources in the world (Barlow et al., 2018). Forest ecosystems cover most of the world’s tropical regions. They are the primary source of ESs supply in the tropics,

but their ESs supply capacity is rapidly declining as the intensity of human activities and the demand for product supply keep increasing (Watson et al., 2018; Hoang and Kanemoto, 2021). Recently, some studies have been conducted on forest ecosystems in tropical regions such as Amazon Plain (Navrud and Strand, 2018; Piponiot et al., 2019) and Congo Basin (Cuni-Sanchez et al., 2019). In China, relevant studies were mainly focused on the tropical rainforest in Xishuangbanna, Yunnan Province (Liu et al., 2019; Fang et al., 2020).

Hainan tropical rainforest is the most concentrated, best preserved, and largest contiguity of continental island tropical rainforest in China. It has the world’s unique plant and animal species and germplasm gene bank; it is the only habitat for critically endangered species such as the Hainan gibbon (*Nomascus hainanus*) in the world; and it is also the ecological safety barrier of Hainan Island. The dense tropical rainforest is the primary source of ESs supply on Hainan Island and is an essential ecosystem with national representation and global conservation significance. On 12 October 2021, Hainan Tropical Rainforest National Park (HTRNP) was officially established as one of the five national parks in China at the 15th Conference of the Parties (COP 15) Leaders’ Summit of the United Nations Convention on Biological Diversity (CBD). Compared to other countries, the national park construction in China started late, and due to the remote location and unique island environment of Hainan Island, there need to be more relevant studies on the ESs within the HTRNP. Recently, Li L. et al. (2022) analyzed the spatial autocorrelation in the ESVs and land-use types in HTRNP in 2018 using the value equivalent conversion method proposed by Xie et al. (2015), advancing the research process of ESV in HTRNP. However, this method is mainly based on assigning values to each landscape type to calculate ESVs, and its assignment is mainly based on the knowledge and experience of experts, which has a certain degree of subjectivity and uncertainty (Chen et al., 2020). Therefore, to more objectively quantify the correlation between ESVs and landscape patterns, this study aims to: (1) explore the spatial-temporal changes of HTRNP’s landscape patterns during 1980–2020; (2) quantitatively assess the spatial-temporal changes of ESs in HTRNP and the trends of ESVs during 1980–2020; and (3) explore the responses of ESVs to landscape pattern changes in HTRNP during 1980–2020.

2. Materials and methods

2.1. Study area

Hainan Tropical Rainforest National Park (HTRNP) is located in the central mountainous region of Hainan Island, China (Figure 1) (18°33′16″–19°14′16″N, 108°44′32″–110°04′43″E). The whole park reaches nine cities and counties of Wuzhishan, Qiongzong, Baisha, Dongfang, Lingshui, Changjiang, Ledong, Baoting, and Wanning, covering the five National Nature Reserves (NNRs) of Wuzhishan (WZS), Yinggeling (YGL), Jianfengling (JFL), Bawangling (BWL), and Diaoluoshan (DLS), with a total area of 439,800 hm², accounting for about 14.28% of the island’s land area. HTRNP has a tropical maritime monsoon climate with an average annual temperature between 22.5 and 26.0°C, average

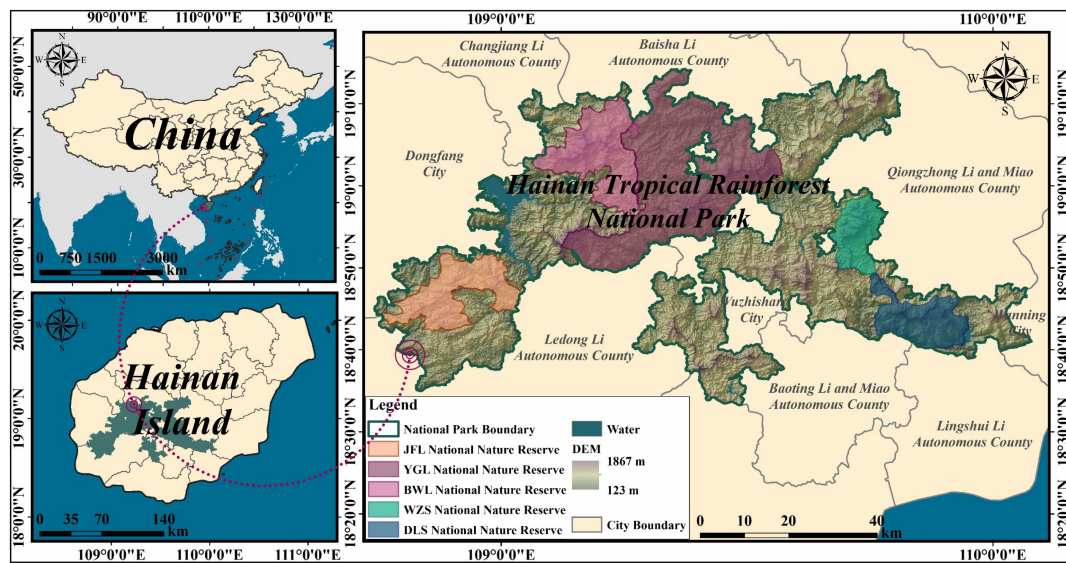


FIGURE 1

Location of the study area. JFL, Jianfengling; YGL, Yinggeling; BWL, Bawangling; WZS, Wuzhishan; DLS, Diaoluoshan.

annual precipitation of 1,759 mm, and annual sunshine hours between 2,000 and 2,700 h.

The unique geographical and climatic environment has shaped China's precious tropical rainforest ecosystem. Since the establishment of Hainan as a province in 1988, the implementation of a series of strategies, such as the construction of Hainan International Tourism Island, has promoted the economic development of cities and counties, which is bound to bring a certain degree of impacts on the landscape patterns of the HTRNP, and then affect some essential ESs related to human well-being. Therefore, it is urgent to quantitatively assess the landscape pattern changes in the HTRNP and its impacts on the critical ESs benefits.

2.2. Data sources and processing

Multi-source datasets were adopted in this study (Table 1). The land use/land cover (LULC) data comes from China's Multi-Period Land Use/Land Cover Remote Sensing Monitoring Dataset (CNLUCC) (Xu et al., 2018), and the spatial resolution is 30 m. We unified all the raster data to a spatial resolution of 30 m based on the ArcGIS v10.2 platform, and the projection coordinate system was unified to WGS_1984_Albers. The framework of this study is shown in Figure 2.

2.3. Landscape patterns analysis

2.3.1. Analysis of landscape type changes

Based on the LULC data, the landscape types of HTRNP were divided into five categories: cultivated land, forestland, grassland, water, and construction land. This study used the transfer matrix to analyze the landscape types transition in two adjacent time nodes (1980–1990, 1990–2000, 2000–2010, and 2010–2020) during 1980–2020.

2.3.2. Analysis of landscape index changes

Based on the actual situation of HTRNP and related study (Li L. et al., 2022), ten landscape indices were selected from Landscape and Class levels: percent of landscape (PLAND), number of patches (NP), patch density (PD), mean patch size (MPS), landscape shape index (LSI), largest patch index (LPI), Shannon's diversity index (SHDI), Shannon's evenness index (SHEI), contagion (CONTAG), and aggregation index (AI). These indices were calculated based on Fragstats v4.2 platform.

2.4. ES indicators selection and assessment

With reference to the ES classification system of The Economic of Ecosystems and Biodiversity (TEEB), and considering the availability and accessibility of data, this study finally selected five important ES indicators based on the characteristics of HTRNP: (1) water supply (WS) and water purification (WP): HTRNP is the source of three major rivers (Nandu, Changhua, and Wanquan) and the primary water source of two major reservoirs (Songtao and Daguangba) on Hainan Island, the WS and WP services of HTRNP is essential for maintaining and regulating the hydrological services of island-wide ecosystems (Li A. et al., 2022); (2) carbon storage (CS), soil retention (SR), and habitat quality (HQ): HTRNP has preserved the largest tropical rainforest and monsoon rainforest ecosystem in China, it is not only the most significant carbon pool of Hainan Island, but also plays a vital role in soil conservation and biodiversity protection (Yu et al., 2016); the abundant rainfall in HTRNP increases the potential risk of soil erosion and poses a threat to biological habitats. The Integrated Valuation of Ecosystem Services and Tradeoffs (InVEST) (Tallis and Polasky, 2009; Sharp et al., 2016) model has been widely used for the ESs assessment, so we applied InVEST v3.12 model to evaluate the biophysical values of the above five ESs. And referring to "The Technical Guideline

TABLE 1 Data information.

| Name | Year | Spatial resolution/Format | Source | Application |
|---|------------------------------|---------------------------|---|--------------------|
| Land use/land cover (LULC) | 1980, 1990, 2000, 2010, 2020 | 30 m/Raster | Resource and Environment Science and Data Center (http://www.resdc.cn/) | WS, WP, CS, SR, HQ |
| Digital elevation model (ASTER GDEM V3) | 2009 (published in 2019) | 30 m/Raster | Geospatial Data Cloud (http://www.gscloud.cn) | WS, WP, SR |
| Annual precipitation | 1980, 1990, 2000, 2010, 2020 | 1 km/Raster | Resource and Environment Science and Data Center (http://www.resdc.cn/) | WS, WP, SR |
| Evapotranspiration | 1991–2020 | 30 m/Raster | Institute of Mountain Hazards and Environment, CAS | WS |
| Soil | 2009 | 1 km/Raster | Chinese soil data set based on world soil database (HWSD) (http://www.ncdc.ac.cn) | WS, SR |
| Road | 2019 | –/Vector | OpenStreetMap (https://www.openstreetmap.org) | HQ |

WS, water supply; WP, water purification; CS, carbon storage; SR, soil retention; HQ, habitat quality.

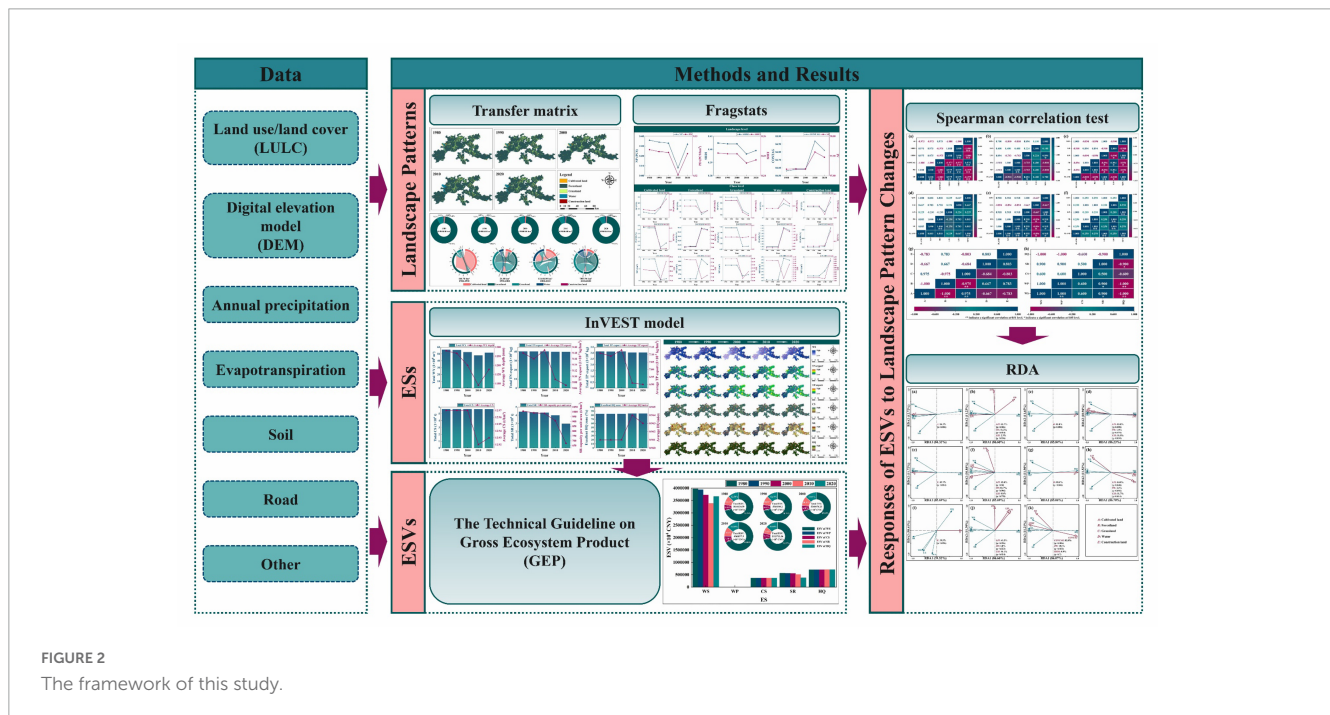


FIGURE 2 The framework of this study.

on Gross Ecosystem Product (GEP)” issued by the Ministry of Ecology and Environment of the People’s Republic of China in 2020, and related research (Chen et al., 2021), the assessment methods (including biophysical and monetary values) of the five ES indicators for HTRNP were established (Table 2).

2.4.1. Water supply

The biophysical value of WS was assessed using the AWY module. This module is based on the water balance principle and considers several factors, such as transpiration, evaporation, and precipitation. The calculation formula is as follows:

$$Y_{xj} = (1 - \frac{AET_{xj}}{P_x}) \times P_x$$

where Y_{xj} is the annual water yield on the pixel x of the landscape type j (mm); AET_{xj} is the actual annual evapotranspiration on the pixel x of the landscape type j (mm); P_x is the annual precipitation on the pixel x (mm) (Qi et al., 2019). The maximum root depth (Root_depth), plant evapotranspiration coefficient (K_c), and actual evapotranspiration value (LULC_veg) in the biophysical coefficient table (Supplementary Table 1) were set according to Zheng et al.’s (2019) research on the central mountainous region of Hainan Island. Zhang’s coefficients for each year were set by referring to the measured data of the Fucai hydrological station in HTRNP (Li A. et al., 2022) after several adjustments. The monetary value of WS was assessed using Alternative costing method. The calculation formula is as follows:

$$V_{ws} = Q_{ws} \times C$$

TABLE 2 Ecosystem service indicators and assessment methods for HTRNP.

| First category of ES indicators | Second category of ES indicators | Biophysical value assessment methods | Monetary value assessment methods |
|---------------------------------|----------------------------------|---|-----------------------------------|
| Provisioning service | Water supply (WS) | InVEST model Annual Water Yield (AWY) module | Alternative costing |
| Regulating service | Water purification (WP) | InVEST model Nutrient Delivery Ratio (NDR) module | Alternative costing |
| | Carbon storage (CS) | InVEST model Carbon Storage and Sequestration (CSS) module | Alternative costing, Carbon tax |
| | Soil retention (SR) | InVEST model Sediment Delivery Ratio (SDR) module | Alternative costing |
| Habitat service | Habitat quality (HQ) | InVEST model Habitat Quality (HQ) module | Excellent HQ region's area |

ES, ecosystem service; InVEST model, Integrated Valuation of Ecosystem Services and Tradeoffs model.

where V_{ws} is the monetary value of WS (CNY/a); Q_{ws} is the total annual water supply (m^3/a); C is the engineering cost of reservoir constructing per unit capacity (CNY/ m^3). According to the “Yearbook of China water resources,” the average reservoir capacity cost is 2.17 CNY/ m^3 , then C was calculated as 7.0547 CNY/ m^3 based on the 2009 price index (3.251) (Fang et al., 2013).

2.4.2. Water purification

The biophysical value of WP was assessed using the NDR module, which inversely characterizes the WP service function by the total nitrogen (TN) and total phosphorus (TP) exports. The higher the TN and TP exports per unit area, the weaker the WP service function. The calculation formula is as follows:

$$ALV_x = HSS_x \times pol_x$$

$$HSS_x = \lambda_x / \bar{\lambda}_w$$

where ALV_x is the adjusted loading value on the pixel x ; pol_x is the export coefficient on the pixel x ; HSS_x is the hydrologic sensitivity score on the pixel x , λ_x is the runoff index on the pixel x , $\bar{\lambda}_w$ is the average runoff index in the watershed of interest (Qi et al., 2019). Nitrogen (N) and phosphorus (P) export coefficients and retention efficiency (Supplementary Table 2) for landscape types were set with reference to relevant studies (Zhe et al., 2013; Zheng et al., 2019). The monetary value of WP was assessed using Alternative costing method. The calculation formula is as follows:

$$V_{wp} = \sum T_N \times P_N + \sum T_P \times P_P$$

where V_{wp} is the monetary value of WP (CNY/a); T_N and T_P are the total amount of TN and TP purification (t/a); P_N and P_P are the purification unit-prices of TN and TP (CNY/t), and the values are 1,750 and 2,800 CNY/t, respectively, according to the “Levy standard of pollution discharge fees and calculation methods” of the National Development and Reform Commission of China (Fan and Li, 2020).

2.4.3. Carbon storage

The biophysical value of CS was assessed using the CSS module, which estimates CS based on each landscape type and its corresponding four primary carbon pools. The calculation formula

is as follows:

$$C_{total} = C_{above} + C_{below} + C_{soil} + C_{dead}$$

where C_{total} is the total CS (t/ hm^2); C_{above} , C_{below} , C_{soil} , and C_{dead} are aboveground CS (t/ hm^2), belowground CS (t/ hm^2), soil CS (t/ hm^2), and dead organic CS (t/ hm^2), respectively. As the vegetation of HTRNP is mainly evergreen broad-leaved species of zonal forest type, its dead organic CS is tiny and difficult to estimate (Gong et al., 2022). This part of CS was not calculated in this study. Other three types of carbon density were set (Supplementary Table 3) with reference to Liu et al.'s (2022) study. The monetary value of CS was assessed using a combination of Alternative costing and Carbon tax methods. The calculation formula is as follows:

$$V_{cs} = (272.65C_t + 1017.675C_t) / 2$$

where V_{cs} is the monetary value of CS (CNY/a); C_t is the total CS (t/a). To obtain more accurate monetary value assessment results, this study referred to Wang et al.'s (2017) study, the unit-price of forest carbon sink in Alternative costing method used the arithmetic average of four unit-prices (251.40, 260.90, 273.30, and 305.00 CNY/t); the Carbon tax method used the international Swedish carbon tax rate (150 USD/t = 1,017.675 CNY/t, the exchange rate was calculated as 100 USD = 678.45 CNY on 29 January 2023).

2.4.4. Soil retention

The SDR module assesses SR's biophysical value based on the Revised Universal Soil Loss Equation (RUSLE). The calculation formula is as follows:

$$A_x = R_x \times K_x \times LS_x \times (1 - C_x \times P_x)$$

$$R_j = 0.0534P_j^{1.6548}$$

$$K = (-0.01383 + 0.51575K_{EPIIC}) \times 0.1317$$

where A_x is the SR amount on the pixel x (t- hm^{-2} -a $^{-1}$); R_x is the rainfall erosivity factor on the pixel x (MJ- mm - hm^{-2} - h^{-1} -a $^{-1}$); K_x is the soil erodibility factor on the pixel x (t- hm^2 -h- hm^{-2} -MJ $^{-1}$ - mm^{-1}); LS_x is the topographical factor on the pixel x ; C_x is the crop-management factor on the pixel

x ; P_x is the support practice factor (Qi et al., 2019). R was calculated using the rainfall erosion force model (Zhang and Fu, 2003), R_j is the rainfall erosion force in year j ($\text{MJ}\cdot\text{mm}\cdot\text{hm}^{-2}\cdot\text{h}^{-1}\cdot\text{a}^{-1}$), P_j is the rainfall in year j (mm). K was calculated using the Erosion-Productivity Impact Calculator (EPIC) model (Williams, 1995), the K_{EPIC} was corrected according to Zhang et al. (2008). The values of C and P were set (Supplementary Table 4) according to the relevant studies (Xiao, 1999; Zheng et al., 2019). The monetary value of SR (including the value of both sedimentation reduction and non-point source pollution reduction) assessed using the Alternative costing method. The calculation formula is as follows:

$$V_{sr} = V_{sd} + V_{dpd}$$

$$V_{sd} = \lambda \times (Q_{sr}/\rho) \times C$$

$$V_{dpd} = \sum_{i=1}^2 Q_{sr} \times C_i \times P_i$$

where V_{sr} is the monetary value of SR (CNY/a); V_{sd} is the value of sedimentation reduction (CNY/a); V_{dpd} is the value of non-point source pollution reduction (CNY/a); λ is the sedimentation coefficient, taking the value of 0.24 (Sheng et al., 2010); Q_{sr} is the SR amount (t/a); C is the cost of reservoir desilting project per unit area (CNY/m³), according to the “The building built water engineering budget norm” of the Ministry of Water Resources of the People’s Republic of China, the value of C is 17.63 CNY/m³ (Yu et al., 2020); ρ is the soil capacity (t/m³), according to the average of the measured data of each forest ecosystem type in the central mountainous region of Hainan island in 2008, the value of ρ is 1.28 t/m³ (Liu et al., 2009); C_i is the pure content of N (or P) in soil (%), and it was determined that the content of N and P in soil of China are 0.370 and 0.108%, respectively (Wang L. et al., 2017); P_i is the degradation cost of N (or P), according to the “Levy standard of pollution discharge fees and calculation methods,” the degradation costs of N and P are 1,750 and 2,800 CNY/t, respectively (Fan and Li, 2020).

2.4.5. Habitat quality

The biophysical value of HQ was assessed using the HQ module. The value of the HQ index is in the range of [0,1], and the higher value indicates the higher level of biodiversity. The calculation formula is as follows:

$$Q_{xj} = H_j \left(1 - \frac{D_{xj}^z}{D_{xj}^z + K^z} \right)$$

where Q_{xj} is the HQ on the pixel x of the landscape type j ; H_j is the habitat suitability of the landscape type j ; D_{xj} is the total threat level on the pixel x of the landscape type j ; K is the half-saturation coefficient, generally taking a value of 0.5; z is a scaling factor, generally taking a value of 2.5 (Yang et al., 2021). Referring to the studies on HTRNP and its neighboring regions (Lei et al., 2022; Yao et al., 2022), paddy fields, dry land, rural residential areas, other construction lands, and expressways were selected as threat factors in this study. The impact distance and weight of the threat factors (Supplementary Table 5) and the sensitivity of each landscape type (Supplementary Table 6) were set with reference to the model

manual and the above studies. Referring to related research (Xiao et al., 2014; Sun et al., 2019), the monetary value of HQ was assessed based on the area of excellent HQ regions, and the ecological benefit of the excellent HQ region is about 191.28×10^4 CNY/km². The excellent HQ regions were obtained by referring to Lei et al.’s (2022) study using the Natural Breaks method to classify the HQ spatial distribution into four classes (Poor: 0–0.3, Medium: 0.3–0.7, Good: 0.7–0.9, and Excellent: 0.9–1.0).

2.5. Correlation mechanism analysis between ESVs and landscape patterns

2.5.1. Correlation test between variables

Testing whether there is a correlation between landscape indices and various types of ESVs is a critical a priori step in exploring the correlation between ESVs and landscape pattern changes, to test whether correlations exist among variables, whether the direction and magnitude of the correlations are as expected, and whether they apply to subsequent more complex multivariate analyses (Cen, 2016; Ge, 2020).

2.5.2. Ranking analysis of the correlation between ESVs and landscape patterns

The ranking analysis is widely used in ecological studies to explain the response relationships between species and environmental variables, this method can effectively downscale the multi-dimensional information, and its analysis results are concise and intuitive (Legendre, 2008; Cen, 2016). According to the results of DCA (length of gradient <3), this study applied the Redundancy Analysis (RDA) based on the Canoco v5.0 platform to rank the correlation between ESVs and landscape patterns. The RDA is a ranking analysis method combining regression and Principal Component Analysis (PCA). It is an extension of multiple regression analysis and can be used to model multivariate response data. The RDA ranking chart can visualize the relationship between environment and response variables (Rao et al., 2016). The angle between their arrows reflects the correlation between them: when the angle <90°, it indicates a positive correlation between the variables, and the smaller the angle, the stronger the positive correlation; when the angle >90°, it indicates a negative correlation between the variables, and the larger the angle, the stronger the negative correlation; when the angle = 90°, it shows that the variables are not correlated with each other (Li C. et al., 2022).

3. Results

3.1. Landscape pattern changes

3.1.1. Landscape type changes from 1980 to 2020

From both the distribution (Figure 3) and proportion (Figure 4) of landscape types, forestland is the most dominant landscape type in the HTRNP, followed by grassland, and construction land occupies a minor proportion. During 1980–2020, the proportion of forestland fluctuated between 89.86 and

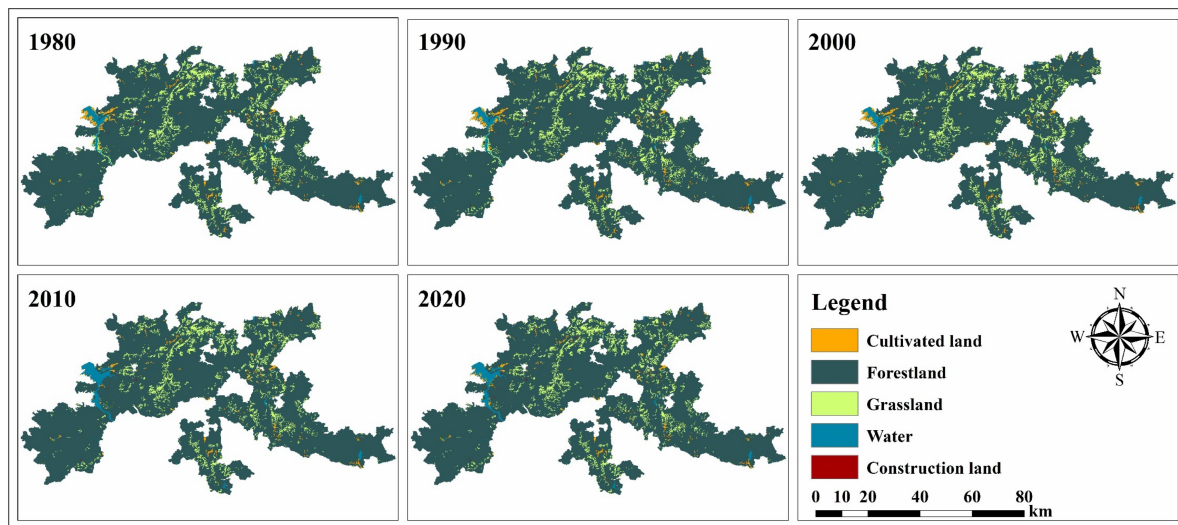


FIGURE 3 Spatial distribution of landscape types in HTRNP during 1980–2020.

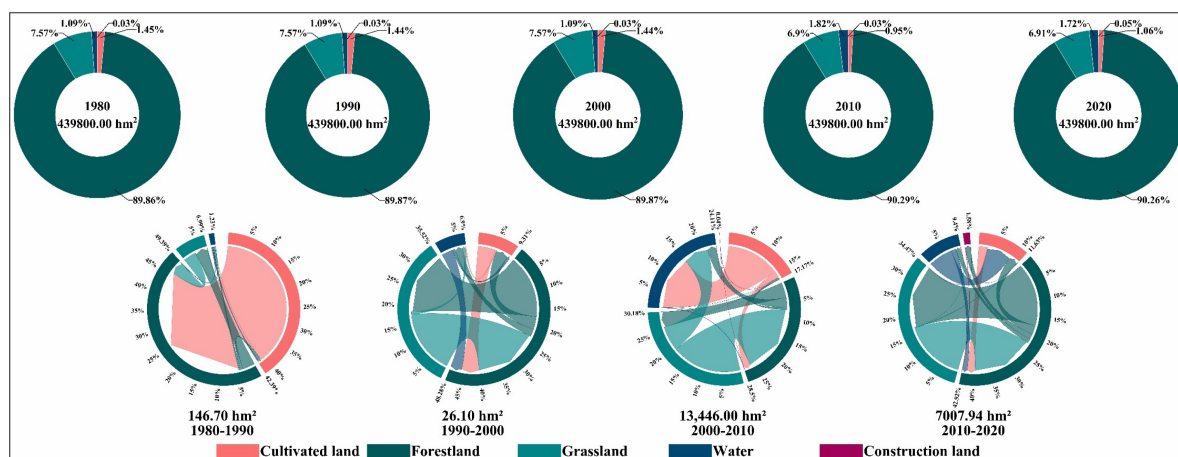


FIGURE 4 Landscape type changes in HTRNP during 1980–2020.

90.29%, with little overall change; the proportion of cultivated land, grassland, and water changed relatively significantly. The conversion between different landscape types became frequent after 2000, especially during 2000–2010. The total area conversion reached 13,446.00 hm² and then gradually eased after 2010.

(1) During 2000–2010, grassland, cultivated land, and forestland areas were transferred out more obviously, accounting for 52.06, 33.18, and 14.72% of the total area transferred out, respectively. Although forestland was one of the primary sources of transfer out area, its proportion showed positive growth because of the significant area input of grassland and cultivated land (Figure 4). The conversions of cultivated land in the northwest and grassland in the southeast to water and forestland, respectively, were evident (Figure 3). (2) The magnitude of changes in landscape types during 2010–2020 was less than in the previous period (Figure 4), and spatially (Figure 3), only the conversion of part of the northwestern water to cultivated land was slightly

noticeable. Although the conversion between forestland and grassland was apparent (Figure 4), the main areas' conversion was limited between these two types, and the number of areas transferred between them was similar. Hence, the changes in the proportion of these two types were relatively small.

3.1.2. Landscape index changes from 1980 to 2020

During 1980–2020, at the Landscape level (Figure 5): NP and PD showed a trend of “slow decline – rapid decline – rapid rise,” with a slight overall decline, indicating that landscape fragmentation and heterogeneity of HTRNP tended to decline; SHDI and SHEI showed a trend of “slow decline – rapid decline – slow rise,” with an overall decline, indicating that the homogeneity of the HTRNP’s landscape decreased, the dominant landscape patch types tended to be prominent, and the distribution of landscape patch types in HTRNP tended to be uneven, which may be related

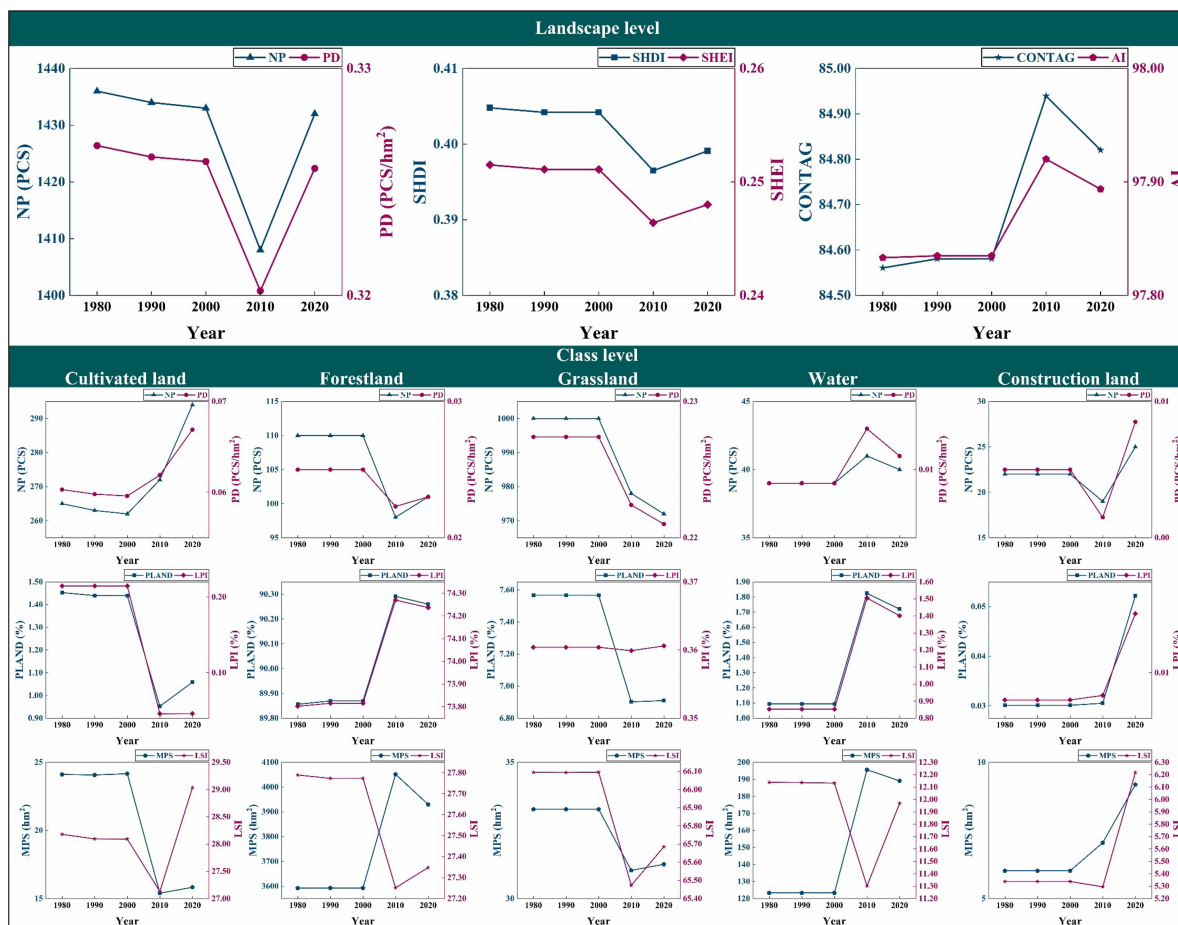


FIGURE 5 Landscape index changes in HTRNP during 1980–2020. PLAND, percent of landscape; NP, number of patches; PD, patch density; MPS, mean patch size; LSI, landscape shape index; LPI, largest patch index; SHDI, Shannon's diversity index; SHEI, Shannon's evenness index; CONTAG, contagion; AI, aggregation index.

to the shrinkage of both grassland and cultivated land and the expansion of both forestland and water. CONTAG and AI showed a trend of “slow rise – rapid rise – slow decline,” these two indices tended to increase overall, indicating that the connectivity of the dominant landscape in HTRNP was enhanced, and the degree of landscape agglomeration was increased.

At the Class level (**Figure 5**): (1) Cultivated land: NP and PD tended to increase, PLAND, LPI, and MPS tended to decrease, indicating that the cultivated land tended to be fragmented and its landscape dominance decreased; LSI tended to increase, indicating that the landscape shape tended to be complex. (2) Forestland: NP and PD tended to decrease, indicating an increase in forestland aggregation; the three indices of PLAND, LPI, and MPS of forestland were the highest among the five landscape types, and all tended to increase, indicating the landscape pattern of HTRNP were dominated by large patches of forestland, and the landscape dominance of forestland tended to increase; LSI tended to decrease, indicating its landscape shape become more regularized. (3) Grassland: grassland had the highest NP and PD among the five landscape types, indicating the highest degree of fragmentation in grassland landscape, but its fragmentation tended to decrease; LPI changed less, PLAND and MPS tended to

decrease, indicating a decrease in its fragmentation was related to the conversion of some small scattered patches to other landscape patch types; LSI tended to decrease, indicating that the landscape shape tended to be regularized. (4) Water: NP and PD tended to increase but at a lower rate; PLAND, LPI, and MPS all tended to increase, indicating an increase in landscape dominance; LSI tended to decrease in general, indicating that the landscape shape tended to be regularized. (5) Construction land: NP, PD, PLAND, LPI, and MPS increased slightly, indicating its area was increasing in fragmented patches; LSI tended to increase, indicating its shape became complex. In summary, landscape indices at both levels changed significantly during 2000–2020.

3.2. Spatial-temporal changes of ESs

3.2.1. Temporal changes of ESs from 1980 to 2020

All the five ESs of HTRNP showed varying degrees of trends during 1980–2020 (**Figure 6**).

(1) WS: WS's biophysical value decreased continuously during 1980–2010; the decrease was more evident during 1990–2010,

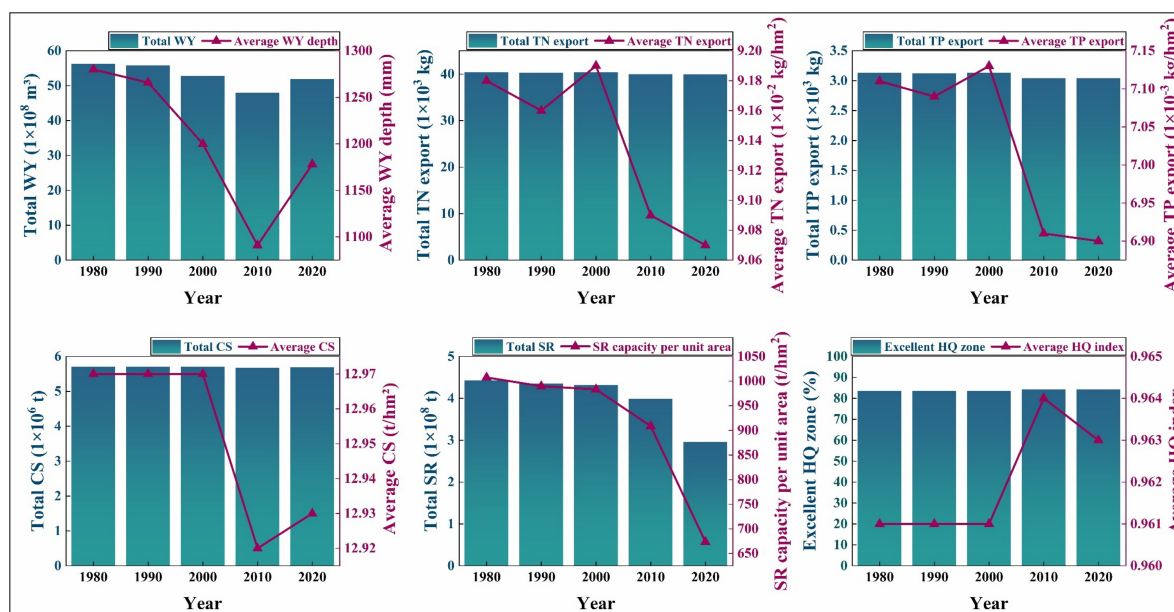


FIGURE 6

Temporal changes of ESs in HTRNP during 1980–2020. WY, water yield; TN, total nitrogen; TP, total phosphorus; CS, carbon storage; SR, soil retention; HQ, habitat quality.

the total WY decreased by 14.16%, and the average WY depth decreased from 1,265.83 to 1,090.93 mm; it rebounded after 2010. There has been a declining trend in WS over the past 40 years, with total annual WY decreasing by 7.82%. (2) WP: the average TN and TP exports both decreased rapidly during 2000–2010, with the average TN export decreasing from 9.19×10^{-2} kg/hm² to 9.09×10^{-2} kg/hm² and the average TP export decreasing from 7.13×10^{-3} kg/hm² to 6.91×10^{-3} kg/hm². The total exports of both TN and TP had decreased slightly over the past 40 years, by 1.24 and 2.88%, respectively. (3) CS: the average CS declined rapidly during 2000–2010, from 12.97 t/hm² to 12.92 t/hm², and the total CS decreased by 0.53%; it rebounded slightly after 2010. There has been a slight overall downward trend in CS over the past 40 years, with a total reduction of 0.35%. (4) SR: the biophysical value of SR decreased significantly during 2010–2020, with a 25.81% decrease in total SR and a decrease in SR capacity per unit area from 908.68 t/hm² to 673.60 t/hm². SR decreased from 1980 to 2020, and the total SR decreased by 33.18%. (5) HQ: the biophysical value of HQ rose rapidly during 2000–2010, with the average HQ index peaking at 0.964; it dropped slightly to 0.963 after 2010. The overall HQ remained high and tended to increase during 1980–2020, the proportion of excellent HQ zone remained above 80%, and the average HQ index remained above 0.960.

3.2.2. Spatial changes of ESs from 1980 to 2020

The mean values of ESs at the sub-watershed scale were calculated based on the Zonal Statistics tool of ArcGIS v10.2 platform, and the ESs were normalized from 0 to 1 (Low to High) for each year to facilitate comparison across years (Xia et al., 2023). All five ESs of HTRNP showed different degrees of spatial heterogeneity during 1980–2020 (Figure 7).

(1) WS: the spatial heterogeneity of WS is “high in the east and low in the west.” This spatial heterogeneity tended to be

significant during 2000–2010, the WS in the southwestern region (including JFL NNR) continued to decrease, and the low-value regions expanded toward the BWL and YGL NNRs in the central region. This trend decreased in 2020. The high-value regions were mainly concentrated in the southeast (including WZS and DLS NNRs). (2) WP: the spatial distribution of both TN and TP exports showed a gradient pattern increasing from the southwestern region (including JFL NNR) to the central region (including BWL and YGL NNRs) and then to the southeastern region (including WZS and DLS NNRs). The high-value regions in the northwest showed a transformation trend to the low-value regions. (3) CS: CS’s spatial heterogeneity did not vary significantly, the low-value regions were concentrated in the northwest, and the high-value regions were concentrated in the southwest (including JFL NNR). (4) SR: SR’s spatial heterogeneity was observed. The low-value regions in the southwest (including JFL NNR) showed a significant expansion during 2000–2010. This trend decreased in 2020. (5) HQ: the spatial heterogeneity of HQ was not observed and did not change significantly. Relatively, the HQ in the northwestern region was slightly lower.

3.3. ESV changes from 1980 to 2020

The total ESV has decreased over the past 40 years (Figure 8), with the most significant decrease during 2000–2010 and a slight rebound in 2020, with a total reduction of $494,419.03 \times 10^4$ CNY. The trends of ESVs are the same as those of ESs: (1) WS’s ESV tended to decrease, but its value weight was still the highest among all ESVs, which may be related to the particular topography and climate of HTRNP: the high altitude and rugged terrain of the HTRNP have a lifting effect on moist air currents, resulting in significant rainfall, and the high altitude also results in low

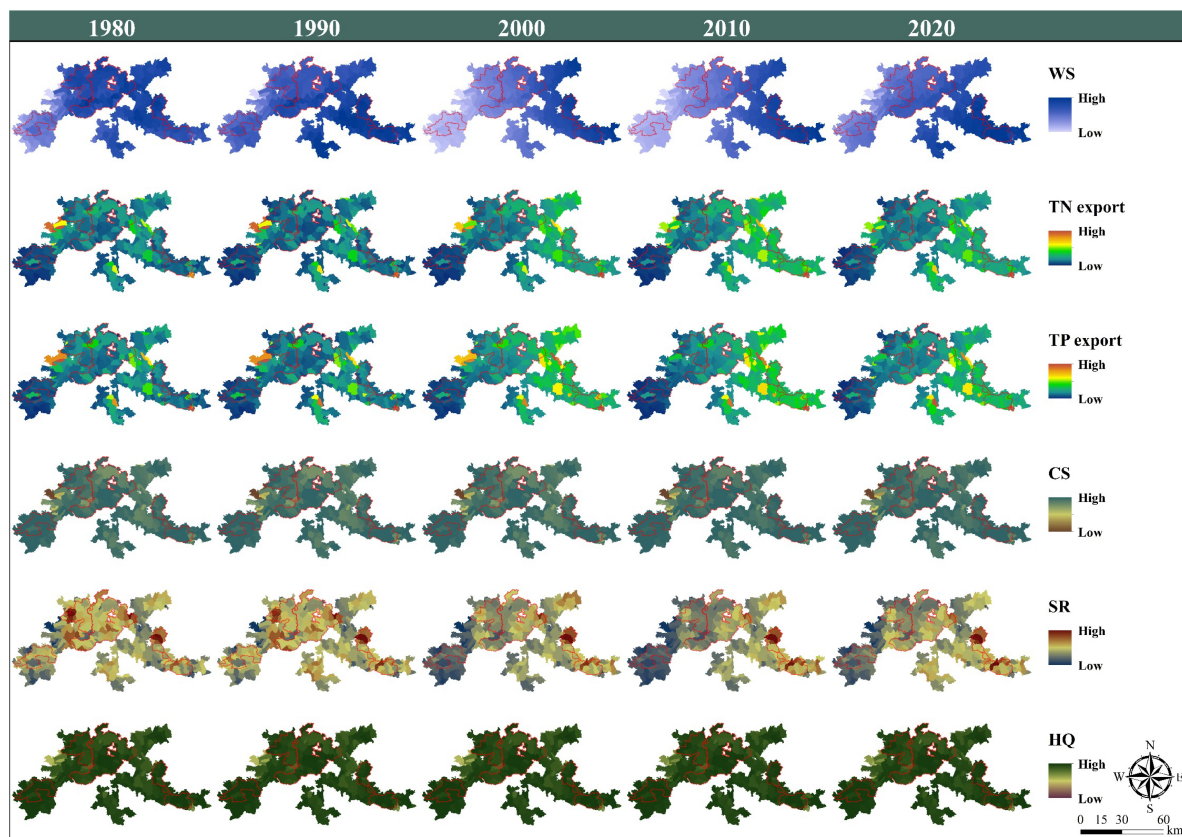


FIGURE 7

Spatial patterns of ESs in HTRNP during 1980–2020. WS, water supply; TN, total nitrogen; TP, total phosphorus; CS, carbon storage; SR, soil retention; HQ, habitat quality.

evapotranspiration, all of which contribute to higher WS (Xia et al., 2023). (2) WP's ESV showed a slight decrease, its value weight was almost 0%, and this may be related to the low TN and TP loads in HTRNP: most of the regions in the HTRNP are sloping and unsuitable for cultivation, so the area of cultivated land is relatively small, resulting in less nitrogen and phosphorus loading from agricultural surface runoff, and thus the amount of purification is less, leading to a low ESV of WP Zhe et al. (2013). (3) CS's ESV declined slightly. Its value weight fluctuated around 7% with insignificant changes. (4) SR's ESV continued to decrease, with a significant drop during 2010–2020, and its value weight plummeted to about 7%, close to that of CS. (5) HQ's ESV tended to increase slightly, and its value weight tended to rise, second only to WS. This phenomenon demonstrated the overall better HQ of HTRNP and indicated that the HQ service was gradually being valued.

3.4. Analysis of the correlation mechanism between ESVs and landscape patterns

3.4.1. Correlation test between variables

The landscape indices, landscape areas, and ESVs of HTRNP during 1980–2020 were used as data sources to test the correlation between these variables. The correlation test was performed based

on the IBM SPSS Statistics v26 platform, using the Spearman correlation coefficient as a measure and a two-tailed *t*-test for the significance of the correlation coefficient. The results showed (Supplementary Figure 1) that the variables had different degrees of correlation.

Based on the previous analysis of the HTRNP's landscape pattern changes, it can be noted that the trends between some of the indices are very similar, indicating that there may be some degree of correlation between them. The strong correlation between indices will result in indices that do not satisfy the statistical properties of mutual independence, causing duplication and redundancy in the mathematical and theoretical significance of subsequent studies, thus affecting the accuracy of the results (Cen, 2016; Ge, 2020). Therefore, in this study, the landscape indices with low correlations were further screened based on the results of the correlation test for subsequent ranking analysis: (1) Landscape level: PD, SHDI, and CONTAG; (2) Class level: PD, LPI, and LSI.

3.4.2. Ranking analysis of the correlation between ESVs and landscape patterns

The RDA ranking analysis (Figure 9) was conducted based on the Canoco v5.0 platform using ESVs as response variables and the landscape areas and indices as environmental variables. Based on the correlation test results between landscape indices, the environmental variable groups are as follows: (1) Landscape level: PD, SHDI, and CONTAG; (2) Class level: LPI, PD, and LSI.

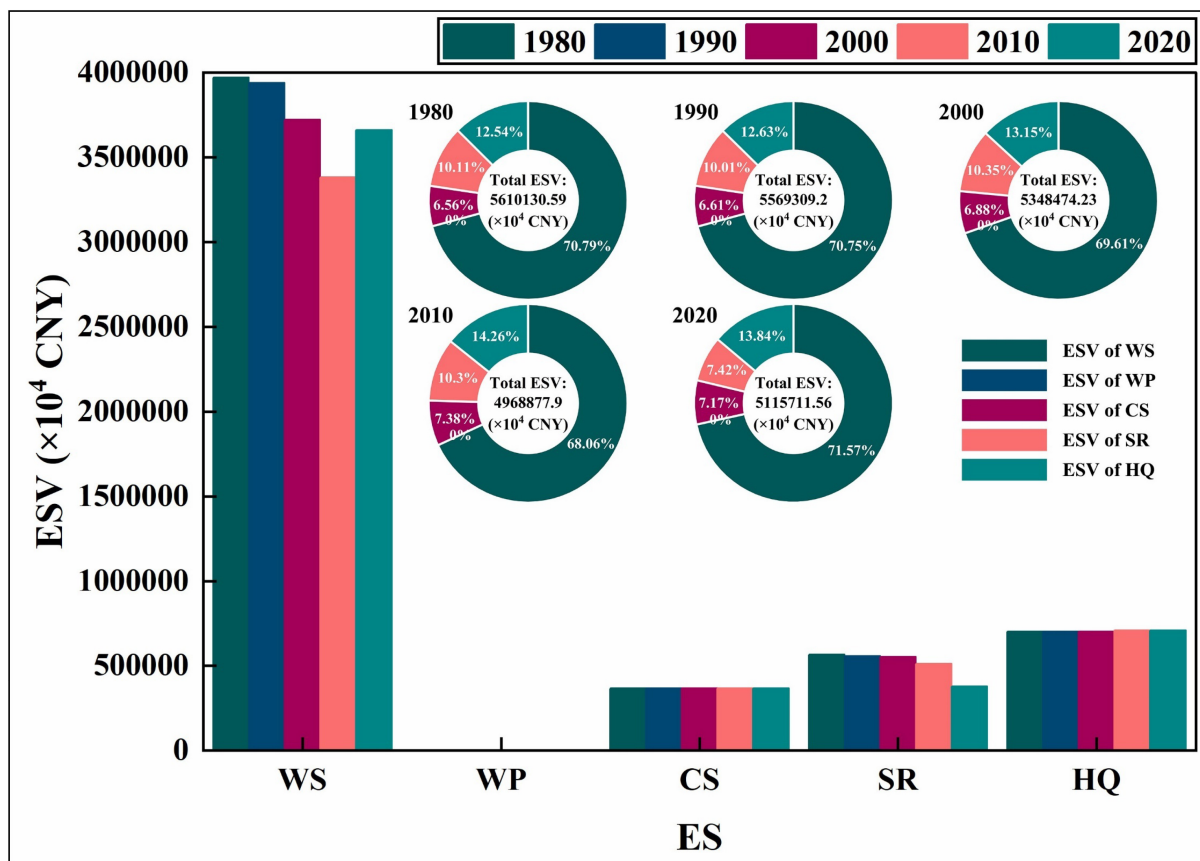


FIGURE 8 Ecosystem service value changes in HTRNP during 1980–2020. ES, ecosystem service; ESV, ecosystem service value; WS, water supply; WP, water purification; CS, carbon storage; SR, soil retention; HQ, habitat quality.

(1) The changes of landscape types over the past 40 years have impacted ESVs. The explanatory degree of cultivated land (84.3%), forestland (85.8%), grassland (85.7%), and water (85.1%) areas are all higher to ESVs, indicating that changes in these four landscape types had significant effects on ESVs. In comparison, the explanatory degree of construction land (39.5%) area is lower, indicating that its changes had weaker effects on ESVs, which may be related to its small area. WP and CS have a strong positive correlation with the areas of grassland and cultivated land and a strong negative correlation with the areas of forestland and water; SR has a strong negative correlation with the area of construction land; HQ has a strong positive correlation with the areas of forestland and water and a strong negative correlation with the areas of grassland and cultivated land.

(2) At the Class level: landscape indices' effects on ESVs across landscape types vary.

Cultivated land: the explanation degree of LPI to ESVs is the highest, reaching 85.7%, followed by PD; LSI has the lowest explanatory degree and did not explain changes in ESVs significantly ($p > 0.10$), and also had a weak correlation with ESVs. WP-LPI and CS-LPI have strong positive correlations, while HQ-LPI and SR-PD have strong negative correlations.

Forestland: the explanation degree of LPI to ESVs is the highest, reaching 85.8%, followed by LSI; PD has the lowest explanatory degree and did not explain changes in ESVs significantly

($p > 0.10$). WP-LSI, CS-LSI, and HQ-LPI have strong positive correlations, while WP-LPI, CS-LPI, and HQ-LSI have strong negative correlations.

Grassland: the explanation degree of PD to ESVs is the highest, reaching 83.7%, followed by LPI; LSI has the lowest explanatory degree and did not explain changes in ESVs significantly ($p > 0.10$). WP-PD and CS-PD have strong positive correlations, while HQ-PD has strong negative correlations.

Water: the explanation degree of LPI to ESVs is the highest, reaching 84.9%, followed by LSI; PD has the lowest explanatory degree. HQ-LPI has strong positive correlations, while WP-LPI and CS-LPI have strong negative correlations.

Construction land: compared with other landscape types, the explanatory degrees of landscape indices of construction land to ESVs are lower. The index with the highest explanatory degree is LSI (explanatory degree only reached 56.1%), followed by LPI; PD has the lowest explanatory degree and did not explain changes in ESVs significantly ($p > 0.10$). SR-LSI and SR-LPI have strong negative correlations.

(3) At the Landscape level: the explanation degree of CONTAG to ESVs is the highest, reaching 82.0%, followed by PD; SHDI has the lowest explanatory degree and did not explain changes in ESVs significantly ($p > 0.10$). HQ-CONTAG has strong positive correlations, while WP-CONTAG and CS-CONTAG have strong negative correlations.

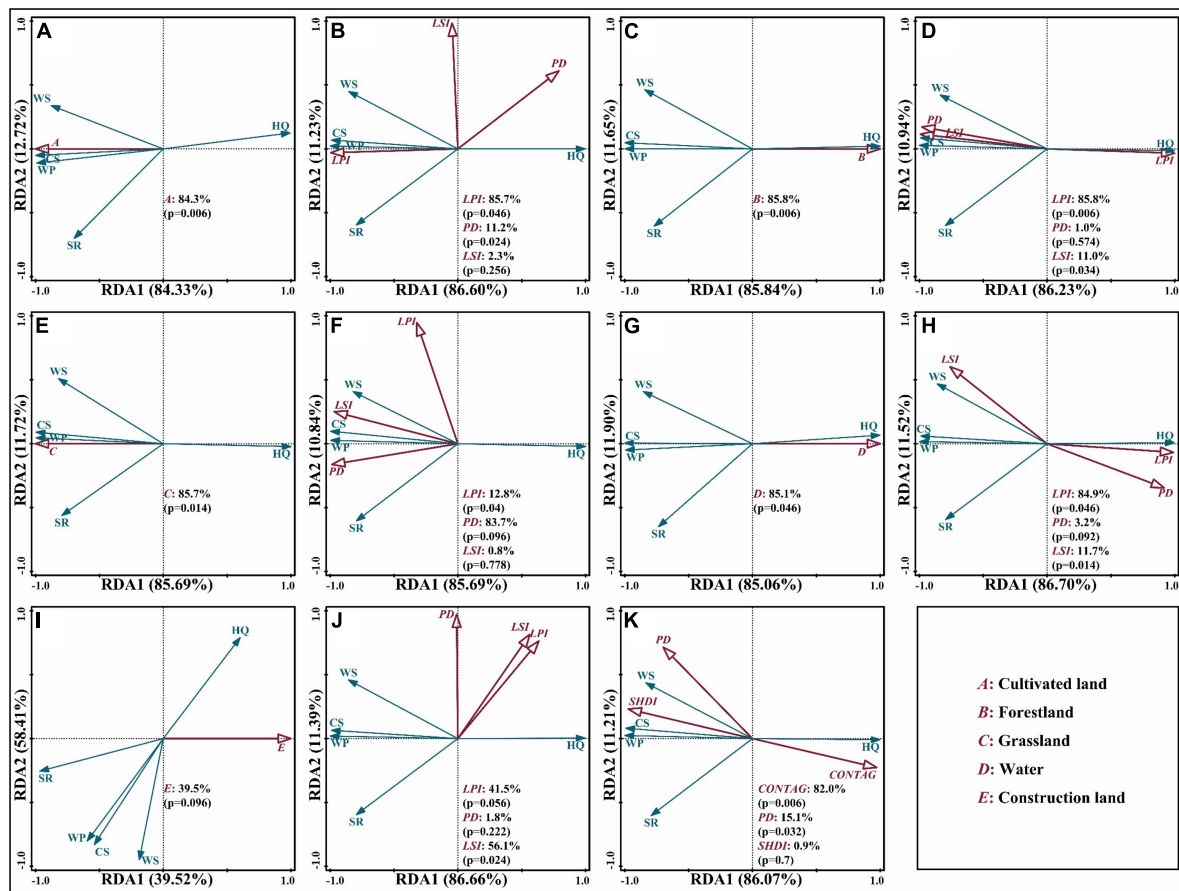


FIGURE 9 Redundancy analysis ranking chart. (A) cultivated land area; (B) landscape indices of cultivated land; (C) forestland area; (D) landscape indices of forestland; (E) grassland area; (F) landscape indices of grassland; (G) water area; (H) landscape indices of water; (I) construction land area; (J) landscape indices of construction land; (K) landscape indices at landscape level. WS, water supply; WP, water purification; CS, carbon storage; SR, soil retention; HQ, habitat quality; PD, patch density; SHDI, Shannon’s diversity index; CONTAG, contagion; LPI, largest patch index; LSI, landscape shape index.

4. Discussion

4.1. Responses of ESVs to landscape pattern changes

The period 2000–2020 is a period of more pronounced changes in landscape patterns and ESVs of HTRNP, the landscape pattern changes in the four landscape types of cultivated land, forestland, grassland, and water had significant effects on the three types of ESVs: WP, CS, and HQ.

For WP’s ESV, the increases in areas and landscape dominance of both forestland and water had adverse inhibitory effects on WP’s ESV. As mentioned previously, the WP’s ESV in HTRNP is strongly influenced by loads of TN and TP, from which it can be inferred that the decrease of WP’s ESV may be related to the decrease of the total load. Different landscape types have different TN and TP loads per unit area: water has less TN and TP loads per unit area than cultivated land, and forestland has less TN and TP loads per unit area than grassland. During 2000–2010, as a result of the Daguangba Reservoir construction and tropical economic forest planting (Han et al., 2022; Li A. et al., 2022), cultivated land was

converted to water mainly in the northwestern region in the form of aggregated large patches, and grassland was converted to forestland mainly in the southeastern region in the form of scattered small patches, resulted in increases in the areas and landscape dominance of both water and forestland (Figure 10A), and the decrease in total loads that was greater than the decrease in total exports, which ultimately led to the decrease in WP’s ESV.

The response of CS’s ESV to the landscape pattern changes was similar to that of WP’s ESV. Although the expansion of forestland has driven CS growth, it was insufficient to compensate for the loss of CS due to the shrinkage of cultivated land and grassland. Thus, the CS’s ESV showed a slightly decreasing trend.

The increases in areas and landscape dominance of forestland and water significantly affected HQ’s ESV. As their areas and landscape dominance increased, the landscape connectivity in HTRNP was enhanced, promoting the formation of intact habitats. Thus, the HQ’s ESV showed an increasing trend.

For HTRNP, although the decreases in cultivated land area and its LPI, grassland area and its PD led to the decrease of WP’s ESV, from a macro perspective, it reduced the water purification pressure of HTRNP. This finding is consistent with the conclusion of Xia et al. (2021). The areas and LPIs of forestland and water showed

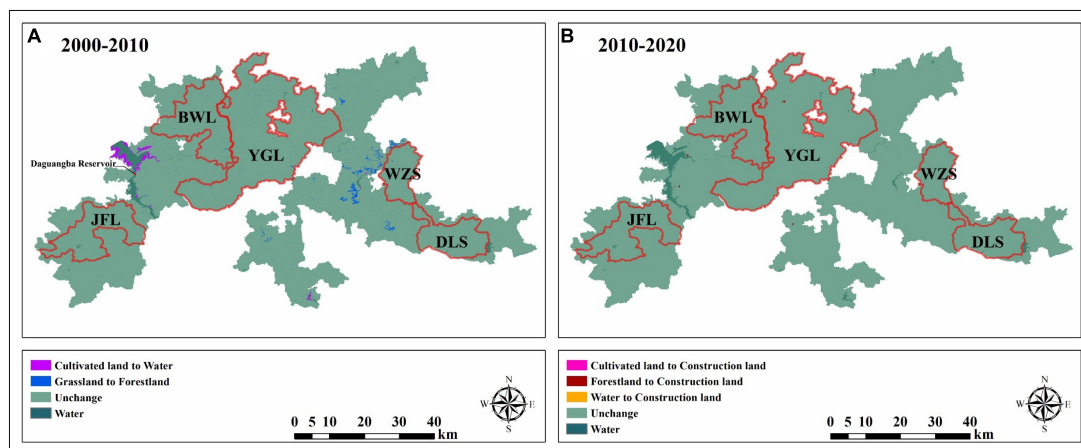


FIGURE 10

Spatial changes in landscape types of HTRNP. (A) Spatial changes in landscape types during 2000–2010; (B) spatial changes in landscape types during 2010–2020. JFL, Jianfengling; YGL, Yinggeling; BWL, Bawangling; WZS, Wuzhishan; DLS, Diaoluoshan.

significant positive driving effects on HQ's ESV, cultivated land area and LPI, grassland area and PD showed significant adverse inhibitory effects on HQ's ESV. These findings are consistent with the conclusions of Dai et al. (2019) and Mandal and Chatterjee (2021).

For WS's ESV, the increases in areas and landscape dominance of both forestland and water had adverse inhibitory effects, resulting in a decrease in WS's ESV. This may be related to the difference in the ability of different landscape types to intercept surface runoff: the water yield of cultivated land and grassland is generally more significant than that of water and forestland because their ability to impound surface runoff is weaker than that of water and forestland (Li A. et al., 2022). Therefore, WS's ESV tended to decrease with the conversion of cultivated land to water and grassland to forestland. In 2010, the construction of International Tourism Island in Hainan Province was officially elevated to a national strategy, converting some forestland to construction land in HTRNP (Li, 2022). For SR's ESV, the increase in the area and the shape complexity of construction land after 2010 had a slightly significant negative inhibitory effect on SR's ESV. However, the effect degree was limited, which may be related to its small expansion scale (Figure 10B). In addition, the increasing fragmentation of cultivated land also had a slightly significant negative inhibitory effect on the SR's ESV, which is consistent with the conclusion of Xia et al. (2021). This may be due to the increased soil erosion caused by cultivated land fragmentation (Mitchell et al., 2015). Compared with other ESs, the factors affecting WS and SR services are more comprehensive and complex, these two ESs are not only affected by the landscape pattern changes but also related to various factors such as precipitation and topography, so the responses of these two ESVs to the landscape pattern changes were not very significant (Rao et al., 2013).

At the overall landscape level, the increase in CONTAG had a significant positive driving effect on HQ's ESV. PD showed a negative correlation with HQ's ESV, similar to the conclusion of Zhang et al. (2022). As the basal landscape type of HTRNP, the changes of forestland had a certain degree of guiding effect on the overall landscape pattern changes of HTRNP. As the scale, dominance, aggregation, and connectivity of the forestland have

increased over the past 40 years, the aggregation and connectivity of the landscape in HTRNP have increased, which promoted the improvement of the biological HQ in the park. Due to the guiding effect of forestland's landscape changes, the increase in CONTAG had adverse inhibitory effects on the ESVs of WP, CS, WS, and SR to varying degrees, similar to the conclusions of Ma et al. (2022).

4.2. Implications for ecosystem management in HTRNP

Rubber plantations are often an essential economic source in tropical regions of China, especially for people living near ecological reserves. However, expanding plantations may pose a potential threat to landscape connectivity. The conclusions of Liu et al. (2017) and Hu et al. (2021) for the Xishuangbanna tropical rainforest region are broadly consistent. I.e., the rapid expansion of plantations has led to a significant decline in landscape connectivity, with significant negative impacts on ESVs. The rubber industry is also one of the main economic pillars of Hainan Province, and some plantations are distributed in the HTRNP. In order to improve the economic conditions of the residents, the scales of plantations were expanded, resulting in some scattered grassland patches in the park being invaded by rubber forests. However, from the overall results, the expansion of these plantations did not significantly affect the landscape connectivity of HTRNP, which may be related to the enhancement of local ecosystem protection and the improvement of conservation methods: the five NNRs of BWL, JFL, WZS, DLS, and YGL were established successively, which further strengthened the protection of ecosystem within the scope of the reserves. Thus, even from 2000 to 2010, there were no significant changes in landscape patterns within these five NNRs (Figure 10A); "The Hainan Tropical Rainforest National Park System Pilot Program" adopted in 2019 had connected these five NNRs into a single piece, initially establishing a relatively complete HTRNP system. The implementation of these conservation policies is the main reason for the maintenance of HTRNP's landscape connectivity. These conservation measures should be maintained and improved in the

future management of the park's ecosystems. Rubber plantation is still one of the primary economic sources to maintain the residents' survival. Its expansion trend may continue in the short term. The areas of low importance and unavailable for wildlife in the park should be the leading site for future plantation expansion (Liu et al., 2017), and the expansion scale should be strictly restricted.

Based on the results of this study, it can be surmised that: if the cultivated land area expands in the form of large patches and the grassland area expands in the form of scattered small patches, the water purification pressure of HTRNP will increase, which is not conducive to the sustainable development of its ecosystems. For HTRNP, WP's ESV is more suitable as a negative indicator to monitor nitrogen and phosphorus loads. As the primary source of nitrogen and phosphorus loads, controlling the cultivated land patch size within a reasonable range is necessary. We proposed to gradually convert some unproductive cultivated land into grassland or forestland, which will not only reduce the pressure of water purification in the park but also help to enhance the connectivity and integrity of grassland and forestland, thus improving the ESVs of CS and HQ; some of the retained cultivated land can be converted to increase the CS in the soil through conservation tillage with cover crops, which will also help to improve the CS's ESV (Martín et al., 2016). In addition, controlling the conversion of cultivated land to water, reducing the size of construction land patches, and the complexity of their shapes will help to curb the decline of both WS and SR ESVs to some extent.

Hainan is a province based on ecology. The construction of HTRNP is not only one of the landmark projects of Hainan Province to promote the construction of the national ecological civilization pilot zone but also a concrete practice to explore the path of transforming clear waters and green mountains into mountains of gold and silver for realization. The monetization of ES helps people to link ES with human well-being better and raise awareness and attention to ES. In recent years, assessments on the Gross Ecosystem Product (GEP) of the HTRNP have been gradually conducted. Chen et al. (2021) conducted a preliminary assessment of the HTRNP's GEP in 2019. In 2023, Hainan Province launched the construction of the HTRNP's ecosystem positioning observation network system, aiming to meet the construction needs of HTRNP further. Since the HTRNP was officially selected as one of the first five national parks in China in 2021, the conservation effectiveness of the ecosystem in the park and its ES benefits have received increasing attention. This study analyzed the spatial-temporal changes of five essential ESs in HTRNP over the past 40 years. And revealed the responses of ESVs to landscape pattern changes, further complementing and improving the related studies on the HTRNP. The results can provide some references for future ecosystem management and optimization to improve the overall ES benefits of the HTRNP continuously.

4.3. Limitations and perspectives

The diversity of ES assessment methods, the subjectivity of parameter selection, and the multi-source nature of the data are the main influencing factors that lead to different ES assessment results for the same region in many studies. For example, in the

CS assessment, some studies have reached different conclusions on CS services in Hainan Island, Ren et al. (2014) suggested that these differences may be related to some factors, such as the different methods of CS calculation adopted by the studies and the different carbon concentration factors used (Wang et al., 2001; Cao et al., 2002). Other ES assessments, such as WS, WP, SR, and HQ, are also affected by similar factors. In addition, there are similar problems with the ESVs' assessments: Lei et al. (2020) used the revised unit area value equivalent factor method to assess the ESVs of Hainan Island during 1980–2018, which differed significantly from Xie et al. (2015). In this study, relevant parameters were selected and set using the relevant studies on the HTRNP and its neighboring regions as the primary reference to maximize the closeness of the assessment results to the actual situation of HTRNP. However, as the construction of the national park in China is at an initial stage, there are few studies for reference on ESs of HTRNP. The setting of relevant parameters is mainly based on studies in neighboring regions, inevitably resulting in discrepancies between the research results and the actual situation. Besides, this study used first-class landscape types to assess the ESs. The results may be slightly rough. Therefore, the landscape types of HTRNP need to be further refined in subsequent studies. For example, its landscape types can be divided into evergreen broad-leaved forests, deciduous broad-leaved forests, etc., to further explore the differences in ESs supply capacity among different plant cover types.

5. Conclusion

This study analyzed the changes of landscape patterns, ESs, and ESVs in the HTRNP during 1980–2020 and further explored the responses of ESVs to the landscape pattern changes. The results revealed that:

1. Forestland is the most dominant landscape type in HTRNP, followed by grassland. The landscape pattern changed significantly after 2000, with the conversions of cultivated land to water in the form of large patches and grassland to forestland in the form of scattered small patches, the landscape dominance and connectivity of both forestland and water increased, and the overall landscape agglomeration and connectivity tended to increase.
2. WS, WP, CS, and SR services tended to weaken, and HQ service tended to strengthen. The spatial heterogeneities of WS and SR changed significantly over time. The four ESVs of WS, HQ, SR, and CS are the main contributors to the total ESV of HTRNP. Over the past 40 years, the four ESVs of WS, WP, SR, and CS showed a decreasing trend; the HQ's ESV tended to increase; and the total ESV tended to decrease.
3. With the transfer of some cultivated land patches and grassland patches to water and forestland in different forms, respectively, the areas and dominance of both forestland and water tended to increase, which was the main reason that HQ's ESV tended to increase, and WP's ESV and CS's ESV tended to decrease. The construction land scale was relatively small, so its impacts on ESVs were limited. The responses of both WS's ESV and SR's ESV to the landscape pattern changes were not very significant due to topographic and climatic factors.

Data availability statement

The original contributions presented in this study are included in the article/**Supplementary material**, further inquiries can be directed to the corresponding author.

Author contributions

XL and HF: conceptualization and methodology. XL: software, formal analysis, and writing—original draft preparation. HF: writing—review and editing, supervision, and funding acquisition. Both authors had read and agreed to the published version of the manuscript.

Funding

This research was funded by the Hainan Provincial Natural Science Foundation of China (Grant No. 421MS015).

References

- Arowolo, A. O., Deng, X., Olatunji, O. A., and Obayelu, A. E. (2018). Assessing changes in the value of ecosystem services in response to land-use/land-cover dynamics in Nigeria. *Sci. Total Environ.* 636, 597–609. doi: 10.1016/j.scitotenv.2018.04.277
- Aryal, K., Maraseni, T., and Apan, A. (2022). How much do we know about trade-offs in ecosystem services? A systematic review of empirical research observations. *Sci. Total Environ.* 806:151229. doi: 10.1016/j.scitotenv.2021.151229
- Ayensu, E., Van Claassen, D. R., Collins, M., Dearing, A., Fresco, L., Gadgil, M., et al. (1999). International ecosystem assessment. *Science* 286, 685–686.
- Barlow, J., França, F., Gardner, T. A., Hicks, C. C., Lennox, G. D., Berenguer, E., et al. (2018). The future of hyperdiverse tropical ecosystems. *Nature* 559, 517–526. doi: 10.1038/s41586-018-0301-1
- Baude, M., Meyer, B. C., and Schindewolf, M. (2019). Land use change in an agricultural landscape causing degradation of soil based ecosystem services. *Sci. Total Environ.* 659, 1526–1536. doi: 10.1016/j.scitotenv.2018.12.455
- Campbell, E. T., and Tilley, D. R. (2014). The eco-price: How environmental emery equates to currency. *Ecosyst. Serv.* 7, 128–140. doi: 10.1016/j.ecoser.2013.12.002
- Cao, J., Zhang, Y., and Liu, Y. (2002). Changes in forest biomass carbon storage in Hainan Island over the last 20 years. *Geogr. Res.* 21, 551–560. doi: 10.11821/yj2002050003
- Cen, X. (2016). *Correlation analysis and optimization between land use landscape patterns and ecosystem service values – a case study of South Coast of Hangzhou Bay*. Ph.D. thesis. Hangzhou: Zhejiang University.
- Chen, W., Zhao, H., Li, J., Zhu, L., Wang, Z., and Zeng, J. (2020). Land use transitions and the associated impacts on ecosystem services in the Middle Reaches of the Yangtze River Economic Belt in China based on the geo-informatic Tupu method. *Sci. Total Environ.* 701:134690. doi: 10.1016/j.scitotenv.2019.134690
- Chen, Z.-Z., Lei, J.-R., Wu, T.-T., Chen, D.-X., Zhou, Z., Li, Y.-L., et al. (2021). Gross ecosystem product accounting of national park: Taking Hainan Tropical Rainforest National Park as an example. *J. Appl. Ecol.* 32, 3883–3892. doi: 10.13287/j.1001-9332.202111.010
- Costanza, R., d'Arge, R., De Groot, R., Farber, S., Grasso, M., Hannon, B., et al. (1997). The value of the world's ecosystem services and natural capital. *Nature* 387, 253–260.
- Cuni-Sanchez, A., Imani, G., Bulonvu, F., Batumike, R., Baruka, G., Burgess, N. D., et al. (2019). Social perceptions of forest ecosystem services in the Democratic Republic of Congo. *Hum. Ecol.* 47, 839–853. doi: 10.1007/s10745-019-00115-6
- Dai, L., Li, S., Lewis, B. J., Wu, J., Yu, D., Zhou, W., et al. (2019). The influence of land use change on the spatial-temporal variability of habitat quality between 1990 and 2010 in Northeast China. *J. For. Res.* 30, 2227–2236. doi: 10.1007/s11676-018-0771-x
- De Groot, R., Brander, L., Van Der Ploeg, S., Costanza, R., Bernard, F., Braat, L., et al. (2012). Global estimates of the value of ecosystems and their services in monetary units. *Ecosyst. Serv.* 1, 50–61. doi: 10.1016/j.ecoser.2012.07.005
- Fairhead, J., Leach, M., and Scoones, I. (2012). Green grabbing: A new appropriation of nature? *J. Peasant Stud.* 39, 237–261.
- Fan, Z., and Li, W. (2020). Research on the realization mechanism of ecological product value—a case study of Guizhou Province. *J. Hebei Geo. Univ.* 43, 82–90. doi: 10.3390/ijerph19105892
- Fang, F., Chen, Y., Liang, J., and Fu, X. (2013). Construction benefit evaluation of coastal shelter forest system in Hainan province. *J. Central South Univ. For. Technol.* 33, 115–119. doi: 10.1016/j.ecolind.2022.109119
- Fang, Z., Bai, Y., Jiang, B., Alatalo, J. M., Liu, G., and Wang, H. (2020). Quantifying variations in ecosystem services in altitude-associated vegetation types in a tropical region of China. *Sci. Total Environ.* 726:138565. doi: 10.1016/j.scitotenv.2020.138565
- Ge, Y. (2020). *Evolution and optimization of green space pattern in the second green belt of Beijing municipality area based on ecosystem services evaluation*. Ph.D. thesis. Beijing: Beijing Forestry University.
- Gong, W., Duan, X., Sun, Y., Zhang, Y., Ji, P., Tong, X., et al. (2022). Multi-scenario simulation of land use/cover change and carbon storage assessment in Hainan coastal zone from perspective of free trade port construction. *J. Clean. Prod.* 12:135630. doi: 10.1016/j.jclepro.2022.135630
- Guo, Z., Xiao, X., Gan, Y., and Zheng, Y. (2001). Ecosystem functions, services and their values—a case study in Xingshan County of China. *Ecol. Econ.* 38, 141–154. doi: 10.1016/S0921-8009(01)00154-9
- Guswa, A. J., Brauman, K. A., Brown, C., Hamel, P., Keeler, B. L., and Sayre, S. S. (2014). Ecosystem services: Challenges and opportunities for hydrologic modeling to support decision making. *Water Resour. Res.* 50, 4535–4544. doi: 10.1002/2014WR015497
- Han, N., Yu, M., and Jia, P. (2022). Multi-scenario landscape ecological risk simulation for sustainable development goals: A case study on the central mountainous area of Hainan Island. *Int. J. Environ. Res. Public Health* 19:4030. doi: 10.3390/ijerph19074030
- Hernández-Morcillo, M., Plieninger, T., and Bieling, C. (2013). An empirical review of cultural ecosystem service indicators. *Ecol. Indic.* 29, 434–444. doi: 10.1016/j.ecolind.2013.01.013

Conflict of interest

The authors declare that the research was conducted in the absence of any commercial or financial relationships that could be construed as a potential conflict of interest.

Publisher's note

All claims expressed in this article are solely those of the authors and do not necessarily represent those of their affiliated organizations, or those of the publisher, the editors and the reviewers. Any product that may be evaluated in this article, or claim that may be made by its manufacturer, is not guaranteed or endorsed by the publisher.

Supplementary material

The Supplementary Material for this article can be found online at: <https://www.frontiersin.org/articles/10.3389/ffgc.2023.1242068/full#supplementary-material>

- Hoang, N. T., and Kanemoto, K. (2021). Mapping the deforestation footprint of nations reveals growing threat to tropical forests. *Nat. Ecol. Evol.* 5, 845–853. doi: 10.1038/s41559-021-01417-z
- Hou, L., Wu, F., and Xie, X. (2020). The spatial characteristics and relationships between landscape pattern and ecosystem service value along an urban-rural gradient in Xi'an city, China. *Ecol. Indic.* 108:105720. doi: 10.1016/j.ecolind.2019.105720
- Hu, Z., Yang, X., Yang, J., Yuan, J., and Zhang, Z. (2021). Linking landscape pattern, ecosystem service value, and human well-being in Xishuangbanna, southwest China: Insights from a coupling coordination model. *Glob. Ecol. Conserv.* 27:e01583. doi: 10.1016/j.gecco.2021.e01583
- Kemkes, R. J., Farley, J., and Koliba, C. J. (2010). Determining when payments are an effective policy approach to ecosystem service provision. *Ecol. Econ.* 69, 2069–2074. doi: 10.1016/j.ecolecon.2009.11.032
- Kertész, Á., Nagy, L. A., and Balázs, B. (2019). Effect of land use change on ecosystem services in Lake Balaton Catchment. *Land Use Policy* 80, 430–438. doi: 10.1007/s42977-020-00032-6
- Kroeger, T., and Casey, F. (2007). An assessment of market-based approaches to providing ecosystem services on agricultural lands. *Ecol. Econ.* 64, 321–332. doi: 10.1016/j.ecolecon.2007.07.021
- Kubiszewski, I., Costanza, R., Anderson, S., and Sutton, P. (2020). “The future value of ecosystem services: Global scenarios and national implications,” in *Environmental assessments*, ed. K. N. Ninan (Cheltenham: Edward Elgar Publishing). doi: 10.1016/j.ecoser.2017.05.004
- Lawler, J. J., Lewis, D. J., Nelson, E., Plantinga, A. J., Polasky, S., Withey, J. C., et al. (2014). Projected land-use change impacts on ecosystem services in the United States. *Proc. Natl. Acad. Sci. U.S.A.* 111, 7492–7497.
- Legendre, P. (2008). Studying beta diversity: Ecological variation partitioning by multiple regression and canonical analysis. *J. Plant Ecol.* 1, 3–8.
- Lei, J., Chen, Z., Chen, X., Li, Y., and Wu, T. (2020). Spatio-temporal changes of land use and ecosystem services value in Hainan Island from 1980 to 2018. *Acta Ecol. Sin.* 40, 4760–4773. doi: 10.1093/jpe/rtm001
- Lei, J.-R., Chen, Y.-Q., Chen, Z.-Z., Chen, X.-H., Wu, T.-T., and Li, Y.-L. (2022). Spatiotemporal evolution of habitat quality in three basins of Hainan Island based on InVEST model. *J. Appl. Ecol.* 33, 2511–2520. doi: 10.13287/j.1001-9332.202209.019
- Li, A., Ye, C., Zhu, L., Wang, Y., Liang, X., and Zou, Y. (2022). Impact from land use/land cover change on function of water yield service: A case study on National Park of Hainan Tropical Rainforest. *Water Resour. Hydropower Eng.* 53, 36–45. doi: 10.3389/ffgc.2023.1131264/full
- Li, C., Zhao, J., Zhuang, Z., and Gu, S. (2022). Spatiotemporal dynamics and influencing factors of ecosystem service trade-offs in the Yangtze River Delta urban agglomeration. *Acta Ecol. Sin.* 14, 1–13. doi: 10.3390/land12040929
- Li, J., Zhou, K., Xie, B., and Xiao, J. (2021). Impact of landscape pattern change on water-related ecosystem services: Comprehensive analysis based on heterogeneity perspective. *Ecol. Indic.* 133:108372. doi: 10.1016/j.ecolind.2021.108372
- Li, L. (2022). *Analysis of landscape pattern and spatio-temporal change for ecosystem service value in Hainan tropical rain Forest National Park*. Ph.D. thesis. Hainan: Hainan University.
- Li, L., Tang, H., Lei, J., and Song, X. (2022). Spatial autocorrelation in land use type and ecosystem service value in Hainan Tropical Rain Forest National Park. *Ecol. Indic.* 137:108727. doi: 10.1016/j.ecolind.2022.108727
- Liu, J., Chen, Q., Peng, Y., and Hu, X. (2009). Forest ecosystem services and their valuation in the central mountainous areas of Hainan. *Ecol. Econ.* 2, 24–30.
- Liu, P., Li, W., Yu, Y., Tang, R., Guo, X., Wang, B., et al. (2019). How much will cash forest encroachment in rainforests cost? A case from valuation to payment for ecosystem services in China. *Ecosyst. Serv.* 38:100949. doi: 10.1016/j.ecoser.2019.100949
- Liu, Q., Yang, D., Cao, L., and Anderson, B. (2022). Assessment and prediction of carbon storage based on land use/land cover dynamics in the tropics: A case study of Hainan Island, China. *Land* 11:244. doi: 10.3390/land11020244
- Liu, S., Yin, Y., Liu, X., Cheng, F., Yang, J., Li, J., et al. (2017). Ecosystem Services and landscape change associated with plantation expansion in a tropical rainforest region of Southwest China. *Ecol. Model.* 353, 129–138. doi: 10.1016/j.ecolmodel.2016.03.009
- Loomisa, J., Kenth, P., Strangec, L., Fausch, K., and Coviche, A. (2018). “Measuring the total economic value of restoring ecosystem services in an impaired river basin: Results from a contingent valuation survey,” in *Economics of water resources*, eds A. Dinar and Y. Tsur (London: Routledge).
- Ma, S., Wang, L. J., Wang, H. Y., Zhang, X., and Jiang, J. (2022). Spatial heterogeneity of ecosystem services in response to landscape patterns under the Grain for Green Program: A case-study in Kaihua County, China. *Land Degrad. Dev.* 33, 1901–1916. doi: 10.1002/ldr.4272
- Mandal, M., and Chatterjee, N. D. (2021). Spatial alteration of fragmented forest landscape for improving structural quality of habitat: A case study from Radhanagar Forest Range, Bankura District, West Bengal, India. *Geol. Ecol. Landsc.* 5, 252–259.
- Martin, J. R., Álvaro-Fuentes, J., Gonzalo, J., Gil, C., Ramos-Miras, J. J., Corbí, J. G., et al. (2016). Assessment of the soil organic carbon stock in Spain. *Geoderma* 264, 117–125. doi: 10.1016/j.geoderma.2015.10.010
- Millennium Ecosystem Assessment (2005). *Ecosystems and human well-being*, Vol. 5. Washington, DC: Island press.
- Mitchell, M. G., Suarez-Castro, A. F., Martinez-Harms, M., Maron, M., McAlpine, C., Gaston, K. J., et al. (2015). Reframing landscape fragmentation's effects on ecosystem services. *Trends Ecol. Evol.* 30, 190–198. doi: 10.1016/j.tree.2015.01.011
- Navrud, S., and Strand, J. (2018). Valuing global ecosystem services: What do European experts say? Applying the Delphi method to contingent valuation of the Amazon rainforest. *Environ. Resour. Econ.* 70, 249–269. doi: 10.1007/s10640-017-0119-6
- Piponiot, C., Rutishauser, E., Derroire, G., Putz, F. E., Sist, P., West, T. A., et al. (2019). Optimal strategies for ecosystem services provision in Amazonian production forests. *Environ. Res. Lett.* 14:124090.
- Qi, W., Li, H., Zhang, Q., and Zhang, K. (2019). Forest restoration efforts drive changes in land-use/land-cover and water-related ecosystem services in China's Han River basin. *Ecol. Eng.* 126, 64–73.
- Rao, E., Xiao, Y., Ouyang, Z., and Zheng, H. (2013). Spatial characteristics of soil conservation service and its impact factors in Hainan Island. *Acta Ecol. Sin.* 33, 746–755.
- Rao, E., Xiao, Y., Ouyang, Z., and Zheng, H. (2016). Changes in ecosystem service of soil conservation between 2000 and 2010 and its driving factors in southwestern China. *Chin. Geogr. Sci.* 26, 165–173.
- Ren, H., Li, L., Liu, Q., Wang, X., Li, Y., Hui, D., et al. (2014). Spatial and temporal patterns of carbon storage in forest ecosystems on Hainan island, southern China. *PLoS One* 9:e108163. doi: 10.1371/journal.pone.0108163
- Salzman, J., Bennett, G., Carroll, N., Goldstein, A., and Jenkins, M. (2018). The global status and trends of payments for ecosystem services. *Nat. Sustain.* 1, 136–144.
- Schröter, M., Ring, I., Schröter-Schlaack, C., and Bonn, A. (2019). “The ecosystem service concept: Linking ecosystems and human wellbeing,” in *Atlas of ecosystem services*, eds M. Schröter, A. Bonn, S. Klotz, R. Seppelt, and C. Baessler (Berlin: Springer), 7–11.
- Sharp, R., Tallis, H., Ricketts, T., Guerry, A. D., Wood, S. A., Chaplin-Kramer, R., et al. (2016). *InVEST+ VERSION+ User's guide. The natural capital project*. Stanford: Stanford University.
- Sheng, L., Jin, Y., and Huang, J. (2010). Value estimation of conserving water and soil of ecosystems in China. *J. Nat. Resour.* 25, 1105–1113.
- Sun, X., Li, S., Yu, J., Fang, Y., Zhang, Y., and Cao, M. (2019). Evaluation of ecosystem service value based on land use scenarios: A case study of Qianjiangyuan National Park pilot. *Biodivers. Sci.* 27, 51–63.
- Tallis, H., and Kareiva, P. (2005). Ecosystem services. *Curr. Biol.* 15, R746–R748.
- Tallis, H., and Polasky, S. (2009). Mapping and valuing ecosystem services as an approach for conservation and natural-resource management. *Ann. N. Y. Acad. Sci.* 1162, 265–283.
- Turner, M. G. (1987). Spatial simulation of landscape changes in Georgia: A comparison of 3 transition models. *Landsc. Ecol.* 1, 29–36.
- Wang, L., Xiao, Y., Ouyang, Z., Wei, Q., Bo, W., Zhang, J., et al. (2017). Gross ecosystem product accounting in the national key ecological function area. *China Popul. Resour. Environ.* 27, 146–154. doi: 10.13287/j.1001-9332.202111.017
- Wang, X., Feng, Z., and Ouyang, Z. (2001). Vegetation carbon storage and density of forest ecosystems in China. *J. Appl. Ecol.* 12, 13–16. doi: 10.1186/s40663-019-0210-2
- Wang, X., Wang, X., Zhu, M., Wang, W., Liang, Q., Zou, Y., et al. (2017). Carbon storage and economic assessment of the main forest types vegetation in Hainan. *J. Central South Univ. For. Technol.* 37, 92–98. doi: 10.3390/land11020244
- Wang, Y., Li, X., Zhang, Q., Li, J., and Zhou, X. (2018). Projections of future land use changes: Multiple scenarios-based impacts analysis on ecosystem services for Wuhan city, China. *Ecol. Indic.* 94, 430–445. doi: 10.1016/j.ecolind.2018.06.047
- Wang, Z., Mao, D., Li, L., Jia, M., Dong, Z., Miao, Z., et al. (2015). Quantifying changes in multiple ecosystem services during 1992–2012 in the Sanjiang Plain of China. *Sci. Total Environ.* 514, 119–130. doi: 10.1016/j.scitotenv.2015.01.007
- Watson, J. E., Evans, T., Venter, O., Williams, B., Tulloch, A., Stewart, C., et al. (2018). The exceptional value of intact forest ecosystems. *Nat. Ecol. Evol.* 2, 599–610. doi: 10.1038/s41559-018-0490-x
- Williams, J. R. (1995). “The EPIC model,” in *Computer models of watershed hydrology*, ed. V. P. Singh (Denver, CO: Highlands Ranch).
- Xia, H., Kong, W., Zhou, G., and Sun, O. J. (2021). Impacts of landscape patterns on water-related ecosystem services under natural restoration in Liaohe River Reserve, China. *Sci. Total Environ.* 792:148290. doi: 10.1016/j.scitotenv.2021.148290
- Xia, H., Yuan, S., and Prishchepov, A. V. (2023). Spatial-temporal heterogeneity of ecosystem service interactions and their social-ecological drivers: Implications for spatial planning and management. *Resour. Conserv. Recycl.* 189:106767.
- Xiao, H. (1999). Spatial distribution characteristics of soil erosion in Hainan Island by GIS. *Res. Environ. Sci.* 5, 75–80.

- Xiao, Q., Xiao, Y., Ouyang, Z. Y., Xu, W. H., Xiang, S., and Li, Y. Z. (2014). Value assessment of the function of the forest ecosystem services in Chongqing. *Acta Ecol. Sin.* 34, 216–223.
- Xie, G., Zhang, C., Zhang, C., Xiao, Y., and Lu, C. (2015). The value of ecosystem services in China. *Resour. Sci.* 37, 1740–1746. doi: 10.1007/BF02886190
- Xu, X., Liu, J., Zhang, S., Li, R., Yan, C., and Wu, S. (2018). *China's multi-period land use land cover remote sensing monitoring data set (CNLUCC)*. Beijing: Resource and Environment Data Cloud Platform.
- Yang, Y., Li, M., Feng, X., Yan, H., Su, M., and Wu, M. (2021). Spatiotemporal variation of essential ecosystem services and their trade-off/synergy along with rapid urbanization in the Lower Pearl River Basin, China. *Ecol. Indic.* 133:108439. doi: 10.1016/j.ecolind.2021.108439
- Yao, X., Zhou, L., Wu, T., and Ren, M. (2022). Landscape dynamics and ecological risk of the expressway crossing section in the Hainan Rainforest National Park. *Acta Ecol. Sin.* 42, 6695–6703. doi: 10.3390/land12061114
- Yu, B., Rao, E., Chao, X., Shi, J., Zhang, C., Xu, W., et al. (2016). Evaluating the effectiveness of nature reserves in soil conservation on Hainan Island. *Acta Ecol. Sin.* 36, 3694–3702. doi: 10.3390/f14071293
- Yu, M., Jin, H., and Li, Q. (2020). Gross ecosystem product (GEP) accounting for Chenggong District. *J. West China For. Sci.* 49, 41–55.
- Yushanjiang, A., Zhang, F., and Yu, H. (2018). Quantifying the spatial correlations between landscape pattern and ecosystem service value: A case study in Ebinur Lake Basin, Xinjiang, China. *Ecol. Eng.* 113, 94–104. doi: 10.1016/j.ecoleng.2018.02.005
- Zhang, D., Wang, J., Wang, Y., Xu, L., Zheng, L., Zhang, B., et al. (2022). Is there a spatial relationship between urban landscape pattern and habitat quality? Implication for landscape planning of the yellow river basin. *Int. J. Environ. Res. Public Health* 19:11974. doi: 10.3390/ijerph191911974
- Zhang, K., Shu, A., Xu, X., Yang, Q., and Yu, B. (2008). Soil erodibility and its estimation for agricultural soils in China. *J. Arid Environ.* 72, 1002–1011. doi: 10.1016/j.jaridenv.2007.11.018
- Zhang, W., and Fu, J. (2003). Rainfall erosivity estimation under different rainfall amount. *Resour. Sci.* 25, 35–41.
- Zhe, W., Xin, C., Beibei, L., Jinfeng, C., and Lixu, P. (2013). Risk assessment of nitrogen and phosphorus loads in Hainan Island based on InVEST model. *Chin. J. Trop. Crops* 34, 1791–1797. doi: 10.3390/su142114344
- Zheng, H., Wang, L., Peng, W., Zhang, C., Li, C., Robinson, B. E., et al. (2019). Realizing the values of natural capital for inclusive, sustainable development: Informing China's new ecological development strategy. *Proc. Natl. Acad. Sci. U.S.A.* 116, 8623–8628. doi: 10.1073/pnas.1819501116



OPEN ACCESS

EDITED BY

Janette Bulkan,
University of British Columbia, Canada

REVIEWED BY

Olutosin Ademola Otekunrin,
Federal University of Agriculture, Abeokuta,
Nigeria

*CORRESPONDENCE

Yaqing Han
✉ hanyaqing306@163.com

RECEIVED 27 February 2023

ACCEPTED 31 July 2023

PUBLISHED 11 August 2023

CITATION

Han Y, Wang Q and Wei Y (2023) Are farmers willing to enter the forestry property market? Evidence from collective forest areas in southern China.
Front. For. Glob. Change 6:1147233.
doi: 10.3389/ffgc.2023.1147233

COPYRIGHT

© 2023 Han, Wang and Wei. This is an open-access article distributed under the terms of the [Creative Commons Attribution License \(CC BY\)](https://creativecommons.org/licenses/by/4.0/). The use, distribution or reproduction in other forums is permitted, provided the original author(s) and the copyright owner(s) are credited and that the original publication in this journal is cited, in accordance with accepted academic practice. No use, distribution or reproduction is permitted which does not comply with these terms.

Are farmers willing to enter the forestry property market? Evidence from collective forest areas in southern China

Yaqing Han^{1,2*}, Qiangqiang Wang³ and Yuanzhu Wei²

¹Fujian Social Science Research Base, Financial Risk Management Research Center of Fujian Jiangxia University, Fuzhou, China, ²Research Center for Targeted Poverty Alleviation and Poverty Relapse Prevention, Ningde Normal University, Ningde, China, ³College of Economics and Management, Fujian Agriculture and Forestry University, Fuzhou, China

The Chinese government encourages farmers to enter the forestry property market for forestry property trading and promotes the standardization of the forestry property trading market. Unfortunately, the development of the forestry property market is still very slow. Farmers are the most important subject of mountain and forest management and the micro foundation of forestry property market operation, and their active market participation is the key to the healthy development of forestry property market. Based on the theory of planned behavior, this paper used the survey data of farmers in collective forest areas in three southern provinces of China to reveal the psychological decision-making process of farmers entering the forestry property market by structural equation model (SEM). The research results show that: (1) Farmers' behavioral attitudes (AB), subjective norms (SN) and perceptual behavioral control (PBC) positively influence farmers' willingness to enter the forestry property market. (2) An important reason why farmers' intentions are largely not effectively translated into behavior is the constraint of PBC. (3) Reducing the risk of transfer and maintaining the interests of both parties constitute the main factors of AB, and the greatest external pressure on farmers' willingness to enter the forestry property market comes from the opinions of village collectives. (4) PBC has a significant impact on behavior, where unfamiliarity with the forestry property market is the main factor affecting farmers' PBC. Therefore, the government should further strengthen the propaganda of forestry property right market, improve the market service system, reduce the transaction cost, introduce specific encouragement policies and measures, and effectively consider farmers' interest demands on forestry property trading; in addition, the power of grassroots organizations should be emphasized when formulating forestry property trading policies.

KEYWORDS

forestry property market, theory of planned behavior, farmers' market participation, farmers behavior, structural equation model

1. Introduction

In 2003, the Chinese government launched a new round of reform of the collective forestry rights system, granting farmers the right to use, dispose of and earn income from forest land, and implementing related supporting measures, including issuing forestry property rights certificates and establishing a forestry property market

(Chen and Innes, 2013). As the first province of forestry reform, Fujian took the lead in establishing the Yongan Forestry Element Market. Subsequently, other provinces have also started to build regional forestry property markets. Different provinces have different names for the forestry property market, such as “forestry element market,” “forest rights trading center” and “rural property market,” but their basic functions are the same. The forestry property market is a comprehensive platform for forestry property transactions, where all administrative and financial functions related to forestry activities can be realized, such as forestry property transactions, forest property rights registration, and forestry property mortgage (Yang and Ming, 2006). The establishment of the forestry property market can, on the one hand, promote the flow of property rights of mountain and forest resources to reorganize and revitalize forest resources, and on the other hand, facilitate direct face-to-face negotiations and transactions between the two sides of forestry property transactions (Wang et al., 2007). This not only eliminates many intermediate links in the transaction process, but also reduces the cost of forest rights transactions and the probability of forest rights disputes, and protects the property rights interests of farmers. In addition, the trading platform can also provide relevant consulting services for both parties (Lin et al., 2022a). The forestry property market plays a bridge role in collective forestry property trading activities, which is of great significance to improving the rural property rights trading market.

China has introduced many policies to encourage farmers and other forestry operators to trade on the forest rights trading market. However, the establishment of a sound market system for forest rights trading requires not only state support and policy promotion, but also active market participation by farmers. The majority of farmers is the most important subject of mountain and forest management, and is also the micro-foundation of forestry property market operation. Farmers’ market participation and forestry property market development are interrelated and mutually constrained, and what kind of attitude do farmers have toward forestry property market? Are they willing to enter a more secure and regulated forestry property market when conducting forestry rights transactions? What factors will influence their willingness and behavior? At present, scholars have paid less attention to these questions, and answering the above questions will help promote the healthy and standardized operation and sustainable development of forestry property markets.

At present, scholars have conducted rich research on the issues related to the forestry property market from different research perspectives. From the aspect of institutional guarantee, scholars mainly study the development of the forestry property market from the aspects of market development, institutional design, government function, and legal improvement (Kong and Du, 2008; Xu et al., 2020; Lin et al., 2022b), and believe that a mature forestry property trading market should be diversified in terms of flowing subjects and forms, and have developed intermediary organizations and a perfect policy and legal environment (Xie et al., 2014). From a functional point of view, the forestry property rights system has deficiencies and blind spots, insufficient specification of the system, coordination to be strengthened, and an imperfect matching of the system (Aggarwal et al., 2021). And, based on the process of forestry property transaction, the paper proposes the development and improvement of the government supervision system of forestry property transfer (Xu et al., 2013). In terms of farmers’ behavior,

scholars mainly focus on farmers’ transfer transaction behavior and influencing factors. In terms of the characteristics of farmers’ subjects, they mainly focus on individual characteristics, family characteristics, and factors of forest land resource endowment, etc (Feng and Heerink, 2008; Li, 2011; Tang and Wang, 2013; Deng et al., 2019; Li et al., 2020). A few scholars have also studied other aspects, for example, some scholars have confirmed that transaction costs are an important constraint to agricultural land transfer through the analysis of farm household survey data (Jin and Deininger, 2009; Li and Ito, 2021). In addition, property rights arrangement, risk perception also affects farmers’ land transfer behavior (Deininger et al., 2014; Li et al., 2014; Cheng et al., 2019; Xu et al., 2021). Other scholars argue that factors such as the number of land plots and the accessibility of transportation networks also affect the transfer of agricultural land (Jiang et al., 2019). In addition, some scholars have observed that these studies are based on the assumption that “the objective facts faced by farmers are the basis for their decisions,” but in fact, the decisions made by farmers are based on their cognitive trade-offs, because farmers’ decisions are not only influenced by external objective factors, but also subjective cognitive constraints formed by farmers under specific circumstances (Shi et al., 2022).

In addition, many studies have focused on the application of the theory of planned behavior (TPB) to the behavioral decisions of farm households. TPB is one of the most influential behavior prediction theories in the field of social psychology. Ajzen and Madden (1986) proposed that behavioral attitudes (AB), subjective norms (SN), and perceived behavioral control (PBC) can help predict and explain behavioral intentions (BI) and thus influence individual behavior. As a successful application of the limited rationality assumption of behaviorist psychology to economics, TPB introduces psychological analysis to the study of economic behavior by incorporating individuals’ multidimensional behavioral motivations (including earnings maximization, emotional satisfaction, and social approval) into behavioral explanations and predictions (Chen, 2022). Due to the close relationship between agricultural decision making and social psychology, agricultural economists and social psychologists have widely applied TPB to agricultural research, effectively solving the problem of limited rationality in farmers’ decision making (Yang et al., 2022). This theory has been applied by scholars in various countries to explain cognition and behavior of farmers toward agricultural reform (Donati et al., 2015), homestead transfer (Lu et al., 2022), sustainable agriculture (Sarkar et al., 2022), ecological protection (Yaghoubi Farani et al., 2019), etc. And the significant effects of variables such as perceived benefits, perceived risks, and perceived fairness (Deng et al., 2022) on behavioral attitudes have been confirmed with different cases. Clearly, TPB is a valid analytical framework for supporting research related to sustainable behavior, and there is sufficient evidence that it is feasible in the study of most behaviors (Xie et al., 2013). In this way, the TPB provides a thorough understanding of the formation of the mechanisms of farmers’ willingness to enter the forestry property markets.

The above research results have important theoretical value and practical significance for guiding farmers’ forestry property transfer behavior and regulating the forestry property market. However, there are still two shortcomings in the existing research: firstly, it focuses on whether farmers have property rights trading behavior and the influence of various factors on property rights trading

behavior, but pays less attention to whether farmers are willing to enter the forestry property market for trading; secondly, it is insufficient to analyze the path of transforming farmers' behavior will into actual behavior. In view of this, this paper empirically analyzes the psychological decision-making process of farmers' entry into the forestry property market using farm household survey data under the framework of the theory of planned behavior (TPB) using structural equation modeling (SEM) with three provinces in the collective forestry region of southern China as the study area. It also compares behavioral attitudes, subjective norms and perceptual behavioral controls and their effects on farmers' entry into the forestry property market to better understand the determinants of farmers' behavioral intentions. The research results provide scientific references and policy recommendations for regulating the order of forestry property transactions and promoting the construction of a forestry property market.

2. Theoretical framework and research hypothesis

2.1. Analytical framework construction

The theory of planned behavior (TPB), derived from social psychology, is dedicated to the study of conscious human behavior, and is an important tool for explaining the logical relationship between "cognition-will-behavior" and action (Ajzen, 2020), and provides a complete theoretical and analytical framework for the study of the role of human psychological cognition on behavior. It uses latent variables to construct behavioral determinants, stating that an individual's specific behavior is determined by his behavioral intention (BI), which is influenced by a combination of individual psycho-cognitive factors, namely behavioral attitudes (AB), subjectivity norms (SN), and perceived behavioral control (PBC) (Ajzen, 1991). This paper introduces the theory of planned behavior into the scenario of farmers' forestry property transactions, explores the psychological factors and driving mechanisms of farmers' willingness to enter the forestry property market, and explains the decision-making process of farmers' behavior through the theory of planned behavior. Several scholars have researched and confirmed that the theory of planned behavior can significantly improve the explanatory power and prediction of behavioral intentions in research (Wauters et al., 2010; Borges et al., 2014; Schroeder et al., 2015; Hall et al., 2019). Therefore, based on the theory of planned behavior, we construct a psychological decision model for farmers to enter the forestry property market from three psychological cognitive factors: behavioral attitudes, subjective norms and perceptual behavioral control. The specific model structure is shown in [Figure 1](#).

2.2. Theoretical analysis and research hypothesis

2.2.1. Behavioral attitude

The natural motivation for the formation of subjective behavior is formed through the individual's knowledge, analysis, and judgment of external or internal things, which is a psychological

cognitive process (Biddle et al., 1994). The theory of planned behavior defines behavioral attitudes as general and stable subjective evaluations with distinct tendencies that behavioral individuals hold about performing a behavior (Ajzen and Fishbein, 2008). Many current studies on farm household behavior consider behavioral attitudes as the single most important predictor variable (Deng et al., 2016; Wang et al., 2019). In this paper, we define behavioral attitude as farmers' perceptions of the necessity of entering the forestry property market and their perceptions of their main responsibility when they make forestry property transactions. This is reflected in three aspects: perceived benefits, perceived risks, and perceived utility, i.e., farmers weigh the benefits and risks of entering the forestry property market when making decisions on forestry property transactions. Based on this, we measure farmers' behavioral attitudes toward the forestry property market by six indicators: "farmers believe that entering the forestry property market can improve the efficiency of forestry property transactions and reduce costs (AB1)," "reduce the risk of forestry property transfer (AB2)," "help achieve open, fair and just forestry property transactions (AB3)," "protect the legal rights and interests of both parties to the transactions (AB4)," "help reduce the occurrence of forestry property disputes (AB5)," and "help promote scale management and optimal allocation of production factors (AB6)." Theoretically, farmers' good perceptions of forestry property market in terms of reducing transaction costs and risks and safeguarding the legal rights and interests of both parties to the transaction can increase farmers' willingness to enter the forestry property market. Therefore, this paper proposes hypothesis 1.

H1: Behavioral attitudes (AB) have a significant positive effect on farmers' willingness to enter the forestry property market (PW).

2.2.2. Subjective norms

Subjective norms refer to the individual's subjective judgment on whether other important relations will agree with him to perform a certain behavior, that is, the pressure on an individual to perform a certain behavior (Ajzen and Fishbein, 1977). In simple terms, the subjective norms of the actor are mainly derived from the perceived social norms and the behavioral patterns of the reference population. Park (2000) and Lam et al. (2003) jointly suggest that perceived pressure from social norms and group behavior is more pronounced in the Chinese cultural context, where behavioral norms reinforce the individual's avoidance of criticism and desire to gain recognition through social integration (Park, 2000; Lam et al., 2003). This is even more evident in rural China, which still retains the characteristics of "acquaintance society." In this study, subjective norms are defined as the social normative pressures and governmental constraints that farmers feel when trading forestry property through forestry property markets. When farmers recognize that important people or organizations around them (e.g., family members, village collectives, forestry departments, etc.) support their choice of forestry property markets for trading, they are likely to adopt their opinions to fit the expectations of the surrounding groups and the needs of social development. In addition, the reference to other farmers' norms is also a psychological effect of farmers' own conformity to group behavior to avoid being a "special case." Therefore, this paper

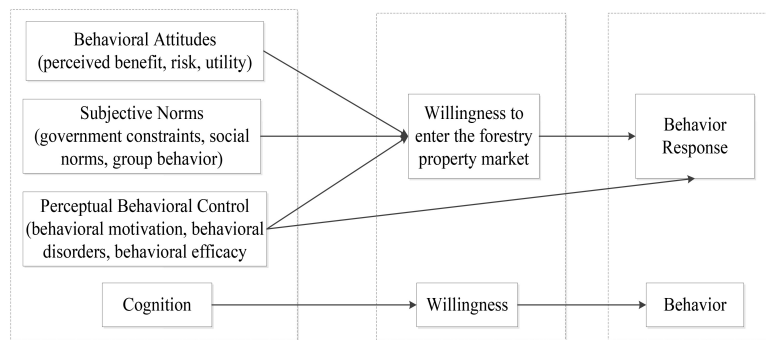


FIGURE 1
Psychological decision model for farmers to enter the forestry property market.

defines the subjective norms of farmers as three factors from social normative pressure, governmental constraint pressure, and group behavior reference. Specifically, the subjective norms are measured by four indicators: “the village collective believes that it should enter the forestry property market for trading (SN1),” “the government or forestry department believes that it should enter the forestry property market for trading (SN2),” “neighboring farmers believe that it should enter the forestry property market for trading (SN3),” and “family members believe that it should enter the forestry property market for trading (SN4).” Usually, the stronger the external pressure felt by farmers, the stronger their willingness to enter the forestry property market for forestry property trading. Therefore, this paper proposes hypothesis 2.

H2: There is a significant positive effect of subjective norms (SN) on farmers’ willingness to enter the forestry property market (PW).

2.2.3. Perceptual behavior control

Ajzen (1991) added perceptual behavioral control to the theory of rational behavior in order to overcome the unreasonable assumption of the individual’s full capacity to act, as a way to reflect the influence of external conditions on the acting subject. Since external behavioral conditions are often difficult to measure directly, he further proposed to characterize the behavioral control situation as perceived by the actor. Behavioral control perceptions are mainly expressed as self-efficacy (Conner and Armitage, 1998), which is the farmer’s perception of the extent of control of his own will and ability. In layman’s terms, this refers to the perception of relevant factors that facilitate or hinder behavioral effects, including three aspects of perceived behavioral motivation, behavioral barriers, and behavioral efficacy (Fishbein and Ajzen, 2011). Self-efficacy reflects the perceived facilitative conditions or implementation barriers that facilitate or hinder farmers’ willingness to enter the forestry property market to some extent. Therefore, this paper measures perceptual behavior control by five indicators: “farmers have sufficient tolerance for forestry property trading risks (PBC1),” “unfamiliarity with the forestry property market processes affects my entry into trading (PBC2),” “the state has good supporting policies (PBC3),” “the degree of regulation of the forestry property trading market (PBC4),” and

“the degree of difficulty in obtaining trading information (PBC5).” If farmers’ perceptual behavioral control is stronger, it means that farmers perceive greater social utility from entering the forestry property market, i.e., higher self-efficacy, and farmers are more inclined to enter forestry property market. Therefore, this paper proposes the following research hypothesis.

H3: Perceived behavioral control (PBC) has a significant positive effect on farmers’ willingness to enter the forestry property market (PW).

H4: Perceived behavioral control (PBC) has a significant positive effect on farmers’ behavior to enter the forestry property market (PB).

3. Materials and methods

3.1. Data collection

The data in this study were derived from the survey of farmers in three southern collective forest areas in Fujian, Zhejiang, and Jiangxi provinces from 2018 to 2020 by our research group. In the survey, we used all farmers who own forest land in these areas as the survey population and conducted the survey using stratified random sampling. Firstly, in the stratified sampling, we identified Fujian, Zhejiang, and Jiangxi provinces as the survey areas among the southern collective forest areas according to the economic development and forest resources. Then, we took 1~2 typical prefecture-level cities from each of the three provinces as the survey areas. It should be noted that the distribution of forest resources in China varies widely, with primary and state-owned forests dominating in the northern regions, while collective forests dominate in the south, with a more even distribution of forest resources. The southern region is the region with the best natural conditions in China, and it’s also the region with historically developed forestry, where planted forests occupy a high proportion and farmers in mountainous areas have the habit of operating forestry. In addition, these three provinces ranked first, third and

TABLE 1 Distribution of samples.

| Cities | Counties | Total sample size | Valid sample size |
|---------------|----------|-------------------|-------------------|
| Sanming | Shaxian | 64 | 52 |
| | Youxi | 75 | 66 |
| Nanping | Jiangle | 82 | 66 |
| | Wuyi | 84 | 65 |
| Quanzhou | Dehua | 66 | 62 |
| Ganzhou | Quannan | 60 | 56 |
| | Anyuan | 57 | 54 |
| Lishui | Songyang | 57 | 44 |
| | Suichang | 59 | 54 |
| Total samples | | 604 | 519 |

sixth in forest cover, while the management species are mainly timber forests, Moso bamboo forests and economic forests. Fujian was the first pilot province in the country to carry out a new round of collective forest rights system reform in 2003, followed by Jiangxi and Zhejiang. The three provinces have adopted different approaches in the construction of forestry property rights market, and it is typical and representative to carry out forestry property rights market-related investigations in these regions.

Secondly, we used a random sampling method to select 2~3 counties in each prefecture-level city, 5~6 townships in each county, and 10~15 sample farm households in each township. The survey was conducted in a one-to-one, face-to-face manner with questionnaires and semi-structured interviews. We obtained a total of 604 questionnaires, and after eliminating invalid questionnaires such as those with incomplete answers and inconsistencies, we finally obtained 519 valid questionnaires, with an effective rate of 85.93%. The distribution of the samples are showed in [Table 1](#). The distribution of the study area is shown in [Figure 2](#).

3.2. Questionnaire design and sample descriptive statistics

We designed the questionnaire from the following aspects: farmers' individual and household characteristics, forest land resource endowment, forest rights trading, farmers' cognition and demand for forestry property market, and farmers' willingness and behavior to enter the forestry property market. Of these, the latter two components were the main data sources for this study. In the cognitive survey, we mainly interviewed farmers' views on the advantages and disadvantages of forestry property market, and assigned "1-5" points according to the five-level Likert scale, indicating "strongly disagree ~ strongly agree." The survey results showed that 66.9% of the farmers think it was necessary to enter the forestry property market for trading. The three advantages of "entering the forestry property market can protect the legitimate rights and interests of both parties," "reduce disputes over forest rights" and "fair, open and just transactions" were the most widely recognized. In the demand survey, we set "What services do you want the forestry property market to provide or improve?" According to the survey results, the top

three businesses in demand were "registration and certification of forest rights," "assessment of forestry assets" and "release of forest rights trading information." The results also reflected the obstacles in realizing the value of forestry resources and the asymmetry of market information.

From the basic characteristics of the sample farmers (as shown in [Table 2](#)), the age of farmers was mainly distributed between 46 and 55 years old, with a sample proportion as high as 48.94%; their education level was concentrated in primary and junior high schools, accounting for 39.7 and 35.5% of the total sample, respectively, and their comprehensive quality and literacy were low; In terms of annual household income, 26.97% of the sample farmers' annual household income is below 50,000, 26.01% of the sample farmers' annual household income is between 50,000 and 100,000, more than half of the total sample farmers have an income below 100,000, and up to 22.35% of the farmers have an income above 200,000, with a serious polarization between farmers with high income and low income; The sample farmers also showed a bifurcation in the size of their woodlands, with 46.82% of farmers with woodlands under 5 hectares, 25.2% of farmers with woodlands over 20 hectares, and 28.08% of farmers with woodlands between 5 and 20 hectares. From the basic situation of the survey sample, it is basically consistent with the current reality of collective forest area farmers, and the data is real, reliable, and representative.

3.3. Research methodology

We used structural equation modeling (SEM) to analyze farmers' willingness to enter the forestry property market and the main influencing factors. Structural equation modeling is a statistical method to explore the relationship and structure between theories and concepts. Using structural equation model can simultaneously simulate the internal logical relationship between multiple factors, and analyze the relationship between multiple causes and multiple effects and the relationship between latent variables. It is a widely used multivariate data analysis tool. SEM provides an analytical tool for latent variables that are difficult to observe directly that can be observed and processed and can incorporate unavoidable errors into the model. SEM is generally represented by a system of linear equations, which is divided into two parts: the measurement model and the structural model. The measurement model reflects the relationship between the latent variables and the observed variables, and the latent variables can be defined by the observed variables through the measurement model; the structural model represents the relationship between the latent variables. The matrix equations of the measurement and structural models and the meanings they represent are shown below.

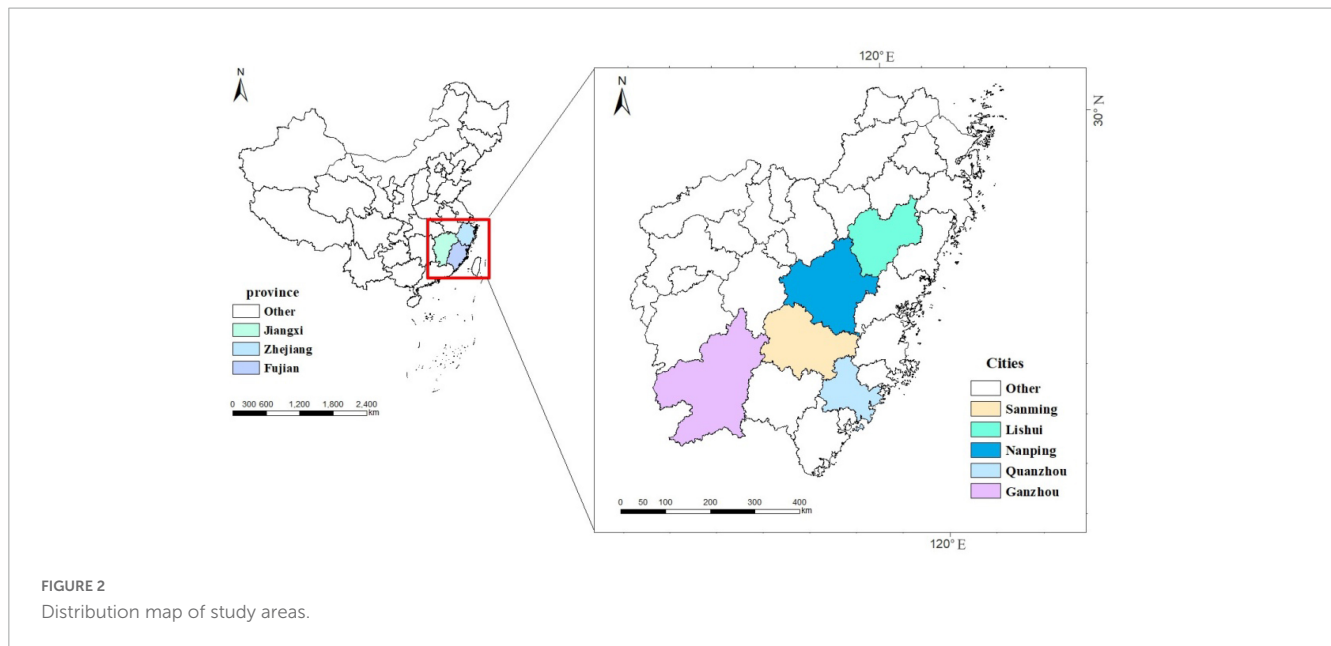
Measurement model:

$$X = \Lambda_X \zeta + \delta \quad (1)$$

$$Y = \Lambda_Y \zeta + \varepsilon \quad (2)$$

Structural model:

$$\eta = \beta \eta \zeta + \Gamma \zeta + \zeta \quad (3)$$



In the above equations, ζ and η are the exogenous latent variables and endogenous latent variables, X is the observed variable of ζ , Y is the observed variable of η , Λ_X is the coefficient linking the variable X to the variable ζ , Λ_Y is the coefficient linking the variable Y to the variable η , δ and ϵ are the errors of the variables X and Y , respectively, β is the regression coefficient of the variable η , Γ is the regression coefficient of the effect of the variable ζ on the variable η , ζ is the error of η .

3.4. Variable selection

Based on the above theoretical analysis, we designed three psychological cognitive factors, including behavioral attitudes, subjective norms, and perceived behavioral control, taking into account the characteristics of the forestry property market and farmers' perspectives. Then, we designed 4–6 observed variables for each latent variable using a 5-point Likert scale, with each item measured according to whether one agrees with the statement, with the number 1 indicating “strongly disagree” and the number 5 indicating “strongly agree,” and the degree of agreement increasing from 1 to 5. The willingness and behavior of farmers to enter the forestry property trading center were dichotomized, with 1 indicating “yes” and 0 indicating “no.” The specific question settings of the scale are shown in [Table 3](#).

3.5. Reliability and validity test

In order to ensure the credibility and validity of the study findings, the scale was tested for reliability and validity, and the results are shown in [Table 4](#). We examined the reliability of the sample data by Cronbach's α and combined reliability, and the Cronbach's α coefficients of the three dimensional observed variables of behavioral attitudes, subjective norms, and perceptual behavioral control were all above 0.8, indicating good agreement of

the measures. Also, the combined reliability of each latent variable is greater than 0.8, and the extracted squared extracted variance of all latent variables is higher than the evaluation criterion of 0.5, indicating that the model has good reliability. In addition, a factor analysis of the sample data using SPSS 24.0 software yielded a Kaiser-Meyer-Olkin value of 0.956 and a cumulative variance contribution of 78.159%. Taken together, the model data were

TABLE 2 Basic characteristics of sample farm households.

| Variable | Classification rule | Frequency | Frequency% |
|---------------------------------|---------------------|-----------|------------|
| Age (year) | < 35 | 13 | 2.51 |
| | 36~45 | 107 | 20.62 |
| | 46~55 | 254 | 48.94 |
| | 56~65 | 106 | 20.42 |
| Household income (Chinese Yuan) | < 50,000 | 140 | 26.97 |
| | 50,000~100,000 | 135 | 26.01 |
| | 100,000~150,000 | 79 | 15.22 |
| | 150,000~200,000 | 49 | 9.44 |
| Education level (year) | > 200,000 | 116 | 22.35 |
| | < 6 | 206 | 39.7 |
| | 6~9 | 184 | 35.5 |
| Forest land size (hectare) | 9~12 | 108 | 20.8 |
| | > 12 | 21 | 4.0 |
| | < 5 | 243 | 46.82 |
| | 5~10 | 67 | 12.98 |
| | 10~15 | 47 | 9.1 |
| | 15~20 | 31 | 6.0 |
| | > 20 | 131 | 25.2 |

TABLE 3 Latent variables, observed variables and code settings.

| Latent variable | Abbr. | Observation variable definition |
|-------------------------------------|-------|---|
| Behavioral attitude (AB) | AB1 | Improve efficiency and reduce costs of forestry property transactions |
| | AB2 | Reduce the risk of forestry property trading |
| | AB3 | Facilitate open, fair and just transactions |
| | AB4 | Protect the legal rights of both parties to the transaction |
| | AB5 | Reduce the occurrence of forestry property disputes |
| | AB6 | Promote large-scale operation and optimal allocation of production factors |
| Subjective norms (SN) | SN1 | The village collective believes that it should enter the forestry property market for trading |
| | SN2 | The government or forestry department thinks it should enter the forestry property market for trading |
| | SN3 | Neighboring farmers think it should enter the forestry property market for trading |
| | SN4 | Family believes it should be traded in the forestry property market |
| Perceptual behavioral control (PBC) | PBC1 | I have sufficient tolerance for trading risk |
| | PBC2 | Unfamiliarity with the forestry property market process affected my entry into the transaction |
| | PBC3 | The country has a very good support policy |
| | PBC4 | The degree of regulation of forestry property trading market |
| | PBC5 | Ease of access to transaction information |
| Willingness (PW) | PW1 | Willingness to enter the forestry property market for forestry property trading |
| Behavior (PB) | PB1 | Access to the forestry property market for forestry property trading |

suitable for factor analysis, and the model had high construct validity.

4. Results and discussions

4.1. Structural equation model fitness test results and model correction

Based on this study’s hypotheses, measurement indicators, and test results, we constructed the structural equation model. The results of the structural equation model fitness test are shown in Table 5. According to the model path coefficients and correction

indices, we revised the model in the order of the correction indices from largest to smallest, and added residual correlations between the variables SN3 and SN4, AB5 and AB6, AB6 and PB1, PBC1 and PBC5, and SN3 and PB1. The cardinality values can be effectively reduced after releasing the correlations between these groups of variables, and the theoretical assumptions are not violated. After the correction, the overall model fitness evaluation indexes all meet the evaluation criteria, indicating that the overall model fit is optimized and the analysis results are more accurate after the parameters are released. The modified structural equation model is shown in Figure 3.

4.2. Estimation results and discussions

Table 6 shows the structural equation model path coefficients. From the table, we can see that the three latent variables that determine the willingness of farmers to enter the forestry property market do not differ greatly in their degree of influence, “AB→PW1,” “SN→PW1,” “PBC→PW1” the three paths influence coefficients of 0.301, 0.338, and 0.341, respectively, and the three are not independently influencing farmers’ willingness to make decisions, but there is a large interaction between them. The path “PBC→PB1” was significant with an effect coefficient of 0.367, indicating that perceptual behavioral control has a significant effect on behavior. The coefficients of the above paths are all significant at the 1% level, indicating that the four research hypotheses proposed in this paper have been verified, while the coefficient of the effect of farmers’ willingness (PW1) on decision-making behavior (PB1) is 0.157, but it is not significant, indicating that the willingness is not completely transformed into behavior, and that the process of transforming farmers’ willingness into behavior is hindered or interfered with by some external factors. In the following section we will discuss the impact of each path specifically.

4.2.1. The effect of AB on farmers’ willingness to enter the forestry property market

Table 6 shows that in the psychological decision-making model of farmers, behavioral attitudes have a positive influence on farmers’ willingness to enter the forestry property market, indicating that the more positive farmers’ behavioral attitudes are, the higher their recognition of the forestry property market and the stronger their willingness to choose, so hypothesis 1 is verified. Hansson et al. (2012) also found a significant positive relationship between indirect attitudes and intentions, indicating that behavioral beliefs about possible outcomes influenced farmers’ intentions.

Among the behavioral attitudes, the loading of AB1 factor loadings amount to 0.809, reflecting farmers’ recognition of the transaction services provided by the forestry property market. The forestry property market generally has multiple comprehensive functions, in addition to organizing transactions and intermediary service. it also has a number of functions such as property rights management and information release (FAO, 2012). Farmers can enjoy one-stop services through the forestry property market, which simplifies the transaction process and improves the efficiency of the transaction, and therefore can stimulate the enthusiasm of farmers. Although many services in the forestry property market are free, there are still some items in some parts of the transaction that require certain fees, which should be reduced as much as

TABLE 4 Reliability and validity test results.

| Latent variable | Cumulative variance contribution rate (%) | Cronbach's α | Combinatorial reliability | Mean refinement variance |
|-----------------|---|---------------------|---------------------------|--------------------------|
| AB | 54.022 | 0.923 | 0.925 | 0.675 |
| SN | 67.028 | 0.830 | 0.827 | 0.645 |
| PBC | 78.159 | 0.809 | 0.812 | 0.528 |

TABLE 5 Evaluation index system and fitting results of the overall SEM suitability.

| Type of index | Abbr. | Acceptable fit values | Fit values | Result |
|------------------------|-------|--|--|--------|
| Absolute fit index | X2/df | < 3.00 | 1.959 | Accept |
| | RMR | < 0.05 | 0.020 | Accept |
| | RMSEA | < 0.05 | 0.043 | Accept |
| | GFI | > 0.90 | 0.954 | Accept |
| | AGFI | > 0.90 | 0.935 | Accept |
| Incremental fit index | NFI | > 0.90 | 0.964 | Accept |
| | RFI | > 0.90 | 0.955 | Accept |
| | IFI | > 0.90 | 0.982 | Accept |
| | TLI | > 0.90 | 0.978 | Accept |
| | CFI | > 0.90 | 0.982 | Accept |
| Parsimonious fit index | PCFI | > 0.50 | 0.780 | Accept |
| | PNFI | > 0.50 | 0.766 | Accept |
| | AIC | Less than both the independent model value and the saturated model value | 301.520 < 306.000 301.520 < 5,990.535 | Accept |
| | CAIC | | 537.856 < 1,109.541 537.856 < 6,079.817 | Accept |

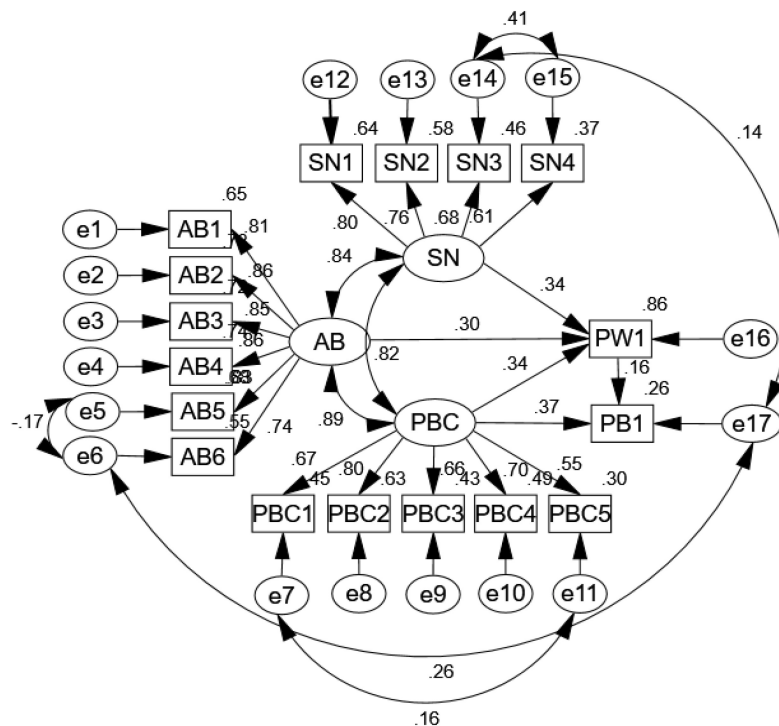


FIGURE 3 Modified structural equation model.

TABLE 6 Estimation results of the SEM.

| Path | Standardized path coefficient | Standard error | Threshold ratio value | Hypothesis test |
|---------------------------|-------------------------------|----------------|-----------------------|-----------------|
| Structural model | | | | |
| AB→PW1 | 0.301*** | 0.091 | 4.315 | H1 accepted |
| SN→PW1 | 0.338*** | 0.067 | 5.991 | H2 accepted |
| PBC→PW1 | 0.341*** | 0.097 | 4.687 | H3 accepted |
| PBC→PB1 | 0.367*** | 0.060 | 3.330 | H4 accepted |
| PW1→PB1 | 0.157 | 0.042 | 1.519 | |
| Measurement models | | | | |
| AB→AB1 | 0.809*** | 0.056 | 18.870 | |
| AB→AB2 | 0.857*** | 0.057 | 20.095 | |
| AB→AB3 | 0.847*** | 0.055 | 19.840 | |
| AB→AB4 | 0.862*** | 0.059 | 20.246 | |
| AB→AB5 | 0.827*** | 0.060 | 17.964 | |
| AB→AB6 | 0.739*** | – | – | |
| SN→SN1 | 0.802*** | – | – | |
| SN→SN2 | 0.764*** | 0.050 | 18.264 | |
| SN→SN3 | 0.682*** | 0.056 | 15.920 | |
| SN→SN4 | 0.609*** | 0.056 | 13.936 | |
| PBC→PBC1 | 0.667*** | 0.062 | 14.057 | |
| PBC→PBC2 | 0.796*** | 0.066 | 16.588 | |
| PBC→PBC3 | 0.657*** | 0.079 | 13.876 | |
| PBC→PBC4 | 0.696 | – | – | |
| PBC→PBC5 | 0.549*** | 0.065 | 11.634 | |

*** indicates 1% significance level.

possible, lower the fee standard, and lower the forest resources assessment fee to attract traders.

AB2 factor loadings amount to 0.857, indicating that the risk of current forestry property trading is an important factor for farmers to choose the trading route, and that most of the current forestry property markets are government forestry department-affiliated institutions with a certain degree of authority, the relevant property rights registration and change procedures for trading are more complete, and the trading risk is relatively low.

AB3 factor loadings amounted to 0.847, indicating that the process through the forestry property market is more open, fair, and equitable than private transactions, and that the standardized transaction procedures play an important role in farmers' willingness and are more likely to be recognized by both sides of the transaction.

The AB4 coefficient reaches 0.862, which indicate that farmers' own rights and interests are the important aspect they consider when making forestry property rights transaction decisions, which largely determines the choice intention. Farmers generally lack a sense of security about the ownership of forestry rights (Liu et al., 2022), therefore, only when their own rights and interests are guaranteed, farmers are willing to trade through the forestry property market. The forestry property market should focus on serving forestry reform, starting with the comprehensive improvement of forestry's ability to serve social and economic development, actively expanding and extending the coverage

of public service platform of forestry production, explore the construction of "forestry remote education service points" covering townships (towns), establish a "forest products information service platform," and optimizing the sharing of scientific and technological information services, so that the majority of farmers, forest enterprises cognitive benefits.

AB5 factor loadings amount to 0.827, indicating that unregulated forestry property transactions are likely to cause related forestry property disputes, while the forestry property market can eliminate related forestry property dispute potential problems, such as confirming whether the subject matter is defective before the transaction, supervising whether the trader is in breach of contract after the transaction, and the transaction process is relatively regulated and complete, avoiding disputes and safeguarding their own interests through regulated transactions. Forest tenure reform has often focused on formalizing the collective rights of communities to forest resources (Duguma et al., 2018), and the establishment of forestry property markets has further facilitated the formalization of forest rights transactions.

AB6 factor loadings amount to 0.739. The new round of forest reform has led to the fragmentation of forest land operations, which has hindered the enhancement of the scale efficiency of forest land operations and the optimal allocation of resources. The emergence of this institution, the forestry property market, has built an interconnected trading platform for both sides of

the transaction, and its role has been recognized by farmers and enhanced their willingness to a large extent.

4.2.2. The influence of SN on farmers' willingness to enter the forestry property market

The path of influence of subjective norms on farmers' willingness to enter the forestry property market is significant, indicating that a farmer feels pressure from the surrounding group when deciding whether to trade through the forestry property market, and this pressure may lead him to make decisions that are consistent with the opinions of others, and hypothesis 2 is tested. Among the subjective normative constructs, the factor loadings of SN1, SN2, SN3, and SN4 are 0.802, 0.764, 0.682, and 0.609, respectively, indicating that norms from different levels have different degrees of influence on farmers' psychological decisions to enter the forestry property market, and the magnitude of their influence is in the following order: village collective or group opinion > government or forestry department opinion > neighboring farmers' opinion > family opinion. This reflects that the influence of organizational-level norms on farmers' decision making is greater than that of individual-level norms.

Before the establishment of the forestry property market in collective forest areas, most of the forestry property transfer transactions were organized by village collectives (Kumar et al., 2015), therefore, the views of village collectives in the transfer transaction activities were regarded as important norms by farmers. After the establishment of the forestry property market, forestry property transfer regulations in some areas stipulate that state or collective forestry property transactions must be transacted through the forestry property market. Farmers are guided by the forestry property transfer policy and have a strong policy perception, which also strengthens their perceived social and policy pressure. On the other hand, the opinions of neighboring groups, such as neighbors or family and friends, may exert pressure on farmers' decisions on transfer transactions, prompting them to make decisions consistent with their opinions; family members' opinions are generally more consistent and are more likely to arise through the influence of external opinions.

4.2.3. The effect of PBC on farmers' willingness to enter the forestry property market

Perceived behavioral control refers to the ability, resources, or implementation barriers that farmers perceive when they perform certain behaviors, which can promote or hinder the willingness and behavior of farmers to some extent (Elsawah et al., 2017). The load coefficient of the effect of perceived behavioral control on farmers' willingness to enter the forestry property market was 0.341 and statistically significant, indicating that perceived behavioral control has a large effect on farmers' willingness and is an important aspect of willingness formation. The load coefficient of the effect of perceptual behavioral control on farmers' behavior was 0.367 and statistically significant, indicating that perceptual behavioral control had a large impact on farmers' behavior, i.e., an important reason why farmers' intentions were not effectively translated into behavior to a large extent was due to the influence of perceptual behavioral control. As reviewed by Jones et al. (2011), literature has focused on the dynamic capacities and abilities of mental models.

Perceived behavioral control includes the ability, resources, or barriers (external factors) to the farmer's choice, which largely constrain the farmer's choice behavior. Among them, the PBC2 factor loading is the largest, at 0.796, indicating that the government's propaganda for the forestry property market is not yet in place, hindering the willingness of farmers to enter. One of the important reasons why forestry property market transactions are insufficient and the function of property rights transactions cannot be effectively played is that farmers do not know much about the stability of forestry reform policy, the function and operation process of forestry property market. The PBC4 factor loading is 0.696, indicating that there are still irregularities in the current forestry property trading market, the forestry property trading process requires forestry departments to provide forestry property registration, change procedures, and other related services, and good and sound market conditions play a positive role in farmers' decision making. The loading of PBC1 factor is 0.667, indicating that farmers' own risk tolerance is one of the important factors in their choice of forestry property trading method. Most farmers are risk-averse (Duan et al., 2021), and forestry property trading faces many uncertain risks, so if farmers perceive that forestry property trading activities through the forestry property market can improve the safety of trading, then their willingness will be higher. The PBC3 factor loading was 0.657, indicating that the support from the state policy has an important guiding effect on farmers' decision making, and the state's support policy can effectively enhance farmers' enthusiasm to participate in the early stages of forestry property trading market establishment. The factor loading of PBC5 is 0.549, which indicates that the information asymmetry between the two sides of the transaction in the forest in rights trading market is prominent, and the forestry property market helps to promote farmers to enter the forestry property market transaction by releasing information about forestry property trading.

4.2.4. Interaction of AB, SN, and PBC

The three latent variables of behavioral attitudes, subjective norms, and perceptual behavioral control are bipartite and interact with each other (Senger et al., 2017). The interaction between behavioral attitude and perceived behavioral control is the strongest, with a loading coefficient of 0.89 between the two latent variables. Farmers who have greater ability and resources to adopt positive attitudes toward forestry property markets have a stronger perception of behavioral control. And farmers with higher perceptions of behavior control expect safer and more secure transaction services and have a more positive attitude toward the forestry property market. The influence between behavioral attitudes and subjective norms is the second most important, with a loading coefficient of 0.84. The choice of forestry property trading method is a rational behavior, which is not only influenced by objective conditions, but also swayed by subjective factors. Farmers' attitudes toward entering the forestry property market interact with subjective norms. The more positive farmers' behavioral attitudes are, the more likely they are to feel pressure from surrounding groups or organizations, and the greater this social pressure is, the greater the influence on their attitudes (Borges and Lansink, 2016). The loading coefficient between subjective norm and perceived behavioral control is 0.82. The stronger the perceived behavioral control, the more adequate the

farmers' conditions are, and the more they want the forestry property trading policy to be recognized by more people, so the subjective norm and perceived behavioral control also influence each other.

5. Study limitations

It is acknowledged that there are some limitations to this study. Firstly, this paper only analyzes the factors influencing farmers' willingness to enter the forestry property market according to the theory of planned behavior. The selected factors are not comprehensive enough, for example, the model does not take the difference of forest land management scale into account. Secondly, due to the large geographical area of China, each province has a different degree of market development. This study only selects Fujian, Jiangxi, and Zhejiang provinces for research, which has certain limitations. Therefore, many future studies can extend this research to provide a research basis for the sustainable development of forestry property market, as well as Chinese experience for the development of forestry property market in other countries in the world.

6. Conclusion and policy recommendations

6.1. Conclusion

This paper combines the theory of planned behavior and structural equation modeling to analyze the psychological decision-making process of farmers' entry into the forestry property market from the perspective of psychological characteristics. The research results show that: (1) Three psychological cognitive factors of farmers' behavioral attitudes, subjective norms, and perceptual behavioral control play an important role in influencing their psychological decision willingness, and the three factors do not independently affect farmers' choice willingness, but have a large interactive effect. (2) An important reason why farmers' willingness is not effectively transformed into behavior is that they are constrained by their own ability and resource endowment, as well as the interference of external factors such as an imperfect forestry property trading market and inadequate policy publicity. (3) Reducing the risk of transfer and protecting the rights and interests of both parties constitute the main factors of behavioral attitudes, and the greatest external pressure on farmers' willingness to enter the forestry property market comes from the opinions of village collectives. (4) Perceptual behavior control has an important restraining effect on behavior, among which unfamiliarity with the forestry property market is the main factor affecting farmers' perceptual behavior control. Farmers are micro subjects of forestry property market, and it is of great practical significance to study farmers' behavioral decisions to enter the forestry property market and to improve farmers' market participation behavior for the healthy development of the forestry property market.

6.2. Policy recommendations

Based on the findings of the study, we propose the following policy recommendations.

First, improve and perfect the service system of forestry property market, and combine multiple supporting policies to protect the vital interests of farmers. Simplify the procedure of forest rights trading, reduce the transaction cost, improve the efficiency of the transaction, and effectively consider the farmers' interest demands on forest rights trading.

Second, cultivate and enhance farmers' awareness of the forestry property market. First of all, we should strengthen the publicity of forestry property market, through the government with the help of public media such as TV, radio, newspapers and magazines, or use modern network, set up websites and other forms to increase the publicity in order to enhance the influence and attractiveness of the market. Secondly, popularize the information related to the forestry property market and enhance the farmers' awareness of the forestry property market.

Third, strengthen the policy guidance to encourage policies to promote the flow of forest rights trading toward standardization. Encourage forest farmers to participate in forest land and forest management and transfer in various ways, such as through forest rights participation, joint operation, development of forestry cooperatives and forest rights mortgage and other forms of property rights transfer. Respect the farmers' right to choose, guide farmers to enter the forestry property market and gradually internalize off-site transactions. In addition, because of the prominent role of village collectives in regulating the flow, the development of forest rights trading policies should also emphasize the power of grassroots organizations.

Data availability statement

The original contributions presented in this study are included in this article/supplementary material, further inquiries can be directed to the corresponding author.

Author contributions

YH and QW: conceptualization, validation, formal analysis, investigation, resources, and data curation. YH and YW: methodology, software, writing—original draft preparation, review and editing, visualization, supervision, project administration, and funding acquisition. All authors have read and agreed to the published version of the manuscript.

Funding

This research was funded by the Major Project of Fujian Provincial Social Science Foundation Base (grant no. FJ2020MJDZ051). Research Center for Targeted Poverty

Alleviation and Poverty Relapse Prevention of Ningde Normal University (grant no. JXH2022086).

Conflict of interest

The authors declare that the research was conducted in the absence of any commercial or financial relationships that could be construed as a potential conflict of interest.

References

- Aggarwal, S., Larson, A., McDermott, C., Katila, P., and Giessen, L. (2021). Tenure reform for better forestry: An unfinished policy agenda. *For. Policy Econ.* 123:102376. doi: 10.1016/j.forpol.2020.102376
- Ajzen, I. (1991). The theory of planned behavior. *Organ. Behav. Hum. Decis. Process.* 50, 179–211. doi: 10.1016/0749-5978(91)90020-T
- Ajzen, I. (2020). The theory of planned behavior: Frequently asked questions. *Hum. Behav. Emerg. Technol.* 2, 314–324. doi: 10.1002/hbe2.195
- Ajzen, I., and Fishbein, M. (1977). Attitude-behavior relations: A theoretical analysis and review of empirical research. *Psychol. Bull.* 84:888. doi: 10.1037/0033-2909.84.5.888
- Ajzen, I., and Fishbein, M. (2008). Scaling and testing multiplicative combinations in the expectancy-value model of attitudes. *J. Appl. Soc. Psychol.* 38, 2222–2247. doi: 10.1111/j.1559-1816.2008.00389.x
- Ajzen, I., and Madden, T. J. (1986). Prediction of goal-directed behavior: Attitudes, intentions, and perceived behavioral control. *J. Exp. Soc. Psychol.* 22, 453–474. doi: 10.1016/0022-1031(86)90045-4
- Biddle, S., Goudas, M., and Page, A. (1994). Social-psychological predictors of self-reported actual and intended physical activity in a university workforce sample. *Br. J. Sports Med.* 28, 160–163. doi: 10.1136/bjism.28.3.160
- Borges, J. A. R., Lansink, A., Ribeiro, C. M., and Lutke, V. (2014). Understanding farmers' intention to adopt improved natural grassland using the theory of planned behavior. *Livestock Sci.* 169, 163–174.
- Borges, J. A. R., and Lansink, A. G. J. M. (2016). Identifying psychological factors that determine cattle farmers' intention to use improved natural grassland. *J. Environ. Psychol.* 45, 89–96. doi: 10.1016/j.jenvp.2015.12.001
- Chen, J., and Innes, J. L. (2013). The implications of new forest tenure reforms and forestry property markets for sustainable forest management and forest certification in China. *J. Environ. Manage.* 129, 206–215. doi: 10.1016/j.jenvman.2013.07.007
- Chen, Q. (2022). Analyzing farmers' cultivated-land-abandonment behavior: Integrating the theory of planned behavior and a structural equation model. *Land* 11:1777. doi: 10.3390/land11101777
- Cheng, W. L., Xu, Y. Y., Zhou, N., He, Z. Z., and Zhang, L. Y. (2019). How did land titling affect china's rural land rental market? Size, composition and efficiency. *Land Use Policy* 82, 609–619. doi: 10.1016/j.landusepol.2018.12.037
- Conner, M., and Armitage, C. J. (1998). Extending the theory of planned behavior: A review and avenues for further research. *J. Appl. Soc. Psychol.* 28, 1429–1464. doi: 10.1111/j.1559-1816.1998.tb01685.x
- Deininger, K., Jin, S. Q., and Xia, F. (2014). Moving off the farm: Land institutions to facilitate structural transformation and agricultural productivity growth in China. *World Dev.* 59, 505–520. doi: 10.1016/j.worlddev.2013.10.009
- Deng, J., Sun, P., Zhao, F., Han, X., Yang, G., and Feng, Y. (2016). Analysis of the ecological conservation behavior of farmers in payment for ecosystem service programs in eco-environmentally fragile areas using social psychology models. *Sci. Total Environ.* 550, 382–390. doi: 10.1016/j.scitotenv.2016.01.152
- Deng, M., Zhang, A., Cheng, C., and Hu, C. (2022). Are villagers willing to enter the rural collective construction land market under the arrangement of transaction rules?—evidence from Ezhou, China. *Land* 11:466. doi: 10.3390/land11040466
- Deng, X., Xu, D. D., Zeng, M., and Qi, Y. B. (2019). Does labor off-farm employment inevitably lead to land rent out? Evidence from china. *J. Mountain Sci.* 16, 689–700. doi: 10.1007/s11629-018-5045-8
- Donati, M., Menozzi, D., and Fioravanzi, M. (2015). Understanding farmers' responses to cap reform. *New Medit* 14, 29–39.
- Duan, W., Hogarth, N. J., Shen, J., Ouyang, B., and Chen, Q. (2021). Household risk preferences and forestland use right transactions in china: Tenure security or price illusion? *Scand. J. For. Res.* 36, 502–512. doi: 10.1080/02827581.2021.1962967
- Duguma, L., Minang, P., Foundjem Tita, D., Parmutia, M., and Piabuo, S. (2018). Prioritizing enablers for effective community forestry in Cameroon. *Ecol. Soc.* 23:1. doi: 10.5751/ES-10242-230301
- Elsawah, S., McLucas, A., and Mazanov, J. (2017). An empirical investigation into the learning effects of management flight simulators: A mental models approach. *Eur. J. Oper. Res.* 259, 262–272. doi: 10.1016/j.ejor.2016.10.011
- FAO (2012). *Success cases and good practices in forest farmer cooperative organizations in china*. Rome: FAO.
- Feng, S., and Heerink, N. (2008). Are farm households' land renting and migration decisions inter-related in rural china? *Njas-Wageningen J. Life Sci.* 55, 345–362. doi: 10.1016/S1573-5214(08)80025-5
- Fishbein, M., and Ajzen, I. (2011). *Predicting and changing behavior: The reasoned action approach*. London: Psychology press. doi: 10.4324/9780203838020
- Hall, A., Turner, L., and Kilpatrick, S. (2019). Using the theory of planned behaviour framework to understand Tasmanian dairy farmer engagement with extension activities to inform future delivery. *J. Agric. Educ. Extens.* 25, 195–210. doi: 10.1080/1389224X.2019.1571422
- Hansson, H., Ferguson, R., and Olofsson, C. (2012). Psychological constructs underlying farmers' decisions to diversify or specialise their businesses - an application of theory of planned behaviour. *J. Agric. Econ.* 63, 465–482. doi: 10.1111/j.1477-9552.2012.00344.x
- Jiang, M., Li, J., Paudel, K. P., and Mi, Y. (2019). Factors affecting agricultural land transfer-out in china: A semiparametric instrumental variable model. *Appl. Econ. Lett.* 26, 1729–1733. doi: 10.1080/13504851.2019.1593929
- Jin, S. Q., and Deininger, K. (2009). Land rental markets in the process of rural structural transformation: Productivity and equity impacts from China. *J. Compar Econ.* 37, 629–646. doi: 10.1016/j.jce.2009.04.005
- Jones, N. A., Ross, H., Lynam, T., Perez, P., and Leitch, A. (2011). Mental models: An interdisciplinary synthesis of theory and methods. *Ecol. Soc.* 16:13. doi: 10.5751/ES-03802-160146
- Kong, F., and Du, L. (2008). Research on regulating the circulation of collective forest property rights. *Issues for. Econ.* 5, 377–384.
- Kumar, K., Singh, N. M., and Kerr, J. M. (2015). Decentralisation and democratic forest reforms in India: Moving to a rights-based approach. *For. Policy Econ.* 51, 1–8. doi: 10.1016/j.forpol.2014.09.018
- Lam, T., Baum, T., and Pine, R. (2003). Moderating effect on new employee's job satisfaction and turnover intentions: The role of subjective norm. *Ann. Tour. Res.* 30, 160–177. doi: 10.1016/S0160-7383(02)00047-6
- Li, J. G., Gao, Y. M., and Zang, J. M. (2014). The impact of farmers' risk awareness on land transfer decision making behavior. *J. Agrotech.* 11, 21–30.
- Li, X., Cirella, G. T., Wen, Y., and Xie, Y. (2020). Farmers' intentions to lease forestland: Evidence from rural china. *Land* 9:78. doi: 10.3390/land9030078
- Li, X., and Ito, J. (2021). An empirical study of land rental development in rural Gansu, China: The role of agricultural cooperatives and transaction costs. *Land Use Policy* 109:105621. doi: 10.1016/j.landusepol.2021.105621
- Li, Z. (2011). Survey on the peasants' will of forest land transfer in the reform of collective forest right system - on the case of 180 peasant households in Lishui city of Zhejiang province. *Asian Agric. Res.* 2:231319.
- Lin, J., Zhang, Q., and Wei, Y. (2022a). Pricing strategy and simulation of forest rights exchange centers based on the two-sided market theory. *Math. Problems Eng.* 2022, 1–9. doi: 10.1155/2022/5766638
- Lin, J., Zhang, Q., Wei, Y., and Nepomuceno, E. G. (2022b). Evolutionary game and simulation in forest rights exchange based on the supplier-demander view. *Math Problems Eng.* 2022:9525675. doi: 10.1155/2022/9525675

Publisher's note

All claims expressed in this article are solely those of the authors and do not necessarily represent those of their affiliated organizations, or those of the publisher, the editors and the reviewers. Any product that may be evaluated in this article, or claim that may be made by its manufacturer, is not guaranteed or endorsed by the publisher.

- Liu, X., Huang, L., Du, J., Xie, F., and Zhu, S. (2022). Forestland transfer between rural households in Jiangxi, China: Differentiated effects of actual and perceived tenure security. *Natl. Resour. Model.* 35:12327. doi: 10.1111/nrm.12327
- Lu, M., Guo, B., Chen, G., Yuan, L., and Xing, R. (2022). A study on the factors influencing farmers' intention to revitalize idle homesteads based on improved TPB framework—analysis of the moderating effect of farmer differentiation. *Sustainability* 14:15759. doi: 10.3390/su142315759
- Park, H. S. (2000). Relationships among attitudes and subjective norms: Testing the theory of reasoned action across cultures. *Commun. Stud.* 51, 162–175. doi: 10.1080/10510970009388516
- Sarkar, A., Wang, H., Rahman, A., Abdul Azim, J., and Hussain Memon, W. (2022). Structural equation model of young farmers' intention to adopt sustainable agriculture: A case study in Bangladesh. *Renew. Agric. Food Syst.* 37, 142–154. doi: 10.1017/S1742170521000429
- Schroeder, L. A., Chaplin, S., and Isselstein, J. (2015). What influences farmers' acceptance of agri-environment schemes? An ex-post application of the 'theory of planned behaviour'. *Landbauforschung* 65, 15–28. doi: 10.3220/LBF1440149868000
- Senger, I., Rossi Borges, J. A., and Dessimon Machado, J. A. (2017). Using the theory of planned behavior to understand the intention of small farmers in diversifying their agricultural production. *J. Rural Stud.* 49, 32–40. doi: 10.1016/j.jrurstud.2016.10.006
- Shi, R., Hou, L., Jia, B., Jin, Y., and Zheng, W. (2022). Effect of policy cognition on the intention of villagers Withdrawal from rural homesteads. *Land* 11:1356. doi: 10.3390/land11081356
- Tang, M., and Wang, F. (2013). Analysis on the willingness of peasant households for forestland use right transfer in the background of collective forest tenure reform: A case study in Guangyuan city in Sichuan province. *Sustain. Agric. Res.* 2:2. doi: 10.5539/sar.v2n2p76
- Wang, G., Innes, J. L., Lei, J., Dai, S., and Wu, S. W. (2007). China's forestry reforms. *Science* 318, 1556–1557. doi: 10.1126/science.1147247
- Wang, H., Li, C., Liu, J., and Zhang, S. (2019). Research on farmers' willingness of land transfer behavior based on food security. *Sustainability* 11:2338. doi: 10.3390/su11082338
- Wauters, E., Biolders, C., Poesen, J., Govers, G., and Mathijs, E. (2010). Adoption of soil conservation practices in Belgium: An examination of the theory of planned behaviour in the agri-environmental domain. *Land Use Policy* 27, 86–94. doi: 10.1016/j.landusepol.2009.02.009
- Xie, M., Yuan, M., and Guo, B. (2013). Study on the rural land transfer behavior based on theory of planned behavior. *Xi'an Univ. Archit. Technol.* 45, 300–304.
- Xie, Y., Cai, Z. J., and Zhang, H. (2014). Multi agent based simulation framework for forest right trade market. *For. Econ.* 4, 37–42.
- Xu, C., Li, L. C., and Cheng, B. D. (2021). The impact of institutions on forestland transfer rents: The case of Zhejiang province in China. *For. Policy Econ.* 123:102354. doi: 10.1016/j.forpol.2020.102354
- Xu, T., Zhang, X., Agrawal, A., and Liu, J. (2020). Decentralizing while centralizing: An explanation of china's collective forestry reform since the 1980s. *For. Policy and Econ.* 119:102268. doi: 10.1016/j.forpol.2020.102268
- Xu, X., Zhang, Y., Li, L., and Yang, S. (2013). Markets for forestland use rights: A case study in southern china. *Land Use Policy* 30, 560–569. doi: 10.1016/j.landusepol.2012.05.001
- Yaghoubi Farani, A., Mohammadi, Y., and Ghahremani, F. (2019). Modeling farmers' responsible environmental attitude and behaviour: A case from Iran. *Environ. Sci. Pollut. Res.* 26, 28146–28161. doi: 10.1007/s11356-019-06040-x
- Yang, X., Zhou, X., and Deng, X. (2022). Modeling farmers' adoption of low-carbon agricultural technology in Jiangnan plain, China: An examination of the theory of planned behavior. *Technol. Forecast. Soc. Change* 180:121726. doi: 10.1016/j.techfore.2022.121726
- Yang, X. J., and Ming, L. (2006). Reform of forest property and forestry factor market construction. *Commerc. Res.* 4, 187–190.



OPEN ACCESS

EDITED BY

Ling Zhang,
Jiangxi Agricultural University, China

REVIEWED BY

Chul-Hee Lim,
Kookmin University, Republic of Korea
Moonil Kim,
Pyongtaek University, Republic of Korea

*CORRESPONDENCE

Hyun-Jun Kim
✉ hjkim0837@chonnam.ac.kr

RECEIVED 24 November 2022

ACCEPTED 12 June 2023

PUBLISHED 02 October 2023

CITATION

Lee S-g and Kim H-J (2023) Spatiotemporal approach for estimating potential CO₂ sequestration by reforestation in the Korean Peninsula. *Front. For. Glob. Change* 6:1106630. doi: 10.3389/ffgc.2023.1106630

COPYRIGHT

© 2023 Lee and Kim. This is an open-access article distributed under the terms of the [Creative Commons Attribution License \(CC BY\)](https://creativecommons.org/licenses/by/4.0/). The use, distribution or reproduction in other forums is permitted, provided the original author(s) and the copyright owner(s) are credited and that the original publication in this journal is cited, in accordance with accepted academic practice. No use, distribution or reproduction is permitted which does not comply with these terms.

Spatiotemporal approach for estimating potential CO₂ sequestration by reforestation in the Korean Peninsula

Sle-gee Lee¹ and Hyun-Jun Kim^{2*}

¹Forest Resource Research Center, Chonnam National University, Gwangju, Republic of Korea,

²Department of Forest Resources, Chonnam National University, Gwangju, Republic of Korea

A forest is one of the carbon sinks in the terrestrial ecosystem; it is a major target for securing CO₂ sequestration to achieve carbon neutrality. Reforestation is a forest management method that could attain carbon fixation and forest degradation recovery at the same time, but quantitative research has not been actively conducted. The purpose of this study is to identify the target areas for reforestation through changes in land cover in the Korean Peninsula and to quantify the potential CO₂ sequestration effect of reforestation. According to the land cover change through satellite imagery, the area of settlements in the Republic of Korea (ROK) was the most dominant (+3,371 km²), and the main change occurred from cropland to settlements. The forest area increased by +1,544 km² from 68,264 km² in the 1980s to 69,809 km² in the late 2010s. The forest decreased by 7,526 km², accounting for 5.68% of the entire land area of the Democratic People's Republic of Korea (DPRK), and cropland increased by 5,222 km² which is 5.12%. Assuming that the target of reforestation is an area whose land cover was a forest in the past and then converted to cropland, wetland, or bare ground, the area of the target decreased as the reference period was applied more recently. As a result of comparing the late 2000s to the late 2010s, the ROK's annual net carbon sequestration due to reforestation is predicted to be 10,833,600 Mg CO₂ yr⁻¹ in 2050 and 20,919,200 Mg CO₂ yr⁻¹ in 2070. In the DPRK, 14,236,800 Mg CO₂ yr⁻¹ in 2050 and 27,490,400 Mg CO₂ yr⁻¹ in 2070 were predicted. Reforestation in the Korean Peninsula was analyzed to have sufficient potential to secure a carbon sink, and the DPRK in particular was analyzed to be able to play a role in overseas reforestation.

KEYWORDS

reforestation, carbon sink, carbon dioxide sequestration, land cover change, forest management scenarios

1. Introduction

A forest is one of the carbon sinks that compose terrestrial ecosystems and plays the highest role in carbon sequestration among other land cover types (Saeed et al., 2016). In particular, reforestation is known as a representative method to enhance the CO₂ sequestration effect by increasing forest biomass along with afforestation (Nevle and Bird, 2008; Wang et al., 2022). As the Paris Agreement in 2012 requires activities to reduce greenhouse gases, the importance of forests has been increasing steadily in land use, land use change, and forestry (LULUCF). Each country makes an effort to expand the carbon sinks to support economic sectors related to energy, industrial processes, agriculture, and waste, which directly affect carbon emissions (Fukushima, 2013; Kim et al., 2021). Indeed,

the Kyoto Protocol indicates that afforestation and reforestation are instruments intended to reduce greenhouse gas emissions (Zomer et al., 2008). The United Nations Framework Convention on Climate Change (UNFCCC) recognizes only afforestation and reforestation as emission reductions in the LULUCF, whereby afforestation is the establishment of trees on the land that has not had a forest on it for more than 50 years, and reforestation is the establishment of trees on the land that has had a forest on it within the last 50 years (UNFCCC, 2002a,b). According to guidelines published by Intergovernmental Panel on Climate Change (IPCC), cropland and settlements are regarded as carbon sources on the surface; therefore, it is possible to secure carbon storage through forest restoration (IPCC, 2006). The atmospheric carbon fixation effect of the carbon reservoir is estimated through annual changes in carbon uptake that are calculated by applying the carbon coefficient and area for each species according to plant growth (Lee S.-g. et al., 2018).

To obtain the emission reduction, time-series land cover change should be preceded, and it is divided into a method using national statistical data and a method based on spatiotemporal activity data according to the IPCC (2003) approach level. To obtain higher scientific reliability, it is recommended to apply spatiotemporal activity data. When these data are absent, a method of replacing them, with national statistical data is proposed. In the case of the Korean Peninsula, various space-based studies have been conducted in the Republic of Korea (ROK), but research on the Democratic People's Republic of Korea (DPRK) is insufficient. The long-term spatiotemporal data analyzed using the same criteria for the Korean Peninsula are from the land cover maps of the ROK's Ministry of Environment classified as Landsat TM (30 m) (<https://egis.me.go.kr/intro/land.do>), it enables a space-based analysis at the level of Approach 3.

The Korean Peninsula had a serious deforestation problem prior to the establishment of a divided government, which comprises the ROK and the DPRK, while a common feature was the large-scale government-led forest restoration projects, which were performed until the 1980s. After the completion of the reforestation phase, the forest area in the ROK has been continuously increasing; however, the DPRK has been gradually converted from forest to cropland (FAO, 2006). Despite the geographical proximity between the two countries, the difference in national policy, according to the economic condition, has caused opposite trends in the changes to the forest area since 1980 (Park and Park, 2012; Song et al., 2017). Recent deforestation in the DPRK, confirmed through satellite imagery, was shown to be more serious than what was reported to the international community by the DPRK (Lee S.-g. et al., 2018; Lim et al., 2019). The degraded forest was converted to cropland for food supply under the DPRK government-led policy, and it was discovered that the target area for restoration would be vast (Lim et al., 2017). The main cause of the DPRK's food shortage is not the lack of cropland, but the lack of financial resources, such as fertilizers, essential for crop growth and the lack of technology required for sustainable farming. Therefore, experts for the DPRK suggest that it does not have the capacity to carry out food production and reforestation on its own. Considering that forest restoration policies have been actively pursued since the

establishment of the Kim Jong-un regime, financial and technical support for the DPRK is required from neighboring countries.

The area of forests has increased in the ROK, but the area of cropland has decreased and the area of settlements has increased. The recent level of deforestation in the DPRK confirmed through satellite imagery is known to be more serious than reported by the international community (Lee S.-g. et al., 2018). This trend has created a difference in the area available for securing additional carbon sinks in the forests within the Korean Peninsula. The ROK urgently needs to increase carbon sinks according to the 2050 Carbon Neutral Plan, but research on fields where non-forests could be converted to forests is insufficient. According to a forest carbon study through reforestation after lumbering in the ROK, 27 million Mg CO₂ yr⁻¹ was predicted in 2050, which does not meet the target of 36 million Mg CO₂ yr⁻¹ of the 2050 Carbon Neutrality Plan (Hong et al., 2022). In this respect, it is urgently necessary to identify the potential for securing additional carbon sinks, and afforestation and reforestation could be realistic alternatives. In contrast, the DPRK's task is to restore forests to solve the problem of land degradation. It is expected that the target area for forest conversion would be wide because the DPRK has a high rate of agricultural land conversion from forests, which means that the restoration of degraded forests could be used as a carbon sink (Lim et al., 2017).

Therefore, this study aims to classify the reforestation target areas in the Korean Peninsula and quantify the potential carbon sequestration effects by reforestation scenarios. The target area of reforestation for the Afforestation and Reforestation Clean Development Mechanism (A/R CDM) is identified by estimating the change in the historical forest area since the 1980s when the difference in land cover trends between the ROK and the DPRK occurs. For the potential carbon sequestration in the future, the hypothesized reforestation scenario is applied and the change over time is estimated. The value of reforestation, which has been underestimated, could be reconsidered and used as a basis for forest policy decisions through the quantification of carbon sink potential.

2. Materials and methods

2.1. Historical land cover changes using satellite images

In this study, reforestation follows the standards of A/R CDM, and it means reforestation on land that was previously forested and then converted to non-forest use. Land cover change through spatial information is essential to meet the eligibility assessment to be selected as a target for afforestation and reforestation (Yoo et al., 2010). Afforestation targets areas that have been non-forested for the past 50 years; there is a limit to the application of the Korean Peninsula because data prior to the 1970s only exist in document statistics. The Korean Peninsula consists of the ROK and the DPRK; however, since 1980, they have possessed contrasting land use patterns. In particular, the trend in forest area change appears in contrast to each other, which causes a difference in the area for carbon sink. In terms of securing CO₂ sequestration

TABLE 1 Information on satellite image data.

| Time | Source image | Spatial resolution | Number of maps |
|-------|------------------------|--------------------|----------------|
| 1980s | Landsat TM (1987–1989) | 30 m | 488 |
| 1990s | Landsat TM (1997–1999) | 30 m | 488 |
| 2000s | Landsat TM (2008–2010) | 30 m | 488 |
| 2010s | Landsat TM (2018–2019) | 30 m | 488 |

through forest conversion, the expected effect will be distinctly different. It could be classified as a reforestation target based on the A/R CDM standard as major changes in the forest of the Korean Peninsula occurred after 1980. Spatial data for estimating land cover change used the 10-year land cover map (1980s, 1990s, 2000s, and 2010s) of the Korean Peninsula officially published by the ROK’s Ministry of Environment (Table 1) (<https://egis.me.go.kr/>). Each data set was established from the Landsat TM imagery for the Korean Peninsula. The spatial resolution is 30 m, and they had more than 70% accuracy for classification (Kang and Choi, 2014). The resolution of the land cover map was applied in units of 30 × 30 m and was matched with the most recent land cover map in 2010. The land cover change was estimated using a time series matrix for each type (Klein et al., 2012). The type of land cover change defines an area that has been converted to settlements, cropland, wetland, bare ground, or water from a forest. The settlements have limitations for reforestation because economic loss occurs in the removal of urbanized land and infrastructure when it converts into a forest. Therefore, cropland, wetland, and bare ground were considered as possible reforestation patches, while settlements and water were classified as impossible for reforestation.

$$f(x) = \frac{1}{\delta\sqrt{2\pi}} e^{-\frac{(x-\mu)^2}{2\delta^2}}, \tag{1}$$

where δ represents the standard deviation, and μ represents the mean value.

2.2. Reforestation scenario

To estimate the effect of carbon sequestration by reforestation in the future, a reforestation scenario was established. The area for reforestation varies depending on when the reference period is established (Teuling et al., 2019). In the land cover change data, the largest reforestation area appears when the reference period is 1980 and the smallest area is derived in 2000 because of the rapid forest decrease in the DPRK. The reference period for the reforestation scenario was 2010 compared with 2020, which shows the smallest area for reforestation in the time series. This is to minimize the burden on food production in the DPRK, and it could support the establishment of a feasible policy that reduces the overestimation. The assumed reforestation area covers the total area of the reforestation derived from each country and applies to the same area annually. The annual reforestation area was derived by dividing the total area of the reforestation target for each country over 70 years from 2031 to 2100, and it was assumed that 5-year-old

TABLE 2 Species growing stock by age of stand.

| Tree species | Growing stock by age class | | | | | | |
|-----------------------------|----------------------------|--------|-------|--------|--------|--------|--------|
| | 10 | 15 | 20 | 25 | 30 | 35 | 40 |
| <i>Pinus densiflora</i> | 34.7 | 62 | 70.2 | 101.85 | 129.25 | 152.05 | 171.05 |
| <i>Pinus koraiensis</i> | 17.2 | 42.7 | 71 | 98.9 | 125.2 | 149.5 | 171.8 |
| <i>Larix kaempferi</i> | 40.5 | 70.7 | 100.7 | 127.7 | 151.6 | 172.8 | 191.7 |
| <i>Pinus rigida</i> | – | 35.8 | 65.6 | 95.5 | 122.5 | 145.5 | 164.6 |
| <i>Chamaecyparis obtuse</i> | – | 49.1 | 90.8 | 126.4 | 153.5 | 173.7 | 189.1 |
| <i>Quercus acutissima</i> | – | 56.6 | 85.3 | 112.7 | 138.7 | 163.1 | 186.3 |
| <i>Quercus mongolica</i> | 37.3 | 66.2 | 92.1 | 113.1 | 131.7 | 148.7 | 164.6 |
| | 45 | 50 | 55 | 60 | 65 | 70 | 75 |
| <i>Pinus densiflora</i> | 187.05 | 200.65 | 212.3 | 222.45 | 231.25 | 239.05 | 245.95 |
| <i>Pinus koraiensis</i> | 192.3 | 211.3 | 228.8 | 245.2 | 260.5 | 275 | 288.8 |
| <i>Larix kaempferi</i> | 208.8 | 224.4 | 238.8 | 252.1 | 264.6 | 276.3 | 287.3 |
| <i>Pinus rigida</i> | 180.4 | 193.5 | 204.4 | 213.8 | 222 | 229.2 | 235.8 |
| <i>Chamaecyparis obtuse</i> | 201.5 | 211.8 | 220.6 | 228.4 | 235.3 | 241.6 | 247.3 |
| <i>Quercus acutissima</i> | 208.3 | 229.1 | 249 | 267.9 | 285.9 | 303.1 | 319.5 |
| <i>Quercus mongolica</i> | 180 | 195 | 209.8 | 224.7 | 239.5 | 254.4 | 269.5 |

woody plants were planted for the annual area. The total amount obtained by reforestation was calculated by the planted amount in the current year and the growing amount generated by tree growth in the previous period (Equation 2). A temporal growing stock by tree age is predicted according to the stand harvest table of the Korea Forest Service (Table 2). The stand yield table presents the growth by site index. As this study targets planting in non-forest areas, overestimation was avoided by applying the growth amount that appears at the lowest status index for each species. In cases of growing stock in 10-aged *Pinus rigida*, *Chamaecyparis obtuse* and *Quercus acutissima* are not known in the ROK, so it is assumed there is half of the growing stock for the 15-age.

$$V_{Total} = V + V_{Reforestation} + V_{t2-t1}, \tag{2}$$

where V_{Total} represents the total forest stock each year, V represents the forest stock prediction without management, $V_{Reforestation}$ represents the volume for the new yearly reforestation, and V_{t2-t1} represents forest accumulation by growth.

2.3. Calculation of CO₂ sequestration

The ROK forest types were reclassified from the forest map made by the Korea Forest Service (<https://map.forest.go.kr/forest/>) to the dominant species, which consists of pure stands, such as *Pinus densiflora*, *Pinus koraiensis*, *Larix kaempferi*, *Pinus rigida*, *Chamaecyparis obtuse*, *Quercus acutissima*, and *Quercus mongolica*, while the tree stock was derived by applying the age of actual vegetation (Hong et al., 2022). These plants are the main species of the Korean Peninsula, and they have an advantage in surviving in a wide and barren environment. It was used as a major afforestation

TABLE 3 Carbon emission factors for the major tree species in the Korean Peninsula.

| Tree species | Basic wood density | Biomass expansion factor | Root/shoot ratio | Carbon fraction |
|-----------------------------|--------------------|--------------------------|------------------|-----------------|
| <i>Pinus densiflora</i> | 0.445 | 1.448 | 0.256 | 0.51 |
| <i>Pinus koraiensis</i> | 0.408 | 1.742 | 0.276 | 0.51 |
| <i>Larix kaempferi</i> | 0.453 | 1.335 | 0.291 | 0.51 |
| <i>Pinus rigida</i> | 0.504 | 1.325 | 0.362 | 0.51 |
| <i>Chamaecyparis obtuse</i> | 0.427 | 1.349 | 0.203 | 0.51 |
| <i>Quercus acutissima</i> | 0.721 | 1.450 | 0.313 | 0.48 |
| <i>Quercus mongolica</i> | 0.663 | 1.603 | 0.388 | 0.48 |

species in the forest reforestation process of the Korean Peninsula in the past. As a result, it constitutes the dominant species on the Korean Peninsula. In the case of the DPRK, the amount of tree stock was calculated using the species distribution data announced by FAO (2020). The prediction of the forest stock change without management was assumed as the baseline for a future period until 2100. The carbon dioxide equations (Equations 3 and 4), which were suggested by IPCC guidelines were applied. The country-specific coefficient derived from the National Institute of Forest Science was used to calculate the effect from 2031 to 2100 when the reforestation will be performed (Table 3) (Son et al., 2010). According to the IPCC method, the carbon stock in the forest sector is derived through the sum of biomass and soil, but a country-specific coefficient that could be used in the Korean Peninsula has only been developed for biomass. To analyze the amount of carbon sequestration in the soil by reforestation in a time series, it is essential to estimate the change after the early and middle periods, but there are insufficient data to calculate this. Therefore, the research subject was limited to biomass in this study. The future annual net CO₂ sequestration is calculated by the predicted baseline and the reforestation effect. The change of stock volume shows a high increasing rate during the early stage of growth and causes a positive effect on the annual net carbon sequestration by reforestation (Başkent et al., 2011; Seo et al., 2018).

$$C = V_{t_j} \times D_j \times BEF_j \times (1 + R) \times CF \quad (3)$$

$$\Delta CO_{2t_i} = \frac{CS_{t_{i+1}} - CS_{t_i}}{t_{i+1} - t_i} \times \frac{44}{12}, \quad (4)$$

where C is carbon stock (Mg C ha⁻¹), V is the stand volume (m³ ha⁻¹), D is the basic density of the wood, BEF is called biomass expansion factor, R is the root-to-shoot ratio, CF is the carbon fraction (IPCC factor = 0.5), t_i is the year, j is the tree species, t_i and t_{i+1} are the annual change in carbon stock (Mg C ha⁻¹ year⁻¹), and $\frac{44}{12}$ is the stoichiometric ratio of CO₂ and C.

3. Results

3.1. Historical land cover changes since the 1980s

As a result of the land cover changes in the Korean Peninsula, a gradual change has occurred during the 30 years since 1980

(Figure 1). Moreover, the forest area decreased from 168,009 km² in the late 1980s to 162,027 km² in the late 2010s, while the settlements increased from 3,630 km² to 7,656 km². The change in the land cover of nations showed different patterns between the ROK and the DPRK (Table 4). In the ROK, the area of forest and settlements has been continuously increasing since 1980, while the cropland is decreasing (Choi et al., 2021). The most distinctive characteristic of land cover change in the ROK is that the area of settlements increased by +3,372 km², resulting in rapid urban expansion and a decrease in agricultural land over the past 30 years. The forest area increased by +1,545 km² from 68,264 km² in the 1980s to 69,809 km² in the late 2010s, indicating that long-term forest management was well implemented. In contrast, there was a clear decrease in forest area and an increase in cropland in the DPRK (Kang and Choi, 2014). The forest decreased by 7,527 km², accounting for 5.68% of the entire land area of the DPRK, and cropland increased by 5,222 km² which is 5.12%. This confirmed, spatially, that the cropland conversion in the DPRK has mainly occurred from the forest. Moreover, spatial distribution demonstrated that the increased cropland gradually widens around the periphery of the forest, meaning that farming in the DPRK has performed at a steeper slope and a higher elevation than in the ROK (Yu et al., 2018). The difference between the countries becomes more pronounced when the land cover is classified into forest and non-forest regions (Figure 2).

3.2. Analysis of reforestation target area

As a result of the reforestation target area, in the past period compared with the current land cover (2020), it was found that the target area decreased as the reference period got closer to the present (Figure 3). The area of reforestation in the ROK was 10,117 km² in the 1980s, 9,812 km² in the 1990s, and 8,880 km² in the 2000s, and there was no significant difference, whereas the reforestation area in the DPRK was 16,586 km² in the 1980s, 14,539 km² in the 1990s, and 11,670 km² in the 2000s. For the purpose of expanding the carbon sink, the largest acquisition would be expected in 1980. However, considering the economic situation of the DPRK, the rapid reforestation of cropland could cause new problems for the food supply. An area, which has been agricultural land for a long time, could easily be degraded as the trees are harvested for fuel (Byeon, 2014; Crespo Cuaresma et al., 2020). In this respect, it is important to minimize the impact of external

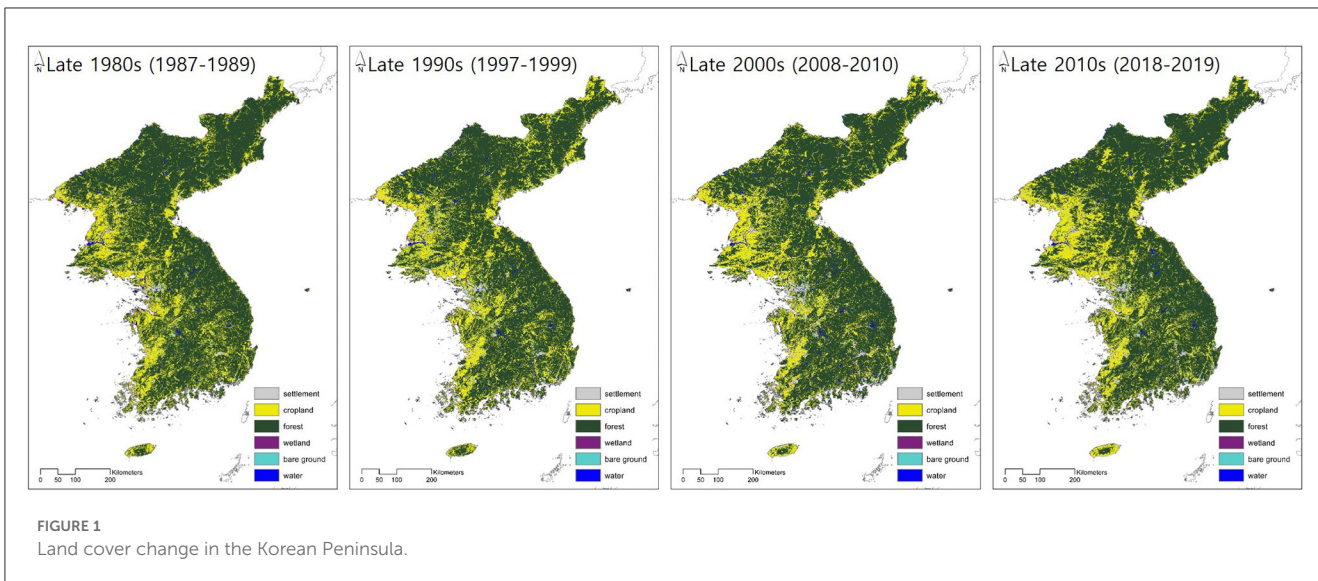


FIGURE 1 Land cover change in the Korean Peninsula.

TABLE 4 Area change for land cover types.

| Land cover change in the Republic of Korea (ROK) (km ²) | | | | | Land cover change in the Democratic People's Republic of Korea (DPRK) (km ²) | | | | |
|---|--------|--------|--------|--------|--|--------|--------|--------|--------|
| Type* | 1980s | 1990s | 2000s | 2010s | Type* | 1980s | 1990s | 2000s | 2010s |
| S | 2,136 | 3,488 | 4,134 | 5,508 | S | 1,493 | 2,129 | 2,084 | 2,148 |
| C | 27,680 | 26,283 | 24,045 | 21,651 | C | 28,383 | 32,600 | 33,120 | 33,605 |
| F | 68,264 | 68,088 | 69,519 | 69,809 | F | 99,744 | 94,029 | 93,950 | 92,217 |
| W | 600 | 396 | 271 | 810 | W | 542 | 396 | 260 | 525 |
| B | 1,234 | 1,641 | 1,566 | 1,492 | B | 991 | 1,919 | 1,244 | 1,664 |
| W | 2,285 | 2,304 | 2,388 | 2,705 | W | 1,593 | 1,650 | 1,995 | 2,244 |

*S, settlement; C, cropland; F, forest; W, wetland; B, bare ground; W, water.

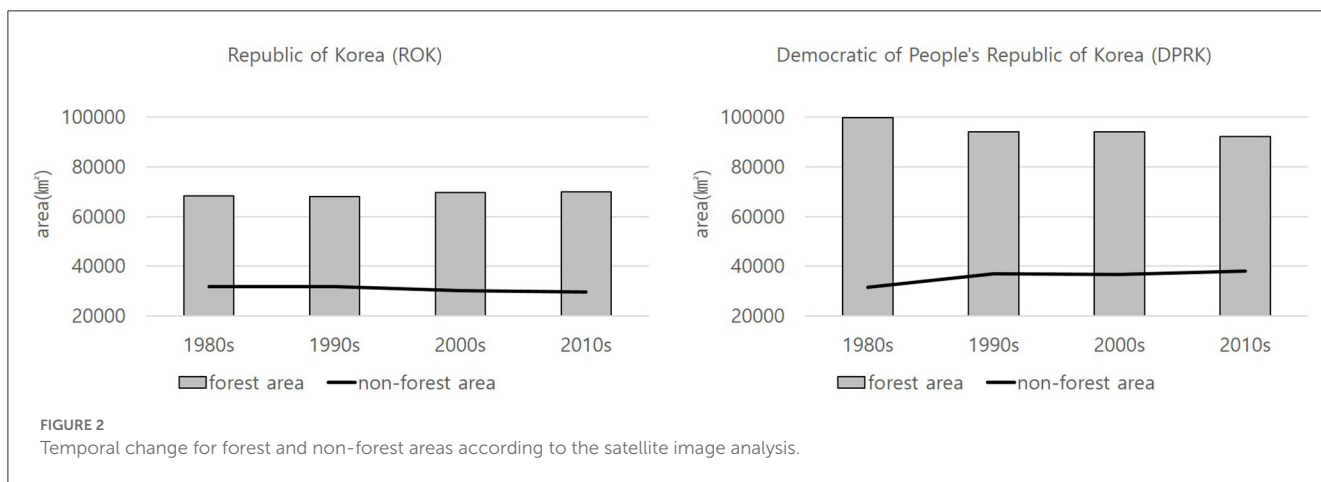
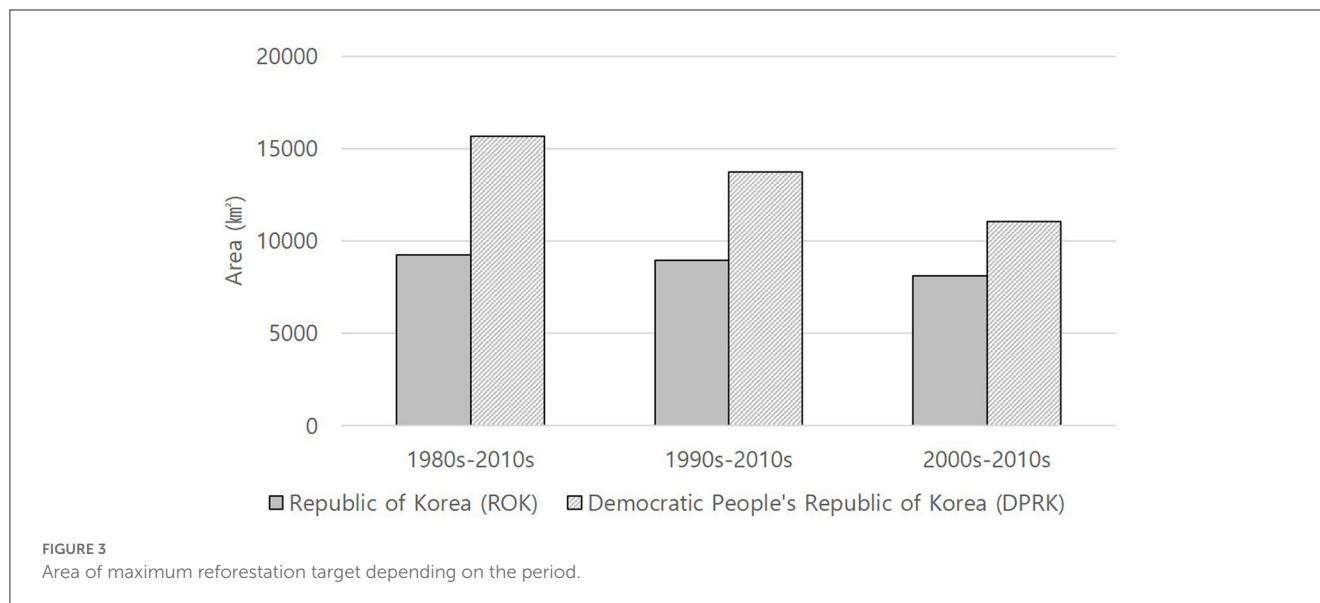


FIGURE 2 Temporal change for forest and non-forest areas according to the satellite image analysis.

factors by selecting a target period close to the present. Considering the ROK, there was no critical difference regardless of the standard reforestation period, and a difference of 4,916 km² was found when comparing the reforestation area between the late 1980s and 2010s in the DPRK. This is an area where about 1.8 billion trees could be planted assuming that 3,000 trees are planted per ha, which is 3.71% of the DPRK's land area.

The spatial distribution of reforestation in the Korean Peninsula shows a different pattern between the ROK and the DPRK, especially when the types of land cover changes were divided into reforestation targets and settlements (Figure 4). If the late 2000s is selected as the reference period, 7,104 km² (79.80%) of the land that could be reforested and 2,248 km² (20.20%) of the land that could not be reforested are found in the ROK. On



the other hand, 11,670 km² (92.97%) of the area is possible and 882 km² (7.03%) of the area is impossible for reforestation in the DPRK. Therefore, the ROK is facing spatial limitations in which reforestation could not be carried out even though forests have been converted to other land covers. In contrast, the DPRK appears to have the conditions for reforestation to be applied in most of the converted areas since the late 1980s.

3.3. Prediction of stand volume and CO₂ changes by reforestation

The annual reforestation area of ROK is 126.8 km², and the DPRK is analyzed to be 166.7 km², which is 1.3 times larger when the reference period set to the late 2000s and the reforestation scenario was applied. As a result of assuming the forest accumulation according to the growth prediction from actual vegetation as a baseline, it is estimated that forest accumulation in the ROK by reforestation calculated at 17,233,460m³ in 2050, 57,848,704m³ in 2070, and 146,087,769m³ in 2100. An increase of ~24.17% is expected through the implementation of the reforestation scenario compared to that of the current forest accumulation of the ROK is estimated to be 604,395,000m³. In the case of the DPRK, it was analyzed that a net acquisition of 22,646,764m³ in 2050, 76,019,899m³ in 2070, and 191,976,252m³ in 2100 was possible. Compared to the DPRK's current forest accumulation of 682,966,400m³, it was analyzed that the maximum potential by reforestation is possible to increase the stand volume by 28.11% compared to the late 2010s (Figure 5).

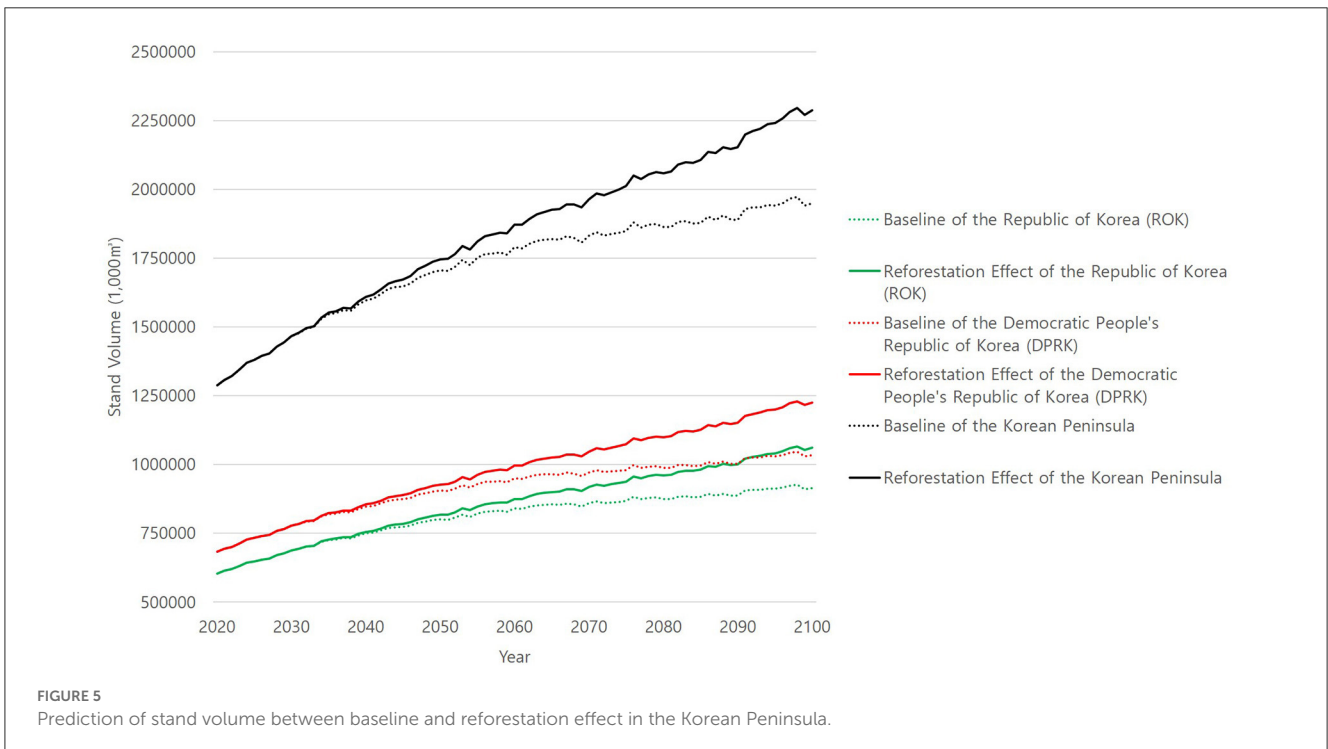
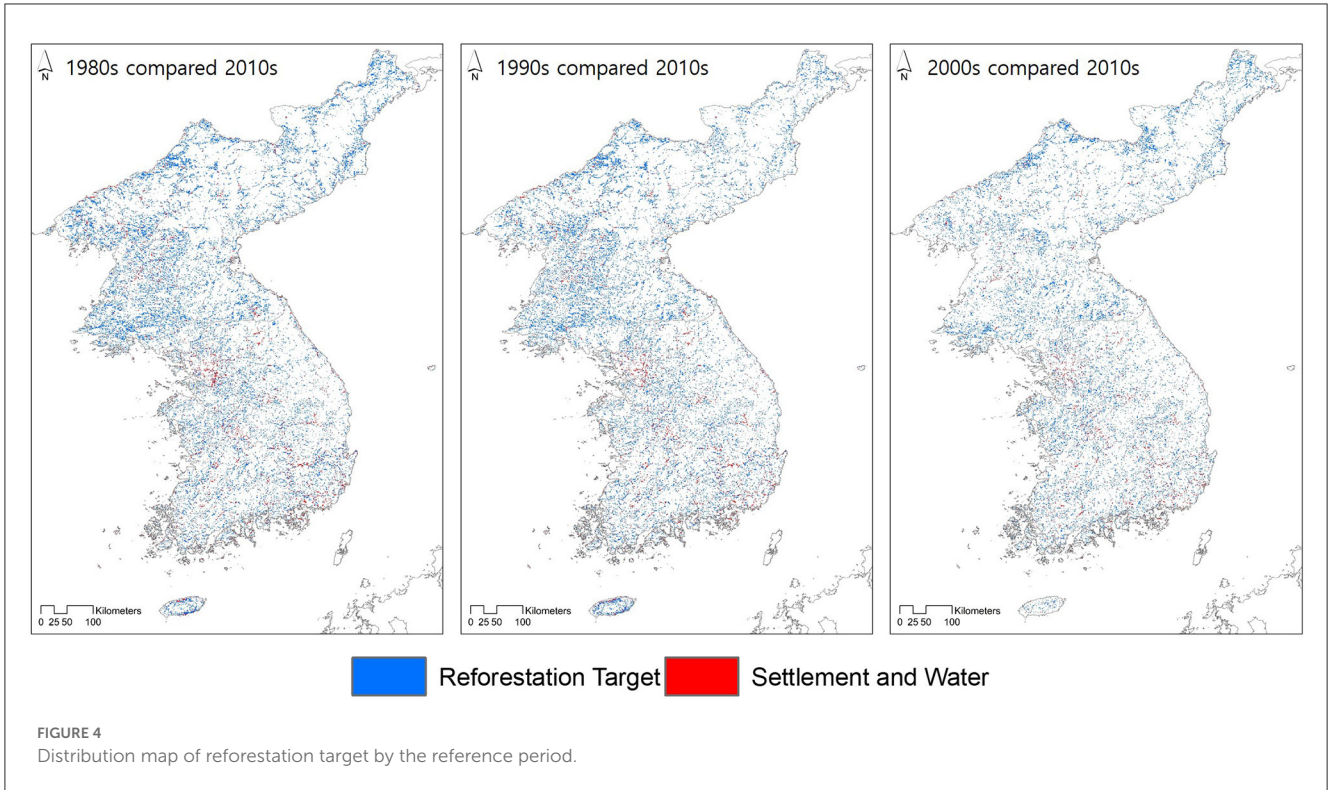
A net annual CO₂ sequestration of 10,833,600 Mg CO₂ year⁻¹ is expected in 2050, with 20,919,200 Mg CO₂ year⁻¹ expected in 2070 in the ROK through the reforestation scenario (Figure 6). Moreover, the DPRK forest was estimated to have a potential net annual carbon sequestration of 14,236,800 Mg CO₂ year⁻¹ in 2050 and 27,490,400 Mg CO₂ year⁻¹ in 2070. The annual net carbon sequestration would be changed according to the area and

period for reforestation because the carbon sequestration effect by reforestation was calculated by including both the increase for tree planting in the current year and the growth of the trees converted to the forest in the previous period. Therefore, it was determined that the potential for carbon sink expansion through reforestation was higher in the DPRK than in the ROK.

4. Discussion

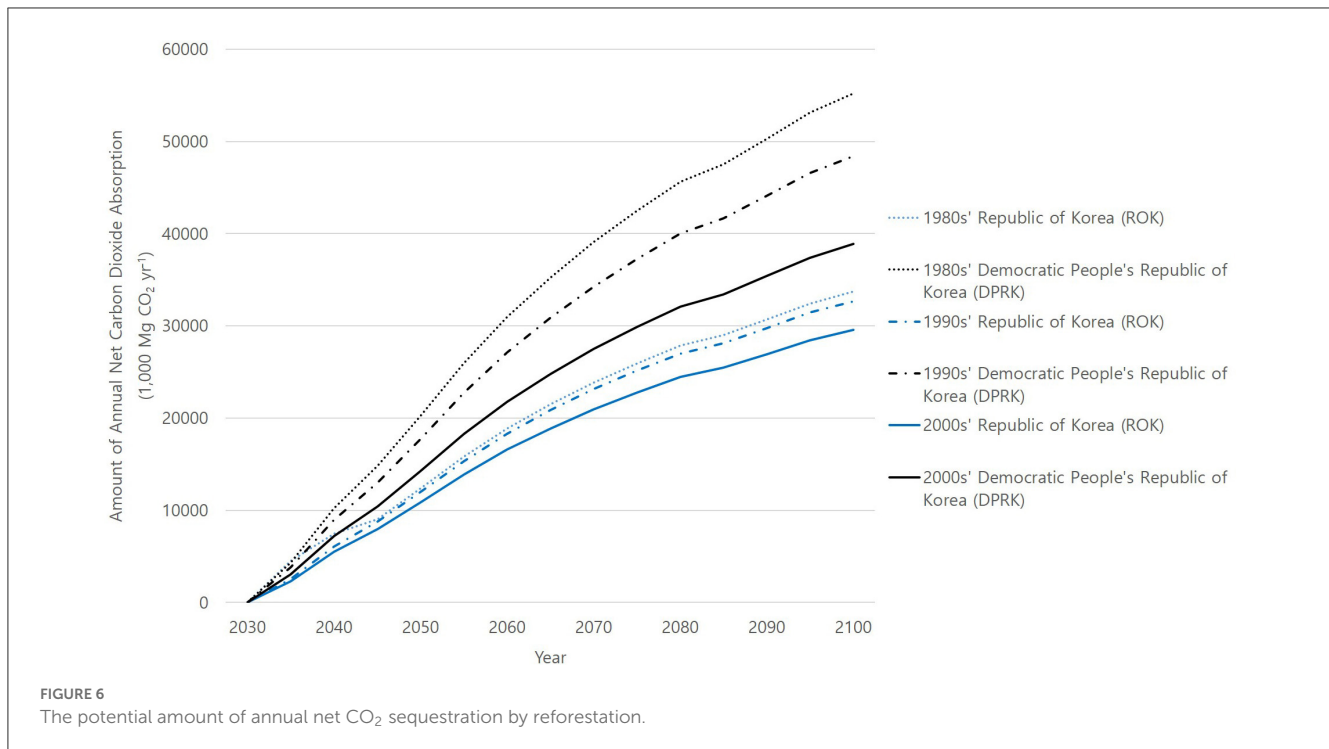
As forests were internationally recognized as carbon sinks, many studies on carbon fixation have been conducted. In this process, the problem of reducing annual carbon sequestration due to forest aging has emerged (Ma et al., 2012; Kim et al., 2022). While studies on forest management have been actively conducted to overcome it, the carbon sequestration effect that could be generated by reforestation has not been presented. The ROK's 2050 Carbon Neutrality Plan emphasizes securing forest carbon sinks. To achieve the target of 34 million tons of carbon sinks by 2050, it is important to apply various forest management methods to reduce the uncertainty of achieving the goal (Yang et al., 2022). The main reasons for the relative lack of research on reforestation are the difficulty of securing the target site, meeting suitability assessment, and long-term forest management. In the case of the ROK, the cost required to secure the site and consultation with the landowner are major issues. Establishing a reforestation plan should be accompanied by an economic analysis of the costs incurred in the process of land purchase and reforestation vs. benefits arising from carbon sequestration.

The DPRK contains uncertainty in the selection of the target site. In the case of the land cover map used in this study, forests were overestimated when compared to the recently published preceding studies (Lee S.-g. et al., 2018; Piao et al., 2021). This is not only a technical problem with image processing but also closely related to land use. In the DPRK, rapid changes in land cover occur due to government-led policies, and a vicious cycle of reckless deforestation and conversion of arable land by



residents continues after achieving the forest greening performance assigned to each region. Therefore, the shooting timing and resolution of images that directly reflect these characteristics could cause differences in image classification. To overcome these limitations, monitoring through short-period imaging of high-resolution satellites should be analyzed on the same method over

a long period of time. Also, in the process of specifying the reforestation target at the implementation level, consideration of land cover changes in the future due to changes in socioeconomic conditions should be included, but there is a limitation in establishing a model due to a lack of data on the DPRK. To develop the socioeconomic scenarios, reliable statistics on spatial-based



population change and urbanization rate are required as mentioned in the socioeconomic path scenario study for the ROK (Song et al., 2018).

As reforestation sites are applied to non-forests in the present, they are likely to be more easily disturbed than forest renewal in terms of continuous forest maintenance. In the A/R CDM, carbon sequestration is calculated through post-planting monitoring and follow-up management, sustainable forest maintenance is the key to being recognized for carbon sequestration. In the DPRK's reforestation process, this problem could be highlighted. When intending to use the DPRK as an overseas reforestation target, international regulations must be followed to enable long-term forest management independent of the unstable political situation. In addition, as the annual reforestation area is achievable when there is no problem with nursery stock supply, seedling production and transportation plans need to be established. There are practical limits to supplying the entire amount required for reforestation from abroad. Mass production of seedlings suitable for local conditions is necessary through advanced technical support and seed supply to local nurseries. In the case of the DPRK, to overcome its own technical limitations, it is receiving support for the construction of nurseries through non-political international organizations, and these facilities will be able to play a major role in supplying seedlings.

5. Conclusion

The Korean Peninsula was an area that was successfully reforested from degraded forest until the 1970s, but changes in land cover occurred due to economic differences after the 1980s.

As a result of analyzing the satellite image data, the ROK was characterized by an increase in the number of settlements and a decrease in cropland, and forests increased by 1,544 km². Since the 1980s, the DPRK has converted forests to cropland, resulting in forest loss of 7,526 km² by the late 2010s. The effect of greening the space converted from past forests to cropland, wetland, and bare ground was analyzed to have an annual net carbon sequestration of 10,833,600 Mg CO₂ year⁻¹ in the ROK and 14,236,800 Mg CO₂ year⁻¹ in the DPRK at 2050. Considering that the forest sector target proposed in the ROK's 2050 Carbon Neutrality Plan is 34,000,000 Mg CO₂ year⁻¹, reforestation is a resource that could be utilized along with carbon enhancement through the renewal of forests maintained as forests. In terms of the international business of securing carbon sinks, the DPRK is free from land ownership issues and has recently been promoting a forest greening policy, so it has a high potential to serve as an overseas target for countries whose forest coverage has reached its limit.

Data availability statement

The original contributions presented in the study are included in the article/supplementary material, further inquiries can be directed to the corresponding author.

Author contributions

S-gL: writing-original draft and data analysis. H-JK: supervision and writing-review and editing. All authors read and agreed to the final version of the manuscript.

Funding

This work was performed with the support of a cooperative research program for agriculture science and technology development (Project No. PJ014923022023) by the Rural Development Administration, the Republic of Korea.

Conflict of interest

The authors declare that the research was conducted in the absence of any commercial or financial relationships

References

- Başkent, E. Z., Keleş, S., Kadiogullari, A. I., and Bingöl, Ö. (2011). Quantifying the effects of forest management strategies on the production of forest values: timber, carbon, oxygen, water, and soil. *Environ. Model. Assess.* 16, 145–152. doi: 10.1007/s10666-010-9238-y
- Byeon, J. (2014). *Forest Change in the DPRK and Strengthen Ability for Recovery*. KAST: Seongnam, Republic of Korea.
- Choi, Y., Lim, C. H., Chung, H. I., Kim, Y., Cho, H. J., Hwang, J., et al. (2021). Forest management can mitigate negative impacts of climate and land-use change on plant biodiversity: Insights from the Republic of Korea. *J. Environ. Manage.* 288, 112400. doi: 10.1016/j.jenvman.2021.112400
- Crespo Cuaresma, J., Danylo, O., Fritz, S., Hofer, M., Kharas, H., and Laso Bayas, J. C. (2020). What do we know about poverty in North Korea?. *Palgrave Commun.* 6, 1–8. doi: 10.1057/s41599-020-0417-4
- FAO (2006). *National Action Plan to combat Desertification / Land degradation in Democratic People's Republic of Korea (2006-2010)*. FAO.
- FAO (2020). *Global Forest Resources Assessment 2020*. FAO.
- Fukushima, T. (2013). The significance of CSR in A/R CDM promotion from the case study of Japan: a focus on corporate forest-related activities and emission trading. *J. For. Res.* 18, 293–304. doi: 10.1007/s10310-012-0351-4
- Hong, M., Song, C., Kim, M., Kim, J., Lee, S. G., Lim, C. H., et al. (2022). Application of integrated Korean forest growth dynamics model to meet NDC target by considering forest management scenarios and budget. *Carbon Balance Manage.* 17, 1–18. doi: 10.1186/s13021-022-00208-8
- IPCC (2003). *Good Practice Guidance for Land Use, Land-Use Change and Forestry*. IPCC/UGES.
- IPCC (2006). *IPCC Guidelines for National Greenhouse Gas Inventory*. Hyama: IPCC/IGES.
- Kang, S., and Choi, W. (2014). Forest cover changes in North Korea since the 1980s. *Reg. Environ. Change* 14, 347–354. doi: 10.1007/s10113-013-0497-4
- Kim, G., Kim, J., Ko, Y., Eyman, O. T. G., Chowdhury, S., Adiwal, J., et al. (2021). How do nature-based solutions improve environmental and socio-economic resilience to achieve the sustainable development goals? reforestation and afforestation cases from the Republic of Korea. *Sustainability* 13, 12171. doi: 10.3390/su132112171
- Kim, H. S., Noulèkoun, F., Noh, N. J., and Son, Y. W. (2022). Future projection of CO₂ absorption and N₂O emissions of the south Korean forests under climate change scenarios: toward net-zero CO₂ emissions by 2050 and beyond. *Forests* 13, 1076. doi: 10.3390/f13071076
- Klein, I., Gessner, U., and Kuenzer, C. (2012). Regional land cover mapping and change detection in Central Asia using MODIS time-series. *Appl. Geograph.* 35, 219–234. doi: 10.1016/j.apgeog.2012.06.016
- Lee, S.-g., Choi, H.-A., Yoo, H., Song, C., Cha, S., Bae, S.-W., et al. (2018). Restoration plan for degraded forest in the democratic people's Republic of Korea considering suitable tree species and spatial distribution. *Sustainability* 10, 856. doi: 10.3390/su10030856
- Lim, C. H., Choi, Y., Kim, M., Jeon, S. W., and Lee, W. K. (2017). Impact of deforestation on agro-environmental variables in cropland, North Korea. *Sustainability* 9, 1354. doi: 10.3390/su9081354
- Lim, C. H., Song, C., Choi, Y., Jeon, S. W., and Lee, W. K. (2019). Decoupling of forest water supply and agricultural water demand attributable to deforestation in North Korea. *J. Environ. Manage.* 248, 109256. doi: 10.1016/j.jenvman.2019.07.027
- Ma, Z., Peng, C., Zhu, Q., Chen, H., Yu, G., Li, W., et al. (2012). Regional drought-induced reduction in the biomass carbon sink of Canada's boreal forests. *Proceed. Nat. Acad. Sci.* 109, 2423–2427. doi: 10.1073/pnas.1111576109
- Nevle, R. J., and Bird, D. K. (2008). Effects of syn-pandemic fire reduction and reforestation in the tropical Americas on atmospheric CO₂ during European conquest. *Palaeogeograph. Palaeoclimatol. Palaeoecol.* 264, 25–38. doi: 10.1016/j.palaeo.2008.03.008
- Park, K. S., and Park, S. Y. (2012). The rehabilitation of North Korea's Devastated Forest: with focus on the case of South Korea. *North Korean Stud.* 8, 133–159. doi: 10.23040/kcdoi.2012.8.1.005
- Piao, Y., Jeong, S., Park, S., and Lee, D. (2021). Analysis of land use and land cover change using time-series data and random forest in North Korea. *Rem. Sens.* 13, 3501. doi: 10.3390/rs13173501
- Saeed, S., Ashraf, M. I., Ahmad, A., and Rahman, Z. (2016). The Bela forest ecosystem of district Jhelum, a potential carbon sink. *Pak. J. Bot.* 48, 121–129.
- Seo, Y., Lee, D., and Choi, J. (2018). Growth pattern analysis of major coniferous tree species in South Korea. *Forest Sci. Technol.* 14, 1–6. doi: 10.1080/21580103.2017.1409660
- Son, Y. M., Lee, G. H., Kim, R., Pyo, J. K., Park, I. H., Son, Y. W., et al. (2010). Carbon emission factors by major tree species for forest greenhouse gas inventory. *Seoul 2010*, 2658.
- Song, C., Kim, S. J., Moon, J., Lee, S. J., Lee, W., Kim, N., et al. (2017). Classification of global land development phases by forest and GDP changes for appropriate land management in the mid-latitude. *Sustainability* 9, 1342. doi: 10.3390/su9081342
- Song, C., Yoo, S., Kim, M., Lim, C. H., Kim, J., Kim, S. J., et al. (2018). Estimation of future land cover considering shared socioeconomic pathways using scenario generators. *J. Clim. Change Res.* 9, 223–234. doi: 10.15531/KSCCR.2018.9.3.223
- Teuling, A. J., De Badts, E. A., Jansen, F. A., Fuchs, R., Buitink, J., Hoek van Dijke, A. J., et al. (2019). Climate change, reforestation/afforestation, and urbanization impacts on evapotranspiration and streamflow in Europe. *Hydrol. Earth Syst. Sci.* 23, 3631–3652. doi: 10.5194/hess-23-3631-2019
- UNFCCC (2002a). *Report of the Conference of the Parties on its Seventh Session, Held in Marrakech from 29 October–10 November 2001*. Addendum Part Two: Action Taken by the Conference of the Parties, vol I (FCCC/CP/2001/13/Add. 1). United Nations Framework Convention on Climate Change Secretariat, Bonn, Germany
- UNFCCC (2002b). *Report of the Conference of the Parties on its Seventh Session, Held in Marrakech from 29 October–10 November 2001*. Addendum Part Two: Action Taken by the Conference of the Parties, vol II (FCCC/CP/2001/13/Add. 1). United Nations Framework Convention on Climate Change Secretariat, Bonn, Germany
- Wang, B., Waters, C., Anwar, M. R., Cowie, A., Li Liu, D., Summers, D., et al. (2022). Future climate impacts on forest growth and implications for carbon sequestration through reforestation in southeast Australia. *J. Environ. Manage.* 302, 113964. doi: 10.1016/j.jenvman.2021.113964
- Yang, C., Kwon, H., Bang, B., Jeong, S., and Lee, U. (2022). Role of biomass as low-carbon energy source in the era of net zero emissions. *Fuel* 328, 125206. doi: 10.1016/j.fuel.2022.125206
- Yoo, S. H., Cho, Y., Son, Y., and Lee, W. K. (2010). A policy recommendation for the successful CDM A/R Projects. *J. Energy Clim. Chang.* 5, 51–64.

that could be construed as a potential conflict of interest.

Publisher's note

All claims expressed in this article are solely those of the authors and do not necessarily represent those of their affiliated organizations, or those of the publisher, the editors and the reviewers. Any product that may be evaluated in this article, or claim that may be made by its manufacturer, is not guaranteed or endorsed by the publisher.

Yu, H., Zhang, B., and Wang, Z. (2018). Comparative study on changes of croplands between North Korea and South Korea during 1990–2015. *Chinese Geographic. Sci.* 28, 920–934. doi: 10.1007/s11769-018-0985-z

Zomer, R. J., Trabucco, A., Bossio, D. A., and Verchot, L. V. (2008). Climate change mitigation: a spatial analysis of global land suitability for clean development mechanism afforestation and reforestation. *Agricult. Ecosyst. Environ.* 126, 67–80. doi: 10.1016/j.agee.2008.01.014



OPEN ACCESS

EDITED BY

Ling Zhang,
Jiangxi Agricultural University, China

REVIEWED BY

Dianming Wu,
East China Normal University, China
Clément Stahl,
Délégation Ile-de-France Sud (CNRS), France

*CORRESPONDENCE

Xinming Wang
✉ wangxm@gig.ac.cn

RECEIVED 17 July 2023

ACCEPTED 28 September 2023

PUBLISHED 12 October 2023

CITATION

Mu Z, Zeng J, Zhang Y, Song W, Pang W, Yi Z, Asensio D, Llusà J, Peñuelas J and Wang X (2023) Soil uptake of isoprenoids in a *Eucalyptus urophylla* plantation forest in subtropical China.
Front. For. Glob. Change 6:1260327.
doi: 10.3389/ffgc.2023.1260327

COPYRIGHT

© 2023 Mu, Zeng, Zhang, Song, Pang, Yi, Asensio, Llusà, Peñuelas and Wang. This is an open-access article distributed under the terms of the [Creative Commons Attribution License \(CC BY\)](https://creativecommons.org/licenses/by/4.0/). The use, distribution or reproduction in other forums is permitted, provided the original author(s) and the copyright owner(s) are credited and that the original publication in this journal is cited, in accordance with accepted academic practice. No use, distribution or reproduction is permitted which does not comply with these terms.

Soil uptake of isoprenoids in a *Eucalyptus urophylla* plantation forest in subtropical China

Zhaobin Mu^{1,2,3,4}, Jianqiang Zeng^{1,2,5}, Yanli Zhang^{1,2}, Wei Song^{1,2}, Weihua Pang^{1,2,5}, Zhigang Yi⁶, Dolores Asensio^{3,7}, Joan Llusà^{3,4}, Josep Peñuelas^{3,4} and Xinming Wang^{1,2,5*}

¹State Key Laboratory of Organic Geochemistry and Guangdong Key Laboratory of Environmental Protection and Resources Utilization, Guangzhou Institute of Geochemistry, Chinese Academy of Sciences, Guangzhou, China, ²CAS Center for Excellence in Deep Earth Science, Guangzhou, China, ³CSIC, Global Ecology Unit CREAM-CSIC-UAB, Barcelona, Spain, ⁴CREAF, Barcelona, Spain, ⁵College of Resources and Environment, University of Chinese Academy of Sciences, Beijing, China, ⁶Fujian Provincial Key Laboratory of Soil Environmental Health and Regulation, College of Resources and Environment, Fujian Agriculture and Forestry University, Fuzhou, China, ⁷Faculty of Science and Technology, Free University of Bozen-Bolzano, Bolzano, Italy

The exchange of isoprenoids, which includes isoprene, monoterpenes, and sesquiterpenes, between ecosystem soils and the atmosphere plays a significant role in soil ecology and atmospheric chemistry. However, research on flux exchange rates in subtropical ecosystems has been limited, as previous studies have mainly focused on temperate and boreal environments. In this study, we aimed to quantify the exchange of isoprenoids between the soil (with or without surface litter) and the atmosphere in a subtropical *Eucalyptus urophylla* plantation forest during the daytime in the wet season of subtropical China. Additionally, we investigated the influence of soil and litter variables on the fluxes of isoprenoids. Our results unveiled the exchange of isoprene and 17 terpenoid compounds, comprising 11 monoterpenes and 6 sesquiterpenes, between the studied soils and the atmosphere. Interestingly, regardless of the presence of surface litter, the studied soils acted as net sinks for isoprenoids, with isoprene being the most absorbed compound ($-71.84 \pm 8.26 \mu\text{g m}^{-2} \text{ h}^{-1}$). The removal of surface litter had a significant impact on the exchange rates of two monoterpenes (α -pinene and β -pinene), resulting in decreased fluxes. Furthermore, the exchange rates of isoprene were positively correlated with litter dry weight and negatively correlated with soil temperature. The higher exchange rates of monoterpenes and sesquiterpenes were associated with increased levels of soil respiration and the abundance of leaf litter. These findings suggest that, in the context of projected global warming scenarios, the capacity of subtropical soils to act as sinks for isoprenoids is expected to increase in subtropical China. These changes in sink capacity may have implications for regional-scale atmospheric chemistry and ecosystem functioning.

KEYWORDS

soil isoprenoid exchanges, isoprene, dynamic chamber, litter, soil temperature, *Eucalyptus urophylla*, plantation forest, subtropical China

Highlights

- First reported soil isoprene and sesquiterpenes in subtropics.
- Subtropical soils are a significant isoprene sink.
- Microclimate, microbes, and litter drive soil isoprenoid exchanges.
- Positive correlation of the sink with temperature: impacted by climate change.

1. Introduction

Forest soils can emit or absorb biogenic volatile organic compounds (BVOCs) due to a simultaneous occurrence of multiple biological and physico-chemical processes related to soil BVOC dynamics in complex soil environments (Asensio et al., 2007c; Leff and Fierer, 2008; Peñuelas et al., 2014). Isoprenoids and oxygenated BVOCs dominate the bidirectional fluxes between forest soils and the atmosphere (Hellén et al., 2006; Aaltonen et al., 2011, 2013; Mäki et al., 2017). Understanding the direction and magnitude of these fluxes, driven by factors like microclimate and litter, is critical for soil ecology (Wenke et al., 2010; Peñuelas et al., 2014; Svendsen et al., 2018) and atmospheric chemistry (Kramshøj et al., 2016; Nölscher et al., 2016; Tang et al., 2019). Soil BVOC emissions vary depending on ecosystem type, environmental conditions, and season (Tang et al., 2019; Mäki et al., 2019a; Mu et al., 2020). They can originate from litter, microorganisms, and roots, constituting a significant fraction of ecosystem emissions (Aaltonen et al., 2011, 2013; Kreuzwieser and Rennenberg, 2013). Soil can act as a sink or source of BVOCs, impacting their release from the ecosystem (Owen et al., 2007; Kramshøj et al., 2018). Biotic degradation and abiotic processes, such as physical diffusion or adsorption, and chemical reactions influence BVOC exchanges (Insam and Seewald, 2010; Ramirez et al., 2010; Albers et al., 2018; Mu et al., 2020).

Measuring soil BVOC fluxes across different climate zones is crucial. Previous studies focused on temperate and boreal regions (Asensio et al., 2007b,c; Mäki et al., 2019a,b), with limited research in tropical and subtropical forests. Soil BVOC fluxes in these regions remain inconsistent, requiring more data to improve modeling and ecosystem understanding (Bourtsoukidis et al., 2018; Huang et al., 2021; Llusà et al., 2022). Subtropical China, characterized by ideal tree growth conditions, has plantation forests lacking BVOC flux information. *Eucalyptus urophylla*, a significant emitter of isoprenoids, dominates these plantations (Zeng et al., 2022a). In this exploratory pilot study, we quantified isoprenoid exchange rates using a dynamic chamber and investigated their relationship with drivers like temperature, moisture, and respiration in an *E. urophylla* plantation. We aimed to address the knowledge gap regarding soil BVOC fluxes in subtropical forests. Forest soils in subtropical regions, known for their warm and humid climate, play a vital role in commercial forestry plantations (Ming et al., 2014; Wei and Blanco, 2014). These plantations cover a significant portion of the country's forested landscape and are predominantly composed of monoculture coniferous and broadleaved species, including *E. urophylla* (He et al., 2013; Wei and Blanco, 2014; Bai et al., 2021).

Despite the vital role these ecosystems play, there is currently a dearth of information regarding soil BVOC fluxes, particularly from

plantation forests. Remarkably, *E. urophylla* stands out as a significant emitter of isoprenoids in subtropical China, boasting the highest isoprene emission factor among dominant tree species (Zeng et al., 2022a). Consequently, our study aimed to address this knowledge gap by:

Quantifying the exchange rates of isoprenoids, encompassing individual and total monoterpenes (MTs) and sesquiterpenes (SQTs), in addition to isoprene, between the atmosphere and forest soils. We achieved this through the use of a dynamic chamber.

Exploring potential relationships between these exchange rates and various biotic and abiotic factors, such as soil temperature, moisture levels, and respiration, within the *E. urophylla* plantation.

2. Materials and methods

2.1. Study site and experimental design

The study was conducted in a *E. urophylla* plantation forest (22° 39' N, 112° 54' E) located in Heshan, Guangdong Province, southeastern China (see Supplementary Figure S1). The *E. urophylla* trees were artificially planted at the study site and had similar sizes (trunk circumference at breast height: 12–20 cm). The study site experiences a subtropical monsoon climate with an average annual temperature of approximately 21.7°C, and 80% of the mean annual precipitation (approximately 1700 mm) occurs during the wet season (April to September) (Wang et al., 2010). The soils in the study area are classified as Ultisols that developed from sand shales (Fang et al., 2023). The understory vegetation mainly comprised of low-statured species, such as *Dicranopteris pedate*, *Pogonatherum crinitum*, *Mallotus apelta*, *Mikania micrantha*, and *Persicaria chinensis*, which are commonly distributed throughout southeastern China.

A 50 × 50 m study plot was established in the central area of the plantation, and six sampling points were selected randomly within the central 40 × 40 m area, with a distance of more than 10 m between any two points. In each sampling point, two adjacent stainless steel soil collars were inserted into the soil (4 cm) for BVOCs and CO₂ sampling, respectively, approximately 1.5 months before sampling began. The litter and understory vegetation were not removed from the BVOC collars prior to sampling to ensure that the measurements reflected the real-world soil fluxes in field conditions, and to find out the role of litter in the soil exchanges of BVOCs by measuring the fluxes both with and without litter in the sampling campaign. The aboveground parts of the understory vegetation were removed from the CO₂ collars during installation, and litter was removed both during installation and prior to sampling to ensure that the measurements represented belowground soil respiration.

2.2. Isoprenoid sampling

Sampling was conducted in the middle of September 2022, during sunny or slightly cloudy days, between 10:00 and 15:00 h. One or two sampling points were sampled per day. Isoprenoids emitted from the soil were collected using a cylindrical semi-open dynamic chamber (internal diameter: 25 cm; height: 14 cm; volume: 6.8 L) placed over the BVOCs collar (see [Supplementary Figure S2](#)). The chamber and collar were fitted and water-sealed through the slot on the top of the collar. The chamber was constructed with polymethyl methacrylate and coated with fluorinated ethylene propylene (FEP) [Teflon film, (FEP 100, Type 200A; DuPont, United States)] on its inner surface. To promote uniform conditions and prevent condensation buildup inside the chamber, a Teflon fan (Shenzhen Shuangmu Plastic Material Co. Ltd., Shenzhen, China) was affixed to the top of the chamber, and small holes (5 mm I.D.) were drilled in the rim. The circulating air was generated by an air pump (MPU2134-N920-2.08, KNE, Freiburg, Germany) pumping the ambient air near the ground (approximately 18 cm above ground) and was controlled at a rate of 4.2 L min⁻¹ by a mass flow controller (Alicat Scientific, Inc., Tucson, AZ, United States). The circulating air passed through two ozone scrubbers (Na₂S₂O₃, [Helmig et al., 2007](#); [Zeng et al., 2022b](#)) before being drawn into the lower position of the chamber through a random hole at the upper edge (see [Supplementary Figure S3](#)). A three-way valve was used to sample inlet air from circulating air just before entering the chamber, while the outlet air was sampled from the upper position of the chamber through another hole opposite to the previous one. Inlet and outlet air were sampled simultaneously using an automatic sampler (JEC921, Jectec Science and Technology, Co., Ltd., Beijing, China) equipped with two stainless steel cartridges (see [Supplementary Figure S4](#)) filled with adsorbents (150 mg of Tenax TA and 150 mg of Carbograph 5TD, 9, Markes International Ltd., Bridgend, United Kingdom). The sampled air flow rate through the cartridges was 200 mL min⁻¹ for 30 min. The flow rate of circulating air was 4 L min⁻¹, and the residence time of circulating air was approximately 1.7 min during sampling. The sampled cartridges were detached from the automatic sampler, sealed with copper caps, and then stored in a portable refrigerator at 4°C in the field and at -20°C after being taken to the laboratory. Three samplings were conducted at each sampling point, with two of the three samples collected without removing the litter and the third sample collected after removing the litter with great care not to damage the superficial roots. The chamber was initially flushed with ambient air for 10–20 min before each sampling to avoid the influence of artificial disturbance on sampling. Air temperature was measured by a sensor (HC2A-S, Rotronic, Bathersdorf, Switzerland) placed over the chamber. The removed litter was collected and taken to the laboratory for litter composition and dry weight measurements.

2.3. Soil temperature, moisture, and respiration

The LI-6800 gas-exchange system (Li-COR Inc., Lincoln, NE, United States; see [Supplementary Figure S3](#)) was used to determine soil temperature (ST), moisture (v/v; SM), and respiration (SR), with 6–10 replicate measurements taken during each soil BVOC sampling.

Soil respiration was measured using a soil CO₂ collar in a closed system with a soil CO₂ flux chamber (6800-09, Li-COR Inc., Lincoln, NE, United States) connected to the LI-6800. Soil temperature and moisture were measured around the soil BVOC chamber using a Stevens HydraProbe (900-17114, Li-COR Inc., Lincoln, NE, United States) equipped for the 6800-09.

2.4. Surface litter layer

The composition of the surface litter layer was assessed by sorting the collected litter into two fractions: leaf material and other material consisting of small branches, bark material, and understory vegetation. The dry-mass weight of the two fractions was measured after drying for 48 h in an oven at 70°C, resulting in the dry weight of total litter (TDW), leaf material (LDW), and other material (ODW).

2.5. Isoprenoid analysis

Isoprenoid analysis was performed using a gas chromatography-mass selective detector (GC-MSD) system (7890A GC interfaced with a 5975C VL MSD; Agilent Technologies, Inc., California, United States) coupled with an automatic thermal desorption system (TD-100, Markes International Ltd., United Kingdom). The sampled isoprenoids were thermally desorbed from cartridges by the TD-100 at 280°C for 10 min and then transferred by pure helium into a cryogenic trap (U-T11PGC-2S, Markes International Ltd., Bridgend, United Kingdom) at -10°C. The trap was rapidly heated to transfer the isoprenoids to the GC-MSD system with an HP-5MS capillary column (30 m × 0.25 mm × 0.25 μm, Agilent Technologies, CA, United Kingdom). [Zeng et al. \(2022a\)](#) provide a detailed description of the chromatographic method and MSD mode for isoprenoid analysis. The target compounds were identified by comparing their retention times with standards and quantified with standard calibration curves. [Zeng et al. \(2022b\)](#) provide a detailed description of the identification and quantification of isoprenoids.

The soil isoprenoids fluxes (E , μg m⁻² h⁻¹) were calculated as μg of isoprenoids per square meter and hour using the following formula:

$$E = F \times 60 \text{ min h}^{-1} \times (C_{\text{out}} - C_{\text{in}}) / (1,000 \text{ ng } \mu\text{g}^{-1} \times A)$$

Here, F (L min⁻¹) represents the flow rate of circulating air, C_{in} (ng L⁻¹) and C_{out} (ng L⁻¹) represent the isoprenoid concentrations of inlet and outlet air, respectively, and A (m²) represents the area of soil surface enclosed by the sampling chamber.

The litter isoprenoids fluxes (E_{litter} , ng g⁻¹ h⁻¹) were calculated as ng of isoprenoids per gram and hour using the following formula:

$$E_{\text{litter}} = F \times 60 \text{ min h}^{-1} \times (C_{\text{with litter}} - C_{\text{without litter}}) / W$$

Here, $C_{\text{with litter}}$ (ng L⁻¹) is the difference between the concentrations of inlet and outlet air in samplings with litter, $C_{\text{without litter}}$ (ng L⁻¹) is the difference between the concentrations of inlet and outlet air in samplings without litter, and W (g) is the dry mass of the total litter collected in the sampling chamber.

2.6. Statistical analyses

To test for statistical differences between samplings with and without litter, a student's *t*-test was conducted and significance was set at $p < 0.05$. The associations between soil or litter variables and isoprenoid exchanges, ambient isoprenoid concentrations and isoprenoid exchanges were tested using Pearson correlation analysis. Pearson correlation coefficient (*r*) between soil or litter variables and isoprenoid exchanges were represented in a heatmap using the reshape2 package in R (v. 4.1.1). A principal component analysis (PCA) was performed with the FactoMineR and factoextra packages in R to visualize the multivariate correlations between the previously standardized variables. Vector variables were marked as isoprenoid exchanges and soil or litter variables. The ggplot2 package was used for visualization in R.

3. Results

3.1. Soil and litter variables

The mean soil temperatures at the sampling points ranged between $30.34 \pm 0.25^\circ\text{C}$ and $33.38 \pm 0.53^\circ\text{C}$, and the mean soil moisture (v/v) ranged between $6.88 \pm 1.41\%$ and $19.20 \pm 1.05\%$ (Supplementary Figures S5A,B). The mean soil respiration ranged between $2.07 \pm 0.10 \mu\text{mol m}^{-2} \text{s}^{-1}$ and $3.05 \pm 0.17 \mu\text{mol m}^{-2} \text{s}^{-1}$ (Supplementary Figure S5C). The mean values for soil temperature, moisture, and respiration across all sampling points were $32.02 \pm 0.49^\circ\text{C}$, $11.89 \pm 1.78\%$, and $2.53 \pm 0.14 \mu\text{mol m}^{-2} \text{s}^{-1}$, respectively. The litter collected from the surface layer of the sampling points was measured for dry weight, which ranged between 9.39 g and 32.09 g with an average of $18.61 \pm 3.33 \text{g}$. The dry weight of leaf material ranged between 4.38 g and 16.73 g with an average of $9.35 \pm 2.21 \text{g}$ (Supplementary Figure S6).

3.2. Soil isoprenoid fluxes

We observed net uptakes of isoprene ($-71.84 \pm 8.26 \mu\text{g m}^{-2} \text{h}^{-1}$), monoterpenes ($-6.20 \pm 13.98 \mu\text{g m}^{-2} \text{h}^{-1}$), and sesquiterpenes ($-6.19 \pm 3.23 \mu\text{g m}^{-2} \text{h}^{-1}$), with isoprene being the most absorbed compound (Figure 1A). The removal of the surface layer litter marginally increased total monoterpene uptakes ($p = 0.09$; Supplementary Table S1), coinciding with higher uptakes of α -pinene ($p < 0.05$; Figure 1B), β -pinene ($p < 0.05$; Figure 1B), and limonene ($p = 0.06$; Supplementary Table S1).

We detected 17 terpenoid compounds, including 11 monoterpenes and 6 sesquiterpenes. The fluxes of monoterpenes were dominated by α -pinene, β -pinene, α -phellandrene, limonene, 1,8-cineole, and trans-ocimene, with mean values above $1 \mu\text{g m}^{-2} \text{h}^{-1}$ (Figures 1B, 2). Regardless of the presence of litter, α -pinene, 1,8-cineole, and trans-ocimene were net absorbed, and α -phellandrene was net emitted. β -pinene and limonene were only net absorbed after removing the surface layer litter. The fluxes of individual sesquiterpenes showed similar magnitudes, with α -longipinene, α -copaene, aromadendrene, and alloaromadendrene being absorbed and β -caryophyllene and α -humulene being emitted (Figures 1C, 2).

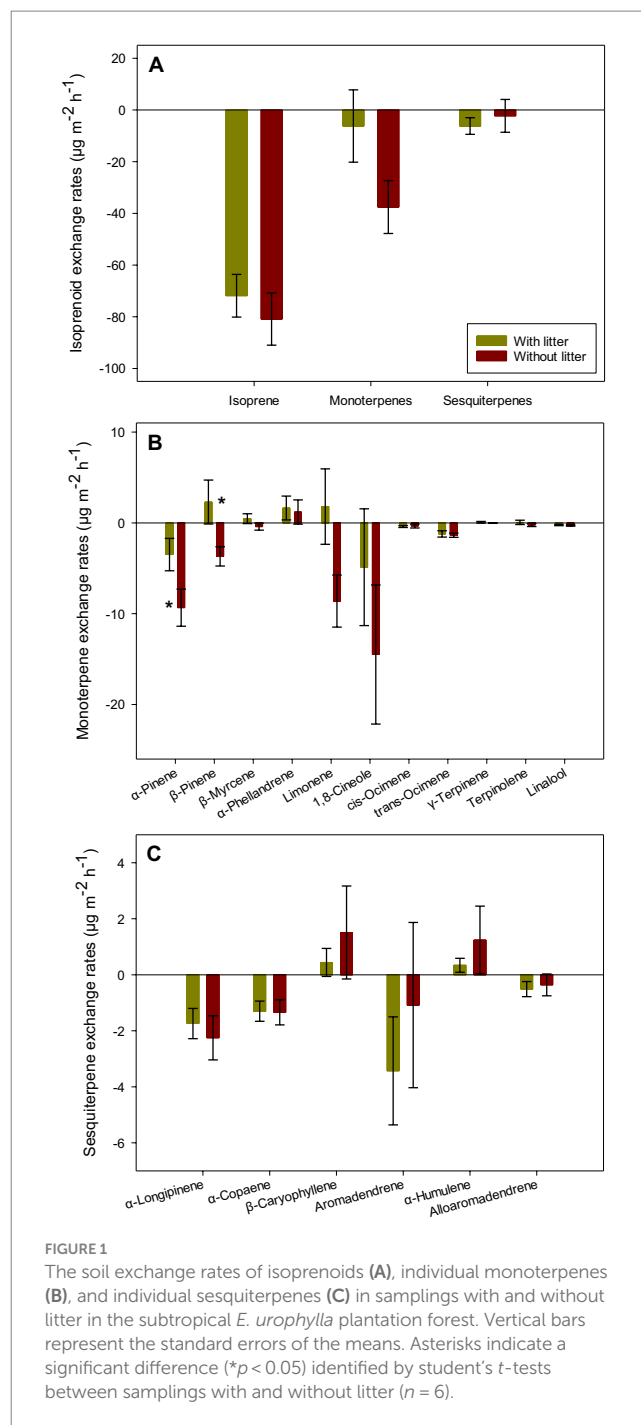


FIGURE 1
The soil exchange rates of isoprenoids (A), individual monoterpenes (B), and individual sesquiterpenes (C) in samplings with and without litter in the subtropical *E. urophylla* plantation forest. Vertical bars represent the standard errors of the means. Asterisks indicate a significant difference ($*p < 0.05$) identified by student's *t*-tests between samplings with and without litter ($n = 6$).

3.3. Litter isoprenoid fluxes

The litter in the surface layer emitted a net amount of isoprene ($67.80 \pm 16.36 \text{ng g}^{-1} \text{h}^{-1}$) and monoterpenes ($109.09 \pm 41.75 \text{ng g}^{-1} \text{h}^{-1}$) while also taking in sesquiterpenes ($-12.64 \pm 14.98 \text{ng g}^{-1} \text{h}^{-1}$; Figure 3A). The dominant contributors to the fluxes of monoterpenes were α -pinene, β -pinene, limonene, and 1,8-cineole, with mean values exceeding $10 \text{ng g}^{-1} \text{h}^{-1}$ (Figure 3B). The fluxes of sesquiterpenes were dominated by aromadendrene ($8.27 \pm 7.12 \text{ng g}^{-1} \text{h}^{-1}$; Figure 3B).

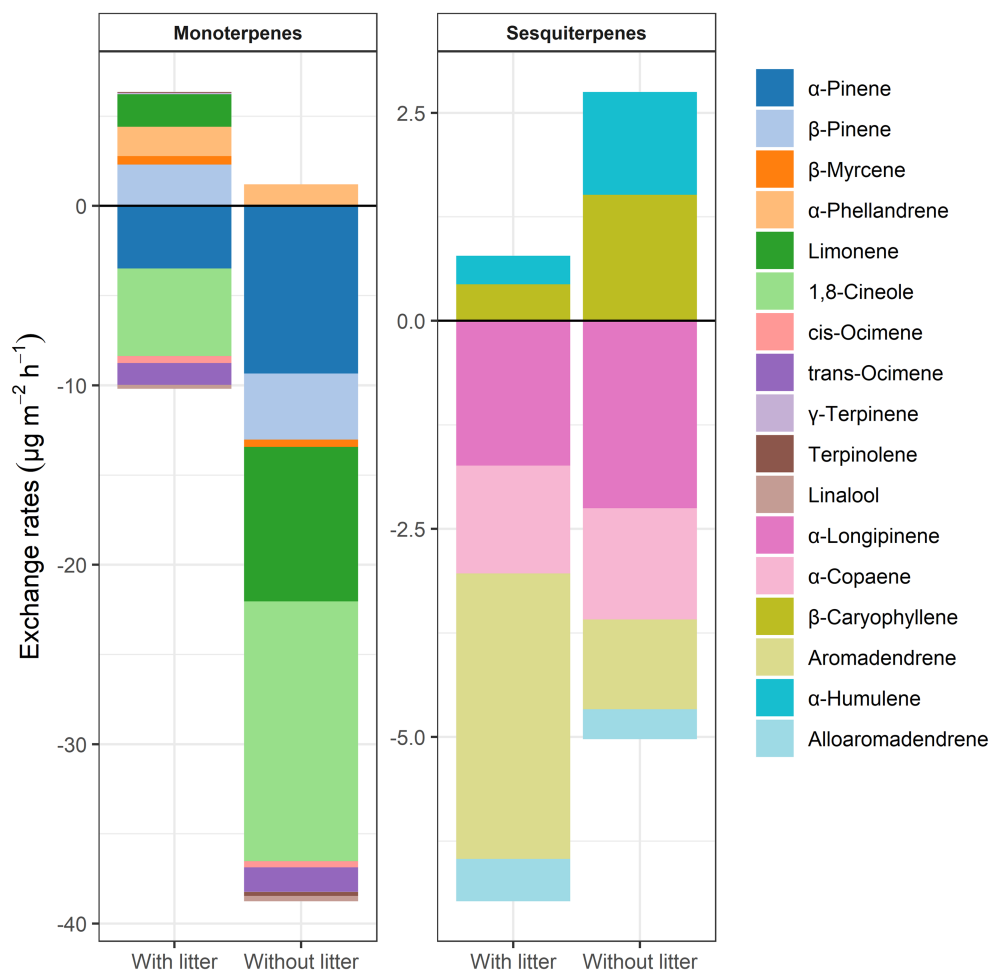


FIGURE 2 Distribution of soil monoterpene and sesquiterpene exchanges in samplings with and without litter in the subtropical *E. urophylla* plantation forest.

3.4. Associations of soil isoprenoid fluxes with soil and litter variables

The Pearson correlation analysis identified strong correlations ($r > 0.60$ and $p < 0.05$) between isoprenoid fluxes and soil or litter variables (Figure 4 and Supplementary Table S2). The fluxes of isoprene, 1,8-cineole, cis-ocimene, and α -longipinene were negatively correlated with soil temperature, whereas the fluxes of α -pinene, α -phellandrene, 1,8-cineole, cis-ocimene, terpinolene, total monoterpenes, α -longipinene, α -copaene, alloaromadendrene, and total sesquiterpenes were positively correlated with soil respiration.

Moreover, the fluxes of isoprene, α -pinene, 1,8-cineole, cis-ocimene, trans-ocimene, terpinolene, total monoterpenes, and α -longipinene were positively correlated with the dry weight of litter. Additionally, the fluxes of α -pinene, α -phellandrene, 1,8-cineole, terpinolene, total monoterpenes, α -longipinene, alloaromadendrene, and total sesquiterpenes increased with higher levels of leaf material mass, whereas the increases in fluxes of isoprene were correlated with higher levels of non-leaf materials.

The first (PC1) and second (PC2) principal components of the PCA explained 56% and 23% of the total variance, respectively, (Figure 5). The fluxes of isoprene and two terpene groups, along

with soil respiration and temperature, total dry weight of litter mainly contributed to PC1, while the two dry weights of litter fraction and soil moisture mainly contributed to PC2. The fluxes of isoprene were positively correlated with the total dry weight of litter and soil respiration and negatively with soil temperature. The fluxes of the two terpene groups were positively correlated with soil respiration, the total dry weight of litter and the dry weight of leaf materials.

3.5. Ambient isoprenoid concentrations

Mean ground-level concentrations (C_{in}) of isoprene, monoterpenes, and sesquiterpenes were 17.47 ± 2.38 , 14.07 ± 2.27 , and $2.89 \pm 0.55 \text{ ng L}^{-1}$, respectively (Supplementary Figure S7A). The ambient concentrations of terpene compounds were dominated by α -pinene, β -pinene, limonene, 1,8-cineole, and aromadendrene, with mean values above 1 ng L^{-1} (Supplementary Figure S7B). The fluxes of isoprene, total monoterpenes, total sesquiterpenes, α -pinene, 1,8-cineole, cis-ocimene, trans-ocimene, γ -terpinene, terpinolene, α -longipinene, α -copaene, β -caryophyllene, aromadendrene, and alloaromadendrene were negatively correlated

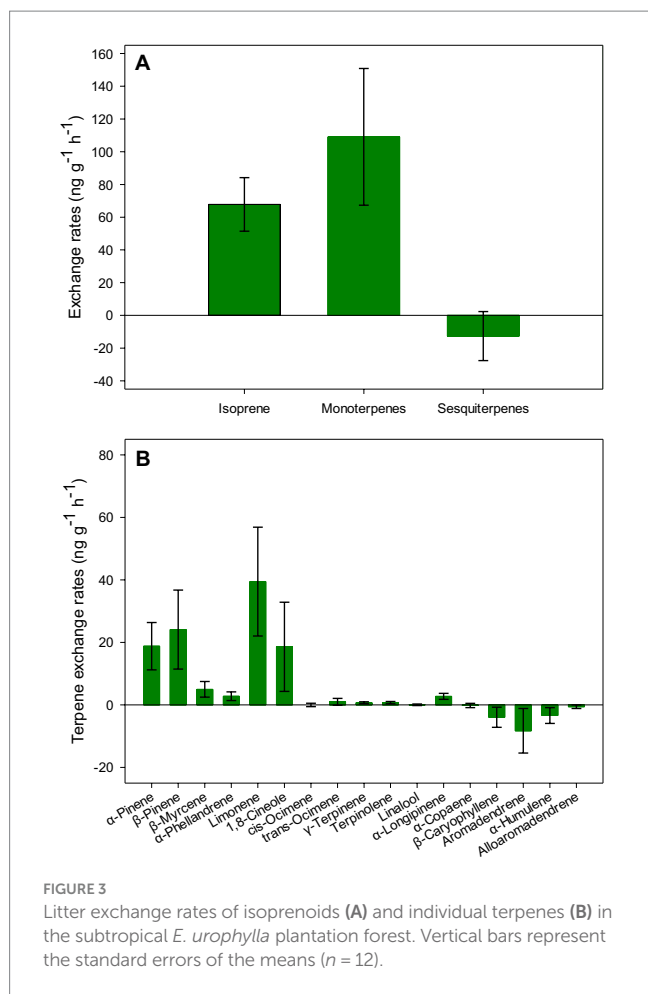


FIGURE 3
Litter exchange rates of isoprenoids (A) and individual terpenes (B) in the subtropical *E. urophylla* plantation forest. Vertical bars represent the standard errors of the means ($n = 12$).

with their ambient concentrations, respectively ($r > 0.60$ and $p < 0.05$; [Supplementary Table S3](#)).

4. Discussion

4.1. Soil isoprenoid fluxes in a subtropical *Eucalyptus urophylla* plantation forest

The isoprenoids fluxes recorded in this study showed that forest soils acted as sinks for isoprenoids, with net adsorption of isoprene occurring at high rates. This net isoprene adsorption was observed regardless of the presence of surface litter, consistent with previous studies reporting that soils act as a sink for isoprene (Cleveland and Yavitt, 1997, 1998; Pegoraro et al., 2005; Gray et al., 2015; Trowbridge et al., 2020). The surface litter layer was found to play a minor role in soil isoprene fluxes (Figure 1A). While low net isoprene emissions have been reported in some forest soils (Purser et al., 2021), significant emissions are rare (Rinnan and Albers, 2020). Isoprene is thought to be produced in soils as a microbial metabolite (Veres et al., 2014), and understorey vegetation such as grasses and mosses can contribute to soil emissions, leading to a small net isoprene emission in some ecosystems (Purser et al., 2021). Isoprene can also be consumed as a carbon and energy source for isoprene-degrading microbes (Cleveland and Yavitt, 1997; Pegoraro et al., 2005; Lin et al., 2007). The large

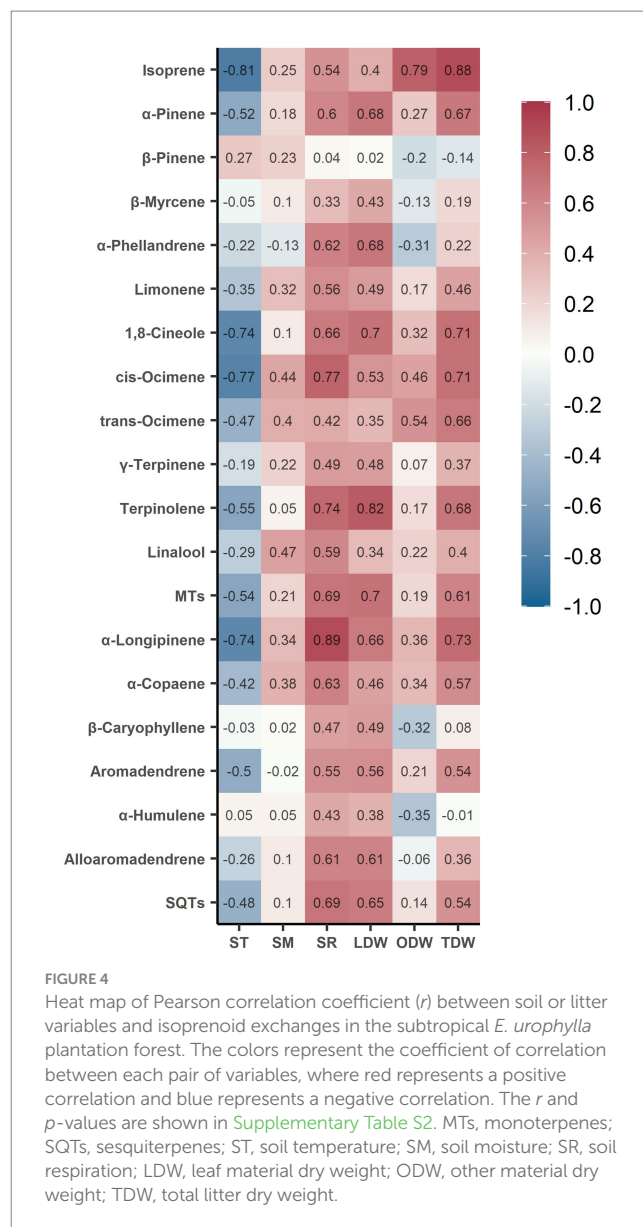
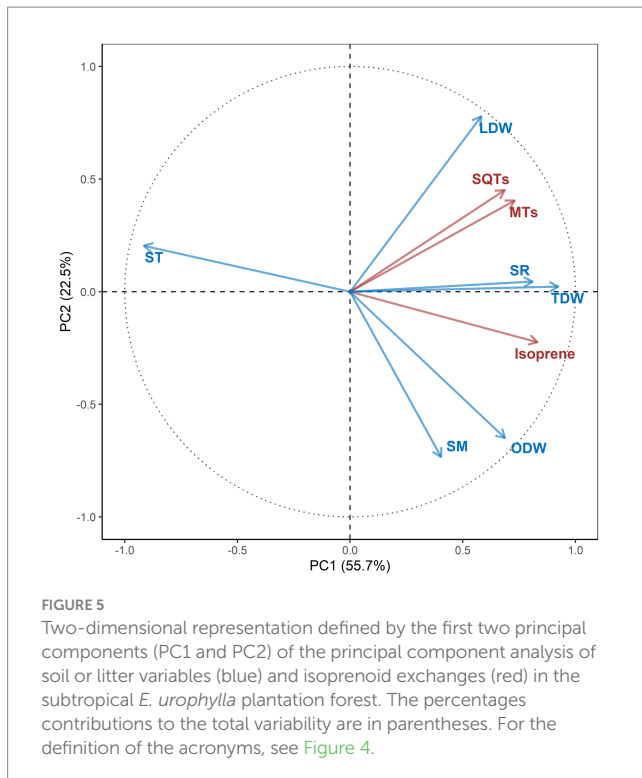


FIGURE 4
Heat map of Pearson correlation coefficient (r) between soil or litter variables and isoprenoid exchanges in the subtropical *E. urophylla* plantation forest. The colors represent the coefficient of correlation between each pair of variables, where red represents a positive correlation and blue represents a negative correlation. The r and p -values are shown in [Supplementary Table S2](#). MTs, monoterpenes; SQTs, sesquiterpenes; ST, soil temperature; SM, soil moisture; SR, soil respiration; LDW, leaf material dry weight; ODW, other material dry weight; TDW, total litter dry weight.

microbial consumption of isoprene that exceeds its production could cause net uptake of isoprene in soils. However, the high uptake of isoprene in this study could be partly due to a large isoprene concentration gradient between the atmosphere and the soil, as the high ambient isoprene concentrations ($17.47 \pm 2.38 \text{ ng L}^{-1}$; [Supplementary Figure S7A](#)) observed in the study site and *E. urophylla* has a large emission factor of isoprene as reported in other studies in subtropical China (Zeng et al., 2022a).

In this study, forest soils acted as sinks for monoterpenes with large variations in fluxes that indicate the possibility of low emissions (Figure 1A). The surface litter layer served as a source of monoterpenes, with emissions ($109.09 \pm 41.75 \text{ ng g}^{-1} \text{ h}^{-1}$; [Figure 3A](#)) around one-tenth of the emission factor ($1.02 \pm 0.65 \text{ } \mu\text{g g}^{-1} \text{ h}^{-1}$; Zeng et al., 2022a) of *E. urophylla* reported in subtropical China. This contrasts with previous results from tropical and subtropical soils, where the presence of surface litter did not affect soil monoterpene exchanges (Huang et al., 2021; Llusia et al., 2022), although the emitted monoterpenes may hardly escape from the litter-soil layer due



to higher soil uptakes of monoterpenes in this study. However, upward fluxes may occur when a large amount of litter (especially leaf litter, see below) covers the soil surface, leading to monoterpene production in the surface litter layer that exceeds soil uptakes of monoterpenes. The net monoterpene adsorption observed here contrasts with net emissions observed in other subtropical or tropical ecosystems, such as $10.4 \pm 2.93 \mu\text{g m}^{-2} \text{ h}^{-1}$ in two tropical forests of French Guiana (Llusià et al., 2022), and $15.0 \pm 15.3 \mu\text{g m}^{-2} \text{ h}^{-1}$ in a *Eucalyptus gunnii* plantation in the United Kingdom (Purser et al., 2021). The emitted monoterpenes could originate from litter, whose emissions are associated with storage pools (Greenberg et al., 2012; Staudt et al., 2019) and microbial decomposition (Gray et al., 2010; Viros et al., 2021), and from soils where plant root systems (Nishida et al., 2005; Purser et al., 2021) and soil microbial communities (Asensio et al., 2008a; Ramirez et al., 2010) are major sources. Like isoprene, microbial uptake of monoterpenes was also widely reported and well understood (Insam and Seewald, 2010; Ramirez et al., 2010; Peñuelas et al., 2014; Tang et al., 2019). This consumption process may dominate monoterpene fluxes, leading to the small net adsorption observed here.

In this study, sesquiterpenes were found to be net adsorbed at rates similar to those of monoterpenes, with the surface litter layer and soil both acting as sinks for sesquiterpenes (Figures 1A, 3A). However, the adsorption rates ($6.19 \pm 3.23 \mu\text{g m}^{-2} \text{ h}^{-1}$; Figure 1A) were much lower compared to those observed in tropical forests of French Guiana ($65.97 \pm 21.15 \mu\text{g m}^{-2} \text{ h}^{-1}$; Llusià et al., 2022), and this contrasts with the strong sesquiterpene emissions that can be of comparable magnitude to canopy emissions recorded from Amazonian soils (Bourtsoukidis et al., 2018). Like monoterpenes, sesquiterpenes have been shown to be released from litter (Isidorov et al., 2003; Svendsen et al., 2018), microorganisms (Horváth et al., 2012; Mäki et al., 2017; Bourtsoukidis et al., 2018), and roots (Lin et al., 2007; Asensio et al., 2007a, 2008b). However, studies identifying soils as sinks for

sesquiterpenes are scarce (Tang et al., 2019; Llusià et al., 2022). Llusià et al. (2022) attributed the net sinks of sesquiterpenes to the effects of biological factors, such as microbial consumption of soil-litter sesquiterpenes, and physical factors, such as high sesquiterpene concentration gradients between the atmosphere and soil air. These factors favor downward fluxes of sesquiterpenes and may also contribute to the small net adsorption observed in this study.

4.2. Abiotic and biotic controls of soil isoprenoid fluxes in the plantation forest

The fluxes of isoprene, total monoterpenes (i.e., 1,8-cineole and cis-ocimene), and total sesquiterpenes (i.e., α -longipinene and aromadendrene) were negatively correlated with soil temperature in our study (Figures 4, 5). Our results suggest that a linear relationship, as found in some temperate forest soils (Trowbridge et al., 2020), is sufficient to explain isoprene fluxes ($r = -0.81$ and $p < 0.001$; Figure 4 and Supplementary Table S2). This contrasts with the decrease in the observed rate of isoprene uptake from temperate forest soils at high temperature ($>30^\circ\text{C}$, Cleveland and Yavitt, 1998). The significant negative linear correlation between monoterpene fluxes and soil temperature was consistent with results found in subtropical pine and broad-leaved forest soils (Huang et al., 2021) and temperate forest soils (Trowbridge et al., 2020). However, significant correlations of soil temperature with monoterpenes and sesquiterpenes contrast with the finding that neither terpene group correlated with soil temperature in tropical forest soils (Llusià et al., 2022). These results suggest that isoprenoid emission rates decreased and/or uptake rates increased with increasing temperature, indicating that the soil capacity of isoprenoid sink is expected to increase due to global warming in subtropical China (IPCC, 2014; Zhang et al., 2019).

The isoprenoid fluxes were generally not correlated with soil moisture in this study (Figures 4, 5), and the lack of association for soil monoterpene fluxes was also found in previous studies conducted in subtropical forests (Huang et al., 2021). Similarly, Llusià et al. (2022) reported weak associations between the exchanges of monoterpenes ($r = 0.45$, $p < 0.01$) and sesquiterpenes ($r = -0.38$, $p < 0.01$) and soil moisture in tropical forest soils. An increase in soil moisture can increase microbial activity at low soil moisture content, but also decrease the amount of gas accessible to soil microbes (Cleveland and Yavitt, 1997; Asensio et al., 2007a; Tang et al., 2019), leading to increased (Asensio et al., 2007a) or decreased (Trowbridge et al., 2020) uptake of isoprenoids, as observed in temperate and Mediterranean forest soils. However, changes in soil moisture may have less effect on warmer and wetter subtropical and tropical ecosystems than in temperate ecosystems. Nevertheless, isoprenoids are hydrophobic VOCs, and their soil fluxes may be less dependent on soil moisture than those of hydrophilic VOCs (e.g., acetic acid, acetaldehyde, acetone; Seco et al., 2007; Baggesen et al., 2022), which could also contribute to the low correlation with soil moisture.

The fluxes of isoprene, total monoterpenes (i.e., cis-ocimene and terpinolene), and total sesquiterpenes (i.e., α -longipinene and α -copaene) were all positively correlated with soil respiration (Figures 4, 5). The positive correlation between soil isoprenoid fluxes and respiration may indicate that increases in microbial activity could promote isoprenoid production to a greater degree than consumption and/or mineralization in ecosystem soils. This result contrasts with the

negative or insignificant relationship between some monoterpenes of forest soils and soil respiration reported in previous studies (Leff and Fierer, 2008; Huang et al., 2021). It has been shown that soil isoprenoid flux depends on the metabolic activities of microbes (Cleveland and Yavitt, 1998; Albers et al., 2018), while both isoprenoid production and consumption associated with microbes usually occur simultaneously (Insam and Seewald, 2010; Peñuelas et al., 2014). Nevertheless, the CO₂ and isoprenoid fluxes were also a result of root activity (Gray et al., 2014; Tang et al., 2019; Mu et al., 2022). Thus, the highly variable correlation between soil isoprenoid flux and respiration among ecosystem soils may be explained by differences in their microbial community composition.

The fluxes of isoprene, total monoterpenes (i.e., 1,8-cineole and cis-ocimene), and total sesquiterpenes (i.e., α -longipinene and α -copaene) were all positively correlated with total litter dry weight (Figures 4, 5), which points to an effect of the litter layer on soil isoprenoid fluxes. The fluxes of the two terpene groups showed a strong correlation with leaf litter, indicating that their emissions mainly originated from the evaporation of stored terpenes in leaf litter, as *E. urophylla* is a terpene-storing species (Külheim et al., 2015). Meanwhile, isoprene fluxes were more correlated with non-leaf litter (branches, barks, and understory vegetation), indicating that their fluxes may be more related to microbe-mediated decomposition of plant residues (Sivy et al., 2002; Mancuso et al., 2015) and/or adsorption-desorption processes in the litter layer. Thus, these results highlight the relevance of studying the effects of litter composition on soil isoprenoid fluxes (Purser et al., 2021).

4.3. Methodological considerations

The soil BVOCs were sampled using a soil BVOC dynamic chamber that evolved from a recent dynamic chamber (Zeng et al., 2022b) designed and well-characterized for measuring branch-scale BVOC emissions. The short residence time (approximately 1.7 min) and ozone-scrubbed circulating air could reduce the adsorptive and reactive loss in samplings. The inlet and outlet air were sampled simultaneously at a constant flow rate (200 mL min⁻¹) to avoid environmental and instrumental disturbance. The isoprenoids were identified with authentic standards and quantified with compound-specific standard calibration curves to ensure high accuracy of results.

The field sampling was conducted exclusively during the hottest and wettest period of the year, spanning from June to September. This limited sampling period may not accurately represent the field conditions throughout the entire year, consequently constraining the scope of our study. For instance, our findings enable us to conclude that subtropical soils possess the capacity to absorb isoprenoids, with this absorption capacity being particularly robust during wet seasons. However, our study falls short of providing a comprehensive assessment of net soil isoprenoid fluxes across all seasons of the year. The soil variables (temperature, moisture, and respiration) were measured only during the BVOC sampling rather than throughout the month or season, which leads to uncertainties in the correlation analysis, as the effects of soil variables on BVOC fluxes may not be instantaneous. Moreover, it is important to consider that our results may have been affected by the ambient concentrations of isoprenoids.

Elevated ambient concentrations tend to promote downward fluxes for most compounds examined in this study (Supplementary Table S3). This influence of ambient concentrations is particularly noteworthy in the case of isoprene, owing to its notably high ambient concentrations (17.47 ± 2.38 ng L⁻¹; Supplementary Figure S7A). Additionally, there is a strong correlation between ambient concentrations and exchange rates ($r = -0.96$ and $p < 0.001$; Supplementary Table S3), which likely contributes to the substantial net absorption of isoprene observed in our study. Furthermore, we hypothesize that the soil's ability to serve as a sink for isoprenoids may be regulated by soil microbes. To gain a more comprehensive understanding of soil BVOCs in subtropical ecosystems and to accurately characterize and project this sink capacity, it is advisable to incorporate additional microbial indicators, especially microbial biomass and community data. A deeper comprehension of the roles played by ambient concentrations and soil microbes in soil-atmosphere isoprenoid exchanges within subtropical ecosystems is essential. This understanding will enhance our capacity to unlock the full potential of soil BVOC carbon sinks, potentially contributing to climate change mitigation efforts. The method does have other limitations; however, through this exploratory pilot study, we have gained primary insight into the complex mechanisms controlling the variability of soil BVOC fluxes in subtropical ecosystems.

5. Conclusion

Our results demonstrate the capacity of subtropical soils to absorb isoprenoids, emphasizing the importance of incorporating this data into models for soil biogenic volatile organic compounds (BVOCs). Our study reiterates the crucial roles played by soil microclimate, microbes, and litter as drivers of isoprenoid exchanges between soils and the atmosphere. The direction and magnitude of these fluxes are often determined by the combined effects of these factors. However, to gain a deeper understanding of the complex mechanisms governing the variability of soil BVOC fluxes, further research involving long-term field measurements and laboratory incubation experiments is essential. Our investigation reveals that under current conditions, the subtropical soils in our study function as significant net sinks for isoprene. This phenomenon can be attributed to various biological and physical factors, including the microbial consumption of soil-litter volatiles and the presence of high atmospheric isoprene concentrations, which promote isoprene uptake by the soil. However, as temperatures increase in the future, along with adequate moisture levels, the consumption of soil-litter isoprenoids by soil microbial communities may intensify, leading to a decrease in soil isoprenoid exchange rates. Consequently, we anticipate that the soil's capacity to act as a sink for isoprenoids will increase due to climate change in subtropical regions of China.

Data availability statement

The original contributions presented in the study are included in the article/Supplementary material, further inquiries can be directed to the corresponding author.

Author contributions

ZM: Conceptualization, Data curation, Formal analysis, Investigation, Methodology, Software, Visualization, Writing – original draft, Writing – review & editing. JZ: Data curation, Formal analysis, Investigation, Methodology, Writing – review & editing. YZ: Funding acquisition, Methodology, Validation, Writing – review & editing, Resources. WS: Data curation, Formal analysis, Investigation, Writing – review & editing. WP: Data curation, Formal analysis, Investigation, Writing – review & editing. ZY: Validation, Writing – review & editing. DA: Validation, Writing – review & editing. JL: Validation, Writing – review & editing. JP: Funding acquisition, Validation, Writing – review & editing. XW: Conceptualization, Funding acquisition, Methodology, Project administration, Resources, Supervision, Validation, Writing – review & editing.

Funding

The author(s) declare financial support was received for the research, authorship, and/or publication of this article. This work was supported by the National Natural Science Foundation of China (Nos. 42022023 and 42321003), the Hong Kong Research Grant Council (No. T24-504/17-N), the Department of Science and Technology of Guangdong (No. 2023B1212060049), the Guangzhou Municipal Science and Technology Bureau (No. 202206010057), the TED2021-132627B-I00 grant funded by the Spanish MCIN, AEI/10.13039/501100011033 and the European Union NextGenerationEU/PRTR, the Fundación Ramón Areces grant

References

- Aaltonen, H., Aalto, J., Kolari, P., Pihlatie, M., Pumpanen, J., Kulmala, M., et al. (2013). Continuous VOC flux measurements on boreal forest floor. *Plant Soil* 369, 241–256. doi: 10.1007/s11104-012-1553-4
- Aaltonen, H., Pumpanen, J., Pihlatie, M., Hakola, H., Hellén, H., Kulmala, L., et al. (2011). Boreal pine forest floor biogenic volatile organic compound emissions peak in early summer and autumn. *Agric. For. Meteorol.* 151, 682–691. doi: 10.1016/j.agrformet.2010.12.010
- Albers, C. N., Kramshøj, M., and Rinnan, R. (2018). Rapid mineralization of biogenic volatile organic compounds in temperate and Arctic soils. *Biogeosciences* 15, 3591–3601. doi: 10.5194/bg-15-3591-2018
- Asensio, D., Owen, S. M., Llusà, J., and Peñuelas, J. (2008a). The distribution of volatile isoprenoids in the soil horizons around *Pinus halepensis* trees. *Soil Biol. Biochem.* 40, 2937–2947. doi: 10.1016/j.soilbio.2008.08.008
- Asensio, D., Peñuelas, J., Filella, I., and Llusà, J. (2007a). On-line screening of soil VOCs exchange responses to moisture, temperature and root presence. *Plant Soil* 291, 249–261. doi: 10.1007/s11104-006-9190-4
- Asensio, D., Peñuelas, J., Llusà, J., Ogaya, R., and Filella, I. (2007b). Interannual and interseasonal soil CO₂ efflux and VOC exchange rates in a Mediterranean holm oak forest in response to experimental drought. *Soil Biol. Biochem.* 39, 2471–2484. doi: 10.1016/j.soilbio.2007.04.019
- Asensio, D., Peñuelas, J., Ogaya, R., and Llusà, J. (2007c). Seasonal soil VOC exchange rates in a Mediterranean holm oak forest and their responses to drought conditions. *Atmos. Environ.* 41, 2456–2466. doi: 10.1016/j.atmosenv.2006.05.007
- Asensio, D., Peñuelas, J., Prieto, P., Estiarte, M., Filella, I., and Llusà, J. (2008b). Interannual and seasonal changes in the soil exchange rates of monoterpenes and other VOCs in a Mediterranean shrubland. *Eur. J. Soil Sci.* 59, 878–891. doi: 10.1111/j.1365-2389.2008.01057.x
- Baggesen, N. S., Davie-Martin, C. L., Seco, R., Holst, T., and Rinnan, R. (2022). Bidirectional exchange of biogenic volatile organic compounds in subarctic heath mesocosms during autumn climate scenarios. *J. Geophys. Res. Biogeosci.* 127:e2021JG006688. doi: 10.1029/2021JG006688
- Bai, Y., Zhou, Y., Du, J., Zhang, X., and Di, N. (2021). Effects of a broadleaf-oriented transformation of coniferous plantations on the hydrological characteristics of litter

CIVP20A6621, and the Catalan Government grant SGR 2021-1333. ZM also acknowledges the financial support from the Guangdong Provincial Postdoctoral Talent-Introduction Program.

Conflict of interest

The authors declare that the research was conducted in the absence of any commercial or financial relationships that could be construed as a potential conflict of interest.

The author(s) declared that they were an editorial board member of *Frontiers*, at the time of submission. This had no impact on the peer review process and the final decision.

Publisher's note

All claims expressed in this article are solely those of the authors and do not necessarily represent those of their affiliated organizations, or those of the publisher, the editors and the reviewers. Any product that may be evaluated in this article, or claim that may be made by its manufacturer, is not guaranteed or endorsed by the publisher.

Supplementary material

The Supplementary material for this article can be found online at: <https://www.frontiersin.org/articles/10.3389/ffgc.2023.1260327/full#supplementary-material>

layers in subtropical China. *Glob. Ecol. Conserv.* 25:e01400. doi: 10.1016/j.gecco.2020.e01400

Bourtsoukidis, E., Behrendt, T., Yañez-Serrano, A. M., Hellén, H., Diamantopoulos, E., Catão, E., et al. (2018). Strong sesquiterpene emissions from Amazonian soils. *Nat. Commun.* 9:2226. doi: 10.1038/s41467-018-04658-y

Cleveland, C. C., and Yavitt, J. B. (1997). Consumption of atmospheric isoprene in soil. *Geophys. Res. Lett.* 24, 2379–2382. doi: 10.1029/97GL02451

Cleveland, C. C., and Yavitt, J. B. (1998). Microbial consumption of atmospheric isoprene in a temperate forest soil. *Appl. Environ. Microbiol.* 64, 172–177. doi: 10.1128/AEM.64.1.172-177.1998

Fang, J., Tan, X., Yang, Z., Shen, W., and Peñuelas, J. (2023). Contrasting terpene emissions from canopy and understory vegetation in response to increases in nitrogen deposition and seasonal changes in precipitation. *Environ. Pollut.* 317:120800. doi: 10.1016/j.envpol.2022.120800

Gray, C. M., Helmig, D., and Fierer, N. (2015). Bacteria and fungi associated with isoprene consumption in soil. *Elem. Sci. Anth.* 3:000053. doi: 10.12952/journal.elementa.000053

Gray, C. M., Monson, R. K., and Fierer, N. (2010). Emissions of volatile organic compounds during the decomposition of plant litter. *J. Geophys. Res. Biogeosci.* 115:G03015. doi: 10.1029/2010JG001291

Gray, C. M., Monson, R. K., and Fierer, N. (2014). Biotic and abiotic controls on biogenic volatile organic compound fluxes from a subalpine forest floor. *J. Geophys. Res. Biogeosci.* 119, 547–556. doi: 10.1002/2013JG002575

Greenberg, J. P., Asensio, D., Turnipseed, A., Guenther, A. B., Karl, T., and Gochis, D. (2012). Contribution of leaf and needle litter to whole ecosystem BVOC fluxes. *Atmos. Environ.* 59, 302–311. doi: 10.1016/j.atmosenv.2012.04.038

He, Y., Qin, L., Li, Z., Liang, X., Shao, M., and Tan, L. (2013). Carbon storage capacity of monoculture and mixed-species plantations in subtropical China. *For. Ecol. Manag.* 295, 193–198. doi: 10.1016/j.foreco.2013.01.020

Hellén, H., Hakola, H., Pystynen, K. H., Rinne, J., and Haapanala, S. (2006). C₂–C₁₀ hydrocarbon emissions from a boreal wetland and forest floor. *Biogeosciences* 3, 167–174. doi: 10.5194/bg-3-167-2006

- Helmig, D., Ortega, J., Duhl, T., Tanner, D., Guenther, A., Harley, P., et al. (2007). Sesquiterpene emissions from pine trees—identifications, emission rates and flux estimates for the contiguous United States. *Environ. Sci. Technol.* 41, 1545–1553. doi: 10.1021/es0618907
- Horváth, E., Hoffer, A., Sebők, F., Dobolyi, C., Szoboszlai, S., Kriszt, B., et al. (2012). Experimental evidence for direct sesquiterpene emission from soils. *J. Geophys. Res.* 117:D15304. doi: 10.1029/2012JD017781
- Huang, X., Zheng, L., Guo, P., and Yi, Z. (2021). Nitrogen addition inhibits total monoterpene emissions in subtropical forest floor of South China. *Soil Ecol. Lett.* 3, 63–72. doi: 10.1007/s42832-020-0056-0
- Insam, H., and Seewald, M. S. A. (2010). Volatile organic compounds (VOCs) in soils. *Biol. Fertil. Soils* 46, 199–213. doi: 10.1007/s00374-010-0442-3
- IPCC (2014). “Climate change 2014: impacts, adaptation, and vulnerability. Part A: global and sectoral aspects” in *Contribution of working group II to the fifth assessment report of the intergovernmental panel on climate change* (New York: Oxford University Press)
- Isidorov, V. A., Vinogorova, V. T., and Rafalowski, K. (2003). HS-SPME analysis of volatile organic compounds of coniferous needle litter. *Atmos. Environ.* 37, 4645–4650. doi: 10.1016/j.atmosenv.2003.07.005
- Kramshøj, M., Albers, C. N., Holst, T., Holzinger, R., Elberling, B., and Rinnan, R. (2018). Biogenic volatile release from permafrost thaw is determined by the soil microbial sink. *Nat. Commun.* 9:3412. doi: 10.1038/s41467-018-05824-y
- Kramshøj, M., Vedel-Petersen, I., Schollert, M., Rinnan, A., Nymand, J., Ro-Poulsen, H., et al. (2016). Large increases in Arctic biogenic volatile emissions are a direct effect of warming. *Nat. Geosci.* 9, 349–352. doi: 10.1038/ngeo2692
- Kreuzwieser, J., and Rennenberg, H. (2013). “Flooding-driven emissions from trees” in *Biology, controls and models of free volatile organic compound emissions*. eds. Ü. Niinemets and R. K. Monson (Dordrecht: Springer), 237–252.
- Külheim, C., Padovan, A., Hefer, C., Krause, S. T., Köllner, T. G., Myburg, A. A., et al. (2015). The Eucalyptus terpene synthase gene family. *BMC Genomics* 16:450. doi: 10.1186/s12864-015-1598-x
- Leff, J. W., and Fierer, N. (2008). Volatile organic compound (VOC) emissions from soil and litter samples. *Soil Biol. Biochem.* 40, 1629–1636. doi: 10.1016/j.soilbio.2008.01.018
- Lin, C., Owen, S. M., and Peñuelas, J. (2007). Volatile organic compounds in the roots and rhizosphere of *Pinus* spp. *Soil Biol. Biochem.* 39, 951–960. doi: 10.1016/j.soilbio.2006.11.007
- Llusà, J., Asensio, D., Sardans, J., Filella, I., Peguero, G., Grau, O., et al. (2022). Contrasting nitrogen and phosphorus fertilization effects on soil terpene exchanges in a tropical forest. *Sci. Total Environ.* 802:149769. doi: 10.1016/j.scitotenv.2021.149769
- Mäki, M., Aalto, J., Hellén, H., Pihlatie, M., and Bäck, J. (2019a). Interannual and seasonal dynamics of volatile organic compound fluxes from the boreal forest floor. *Front. Plant Sci.* 10:191. doi: 10.3389/fpls.2019.00191
- Mäki, M., Aaltonen, H., Heinonsalo, J., Hellén, H., Pumpanen, J., and Bäck, J. (2019b). Boreal forest soil is a significant and diverse source of volatile organic compounds. *Plant Soil* 441, 89–110. doi: 10.1007/s11104-019-04092-z
- Mäki, M., Heinonsalo, J., Hellén, H., and Bäck, J. (2017). Contribution of understory vegetation and soil processes to boreal forest isoprenoid exchange. *Biogeosciences* 14, 1055–1073. doi: 10.5194/bg-14-1055-2017
- Mancuso, S., Taiti, C., Bazihizina, N., Costa, C., Menesatti, P., Giagnoni, L., et al. (2015). Soil volatile analysis by proton transfer reaction-time of flight mass spectrometry (PTR-TOF-MS). *Appl. Soil Ecol.* 86, 182–191. doi: 10.1016/j.apsoil.2014.10.018
- Ming, A., Jia, H., Zhao, J., Tao, Y., and Li, Y. (2014). Above- and below-ground carbon stocks in an indigenous tree (*Mytilaria laosensis*) plantation chronosequence in subtropical China. *PLoS One* 9:e109730. doi: 10.1371/journal.pone.0109730
- Mu, Z., Asensio, D., Llusà, J., Filella, I., Ogaya, R., Yi, Z., et al. (2022). Annual and seasonal variations in soil volatile organic compound concentrations in a Mediterranean shrubland and holm oak forest. *Geoderma* 405:115401. doi: 10.1016/j.geoderma.2021.115401
- Mu, Z., Llusà, J., and Peñuelas, J. (2020). Ground level isoprenoid exchanges associated with *Pinus pinea* trees in a Mediterranean turf. *Atmosphere* 11:809. doi: 10.3390/atmos11080809
- Nishida, N., Tamotsu, S., Nagata, N., Saito, C., and Sakai, A. (2005). Allelopathic effects of volatile monoterpenoids produced by *Salvia leucophylla*: inhibition of cell proliferation and DNA synthesis in the root apical meristem of *Brassica campestris* seedlings. *J. Chem. Ecol.* 31, 1187–1203. doi: 10.1007/s10886-005-4256-y
- Nölscher, A. C., Yañez-Serrano, A. M., Wolff, S., de Araujo, A. C., Lavrič, J. V., Kesselmeier, J., et al. (2016). Unexpected seasonality in quantity and composition of Amazon rainforest air reactivity. *Nat. Commun.* 7:10383. doi: 10.1038/ncomms10383
- Owen, S. M., Clark, S., Pompe, M., and Semple, K. T. (2007). Biogenic volatile organic compounds as potential carbon sources for microbial communities in soil from the rhizosphere of *Populus tremula*. *FEMS Microbiol. Lett.* 268, 34–39. doi: 10.1111/j.1574-6968.2006.00602.x
- Pegoraro, E., Abrell, L., Haren, J. V., Barron-Gafford, G., Grieve, K. A., Malhi, Y., et al. (2005). The effect of elevated atmospheric CO₂ and drought on sources and sinks of isoprene in a temperate and tropical rainforest mesocosm. *Glob. Chang. Biol.* 11, 1234–1246. doi: 10.1111/j.1365-2486.2005.00986.x
- Peñuelas, J., Asensio, D., Tholl, D., Wenke, K., Rosenkranz, M., Piechulla, B., et al. (2014). Biogenic volatile emissions from the soil. *Plant Cell Environ.* 37, 1866–1891. doi: 10.1111/pce.12340
- Purser, G., Drewer, J., Morison, J. I. L., and Heal, M. R. (2021). A first assessment of the sources of isoprene and monoterpene emissions from a short-rotation coppice *Eucalyptus gunnii* bioenergy plantation in the United Kingdom. *Atmos. Environ.* 262:118617. doi: 10.1016/j.atmosenv.2021.118617
- Ramirez, K. S., Lauber, C. L., and Fierer, N. (2010). Microbial consumption and production of volatile organic compounds at the soil-litter interface. *Biogeochemistry* 99, 97–107. doi: 10.1007/s10533-009-9393-x
- Rinnan, R., and Albers, C. N. (2020). Soil uptake of volatile organic compounds: ubiquitous and underestimated? *J. Geophys. Res. Biogeosci.* 125:e2020JG005773. doi: 10.1029/2020JG005773
- Seco, R., Peñuelas, J., and Filella, I. (2007). Short-chain oxygenated VOCs: emission and uptake by plants and atmospheric sources, sinks, and concentrations. *Atmos. Environ.* 41, 2477–2499. doi: 10.1016/j.atmosenv.2006.11.029
- Sivy, T. L., Shirk, M. C., and Fall, R. (2002). Isoprene synthase activity parallels fluctuations of isoprene release during growth of *Bacillus subtilis*. *Biochem. Biophys. Res. Commun.* 294, 71–75. doi: 10.1016/S0006-291X(02)00435-7
- Staudt, M., Byron, J., Piquemal, K., and Williams, J. (2019). Compartment specific chiral pinene emissions identified in a maritime pine forest. *Sci. Total Environ.* 654, 1158–1166. doi: 10.1016/j.scitotenv.2018.11.146
- Svendsen, S. H., Priemé, A., Voriskova, J., Kramshøj, M., Schostag, M., Jacobsen, C. S., et al. (2018). Emissions of biogenic volatile organic compounds from arctic shrub litter are coupled with changes in the bacterial community composition. *Soil Biol. Biochem.* 120, 80–90. doi: 10.1016/j.soilbio.2018.02.001
- Tang, J., Schurgers, G., and Rinnan, R. (2019). Process understanding of soil BVOC fluxes in natural ecosystems: a review. *Rev. Geophys.* 57, 966–986. doi: 10.1029/2018RG000634
- Trowbridge, A. M., Stoy, P. C., and Phillips, R. P. (2020). Soil biogenic volatile organic compound flux in a mixed hardwood forest: net uptake at warmer temperatures and the importance of mycorrhizal associations. *J. Geophys. Res. Biogeosci.* 125:e2019JG005479. doi: 10.1029/2019JG005479
- Veres, P. R., Behrendt, T., Klaphor, A., Meixner, F. X., and Williams, J. (2014). Volatile organic compound emissions from soil: using proton-transfer-reaction time-of-flight mass spectrometry (PTR-TOF-MS) for the real time observation of microbial processes. *Biogeosci. Discuss.* 11, 12009–12038. doi: 10.5194/bgd-11-12009-2014
- Viros, J., Santonja, M., Temime-Roussel, B., Wortham, H., Fernandez, C., and Ormeño, E. (2021). Volatilome of Aleppo pine litter over decomposition process. *Ecol. Evol.* 11, 6862–6880. doi: 10.1002/ece3.7533
- Wang, F., Li, Z., Xia, H., Zou, B., Li, N., Liu, J., et al. (2010). Effects of nitrogen-fixing and non-nitrogen-fixing tree species on soil properties and nitrogen transformation during forest restoration in southern China. *Soil Sci. Plant Nutr.* 56, 297–306. doi: 10.1111/j.1747-0765.2010.00454.x
- Wei, X., and Blanco, J. A. (2014). Significant increase in ecosystem C can be achieved with sustainable forest management in subtropical plantation forests. *PLoS One* 9:e89688. doi: 10.1371/journal.pone.0089688
- Wenke, K., Kai, M., and Piechulla, B. (2010). Belowground volatiles facilitate interactions between plant roots and soil organisms. *Planta* 231, 499–506. doi: 10.1007/s00425-009-1076-2
- Zeng, J., Song, W., Zhang, Y., Mu, Z., Pang, W., Zhang, H., et al. (2022a). Emissions of isoprenoids from dominant tree species in subtropical China. *Front. For. Glob. Change* 5:1089676. doi: 10.3389/ffgc.2022.1089676
- Zeng, J., Zhang, Y., Zhang, H., Song, W., Wu, Z., and Wang, X. (2022b). Design and characterization of a semi-open dynamic chamber for measuring biogenic volatile organic compound (BVOC) emissions from plants. *Atmos. Meas. Tech.* 15, 79–93. doi: 10.5194/amt-15-79-2022
- Zhang, Y., You, Q., Mao, G., Chen, C., and Ye, Z. (2019). Short-term concurrent drought and heatwave frequency with 1.5 and 2.0°C global warming in humid subtropical basins: a case study in the Gan River Basin, China. *Clim. Dynam.* 52, 4621–4641. doi: 10.1007/s00382-018-4398-6



OPEN ACCESS

EDITED BY

Ling Zhang,
Jiangxi Agricultural University, China

REVIEWED BY

Junzhou Zhang,
Lanzhou University, China
Tianyi Zhan,
Nanjing Forestry University, China
Yunlin Zhang,
Guizhou Education University, China

*CORRESPONDENCE

Keyan Fang
✉ kfang@fjnu.edu.cn

†These authors have contributed equally to this work

RECEIVED 18 May 2023

ACCEPTED 25 September 2023

PUBLISHED 18 October 2023

CITATION

Wang C, Zheng Z, Zhou F, Liu X, Fonti P, Gao J and Fang K (2023) Intra-annual dynamic of opposite and compression wood formation of *Pinus massoniana* Lamb. in humid subtropical China.

Front. For. Glob. Change 6:1224838.
doi: 10.3389/ffgc.2023.1224838

COPYRIGHT

© 2023 Wang, Zheng, Zhou, Liu, Fonti, Gao and Fang. This is an open-access article distributed under the terms of the [Creative Commons Attribution License \(CC BY\)](https://creativecommons.org/licenses/by/4.0/). The use, distribution or reproduction in other forums is permitted, provided the original author(s) and the copyright owner(s) are credited and that the original publication in this journal is cited, in accordance with accepted academic practice. No use, distribution or reproduction is permitted which does not comply with these terms.

Intra-annual dynamic of opposite and compression wood formation of *Pinus massoniana* Lamb. in humid subtropical China

Chunsong Wang^{1†}, Zhuangpeng Zheng^{1,2†}, Feifei Zhou¹, Xinsheng Liu³, Patrick Fonti⁴, Jiani Gao¹ and Keyan Fang^{1*}

¹Key Laboratory of Humid Subtropical Eco-Geographical Process (Ministry of Education), College of Geographical Sciences, Fujian Normal University, Fuzhou, China, ²School of Tourism and Historical Culture, Zhaoqing University, Zhaoqing, China, ³Key Laboratory of Earth Surface Processes and Regional Response in the Yangtze-Huaihe River Basin, School of Geography and Tourism, Anhui Normal University, Wuhu, China, ⁴Swiss Federal Institute for Forest, Snow and Landscape Research WSL, Birmensdorf, Switzerland

Radial growth of trees can result in opposite wood (OW) and compression wood (CW) due to the varying impact of stem mechanical stress, such as that caused by gravity or wind. Previous research has identified higher xylem production in CW compared to OW. Yet, it remains unclear whether the difference in the number of xylem cells between OW and CW results from differences in growth rate or the duration of xylem cells. In this study, we collected wood microcores on a weekly basis from March 2019 to January 2020 in *Pinus massoniana* Lamb. located on a steep slope. Our objective was to compare the dynamic of cambial activity and resulting cellular anatomical parameters between OW and CW in a humid subtropical environment. Our results showed that the xylem phenology of OW and CW was generally consistent with the xylem cell division process beginning in early March and ceasing in November. The last latewood cell completed its differentiation at the end of December. The response of wood formation dynamics to climate was consistent in both OW and CW. Moreover, both wood types exhibited a limited development of the enlargement phase due to the heat and drought during the summer. The rate of cell division was responsible for 90.7% of the variability in the number of xylem cells. The CW xylem obtained a larger number of cells by increasing the rate of cell division and displayed thinner earlywood cells with larger lumens than OW cells. Our findings showed that the xylem of conifer species responds to mechanical stress by accelerating the cell division rate. As a result, we suggest calculating the ratio between OW and CW widths to reconstruct wind stress changes rather than calculating the residuals used in the current study.

KEYWORDS

microcore, compression wood, tree rings, wood anatomy, xylogenesis, subtropical China

1. Introduction

Trees form annual rings due to the seasonal changes that occur within a year (Little and Bonga, 1974). The cambium, which is the tissue responsible for the production of new wooden cells, typically remains active from spring to autumn (Campoy et al., 2011; Singh et al., 2017). Environmental conditions before or during the growing season can directly influence the characteristics of the cells produced and the consequent functioning of xylem (Kellomäki and Wang, 2001; Rathgeber et al., 2016; Castagneri et al., 2017). Tree rings can provide insight into past climate conditions, for example, missing rings may indicate very cool summers (George and Anchukaitis, 2015) and intra-annual density fluctuations (IADFs) indicating extreme climate events during the growing season (De Micco et al., 2016; Zhang et al., 2020; Gao et al., 2021). The dynamics of tree growth can reflect past environmental changes and play a significant role in global change (Frank et al., 2022).

However, xylem cells within the same annual rings may exhibit distinct characteristics in different directions. For instance, mechanical stress, such as snow pressure or prevailing winds can cause the generation of specific wood structures, known as “reaction wood” (Sultana and Rahman, 2013). This type of wood induces asymmetric growth patterns (Groover, 2016) and is responsible for controlling the response to mechanical stress in conifers, unlike tension wood in hardwood species (Telewski, 2016). Current research indicates that the formation mechanism of compression wood (CW) is highly intricate and regulated by gravity, plant hormones, and gene expression (Du and Yamamoto, 2007; Yamashita et al., 2007, 2009). However, it is relatively clear that when trees experience mechanical stress that causes tilting, they adapt to the gravitational force, resulting in CW formation (Yamashita et al., 2007; Sultana and Rahman, 2013). The composition and structure of the CW's cell wall undergo significant changes. Notably, CW exhibits an increase in cellulose content, and the content and composition of lignin also undergo alterations (Peng et al., 2019; Wang et al., 2020). CW is characterized by thicker cells with a gelatinous layer produced in the compressed stem region, leading to stiffer mechanical characteristics (Donaldson, 2001). Moreover, annual rings in the compressed stem region are usually larger and contain more cells than those on the opposite side of the stem (OW, opposite wood) (Donaldson et al., 2004).

The reconstruction of mechanical stress relies on the asymmetric growth of the stem, which typically indicates the timing and strength of the stem eccentricity (Zhang et al., 2017; Fang et al., 2022a). For example, Fang et al. (2022b) have proposed a method to reconstruct wind speed by analyzing shifts in the geometric center of tree rings. Although there is significant interest in comprehending the drivers of wood formation, particularly in response to climate, the formation of reaction wood has received little attention (Palombo et al., 2018). Therefore, quantifying and comprehending the differences between CW and OW or other types of wood could provide valuable insights into wood formation processes. Moreover, it could improve the use of annually datable markers in mechanical events-related reconstruction.

In this study, we investigated the intra-annual xylem formation dynamics of *Pinus massoniana* Lamb. in both OW and CW as well as their responses to climate and mechanical stress using microcore monitoring. We hypothesized that the intra-annual

xylem formation dynamics and climate responses would exhibit similarities between OW and CW and that xylem would respond to mechanical stress by accelerating the rate of cell division. Specifically, our tasks were as follows: to (a) obtain the intra-annual xylem formation dynamics of *P. massoniana* Lamb. in both OW and CW and analyze the response of xylem cell dynamics to climate; (b) compare the anatomical characteristics of xylem cells in OW and CW; and (c) investigate the effect of the duration and rate of cell division on the number of xylem cells. By doing so, we hope to gain a better understanding of the physiological mechanisms underlying differential growth in a tree of different aspects. Results obtained could help to verify or propose a methodology for reconstructing regional wind speed.

2. Materials and methods

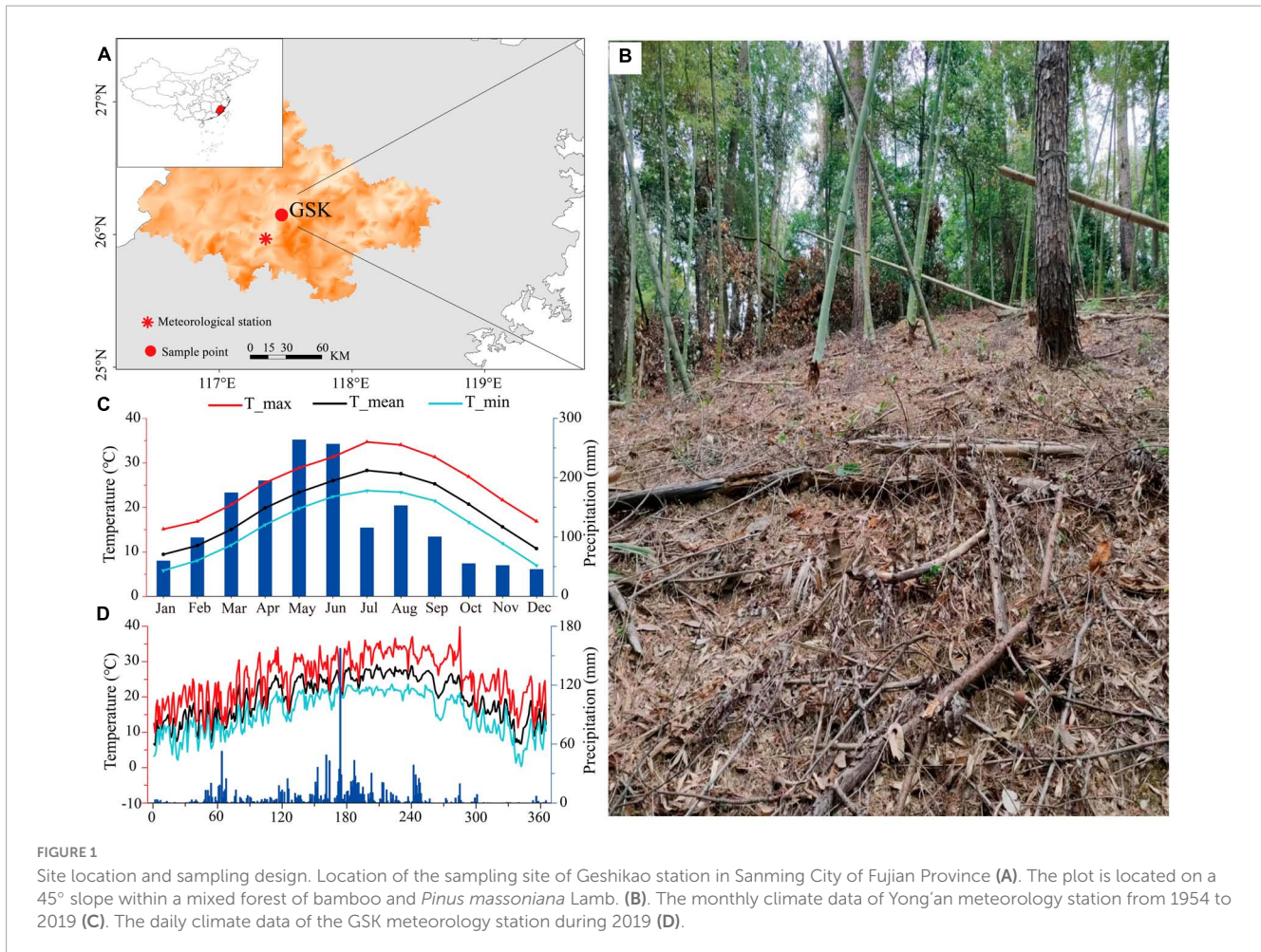
2.1. Study region

This study was conducted at the Geshikao (GSK) nature reserve in Sanming City, Fujian Province (26°9'13"N, 117°28'19"E, 320 m above sea level), which is a permanent monitoring site in the humid subtropical region of China (Figure 1A). Specifically, the site is located on a steep hill (slope angle of ca. 50°) in a mixed forest of bamboo and *P. massoniana* Lamb. and is 3 km away from the GSK field station (Figure 1B). The main soil type in the study area is mountain red soil followed by mountain yellow soil and purple soil.

The mean annual temperature at the study site between 1954 and 2019 was 19.46°C, with the warmest and coldest monthly mean temperatures of 34.72 and 5.84°C being recorded in July and January, respectively. Annual precipitation at the site is 1,573 mm, roughly 75% of which is received from March to August (data from Yong'an meteorological station) (Figure 1C). Yong'an meteorological station is 25.5 km away from the monitoring site. Daily mean, maximum, and minimum air temperatures, as well as total precipitation, were collected by the micro-automatic meteorological station at the GSK field station (Figure 1D). The daily-scale meteorological data was simultaneously monitored with a 3-m high automated weather station (KME101, LSI-LASTEM, Milan, Italy). A set of probes for measuring air temperature (Ta; KME101, accuracy ± 0.2°C) and precipitation (P; DQA230.1#C, resolution 0.2 mm).

2.2. Tree selection and sample preparation

Four healthy *P. massoniana* Lamb. trees were selected. The monitored trees had an average diameter at breast height (DBH) of 37.7 ± 5.5 cm, height of 13.9 ± 1 m, and tree age of 45 ± 2 years. The sample size and tree parameters met the requirements of a micro-sampling study (Nehrbass-Ahles et al., 2014; Huang et al., 2018). From 11 March 2019 to 10 January 2020, weekly samples were taken at breast height (i.e., 1.3 m above the ground) using a Trephor (Rossi et al., 2006). Microcores were collected from both the CW (the widest tree rings) and the OW (the narrowest tree rings) (as seen in Supplementary Figure 2). Each core had a diameter of 2 mm and a length of 2–3 cm that contained at least two intact xylem and lamellar bands with adjacent phloem



(Zheng et al., 2021). To maximize the use of limited sampling locations and minimize influences between adjacent sample areas, samples were taken in a zigzag pattern around the trunk, with a minimum distance of 5 cm between each sample (Supplementary Figure 3). A total of 360 samples were collected and immediately stored in a mixed solution of 70% alcohol and glacial acetic acid (mixing ratio: 9:1). In the laboratory, samples were dehydrated in different concentrations of alcohol (70, 90, 95, and 100%), soaked in limonene, and finally embedded in paraffin. Transverse sections of 12 μm were cut using a rotary microtome and stained with safranin and Astra blue (Li et al., 2019).

2.3. Cell types and anatomical parameters

The three continuous columns of cell counts showing good quality and absence of disturbances were selected for the measurements of each sample, and the cells were identified as cambium cells, enlargement cells, wall thickening cells, and mature cells (Rathgeber et al., 2016). The average weekly number of cells in each differentiation phase was then expressed as a function of day of the year (DOY) (Rathgeber, 2012). The cambium cells are typically flattened and have very thin walls, and enlargement cells have an irregular radial diameter and are at least two

times larger than cambium cells. Wall-thickening cells appear shiny under polarized light compared to enlargement cells, and mature cells are red-stained by safranin and have mature tubular cells (Camarero et al., 2010; Ren et al., 2018; Supplementary Figure 4). The onset of radial stem growth was determined by the appearance of the first enlargement cells, and radial stem growth was considered completed when wall-thickening cells no longer appeared (Rossi et al., 2006).

Using ImageJ (National Institutes of Health, Bethesda, MD, USA), we measured the cell anatomical parameters of the last collected samples after the end of the growing season (i.e., on 10 January 2020; DOY 375). These included the radial parameters: double cell wall thickness (2CWT), radial lumen diameter (LD), lumen area (LA), cell area (CA), and cell number (Num). Cell wall area (CWA) was calculated as the difference between the CA and LAs (Cuny et al., 2019). According to Mork's criterion (Denne, 1989), we divided mature cells into earlywood cells ($2\text{CWT}/\text{LD} < 0.5$) and latewood cells ($2\text{CWT}/\text{LD} \geq 0.5$).

2.4. Statistics and analysis

The number of cells can differ largely between aspects due to differences in growth rate. Therefore, standardization of the number of xylem cells was necessary. This can be achieved by using

the number of cambium xylem cells of the previous tree ring width as a reference (Rossi et al., 2006; Zhang et al., 2018). The formula used for this standardization is as follows:

$$nc_i = ncm_i \times rw_m / rw_s \quad (1)$$

where nc_i is the standardized number of xylem cells, ncm_i is the measured number of xylem cells, rw_m is the mean width of the previous tree rings for all samples, and rw_s is the width of the previous tree rings for each sample (Zheng et al., 2021).

Different from the simple unimodal growth characteristics in the alpine region, the radial growth in the humid subtropical region has a complex growth pattern (Huang et al., 2018; Liu et al., 2019; Zheng et al., 2021). Given that generalized additive models (GAMs) are data-driven, they are better able to describe complex intra-annual wood formation dynamics than traditional Gompertz functions (Cuny et al., 2013). So, we used GAMs to model the growth of cambium xylem cells (enlargement + wall thickening + mature cells) in both the CW and OW of each tree. The model is represented by the equation

$$E(y/x_1) = f(x_1) \quad (2)$$

In the equation, y is the response variable (the number of cambium xylem cells), x_1 is the DOY and f represents the smoothing function. The Poisson link function is used given that the response variable is a count variable. Its derivative was further calculated to obtain the rate of cell division (Huang et al., 2018).

A model is constructed to demonstrate the correlation between the number of cambium xylem cells (N_{cell}), the mean rate (r_m), and the duration (Δt_E) of cell production. The N_{cell} is the median number of cells remaining in the sample after the cells have stopped dividing. The r_m is the average of the rate of cell division, and the Δt_E is calculated from observations, which represents the duration of cell division, from the emergence to the disappearance of enlarged cells (Rathgeber et al., 2011; Ren et al., 2019):

$$N_{cell} = f(r_m \times \Delta t_E) \quad (3)$$

Before determining the correlation between the number or rate of cells at different times and climate records, average meteorological variables were calculated over a 7- and 10-day period preceding the sampling date. This is because xylem cell growth is affected by climate with a lag effect (Prislan et al., 2016). The variations in key times of xylem phenology and wood anatomy between CW and OW were identified using ANOVA and Tukey's test. Normality was confirmed for all critical dates before using ANOVA.

3. Results

3.1. Xylem cell dynamics and their response to climate

The seasonal dynamic of xylem cell numbers at different phase in both CW and OW were very similar. Cambial cells enlarged in early March and stopped dividing in November. The number of cambium cells fluctuated between three and seven throughout the growing season at both wood types and stabilized at ca. five at the end of the xylem enlargement phase (Figure 2A). At the initial

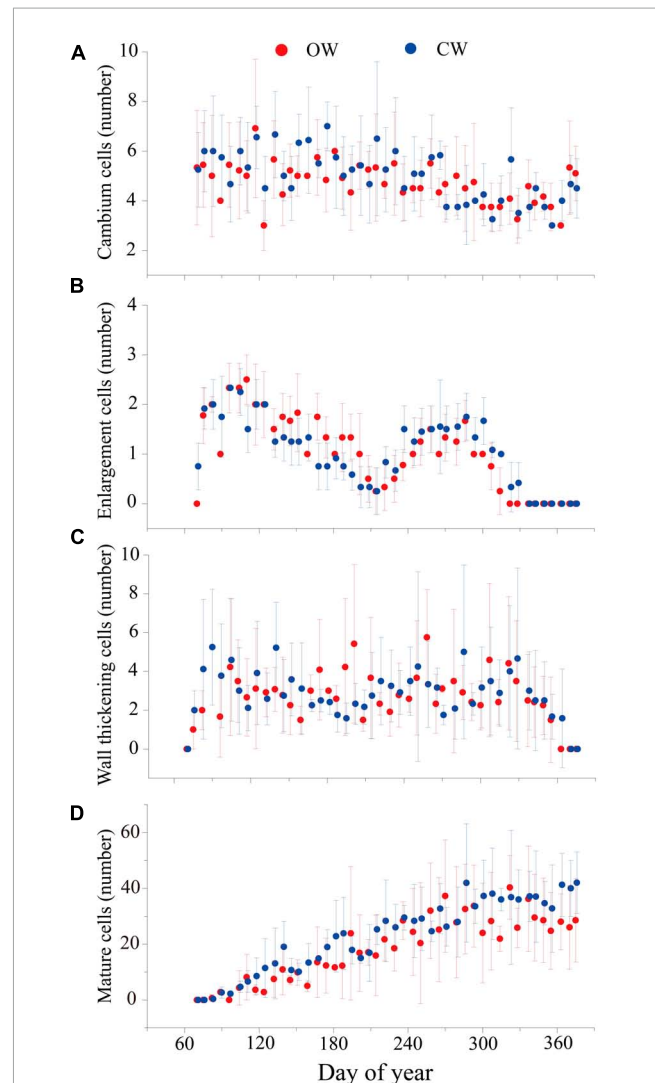


FIGURE 2

Number of cambium cells (A), enlargement cells (B), wall thickening cells (C), and mature cells (D) of OW (red) and CW (blue) of *Pinus massoniana* Lamb. during 2019 at GSK field station. The dots and the bars represent the mean cell number and standard errors among the four selected trees, respectively.

sampling date (March 11, DOY 70), CW samples already presented cells in the enlargement phase, indicating that the cambium had begun to activate before the first date. In contrast, the OW cambium did not activate until the second sampling date (March 16, DOY 75). The seasonal dynamic of the enlarged cells exhibited a bimodal pattern. The enlarged cells reached a first growth peak in early April (DOY 100), and then gradually decreased until a secondary growth peak occurred in early October (DOY 280) (Figure 2B). The bimodal pattern in the wall thickening phase was less evident (Figure 2C), while the intra-annual dynamics of mature cells are characterized by a single “S” shaped change (Figure 2D).

The response of xylem cell numbers at different phase to climatic factors (minimum, mean and maximum temperatures, and precipitation) was highly consistent between CW and OW. The effects of temperature and precipitation on xylem cell numbers between CW and OW were independent of time periods. Precipitation had a weak promoting effect on cells in the mature

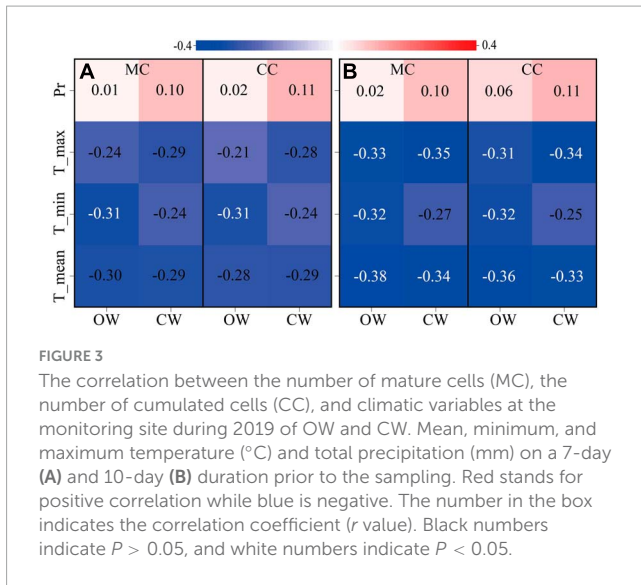


FIGURE 3
The correlation between the number of mature cells (MC), the number of cumulated cells (CC), and climatic variables at the monitoring site during 2019 of OW and CW. Mean, minimum, and maximum temperature (°C) and total precipitation (mm) on a 7-day (A) and 10-day (B) duration prior to the sampling. Red stands for positive correlation while blue is negative. The number in the box indicates the correlation coefficient (*r* value). Black numbers indicate $P > 0.05$, and white numbers indicate $P < 0.05$.

phase and the cumulated cells ($P > 0.05$). Temperature had an inhibiting effect on cells in the mature phase and the cumulated cells ($P > 0.05$), while the temperature 10 days before sampling significantly inhibited cells in the mature phase and the cumulated cells ($P < 0.05$) (Figure 3).

3.2. Phenological timing and the rate of xylem cell division

The phenological timings between OW and CW were insignificantly different, while the rate of xylem cell division was significantly different. The cambium activates at DOY 75 ± 3 (OW) and DOY 73 ± 5 (CW), and cell division ended at DOY 307 ± 5 (OW) and DOY 321 ± 7 (CW), leading to Δt_E of 232 ± 8 days (OW) and 248 ± 12 days (CW), respectively. The first latewood cells appeared at DOY 193 ± 18 (OW) and DOY 179 ± 8 (CW), respectively. The date of first appearance of cell wall thickening cells was on DOY 82 ± 10 (OW) and DOY 79 ± 8 (CW). The cambium entered the dormancy stage at DOY 352 ± 3 (OW) and DOY 359 ± 5 (CW), respectively. There was no significant difference in the growing season length between OW and CW (279 ± 13 and 284 ± 13 days for OW and CW, respectively; Table 1). The GAMs model explained 80.9% (83.9%) of the intra-annual dynamics of xylem cells at the OW (CW) (Figure 4A). The seasonal dynamics of the cell division rate showed a bimodal shape, with the cell division rate reaching a first growth peak in early March and a second growth peak in the middle of September (Figure 4B). The r_m for OW was 0.126 cells/day and the r_m for CW was 0.154 cells/day. When compared to OW, xylem cell production and r_m of CW

increased by 22.2 and 24.8%, respectively. However, the Δt_E for CW was only 6% longer than OW.

The response of cell production rates at different periods (earlywood phase or latewood phase) to climatic factors (minimum, mean and maximum temperatures, and precipitation) was highly consistent between CW and OW. During earlywood formation, temperature and precipitation did not significantly affect the xylem cell division rate during earlywood formation, while the precipitation the 10 days before sampling significantly promoted the production rate of earlywood cells ($P < 0.05$). However, during latewood growth temperature significantly facilitated the rate of cell production. The mean temperature of 7 days before sampling and both the mean and maximum temperature 10 days before sampling significantly promoted the latewood cell production rate ($P < 0.05$) (Figure 5).

3.3. Rate and duration of wood production

A physical model was constructed to determine whether xylem cell production is controlled by r_m or Δt_E . The model, which was based on N_{cell} , r_m , and Δt_E , was found to have a good fit (COD = 70.2%) (Figure 6A). Sensitivity analysis of the model revealed that an increase in r_m resulted in a corresponding increase in N_{cell} , while Δt_E had a minor effect on N_{cell} (Figure 6B). The model indicated that a majority portion (90.7%) of the variability in N_{cell} was attributed to r_m . When r_m remains constant at the mean and Δt_E varies around its mean by twice its standard deviation, N_{cell} varies only in the range of 36.5–39.2 cells (a range of variation of 2.7 cells). Similarly, when Δt_E was constant at its mean and r_m varied around its mean within twice its standard deviation, N_{cell} varied within a range of 24.6–51.1 cells (a range of variation of 26.5 cells).

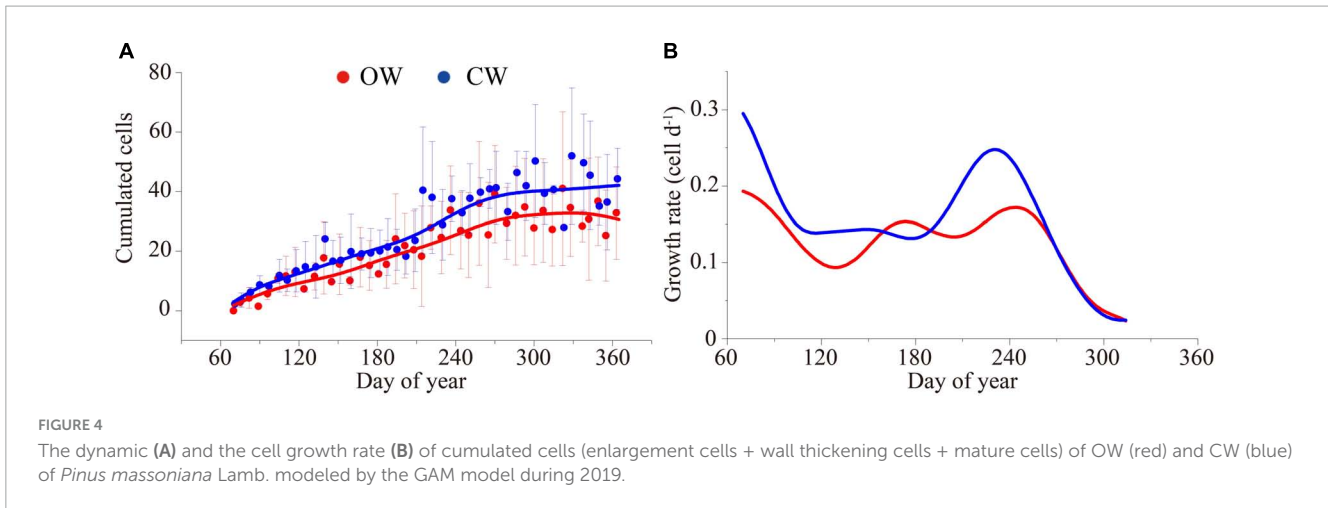
3.4. The cellular anatomy between OW and CW

A comparison of microcore sections revealed differences in xylem cell anatomy between CW and OW (Supplementary Figures 2B, C). Compared to OW, CW earlywood cells exhibited distinct anatomical changes. Specifically, compared to OW earlywood cells, the 2CWT of CW was slightly thinner ($P > 0.05$); the LD of CW earlywood cells was significantly larger ($P < 0.05$); the LA and CA were larger but insignificant ($P > 0.05$); and the CWA and Num increased significantly ($P < 0.05$) (Figures 7A, C, E, G, I, K). Compared to OW, CW had smaller 2CWT, LA, CWA, LD, and CA but a higher number of latewood cells. However, it is worth noting that none of the differences in latewood anatomy

TABLE 1 Critical dates of xylem phenology between OW (opposite wood) and CW (compressed wood) of *Pinus massoniana* Lamb.

| Type | EC onset (DOY) | EC end (DOY) | WT onset (DOY) | Xylem end (DOY) | Lw onset (DOY) | Duration of cell division (day) | Duration of growing season (day) |
|------|----------------|---------------|----------------|-----------------|----------------|---------------------------------|----------------------------------|
| OW | 75 ± 3^A | 307 ± 5^A | 82 ± 10^A | 352 ± 3^A | 193 ± 18^A | 232 ± 8^A | 279 ± 13^A |
| CW | 73 ± 5^A | 321 ± 7^A | 79 ± 8^A | 359 ± 5^A | 179 ± 8^A | 248 ± 12^A | 284 ± 13^A |

Numerical values are mean \pm standard error. The same letters are not statistically different at 0.05 probability. EC indicates the phase of the enlargement cell; WT indicates the phase of the wall thickening cell; Lw indicates the phase of latewood.



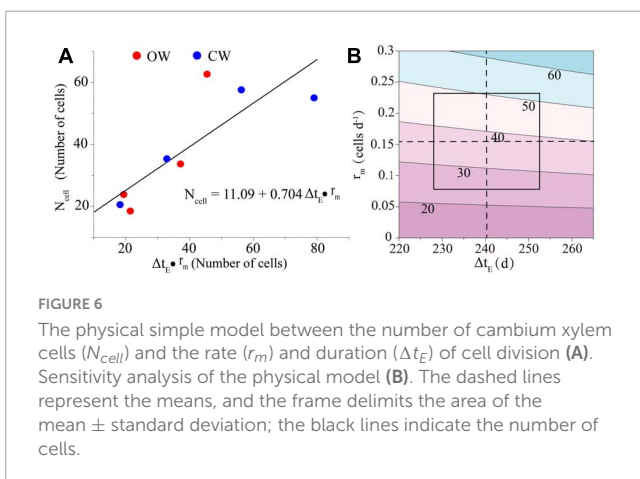
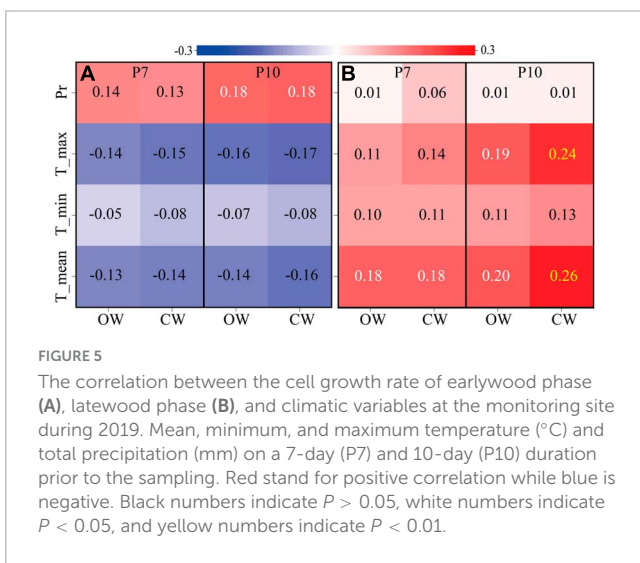
were significant (Figures 7B, D, F, H, J, L). When comparing the morphology of earlywood to latewood cells, it was observed that earlywood cells in CW had larger cells with thinner walls and larger lumens, while latewood cells were significantly smaller with thicker walls and smaller lumens.

4. Discussion

4.1. Dry and hot summer climate induces bimodal growth

In this study, xylem cell division of *P. massoniana* Lamb. began in March and ceased in November. The growth duration was prolonged by 3–4 months compared to coniferous species in cold environments (Rossi et al., 2016) but was consistent with the findings of Huang et al. (2018) and Zheng et al. (2021) who reported that the regional climate plays a significant role in wood formation processes of subtropical conifers. A humid and warm climate is optimal for leaf photosynthesis, which will further promote the radial growth of trees (Ding et al., 2021). When favorable conditions occur in the spring, cambium cells begin to divide and expand (Li et al., 2017). Turgor within the cells is essential to maintain the expansion pressure required for division and expansion, and the availability of water plays a crucial role at this stage (as seen in Supplementary Figure 1; Cabon et al., 2020). At the early and late stages of cell expansion, the temperature in the study area is already high, but the low precipitation levels do not effectively replenish soil moisture, which has an inhibiting effect on the production of expanding cells (Song et al., 2022).

It is worth noting that the seasonal dynamic of xylem cells at the enlargement and wall thickening phase of *P. massoniana* Lamb. in the study area presented a bimodal pattern, which is in line with previous reports in the Mediterranean region that is driven by seasonal changes in water availability (Pacheco et al., 2016; Campelo et al., 2018). Radial growth of *P. massoniana* Lamb. in the study area is affected by summer heat and drought (Li et al., 2016). Studies using tree-ring isotopes and dendrometer measurements suggest that tree growth of subtropical conifers is constrained by summer heat and drought (Liu et al., 2019; Bing et al., 2022), leading to the bimodal seasonal growth patterns of trees in humid subtropical China. As the latewood cells develop, the regulation of cell production rates transitions from being solely dependent on precipitation to becoming modulated by temperature. The occurrence of summer drought results in decreased activity of the cambium or even dormancy, which subsequently causes a seasonal alteration in limiting factors that



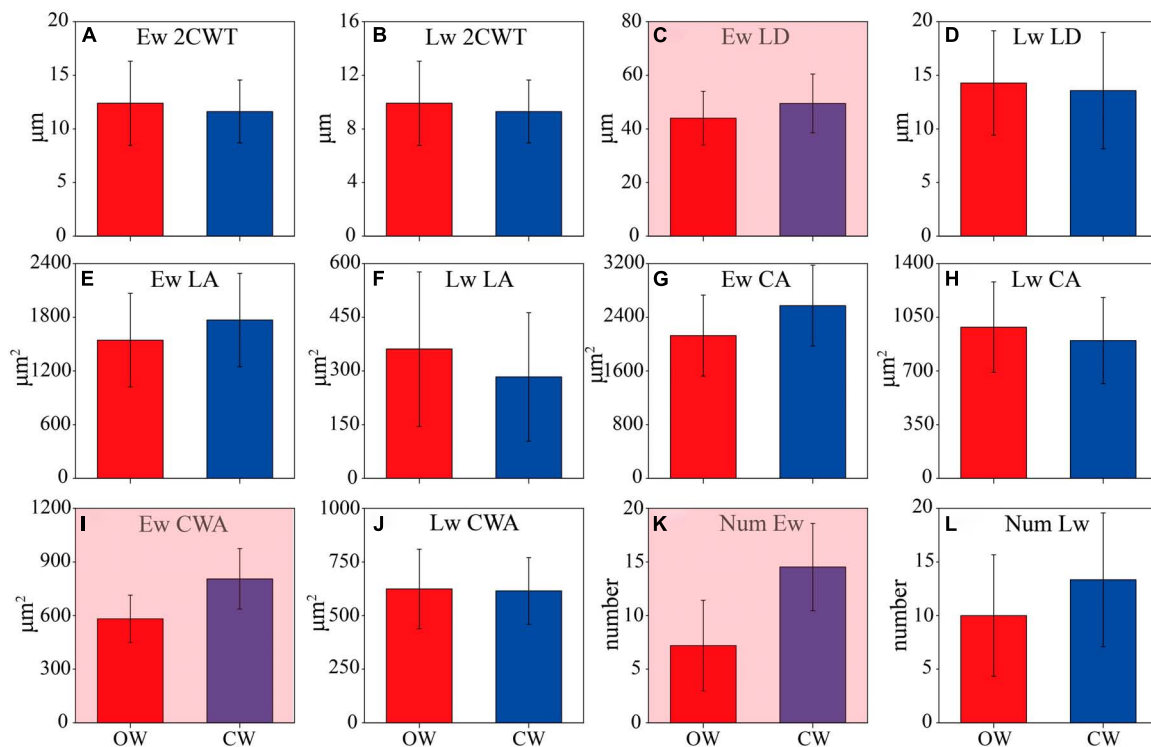


FIGURE 7

Comparison of the wood anatomical parameters between opposite wood (OW, red) and compressed wood (CW, blue). Double cell wall thickness (2CWT), radial lumen diameter (LD), lumen area (LA), cell area (CA), cell wall area (CWA), and number (Num) of earlywood (Ew) (A,C,E,G,I,K) and latewood (Lw) (B,D,F,H,J,L). Numerical values are mean \pm standard error. Shades of red indicate a significant difference at 0.05 probability.

restrict the growth rate of xylem cells (Carteni et al., 2018; Liu X. et al., 2018).

4.2. The influence of mechanical stress on xylem formation

Several studies have suggested that wood production is correlated with the length of the growing season (Rossi et al., 2012; Liu S. et al., 2018; Camarero et al., 2022). However, others contend that wood production may be more strongly influenced by the rate of cell production rather than growing season length (Ren et al., 2019; Jiang et al., 2021). Our research demonstrated that a faster rate cell production leads to larger wood production on the CW. The tree-ring of *P. massoniana* Lamb. exhibits evident eccentricity in order to regain their upright position via maintaining balance (Bamber, 2001; Donaldson and Singh, 2013). The tree growth responds to mechanical stress in different aspects by changing the rate of cell production.

During the sampling process, it was observed that on steep slopes, the branches of *P. massoniana* Lamb. were primarily located on the downhill side, and the young leaves and shoots of the canopy were the main sites of phytohormone production (Huang et al., 2014; Ding et al., 2021), indicating that phytohormones play a significant role in the xylem formation of coniferous species (Guo et al., 2022). Studies have shown that the concentration of phytohormones in the trunk affects the rate of division and differentiation, size, and lignin accumulation in xylem cells

(Perrot-Rechenmann, 2010; Sorce et al., 2013; Rathgeber et al., 2016; Buttò et al., 2020). At the start of xylem activity, before the plant begins to sprout, there is no difference in phytohormone concentration between OW and CW, and the timing of xylem initiation is also similar. As leaf extension and maturation occur, phytohormones are enriched at CW and xylem cells are rapidly produced and expanded (Rossi et al., 2009; Guo et al., 2022), influencing tubular cell lumen and CWA (Majda and Robert, 2018). As a result, earlywood cells at CW are significantly larger in lumen and CWA than at OW. The transition from earlywood to latewood in xylem cells occurs after leaf bursting and extension is completed (Fajstavr et al., 2019), when phytohormone concentrations in the stem are at low levels and a slight reduction in cell size at CW occurs due to gravity (Tarmian and Azadfallah, 2009; Palombo et al., 2018). This leads to a significant increase in the size and number of xylem earlywood cells at CW.

4.3. Differences in wood production between OW and CW

Previous studies have used the difference of tree ring width between the opposite and compression sides (CW-OW) to quantify the effect of wind stress on trees (Fang et al., 2022a). This method extracts a composite signal that encompasses a prolonged growing season and increased growth rate, operating under the premise that xylem production is co-regulated by the duration of the growing season and the growth rate (Rossi et al., 2012;

Camarero et al., 2022). In our study, we found that the greater accumulation of xylem cells on the CW side was primarily due to a higher rate of cell production rather than the duration of xylem cell production. The xylem formation process was found to be consistent between OW and CW in response to climate, with the CW side responding to mechanical stress by accelerating its cell division rate. Therefore, we suggest that the impact of external stress on trees can be studied by considering the ratio between the two sides simultaneously. When reconstructing regional wind speeds, using the ratio chronology will provide a more accurate reflection of wind speed changes than a difference chronology.

However, the physiological response of trees to prevailing winds is complex, as wind not only generates mechanical stresses in different directions compared to the steady mechanical stresses generated by gravity but also accelerates related physiological processes such as leaf transpiration (Telewski, 2012; Mitchell, 2013). Therefore, we recommend that future studies to accurately understand the effects of strong winds on wood formation in different directions within trees should include monitoring of multiple tree species in strong wind conditions to further clarify the effects of wind speed on tree growth and cambium activity.

5. Conclusion

This study investigates the dynamics of xylem formation in *P. massoniana* Lamb. and compares the phenological and anatomical characteristics of trees growing on steep slopes facing opposite directions (OW and CW) in the humid subtropics. Our findings demonstrate that xylem formation responds similarly to climate in both OW and CW. Moreover, the number of cells in the enlargement phase was limited by summer drought in *P. massoniana* Lamb. in both directions. We observed that the cell division rate of xylem cells in CW was accelerated, due to the effect of gravity, although there was no significant difference in cell division time. The earlywood cells in CW had larger cell lumens and thinner cell walls, while the latewood cells had smaller cell lumens and thicker cell walls. These differences in cellular anatomical parameters suggest that phytohormones may influence xylem cell morphology. The results of our study imply that trees growing in locations with different mechanical stress primarily modify the rate of cell division. So, we suggest calculating the ratio between OW and CW widths to reconstruct wind stress changes rather than calculating the residuals used in the current study.

Data availability statement

The raw data supporting the conclusions of this article will be made available by the authors, without undue reservation.

References

- Bamber, R. K. (2001). A general theory for the origin of growth stresses in reaction wood: How trees stay upright. *JAWA J.* 22, 205–212. doi: 10.1163/22941932-90000279
- Bing, X., Fang, K., Gong, X., Wang, W., Xu, C., Li, M., et al. (2022). The intra-annual intrinsic water use efficiency dynamics based on an improved model. *Clim. Change* 172:16. doi: 10.1007/s10584-022-03368-1

Author contributions

KE, ZZ, and FZ designed the experiment. CW and ZZ performed the material preparation, data collection, and analysis. CW wrote the first draft of the manuscript. XL, PF, and JG commented on previous versions of the manuscript. All authors contributed to the preparation of the manuscript, and read and approved the final manuscript.

Funding

We acknowledged support from the National Natural Science Foundation of China (41971022, 42101082, 41888101, and 41772180), the Strategic Priority Research Program of the Chinese Academy of Sciences (XDB26020000), the fellowship for Youth Talent Support Program of Fujian Province, and the innovation team project (IRTL1705).

Acknowledgments

We thank Meiqing Yang and Ping Chen for their help during field sampling.

Conflict of interest

The authors declare that the research was conducted in the absence of any commercial or financial relationships that could be construed as a potential conflict of interest.

Publisher's note

All claims expressed in this article are solely those of the authors and do not necessarily represent those of their affiliated organizations, or those of the publisher, the editors and the reviewers. Any product that may be evaluated in this article, or claim that may be made by its manufacturer, is not guaranteed or endorsed by the publisher.

Supplementary material

The Supplementary Material for this article can be found online at: <https://www.frontiersin.org/articles/10.3389/ffgc.2023.1224838/full#supplementary-material>

- Buttò, V., Deslauriers, A., Rossi, S., Rozenberg, P., Shishov, V., and Morin, H. (2020). The role of plant hormones in tree-ring formation. *Trees* 34, 315–335. doi: 10.1007/s00468-019-01940-4
- Cabon, A., Fernández-de-Uña, L., Gea-Izquierdo, G., Meinzer, F. C., Woodruff, D. R., Martínez-Vilalta, J., et al. (2020). Water potential control of turgor-driven tracheid enlargement in Scots pine at its xeric distribution edge. *N. Phytol.* 225, 209–221. doi: 10.1111/nph.16146
- Camarero, J. J., Campelo, F., Colangelo, M., Valeriano, C., Knorre, A., Solé, G., et al. (2022). Decoupled leaf-wood phenology in two pine species from contrasting climates: Longer growing seasons do not mean more radial growth. *Agric. For. Meteorol.* 327:109223. doi: 10.1016/j.agrformet.2022.109223
- Camarero, J. J., Olano, J. M., and Parras, A. (2010). Plastic bimodal xylogenesis in conifers from continental Mediterranean climates. *N. Phytol.* 185, 471–480. doi: 10.1111/j.1469-8137.2009.03073.x
- Campelo, F., Gutiérrez, E., Ribas, M., Sánchez-Salguero, R., Nabais, C., and Camarero, J. J. (2018). The facultative bimodal growth pattern in *Quercus ilex*—a simple model to predict sub-seasonal and inter-annual growth. *Dendrochronologia* 49, 77–88. doi: 10.1016/j.dendro.2018.03.001
- Campoy, J. A., Ruiz, D., and Egea, J. (2011). Dormancy in temperate fruit trees in a global warming context: A review. *Sci. Hortic.* 130, 357–372. doi: 10.1016/j.scienta.2011.07.011
- Carteni, F., Deslauriers, A., Rossi, S., Morin, H., De Micco, V., Mazzoleni, S., et al. (2018). The physiological mechanisms behind the earlywood-to-latewood transition: A process-based modeling approach. *Front. Plant Sci.* 9:1053. doi: 10.3389/fpls.2018.101053
- Castagneri, D., Fonti, P., von Arx, G., and Carrer, M. (2017). How does climate influence xylem morphogenesis over the growing season? Insights from long-term intra-ring anatomy in *Picea abies*. *Ann. Bot.* 119, 1011–1020. doi: 10.1093/aob/mcw274
- Cuny, H. E., Fonti, P., Rathgeber, C. B., von Arx, G., Peters, R. L., and Frank, D. C. (2019). Couplings in cell differentiation kinetics mitigate air temperature influence on conifer wood anatomy. *Plant Cell Environ.* 42, 1222–1232. doi: 10.1111/pce.13464
- Cuny, H. E., Rathgeber, C. B., Kiessé, T. S., Hartmann, F. P., Barbeito, I., and Fournier, M. (2013). Generalized additive models reveal the intrinsic complexity of wood formation dynamics. *J. Exp. Bot.* 64, 1983–1994. doi: 10.1093/jxb/ert057
- De Micco, V., Campelo, F., De Luis, M., Bräuning, A., Grabner, M., Battipaglia, G., et al. (2016). Intra-annual density fluctuations in tree rings: How, when, where, and why? *IAWA J.* 37, 232–259. doi: 10.1163/22941932-20160132
- Denne, M. P. (1989). Definition of latewood according to Mork (1928). *IAWA J.* 10, 59–62. doi: 10.1163/22941932-90001112
- Ding, X., Jiang, Y., Xue, F., Zhang, Y., Wang, M., Kang, M., et al. (2021). Intra-annual growth dynamics of *Picea meyeri* needles, shoots, and stems on Luya Mountain, North-central China. *Trees* 35, 637–648. doi: 10.1007/s00468-020-02065-9
- Donaldson, L. A. (2001). Lignification and lignin topochemistry—an ultrastructural view. *Phytochemistry* 57, 859–873. doi: 10.1016/S0031-9422(01)00049-8
- Donaldson, L. A., Grace, J., and Downes, G. M. (2004). Within-tree variation in anatomical properties of compression wood in radiata pine. *IAWA J.* 25, 253–271. doi: 10.1163/22941932-90000364
- Donaldson, L. A., and Singh, A. P. (2013). “Formation and structure of compression wood,” in *Cellular aspects of wood formation*, ed. J. Fromm (Berlin: Springer Berlin Heidelberg), 225–256. doi: 10.1007/978-3-642-36491-4_9
- Du, S., and Yamamoto, F. (2007). An overview of the biology of reaction wood formation. *J. Integr. Plant Biol.* 49, 131–143. doi: 10.1111/j.1744-7909.2007.00427.x
- Fajstavr, M., Bednářová, E., Nezval, O., Giagli, K., Gryc, V., Vavrčik, H., et al. (2019). How needle phenology indicates the changes of xylem cell formation during drought stress in *Pinus sylvestris* L. *Dendrochronologia* 56:125600. doi: 10.1016/j.dendro.2019.05.004
- Fang, K., Bai, M., Azorin-Molina, C., Dong, Z., Camarero, J. J., Zheng, Z., et al. (2022a). Wind speed reconstruction from a tree-ring difference index in northeastern Inner Mongolia. *Dendrochronologia* 72:125938. doi: 10.1016/j.dendro.2022.125938
- Fang, K., He, M., Bai, M., Dong, Z., Linderholm, H. W., Azorin-Molina, C., et al. (2022b). The potential to use variations in tree-ring geometric center to estimate past wind speed change. *Nat. Hazards Res.* 2, 132–137. doi: 10.1016/j.nhres.2022.04.004
- Frank, D., Fang, K., and Fonti, P. (2022). “Dendrochronology: Fundamentals and innovations,” in *Stable isotopes in tree rings. Tree physiology*, Vol. 8, eds R. T. W. Siegwolf, J. R. Brooks, J. Roden, and M. Saurer (Cham: Springer), doi: 10.1007/978-3-030-92698-4_2
- Gao, J., Rossi, S., and Yang, B. (2021). Origin of intra-annual density fluctuations in a semi-arid area of Northwestern China. *Front. Plant Sci.* 12:777753. doi: 10.3389/fpls.2021.777753
- George, S. S., and Anchukaitis, K. J. (2015). On the AD 1815 tabora eruption and the matter of misplaced tree rings. *Past Glob. Changes Magaz.* 23, 60–61. doi: 10.1002/jgrd.50692
- Groover, A. (2016). Gravitropisms and reaction woods of forest trees—evolution, functions and mechanisms. *N. Phytol.* 211, 790–802. doi: 10.1111/nph.13968
- Guo, X., Huang, J. G., Buttò, V., Luo, D., Shen, C., Li, J., et al. (2022). Auxin concentration and xylem production of *Pinus massoniana* in a subtropical forest in south China. *Tree Physiol.* 42, 317–324. doi: 10.1093/treephys/tpab110
- Huang, J. G., Deslauriers, A., and Rossi, S. (2014). Xylem formation can be modeled statistically as a function of primary growth and cambium activity. *N. Phytol.* 203, 831–841. doi: 10.1111/nph.12859
- Huang, J. G., Guo, X., Rossi, S., Zhai, L., Yu, B., Zhang, S., et al. (2018). Intra-annual wood formation of subtropical Chinese red pine shows better growth in dry season than wet season. *Tree Physiol.* 38, 1225–1236. doi: 10.1093/treephys/tpy046
- Jiang, Y., Zhang, X., Chhin, S., and Zhang, J. (2021). A bimodal pattern and age-related growth of intra-annual wood cell development of Chinese fir in subtropical China. *Front. Plant Sci.* 12:757438. doi: 10.3389/fpls.2021.757438
- Kellomäki, S., and Wang, K. Y. (2001). Growth and resource use of birch seedlings under elevated carbon dioxide and temperature. *Ann. Bot.* 87, 669–682. doi: 10.1006/anbo.2001.1393
- Li, X., Liang, E., Gričar, J., Rossi, S., Čufar, K., and Ellison, A. M. (2017). Critical minimum temperature limits xylogenesis and maintains treelines on the southeastern Tibetan Plateau. *Sci. Bull.* 62, 804–812. doi: 10.1016/j.scib.2017.04.025
- Li, X., Rossi, S., and Liang, E. (2019). The onset of xylogenesis in Smith fir is not related to outer bark thickness. *Am. J. Bot.* 106, 1386–1391.
- Li, Y., Fang, K., Cao, C., Li, D., Zhou, F., Dong, Z., et al. (2016). A tree-ring chronology spanning 210 years in the coastal area of southeastern China, and its relationship with climate change. *Clim. Res.* 67, 209–220. doi: 10.3354/cr01376
- Little, C. H. A., and Bonga, J. M. (1974). Rest in the cambium of *Abies balsamea*. *Can. J. Bot.* 52, 1723–1730. doi: 10.1139/b74-224
- Liu, S., Li, X., Rossi, S., Wang, L., Li, W., Liang, E., et al. (2018). Differences in xylogenesis between dominant and suppressed trees. *Am. J. Bot.* 105, 950–956. doi: 10.1002/ajb2.1089
- Liu, X., Nie, Y., and Wen, F. (2018). Seasonal dynamics of stem radial increment of *Pinus taiwanensis* Hayata and its response to environmental factors in the Lushan Mountains, Southeastern China. *Forests* 9:387. doi: 10.3390/f9070387
- Liu, X., Wang, C., and Zhao, J. (2019). Seasonal drought effects on intra-annual stem growth of *Taiwan Pine* along an elevational gradient in subtropical China. *Forests* 10:1128. doi: 10.3390/f10121128
- Majda, M., and Robert, S. (2018). The role of auxin in cell wall expansion. *Int. J. Mol. Sci.* 19:951. doi: 10.3390/ijms19040951
- Mitchell, S. J. (2013). Wind as a natural disturbance agent in forests: A synthesis. *For. Int. For. Res.* 86, 147–157. doi: 10.1093/forestry/cps058
- Nehrbass-Ahles, C., Babst, F., Klesse, S., Nötzli, M., Bouriaud, O., Neukom, R., et al. (2014). The influence of sampling design on tree ring-based quantification of forest growth. *Glob. Change Biol.* 20, 2867–2885. doi: 10.1111/gcb.12599
- Pacheco, A., Camarero, J. J., and Carrer, M. (2016). Linking wood anatomy and xylogenesis allows pinpointing of climate and drought influences on growth of coexisting conifers in continental Mediterranean climate. *Tree Physiol.* 36, 502–512. doi: 10.1093/treephys/tpv125
- Palombo, C., Fonti, P., Lasserre, B., Cherubini, P., Marchetti, M., and Tognetti, R. (2018). Xylogenesis of compression and opposite wood in mountain pine at a Mediterranean treeline. *Ann. For. Sci.* 75:93. doi: 10.1007/s13595-018-0773-z
- Peng, H., Salmén, L., Stevanic, J. S., and Lu, J. (2019). Structural organization of the cell wall polymers in compression wood as revealed by FTIR microspectroscopy. *Planta* 250, 163–171. doi: 10.1007/s00425-019-03158-7
- Perrot-Rechenmann, C. (2010). Cellular responses to auxin: Division versus expansion. *Cold Spring Harb. Perspect. Biol.* 2:a001446. doi: 10.1101/cshperspect.a001446
- Prislan, P., Gričar, J., De Luis, M., Novak, K., Martínez del Castillo, E., Schmitt, U., et al. (2016). Annual cambial rhythm in *Pinus halepensis* and *Pinus sylvestris* as indicator for climate adaptation. *Front. Plant Sci.* 7:1923. doi: 10.3389/fpls.2016.01923
- Rathgeber, C. B. K. (2012). *Cambial activity and wood formation: Data manipulation, visualisation and analysis using R. R package version 1.4-1.*
- Rathgeber, C. B., Cuny, H. E., and Fonti, P. (2016). Biological basis of tree-ring formation: A crash course. *Front. Plant Sci.* 7:734. doi: 10.3389/fpls.2016.00734
- Rathgeber, C. B., Rossi, S., and Bontemps, J. D. (2011). Cambial activity related to tree size in a mature silver-fir plantation. *Ann. Bot.* 108, 429–438. doi: 10.1093/aob/mtr168
- Ren, P., Rossi, S., Camarero, J. J., Ellison, A. M., Liang, E., and Peñuelas, J. (2018). Critical temperature and precipitation thresholds for the onset of xylogenesis of *Juniperus przewalskii* in a semi-arid area of the north-eastern Tibetan Plateau. *Ann. Bot.* 121, 617–624. doi: 10.1093/aob/mcx188
- Ren, P., Ziaco, E., Rossi, S., Biondi, F., Prislan, P., and Liang, E. (2019). Growth rate rather than growing season length determines wood biomass in dry environments. *Agric. For. Meteorol.* 271, 46–53. doi: 10.1016/j.agrformet.2019.02.031
- Rossi, S., Anfodillo, T., and Menardi, R. (2006). Trephor: A new tool for sampling microcores from tree stems. *IAWA J.* 27, 89–97. doi: 10.1163/22941932-90000139

- Rossi, S., Anfodillo, T., Čufar, K., Cuny, H. E., Deslauriers, A., Fonti, P., et al. (2016). Pattern of xylem phenology in conifers of cold ecosystems at the Northern Hemisphere. *Glob. Change Biol.* 22, 3804–3813. doi: 10.1111/gcb.13317
- Rossi, S., Morin, H., and Deslauriers, A. (2012). Causes and correlations in cambium phenology: Towards an integrated framework of xylogenesis. *J. Exp. Bot.* 63, 2117–2126. doi: 10.1093/jxb/err423
- Rossi, S., Rathgeber, C. B., and Deslauriers, A. (2009). Comparing needle and shoot phenology with xylem development on three conifer species in Italy. *Ann. For. Sci.* 66:206. doi: 10.1051/forest/2008088
- Singh, R. K., Svystun, T., AlDahmash, B., Jönsson, A. M., and Bhalerao, R. P. (2017). Photoperiod-and temperature-mediated control of phenology in trees—a molecular perspective. *N. Phytol.* 213, 511–524. doi: 10.1111/nph.14346
- Song, W., Zhao, B., Mu, C., Ballikaya, P., Cherubini, P., and Wang, X. (2022). Moisture availability influences the formation and characteristics of earlywood of *Pinus tabulaeformis* more than latewood in northern China. *Agric. For. Meteorol.* 327:109219. doi: 10.1016/j.agrformet.2022.109219
- Sorce, C., Giovannelli, A., Sebastiani, L., and Anfodillo, T. (2013). Hormonal signals involved in the regulation of cambial activity, xylogenesis and vessel patterning in trees. *Plant Cell Rep.* 32, 885–898. doi: 10.1007/s00299-013-1431-4
- Sultana, R. S., and Rahman, M. (2013). A review on structures of secondary wall in reaction wood fiber of hardwood species. *Plant* 1, 54–59. doi: 10.11648/j.plant.20130105.12
- Tarmian, A., and Azadfallah, M. (2009). Variation of cell features and chemical composition in spruce consisting of opposite, normal, and compression wood. *Bioresources* 4, 194–204. doi: 10.1515/HF.2009.036
- Telewski, F. W. (2012). Is windswept tree growth negative thigmotropism? *Plant Sci.* 184, 20–28. doi: 10.1016/j.plantsci.2011.12.001
- Telewski, F. W. (2016). “Flexure wood: Mechanical stress induced secondary xylem formation,” in *Secondary xylem biology*, (Cambridge, MA: Academic Press), 73–91. doi: 10.1016/B978-0-12-802185-9.00005-X
- Wang, D., Lin, L., and Fu, F. (2020). Deformation mechanisms of wood cell walls under tensile loading: A comparative study of compression wood (CW) and normal wood (NW). *Cellulose* 27, 4161–4172. doi: 10.1007/s10570-020-03095-9
- Yamashita, S., Yoshida, M., and Yamamoto, H. (2009). Relationship between development of compression wood and gene expression. *Plant Sci.* 176, 729–735. doi: 10.1016/j.plantsci.2009.02.017
- Yamashita, S., Yoshida, M., Takayama, S., and Okuyama, T. (2007). Stem-righting mechanism in gymnosperm trees deduced from limitations in compression wood development. *Ann. Bot.* 99, 487–493. doi: 10.1093/aob/mcl270
- Zhang, J., Alexander, M. R., Gou, X., Deslauriers, A., Fonti, P., Zhang, F., et al. (2020). Extended xylogenesis and stem biomass production in *Juniperus przewalskii* Kom. during extreme late-season climatic events. *Ann. For. Sci.* 77:99. doi: 10.1007/s13595-020-01008-1
- Zhang, J., Gou, X., Pederson, N., Zhang, F., Niu, H., Zhao, S., et al. (2018). Cambial phenology in *Juniperus przewalskii* along different altitudinal gradients in a cold and arid region. *Tree Physiol.* 38, 840–852. doi: 10.1093/treephys/tpx160
- Zhang, Y., Fang, K., Zhou, F., Dong, Z., Li, Y., and Zhang, P. (2017). Reconstruction of soil erosion rates from exposed roots in southeast China. *Asian Geogr.* 34, 91–105. doi: 10.1080/10225706.2017.1351380
- Zheng, Z., Zhou, F., Fonti, P., Ren, P., Li, X., Miao, G., et al. (2021). Intra-annual wood formation of *Cryptomeria fortunei* and *Cunninghamia lanceolata* in humid subtropical China. *Front. Ecol. Evol.* 9:733974. doi: 10.3389/fevo.2021.733974



OPEN ACCESS

EDITED BY

Ling Zhang,
Jiangxi Agricultural University, China

REVIEWED BY

Lydie-Stella Koutika,
CRDPI, Republic of Congo
Mauricio Zagatto,
DungTech Biofertilizers, Brazil

*CORRESPONDENCE

Shaoming Ye
✉ yshaoming@163.com

RECEIVED 30 July 2023

ACCEPTED 03 October 2023

PUBLISHED 23 November 2023

CITATION

Cui Y, Yan Y, Wang S, Zhang H, He Y, Jiang C,
Fan R and Ye S (2023) Mixed *Eucalyptus*
plantations in subtropical China enhance
phosphorus accumulation and transformation
in soil aggregates.
Front. For. Glob. Change 6:1269487.
doi: 10.3389/ffgc.2023.1269487

COPYRIGHT

© 2023 Cui, Yan, Wang, Zhang, He, Jiang, Fan
and Ye. This is an open-access article
distributed under the terms of the [Creative
Commons Attribution License \(CC BY\)](https://creativecommons.org/licenses/by/4.0/). The
use, distribution or reproduction in other
forums is permitted, provided the original
author(s) and the copyright owner(s) are
credited and that the original publication in this
journal is cited, in accordance with accepted
academic practice. No use, distribution or
reproduction is permitted which does not
comply with these terms.

Mixed *Eucalyptus* plantations in subtropical China enhance phosphorus accumulation and transformation in soil aggregates

Yuhong Cui¹, Yu Yan¹, Shengqiang Wang¹, Han Zhang¹, Yaqin He¹,
Chenyang Jiang¹, Rongyuan Fan¹ and Shaoming Ye^{1,2,3*}

¹College of Forestry, Guangxi University, Nanning, China, ²Guangxi Key Laboratory of Forest Ecology and Conservation, Nanning, China, ³Guangxi Colleges and Universities Key Laboratory for Cultivation and Utilization of Subtropical Forest Plantation, Nanning, China

Introduction: The production of *Eucalyptus*, a principal economic tree genus in China, is faced with challenges related to soil phosphorus (P) limitations. In this study, we explore variations in phosphorus content, storage, and transformation in *Eucalyptus* forests. We hypothesize that mixed forests augment soil aggregate stability and P content and that microaggregates are pivotal in determining P differences between mixed and pure forests. Additionally, we posit that mixed forests foster P transformation, enhancing its efficacy in the soil. Current research on the distribution and transformation of soil total P (TP) and P fractions at the soil aggregate level is limited.

Methods: In this study, we selected soil from a *Eucalyptus-Mytilaria laosensis* Lecomte mixed forest, *Eucalyptus-Erythrophleum fordii* Oliv mixed forest, and pure *Eucalyptus* forest in Chongzuo County, Guangxi, China, as the research objects. Using a dry-sieving method, we divided the soil collected *in situ* from the 0–40 cm layer into aggregates of >2, 1–2, 0.25–1, and <0.25 mm particle sizes, measured the TP and P fractions (resin-extractable inorganic P, bicarbonate-extractable inorganic P, bicarbonate-extractable organic P, sodium hydroxide-extractable inorganic P, sodium hydroxide-extractable organic P, dilute hydrochloric acid-extractable P, concentrated hydrochloric acid extractable inorganic P, concentrated hydrochloric acid-extractable organic P and residue-P) in different aggregates, and used redundancy analysis and PLS SEM to reveal key factors affecting soil P accumulation and transformation.

Results: The results showed that compared to pure *Eucalyptus* forests, mixed *Eucalyptus* forests significantly enhanced the stability of soil aggregates and the content and storage of phosphorus, especially the *Eucalyptus-Mytilaria laosensis* mixed forest. The content of total soil phosphorus and its fractions decreased with increasing aggregate particle size, while the opposite trend was observed for stored P, with aggregates <0.25 mm being the main fraction influencing soil phosphorus accumulation. The transformation process of P fractions was primarily constrained by dissolution rates, mineralization rates, biological activity, including the action of microbes, fungi, and plant–root interactions, and other factors.

Discussion: Mixed forests increased the transformation of phosphorus in soil aggregates, effectively enhancing the availability of soil phosphorus. In summary, this study provides important evidence for the systematic management of subtropical artificial *Eucalyptus* forests and the sustainable utilization of soil resources.

KEYWORDS

Eucalyptus, mixed forest, soil aggregates, phosphorus fractions, phosphorus transformation

1 Introduction

Plantations are considered one of the most widely distributed forest types worldwide, these forests play a crucial role in alleviating land degradation, mitigating the impacts of climate change, reducing air pollution, and curtailing the loss of biodiversity (Yang et al., 2021). Among different plantations, *Eucalyptus*, which is characterized by rapid growth rates, high productivity, and strong adaptability, is cultivated worldwide to meet the global demand for timber and wood products. *Eucalyptus* species are grown in more than 90 countries, with China ranking second globally in terms of plantation area, next only to Brazil (Wei et al., 2022; Hutapea et al., 2023). The Guangxi Zhuang Autonomous Region in China has become a principal region for *Eucalyptus* plantations in China due to its advantageous geographical location and favorable climatic conditions (Zhao et al., 2018). At present, these plantations are mainly monocultures, with intensive management involving short rotations and continuous rotations (Huang et al., 2017). However, continuous cropping has led to severe soil nutrient losses, especially with respect to phosphorus (P) (Liu et al., 1998; Sicardi et al., 2004). Given that P significantly affects timber production efficiency, high amounts of phosphate fertilizers are often used to ensure high yield and sustainable forest production (Laclau et al., 2013; Bazani et al., 2014). However, this increases economic costs and leads to ecological problems such as soil acidification and groundwater pollution, generating negative environmental impacts (Goncalves et al., 1997). To address ongoing challenges associated with declining soil quality and reduced productivity in *Eucalyptus* plantations, experts advocate for a transition from monocultures to mixed forests (Guo et al., 2022). Specifically, incorporating native tree species, such as *Mytilaria laosensis* and *Erythrophleum fordii*, alongside *Eucalyptus* has been shown to be an effective approach. Recent studies highlight that these mixed plantations not only improve soil chemical properties by enriching the soil with vital nutrients but also enhance soil physical structure, leading to improved water retention and reduced soil erosion (Luo et al., 2015; Dawud et al., 2016; Zhang Q. et al., 2021; Zhang Y. et al., 2021). Furthermore, these mixed ecosystems have demonstrated markedly higher microbial diversity relative to monoculture systems, which results in improved nutrient cycling and overall soil health (Xu et al., 2020; Zhang et al., 2022; Formaglio et al., 2023).

Phosphorus is an essential macronutrient for forest ecosystems, with timber yields largely depending on the fulfillment of forestland P demands (Yang et al., 2019). Weathered soils in subtropical regions typically supply several times the amount of unstable inorganic phosphorus (Pi) needed by vegetation annually (Yang et al., 2011). Phosphorus is considered one of the nutrients that most limits the productivity of tropical and subtropical forests (Sullivan et al., 2014). This is because approximately 95%–99% of soil total P exists in insoluble or unavailable forms that plants cannot directly utilize (Richardson and Simpson, 2011). To better study soil P and improve plant P utilization rates, Hedley et al. (1982) developed a method for continuous P extraction or fractionation to characterize the different organic and inorganic fractions of P in soil based on solubility. This method has become widely accepted and used for characterizing P forms in soil (Condrón and Newman, 2011). Later, Tiessen and Moir (2007) improved Hedley's et al. method, categorizing P into nine fractions. Among these, resin-extractable inorganic P (resin-Pi) is

generally considered the most readily available form of P in soil for plant absorption and use, as it exists in the soil solution and can be directly absorbed by plant roots (Costa et al., 2016). Therefore, the content and availability of resin-Pi are important for plant growth. If the soil contains high amounts of resin-Pi, *Eucalyptus* can usually obtain sufficient P to grow and develop (Yang et al., 2011). After resin-Pi is consumed, it can be replenished from lower solubility P pools through desorption, dissolution, and mineralization (Tiessen and Moir, 2007). Bicarbonate-extractable inorganic P ($\text{NaHCO}_3\text{-Pi}$) is another form of inorganic P that is easily absorbed by plants. If the soil contains ample $\text{NaHCO}_3\text{-Pi}$, then plants can obtain sufficient P, which can stimulate growth (Yang et al., 2011). Bicarbonate-extractable organic P ($\text{NaHCO}_3\text{-Po}$) must be microbially decomposed before it can be utilized by plants. Its impact on *Eucalyptus* growth depends on the decomposition rate of organic P and the plant's P demand (Tiessen and Moir, 2007). Sodium hydroxide-extractable inorganic P (NaOH-Pi) and sodium hydroxide-extractable organic P (NaOH-Po) typically exist as iron phosphates and aluminum phosphates (Hunt et al., 2007). They have smaller impacts on *Eucalyptus* growth than resin-Pi, $\text{NaHCO}_3\text{-Pi}$ and $\text{NaHCO}_3\text{-Po}$, as these P compounds have low solubility and require a certain period of desorption, dissolution, and mineralization to be available for plant use (Bunemann, 2008). Dilute hydrochloric acid-extractable P (Dil. HCl-P) represents native mineral P pools bound to calcium, which can be utilized by plants after a long period of weathering (Yang et al., 2011). Other P fractions have low solubility and represent the most inaccessible occluded P pools for plants, requiring long-term weathering for plant uptake (Condrón and Newman, 2011). Research has underscored that within mixed forests, *Mytilaria laosensis* and *Erythrophleum fordii* possess the capacity to access phosphorus from deep soil strata due to their expansive and deep root systems (Luo et al., 2015; Zhang Q. et al., 2021; Zhang Y. et al., 2021). However, the reasons for the enhanced phosphorus acquisition efficiency of these woodlands is still poorly understood. In this context, the enhanced Hedley method can be used to study diverse phosphorus fractions in soil and provide insights into phosphorus efficacy in subtropical forest ecosystems, such as *Eucalyptus* plantations (Johnson et al., 2003).

Notably, current research on P in mixed *Eucalyptus* forests mainly focuses on entire soil layers, and studies at the microscopic level of soil aggregates are relatively limited. Soil aggregates are the basic units of the soil structure, affecting its physical, chemical, and biological properties (Six et al., 2004). The quantity and quality of soil aggregates reflect the soil's nutrient supply and storage capabilities (Mustafa et al., 2020). The stability of soil aggregates is an important index that is closely related to soil P storage and nutrient recovery (Song et al., 2019). According to the formation and stabilization mechanisms of soil aggregates, they are divided into large aggregates (>0.25 mm) and microaggregates (≤ 0.25 mm) (Alag and Yilmaz, 2009). Aggregates serve as an important compartment for soil P storage and effective utilization. Aggregates of different particle sizes show significant differences in P adsorption, retention, and supply capabilities, which in turn affect the transformation and distribution of different P fractions (Song et al., 2019). Much research has been focused on soil aggregates and organic carbon (Cao et al., 2021; Li et al., 2021), but the related features of P fractions in aggregates are not clear. While a few studies exist on the effects of aggregate size on P, they are not comprehensive (Sun and Xiong, 1998; Rubk et al., 1999). Furthermore, the formation and stabilization processes of aggregates are influenced

by both natural conditions and human activities, leading to differences in the number and quality of soil aggregates in different regions (Six et al., 2002; Cooper et al., 2020; Liu et al., 2021). Therefore, evaluating differences in P fraction content and transformation in the soil of subtropical pure and mixed *Eucalyptus* forests from the perspective of aggregates has important practical value for elucidating the retention and release mechanisms of P in soil aggregates during the management of *Eucalyptus* plantations.

In this study, variations in phosphorus content, storage, and transformation within soil aggregates were examined across various *Eucalyptus* forest types. Based on previous research, this study proposes three hypotheses: (1) mixed forests show higher stability of soil aggregates and the content and storage of P in soil aggregates relative to pure forests; (2) microaggregates are the main factors leading to differences in total P and P fraction content between mixed forest and pure forest soils; and (3) mixed forests promote P transformation to enhance the effectiveness of P in the soil. In response to these hypotheses, we set the following research objectives: (1) to determine the impact of mixed forests on the stability, content, and storage of P in soil aggregates; (2) to elucidate the role of microaggregates in driving differences in total P and its fractions between mixed and pure forest soils; and (3) to analyze the degree and mechanisms through which mixed forests affect P transformation. To achieve these objectives, we performed a meticulous and systematic evaluation of data collected from a comprehensive set of field surveys and laboratory experiments.

2 Materials and methods

2.1 Study site

The study area is located in the Qing Mountain Experimental Field of the Experimental Center of Tropical Forestry, Chinese Academy of Forestry in Pingxiang County, Guangxi Zhuang Autonomous Region, China (21°57′–22° 19′N, 106°39′–106° 59′E) (Figure 1). The climate of the region is mainly subtropical monsoon, with an annual average rainfall of 1,500 mm and an average annual temperature of 18.8°C. The topography is dominated by low mountains and hills, with a slope of 20–22° and an altitude of 500–900 m. The soil type of this region is mainly Latosol (IUSS Working Group, 2014), with sedimentary rocks as the native rock. Currently, the Tropical Forestry Center has 6,000 hectares of experimental and demonstration forests with valuable and high-quality broad-leaved tree species, mainly *Eucalyptus* and *Pinus massoniana* Lamb., as well as tree species such as *Mytilaria laosensis*, *Erythrophleum fordii*, *Castanopsis hystrix*, *Tectona grandis*, *Betula alnoides*, *Michelia gioii*, and *Dalbergia odorifera*.

2.2 Experimental design

After field surveys, we selected a *Eucalyptus-Mytilaria laosensis* mixed forest (stand type I), a *Eucalyptus-Erythrophleum fordii* mixed forest (stand type II), and a pure *Eucalyptus* forest (stand type III) (Table 1) with similar site conditions with respect to soil type, parent material, altitude, slope, and aspect. All three types of forests were established on barren forestland in March 2012 by full reclamation

and afforestation, with a planting density of approximately 1,666 plants·ha⁻¹. The ratio of *Eucalyptus* to other mixed species in the mixed forests was 2:1, with a spacing of approximately 2 m × 3 m. For the first 3 years after afforestation, fertilization and weeding were carried out once per year, with a fertilizer application of 840 kg·ha⁻¹ (fertilizer composition: N: 31%, P: 10%, K: 10%, B: <0.5% and Zn: <0.5%). Afterward, the plantation managers employed a near-natural management strategy, emphasizing natural tree regeneration, minimal chemical intervention, and selective thinning to closely simulate natural forest conditions and limit human interference. A completely randomized design was adopted in this study: five 20 m × 20 m standard plots were set up in each of the three stand types, totaling 15 plots (3 stand types × 5 repetitions) (Figure 1). The distance between adjacent plots was greater than 1,000 m to prevent pseudoreplication and to reduce spatial autocorrelation. In each plot, a subplot (S = 20 m × 20 m) was randomly established at a distance >50 m from the forest edge.

2.3 Litter and soil sampling

Sampling was conducted in October 2021 for this study. Before soil sampling, 5 litter samples were collected from the surface of each of 5 random subplots (1 m × 1 m) and placed in plastic bags. Then, the 5 litter samples were combined into a composite litter sample. The 15 composite litter samples were dried at 80°C to a constant weight and were weighed after drying. Soil samples were collected from the same locations as the litter samples; 5 soil samples were collected with a spade and combined into a composite soil sample. The 30 (3 types of forest × 2 soil layers × 5 replicates) composite soil samples were carefully separated into natural aggregates. Then, a 5 mm sieve was used to remove small stones, coarse roots, and animal remains. Finally, the sieved soil aggregates (<5 mm) were further used for the classification of aggregates of various particle sizes. From each plot, 5 soil samples from each soil layer within 5 small subplots were collected with a ring knife (depth = 50 mm, Ø = 50.46 mm, V = 100 cm⁻³) to measure bulk density, pH, and P fraction content.

2.4 Soil aggregate separation

The Savinov dry-sieving method (Wang et al., 2021) was used for soil aggregate separation. Air-dried soil samples (500 g) were sieved using sieves with apertures of 2 mm, 1 mm, and 0.25 mm that were vertically oscillated at a rate of 5 cm s⁻¹ for 20 min. This resulted in the separation of aggregates of four grain sizes, namely, large soil aggregates (>2 mm), medium aggregates (1–2 mm), fine aggregates (0.25–1 mm), and microaggregates (<0.25 mm) (Table 2). The contents of clay particles and P fractions in the aggregates of each particle size were determined.

2.5 Soil property analyses

Before analyzing soil properties, we air-dried the soil samples at room temperature and then weighed them. A cutting ring was used to determine the soil bulk density (Lu, 2000). Soil porosity was measured using the ring knife method (Lu, 2000). Soil pH was determined by a

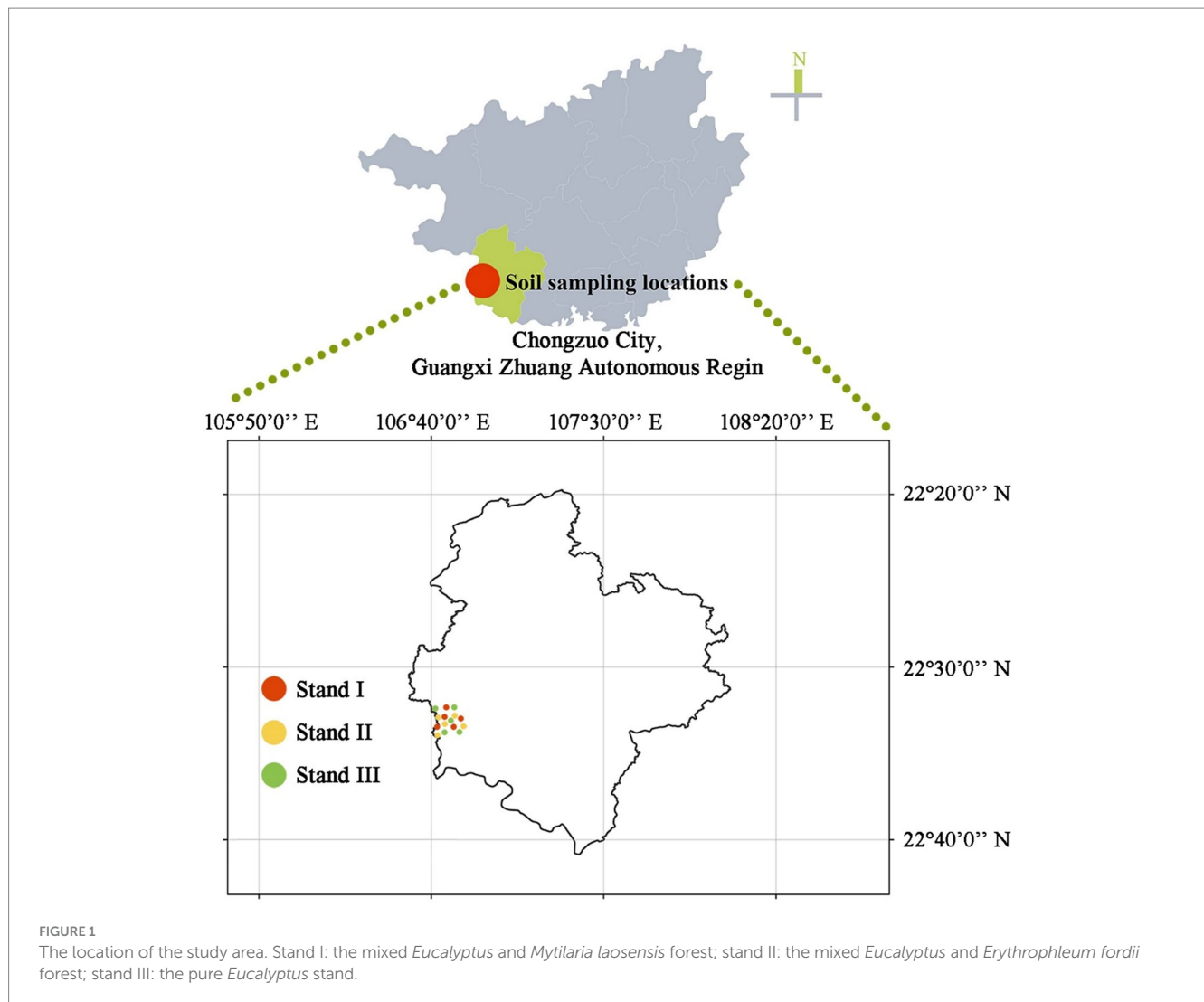


TABLE 1 Basic information for sample plots.

| Stand type | I | II | III |
|--|--------------------|--------------------|--------------------|
| Altitude (m) | 240–245 | 245–255 | 245–260 |
| Gradient (°) | 26–30 | 23–27 | 25–32 |
| Aspect | South-facing slope | South-facing slope | South-facing slope |
| Position | Upslope | Upslope | Upslope |
| Soil type | Latosol | Lateritic red soil | Lateritic red soil |
| Canopy density | 0.8 | 0.9 | 0.8 |
| Litterfall amount (g m ⁻²) | 410.80 ± 21.82 B | 491.80 ± 16.57 A | 246.40 ± 10.50 C |

I: The mixed *Eucalyptus* and *Mytilaria laosensis* forest; II: the mixed *Eucalyptus* and *Erythropheum fordii* forest; III: the pure *Eucalyptus* forest.

potentiometric method (Lu, 2000). A pycnometer (TM 85, Veichi, China) was used to measure soil clay content (Lu, 2000). Determination of soil organic carbon content was performed using the potassium dichromate-external heating method (Lu, 2000).

The sequential fractionation of P fractions was carried out in reference to the meth Sequential fractionation of P fractions was carried out based on the methods of Hedley et al. (1982) and Tiessen and Moir (2007), in which P is separated into various forms through a series of extractions. The extraction process was as follows: 0.5 g of soil was sequentially added to 30 mL H₂O and a 2 cm² ion-exchange resin film, followed by different extractants, i.e., 0.5 mol L⁻¹ NaHCO₃, 0.1 mol L⁻¹ NaOH, 1 mol L⁻¹ HCl, and 11.3 mol L⁻¹ HCl. Each extract was shaken at 60 rpm for 16 h and then centrifuged at 4,000 rpm for 20 min. The supernatant was collected as the sample to be tested for these fractions. Then, the next extractant was added to the precipitated soil sample. Thus, the following soil fractions were sequentially extracted: resin-P, NaHCO₃-Pi, NaHCO₃-Po, NaOH-Pi, NaOH-Po, Dil. HCl-P, concentrated hydrochloric acid-extractable inorganic P (conc. HCl-Pi), concentrated hydrochloric acid-extractable organic P (conc. HCl-Po) and residue P.

2.6 Statistical analysis

The mean weight diameter (MWD, mm) and geometric mean diameter (GMD, mm) are key indicators to evaluate soil aggregate

TABLE 2 Litterfall and soil properties as influenced by aggregate size and stand type in *Eucalyptus* plantations.

| Index | Litter | 0–20 cm | | | 20–40 cm | | |
|---|----------------|---------|------------------|-------|----------|----|-------|
| | Stand type (S) | S | Aggregate size A | S × A | S | A | S × A |
| Litterfall quantity (g m ⁻²) | ✓✓ | | | | | | |
| Bulk density (g cm ⁻³) | | ✓✓ | | | ✓✓ | | |
| Total porosity (%) | | ✓✓ | | | ✓✓ | | |
| pH | | ✓✓ | | | ✓✓ | | |
| MWD | | ✓✓ | ✓✓ | ✓✓ | ✓✓ | ✓✓ | ✓✓ |
| GMD | | ✓✓ | ✓✓ | ✓✓ | ✓✓ | ✓✓ | ✓✓ |
| TOC (mg kg ⁻¹) | | ✓✓ | ✓✓ | × | ✓✓ | ✓✓ | × |
| TP (mg kg ⁻¹) | | ✓✓ | ✓✓ | × | ✓✓ | × | × |
| Resin-Pi (mg kg ⁻¹) | | ✓✓ | ✓✓ | ✓✓ | ✓✓ | ✓✓ | ✓✓ |
| NaHCO ₃ -Pi (mg kg ⁻¹) | | ✓✓ | ✓✓ | × | ✓✓ | ✓✓ | × |
| NaHCO ₃ -Po (mg kg ⁻¹) | | ✓✓ | ✓ | × | ✓✓ | ✓✓ | ✓✓ |
| NaOH-Pi (mg kg ⁻¹) | | ✓✓ | ✓✓ | × | ✓✓ | ✓ | × |
| NaOH-Po (mg kg ⁻¹) | | ✓✓ | ✓✓ | ✓ | ✓✓ | ✓✓ | × |
| Dil. HCl-P (mg kg ⁻¹) | | ✓✓ | ✓✓ | ✓✓ | ✓✓ | ✓✓ | ✓✓ |
| Conc. HCl-Pi (mg kg ⁻¹) | | ✓✓ | ✓✓ | × | × | ✓✓ | × |
| Conc. HCl-Po (mg kg ⁻¹) | | ✓✓ | ✓✓ | × | × | ✓✓ | × |
| Residue-P (mg kg ⁻¹) | | ✓✓ | ✓✓ | × | ✓✓ | ✓✓ | × |
| TPS (mg m ⁻²) | | ✓✓ | ✓✓ | ✓✓ | ✓✓ | ✓✓ | ✓✓ |
| Resin-PiS (mg m ⁻²) | | ✓✓ | ✓✓ | ✓✓ | ✓✓ | ✓✓ | ✓✓ |
| NaHCO ₃ -PiS (mg m ⁻²) | | ✓✓ | ✓✓ | ✓✓ | ✓✓ | ✓✓ | ✓✓ |
| NaHCO ₃ -PoS (mg m ⁻²) | | ✓✓ | ✓✓ | ✓✓ | ✓✓ | ✓✓ | ✓✓ |
| NaOH-PiS (mg m ⁻²) | | ✓✓ | ✓✓ | ✓✓ | ✓✓ | ✓✓ | ✓✓ |
| NaOH-PoS (mg m ⁻²) | | ✓✓ | ✓✓ | ✓✓ | ✓✓ | ✓✓ | ✓✓ |
| Dil. HCl-PS (mg m ⁻²) | | ✓✓ | ✓✓ | ✓✓ | × | ✓✓ | ✓✓ |
| Conc. HCl-PiS (mg m ⁻²) | | ✓✓ | ✓✓ | ✓✓ | × | ✓✓ | ✓✓ |
| Conc. HCl-PoS (mg m ⁻²) | | ✓✓ | ✓✓ | ✓✓ | × | ✓✓ | ✓✓ |
| Residue-PS (mg m ⁻²) | | ✓✓ | ✓✓ | ✓✓ | ✓✓ | ✓✓ | ✓✓ |

“x” represents a nonsignificant difference ($p > 0.05$); S, stand type; A, aggregate size. MWD and GMD indicate the mean weight diameter and geometric mean diameter, respectively; TP, soil total P content; Resin-Pi, resin-extractable inorganic P content; NaHCO₃-Pi, resin-extractable inorganic P content; NaHCO₃-Po, bicarbonate-extractable organic P content; NaOH-Pi, sodium hydroxide-extractable inorganic P content; NaOH-Po, sodium hydroxide-extractable organic P content; Dil. HCl-P, dilute hydrochloric acid-extractable P content; conc. HCl-Pi, concentrated hydrochloric acid-extractable inorganic P content; conc. HCl-Po, concentrated hydrochloric acid-extractable organic P content; Residue-P, residue P content; TPS, soil total P stock; Resin-PiS, resin-extractable inorganic P stock; NaHCO₃-PiS, resin-extractable inorganic P stock; NaHCO₃-PoS, bicarbonate-extractable organic P stock; NaOH-PiS, sodium hydroxide-extractable inorganic P stock; NaOH-PoS, sodium hydroxide-extractable organic P stock; Dil. HCl-PS, dilute hydrochloric acid-extractable P stock; conc. HCl-PiS, concentrated hydrochloric acid-extractable inorganic P stock; conc. HCl-PoS, concentrated hydrochloric acid-extractable organic P stock; “x” represents a nonsignificant difference ($p > 0.05$); “✓” and “✓✓” represent significant differences at $p < 0.05$ and $p < 0.01$, respectively.

stability, and the calculation formulas for MWD and GMD are as follows (Zhang Q. et al., 2021; Zhang Y. et al., 2021):

$$MWD = \sum_{i=1}^n \bar{x}_i w_i \tag{1}$$

$$GMD = \exp \left[\frac{\sum_{i=1}^n w_i \ln \bar{x}_i}{\sum_{i=1}^n w_i} \right] \tag{2}$$

where \bar{x}_i is the average diameter of aggregates in each grade (mm) and w_i is the weight percentage of aggregates in each grade (%).

The total P storage (TPS, g m⁻²) calculation formula is (Wang et al., 2020):

$$TPS = \sum_{i=1}^4 (w_i \times TP_i) \times B_d \times H \times 10 \tag{3}$$

where w_i is the mass ratio of aggregates of different sizes to total aggregates; TP_i is the total P content of the i th aggregate size (g kg⁻¹); B is the soil bulk density (g cm⁻³); H is the soil layer thickness (cm); and 10 is the unit conversion factor. Similarly, stored soil resin-Pi, NaHCO₃-Pi, NaHCO₃-Po, NaOH-Pi, NaOH-Po, Dil-HCl-P, conc. HCl-Pi, conc. HCl-Po, and residue-P was calculated in the same way.

We identified two main variables in this study: stand type and aggregate size. Therefore, statistical analysis was conducted according to soil depth. Statistical analysis was performed using SPSS 22.0 (SPSS Inc., Chicago, IL, United States). The Shapiro–Wilk test was used to check the normality of the data before variance analysis was conducted. The Levene method was used to test variance homogeneity. One-way analysis of variance (ANOVA) was used to test the impact of stand type on litter mass and soil physicochemical properties. Two-way ANOVA was used to test the impact of stand type, aggregate size, and their interaction on soil aggregate physicochemical characteristics. Subsequently, the Tukey HSD *post hoc* test was used to test the significance of differences. $p < 0.05$ indicated that the difference was statistically significant. CANOCO 5.0 (CANOCO Inc., Shanghai, China) was used to conduct redundancy analysis to test the impact of soil aggregate parameters on P content and storage in the soil. In addition, a partial least squares structural equation model was constructed using Smart PLS 3.0 (SmartPLS GmbH Inc., Oststeinbek, Germany) to predict the P transformation patterns in different stand types. We used the coefficient of determination (R^2) and cross-validated redundancy (Q^2) to evaluate the structural model. R^2 measures the relationship between the explained variance of latent variables and total variance (Chin, 1998). R^2 values of 0.670, 0.333, and 0.190 indicate high, medium, and low explanatory rates, respectively (Diamantopoulos and Sigauw, 2006). Q^2 measures the predictive relevance of a specific structural model (An et al., 2010; Hair et al., 2019).

3 Results

3.1 Litter mass and overall soil physicochemical properties

The litter mass and total soil porosity of stand types I and II were significantly higher than those of stand type III ($p < 0.05$), whereas soil bulk density and pH showed the opposite trend (Table 3). In the 0–20 cm soil layer, the contents of TOC, TP, resin-Pi, and NaHCO_3 -Pi in stand type I were significantly higher than those in stand types II and III. The contents of NaHCO_3 -Po, NaOH-Pi, NaOH-Po, Dil. HCl-P, conc. HCl-Pi, conc. HCl-Po and residue-P in stand types I and II were significantly higher than those in stand type III ($p < 0.05$). In the 20–40 cm soil layer, the TP, resin-Pi, NaHCO_3 -Pi, and NaHCO_3 -Po contents in stand type I were significantly higher than those in stand types II and III. The contents of NaOH-Pi, NaOH-Po, and residue-P in stand types I and II were significantly higher than those in stand type III ($p < 0.05$). However, there were no significant differences in the contents of Dil. HCl-P, conc. HCl-Pi, and conc. HCl-Po among the three types of forests. Additionally, the total soil porosity, TP, and P fraction contents of all three stand types decreased with increasing soil depth, while the soil bulk density and pH increased with increasing soil depth.

3.2 Distribution and stability characteristics of soil aggregates

In both the 0–20 cm and 20–40 cm soil layers, the proportion of aggregates with a diameter of >2 mm in stand types I and II was

significantly higher than that in stand type III ($p < 0.05$), while the proportion of aggregates with a diameter of <0.25 mm exhibited the opposite trend (Table 4). All three stand types were predominantly characterized by aggregates >2 mm in diameter, with proportions significantly different from those of other aggregates ($p < 0.05$), ranging from 54.10% to 69.58%. Simultaneously, in both soil layers, the mean weight diameter (MWD) and geometric mean diameter (GMD) of stand types I and II were significantly higher than those of stand type III ($p < 0.05$).

3.3 Total P and its fractions in soil aggregates: content, storage and contribution

In this study, we undertook an in-depth analysis to elucidate the distribution and storage of multiple phosphorus components across varying forest stand types and soil particle sizes. At the aggregate level, our experimental findings suggest that the content of diverse phosphorus fractions is principally confined to 0.25–1 mm aggregates in each type of forest stand (Figure 2). However, phosphorus storage exhibits a different distribution pattern; reserves are primarily localized in aggregates greater than 2 mm for all stand types under consideration. Regarding the relative contribution of aggregate sizes to phosphorus content, it was observed that aggregates larger than 2 mm in size play a significantly more prominent role than their smaller-sized counterparts, although there are particular phosphorus components that show exceptions to this trend ($p < 0.05$) (Figure 3). From a stand type perspective, our data consistently demonstrate that stand type I exhibits appreciably higher levels of both phosphorus content and storage compared to stand type III. This marked discrepancy is observable across two distinct soil strata, namely, the 0–20 cm and 20–40 cm layers. One commonality that was observed across all stand types and soil depths was a consistent decline in both phosphorus content and storage with increasing soil depth.

3.4 Relationship between soil aggregate characteristics and P content

The RDA results showed (Figure 4) that in the two soil layers studied, soil aggregate characteristics explained 93.83% and 98.41% of the soil P content. Aggregates with a diameter of <0.25 mm were the most critical factor affecting the soil P content in the 0–20 cm layer, explaining 82.70% of the variance, followed by aggregates with diameters of 0.25–1 mm and the MWD. Aggregates with a diameter of <0.25 mm were also the most critical factor affecting the soil P content in the 20–40 cm layer, explaining 30.70% of the variance, followed by aggregates with diameters of 1–2 mm and the MWD. Additionally, in the upper soil stratum of 0–20 cm, there was a positive correlation between each phosphorus component and parameters such as GMD and MWD, as well as with aggregates larger than 2 mm. In the 20–40 cm layer, a similar positive correlation was observed for most phosphorus components with GMD, MWD, and aggregates exceeding 2 mm in size. However, it is noteworthy that only Dil. HCl-P and Conc. HCl-Po exhibited a positive association with aggregates sized between 0.25–1 mm at this depth.

3.5 P fraction transformation characteristics in different stand types

Based on the PLS-SEM results, the direct and indirect impacts of various P fractions on resin-Pi in the three stand types were

identified, each showing different P fraction transformation characteristics (Figure 5). For instance, in stand type I, resin-Pi was directly and positively influenced by $\text{NaHCO}_3\text{-Pi}$ (total effect = 0.659), $\text{NaHCO}_3\text{-Po}$ (total effect = 0.459), and Dil. HCl-P (total effect = 0.758) and directly and negatively influenced by

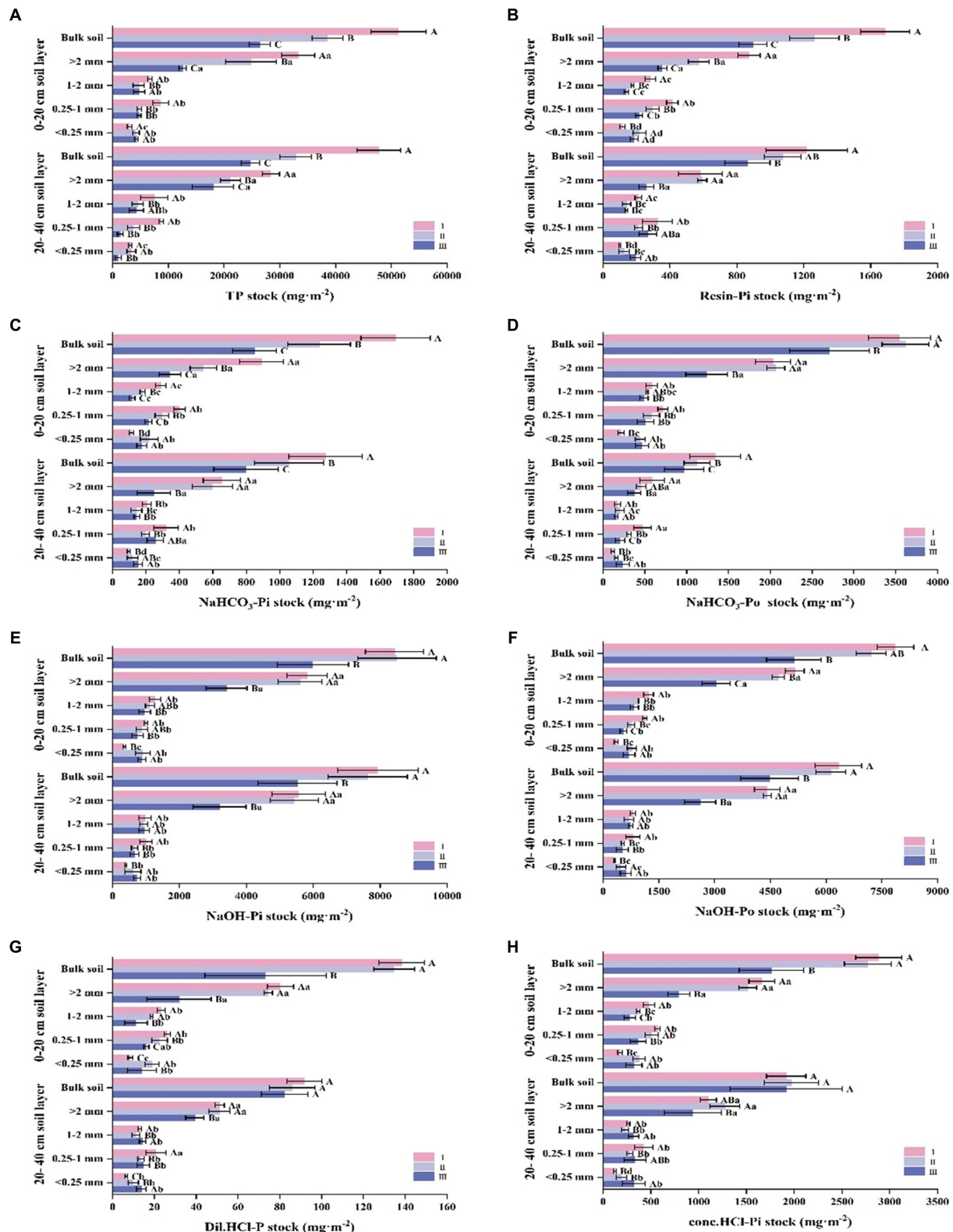


FIGURE 2 (Continued)

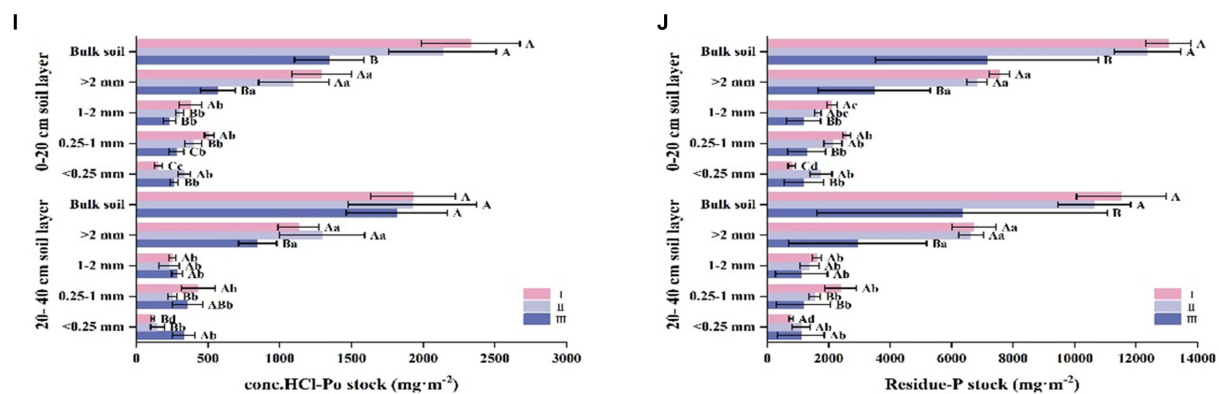


FIGURE 2

Stock of phosphorus components in soil aggregates of different *Eucalyptus* forest types. In different types of artificial *Eucalyptus* forest stands, the stocks of aggregate-related resin-extractable inorganic P (resin-Pi), bicarbonate-extractable inorganic P (NaHCO_3 -Pi), bicarbonate-extractable organic P (NaHCO_3 -Po), sodium hydroxide-extractable inorganic P (NaOH -Pi), sodium hydroxide-extractable organic P (NaOH -Po), dilute hydrochloric acid-extractable P (Dil. HCl-P), concentrated hydrochloric acid-extractable inorganic P (conc. HCl-Pi), concentrated hydrochloric acid-extractable organic P (conc. HCl-Po), and residual P (residue-P) were examined. Different uppercase letters indicate significant differences between different stand types ($p < 0.05$), and different lowercase letters indicate significant differences in aggregate particle size within the same stand type ($p < 0.05$).

NaOH -Po (total effect = -0.245). In stand type II, resin-Pi was directly and positively influenced by NaHCO_3 -Po (total effect = 0.559) and NaOH -Po (total effect = 0.506) and directly and negatively influenced by NaHCO_3 -Pi (total effect = -0.483). In stand type III, resin-Pi was directly and positively influenced by NaHCO_3 -Pi (total effect = 0.666), NaHCO_3 -Po (total effect = 0.203), and occluded-P (total effect = 0.649) and directly and negatively influenced by NaOH -Po (total effect = -0.483). Other P fractions indirectly affected resin-Pi through differential regulation. Furthermore, apart from the impacts of various P fractions on resin-Pi, other fixed P transformation pathways existed in the three stand types. For example, occluded-P transformed into Dil. HCl-P and NaOH -Pi, Dil. HCl-P transformed into NaOH -Po, and NaOH -Po transformed into NaHCO_3 -Po. In the three stand types, the R^2 values of the P fractions all followed the trend of stand type I > stand type II > stand type III and were all above 0.670. The mixed forest model had a higher explanatory rate than the pure forest model, and the Q^2 value displayed a similar pattern.

4 Discussion

4.1 Effects of mixed forests on soil aggregate stability and P distribution

Soil aggregates are the basic units of soil structure, and their distribution determines the size distribution of soil pores, which in turn influences the cycling of material and energy at the aggregate scale. Well-aggregated soil fosters good water cycling, absorption and plant growth and enables the sustainability of forest plantations (Dal Ferro et al., 2012; Gao et al., 2022). Aggregate composition and stability are critical for assessing soil structure, which in turn affects nutrient supply, storage, and erosion resistance (Fattet et al., 2011). Larger aggregates improve soil stability and pore structure, while an increase in microaggregates can elevate the risk of soil erosion (Zhang et al., 2008; Wang et al., 2022).

In our study, we found that mixed *Eucalyptus-Mytilaria laosensis* and *Eucalyptus-Erythrophleum fordii* forests have better soil aggregate stability than pure *Eucalyptus* forests. This is due to higher TOC and litter levels, which enhance large aggregate formation and reduce erosion. Consequently, these mixed forests showed improved soil quality metrics, such as higher MWD and GMD of aggregates (Al-Kaisi et al., 2014; Giumbelli et al., 2020) (Table 4). The physical and chemical attributes of soil structure and biological factors play a pivotal role in determining soil stability (Wang et al., 2022). In mixed *Eucalyptus* forests, increased plant diversity often supports a broader range of soil fauna and flora. This biodiversity can lead to enhanced soil aggregation through the combined action of various organisms (He et al., 2023). For instance, the burrowing activities of larger soil animals, such as earthworms, can create channels in soils, facilitating root growth and water movement (Mao et al., 2022). Furthermore, in mixed forests, the presence of diverse plants can lead to richer fungal networks or mycorrhizae, which help to bind soil particles into stable aggregates (Tang and Wang, 2022). Mixed forests also play a pivotal role in addressing the triple planetary crises. The introduction of diverse mixed plantations can contribute to reducing biodiversity losses by providing varied habitats and promoting ecosystem balance. Additionally, increased carbon sequestration in both the biomass and well-aggregated soil of mixed plantations directly contributes to the mitigation of climate change effects. While in our research, we did not directly investigate the effects of mixed forests on air pollution, it is worth noting that healthy forests can act as filters, capturing pollutants and improving air quality.

P is an essential nutrients for plant growth, and soil P levels determine the growth status of plants (Yang et al., 2019). At the aggregate level, this study revealed that TP, resin-Pi, NaHCO_3 -Pi, NaHCO_3 -Po, Dil. HCl-P, conc. HCl-Pi, conc. HCl-Po, and residue-P contents were mainly distributed in aggregates 0.25–1 mm and <0.25 mm in size (Figure 6). This may indicate that smaller aggregates have a stronger adsorption capacity for P than NaOH -Pi and NaOH -Po, as smaller aggregates have larger specific surface areas and provide more binding sites for P (Egan et al., 2018). In addition, the

TABLE 3 Litter and bulk soil properties.

| Index | 0–20 cm soil layer | | | 20–40 cm soil layer | | |
|---|--------------------|------------------|------------------|---------------------|----------------|----------------|
| | Stand I | Stand II | Stand III | Stand I | Stand II | Stand III |
| Litterfall amount (g m ⁻²) | 410.80 ± 21.82 B | 491.80 ± 16.57 A | 246.40 ± 10.50 C | | | |
| Soil texture | Clay | Clay | Clay | Clay | Clay | Clay |
| Bulk density (g cm ⁻³) | 1.03 ± 0.03 B | 1.22 ± 0.01 AB | 1.29 ± 0.07 A | 1.31 ± 0.01 C | 1.40 ± 0.02 B | 1.48 ± 0.01 A |
| Total porosity (%) | 54.12 ± 0.43 A | 53.64 ± 0.32 A | 50.22 ± 0.63 B | 52.64 ± 0.83 A | 52.34 ± 0.45 A | 49.19 ± 0.38 B |
| pH | 4.40 ± 0.01 A | 4.35 ± 0.01 B | 4.30 ± 0.01 C | 4.42 ± 0.01 A | 4.36 ± 0.01 B | 4.31 ± 0.01 C |
| TOC (g kg ⁻¹) | 17.41 ± 0.66 A | 15.04 ± 0.56 B | 14.88 ± 0.67 B | 12.08 ± 0.41 A | 7.93 ± 0.87 B | 7.88 ± 0.89 B |
| TP (g kg ⁻¹) | 0.19 ± 0.01 A | 0.14 ± 0.01 B | 0.13 ± 0.00 B | 0.18 ± 0.01 A | 0.12 ± 0.01 B | 0.11 ± 0.01 B |
| C:P | 92.03 ± 3.05 C | 108.64 ± 6.46 B | 115.60 ± 3.93 A | 67.63 ± 2.93 B | 70.49 ± 8.47 A | 71.43 ± 2.76 A |
| Resin-Pi (mg kg ⁻¹) | 6.71 ± 1.75 A | 5.17 ± 1.12 B | 4.34 ± 0.79 C | 4.26 ± 0.89 A | 3.84 ± 0.82 B | 3.29 ± 0.64 C |
| NaHCO ₃ -Pi (mg kg ⁻¹) | 6.72 ± 0.50 A | 5.05 ± 0.52 B | 4.11 ± 0.64 C | 4.47 ± 0.45 A | 3.76 ± 0.41 B | 3.05 ± 0.60 C |
| NaHCO ₃ -Po (mg kg ⁻¹) | 14.09 ± 2.24 A | 14.80 ± 1.30 A | 13.08 ± 1.34 B | 4.73 ± 1.56 A | 4.03 ± 1.38 B | 3.68 ± 0.64 C |
| NaOH-Pi (mg kg ⁻¹) | 33.59 ± 2.98 A | 34.72 ± 3.73 A | 28.93 ± 3.96 B | 27.88 ± 2.88 A | 27.22 ± 3.27 A | 21.06 ± 3.63 B |
| NaOH-Po (mg kg ⁻¹) | 30.42 ± 5.31 A | 29.49 ± 5.26 A | 24.82 ± 2.47 B | 22.27 ± 4.14 A | 21.87 ± 4.07 A | 17.05 ± 3.32 B |
| Dil. HCl-P (mg kg ⁻¹) | 0.55 ± 0.01 A | 0.55 ± 0.02 A | 0.35 ± 0.13 B | 0.32 ± 0.01 A | 0.31 ± 0.01 A | 0.31 ± 0.02 A |
| conc. HCl-Pi (mg kg ⁻¹) | 11.47 ± 1.77 A | 11.33 ± 2.32 A | 8.50 ± 1.47 B | 6.74 ± 1.41 A | 7.04 ± 1.59 A | 7.26 ± 1.69 A |
| conc. HCl-Po (mg kg ⁻¹) | 9.25 ± 1.04 A | 8.78 ± 1.42 A | 6.50 ± 0.84 B | 6.77 ± 0.73 A | 6.87 ± 1.17 A | 6.91 ± 0.85 A |
| Residue-P (mg kg ⁻¹) | 52.01 ± 7.84 A | 50.53 ± 7.76 A | 45.93 ± 7.23 B | 40.47 ± 6.18 A | 37.98 ± 5.90 A | 32.79 ± 5.30 B |

The data are presented as the mean ± standard deviation of 5 replicates. I, II, and III represent *Eucalyptus-Mytilaria laosensis* mixed forest, *Eucalyptus-Erythrophleum fordii* mixed forest, and *Eucalyptus* pure forest, respectively. The capital letters indicate a significant difference among different forest stand types ($p < 0.05$).

TABLE 4 Distribution and stability of soil aggregates as influenced by stand type in *Eucalyptus* plantations.

| Index | 0–20 cm soil Layer | | | 20–40 cm soil Layer | | |
|-----------|--------------------|-----------------|-----------------|---------------------|-----------------|-----------------|
| | Stand I | Stand II | Stand III | Stand I | Stand II | Stand III |
| >2 mm | 65.49 ± 1.61 Aa | 63.25 ± 0.95 Aa | 54.13 ± 1.93 Ba | 67.10 ± 2.17 Aa | 69.58 ± 0.23 Aa | 54.10 ± 3.36 Ba |
| 1–2 mm | 15.42 ± 0.97 ABb | 13.39 ± 0.09 Bb | 16.30 ± 0.59 Ab | 13.18 ± 0.25 Bb | 12.11 ± 1.33 Bb | 17.55 ± 0.59 Ab |
| 0.25–1 mm | 14.06 ± 0.25 Ab | 12.45 ± 0.95 Ab | 13.95 ± 0.95 Ab | 14.19 ± 1.75 Ab | 9.51 ± 0.49 Ab | 13.74 ± 1.65 Ab |
| <0.25 mm | 5.03 ± 0.39 Cc | 10.92 ± 0.73 Bb | 15.39 ± 1.02 Ab | 5.53 ± 0.28 Bc | 8.79 ± 1.52 Bb | 14.69 ± 1.26 Ab |
| MWD | 4.25 ± 0.08 A | 4.09 ± 0.06 A | 3.60 ± 0.11 B | 4.32 ± 0.21 A | 4.43 ± 0.05 A | 3.61 ± 0.18 B |
| GMD | 2.90 ± 0.10 A | 2.47 ± 0.12 B | 1.92 ± 0.19 C | 2.94 ± 0.15 A | 2.92 ± 0.12 A | 1.97 ± 0.17 B |

Data are the mean of 5 replicates ± standard deviations. I, II, and III represent mixed plantations of *Eucalyptus* and *Mytilaria laosensis* and of *Eucalyptus* and *Erythrophleum fordii* and a pure *Eucalyptus* plantation. Different capital letters indicate significant differences ($p < 0.05$) among aggregates of different sizes.

fine-grained minerals in soil, mainly contained in small aggregates, provide protection for most organic matter through physical retention, thereby enhancing the adsorption capacity of small aggregates for organic P (Adesodun et al., 2007). NaOH-Pi and NaOH-Po are primarily distributed in >2 mm and 1–2 mm aggregates (Figure 6) because they are easily precipitated or adsorbed by amorphous Al and

Fe in the soil (Tiessen et al., 1984; Barrow, 2015). Studies report that Al³⁺ and Fe²⁺ in the soil are mainly distributed within these aggregates (Wang et al., 2022). Many studies have shown that mixed forests significantly improve soil nutrient conditions, including soil P content (Huang et al., 2013; He et al., 2023). Our study also showed that the total P and its fractions in the soil of the *Eucalyptus-Mytilaria laosensis*

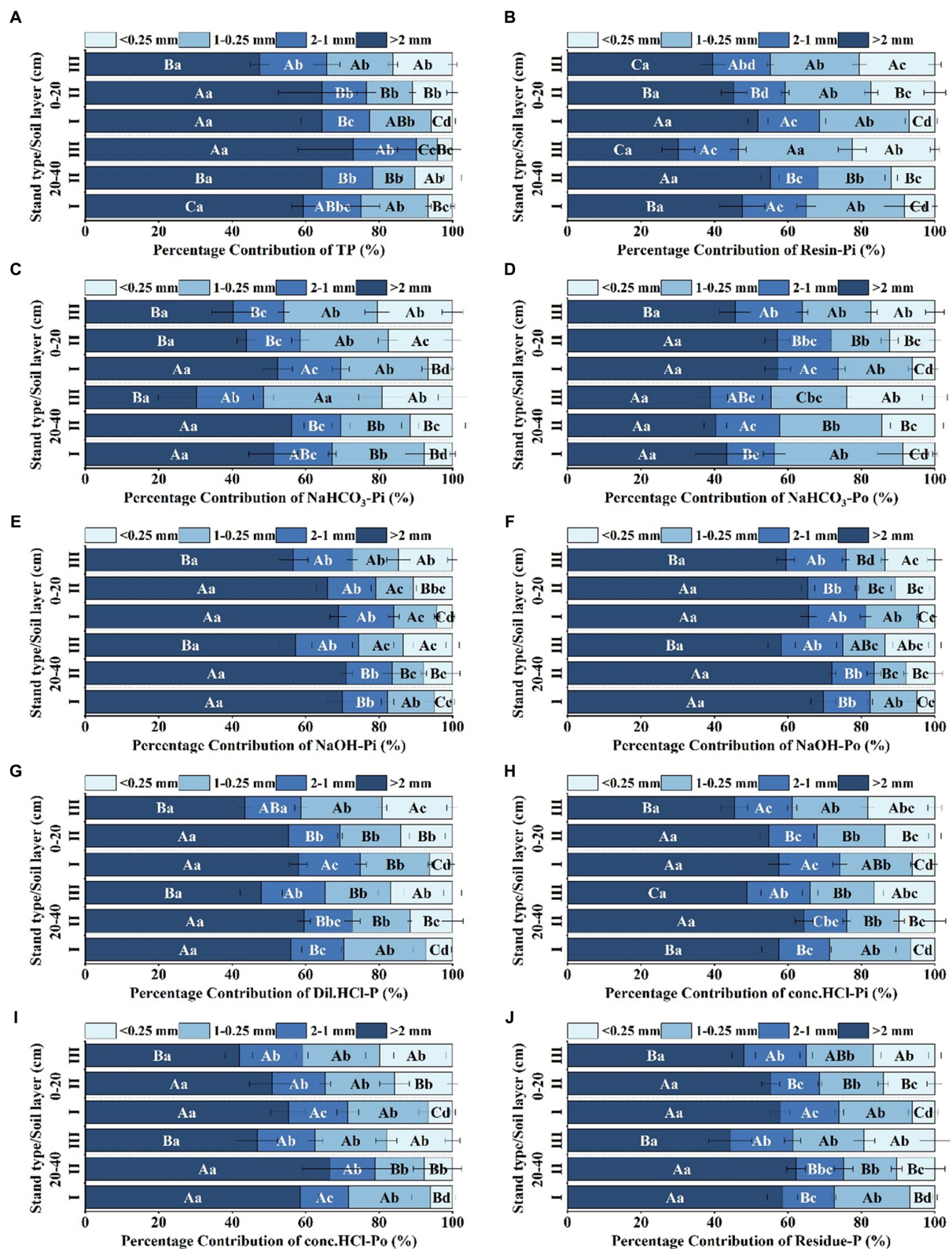
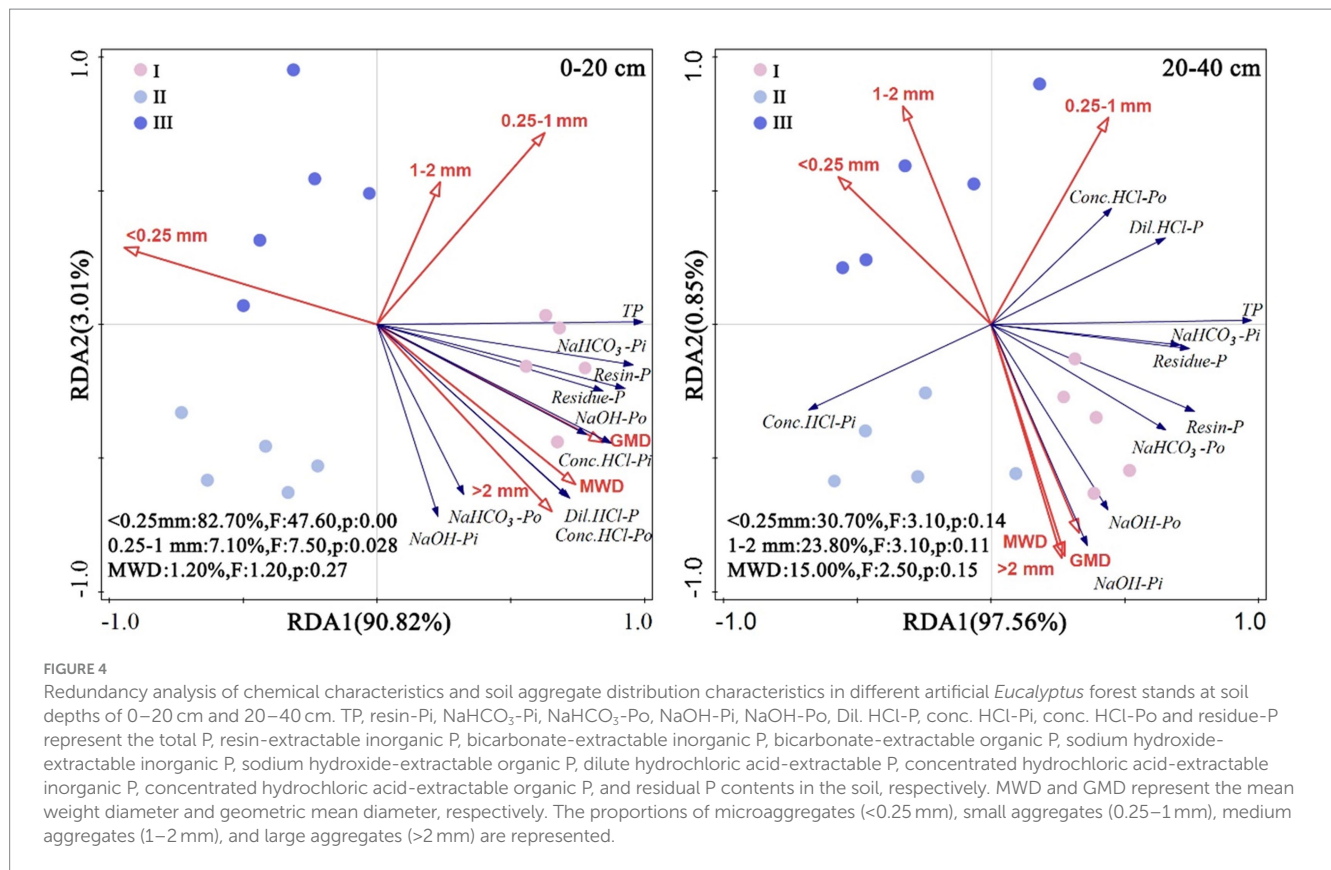


FIGURE 3
 Contribution rate of phosphorus components in soil aggregates of different *Eucalyptus* forest types. The contribution rate of the aggregate reserves of resin-extractable inorganic P (resin-Pi), bicarbonate-extractable inorganic P (NaHCO₃-Pi), bicarbonate-extractable organic P (NaHCO₃-Po), sodium hydroxide-extractable inorganic P (NaOH-Pi), sodium hydroxide-extractable organic P (NaOH-Po), dilute hydrochloric acid-extractable P (Dil. HCl-P), concentrated hydrochloric acid-extractable inorganic P (conc. HCl-Pi), concentrated hydrochloric acid-extractable organic P (conc. HCl-Po), and residual P (residue-P) in aggregates of different particle sizes across various artificial *Eucalyptus* forest stand types. Different uppercase letters indicate significant differences between different stand types ($p < 0.05$), and different lowercase letters indicate significant differences in aggregate particle size within the same stand type ($p < 0.05$).



and *Eucalyptus-Erythrophleum fordii* mixed forests were generally significantly higher than those in the pure *Eucalyptus* forest (Figure 6). This is because decomposition of plant litter is a major source of soil P, which not only directly replenishes P in the soil but also promotes P mineralization and weathering in the soil by promoting soil microbial proliferation and enzyme activity (Stewart and Tiessen, 1987; Frossard et al., 2000). Moreover, mixed forests have more diverse litter, which often provides a greater array of enzymes and microbial communities than litter from pure forests, further enhancing nutrient cycling (Vitousek et al., 2010; Kerdraon et al., 2020; Sayer et al., 2020). Beyond chemical interactions, dynamic interactions among biological processes—including root activity, intricate microbial associations, and soil fauna behavior—come together in mixed forests. This diversity enriches the soil environment, amplifying P availability (Turner and Engelbrecht, 2011; Gao et al., 2022). Moreover, the heterogeneous root architectures and penetration depths inherent to mixed plantations enable plant access to varied P stores throughout the soil strata, facilitating holistic nutrient cycling (Liu and Liu, 2012; He et al., 2023; Yan et al., 2023). Furthermore, the intertwined relationships that exist between the physical, chemical, and biological factors involved in soil health are magnified in mixed-species plantations. The combined effects of varied root systems, diverse microbial communities, and soil fauna activities result in a robust and resilient soil environment that is optimal for supporting forest plantations (Zhao and Hu, 2022). For instance, a balanced C:P ratio, influenced by decomposition rates and microbial activities, indicates effective nutrient cycling, and studies have pointed to the crucial role it plays in determining the mineralization capacity of soil P (Zeng et al., 2015; Zhang et al., 2023). Our study results indicate that the C:P

ratio in the mixed forests was lower than that in the pure forest, which increases the soil's P mineralization capacity (Table 3). According to a study by Six et al. (2004), changes in soil bulk density and porosity affect aeration and the permeability of soil. Excessively high soil bulk density or soil porosity that is very low can indirectly lead to a decrease in soil P content. In this study, creating mixed forests reduced soil bulk density and increased soil porosity (Table 3), which also resulted in a higher P content in mixed forests than in pure forests. In heterogeneous forest ecosystems, such as mixed forests, the activities of soil arthropods, such as centipedes and woodlice, have a significant impact on soil structural integrity. Centipedes, while hunting for prey, navigate through soil particles, inadvertently aerating the soil and creating minute passageways. Moreover, woodlice, by feeding on decaying plant material, contribute to the formation of stable soil aggregates by excreting fine particulate organic matter. This combination of activities from diverse fauna results in a well-structured soil with enhanced porosity, which in turn facilitates better water storage, gas exchange, and root exploration, fortifying ecosystem resilience and health (Kuperman, 1996; Yang et al., 2023).

The distribution of P reserves are closely related to the P content of soil aggregates of different particle sizes, the composition ratio of soil aggregates, and soil bulk density (Tamura et al., 2017). Therefore, in this study, total P (TP) and its reserves in all three types of forests exhibited a pattern in which they were significantly higher in the mixed forests than in the pure forest, and the reserves were mainly concentrated in aggregates with particle sizes >2 mm. Except for the 20–40 cm soil layer in stand type III, where the contribution rates of resin-Pi and NaHCO₃-Pi in the >2 mm aggregates were not significantly different from those in the

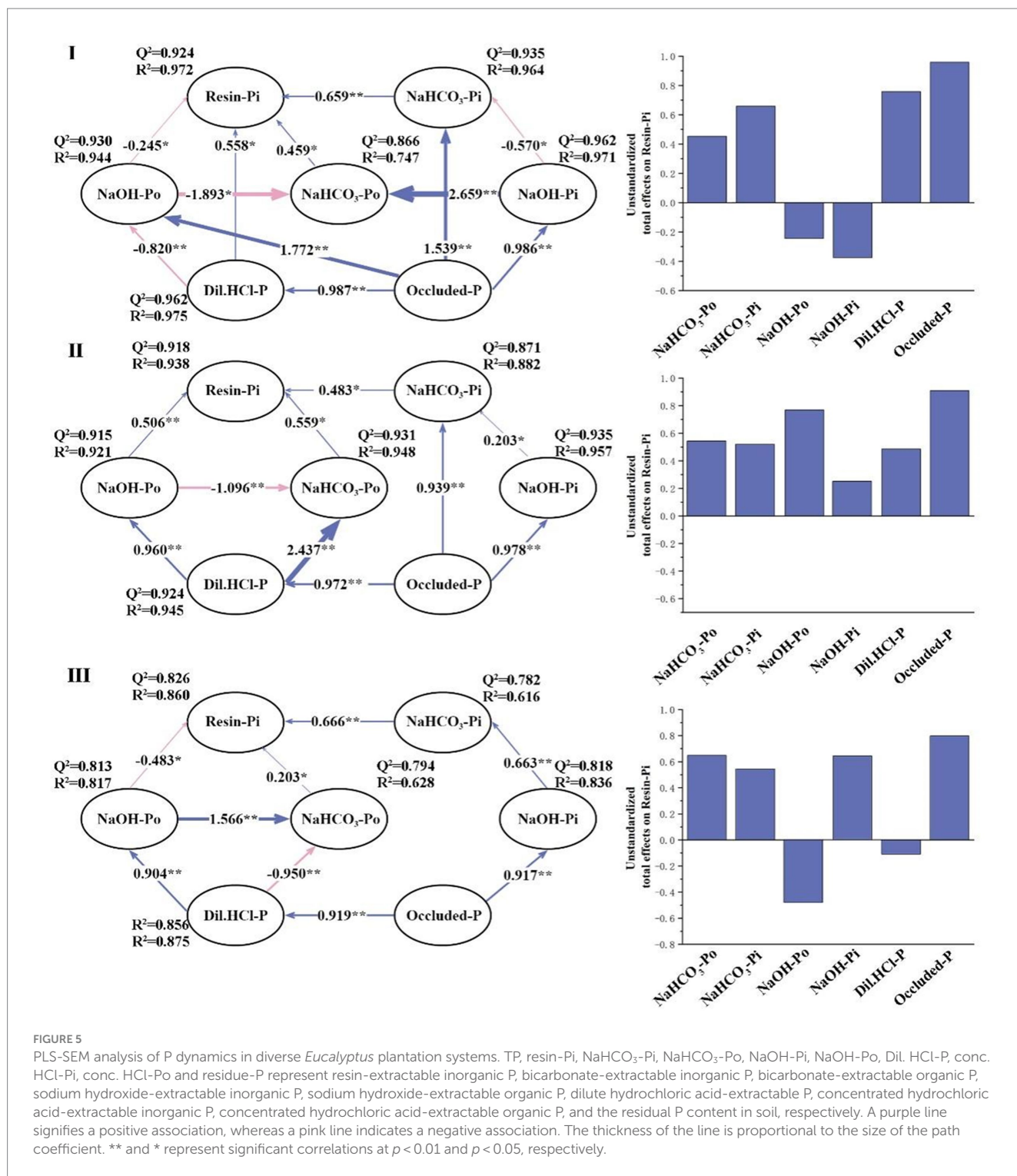


FIGURE 5
PLS-SEM analysis of P dynamics in diverse *Eucalyptus* plantation systems. TP, resin-Pi, NaHCO₃-Pi, NaHCO₃-Po, NaOH-Pi, NaOH-Po, Dil. HCl-P, conc. HCl-Pi, conc. HCl-Po and residue-P represent resin-extractable inorganic P, bicarbonate-extractable inorganic P, bicarbonate-extractable organic P, sodium hydroxide-extractable inorganic P, sodium hydroxide-extractable organic P, dilute hydrochloric acid-extractable P, concentrated hydrochloric acid-extractable inorganic P, concentrated hydrochloric acid-extractable organic P, and the residual P content in soil, respectively. A purple line signifies a positive association, whereas a pink line indicates a negative association. The thickness of the line is proportional to the size of the path coefficient. ** and * represent significant correlations at $p < 0.01$ and $p < 0.05$, respectively.

0.25–1 mm aggregates, the P fractions all showed that the contribution rate of the >2 mm aggregates was significantly higher than that of other particle sizes ($p < 0.05$). This indicates that in all types of forests, >2 mm aggregates were the main carriers of stored P, which is consistent with the research results of He et al. (2023). The total P and P reserves in >2 mm aggregates in stand types I and II were generally significantly higher than those in stand type III. The above results indicate that mixed planting improved the stability of soil aggregates and increased the content and reserves of

total P and its fractions in soil aggregates. The above results support hypothesis (1) in this study.

4.2 The influence of mixed forests on P accumulation

Soil P content is closely related to the formation and stability of soil aggregates. In this study, mixed forests had a positive impact on

soil P accumulation by affecting the formation and stability of soil aggregates (Wang et al., 2021). Some research has revealed that microaggregates contain more active organic P and easily

mineralizable organic P (Rubk et al., 1999). In red soil, organic P mainly exists in particles <0.005 mm, and the content of different organic P fractions increases with decreasing particle size. Expanding

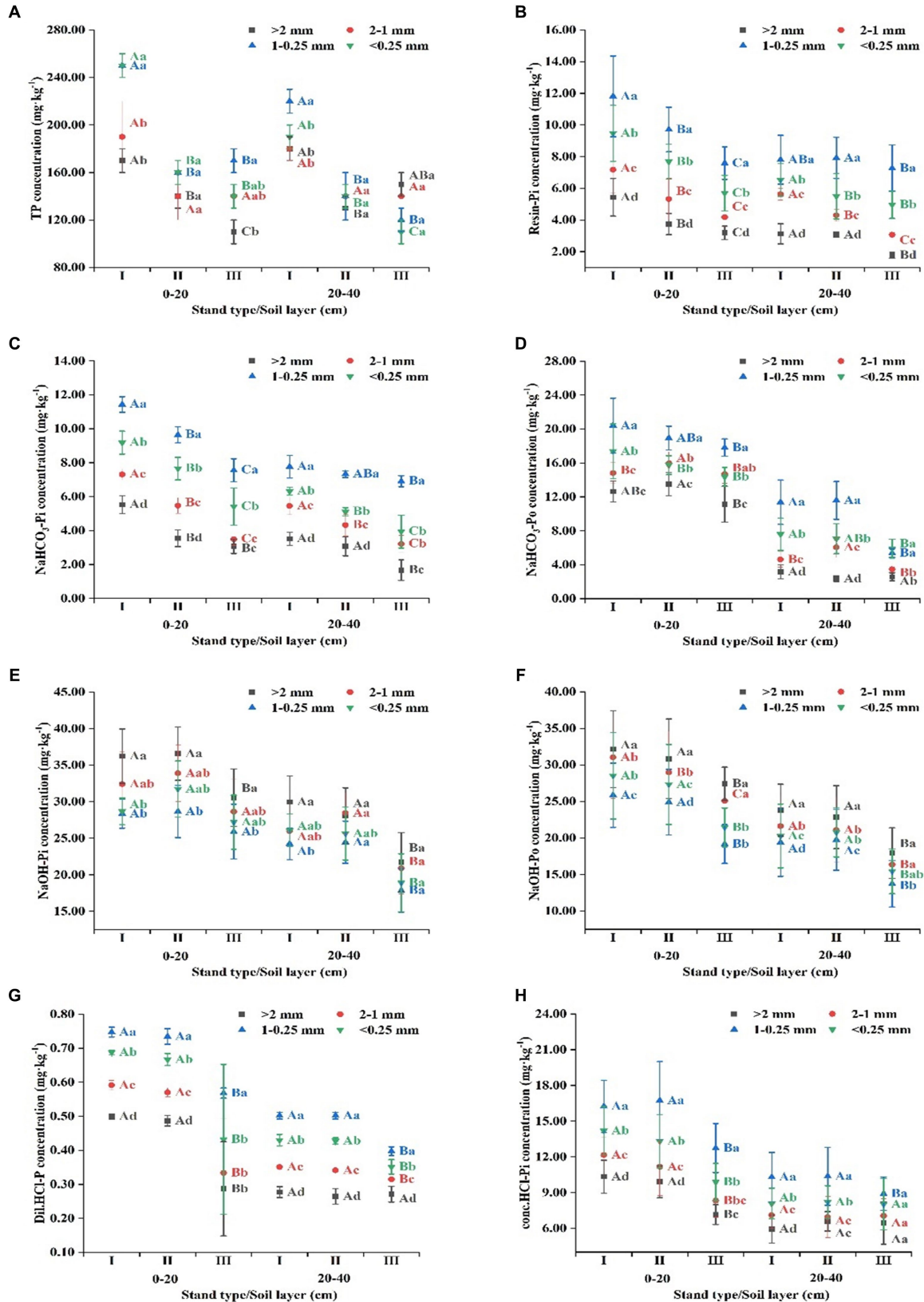
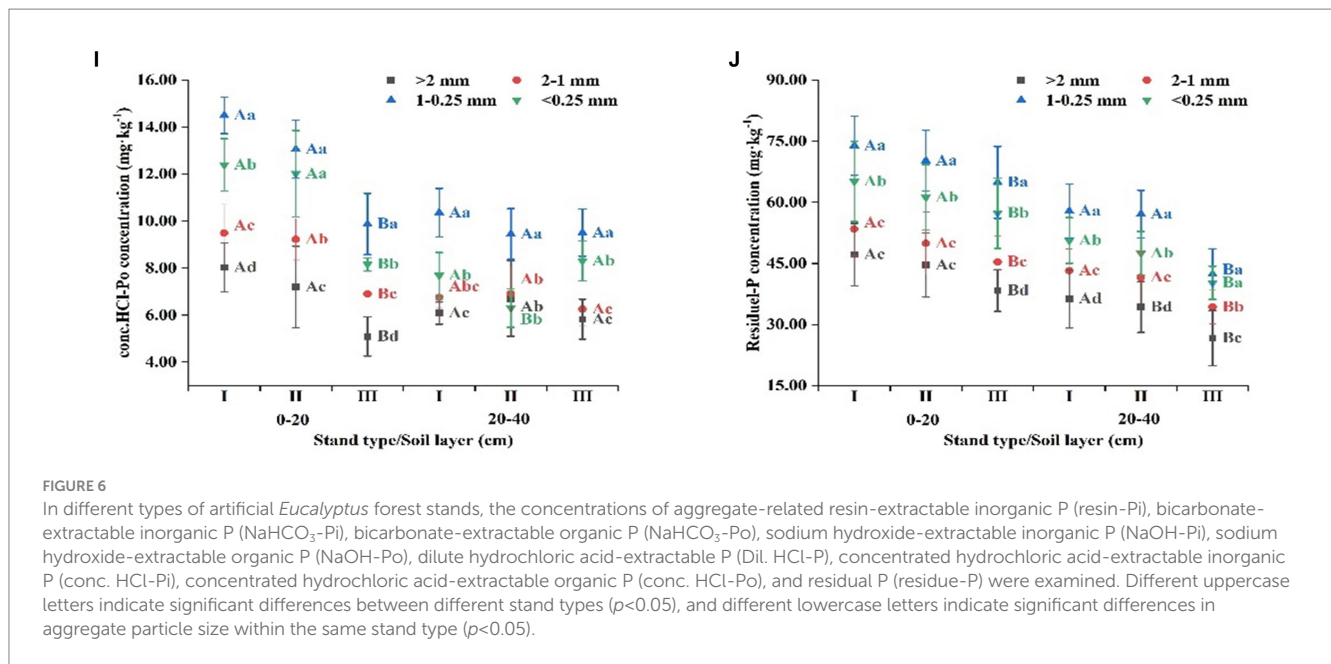


FIGURE 6 (Continued)



on this concept, it is plausible that the biological complexity of mixed forests, characterized by varied root systems and rich microbial diversity, is particularly favorable for facilitating the formation of microaggregates. Root exudates, coupled with varied microbial interactions, can dynamically modify the soil physicochemical landscape. Such alterations can, in turn, promote the formation of microaggregates, thereby amplifying a soil's potential for P sequestration. Therefore, it is believed that increasing the proportion of soil microaggregates can have a positive impact on soil P accumulation (Sun and Xiong, 1998).

However, the results of this study present the opposite trends. The RDA (Figure 4) results showed that in both soil layers, the proportion of aggregates with particle sizes <0.25 mm had a negative impact on soil P accumulation and was the most significant influential factor. This is because large aggregates endow the soil with larger pore structures and are rich in organic matter; therefore, they are capable of forming a microenvironment suitable for P retention and accumulation, while the role of aggregates with particle sizes of <0.25 mm is the opposite (Zhang et al., 2008).

Furthermore, aggregates with particle sizes <0.25 mm increase the risk of soil erosion. Under rainfall or surface runoff, P in a soil is more likely to be lost (Giumbelli et al., 2020). However, the RDA (Figure 4) results showed that mean weight diameter (MWD) was the factor with the greatest positive impact on soil P accumulation. This is because the MWD is related to soil consolidation, erosion resistance, aeration, permeability, etc., and soils with larger particle sizes generally have lower degrees of consolidation and good permeability, which is beneficial for the activity of soil microorganisms and root growth. On the one hand, a good soil structure is conducive to the storage and accumulation of P, and on the other hand, microbial activity and root growth promote the decomposition of organic matter in the soil, thereby increasing P content (Song et al., 2019). Therefore, mixed forests had a positive effect on soil P accumulation by reducing the proportion of aggregates with particle sizes <0.25 mm and by improving the soil MWD value. The above results support hypothesis (2).

4.3 The influence of mixed forests on soil P transformation

Currently, there is limited research on how mixed forests influence soil P transformation. Thus, we attempted to explore this through partial least squares structural equation modeling (PLS-SEM). In research by Tiessen and Moir (2007), the P in soil was divided into nine fractions according to solubility. Resin-Pi and NaHCO₃-Pi represent the two fractions that have the highest solubility and can be directly absorbed and utilized by plants. Their contents are directly related to plant growth (Yang et al., 2011). The remaining fractions, including NaHCO₃-Po, NaOH-Pi, NaOH-Po, Dil. HCl-P, and occluded-P (conc. HCl-Pi, conc. HCl-Po, residue-P), have decreased solubility, and not all of these fractions can be directly absorbed and utilized by plants—they need to be desorbed, dissolved, and mineralized into fractions with higher solubility to be utilized by plants (Condrón and Newman, 2011).

We conducted PLS-SEM based on this, and according to evaluations of the model, all three models showed excellent interpretability and predictability. The R^2 values were generally higher than 0.67, indicating that the model had strong explanatory power for the data. The Q^2 values were generally higher than 0.8, indicating that the model had good predictive ability (Figure 5). Overall, these results demonstrate that our model is effective and reliable.

Our findings revealed that in comparison to NaHCO₃-Pi, NaHCO₃-Po has a lower degree of total influence on resin-Pi. This differential effect arises because NaHCO₃-Po must be microbially decomposed prior to its conversion into resin-Pi (Reed et al., 2011, 2015). Notably, soil microbiota, particularly fungi and bacteria, play a pivotal role in these transformation processes. Certain soil fungi, including mycorrhizal associations, have been shown to enhance the mobilization and uptake of phosphorus fractions, including those bound organically (Olander and Vitousek, 2004; Tiessen and Moir, 2007; Spohn and Kuzyakov, 2013).

Among the three models analyzed, the influence of $\text{NaHCO}_3\text{-P}$ in mixed forests surpassed that in pure forests. This suggests that mixed forestry practices amplify microbial decomposition rates, thereby accelerating the conversion of $\text{NaHCO}_3\text{-Po}$ into resin-Pi. Notably, microbial communities enriched by the diversity of mixed forests could expedite this transformation. For example, bacterial communities, particularly phosphobacteria, are known to release specific enzymes, such as phosphatases, which facilitate the hydrolysis of organic P, making it available for plant uptake (Wan et al., 2020).

NaOH-Pi and NaOH-Po had minimal direct impacts on resin-Pi and instead indirectly influenced resin-Pi through $\text{NaHCO}_3\text{-Pi}$ or $\text{NaHCO}_3\text{-Po}$. This is primarily due to two reasons: one is the low solubility of NaOH-P , which limits its transformation rate (Bunemann, 2008), and the second is that most of the P released by mineralization is absorbed by Al/Fe minerals in the soil (Tiessen et al., 1984; Barrow, 2015).

Mixed forests evidently mitigate the effect of Al/Fe minerals on the transformation of NaOH-P . The enhanced soil aeration and permeability within these mixed forests favor the weathering of highly insoluble P fractions, such as Dil. HCl-P and occluded-P (Song et al., 2019). The diverse root exudates and microbial interactions within these forests, including those with *Miscanthus* and *Cassia*, can result in the production of organic acids and enzymes, modulating soil properties and in turn augmenting the solubility of P fractions (Liu and Liu, 2012; Gao et al., 2022; Yan et al., 2023).

Fractions with extremely low solubility, Dil. HCl-P and occluded-P, in forests I and II directly impacted resin-Pi or $\text{NaHCO}_3\text{-Pi}$, whereas in forest III, the influence was only indirect via NaOH-P . This is because compared to pure forests, aeration and permeability are better in mixed forest soil, which facilitates the weathering of P fractions with extremely low solubility (Song et al., 2019). Additionally, the diverse microbial community that exists within mixed forests could be pivotal in mineralizing organic P forms. Bacterial phosphatases and fungal exoenzymes play a synergistic role in the mineralization of organic P, making it accessible to plants (Zhou et al., 2020).

In summary, mixed forests promote the transformation of soil P fractions into resin-Pi, increasing the effectiveness of soil P. These results support our third hypothesis.

5 Conclusion

Our research results clearly demonstrate that mixed forest cultivation significantly improved the stability of soil aggregates and the content and reserves of P, especially in the case of mixed *Eucalyptus-Mytilaria laosensis* forests. Additionally, soil aggregates with a particle size of less than 0.25 mm played a key role in influencing soil P accumulation. The mixed forests promoted the transformation of P in soil aggregates, thereby effectively enhancing the availability of soil P.

Notably, the positive influence of mixed forest cultivation is promising for the restoration of degraded lands, addressing the pervasive issue of soil degradation that affects vast areas globally. By stabilizing soil structures and enhancing nutrient content, mixed plantations can play a significant role in rehabilitating such lands, offering a solution to this pressing environmental challenge.

Overall, these results not only contribute to improving soil fertility management but also promote progress in soil P research, particularly on the distribution and transformation of P and its fractions at the soil aggregate level. In future investigations, diverse mixed forest combinations should be considered to provide a more holistic understanding of the influence of species mixing on soil P dynamics, and biological factors influencing these mixed plantations should also be explored in greater detail. By integrating insights from the complex interplay of soil microbes, fungi, and their interactions with plant roots, we can further refine and optimize management strategies for *Eucalyptus* plantations. It is imperative to consider these biological elements to truly create a sustainable forest management framework that promotes both soil health and overall environmental well-being.

Data availability statement

The original contributions presented in the study are included in the article/supplementary material, further inquiries can be directed to the corresponding author.

Author contributions

YC: Writing – review & editing, Conceptualization, Data curation, Formal analysis, Investigation, Methodology, Project administration, Software, Supervision, Validation, Visualization, Writing – original draft. YY: Conceptualization, Data curation, Investigation, Methodology, Supervision, Validation, Visualization, Writing – review & editing. SW: Methodology, Supervision, Validation, Writing – review & editing, Formal analysis. HZ: Formal analysis, Methodology, Supervision, Validation, Writing – review & editing, Investigation, Software. YH: Formal analysis, Investigation, Methodology, Supervision, Validation, Writing – review & editing. CJ: Investigation, Writing – review & editing. RF: Investigation, Writing – review & editing. SY: Writing – review & editing, Funding acquisition, Resources.

Funding

The author(s) declare financial support was received for the research, authorship, and/or publication of this article. This research was supported by the National Natural Science Foundation of China (Grant number: 32260382).

Acknowledgments

Insightful comments from American Journal Experts (www.aje.cn) helped us improve the grammar and phrasing in this manuscript.

Conflict of interest

The authors declare that the research was conducted in the absence of any commercial or financial relationships that could be construed as a potential conflict of interest.

Publisher's note

All claims expressed in this article are solely those of the authors and do not necessarily represent those of their affiliated

organizations, or those of the publisher, the editors and the reviewers. Any product that may be evaluated in this article, or claim that may be made by its manufacturer, is not guaranteed or endorsed by the publisher.

References

- Adesodun, J. K., Adeyemi, E. F., and Oyegoke, C. O. (2007). Distribution of nutrient elements within water-stable aggregates of two tropical agro-ecological soils under different land uses. *Soil Tillage Res.* 92, 190–197. doi: 10.1016/j.still.2006.03.003
- Alag, Z. Z., and Yilmaz, E. (2009). Effects of different sources of organic matter on soil aggregate formation and stability: a laboratory study on a lithic Rhodoxeralf from Turkey. *Soil Tillage Res.* 103, 419–424. doi: 10.1016/j.still.2008.12.006
- Al-Kaisi, M. M., Douelle, A., and Kwaw-Mensah, D. (2014). Soil micro-aggregate and macroaggregate decay over time and soil carbon change as influenced by different tillage systems. *J. Soil Water Conserv.* 69, 574–580. doi: 10.2489/jswc.69.6.574
- An, S., Mentler, A., Mayer, H., and Blum, W. E. H. (2010). Soil aggregation, aggregate stability, organic carbon and nitrogen in different soil aggregate fractions under forest and shrub vegetation on the Loess Plateau, China. *Catena* 81, 226–233. doi: 10.1016/j.catena.2010.04.002
- Barrow, N. (2015). A mechanistic model for describing the sorption and desorption of phosphate by soil. *Eur. J. Soil Sci.* 66, 9–18. doi: 10.1111/ejss.12198_2
- Bazani, J. H., Gonçalves, J. L. M., and Rocha, J. H. T. (2014). Nutrição fosfatada em plantações de eucalipto. *Info. Agron.* 148, 1–11. doi: 10.11606/d.11.2014.tde-11112014-160156
- Bunemann, E. K. (2008). Enzyme additions as a tool to assess the potential bioavailability of organically bound nutrients. *Soil Biol. Biochem.* 40, 2116–2129. doi: 10.1016/j.soilbio.2008.03.001
- Cao, S., Zhou, Y. Z., Zhou, Y. Y., Zhou, X., and Zhou, W. (2021). Soil organic carbon and soil aggregate stability associated with aggregate fractions in a chronosequence of citrus orchards plantations. *J. Environ. Manag.* 293:112847. doi: 10.1016/j.jenvman.2021.112847
- Chin, W. W. (1998). “The partial least squares approach to structural equation modeling” in *Modern methods for business research*. ed. G. A. Marcoulides (Mahwah, NJ: Lawrence Erlbaum Associates), 1295–1336.
- Condrón, L. M., and Newman, S. (2011). Revisiting the fundamentals of phosphorus fractionation of sediments and soils. *J. Soils Sediments* 11, 830–840. doi: 10.1007/s11368-011-0363-2
- Cooper, J., Greenberg, I., Ludwig, B., Hippich, L., Fischer, D., Glaser, B., et al. (2020). Effect of biochar and compost on soil properties and organic matter in aggregate size fractions under field conditions. *Agric. Ecosyst. Environ.* 295:106882:106882. doi: 10.1016/j.agee.2020.106882
- Costa, M. G., Gama-Rodrigues, A. C., Gonçalves, J. L. M., Gama-Rodrigues, E., Sales, M., and Aleixo, S. (2016). Labile and non-labile fractions of phosphorus and its transformations in soil under Eucalyptus plantations, Brazil. *Forests* 7:15. doi: 10.3390/f7010015
- Dal Ferro, N., Berti, A., Francioso, O., Ferrari, E., Matthews, G. P., and Morari, F. (2012). Investigating the effects of wettability and pore size distribution on aggregate stability: the role of soil organic matter and the humic fraction. *Eur. J. Soil Sci.* 63, 152–164. doi: 10.1111/j.1365-2389.2012.01427.x
- Dawud, S. M., Raulund-Rasmussen, K., Domisch, T., Finér, L., Jaroszewicz, B., and Vesterdal, L. (2016). Is tree species diversity or species identity the more important driver of soil carbon stocks, C/N ratio, and pH? *Ecosystems* 19, 645–660. doi: 10.1007/s10021-016-9958-1
- Diamantopoulos, A., and Siguaw, J. A. (2006). Formative versus reflective indicators in organizational measure development: a comparison and empirical illustration. *Br. J. Manag.* 17, 263–282. doi: 10.1111/j.1467-8551.2006.00500.x
- Egan, G., Crawley, M. J., and Fornara, D. A. (2018). Effects of long-term grassland management on the carbon and nitrogen pools of different soil aggregate fractions. *Sci. Total Environ.* 614, 810–819. doi: 10.1016/j.scitotenv.2017.09.165
- Fattet, M., Fu, Y., Ghestem, M., Ma, W., Foulonneau, M., Nespoulous, J., et al. (2011). Effects of vegetation type on soil resistance to erosion: relationship between aggregate stability and shear strength. *Catena* 87, 60–69. doi: 10.1016/j.catena.2011.05.006
- Formaglio, G., Krusche, A. V., Mareschal, L., Bouillet, J. P., Gonçalves, J. L. M., Nouvellon, Y., et al. (2023). Planting nitrogen-fixing trees in tropical Eucalyptus plantations does not increase nutrient losses through drainage. *For. Ecol. Manag.* 537:120940. doi: 10.1016/j.foreco.2023.120940
- Frossard, E., Condrón, L. M., Oberson, A., Sinaj, S., and Fardeau, J. C. (2000). Processes governing phosphorus availability in temperate soils. *J. Environ. Qual.* 29, 15–23. doi: 10.2134/jeq2000.00472425002900010003x
- Gao, G., Huang, X., Xu, H., Wang, Y., Shen, W., Zhang, W., et al. (2022). Conversion of pure Chinese fir plantation to multi-layered mixed plantation enhances the soil aggregate stability by regulating microbial communities in subtropical China. *For. Ecosyst.* 9:100078. doi: 10.1016/j.fecs.2022.100078
- Giumbelli, L. D., Loss, A., Ventura, B. S., dos Santos, E., Almeida, J., de Cássia Piccolo, M., et al. (2020). Aggregation index, carbon, nitrogen, and natural abundance of ¹³C and ¹⁵N in soil aggregates and bulk soil cultivated with onion under crop successions and rotations. *Soil Res.* 58:622. doi: 10.1071/SR19346
- Goncalves, J. L. M., Barros, N. F., Nambiar, E. K. S., and Novais, R. F. (1997). “Soil and stand management for short-rotation plantations” in *Management of Soil, nutrients and water in tropical plantation forests*. eds. E. K. S. Nambiar and A. G. Brown (Canberra: Australian Centre for International Agricultural Research), 379–418.
- Guo, J. H., Feng, H. L., McNie, P., Wang, W., Peng, C., Feng, L., et al. (2022). The effect of the conversion from natural broadleaved forests into Chinese fir (*Cunninghamia lanceolata* (Lamb.) Hook.) plantations on soil microbial communities and nitrogen functional genes. *Forests* 13:158. doi: 10.3390/f13020158
- Hair, J. F., Risher, J. J., Sarstedt, M., and Ringle, C. M. (2019). When to use and how to report the results of PLS-SEM. *Eur. Bus. Rev.* 31, 2–24. doi: 10.1108/EBR-11-2018-0203
- He, Y., Zhang, Q., Jiang, C., Lan, Y., Zhang, H., and Ye, S. (2023). Mixed planting improves soil aggregate stability and aggregate-associated C-N-P accumulation in subtropical China. *Front. For. Glob. Change* 6:1141953. doi: 10.3389/ffgc.2023.1141953
- Hedley, M. J., Stewart, J. W. B., and Chauhan, B. S. (1982). Changes in inorganic and organic soil-phosphorus fractions induced by cultivation practices and by laboratory incubations. *Soil Sci. Soc. Am. J.* 46, 970–976. doi: 10.2136/sssaj1982.03615995004600050017x
- Huang, W. J., Liu, J. X., Wang, Y. P., Zhou, G., Han, T., and Li, Y. (2013). Increasing phosphorus limitation along three successional forests in southern China. *Plant Soil* 364, 181–191. doi: 10.1007/s11104-012-1355-8
- Huang, X., Liu, S., You, Y., Wang, H., and Wang, J. (2017). Microbial community and associated enzymes activity influence soil carbon chemical composition in *Eucalyptus urophylla* plantation with mixing N₂-fixing species in subtropical China. *Plant Soil* 414, 199–212. doi: 10.1007/s11104-016-3117-5
- Hunt, J. F., Ohno, T., He, Z., Honeycutt, C. W., and Dail, D. B. (2007). Inhibition of phosphorus sorption to goethite, gibbsite, and kaolin by fresh and decomposed organic matter. *Biol. Fertil. Soils* 44, 277–288. doi: 10.1007/s00374-007-0202-1
- Hutapea, F. J., Weston, C. J., Mendham, D., and Volkova, L. (2023). Sustainable management of *Eucalyptus pellita* plantations: a review. *For. Ecol. Manag.* 537:120941. doi: 10.1016/j.foreco.2023.120941
- IUSS Working Group (2014). “World reference base for soil resources 2014” in *International soil classification system for naming soils and creating legends for soil maps*. *World soil resources reports no. 106* (Rome: FAO)
- Johnson, A. H., Frizano, J., and Vann, D. R. (2003). Biogeochemical implications of labile phosphorus in forest soils determined by the Hedley fractionation procedure. *Oecologia* 135, 487–499. doi: 10.1007/s00442-002-1164-5
- Kerdraon, D., Drewer, J., Chung, A. Y. C., Majalap, N., Slade, E. M., Bréchet, L., et al. (2020). Litter inputs, but not litter diversity, maintain soil processes in degraded tropical forests-across-continental comparison. *Front. For. Glob. Change.* 2:90. doi: 10.3389/ffgc.2019.00090
- Kuperman, R. G. (1996) *Relationships between soil properties and community structure of soil macroinvertebrates in oak-history forests along an acidic deposition gradient*. United States: UNT Digital Library.
- Laclau, J. P., Goncalves, J. L. D., and Stape, J. L. (2013). Perspectives for the management of eucalypt plantations under biotic and abiotic stresses. *For. Ecol. Manag.* 301, 1–5. doi: 10.1016/j.foreco.2013.03.007
- Li, Y. P., Wang, J., and Shao, M. A. (2021). Application of earthworm cast improves soil aggregation and aggregate-associated carbon stability in typical soils from Loess Plateau. *J. Environ. Manag.* 278:111504. doi: 10.1016/j.jenvman.2020.111504
- Liu, D. D., Ju, W. L., Jin, X. L., Li, M., Shen, G., Duan, C., et al. (2021). Associated soil aggregate nutrients and controlling factors on aggregate stability in semiarid grassland under different grazing prohibition timeframes. *Sci. Total Environ.* 777:146104. doi: 10.1016/j.scitotenv.2021.146104
- Liu, S. R., Li, X. M., and Niu, L. M. (1998). The degradation of soil fertility in pure larch plantation in the northeastern part of China. *Ecol. Eng.* 10, 75–86. doi: 10.1016/S0925-8574(97)10024-6
- Liu, E., and Liu, S. R. (2012). The research of carbon storage and distribution feature of the *Mytilaria laosensis* plantation in south sub-tropical area. *Acta Ecol. Sin.* 32, 5103–5109. doi: 10.5846/stxb201108141190

- Lu, R., (2000). *Analysis of soil agrochemistry*. Chinese Agricultural Science and Technology Press, Beijing.
- Luo, D., Shi, Z. M., Wang, W. X., Shirong, L., Lihua, L., Angang, M., et al. (2015). Carbon and nitrogen storage in monoculture and mixed young plantation stands of *Erythrophleum fordii* and *Pinus massoniana* in subtropical China. *Acta Ecol. Sin.* 35:9. doi: 10.5846/stxb201401030018
- Mao, L., Ye, S., and Wang, S. (2022). Soil nutrient contents and stoichiometry within aggregate size classes varied with tea plantation age and soil depth in southern Guangxi in China. *Soil* 8, 487–505. doi: 10.5194/soil-8-487-2022
- Mustafa, A., Minggang, X., Ali Shah, S. A., Abrar, M. M., Nan, S., Baoren, W., et al. (2020). Soil aggregation and soil aggregate stability regulate organic carbon and nitrogen storage in a red soil of southern China. *J. Environ. Manag.* 270:110894. doi: 10.1016/j.jenvman.2020.110894
- Olander, L. P., and Vitousek, P. M. (2004). Biological and geochemical sinks for phosphorus in soil from a wet tropical forest. *Ecosystems* 7, 404–419. doi: 10.1007/s10021-004-0264-y
- Reed, S. C., Townsend, A. R., Taylor, P. G., and Cleveland, C. C. (2011). “Phosphorus cycling in tropical forests growing on highly weathered soils” in *Phosphorus in action: biological processes in soil phosphorus cycling, soil biology* 26. eds. E. K. Bünenmann, E. Frossard and A. Oberson (Berlin, German: Springer), 339–369.
- Reed, S. C., Yang, X., and Thornton, P. E. (2015). Incorporating phosphorus cycling into global modeling efforts: a worthwhile, tractable endeavor. *New Phytol.* 208, 324–329. doi: 10.1111/nph.13521
- Richardson, A. E., and Simpson, R. J. (2011). Soil microorganisms mediating phosphorus availability. *Plant Physiol.* 156, 989–996. doi: 10.1104/pp.111.175448
- Rubk, G. H., Guggenberger, G., Zech, W., and Christensen, B. T. (1999). Organic phosphorus in soil size separates characterized by phosphorus-31 nuclear magnetic resonance and resin extraction. *Soil Sci. Soc. Am. J.* 63, 1123–1132. doi: 10.2136/sssaj1999.6351123x
- Sayer, E. J., Rodtassana, C., Sheldrake, M., Bréchet, L. M., Ashford, O. S., Lopez-Sangil, L., et al. (2020). Chapter five-revisiting nutrient cycling by litterfall-insights from 15 years of litter manipulation in old-growth lowland tropical forest. *Adv. Ecol. Res.* 62, 173–223. doi: 10.1016/bs.aecr.2020.01.002
- Sicardi, M., García-Pérchac, F., and Frioni, L. (2004). Soil microbial indicators sensitive to land use conversion from pastures to commercial *Eucalyptus grandis* (Hill ex Maiden) plantations in Uruguay. *Appl. Soil Ecol.* 27, 125–133. doi: 10.1016/j.apsoil.2004.05.004
- Six, J., Bossuyt, H., Degryze, S., and Deneff, K. (2004). A history of research on the link between (micro)aggregates, soil biota, and soil organic matter dynamics. *Soil Tillage Res.* 79, 7–31. doi: 10.1016/j.still.2004.03.008
- Six, J., Conant, R. T., Paul, E. A., and Paustian, K. (2002). Stabilization mechanisms of soil organic matter: implications for C-saturation of soils. *Plant Soil* 241, 155–176. doi: 10.1023/A:1016125726789
- Song, L. Q., Wang, Y. D., Li, D. C., Zhang, H. M., Lou, Y. L., Dou, B. K., et al. (2019). Long-term effects of natural restoration on C:N:P ecological stoichiometry in aggregates of red soil. *Chin. J. Ecol.* 38, 1707–1715. doi: 10.13292/j.1000-4890.201906.011
- Spohn, M., and Kuzuyakov, Y. (2013). Phosphorus mineralization can be driven by microbial need for carbon. *Soil Biol. Biochem.* 61, 69–75. doi: 10.1016/j.soilbio.2013.02.013
- Stewart, J. W. B., and Tiessen, H. (1987). Dynamics of soil organic phosphorus. *Biogeochemistry* 4, 41–60. doi: 10.1007/BF02187361
- Sullivan, B. W., Alvarez-Clare, S., Castle, S. C., Porder, S., Reed, S. C., Schreeg, L., et al. (2014). Assessing nutrient limitation in complex forested ecosystems: alternatives to large-scale fertilization experiments. *Ecology* 95, 668–681. doi: 10.1890/13-0825.1
- Sun, H., and Xiong, D. X. (1998). Study on organic phosphorus in Shajiang black soil and its organic inorganic complex in southern Shandong. *Chin. J. Soil Sci.* 2, 14–17. doi: 10.19336/j.cnki.trtb.1998.02.005
- Tamura, M., Suseela, V., Simpson, M., Powell, B., and Tharayil, N. (2017). Plant litter chemistry alters the content and composition of organic carbon associated with soil mineral and aggregate fractions in invaded ecosystems. *Glob. Change Biol. Bioenergy* 23, 4002–4018. doi: 10.1111/gcb.13751
- Tang, L., and Wang, S. (2022). Dynamics of soil aggregate-related C-N-P stoichiometric characteristics with stand age and soil depth in Chinese fir plantations. *Land Degrad. Dev.* 8:33. doi: 10.1002/ldr.4217
- Tiessen, H., and Moir, J. O. (2007). “Characterization of available P by sequential extraction” in *Soil sampling and methods of analysis*. eds. M. R. Carter and E. G. Gregorich. 2nd ed (Boca Raton, FL: CRC Press), 293–306.
- Tiessen, H., Stewart, J., and Cole, C. (1984). Pathways of phosphorus transformations in soils of differing pedogenesis. *Soil Sci. Soc. Am. J.* 48, 853–858. doi: 10.2136/sssaj1984.03615995004800040031x
- Turner, B. L., and Engelbrecht, B. M. J. (2011). Soil organic phosphorus in lowland tropical rain forests. *Biogeochemistry* 103, 297–315. doi: 10.1007/s10533-010-9466-x
- Vitousek, P. M., Porder, S., Houlton, B. Z., and Chadwick, O. A. (2010). Terrestrial phosphorus limitation: mechanisms, implications, and nitrogen-phosphorus interactions. *Ecol. Appl.* 20, 5–15. doi: 10.1890/08-0127.1
- Wan, W. J., Xiang, H., Shun, W., Wang, L., Luo, X., Chen, W., et al. (2020). Soil aggregate fractionation and phosphorus fraction driven by long-term fertilization regimes affect the abundance and composition of P-cycling-related bacteria. *Soil Tillage Res.* 196:104475. doi: 10.1016/j.still.2019.104475
- Wang, S., Huang, Y., and Ye, S. (2021). Distribution of organic carbon and nutrients in soil aggregates under different stand types of *Cunninghamia lanceolata* in southern Guangxi of China. *Soil Sci. Plant Nutr.* 67, 427–438. doi: 10.1080/00380768.2021.1932585
- Wang, S. Q., Zhang, Z., and Ye, S. M. (2020). Response of soil fertility characteristics in water-stable aggregates to tea cultivation aggregates to tea cultivation age in hilly region of southern Guangxi, China. *Catena* 191:104578. doi: 10.1016/j.catena.2020.104578
- Wang, S., Zhou, P., Luo, B., and Ye, S. (2022). Stoichiometric characteristics of medium- and micro-elements (Ca, Mg, Fe, and Mn) in soil aggregates as affected by stand age in Chinese fir plantations. *Land Degrad. Dev.* 18, 3991–4003. doi: 10.1002/ldr.4439
- Wei, J. X., Wang, C., He, B., Yuo, Y. M., and Huang, X. M. (2022). Research progress on soil microorganisms in eucalypt forests. *J. Zhejiang A F Univ.* 39, 1144–1154. doi: 10.11833/j.issn.2095-0756.20210701
- Xu, H. D., Yuan, H. J., Yu, M. K., and Cheng, X. (2020). Large macroaggregate properties are sensitive to the conversion of pure plantation to uneven-aged mixed plantations. *Catena* 194:104724. doi: 10.1016/j.catena.2020.104724
- Yan, Y., Cui, Y. H., Fan, R. Y., Pan, C. L., Jiang, C. Y., Hao, J. W., et al. (2023). Soil aggregate stability and distribution characteristics of organic nitrogen components in *Eucalyptus* pure and mixed forests. *J. Cent. South Univ. For. Technol.* 7, 149–158. doi: 10.1016/j.j.cnki.1673-923x.2023.07.015
- Yang, X., Chen, X., and Yang, X. (2019). Effect of organic matter on phosphorus adsorption in a black soil from Northeast China. *Soil Tillage Res.* 187, 85–91. doi: 10.1016/j.still.2018.11.016
- Yang, X., Post, W. M., et al. (2011). Phosphorus transformation as a function of pedogenesis: a synthesis of soil phosphorus data using Hedley fractionation method. *Biogeosciences* 8, 2907–2916. doi: 10.5194/bg-8-2907-2011
- Yang, H. B., Vina, A., Winkler, J. A., Chung, M. G., Huang, Q., Dou, Y., et al. (2021). A global assessment of the impact of individual protected areas on preventing forest loss. *Sci. Total Environ.* 777:145995. doi: 10.1016/j.scitotenv.2021.145995
- Yang, Y., Zhang, Y., Yu, X., and Jia, G. (2023). Soil microorganism regulated aggregate stability and rill erosion resistance under different land uses. *Catena* 228:107176. doi: 10.1016/j.catena.2023.107176
- Zeng, Q., Li, X., Dong, Y. H., Li, Y. Y., Cheng, M., An, S. S., et al. (2015). Ecological stoichiometry characteristics and physical-chemical properties of soils at different latitudes on the loess plateau. *J. Nat. Resour.* 30, 870–879. doi: 10.11849/zrzyxb.2015.05.014
- Zhang, D. J., Li, J. J., Huang, Y. M., Huang, Y., Gao, S., and Zhang, J. (2022). Root-soil facilitation in mixed *Eucalyptus grandis* plantations including nitrogen-fixing species. *For. Ecol. Manag.* 516:120215. doi: 10.1016/j.foreco.2022.120215
- Zhang, Y., Shengzhe, E., Wang, Y., Su, S., Bai, L., Wu, C., et al. (2021). Long-term manure application enhances the stability of aggregates and aggregate-associated carbon by regulating soil physicochemical characteristics. *Catena* 203:105342. doi: 10.1016/j.catena.2021.105342
- Zhang, Q., Wang, S., Huang, Y., Yao, X., He, X., and Ye, S. (2021). Ecological stoichiometry of soil carbon, nitrogen, and phosphorus within soil aggregates of four plantations in different *Cunninghamia lanceolata* stand types. *Acta Bot. Boreali-Occident. Sin.* 41:8. doi: 10.7606/j.issn.1000-4025.2021.06.1028
- Zhang, Z., Wei, C. F., Xie, D. T., Gao, M., and Zeng, X. (2008). Effects of land use patterns on soil aggregate stability in Sichuan Basin, China. *Particology* 6, 157–166. doi: 10.1016/j.partic.2008.03.001
- Zhang, W., You, Y., Su, X., Yan, J., Gao, G., Ming, A., et al. (2023). Introducing N₂-fixing tree species into *Eucalyptus* plantations promotes soil organic carbon sequestration in aggregates by increasing microbial carbon use efficiency. *Catena* 231:107321. doi: 10.1016/j.catena.2023.107321
- Zhao, Y. D., and Hu, X. (2022). How do freeze-thaw cycles affect the soil pore structure in alpine meadows considering soil aggregate and soil column scales? *J. Soil Sci. Plant Nutr.* 22, 4207–4216. doi: 10.1007/s42729-022-01019-z
- Zhao, B. C., Xu, J. D., Chen, B. Y., Cao, X. F., Yuan, T. Q., Wang, S. F., et al. (2018). Selective precipitation and characterization of lignin-carbohydrate complexes (LCCs) from *Eucalyptus*. *Planta* 247, 1077–1087. doi: 10.1007/s00425-018-2842-9
- Zhou, L., Sun, Y. J., Saeed, S., Zhang, B., and Luo, M. (2020). The difference of soil properties between pure and mixed Chinese fir (*Cunninghamia lanceolata*) plantations depends on tree species. *Glob. Ecol. Conserv.* 22:e01009. doi: 10.1016/j.gecco.2020.e01009



OPEN ACCESS

EDITED BY
Peter Fule,
Northern Arizona University, United States

REVIEWED BY
Ronggo Sadono,
Gadjah Mada University, Indonesia
Nophea Sasaki,
Asian Institute of Technology, Thailand

*CORRESPONDENCE
Andres Schmidt
✉ andres.schmidt@oregonstate.edu

RECEIVED 12 May 2023
ACCEPTED 12 February 2024
PUBLISHED 26 February 2024

CITATION
Schmidt A, Ellsworth LM, Boisen GA,
Novita N, Malik A, Gangga A, Albar I,
Dwi Nurhayati A, Putra Ritonga R, Asyhari A
and Kauffman JB (2024) Fire frequency,
intensity, and burn severity in Kalimantan's
threatened Peatland areas over two
Decades.
Front. For. Glob. Change 7:1221797.
doi: 10.3389/ffgc.2024.1221797

COPYRIGHT
© 2024 Schmidt, Ellsworth, Boisen, Novita,
Malik, Gangga, Albar, Dwi Nurhayati, Putra
Ritonga, Asyhari and Kauffman. This is an
open-access article distributed under the
terms of the [Creative Commons Attribution
License \(CC BY\)](https://creativecommons.org/licenses/by/4.0/). The use, distribution or
reproduction in other forums is permitted,
provided the original author(s) and the
copyright owner(s) are credited and that the
original publication in this journal is cited, in
accordance with accepted academic
practice. No use, distribution or reproduction
is permitted which does not comply with
these terms.

Fire frequency, intensity, and burn severity in Kalimantan's threatened Peatland areas over two Decades

Andres Schmidt^{1*}, Lisa M. Ellsworth¹, Grace A. Boisen²,
Nisa Novita³, Anjelita Malik³, Adi Gangga³, Israr Albar⁴,
Ati Dwi Nurhayati⁵, Rasis Putra Ritonga³, Adibtya Asyhari³ and
J. Boone Kauffman⁶

¹Department of Fisheries, Wildlife, and Conservation Sciences, Oregon State University, Corvallis, OR, United States, ²Department of Biological and Ecological Engineering, Oregon State University, Corvallis, OR, United States, ³Yayasan Konservasi Alam Nusantara, Jakarta, Indonesia, ⁴Indonesia Ministry of Environment and Forestry (MoEF), Jakarta, Indonesia, ⁵Faculty of Forestry and Environment, IPB University, Bogor, Indonesia, ⁶Illahee Sciences International, Corvallis, OR, United States

Kalimantan, the Indonesian portion of the Island of Borneo, has an estimated 45,000 km² of tropical peatland and represents one of the largest stocks of tropical peat carbon. However, over the last three decades, the peatlands of Indonesia, and Kalimantan in particular, have been heavily degraded or destroyed by drainage of peatland swamps, deforestation, land cover change for agriculture, and intentional burning. Many studies have examined degradation of peat forests and the associated frequency of fires, often focusing on specific regions of Kalimantan over limited periods. Here, we present our results of a spatially comprehensive, long-term analysis of peatland fires in Kalimantan over more than two decades from early 2001 to the end of 2021. We examined the effects of changing climate conditions, land cover change, and the regulatory framework on the total burned area and frequency and severity of peatland fires over a 21-year period by combining extensive datasets of medium-resolution and high-resolution satellite imagery. Moreover, surface fire intensity was modeled for four dominant land use/land cover types to determine how land use change alters fire behavior. Our results confirm a consistent and strong spatiotemporal correlation between hydro-climatological drivers associated with El Niño conditions on peatland fire frequencies and burned peatland area. Changes in the number of fires and burn severity are visible over time and are caused by a combination of large-scale meteorological patterns and changing regulations. A significant relative increase of the "high" and "very high" severity across all peatland fires in Kalimantan was found for the latest period from 2015 through 2021 by 12.1 and 13.4%, compared to the two previous 7-year periods from 2001 to 2007 period and from 2008 to 2014, respectively, whereas the total peatland area burned decreased in 2015 to 2021 by 28.7% on average compared to the previous periods.

The results underline the importance of a comprehensive approach considering physical aspects of overarching climate conditions while improving political and regulatory frameworks to mitigate the negative effects of burning tropical peatlands.

KEYWORDS

peatland fires, changes in burn severity over 2 decades, satellite analysis of peatland fires, fire frequency in Kalimantan, climate effects on peatland fires

1 Introduction

Indonesia is home to about 23% of the world's tropical peatlands with a large portion of the country's peatland areas (32%, an area of roughly 45,000 km²) located in Kalimantan, the Indonesian portion of the Island of Borneo (Osaki et al., 2016; Xu et al., 2018; Anda et al., 2021). Indonesia's peatland ecosystems represent one of the largest stocks of tropical forest carbon, storing an estimated 57 Gt of carbon (Page et al., 2011; Kiely et al., 2021). However, over the last three decades, the peat forests of Indonesia, and Kalimantan in particular, have been heavily degraded or destroyed by land cover change including the drainage of peatland swamps, deforestation, and human-ignited fires primarily for land clearing.

Analyses from remote sensing imagery indicate that more than half of tropical peatland areas in Malaysia, Sumatra, and Borneo have been converted (Miettinen et al., 2016). Based on the land cover change datasets of the Indonesian Ministry of Environment and Forestry (MoEF), Indonesia has lost about 21% of peat swamp forests mainly due to oil palm and plantation forest development from 2009–2019 (Indonesia Ministry of Environment and Forestry [MoEF], 2020). This anthropogenically induced land use/land cover (LULC) change transformed large portions of the natural peat swamp to agricultural land primarily for oil palm plantations, industrial timber plantation, the cultivation of rice, and the production of rubber (e.g., Ramdani and Hino, 2013; Tacconi and Muttaqin, 2019). The occurrence of peatland fires in Indonesia is driven by a complex combination of overarching meteorological conditions, the political framework, and socio-economic aspects within agricultural communities in peatland areas (Edwards et al., 2020; Silvianingsih et al., 2020). The province of Central Kalimantan in Indonesia, where an estimated 10,000 km² of tropical peat swamp forest was cleared during the Mega Rice project (Law et al., 2015) exhibits the highest density of peatland fires in Southeast Asia (Miettinen et al., 2017).

Degraded peatlands are more prone to recurrent fires (Miettinen et al., 2012). For example, Vetrina and Cochrane (2020) analyzed fire frequencies in Indonesia's two largest peatland regions, Kalimantan and Sumatra during 2001–2018 and found degraded shrublands have the highest rate of annual burning (329 and 236 km² per year, respectively), impeding forest regeneration. LULC change and the conversion to more flammable vegetation increases the risk of intentionally ignited peatland fires spreading beyond their intended extent (Goldstein et al., 2020). Peatland fires have been attributed to negative consequences across all sectors.

In addition to the devastating effects on public health by smoke and haze during intense drought-induced peatland fire seasons in Indonesia (Marlier et al., 2015; Uda et al., 2019) and substantial economic losses (Kiely et al., 2021), the peatland fires also have a strong impact on climate change as massive amounts of carbon stored in aboveground vegetation, roots, and soils are released into the atmosphere (Turetsky et al., 2015; Heymann et al., 2017; Wiggins et al., 2018; Lasslop et al., 2019; Novita et al., 2021; Ribeiro et al., 2021; Volkova et al., 2021), intensified by contributions from long-lasting peat smoldering below the surface (Yokelson et al., 2022).

Hence, a comprehensive assessment of the effects of climate and meteorological conditions on the number and behavior of peatland fires is needed to reveal short-term and long-term patterns in fire frequency and burn severity and to understand how changing LULC alters landscape flammability within Kalimantan's threatened peatland areas and consequently inform land management and regulatory strategies.

In recent years, peatland fire frequency has been in the focus of the scientific community to characterize fire regimes in peatlands and link fire occurrences to climate conditions and anthropogenic actions. This is supported with an ever-growing number of studies using remote sensing data and satellite imagery in combination with process models, machine learning, and refined remote sensing methods on various spatial scales to address the fire frequency and fire-induced land cover changes, focusing on specific regions or distinct periods, respectively, (e.g., Sabani et al., 2019; Gaveau et al., 2021).

Burn severity is another key factor in characterizing fire occurrences and is needed to estimate emissions from the fire and to quantify the recovery potential of vegetation (Turetsky et al., 2015). In addition, the properties of the post-fire vegetation are important factors that define the burning conditions for following fire events (Hoscilo et al., 2013). Many studies have linked spatiotemporal patterns of fire frequency and burn severity and their relationship to land cover changes to address drivers of tropical peatland fire in distinct periods (Vetrina and Cochrane, 2020).

Yet, to the knowledge of the authors, studies emphasizing long-term patterns of fire in response to climate-drivers in tropical peatlands are scarce for Indonesia, especially in Kalimantan, a region with vast peatland coverage and continuous threats of fires within peatland ecosystems.

The Indonesian government has initiated various programs and policies to address peatland fires in Kalimantan. These include efforts to restore degraded peatlands, improve fire prevention and control measures, and promote sustainable land-use practices.

While organized efforts are needed, informed decisions require the knowledge of causes and effects of peatland fire frequency and severity, especially when long-term changes of climate that affect important large-scale meteorological patterns are added to economically driven LULC change. In this study we aim to (1) assess the effect of climate and meteorological conditions on the number and behavior of fires in tropical peatland (2) analyze spatiotemporal patterns in fire frequency and burn severity across all peatland areas of Kalimantan over more than two decades (January 2001 through December 2021) using medium-resolution and high-resolution satellite imagery, (3) model potential surface fire intensity for four dominant land cover types in Kalimantan to better understand how changing LULC alters landscape flammability.

2 Data and methods

2.1 Study area and climate data

Our peatland study region covers an integrated area of 45,000 km² in Kalimantan (**Figure 1**) and was chosen according to the delineation of the PEATMAP landcover dataset (Xu et al., 2018).

To spatiotemporally assess the governing climate conditions that drive fire regime conditions and occurrences over more than two decades (January 2001–December 2021), we used gridded climate data with a spatial resolution 0.1 × 0.1 (ca. 11 km × 11 km in our study region) of the ERA5 - Land Reanalysis data (Muñoz-Sabater et al., 2021) over Kalimantan provided by the European Centre for Medium-Range Weather Forecasts (ECMWF).

We used monthly values of synoptic means of air temperature at 2 m a.g.l. and total precipitation accessible through the ECMWF data repository (Muñoz-Sabater, 2019) to calculate anomalies of air temperature and precipitation with respect to the 21-year study period.

2.2 Moderate resolution thermal anomalies

Moderate Resolution Imaging Spectroradiometer (MODIS, Aqua & Terra) Thermal Anomalies / hotspot data (Ver. 6.1), provided through U.S. Geological Survey (USGS) and the National Aeronautics and Space Administration (NASA), was applied to identify peatland fires in Kalimantan from January 2001 through December 2021. While the corresponding Visible Infrared Imaging Radiometer Suite (VIIRS) captures more small fires, the satellite only launched in October 2011 making the dataset unsuitable for our long-term assessment. Hence, to avoid inconsistencies, only MODIS hotspot data was utilized to identify fires.

We combined the daily MODIS MCD14DL (Collection 6.1) active fire product and the corresponding historic fire product MCD14ML to track fire events detected in peatlands of Kalimantan from 2001 through 2021. The MODIS hotspot dataset provides daily 1 km × 1 km resolution center coordinates of fire events and fire radiative power (FRP) values for high-intensity fire pixels (Giglio et al., 2016). The MODIS hotspot dataset has

been proven suitable to assess fire frequency and burned area in our study region (e.g., Tansey et al., 2008; Albar et al., 2018). The dataset also contains values reflecting the certainty of each thermal anomaly detection. Only data points with a certainty value of ≥85% were considered actual peatland fire events and used for further analyses. Using locations and dates of fire events detected through the MODIS MCD14DL thermal anomaly/hotspot dataset as reference, temporally corresponding and collocated high-resolution (10 m × 10 m to 30 m × 30 m) satellite surface reflectance data was identified and analyzed for long-term pattern recognition in burn severity of peatland fires. The monthly long-term USGS/NASA MCD64A1 Burned Area data product (Version 6.1) was used to trace the amount burned peatland area over time.

The MCD64A1 dataset combines MODIS active fire observations with MODIS surface reflectance imagery providing a global grid with 500 m × 500 m spatial resolution. The dataset contains a classification indicating whether a pixel is a burned area, accompanied by additional information such as burn date and quality assessment values of the uncertainty in days for the date of burn for each data pixel (Giglio et al., 2018). Globally, the data product exhibits a 40.2% commission error and 72.6% omission error after a comparison with corresponding Landsat 8 burned area values based on 558 pre- and post-fire scenes (Boschetti et al., 2019).

Nevertheless, using aggregated Landsat 8 raster data with decreased spatial resolution, the coefficient of determination (R^2) for the MCD64A1 and Landsat 8 burned area data was found to be >0.7 for the linear regression. Hence, while limited by resolution, the global MCD64A1 dataset offers the longest standing reference for burned area assessments.

2.3 High resolution satellite surface reflectance imagery

To cover the 21-year study period as continuously as possible, we combined high resolution imagery from Landsat missions provided through the NASA/USGS Collection 2 / Level 2 data repository (Micijevic et al., 2020) and data from the European Space Agency (ESA) Sentinel-2 A/B satellite mission (Gascon et al., 2014). This comprises Landsat-5 Thematic Mapper (TM), Landsat-7 Enhanced Thematic Mapper Plus (ETM+), Landsat-8 Operational Land Imager (OLI) and Thermal Infrared Sensor (TIRS) multispectral data (e.g., Reuter et al., 2011, 2015; Wulder et al., 2019) as well as data from the Copernicus Sentinel-2 mission (Claverie et al., 2018) for the analyses of burn severity (**Figure 2**). The USGS Landsat 2 / Level-2 collection datafiles are quality filtered and flagged including cloud masking and atmospheric corrections have been applied such as corrections for solar angle and sensor viewing angles (Micijevic et al., 2020; Pinto et al., 2020).

We extracted data sub-grids from the Landsat and Sentinel-2 satellite scenes for each channel for each fire event with a 2 km buffer from the centers of the MODIS hotspot data points. The spatial buffer size was chosen empirically to safely capture the complete extent of all burns while accounting for the spatial accuracy of the MODIS hotspot coordinates. To maximize the availability of high-resolution imagery data from the various Landsat and Sentinel-2 campaigns while accounting for generally

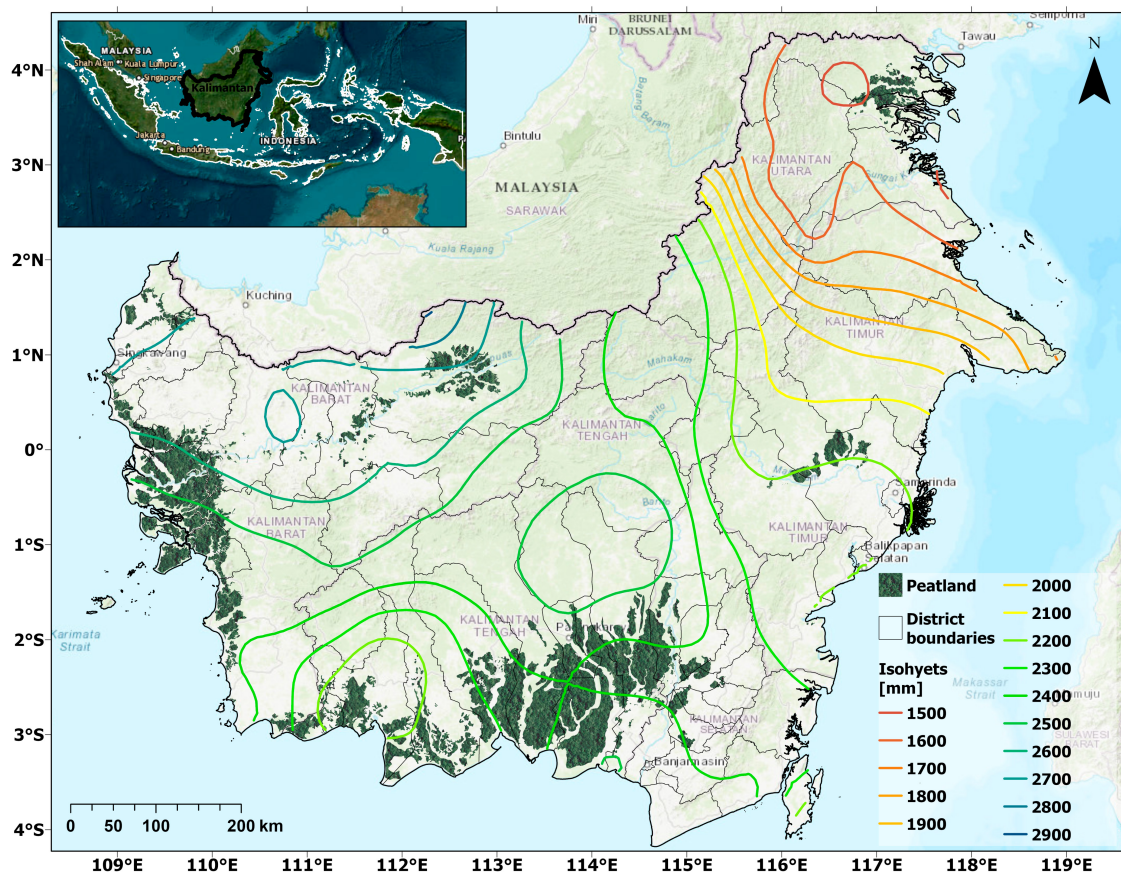


FIGURE 1

Overview of the study region showing the delineated peatland areas (dark green) based on PEATMAP data and the average annual precipitation for the study period from January 2001 to December 2021.

faster regrowth in humid and tropic regions compared to temperate ecosystems, we allowed a window-width of 90 days before and after a fire event for the satellite scenes to be used to capture the pre-fire and post-fire surface reflectance spectra around a specific peatland fire event. The rasters used for the reflectance analyses of burn severity have a spatial resolution of $30\text{ m} \times 30\text{ m}$ for the Landsat imagery and $20\text{ m} \times 20\text{ m}$ for the Sentinel-2 data.

With the study area located in the tropics, cloudiness mostly affects the quality and usability of the Landsat and Sentinel satellite surface reflectance imagery in our study area (e.g., Sudmanns et al., 2019). Hence, to allow for reliable comparison of pre-fire and post-fire reflectance data, hotspot-specific Landsat, and Sentinel-2 sub-grids with more than 2% of the pixels classified as cloud cover (clouds and cloud shadows) in the reflectance data sub-grids were not used for further analyses.

2.4 Burn severity analyses and classification

The differenced Normalized Burn Ratio ($dNBR$) was used to assess aboveground damage to vegetated areas after fires (Brewer et al., 2005). Unharmed vegetation exhibits high reflectance values in the near-infrared (NIR), and low reflectance in the shortwave-infrared (SWIR) band spectrum whereas burnt vegetation shows

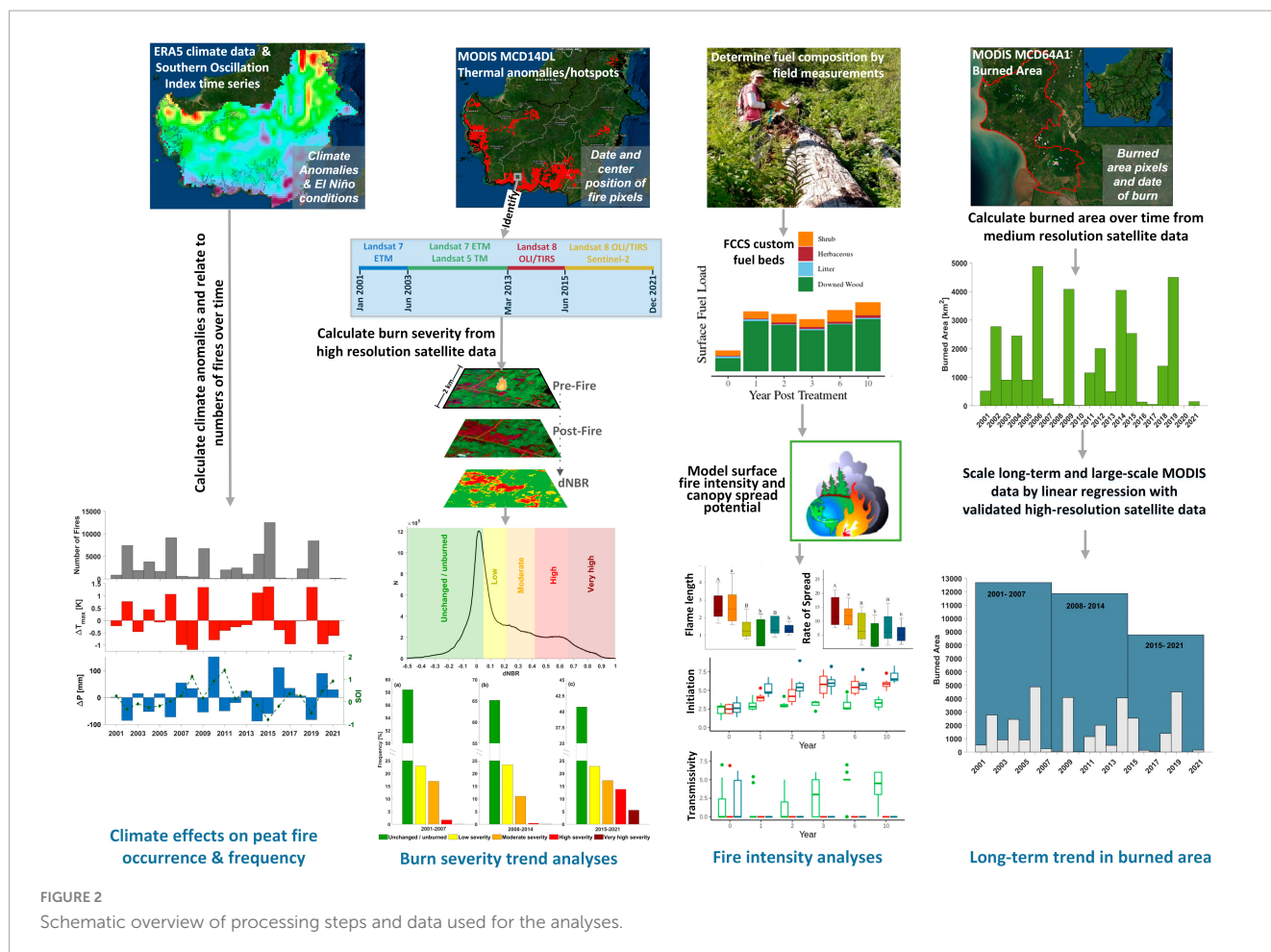
low reflectance in the NIR and high reflectance in the SWIR band. Hence, high NBR (Eq. 1) values indicate healthy unburned vegetation while low NBR values indicate bare ground, charred vegetation, and recently burnt areas. By comparing pre-fire reflectance with post-fire reflectance through the $dNBR$ (Eq. 2), damage to the surface vegetation (i.e., burn severity) can be assessed and classified (e.g., Miller and Yool, 2002; Cocke et al., 2005) following Eqs 1, 2:

$$NBR = \frac{(NIR - SWIR)}{(NIR + SWIR)} \quad (1)$$

$$dNBR = NBR_{pre-fire} - NBR_{post-fire} \quad (2)$$

The NIR and SWIR channel assignments vary slightly with respect to the wavelengths captured based on the satellites' instrumentations. Details regarding the quality, spectral comparability, as well as the classification of channels and respective wavelengths for the various LANDSAT missions used and the Sentinel-2 mission can be found in Chander and Markham (2003), Irons et al. (2012), and Lamquin et al. (2019), for instance.

If more than one pre-fire or post-fire NBR raster sub-grids were available after quality filtering, we used averages of the corresponding NBR datasets. This dampens effects of remaining erroneous pixel values and leads to an overall improved accuracy



compared to corresponding *dNBR* values based on only one pre-fire and one post-fire raster pair (Parks et al., 2018).

For some peatland fire events after 2015, a combination of Sentinel-2 and Landsat-8 data were blended after rescaling the higher resolution rasters to 30 m x 30 m resolution, leading to acceptable deviations compared to using post- and pre-fire spectral data from one set of spectral data. However, using imagery from various satellites/instruments increases the overall accuracy if surface reflectance data closer to an actual fire date can be captured (Quintano et al., 2018).

2.5 Fire intensity modeling

Fire behavior models are important in supporting fire characteristics assessment and fire management (Scott and Burgan, 2005). Those models are built around mathematical equations that predict fire spread (Rothermel, 1972; Prichard et al., 2013) based on the amount, type, and arrangement of burnable material (fuels) and weather conditions. Fire behavior is commonly predicted using models that are parameterized with fuel structure and composition data (i.e., cover, height, biomass) that are collected *in situ* or with existing standard fuel models (Scott and Burgan, 2005; Heinsch and Andrews, 2010). The Fuel Characteristic Classification System (FCCS) in the Fuel and Fire Tool (FFT) (Prichard et al., 2013) allows users to input site-specific fuel and weather data to estimate

potential fire behavior (e.g., rate of spread, flame length), as well as to inform prescribed fire planning and fuel hazard assessments. This model improved upon earlier systems (i.e., BehavePlus, Heinsch and Andrews, 2010) by incorporating a modified version of Rothermel (1972) equations that allowed for greater flexibility in user inputs to fuel loads, ultimately allowing the user to set fuel input parameters to represent a heterogeneous and layered fuel structure (i.e., canopy, sub-canopy, understory, surface fuel, and ground fuel) that more accurately represents field conditions (Sandberg et al., 2008). Modeled fire behavior studies have provided valuable information, in particular, for risk assessments (e.g., Ager et al., 2011; Schmidt et al., 2022) and for comparisons among LULC types or management alternatives (Brose and Wade, 2002; Evans et al., 2015; Parsons et al., 2018; Johnston et al., 2021; Williams et al., 2023).

To estimate the impact that different LULC types (forest, plantation, oil palm, early successional grass and shrubland - hereafter, grassland) have on potential fire intensity, we used the FCCS to build custom fuel models based on field observations and characterized surface fire intensity and canopy fire transmission in FFT. Fuels data were derived from published and government literature and local expert opinion for each LULC type (Novita, 2016; Basuki, 2017). The FFT estimates surface fire intensity using ecosystem-specific fuel data and environmental scenarios (i.e., moisture content through the typical fire season).

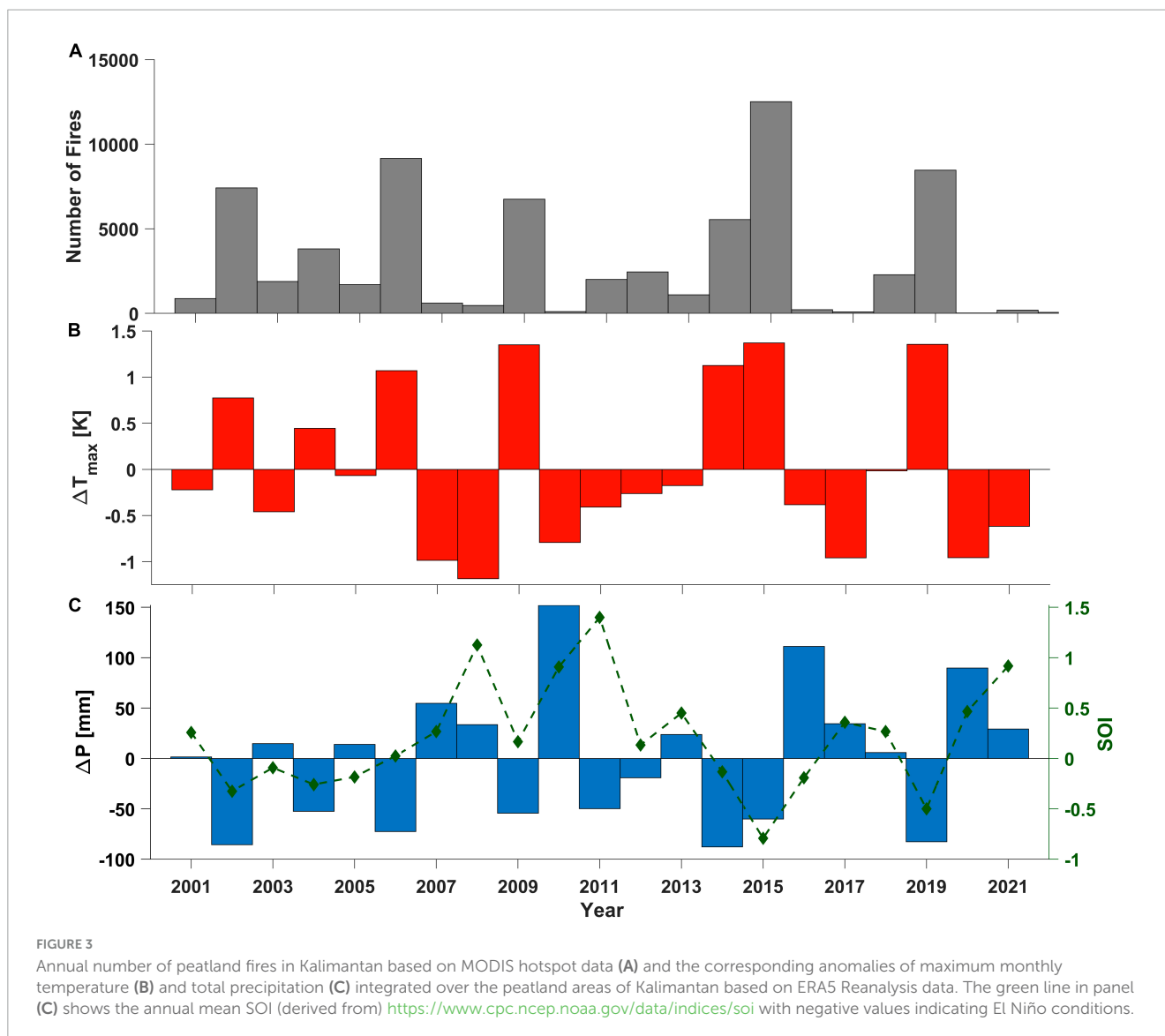


FIGURE 3

Annual number of peatland fires in Kalimantan based on MODIS hotspot data (A) and the corresponding anomalies of maximum monthly temperature (B) and total precipitation (C) integrated over the peatland areas of Kalimantan based on ERA5 Reanalysis data. The green line in panel (C) shows the annual mean SOI (derived from <https://www.cpc.ncep.noaa.gov/data/indices/soi> with negative values indicating El Niño conditions).

TABLE 1 Applied burn severity classification.

| dNBR range | Severity class |
|-------------|--------------------|
| <0.053 | Unchanged/unburned |
| 0.053–0.212 | Low |
| 0.213–0.419 | Moderate |
| 0.420–0.660 | High |
| >0.660 | Very high |

For each ecosystem type, fuel beds were customized to represent the quantity and arrangement of fuel. Details about the customized fuel beds are provided in the **Supplementary material**.

Environmental scenarios in the FFT model were calculated by inclusion of a moisture dampening coefficient, which has a linear relationship with model outputs, such that moist fuels generate reduced fire behavior metrics, and drier fuels result in more intense modeled fire behavior (Prichard et al., 2013). “Moderate” and “extreme” environmental scenarios were chosen to represent

fuel moisture expected as vegetation phenology progresses from burnable, but moderate fire risk (2/3 cured scenarios; D2L2 in FFT), to highest fire risk, when fuels are dry and highly flammable (fully cured scenario; D2L1). Windspeed assumptions used were 6 kph (mild wind conditions) and 32 kph (moderately high wind). Independent model runs were done for each fuel model (forest, plantation, oil palm, grassland) at each wind and fuel moisture scenario. While not all combinations of influencing parameters that occur in reality can be covered, the applied model conditions cover a variety of meteorological and fuel conditions. Model outputs chosen to characterize surface fire intensity included rate of spread (ROS; $m\ min^{-1}$), flame length (FL; m), and reaction intensity (RI; the rate of heat release per unit area of the flaming front; $kW\ m^2\ min^{-1}$) (Byram, 1959; Keeley, 2009).

3 Results and discussion

The results for study’s objectives are consecutively presented in the following sections assessing the effect of climate and

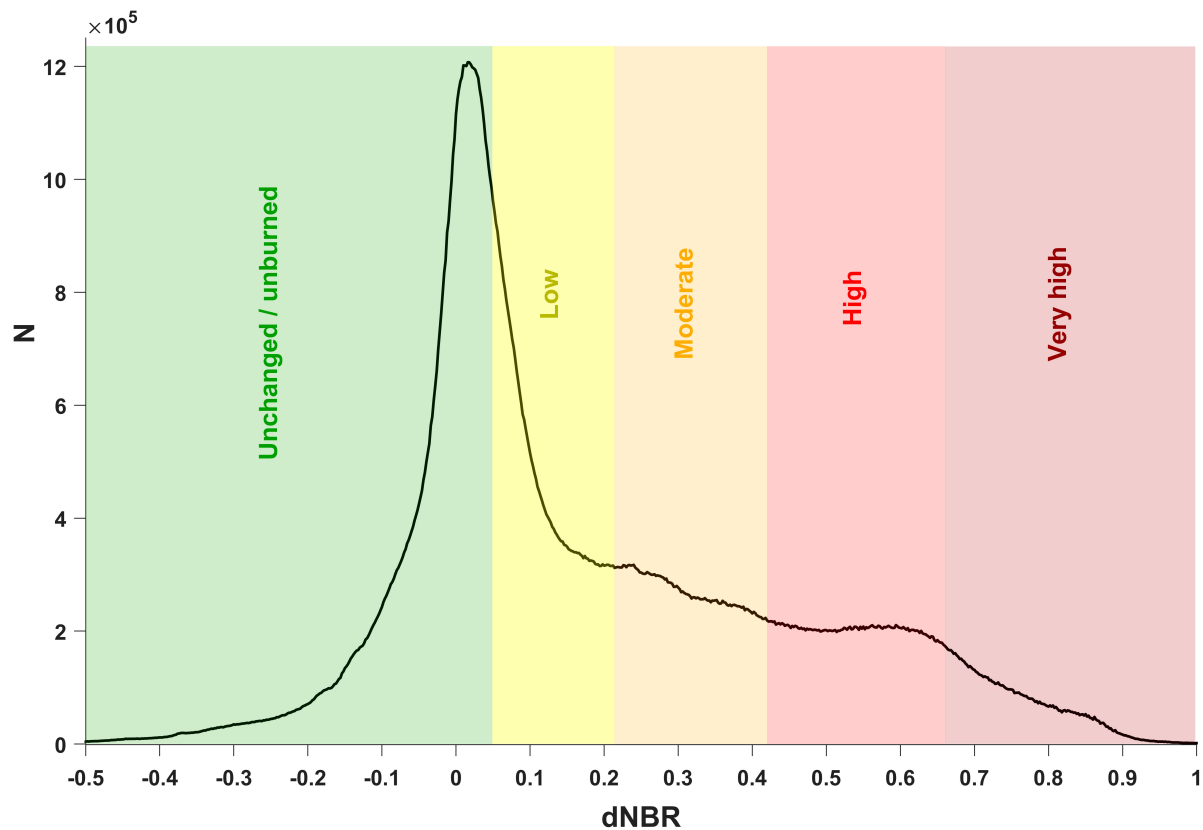


FIGURE 4

Frequency distribution of calculated dNBR pixel values and applied dNBR class boundaries for the burn severity classification of all fires included in the analysis across Kalimantan.

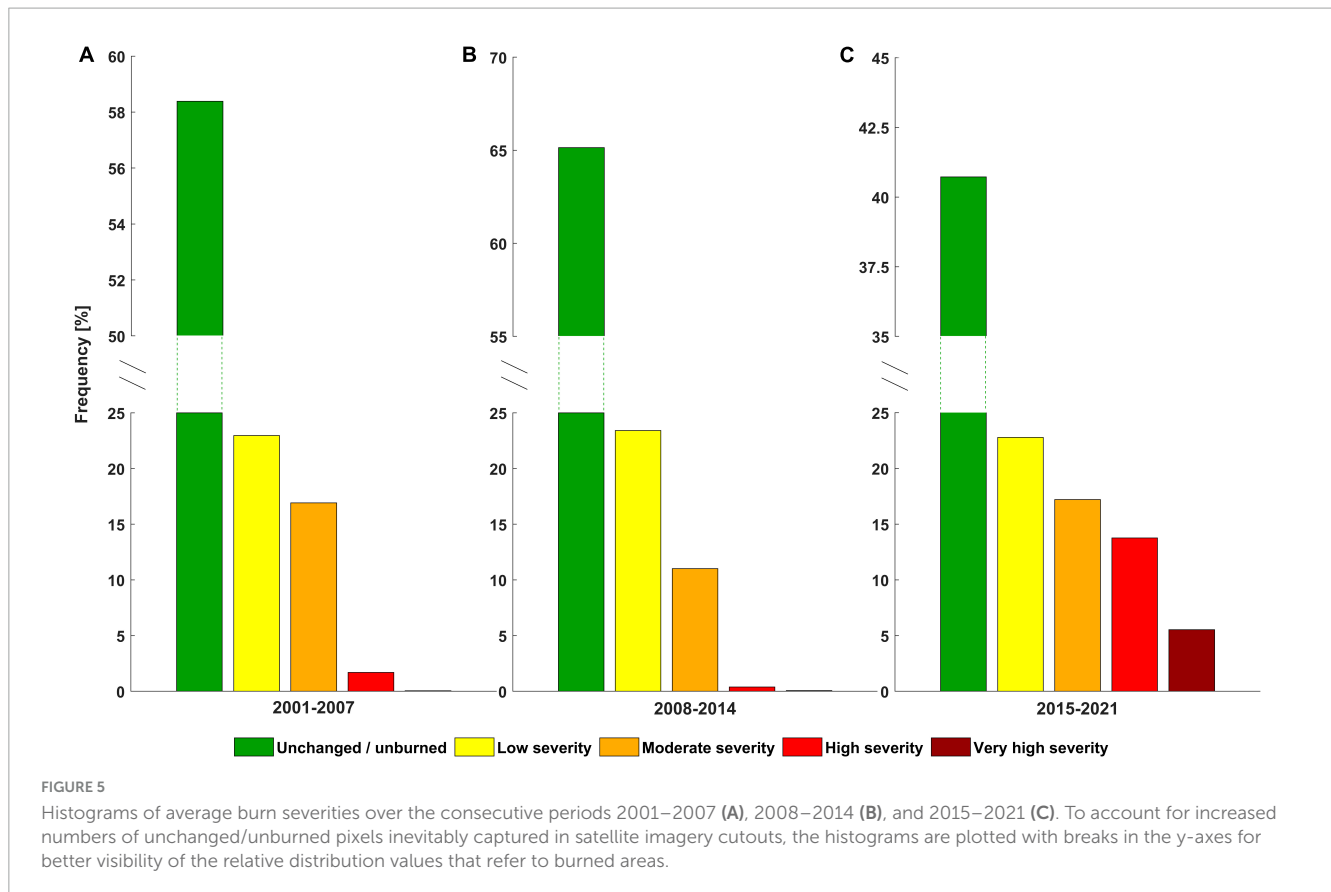
meteorological conditions on the number and behavior of fires in tropical peatland (section “3.1 Dependence of fire frequencies on meteorological conditions”), analyzing long-term spatiotemporal patterns of burn severity and peatland area burned across Kalimantan (sections “3.2 Regional trends in peatland fire burn severity” and “3.3 Assessment of burned peatland area over time”), and model potential surface fire intensity for four dominant land cover types in Kalimantan to better understand how changing LULC alters landscape flammability (section “3.4 Modeled fire intensity”). Furthermore, a short overview of the regulatory framework over the two-decade study period is presented in section “3.5 Timeline of the regulatory framework for peatland fires,” including observed effects on the number of peatland fires.

3.1 Dependence of fire frequencies on meteorological conditions

Using monthly ECMWF ERA5 Land Reanalysis climate data, we calculated annual averages for air temperature and precipitation anomalies spatially integrated over the peatland areas of Kalimantan. The annual deviations from the 21-year average of air temperature in 2 m a.g.l. and precipitation are shown in **Figures 3B, C**, respectively. Increased numbers of fires (**Figure 3A**) occur during years when the precipitation is lower than the average

and the maxima of air temperature at 2 m a.g.l. exceeds the 21-year average value. Accordingly, years with the lower numbers of fires (i.e., 2007, 2008, 2010, 2016, 2017, 2020, and 2021) coincide with the years that exhibit total precipitation amounts above average and air temperature below average, respectively, (**Figures 3A, C**). The interannual variation of rainfall in Indonesia is strongly influenced by the Southern Oscillation index (SOI) and the associated ocean surface temperature variations, with the El Niño–Southern Oscillation (ENSO) affecting the amounts of precipitation during fire season and annual groundwater levels in the tropical peatlands of Kalimantan (**Susilo et al., 2013; Alsepan and Minobe, 2020**). The warmer conditions and reduced water vapor during El-Niño years decreases precipitation resulting in lower peatland groundwater level further increasing the fire susceptibility of degraded and drained peatlands (**Sulaiman et al., 2023**). An increase in the frequency of the El-Niño conditions of the overarching circulation system leads to more frequent, intensely dry fire seasons in Southeast Asia (e.g., **Sun et al., 2020; Tan et al., 2020**). These meteorological conditions that define the fire regime on a regional scale are reflected in the correlations with El Niño conditions and the corresponding number of fire events observed in our study region (e.g., **Chen et al., 2016; Nurhayati et al., 2021**).

We calculated Spearman rank correlation coefficients R_s for the time series of the number of peatland fires, SOI, precipitation anomalies, and air temperature anomalies, confined to the peatland areas of Kalimantan (**Figure 1**). With a 99% confidence level,



the annual number of peatland fires shows significant and strong correlations with the anomalies of precipitation ($R_S = -0.92$), air temperature ($R_S = 0.88$), and SOI values ($R_S = -0.67$), respectively.

Annual averages of the Southern Oscillation Index for our 21-year study period are shown in **Figure 3C**. The negative SOI values are associated with El Niño conditions which lead to changes in large-scale transport of atmospheric moisture in the tropics coupled with intensified dry seasons in our study area. This is noticeable for the period from 2001 through 2006 and 2013 through 2016, for instance, during which also increased numbers of peatland fires were counted across Kalimantan's peatland areas according to the MODIS hotspot data (**Figure 3A**).

This dependence of the number of peatland fires on the SOI also persists during short-term fluctuations in 2002, 2009, and 2016 when drops in the SOI concurred with increasing numbers of peatland fires compared to adjacent years (**Figures 3A, C**).

3.2 Regional trends in peatland fire burn severity

A total of 13,307 peatland fire events with high resolution pre-fire and post-fire surface reflectance data layers captured within 90 days before and after each analyzed fire event were available for our burn severity analyses. We applied a burn severity classification system developed using ground validated assessments of fire damage to the vegetation in combination with satellite imagery based $dNBR$ values in Central Kalimantan to the high-resolution surface reflectance data following **Hoscilo et al. (2013)**. The $dNBR$

classification shows high correlations with corresponding pre-fire and post-fire ground measurements of vegetation parameters such as total woody aboveground biomass, tree density, and numbers of small trees in the affected areas. To increase the bin resolution for higher burn severities, we refined the classification by further separating the “moderate” and “high severity” classes according to **Hoscilo et al. (2013)**, into “moderate,” “high,” and “very high” severity classes using the European Forest Fire Information Service (EFFIS) $dNBR$ classification (e.g., **Liu et al., 2022**) for the higher burn severity classes.

The classification system (**Table 1**) also matches the partitioning of our overall distribution of $dNBR$ pixels frequencies (N) calculated across all fires captured in the 21-year period (**Figure 4**).

Many of the peatland fires were ignited to clear the area for establishment of crops such as oil palm plantations or rice fields. Because we applied a constrained window of 90 days after (or before) a fire, the number of $dNBR$ pixel values potentially affected by post-fire reflectance of already growing crops is kept small but cannot completely be avoided in cases where an increased time interval has to be applied to capture the same area before and after a fire. In order to avoid misinterpretation of altered reflectance spectra caused by anthropogenic LULC change after a fire, we did not include an extra ‘enhanced regrowth’ class for negative $dNBR$ pixels as our analyses focus on the fire damage to the natural peatland vegetation.

To assess long-term changes in fire severity in Kalimantan's peatlands, we aggregated the high-resolution satellite data into three equal periods of 7 years (2001–2007, 2008–2014, and

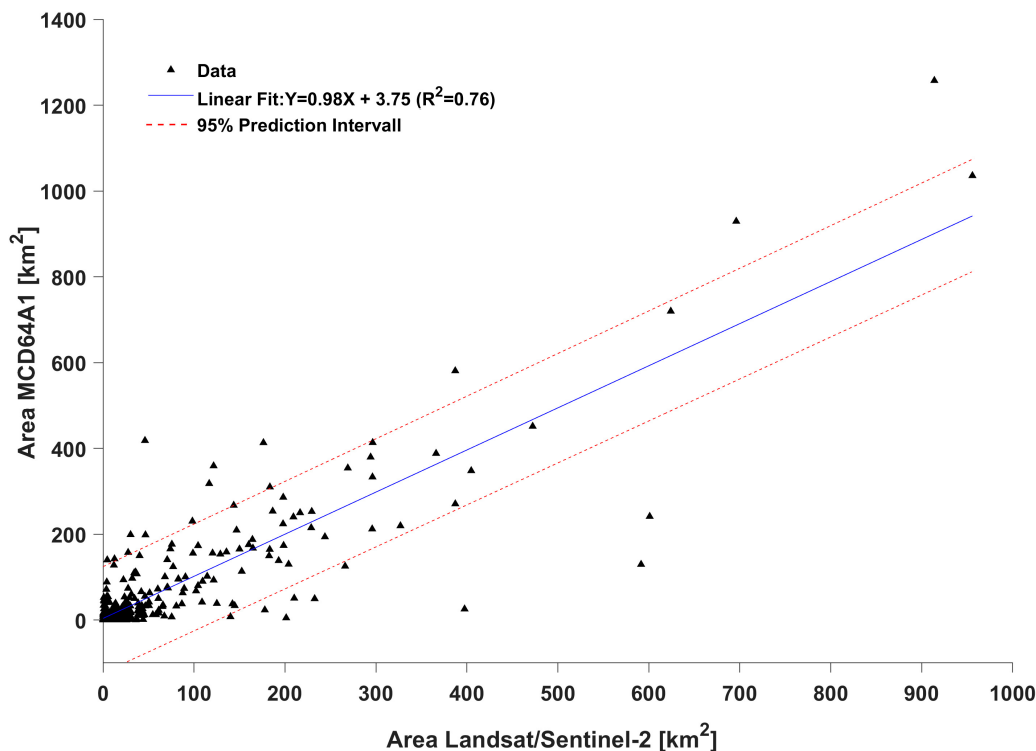


FIGURE 6

Comparison of monthly and annually accumulated burned peatland area of the MODIS MCD64A1 data for the 49 districts and the corresponding area values from high resolution satellite imagery, including the 95% prediction interval based on the regression model.

2015–2021). The selected length of the periods assures that different meteorological conditions with above and below average precipitation and air temperatures are captured within each period (Figure 2). Due to an increasing number of satellite missions and an increasing amount of available imagery over the 21-years, the number of available satellite scenes varies over the 7-year data periods. Therefore, period-specific relative frequencies of burn severity values were calculated to account for changing total numbers that are solely based on an increasing imagery data pool for the later years of our study period.

Figure 5 shows the resulting multi-year histograms of burn-severity, integrated over all peatland fires in Kalimantan with pre- and post-fire high-resolution surface reflectance imagery within each 7-year interval. The fraction of areas with low severity fire damage remains relatively stable with an average of 23.0% ($\sigma = 0.32\%$) across all periods. The portion of pixels with moderate burn damages fluctuates comparatively with $\sigma = 3.5\%$ and percentage values between 11 and 17% (Figure 5).

However, a strong relative increase of the “high” and “very high” severity class allocations is noticeable for the latest period (January 2015 through December 2021) in the *dNBR* frequency distribution (Figure 5C) compared to the two previous 7-year intervals (Figures 5A, B).

The number of pixels with high severity burn damages across all peatland fires in Kalimantan increased by 12.1 and 13.4% compared to the 2001–2007 period and 2008–2014 period, respectively.

While only negligible areas were classified as “very high severity” during the first two periods, 5.5% of burned pixels showed very high severity damage during the 2015–2021 period.

Surface reflectance spectra alone cannot explain why fires result in more severe burn damage. Nevertheless, the highest severity class is nearly unoccupied during the first two 7-year periods (<1%) whereas a noticeable increase in the “highest severity” class is observed for the later periods. The consistent and significant changes in high severity and highest severity burns over time indicate an overall change in the severity of fire damage to the peat vegetation in more recent years. The latest period (Figure 5C) also includes the two extreme years of 2015 and 2019 with large numbers of peatland fires and strongly developed El Niño conditions (Figure 3). Moreover, both extreme years were characterized by persisting dry conditions starting the previous year which led to exceptionally dry fuel beds that in turn increase fire intensity and burn severity (e.g., Davies et al., 2016; Hantson et al., 2017).

3.3 Assessment of burned peatland area over time

Monthly aggregated MCD64A1 burned area grid maps (Ver 6.1, section “2.2 Moderate resolution thermal anomalies”) were applied as long-term data suitable for tracking temporal patterns and relative changes of burned peatland area in Kalimantan. Only grid cell values with a quality flag indicating sufficient valid data in the reflectance time series for the grid cell to be processed were used for the analyses. Using the available spatial resolution of 500 m × 500 m, we classified the corresponding pixel area as

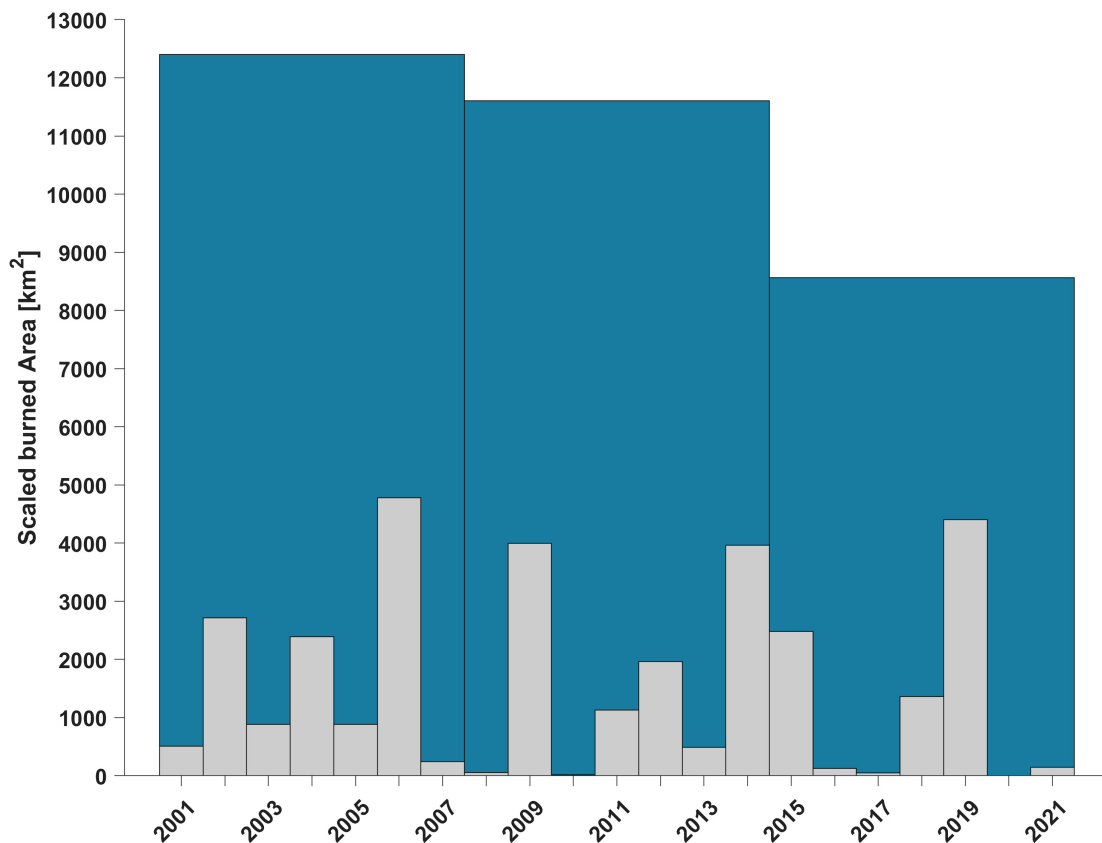


FIGURE 7

Corrected annual and 7-year accumulated burned area values integrated over all peatland areas of Kalimantan.

burned and integrated the areas over each year covering all peatland areas in Kalimantan.

Like all satellite imagery, the MODIS dataset is affected by inherent commission and omission errors and furthermore is affected by its moderate spatial resolution which limits the ability to accurately resolve the area of smaller fires. Hence, to capitalize on the long-term availability and consistency of the MODIS data while accounting for its limited resolution, we used 30 m high resolution imagery to scale MODIS derived long-term values of burned area (Vetrita et al., 2021).

We manually delineated burned areas using LANDSAT8 and Sentinel-2 imagery from 2015 through 2021 capturing the total burned area for 49 districts and cities in Kalimantan (Figure 1). To correct the long-term data for the annual total burned area for Kalimantan, we conducted a linear regression analysis (Roy et al., 2019; Vetrita et al., 2021) comparing annual district-specific sums of MODIS burned area and the corresponding burned area sums, manually delineated using high-resolution imagery from LANDSAT8 and Sentinel-2, for each district.

To account for district-year combinations with delineated monthly burned areas missing and to cover different temporal scales for the comparison, we included monthly and annual sums of delineated burned area values and corresponding MCD64A1 sums for the regression (Figure 6).

District-specific sums of burned areas smaller than 0.25 km² (monthly or annual sums) were removed to account for the

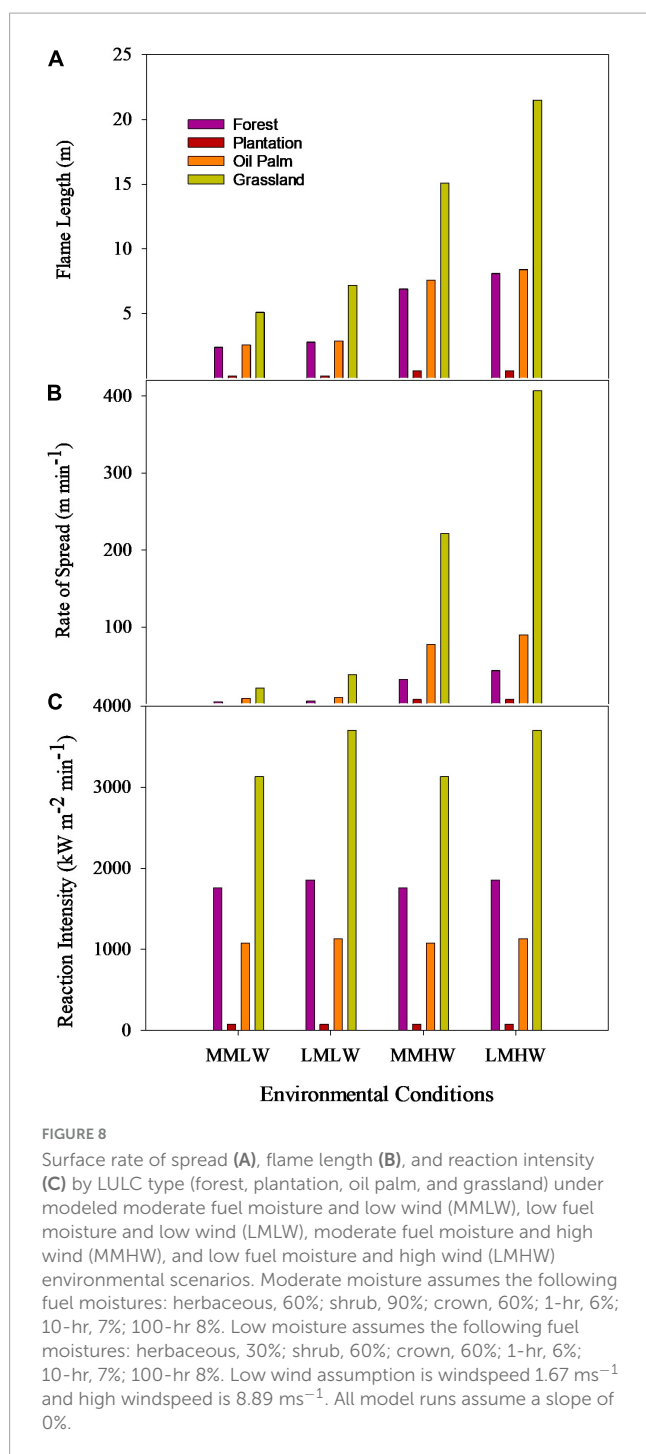
resolution limit of the MODIS data which cannot distinguish areas smaller than 0.25 km².

The annual MODIS MCD64A1 burned area sums were then scaled using the slope and intercept of the linear regression function leading to a corrected burned area assessment over time (Figure 7). Using the regression equation, the burned area totals increased by 1.8% on average, compared to the original MCD64A1 data.

While the portion of high and very high severity burns increased over time (Figure 5), the total area burned decreased over time. The average corrected burned area between 2015 and 2021 was 31 and 26% lower than the previous 7-year averages from 2001 to 2007 and 2008 to 2014, respectively, (Figure 7). With respect to the burned area totals, the results agree with the finding that 12% of the areas in our study region were burned twice over the last two decades, with about 23% of the areas burned more than twice (Vetrita and Cochrane, 2020), dominated by smaller fires intentionally ignited for agricultural conversion.

The annual pattern of the amount of burned peatland area follows the patterns of the annual numbers of fires observed per year (Figures 3A, 6), with exception of the period from 2014 to 2015, where despite an increase of the total number of peatland fires in 2015 compared to the previous year (Figure 3A), the total peatland area burned as captured by the MCD14DL record, decreased in 2015 compared to 2014 (Figure 6).

Potential explanations for the temporal patterns in burn severity and number of fires or total area burned are combinations of climate factors and the effect of the regulatory framework. With



the 7-year periods smoothing out the effects of single years, the 7-year patterns indicate that the climate factors, mostly driven by long-term and large-scale atmospheric circulations, led to increased burn severities. On the other hand, the burned area integrated over the 7-year sections was reduced due to restrictions on the clearing of peatland through burning as imposed by the legislature through changes in environmental laws over time, driven particularly by the 2015 fire season in Kalimantan with the highest number of peatland fires on record (Figure 2). In addition, the very low area of burned peatland during the year 2020 might also be caused at least in part by the COVID-19

pandemic that temporally limited agricultural activities in the region (Gregorio and Ancog, 2020) in combination with the climatic effect of a triple La Niña series in Southeast Asia from 2020-2022 which caused persisting wet conditions that likely contributed to the decline in wildfires in 2021-2022, a phenomenon that had previously occurred from 1973-1975 and 1998-2001, respectively, (e.g., Tangang et al., 2017). The comparisons of the long-term patterns of peatland fire counts, SOI, and meteorological parameters that determine the fire regime confirm the strong effect of large-scale atmospheric circulations and regional meteorological conditions on peatland fire occurrences in Kalimantan over the last two decades.

3.4 Modeled fire intensity

The model results show that flame lengths were low under moderate moisture and low wind conditions but increased substantially in high wind and low fuel moisture scenarios (Figure 8A). Flame lengths were highest in dense early successional grasslands, reaching up to 21.5 m under high wind, low fuel moisture scenarios. Modeled surface flame lengths were higher in oil palm than in the forests that they replace, where low-hanging fronds and stringy bark readily ignite and contribute to the active flaming front (Figure 9), resulting in flame lengths ranging from 2.6 to 8.4 m. Lower flame lengths in forests and plantations were reflective of the lower statured shrubby vegetation that carried the surface fire. As plantations had very little vegetation under the tree canopy, there was sparse fuel to carry surface fire for any moisture or wind scenario.

Oil palm (8.9 m min⁻¹ at low wind and up to 89.8 m min⁻¹ in high wind, low fuel moisture scenarios) and grasslands (38.3 m min⁻¹ at low wind and 406.9 m min⁻¹ in high wind, low moisture) had greatly increased rates of spread (Figure 8B), relative to the primary forests (4.3 m min⁻¹ at low wind and 43.6 m min⁻¹ in high wind, low moisture) that they replaced. In contrast, timber plantations, consisting primarily of *Eucalyptus* and *Acacia* species, had very low rates of modeled surface fire spread (1.1–6.1 m min⁻¹), as there is little fuel under the tree canopies to carry surface fire. Fuel moisture was an important driver of rates of fire spread in all LULC categories except plantations, with modeled fires at low moisture scenarios 16–84% faster than fires at moderate moisture scenarios, with most pronounced differences in the highly flammable grassland LULC type.

Reaction intensity, a measure of the heat per unit area of the flaming front of a surface fire, is dependent on the density of flammable vegetation in each fuel type. Reaction intensities were highest in grassland LULC types, where dense litter accumulates under the live herbaceous vegetation (Figure 9). Dense forest vegetation, with a complex, layered vegetation structure, large, downed wood, and deep peat layers, also had high reaction intensities (Figure 8C). As plantations are a greatly simplified fuel arrangement, containing primarily merchantable timber species without a lot of natural understory vegetation, there was little surface fuel and greatly reduced reaction intensity. Oil palm fields were structurally simplified relative to forests, with less burnable material on the soil surface, and were intermediate in modeled reaction intensities.



FIGURE 9

Photos of field sites (A) forest, (B) plantation, (C) oil palm, and (D) early successional grassland from which fuel models were developed and fire behavior interpreted in Kalimantan, Indonesia.

Overall, the model results confirm the superimposed influence of meteorological conditions and indicate the significant effects of LULC on fire behavior by showing that simulated conversions greatly affect surface fire intensity metrics (rate of spread, flame length, and reaction intensity).

3.5 Timeline of the regulatory framework for peatland fires

The results show that climate conditions had a strong effect on the number of peatland fires in Kalimantan during the last two decades. Due to the strong correlations between driving climatological and meteorological conditions, superimposed effects of regulatory restrictions that restrict the burning of natural peatland for agricultural purposes are inherently difficult to quantify.

Due to intense fire seasons and associated effects on the environment and public health (e.g., [Kiely et al., 2021](#); [Hein et al., 2022](#)), the laws pertaining to the protection of natural peatlands including burn restrictions in Kalimantan changed over time. Following the wildfire season of 1997–1998 when 1,10,000 km² of peatland were burned in Indonesia, and in recognition of the increased risk of wildfire in a warming climate,

the Government of Indonesia established the Directorate of Forest Fire Control (renamed in 2016 to Directorate of Land and Forest Fire Management) under the Ministry of Forestry in 2000.

Current policies on forest and fire management consist of three main activities, fire prevention, suppression, and post-fire recovery. Under these regulations, people are forbidden by law to intentionally burn large areas of land for clearing or agriculture, though there are at times exceptions and inconsistencies between central and provincial regulations.

In 2006, the Indonesian government allowed burning under certain conditions for farmers in Central Kalimantan, but larger scale ignitions of peatland for land clearing remained prohibited for large oil palm plantations in this region. The reduction of burns after 2006 as well as the tempering of the restrictions in 2008, can clearly be tracked in the burn frequency numbers derived from MODIS hotspot observations across Kalimantan ([Figure 3A](#)).

After the extreme fire season of 2015, the government reinstated a complete restriction of prescribed peatland fires for the gain of agricultural land. There has been slow progress in reducing anthropogenic forest and land fire occurrence in Indonesia in the last two decades ([Purnomo et al., 2017](#)). Currently, the Government of Indonesia focuses on fire prevention rather than suppression, using integrated fire prevention patrol, land clearing without burning practices, improving community livelihood, or canal blocking and forest restoration in degraded peatlands,

and improving fire early warning system such as SPARTAN (Sistem Peringatan Kebakaran Hutan dan Lahan). The Indonesian government also established the Peatland Restoration Agency (Badan Restorasi Gambut, BRG) in January 2016 and stipulated a permanent peatland and primary forest conversion moratorium for business permits in August 2019 to address land and fire issues and strengthen Indonesia's commitment to slowing deforestation on peatlands. Later in 2020, BRG was transformed into the Mangrove and Peatland Restoration Agency (Badan Restorasi Gambut dan Mangrove-BRGM) with the purpose of restoring 1.2 million ha of peatlands and 600 thousand ha of mangrove across 13 provinces.

Furthermore, Law No 32/2009, concerning Environmental Protection and Management particularly in Article 69, prohibits clearing of land by burning for every entity. However, as an exception, small, prescribed fires (maximum 2 ha) are allowed in peatland vegetation and categorized as local wisdom practices, as local understanding uses controlled burning to reduce the risk of large wildfires in fire weather with strong or gusty winds and dry fuel conditions.

4 Conclusion

We examined long-term patterns of frequencies, and severities of peatland fires in Kalimantan using medium-resolution and high-resolution satellite imagery over a period of 21 years. Moreover, fire intensity parameters were modeled with regard to conversion from forest to agricultural land uses as has been done for decades in the study region of Kalimantan, Indonesia.

Variations in the number of fires and burn severity are visible over time and are caused by a combination of large-scale meteorological patterns and changing regulations. Our results confirm a strong spatiotemporal correlation between climatological drivers and corresponding peatland fire frequency and burned area, based on noticeable concurrences with spatially and temporally well-defined El Niño-related meteorological extremes. Steep increases of the number of peatland fires were found to be tightly connected to increased air temperature values and reduced precipitation in our study region over the 21-year study period from the beginning of 2001 through the end of 2021.

The results further show a steady, regionally comprehensive increase of burn severity of peatland fires in Kalimantan by 12.8% on average for the latest period from 2015 through 2021 compared to earlier periods of the same length, whereas the total peatland area burned decreased between 2015 and 2021 by 28.7% on average compared to the previous 7-year periods. Our fire model results show an increased fire intensity (elevated flame lengths and rates of spread) for grassland and oil-palm plantations compared to forest stands prior to the LULC conversion. Thus, beyond the release of large amounts of carbon stored above ground and below ground in peatland and the loss of unique tropical ecosystems when peatland is converted to arable land, the decreased fire resilience of degraded peatland and increased proneness to fire of converted areas exacerbates the impacts of a changing climate in this region with increasingly extreme conditions during recurring El Niño periods with higher temperatures and low amounts of precipitation.

As the national Indonesian government holds the highest role as regulator but has little oversight for enforcement, it will be critical for local government to support and uphold policy.

Hence, recommendations for better peatland fire management are (1) more focus on fire prevention activities, (2) alignment and harmonization of government regulations at the national and regional levels, (3) improve availability and accessibility of sufficient funding for pre-fire mitigation, suppression, and post-fire recovery efforts on regional and local scales. Our results show that LULC, regulatory frameworks, and meteorological conditions often driven by larger scale climate patterns all affect the frequency and severity of peatland fires across scales. The ongoing alteration of burn frequencies and severities shown in this study needs to be reassessed frequently while considering ongoing LULC, evolving adaptations of regulations, and a changing climate. Therefore, future studies need to use comprehensive approaches that incorporate the physical aspects of overarching climate conditions as well as political and regulatory frameworks to assess negative effects of burning tropical peatlands. Ultimately, research results can support decision making that leads to a further reduction of tropical peatland burning in Kalimantan.

Data availability statement

Publicly available datasets were analyzed in this study. This data can be found here: <https://www.ecmwf.int/>.

Author contributions

AS: remote sensing analyses, climate data analyses, and writing and editing of manuscript. LE: fire modeling and writing and editing of manuscript. GB: support of fire modeling. NN: writing and editing of manuscript and analyses of political framework data. AM, AG, and AD: writing and editing of manuscript. IA: writing and editing of manuscript and political framework analyses. RP: GIS data preparation and editing of manuscript. AA: editing of manuscript. JK: support of fire modeling and editing of manuscript. All authors contributed to the article and approved the submitted version.

Acknowledgments

We would like to thank the European Centre for Medium-Range Weather Forecasts, the European Space Agency, the National Aeronautics and Space Administration, and the United States Geological Survey for providing essential research products and making the data accessible for the scientific community through their public data repositories. This research was funded through the Bezos Earth Fund under The Nature Conservancy's Applied Science to Catalyze Natural Climate Solutions project.

Conflict of interest

The authors declare that the research was conducted in the absence of any commercial or financial relationships that could be construed as a potential conflict of interest.

Publisher's note

All claims expressed in this article are solely those of the authors and do not necessarily represent those of their affiliated

organizations, or those of the publisher, the editors and the reviewers. Any product that may be evaluated in this article, or claim that may be made by its manufacturer, is not guaranteed or endorsed by the publisher.

Supplementary material

The Supplementary Material for this article can be found online at: <https://www.frontiersin.org/articles/10.3389/ffgc.2024.1221797/full#supplementary-material>

References

- Ager, A., Vaillant, N., and Finney, M. (2011). Integrating fire behavior models and geospatial analysis for wildland fire risk assessment and fuel management planning. *J. Combust.* 2011:572452. doi: 10.1155/2011/572452
- Albar, I., Jaya, I., Saharjo, B., Kuncayho, B., and Vadrevu, K. (2018). "Spatio-temporal analysis of land and forest fires in Indonesia using MODIS active fire dataset," in *Land-atmospheric research applications in south and Southeast Asia*, eds K. Vadrevu, T. Ohara, and C. Justice (Cham: Springer). doi: 10.1007/978-3-319-67474-2_6
- Alsepan, G., and Minobe, S. (2020). Relations between interannual variability of regional-scale Indonesian precipitation and large-scale climate modes during 1960–2007. *J. Clim.* 33, 5271–5291. doi: 10.1175/JCLI-D-19-0811.1
- Anda, M., Ritung, S., Suryani, E., Sukarman, Hikmat, M., Yatno, E., et al. (2021). Revisiting tropical peatlands in Indonesia: Semi-detailed mapping, extent and depth distribution assessment. *Geoderma* 402:115235. doi: 10.1016/j.geoderma.2021.115235
- Basuki, I. (2017). *Carbon dynamics in response to land cover change in tropical Peatlands, Kalimantan, Indonesia*. Corvallis, OR: Oregon State University.
- Boschetti, L., Roy, D., Giglio, L., Huang, H., Zubkova, M., and Humber, M. (2019). Global validation of the collection 6 MODIS burned area product. *Remote Sens. Environ.* 235:111490. doi: 10.1016/j.rse.2019.111490
- Brewer, C., Winne, J., Redmond, R., Opitz, D., and Mangrich, M. (2005). Classifying and mapping wildfire severity: A comparison of methods. *Photogramm. Eng. Remote Sens.* 71, 1311–1320.
- Brose, P., and Wade, D. (2002). Potential fire behavior in pine flatwood forests following three different fuel reduction techniques. *For. Ecol. Manag.* 163, 71–84. doi: 10.1016/S0378-1127(01)00528-X
- Byram, G. (1959). "Combustion of forest fuels," in *Forest fire control and use*, 2nd Edn, eds A. A. Brown and K. P. Davis (New York, NY: McGraw-Hill), 686.
- Chander, G., and Markham, B. (2003). Revised landsat-5 TM radiometric calibration procedures and postcalibration dynamic ranges. *IEEE Trans. Geosci. Remote Sens.* 41, 2674–2677. doi: 10.1109/TGRS.2003.818464
- Chen, C., Lin, H., Yu, J., and Lo, M. (2016). The 2015 Borneo fires: What have we learned from the 1997 and 2006 El Niños? *Environ. Res. Lett.* 11:104003. doi: 10.1088/1748-9326/11/10/104003
- Claverie, M., Ju, J., Masek, J., Dungan, J., Vermote, E., Roger, J., et al. (2018). The Harmonized landsat and sentinel-2 surface reflectance data set. *Remote Sens. Environ.* 219, 145–161. doi: 10.1016/j.rse.2018.09.002
- Cocke, A., Fulé, P., and Crouse, J. (2005). Comparison of burn severity assessments using differenced normalized burn ratio and ground data. *Int. J. Wildland Fire* 14, 189–198. doi: 10.1071/WF04010
- Davies, G., Domènech, R., Gray, A., and Johnson, P. (2016). Vegetation structure and fire weather influence variation in burn severity and fuel consumption during peatland wildfires. *Biogeosciences* 13, 389–398. doi: 10.5194/bg-13-389-2016
- Edwards, R., Naylor, R., Higgins, M., and Falcon, W. (2020). Causes of Indonesia's forest fires. *World Dev.* 127:104717. doi: 10.1016/j.worlddev.2019.104717
- Evans, E., Ellsworth, L., and Litton, C. (2015). Impact of grazing on fine fuels and potential wildfire behaviour in a non-native tropical grassland. *Pac. Conserv. Biol.* 21, 126–132. doi: 10.1071/PC14910
- Gascon, F., Cadau, E., Colin, O., Hoersch, B., Isola, C., Fernández, B., et al. (2014). Copernicus sentinel-2 mission: Products, algorithms and Cal/Val. *Earth Observ. Syst.* 9218:92181E. doi: 10.1117/12.2062260
- Gaveau, D., Descals, A., Salim, M., Sheil, D., and Sloan, S. (2021). Refined burned-area mapping protocol using sentinel-2 data increases estimate of 2019 Indonesian burning. *Earth Syst. Sci. Data* 13, 5353–5368. doi: 10.5194/essd-13-5353-2021
- Giglio, L., Boschetti, L., Roy, D., Humber, M., and Justice, C. (2018). The collection 6 MODIS burned area mapping algorithm and product. *Remote Sens. Environ.* 217, 72–85. doi: 10.1016/j.rse.2018.08.005
- Giglio, L., Schroeder, W., and Justice, C. (2016). The collection 6 MODIS active fire detection algorithm and fire products. *Remote Sens. Environ.* 178, 31–41. doi: 10.1016/j.rse.2016.02.054
- Goldstein, J., Graham, L., Ansori, S., Vetruta, Y., Thomas, A., Applegate, G., et al. (2020). Beyond slash-and-burn: The roles of human activities, altered hydrology and fuels in peat fires in Central Kalimantan, Indonesia. *Singap. J. Trop. Geogr.* 41, 190–208. doi: 10.1111/sjtg.12319
- Gregoria, G., and Ancog, R. (2020). Assessing the impact of the COVID-19 pandemic on agricultural production in Southeast Asia: Toward transformative change in agricultural food systems. *Asian J. Agric. Dev.* 17, 1–13. doi: 10.22004/ag.econ.30378
- Hantson, S., Scheffer, M., Pueyo, S., Xu, C., Lasslop, G., van Nes, E., et al. (2017). Rare, intense, big fires dominate the global tropics under drier conditions. *Sci. Rep.* 7:14374. doi: 10.1038/s41598-017-14654-9
- Hein, L., Spadaro, J., Ostro, B., Hammer, M., Sumarga, E., Salmayenti, R., et al. (2022). The health impacts of Indonesian Peatland fires. *Environ. Health* 21:62. doi: 10.1186/s12940-022-00872-w
- Heinisch, F., and Andrews, P. (2010). *BehavePlus fire modeling system, version 5.0: Design and features*. Fort Collins, CO: U.S. Department of Agriculture, Forest Service, Rocky Mountain Research Station, 111.
- Heymann, J., Reuter, M., Buchwitz, M., Schneising, O., Bovensmann, H., Burrows, J., et al. (2017). CO₂ emission of Indonesian fires in 2015 estimated from satellite-derived atmospheric CO₂ concentrations. *Geophys. Res. Lett.* 44, 1537–1544. doi: 10.1002/2016GL072042
- Hoscilo, A., Tansey, K., and Page, S. (2013). Post-fire vegetation response as a proxy to quantify the magnitude of burn severity in tropical peatland. *Int. J. Remote Sens.* 34, 412–433. doi: 10.1080/01431161.2012.709328
- Indonesia Ministry of Environment and Forestry [MoEF] (2020). *Annual land cover map from 2009–2019*. Jakarta: Indonesia Ministry of Environment and Forestry [MoEF].
- Irons, J., Dwyer, J., and Barsi, J. (2012). The next landsat satellite: The landsat data continuity mission. *Remote Sens. Environ.* 122, 11–21. doi: 10.1016/j.rse.2011.08.026
- Johnston, J., Olszewski, J., Miller, B., Schmidt, M., Vernon, M., and Ellsworth, L. (2021). Mechanical thinning without prescribed fire moderates wildfire behavior in an Eastern Oregon, USA ponderosa pine forest. *For. Ecol. Manag.* 501:119674. doi: 10.1016/j.foreco.2021.119674
- Keeley, J. (2009). Fire intensity, fire severity and burn severity: A brief review and suggested usage. *Int. J. Wildland Fire* 18, 116–126. doi: 10.1071/WF07049
- Kiely, L., Spracklen, D., Arnold, S., Papargyropoulou, E., Conibear, L., Wiedinmyer, C., et al. (2021). Assessing costs of Indonesian fires and the benefits of restoring Peatland. *Nat. Commun.* 12:7044. doi: 10.1038/s41467-021-27353-x
- Lamquin, N., Woolliams, E., Bruniquel, V., Gascon, F., Gorroño, J., Govaerts, Y., et al. (2019). An inter-comparison exercise of Sentinel-2 radiometric validations assessed by independent expert groups. *Remote Sens. Environ.* 233:111369. doi: 10.1016/j.rse.2019.111369
- Lasslop, G., Coppola, A., Voulgarakis, A., Yue, C., and Veraverbeke, S. (2019). Influence of fire on the carbon cycle and climate. *Curr. Clim. Chang. Rep.* 5, 112–123. doi: 10.1007/s40641-019-00128-9

- Law, E., Bryan, B., Meijaard, E., Mallawaarachchi, T., Struebig, M., and Wilson, K. (2015). Ecosystem services from a degraded peatland of Central Kalimantan: Implications for policy, planning, and management. *Ecol. Appl.* 25, 70–87. doi: 10.1890/13-2014.1
- Liu, Q., Fu, B., Chen, Z., Chen, L., Liu, L., Peng, W., et al. (2022). Evaluating effects of post-fire climate and burn severity on the early-term regeneration of forest and shrub communities in the san Gabriel mountains of California from sentinel-2(MSI) images. *Forests* 13:1060. doi: 10.3390/f13071060
- Marlier, M., DeFries, R., Kim, P., Koplitz, S., Jacob, D., Mickley, L., et al. (2015). Fire emissions and regional air quality impacts from fires in oil palm, timber, and logging concessions in Indonesia. *Environ. Res. Lett.* 10:085005. doi: 10.1088/1748-9326/10/8/085005
- Micijevic, E., Haque, O., Barsi, J., Anderson, C., Markham, B., and Rengarajan, R. (2020). Landsat collection 2 radiometric calibration updates. *Earth Observ. Syst. XXV*:115010. doi: 10.1117/12.2570026
- Miettinen, J., Shi, C., and Liew, S. (2012). Two decades of destruction in Southeast Asia's peat swamp forests. *Front. Ecol. Environ.* 10:124–128. doi: 10.1890/10.0236
- Miettinen, J., Shi, C., and Liew, S. (2016). Land cover distribution in the Peatlands of Peninsular Malaysia, Sumatra and Borneo in 2015 with changes since 1990. *Glob. Ecol. Conserv.* 6, 67–78. doi: 10.1016/j.gecco.2016.02.004
- Miettinen, J., Shi, C., and Liew, S. (2017). Fire distribution in Peninsular Malaysia, Sumatra and Borneo in 2015 with special emphasis on Peatland fires. *Environ. Manag.* 60, 747–757. doi: 10.1007/s00267-017-0911-7
- Miller, J., and Yool, S. (2002). Mapping forest post-fire canopy consumption in several overstory types using multi-temporal landsat TM and ETM data. *Remote Sens. Environ.* 82, 481–496. doi: 10.1016/S0034-4257(02)00071-8
- Muñoz-Sabater, J. (2019). ERA5-land monthly averaged data from 1981 to present, Copernicus climate change service (C3S) climate data store (CDS). doi: 10.24381/cds.68d2bb30
- Muñoz-Sabater, J., Dutra, E., Agustí-Panareda, A., Albergel, C., Arduini, G., Balsamo, G., et al. (2021). ERA5-Land: A state-of-the-art global reanalysis dataset for land applications. *Earth Syst. Sci. Data* 13, 4349–4383. doi: 10.5194/essd-13-4349-2021
- Novita, N. (2016). *Carbon stocks and soil greenhouse gas emissions associated with forest conversion to oil palm plantations in Tanjung Puting tropical Peatlands, Indonesia*. Corvallis, OR: Oregon State University.
- Novita, N., Kauffman, J., Hergoualc'h, K., Murdiyasar, D., Tryanto, D., and Jupesta, J. (2021). "Carbon stocks from peat swamp forest and oil palm plantation in central Kalimantan, Indonesia," in *Climate change research, policy and actions in Indonesia*, eds R. Djalante, J. Jupesta, and E. Aldrian (Cham: Springer). doi: 10.1007/978-3-030-55536-8_10
- Nurhayati, A., Saharjo, B., Sundawati, L., Syartinilia, and Cochrane, M. (2021). Forest and Peatland fire dynamics in south Sumatra province. *For. Soc.* 5, 591–603. doi: 10.24259/fs.v5i2.14435
- Osaki, M., Setiadi, B., Takahashi, H., and Evri, M. (2016). "Peatland in Kalimantan," in *Tropical Peatland ecosystems*, eds M. Osaki and N. Tsuji (Tokyo: Springer). doi: 10.1007/978-4-431-55681-7_6
- Page, S., Rieley, J., and Banks, C. (2011). Global and regional importance of the tropical peatland carbon pool. *Glob. Chang. Biol.* 17, 798–818. doi: 10.1111/j.1365-2486.2010.02279.x
- Parks, S., Holsinger, L., Voss, M., Loehman, R., and Robinson, N. (2018). Mean composite fire severity metrics computed with Google earth engine offer improved accuracy and expanded mapping potential. *Remote Sens.* 10:879. doi: 10.3390/rs10060879
- Parsons, R., Pimont, F., Wells, L., Cohn, G., Jolly, W., de Coligny, F., et al. (2018). Modeling thinning effects on fire behavior with STANDFIRE. *Ann. For. Sci.* 75, 1–10. doi: 10.1007/s13595-017-0686-2
- Pinto, C., Cibele Jing, X., and Leigh, L. (2020). evaluation analysis of landsat level-1 and level-2 data products using in situ measurements. *Remote Sens.* 12:2597. doi: 10.3390/rs12162597
- Prichard, S., Sandberg, D., Ottmar, R., Eberhardt, E., Andreu, A., Eagle, P., et al. (2013). *Fuel characteristic classification system version 3.0: Technical documentation*. Portland, OR: U.S. Department of Agriculture, Forest Service, 79. doi: 10.2737/PNW-GTR-887
- Purnomo, H., Shantiko, B., Sitorus, S., Gunawan, H., Achdiawan, R., Kartodihardjo, H., et al. (2017). Fire economy and actor network of forest and land fires in Indonesia. *For. Policy Econ.* 78, 21–31. doi: 10.1016/j.forpol.2017.01.001
- Quintano, C., Fernández-Manso, A., and Fernández-Manso, O. (2018). Combination of Landsat and Sentinel-2 MSI data for initial assessing of burn severity. *Int. J. Appl. Earth Observ. Geoinf.* 64, 221–225. doi: 10.1016/j.jag.2017.09.014
- Ramdani, F., and Hino, M. (2013). Land use changes and GHG emissions from tropical forest conversion by oil palm plantations in Riau Province, Indonesia. *PLoS One* 8:e70323. doi: 10.1371/journal.pone.0070323
- Reuter, D., Irons, J., Lunsford, A., Montanaro, M., Pellerano, F., Richardson, C., et al. (2011). The operational land imager (OLI) and the thermal infrared sensor (TIRS) on the landsat data continuity mission (LDCM). *Proc. SPIE XVII*:804812. doi: 10.1117/12.885963
- Reuter, D., Richardson, C., Pellerano, F., Irons, J., Allen, R., Anderson, M., et al. (2015). The thermal infrared sensor (TIRS) on landsat 8: Design overview and pre-launch characterization. *Remote Sens.* 7, 1135–1153. doi: 10.3390/rs70101135
- Ribeiro, K., Pacheco, F. S., Ferreira, J. W., Sousa-Neto, E. R., Hastie, A., Filho, G. K., et al. (2021). Tropical peatlands and their contribution to the global carbon cycle and climate change. *Glob. Chang. Biol.* 27, 489–505. doi: 10.1111/gcb.15408
- Rothermel, R. (1972). *A mathematical model for predicting fire spread in wildland fuels*. Ogden, UT: U.S. Department of Agriculture, Forest Service, 40.
- Roy, D., Huang, H., Boschetti, L., Giglio, L., Yan, L., Zhang, H., et al. (2019). Landsat-8 and Sentinel-2 burned area mapping – A combined sensor multitemporal change detection approach. *Remote Sens. Environ.* 231:111254. doi: 10.1016/j.rse.2019.111254
- Sabani, W., Rahmadewi, D., Rahmi, K., Priyatna, M., and Kurniawan, E. (2019). Utilization of MODIS data to analyze the forest/land fires frequency and distribution (case study: Central Kalimantan province). *IOP Conf. Ser. Earth Environ. Sci.* 243:012032. doi: 10.1088/1755-1315/243/1/012032
- Sandberg, D., Riccardi, C., and Schaaf, M. (2008). Reformulation of Rothermel's wildland fire behavior model for heterogeneous fuelbeds. *Can. J. For. Res.* 37, 2438–2455. doi: 10.1139/X07-094
- Schmidt, A., Leavell, D., Panches, J., Rocha Ibarra, M., Kagan, J., Creutzburg, M., et al. (2022). A quantitative wildfire risk assessment using a modular approach of geostatistical clustering and regionally distinct valuations of assets—A case study in Oregon. *PLoS One* 17:e0264826. doi: 10.1371/journal.pone.0264826
- Scott, J., and Burgan, R. (2005). *Standard fire behavior fuel models: a comprehensive set for use with Rothermel's surface fire spread model*. Fort Collins, CO: U.S. Department of Agriculture, Forest Service, Rocky Mountain Research Station, 72.
- Silvianingsih, Y., Hairiah, K., Suprayogo, D., and van Noordwijk, M. (2020). Agroforests, swiddening and livelihoods between restored peat domes and river: Effects of the 2015 fire ban in central Kalimantan (Indonesia). *Int. For. Rev.* 22, 382–396. doi: 10.1505/146554820830405645
- Sudmanns, M., Tiede, D., Augustin, H., and Lang, S. (2019). Assessing global Sentinel-2 coverage dynamics and data availability for operational earth observation (EO) applications using the EO-compass. *Int. J. Digit. Earth* 13, 768–784. doi: 10.1080/17538947.2019.1572799
- Sulaiman, A., Osaki, M., Takahashi, H., Yamanaka, M. D., Susanto, R. D., Shimada, S., et al. (2023). Peatland groundwater level in the Indonesian maritime continent as an alert for El Niño and moderate positive Indian Ocean dipole events. *Sci. Rep.* 13:939. doi: 10.1038/s41598-023-27393-x
- Sun, Q., Miao, C., AghaKouchak, A., Mallakpour, I., Ji, D., and Duan, Q. (2020). Possible increased frequency of ENSO-related dry and wet conditions over some major watersheds in a warming climate. *Bull. Am. Meteorol. Soc.* 101, E409–E426. doi: 10.1175/BAMS-D-18-0258.1
- Susilo, G., Yamamoto, K., Imai, T., Ishii, Y., Fukami, H., and Sekine, M. (2013). The effect of ENSO on rainfall characteristics in the tropical peatland areas of central Kalimantan, Indonesia. *Hydrol. Sci. J.* 58, 539–548. doi: 10.1080/02626667.2013.772298
- Tacconi, L., and Muttaqin, M. (2019). Reducing emissions from land use change in Indonesia: An overview. *For. Ecol. Manag.* 108:101979. doi: 10.1016/j.forpol.2019.101979
- Tan, Z., Carrasco, L., and Taylor, D. (2020). Spatial correlates of forest and land fires in Indonesia. *Int. J. Wildland Fire* 29, 1088–1099. doi: 10.1071/WF20036
- Tangang, F., Farzanmanesh, R., Mirzaei, A., Salimun, E., Jamaluddin, A., and Juneng, L. (2017). Characteristics of precipitation extremes in Malaysia associated with El Niño and La Niña events. *Int. J. Climatol.* 37, 696–716. doi: 10.1002/joc.5032
- Tansey, K., Beston, J., Hoscilo, A., Page, S., and Hernández, P. (2008). Relationship between MODIS fire hot spot count and burned area in a degraded tropical peat swamp forest in Central Kalimantan, Indonesia. *J. Geophys. Res. Atmos.* 113:D23. doi: 10.1029/2008JD010717
- Turetsky, M., Benscoter, B., Page, S., Rein, G., van der Werf, G., and Watts, A. (2015). Global vulnerability of peatlands to fire and carbon loss. *Nat. Geosci.* 8, 11–14. doi: 10.1038/ngeo2325
- Uda, S., Hein, L., and Atmoko, D. (2019). Assessing the health impacts of peatland fires: A case study for central Kalimantan, Indonesia. *Environ. Sci. Pollut. Res.* 26, 31315–31327. doi: 10.1007/s11356-019-06264-x
- Vetrita, Y., and Cochrane, M. (2020). Fire frequency and related land-use and land-cover changes in Indonesia's Peatlands. *Remote Sens.* 12:5. doi: 10.3390/rs12010005
- Vetrita, Y., Cochrane, M., Suwarsono, Priyatna, M., Sukowati, K., and Khomarudin, M. (2021). Evaluating accuracy of four MODIS-derived burned area products for tropical peatland and non-peatland fires. *Environ. Res. Lett.* 16:035015. doi: 10.1088/1748-9326/abd3d1
- Volkova, L., Krisnawati, H., Adinugroho, W., Imanuddin, R., Qirom, M., Santosa, P., et al. (2021). Identifying and addressing knowledge gaps for improving greenhouse

gas emissions estimates from tropical peat forest fires. *Sci. Total Environ.* 763:142933. doi: 10.1016/j.scitotenv.2020.142933

Wiggins, E., Czimczik, C., Santos, G., Chen, Y., Xu, X., Holden, S., et al. (2018). Smoke radiocarbon measurements from Indonesian fires provide evidence for burning of millennia-aged peat. *Environ. Res. Lett.* 115, 12419–12424. doi: 10.1073/pnas.1806003115

Williams, C., Ellsworth, L., Strand, E., Reeves, M., Shaff, S., Short, K., et al. (2023). Fuel treatments in shrublands experiencing pinyon and juniper expansion result in trade-offs between desired vegetation and increased fire behavior. *Fire Ecol.* 19:46. doi: 10.1186/s42408-023-00201

Wulder, M., Loveland, T., Roy, D., Crawford, C., Masek, J., Woodcock, C., et al. (2019). Current status of Landsat program, science, and applications. *Remote Sens. Environ.* 225, 127–147. doi: 10.1016/j.rse.2019.02.015

Xu, J., Morris, P., Liu, J., and Holden, J. (2018). PEATMAP: Refining estimates of global peatland distribution based on a meta-analysis. *Catena* 160, 134–140. doi: 10.1016/j.catena.2017.09.010

Yokelson, R., Saharjo, B., Stockwell, C., Putra, E., Jayarathne, T., Akbar, A., et al. (2022). Tropical peat fire emissions: 2019 field measurements in Sumatra and Borneo and synthesis with previous studies. *Atmos. Chem. Phys.* 22, 10173–10194. doi: 10.5194/acp-22-10173-2022



OPEN ACCESS

EDITED BY

Kyung Ah Koo,
Korea Environment Institute,
Republic of Korea

REVIEWED BY

Feng Chen,
Yunnan University, China
Jong Sik Kim,
Chonnam National University,
Republic of Korea

*CORRESPONDENCE

Jeong-Wook Seo
✉ jwseo@chungbuk.ac.kr

RECEIVED 29 July 2023

ACCEPTED 18 March 2024

PUBLISHED 22 April 2024

CITATION

Choi E-B, Park J-H, Sano M, Nakatsuka T and Seo J-W (2024) Summer climate information recorded in tree-ring oxygen isotope chronologies from seven locations in the Republic of Korea.

Front. For. Glob. Change 7:1269346.
doi: 10.3389/ffgc.2024.1269346

COPYRIGHT

© 2024 Choi, Park, Sano, Nakatsuka and Seo. This is an open-access article distributed under the terms of the [Creative Commons Attribution License \(CC BY\)](https://creativecommons.org/licenses/by/4.0/). The use, distribution or reproduction in other forums is permitted, provided the original author(s) and the copyright owner(s) are credited and that the original publication in this journal is cited, in accordance with accepted academic practice. No use, distribution or reproduction is permitted which does not comply with these terms.

Summer climate information recorded in tree-ring oxygen isotope chronologies from seven locations in the Republic of Korea

En-Bi Choi¹, Jun-Hui Park¹, Masaki Sano², Takeshi Nakatsuka³ and Jeong-Wook Seo^{4*}

¹Department of Forest Product, College of Agriculture, Life and Environment Science, Chungbuk National University, Cheongju, Republic of Korea, ²National Museum of Japanese History, Sakura, Japan, ³Graduate School of Environmental Studies, Nagoya University, Nagoya, Japan, ⁴Department of Wood and Paper Science, College of Agriculture, Life and Environment Science, Chungbuk National University, Cheongju, Republic of Korea

The Republic of Korea is characterized by its north-to-south stretch and high mountain ranges along the eastern coast, resulting in terrain with higher elevation in the east and lower in the west. These geographical features typically lead to regional climate differences, either based on latitude or from east to west. In the present study, for effectiveness, the entire Korean peninsula was divided into four regions based on the geographical features: The Northeast Coast (NEC), Central Inland (MI), Southeast Coast (SEC), and South Coast (SC). Two test sites were chosen from each region, except for the SC. The linear relationship between the altitude of sites and the mean oxygen isotope ratio ($\delta^{18}\text{O}$) revealed a negative correlation; the highest (1,447 m a.s.l.) and the lowest altitude (86 m a.s.l.) sites had a mean $\delta^{18}\text{O}$ of 27.03‰ and 29.67‰, respectively. The sites selected from the same region exhibited stronger correlation coefficients (0.75–0.79) and GI_k (Gleichläufigkeit) (74–83%) between the tree-ring oxygen isotope chronologies ($\delta^{18}\text{O}_{\text{TR}}$ chronologies) than those from different regions (0.60–0.69/70–79%). However, subtle variations in pattern were observed in the comparison period during a few selected intervals (approximately 10 years). All the regional $\delta^{18}\text{O}_{\text{TR}}$ chronologies exhibited positive correlations with either June or July temperatures over Korea, whereas negative correlations with regional summer precipitation and SPEI-3. Moreover, the chronologies showed notable negative correlations with the water condition of western Japan. The findings of this study can be used as a scientific reference for the study of variations of rainfall in East Asia using $\delta^{18}\text{O}_{\text{TR}}$ chronology.

KEYWORDS

tree ring, oxygen isotope, precipitation, monsoon, East Asia

1 Introduction

Tree rings typically provide annual information on the growth duration of a tree, and therefore, have been used as a significant indicator in a variety of studies, such as tree adaptation, forest events, dating, and climate reconstruction (Fritts, 1976; Speer, 2010). Apart from the traditional tree-ring width, other ring parameters, such as stable isotopes, density, and cells have also been used in many studies (Fritts et al., 1991; Kirilyanov et al., 2008;

Choi et al., 2020b; Siegwolf et al., 2020; Park et al., 2021; Chen et al., 2023; Lopez-Saez et al., 2023; Xu et al., 2023). One advantage of using the tree-ring width is that it allows simple and straightforward method of analysis. However, this width is also influenced by certain factors in the growing environment (Schweingruber, 1996; Larcher, 2003), such as environmental changes, stand dynamics, competition, soil conditions, and insect damage. In such cases, using tree-ring width chronologies for analysis becomes a challenge. Among the various tree-ring parameters, the stable isotopes in the tree rings become more sensitive during the growth period to the environmental changes, specifically the climatic factors than to net growth (Yakir et al., 1990; Roden et al., 2000; Barbour et al., 2004; Kress et al., 2010; Haupt et al., 2011), which involves the non-climatic factors (McCarroll and Loader, 2004; Liu et al., 2009; Young et al., 2012; Sano et al., 2013; Seo et al., 2017, 2019; Li et al., 2022; Mandy et al., 2023).

The three main elements present in wood and commonly employed in research are the oxygen (^{16}O , ^{18}O), carbon (^{12}C , ^{13}C), and hydrogen (^1H , ^2H) isotopes (Leavitt and Long, 1988; McCarroll and Loader, 2004; Jia et al., 2023; Pandey et al., 2023). Due to different formation mechanisms of these isotopes in the tree rings, each isotope is applied either individually or in combination across various fields (Farquhar et al., 1989; Yakir et al., 1990; Saurer et al., 1997; Roden and Ehleringer, 1999; Roden et al., 2000; Barbour et al., 2004; Saurer and Siegwolf, 2007; Loader et al., 2008; Roden, 2008; Miles et al., 2019; Belmecheri and Lavergne, 2020; Büntgen, 2022). The annual oxygen isotope ratio in a tree ring reflects the isotopic ratio of the water the tree absorbs during its growing season. Such absorption largely depends upon the precipitation during that period. The $\delta^{18}\text{O}_{\text{TR}}$ chronologies are therefore greatly influenced by the precipitation during the growing season, and any change in annual precipitation patterns causes variation in the oxygen isotope ratio in the tree rings (Seo et al., 2019; Choi et al., 2020a; Preechamart et al., 2023; Watanabe et al., 2023). Therefore, the isotopes in different trees of the same species exhibit similar patterns of change in the same climate zone, thereby making it possible to use them in climate analysis and establish tree-ring oxygen isotope chronologies ($\delta^{18}\text{O}_{\text{TR}}$ chronologies) over extensive areas (Baker et al., 2015; Young et al., 2015; Choi et al., 2020a). Additionally, it has been confirmed that although the mean value of the oxygen isotope ratio may differ between tree species due to physiological and spatial characteristics, they exhibit the same pattern (Baker et al., 2015; Loader et al., 2019, 2021; Choi et al., 2020a; Xu et al., 2021; Sano et al., 2022). These advantages of the tree-ring isotopes allow us to establish long-term $\delta^{18}\text{O}_{\text{TR}}$ chronology using data from different tree species over a wide region.

Until now, only four studies in Korea have been published which involved $\delta^{18}\text{O}_{\text{TR}}$ chronology (Seo et al., 2017, 2019; Choi et al., 2020a; Lee et al., 2023). These studies verified that a chronology built using $\delta^{18}\text{O}$ in tree rings between study sites which are about 144 km away can be used as a master chronology for cross-dating (Choi et al., 2020a) regardless of the tree species due to their high synchronization (Seo et al., 2017; Lee et al., 2023). The influence of water condition in western Japan on the $\delta^{18}\text{O}_{\text{TR}}$ chronology in southern Korea had also been reported (Seo et al., 2017). However, since these results were obtained from restricted regions, the data have limited application across the country. Korea spans along north–south direction (33° to 38°), and the terrain is characterized by higher elevation in the east, with developed mountain ranges, and lower

elevations in the west (The Academy of Korean Studies, 2016). Such difference in topography results in difference in the regional climate (Ministry of Land Infrastructure and Transport and National Geography Information Institute, 2020). Therefore, studies using $\delta^{18}\text{O}_{\text{TR}}$ chronology which consider such topographical features are necessary.

The current study was designed under the hypothesis that local climatic condition is influenced by topographical features and its effect on $\delta^{18}\text{O}$ in the tree rings. The main objectives of the present study are to investigate (1) synchronization strength between the $\delta^{18}\text{O}_{\text{TR}}$ chronologies from different regions, (2) climatic information embedded in the regional chronologies, and (3) the role of topographical and/or meteorological features on the results of (1) and (2). The results should play an important role in advancing our strategy for making a dendrochronological research plan using $\delta^{18}\text{O}$ in tree rings.

2 Materials and methods

2.1 Study sites

Korea has several notable topographical features, including (1) an elongated north–south shape, (2) major mountains along the eastern coast (the Taebaek Mountains), and (3) three sides surrounded by ocean (Figure 1). These geographical locations, topographical, and sea distribution characteristics significantly impact the regional climate of Korea. For example, a large temperature difference exists between the northern and southern regions of Korea depending upon the latitude. On the other hand, at the same latitude, the eastern region is cooler in summer and warmer in winter compared to the western region (Ministry of Land Infrastructure and Transport and National Geography Information Institute, 2020). These variations occur because the Taebaek Mountain blocks the cold air from the continent, while the relatively deep East Sea exhibits less fluctuation in the water temperature compared to the Yellow Sea. In the present study, we considered these topographical differences and divided the study areas with respect to latitude and coastal/inland areas. The study sites were subdivided into four regions, namely (1) Northeast Coast (NEC), (2) Mid-Inland (MI), (3) Southeast Coast (SEC), and (4) South Coast (SC) of South Korea. All the sites in these regions were chosen from the National parks located across the country. The NEC comprises Mt. Seoraksan (SA) and Mt. Odaesan (OD), MI consists of Mt. Songnisan (SN) and Mt. Gyeryongsan (GR), SEC includes Mt. Juwangsang (JW) and Mt. Namsan (NS), and SC includes Jirisan (JR) National Park.

According to the monthly mean climate data from 1991 to 2020, the monthly temperature was the lowest in January and highest in August (Figure 1, bottom right). The monthly precipitation was the highest in July and lowest in January (Open MET Data Portal, <https://data.kma.go.kr/resources/html/en/aowdp.html>, accessed on July 15, 2023). During summer, the precipitation reached 710.9 mm, accounting for 54% of the total annual precipitation (1306.3 mm) in the nation. Since the 1980s, the average annual temperature and precipitation of South Korea showed significant increase, and the increase in the average annual precipitation was attributed to the rise in summer precipitation

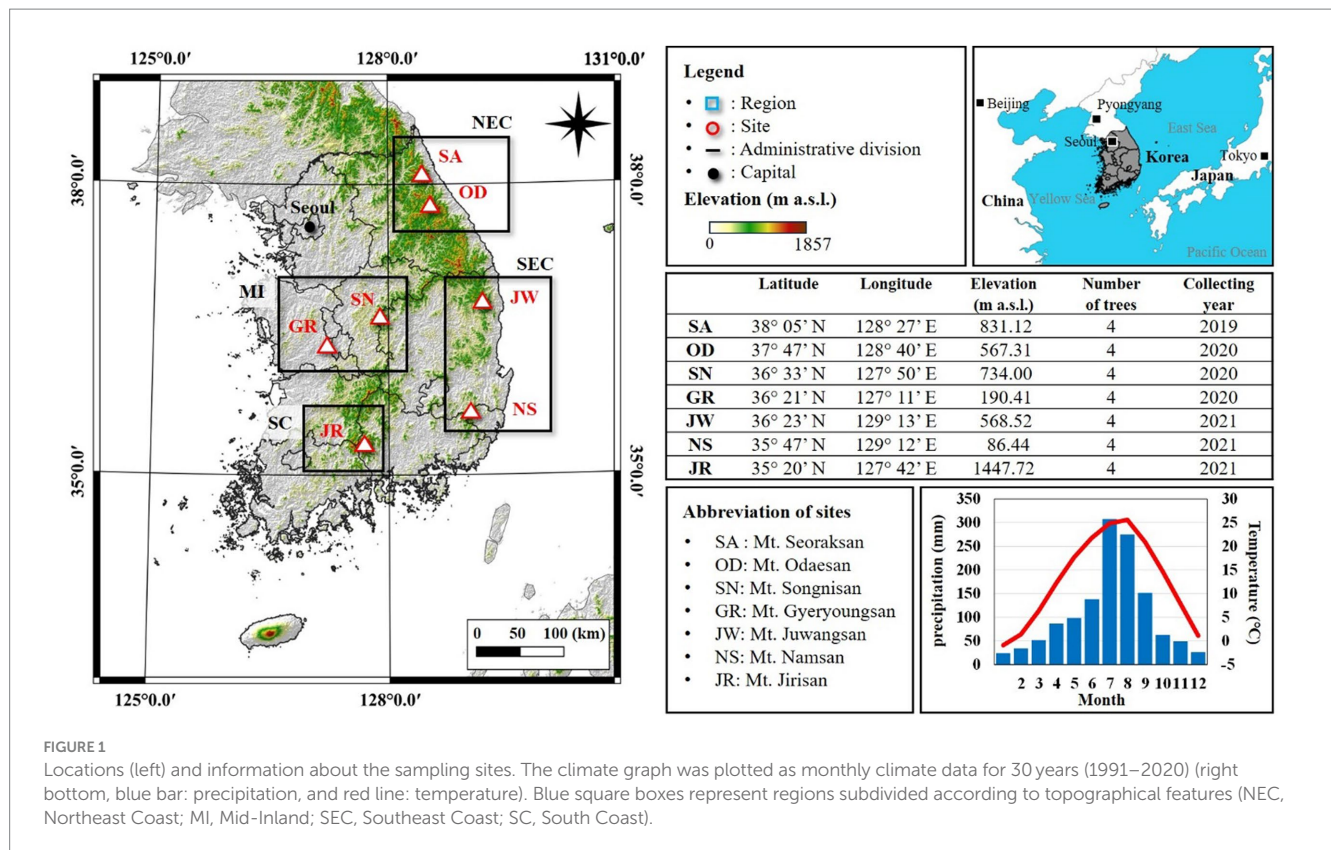


FIGURE 1

Locations (left) and information about the sampling sites. The climate graph was plotted as monthly climate data for 30 years (1991–2020) (right bottom, blue bar: precipitation, and red line: temperature). Blue square boxes represent regions subdivided according to topographical features (NEC, Northeast Coast; MI, Mid-Inland; SEC, Southeast Coast; SC, South Coast).

(National Institute of Meteorological Sciences, 2018; Korea Meteorological Administration, 2020, 2022).

2.2 Tree-ring samples

Pinus densiflora (red pine) was chosen as the sample for the present study which was collected during 2019–2021 (3 years). *P. densiflora* is a coniferous tree species which occupies the largest area (1.5 million ha, 21.9% of all forests) among all the single tree species in South Korea. The red pine is used widely since the ancient times due to its easy accessibility and various applications (Park et al., 2007, 2010; Kim et al., 2013; Kong et al., 2014; Choi et al., 2020a,b). Due to these qualities, the pine forests were designated as protected areas throughout Korea's history (10 C–19 C), and indiscriminate logging is strictly prohibited. In the present study, we have chosen the pine trees in the National parks as the samples because substantial number of tree rings can be obtained from them.

At each study site, cores were collected from minimum 10 trees. A core of 10 mm diameter was extracted for oxygen isotope analysis. All the cores were precisely dated to an accuracy of 0.01 mm using LINTAB (RENNTECH, Germany). Then, tree-ring width chronologies were established which were further used to cross-date each tree, identify any missing or discontinuous rings, and accurately deduce the growth year of each ring. The cross-dating was performed through statistical analysis using the TSAP program (Cook and Kairiukstis, 1990; Speer, 2010). For oxygen isotope measurements, four cores with the longest chronologies and no missing rings were chosen from each study site.

2.3 Tree-ring oxygen isotope chronology

The oxygen isotope ratio was measured for all the selected tree rings. The samples were prepared as described below (Kagawa et al., 2015; Choi et al., 2020a,b). A 1 mm thick plate was first sliced from the selected cores, and α -cellulose was extracted from the plate following Jayme-Wise method (Jayme, 1942; Wise et al., 1946; Green, 1963; Loader et al., 1997; Brendel et al., 2000). From each tree ring of the α -cellulose plate, small specimens weighing between 120 and 250 μ g were obtained and wrapped in silver foil. The oxygen isotope ratio ($^{18}\text{O}/^{16}\text{O}$) in the wrapped samples was measured via pyrolysis using high-temperature conversion elemental analyzer (TC/EA, Thermo Fisher Scientific, Germany) and isotope ratio mass spectrometer (IRMS, Delta V Advantage, Thermo Fisher Scientific, Germany). The ratio was calculated in permil (‰) against Vienna Standard Mean Ocean Water (VSMOW). The measurements were conducted at Nagoya University, Nagoya, Japan.

2.4 Statistical analyses and climate data

The R packages “Dendrochronology Program Library in R (dplR)” and “treeclim” (version 4.3.0) were used for all statistical analyses, namely cross-dating, Expressed Population Singal (EPS), Gleichläufigkeit (Glk) and correlation analysis with climatic parameters, using $\delta^{18}\text{O}_{\text{TR}}$ chronologies. The climatic parameters used in this study include temperature, precipitation, and SPEI-3. Since Korea lacks meteorological data for more than 100 years, the following data were selected for analysis of the climatic factors spanning over the entire study period. For temperature and precipitation, the

TABLE 1 Information about the established $\delta^{18}\text{O}_{\text{TR}}$ chronologies.

| Site | $\delta^{18}\text{O}_{\text{TR}}$ chronology | | | Correlation* | $\delta^{18}\text{O}$ (‰) | EPS** |
|------|--|------------|-----------|--------------------|---------------------------|-------|
| | Length (year) | First year | Last year | Mean (\pm std) | Mean (\pm std) | |
| SA | 210 | 1809 | 2018 | 0.79 (\pm 0.06) | 27.52 (\pm 1.01) | 0.94 |
| OD | 393 | 1628 | 2020 | 0.67 (\pm 0.07) | 29.11 (\pm 1.12) | 0.89 |
| SN | 144 | 1877 | 2020 | 0.66 (\pm 0.06) | 29.04 (\pm 1.08) | 0.89 |
| GR | 126 | 1895 | 2020 | 0.65 (\pm 0.05) | 29.80 (\pm 0.96) | 0.87 |
| JW | 103 | 1918 | 2020 | 0.73 (\pm 0.06) | 27.75 (\pm 1.24) | 0.93 |
| NS | 133 | 1888 | 2020 | 0.58 (\pm 0.06) | 29.67 (\pm 1.12) | 0.86 |
| JR | 250 | 1771 | 2020 | 0.74 (\pm 0.03) | 27.03 (\pm 1.07) | 0.93 |

*: correlation between individual $\delta^{18}\text{O}_{\text{TR}}$ chronologies. **: expressed population signal.

Climatic Research Unit gridded Time Series (CRU T.S.) 4.06 data set from 1901 to 2020 provided by the Centre for Environmental Data Analysis (CEDA) was utilized (Harris et al., 2020). For Standardized Precipitation-Evapotranspiration Index (SPEI), data from 1901 to 2018 provided by Consejo Superior de Investigaciones Científicas (CSIC) were used,¹ and SPEI-3 accumulated in 3-month increments was utilized for the analysis.

3 Results and discussion

3.1 $\delta^{18}\text{O}$ of tree ring

The mean and standard deviation of the oxygen isotope ratio varied across regions (Table 1; Figure 2). The altitude of the sites and mean oxygen isotope ratio showed a linear relationship with negative correlation. Specifically, the higher altitude sites, viz. JR (1,447 m a.s.l.), showed the lowest mean oxygen isotope ratio of 27.03‰, whereas the lower altitude sites, such as NS (86 m a.s.l.) and GR (190 m a.s.l.) showed the highest oxygen isotope ratio of 29.67‰ and 29.80‰, respectively.

The differences in the mean and standard deviation of the oxygen isotope ratio between various tree species are known to be influenced by complicated physiological and biochemical mechanisms (Roden et al., 2000; Sternberg, 2009). However, in our study, since all the $\delta^{18}\text{O}_{\text{TR}}$ chronologies were for the same tree species (*P. densiflora*), it is reasonable to state that the spatial factors of a site played a more significant role than the species characteristics. The oxygen isotope ratio of the tree rings is closely related to the temperature and/or precipitation conditions during the tree-ring formation (Hau et al., 2023). Furthermore, for the oxygen isotope ratio of precipitation, fractionation may appear where the relative concentrations of the isotopes vary owing to various factors, such as altitude effect, latitude effect, rainfall, continental effect, surface temperature, and distance from the ocean (Dansgaard, 1964; Rozanski et al., 1993; Bowen and Wilkinson, 2002; Vuille et al., 2003; Aggarwal et al., 2012).

The altitude effect refers to lower oxygen isotope ratio with increasing altitude which occurs due to Rayleigh distillation (Poage and Chamberlain, 2001). The altitude effect occurs mainly because the

isotopic ratio of precipitation decreases almost linearly with altitude, and trees at higher altitudes rely mostly on precipitation as the water source during the growing season. Moreover, the neutral isotope ratio of freshwater decreases with increasing latitude and altitude (Dansgaard, 1964; Eriksson, 1965; Poage and Chamberlain, 2001; Aggarwal et al., 2012).

3.2 Regional tree-ring $\delta^{18}\text{O}$ chronologies

From the individual $\delta^{18}\text{O}_{\text{TR}}$ chronologies, we constructed seven site $\delta^{18}\text{O}_{\text{TR}}$ chronologies representing the respective sites. The longest site $\delta^{18}\text{O}_{\text{TR}}$ chronology comprised 393 years (1628–2020) for Mt. Odaesan, while the shortest was for 103 years (1918–2020) for Mt. Juwangsan. The expressed population signal (EPS) for all the sites was above 0.85 for the duration of the $\delta^{18}\text{O}_{\text{TR}}$ chronology (Table 1). The mean correlation obtained between the individual oxygen isotope ages was 0.69 (maximum SA: 0.79, minimum NS: 0.58, $p < 0.05$).

The EPS in dendrochronology signifies the explanatory power of an infinite population chronology using finite tree-ring data. Usually, $\text{EPS} > 0.85$ is applied to determine the ability of a chronology to explain a common signal (Briffa and Jones, 1990; Buras, 2017; Siegwolf et al., 2020). In the current study, the EPS of all the 7 sites was above 0.85 for the duration of the $\delta^{18}\text{O}_{\text{TR}}$ chronology. This signifies that the site $\delta^{18}\text{O}_{\text{TR}}$ chronologies can be utilized to explain a common signal such as climate. Typically, dendroisotope studies urge that minimum four trees should be used to obtain meaningful EPS values (> 0.85) for each site (Wigley et al., 1984; Xu et al., 2017; Choi et al., 2020a,b; Li et al., 2020). In the present study, significant $\text{EPS} > 0.85$ was also obtained with four trees for all the sites; EPS between 1918 and 2018 (SA = 0.94, OD = 0.87, SN = 0.89, GR = 0.90, JW = 0.92, NS = 0.85, and JR = 0.93). This indicated that the $\delta^{18}\text{O}_{\text{TR}}$ chronologies strongly share a common signal with each other and meaningful climatological analysis is possible with these data.

The period of overlap among all the site $\delta^{18}\text{O}_{\text{TR}}$ chronologies was from 1918 to 2018, i.e., total 101 years. The standardized site $\delta^{18}\text{O}_{\text{TR}}$ chronologies displayed significant correlations ($p < 0.05$) (Figure 3). The sites in the same region showed higher correlations and Glk values than the sites from different regions, and a clear difference in correlation was observed. Specifically, the correlation and Glk values were 0.75 and 74% between SA and OD in NEC, 0.79 and 83% between SN and GR in MI, and 0.79 and 81% between JW and NS in

¹ <https://spei.csic.es/index.html>

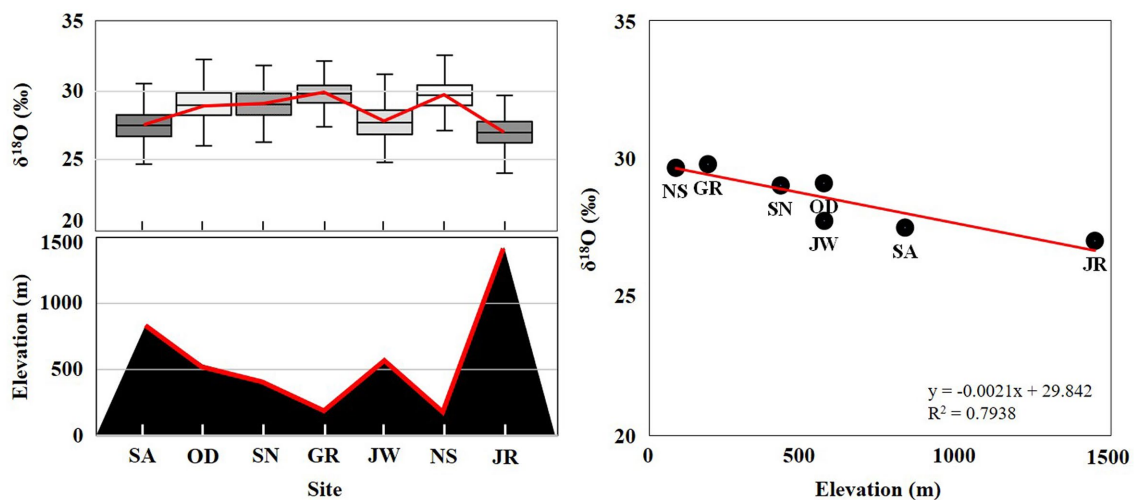


FIGURE 2
Distribution of oxygen isotope ratio according to altitudes of the sites.

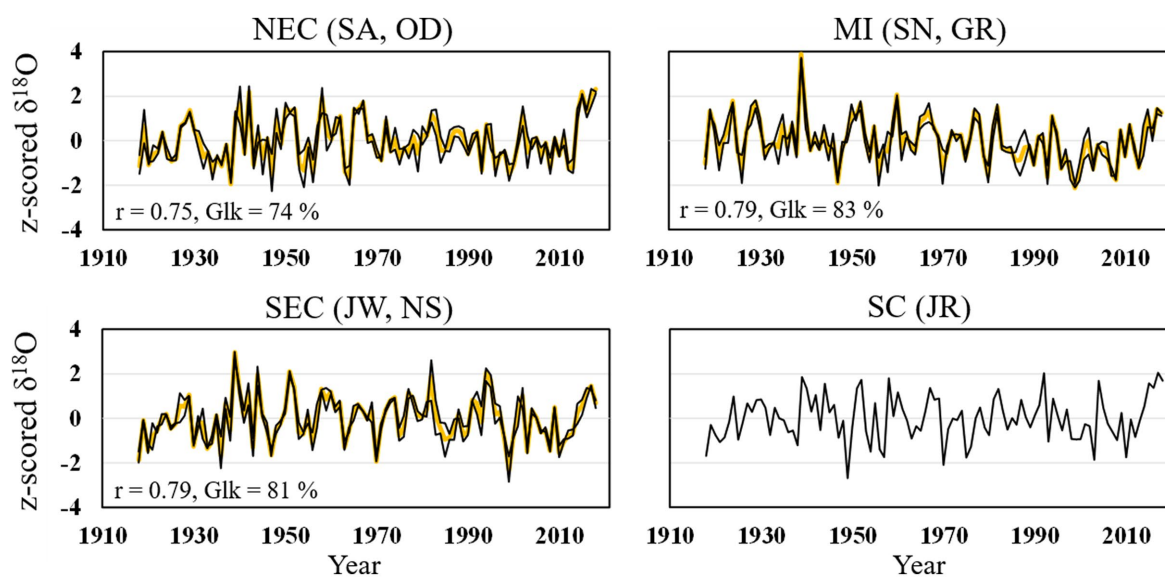


FIGURE 3
Site- $\delta^{18}\text{O}_{\text{TR}}$ chronology (black line) and regional $\delta^{18}\text{O}_{\text{TR}}$ chronology (yellow line).

SEC, respectively ($p < 0.05$). Based on these values, three regional $\delta^{18}\text{O}_{\text{TR}}$ chronologies were constructed. A single site was chosen in the SC; hence, only chronology data from JR were used to construct the SC $\delta^{18}\text{O}_{\text{TR}}$ chronology.

We also examined the correlations between the regional $\delta^{18}\text{O}_{\text{TR}}$ chronologies. Most of the regional $\delta^{18}\text{O}_{\text{TR}}$ chronologies showed statistically significant correlations for the entire comparison period. The NEC exhibited an average correlation and Glk values of 0.64 and 74% with other regions, MI was 0.63 and 77%, SEC was 0.68 and 74%, and SC was 0.65 and 77% ($p < 0.05$). Although the regional $\delta^{18}\text{O}_{\text{TR}}$ chronologies showed statistically significant correlations for the entire period, the regional chronologies displayed certain differences in patterns between them during certain periods

(Figure 4). These subtle differences in patterns during certain periods were attributed to the influence of the same large climatic zone in the study area along with some strong regional climates during certain periods. Therefore, we conducted analyses of climatic factors on a region-by-region basis.

3.3 Climate factors affecting oxygen isotope ratios in tree rings

The regional $\delta^{18}\text{O}_{\text{TR}}$ chronologies were correlated with temperature, precipitation, and SPEI-3 (Figure 5). All the three climatic factors showed significant correlations ($p < 0.05$), but the strongest correlation

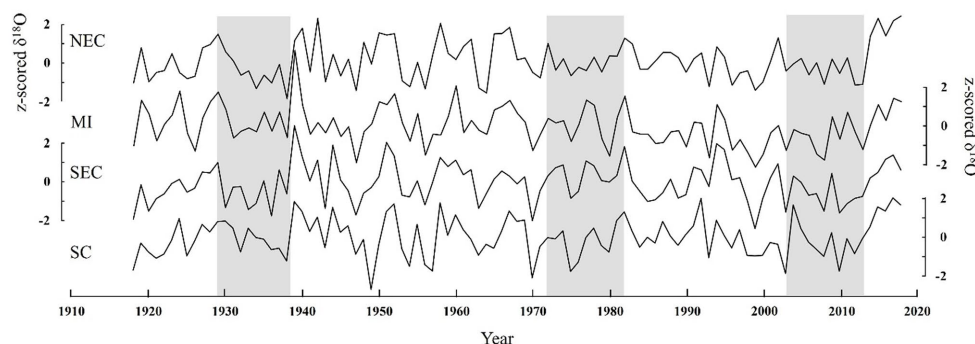


FIGURE 4 Comparison of $\delta^{18}\text{O}_{\text{TR}}$ patterns between the four composed regional $\delta^{18}\text{O}_{\text{TR}}$ chronologies. The gray box indicates the period in which subtle pattern differences were observed.

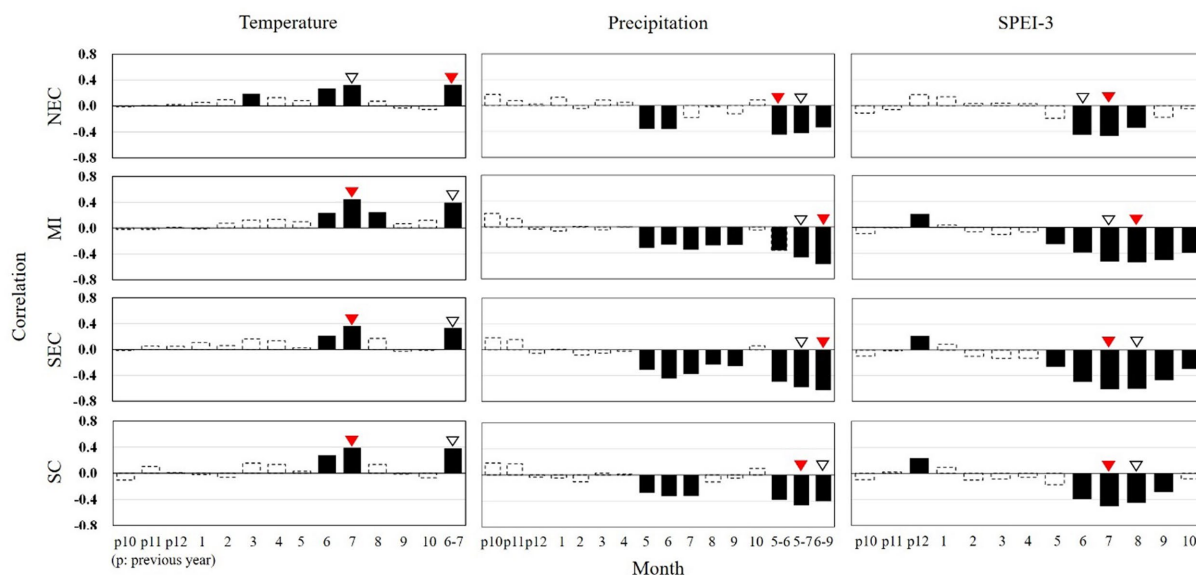


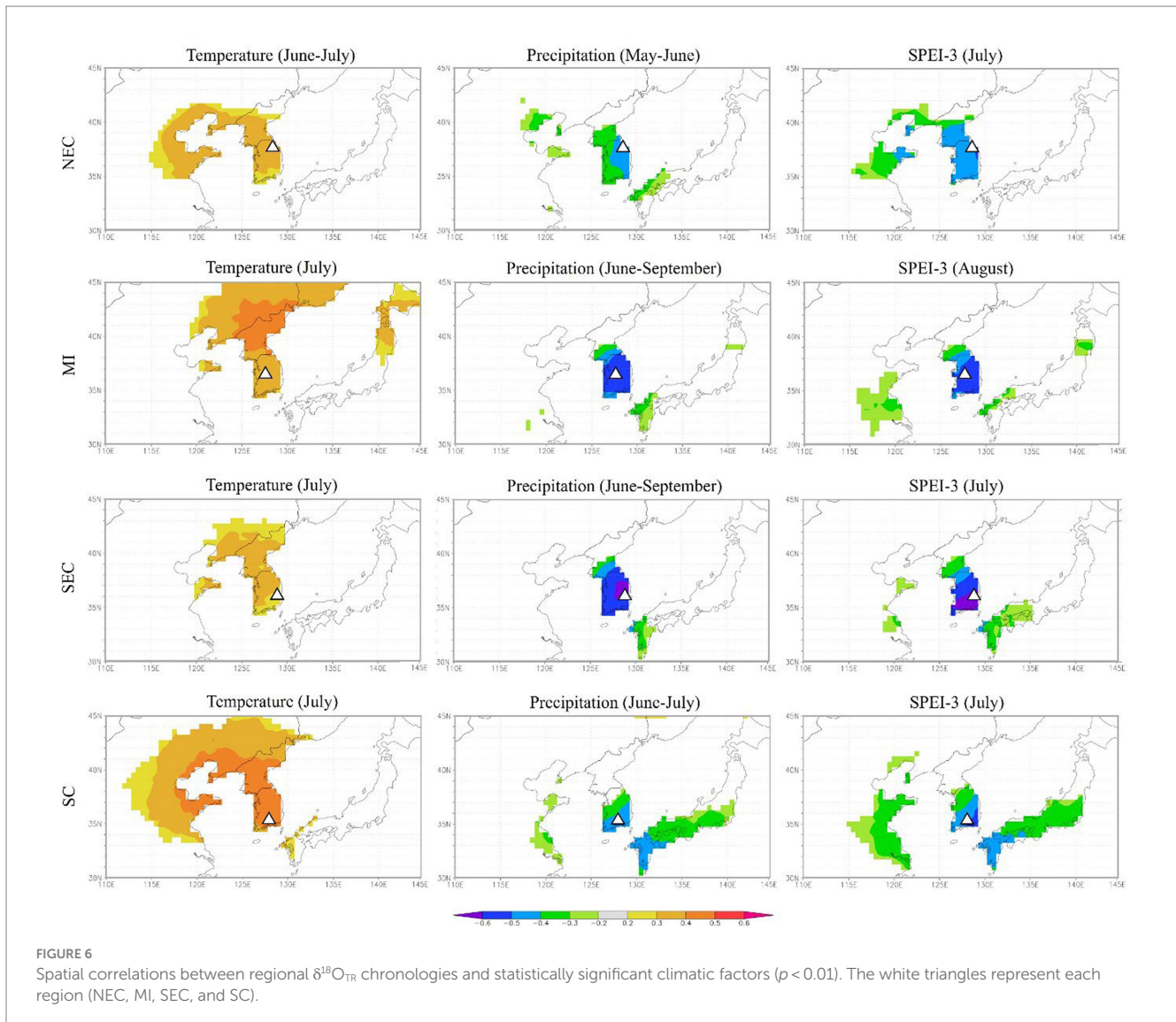
FIGURE 5 Correlation coefficients between regional $\delta^{18}\text{O}_{\text{TR}}$ chronology and climate data (temperature, precipitation, and SPEI-3) (black bar: $p < 0.05$). The red inverted triangle indicates the highest statistical result, and the white inverted triangle represents the second highest statistical value.

coefficient was obtained for SPEI-3. Specifically, all the regional $\delta^{18}\text{O}_{\text{TR}}$ chronologies exhibited positive correlations with summer temperatures, and the strongest correlations were observed in either June or July. The NEC displayed the highest correlation with June–July temperatures ($r = 0.33$), as well as with July ($r = 0.32$). For MI, SEC, and SC, the most significant correlations were observed with the July temperatures ($r_{\text{MI}} = 0.45$, $r_{\text{SEC}} = 0.36$, $r_{\text{SC}} = 0.39$), followed by June–July temperatures ($r_{\text{MI}} = 0.39$, $r_{\text{SEC}} = 0.33$, and $r_{\text{SC}} = 0.38$).

The monthly mean precipitation exhibited higher negative correlations with regional $\delta^{18}\text{O}_{\text{TR}}$ chronologies when the summer precipitation was aggregated by month (Figure 5). This indicated that all the regions were strongly influenced by precipitation during the summer. Specifically, NEC showed a strong negative correlation with the early summer months, May–June ($r_{\text{NEC}} = -0.45$) during the overall summer rainfall period. MI and SEC exhibited significant correlation during the entire summer rainfall period, i.e., from June

to September, with correlation coefficient of -0.57 (r_{MI}) and -0.62 (r_{SEC}), respectively. For NC, the highest correlation was observed between May and July ($r_{\text{SC}} = -0.47$), a significant correlation was also observed from June to September ($r_{\text{SC}} = -0.40$). SPEI-3 showed a strong negative correlation in July or August. NEC, SEC, and SC displayed maximum correlation in July ($r_{\text{NEC}} = -0.47$, $r_{\text{SEC}} = -0.61$, and $r_{\text{SC}} = -0.50$), while MI is most highly correlated in August ($r_{\text{MI}} = -0.54$).

All the regional $\delta^{18}\text{O}_{\text{TR}}$ chronologies presented a significant relationship with climate from May to September. These months are typically characterized by the highest temperatures, the most intense precipitation, and maximum growth of most of the trees in Korea. These findings indicate that temperature and precipitation during summer strongly influence the oxygen isotope ratio of the trees in the studied regions. However, even during summer, the regional differences between the climatic factors, especially the precipitation



were evident. Unlike the other regions, NEC exhibited a significant impact mainly during the early summer precipitation period with specific correlations to temperature in June–July, precipitation in May–June, and SPEI-3 in July.

3.4 Spatial correlations between regional $\delta^{18}\text{O}_{\text{TR}}$ chronologies and climate

Temporal correlation analyses were conducted on the highly correlated periods identified in the previous correlation analysis (Figure 6). A comparison between the regional $\delta^{18}\text{O}_{\text{TR}}$ chronologies and temperature revealed that the tree-ring $\delta^{18}\text{O}_{\text{TR}}$ was governed by the July temperature of Korea, whereas that between the chronologies and precipitation or SPEI-3 was governed by the study site regions. Furthermore MI, SEC, and SC also showed high correlations with western Japan.

Previous studies reported that the $\delta^{18}\text{O}_{\text{TR}}$ chronology of *Taxus cuspidata* from Mt. Jirisan has high correlations with June–July

temperature over Korea and May–July precipitation of the study site and western Japan (Seo et al., 2019; Sano et al., 2022). In another study, using the $\delta^{18}\text{O}$ data from rainfall, Kurita et al. (2009) interpreted that the high correlation with precipitation in western Japan comes from upstream hydrological processes, such as evaporation and condensation (Kurita et al., 2009). The correlations from MI, SCE, and SC in the present study also support the previous findings, i.e., the role of precipitation in the upstream regions of western Japan (Figure 6). As the altitude increases from the south (SC) to the north (MI), the rain clouds move from SC to MI during June–September. Unlike other regions, early summer climate in NEC is normally influenced by high pressure on the Okhotsk Sea (Lee, 1994). Moreover, the precipitation in NEC located in the east of the Taebaek Mountains is higher than that in the west due to the Föhn effect (WMO, 1992; Choi et al., 1997; Kim and Kim, 2013; Park, 2020). The Taebaek Mountains are located along the eastern edge of Korea. Such meteorological characteristics enhances the effect of early summer precipitation on the $\delta^{18}\text{O}$ of the tree rings from NEC (Shin and Lee, 2023).

4 Conclusion

From dendrochronological perspective and based on the comparisons between the seven site $\delta^{18}\text{O}_{\text{TR}}$ chronologies, several conclusions can be drawn. First, the site chronologies can be used for cross-dating even if they are tens to hundreds of kilometers apart, because the chronologies have similar inter-annual variations. Our findings support that any of the site chronologies can be used for cross-dating tree rings from places where there is no long chronology. Second, although the seven site $\delta^{18}\text{O}_{\text{TR}}$ chronologies show reliable synchronization pattern, subtle differences exist between the four regions (NEC, MI, SEC, and SC) due to geographical and/or meteorological characteristics. Therefore, at least these four regions should be considered for dendroclimatological study on reconstructing a local paleoclimate.

Temporal correlation analyses between the regional $\delta^{18}\text{O}_{\text{TR}}$ chronologies and climate data (temperature, precipitation, and SPEI-3) showed different results with respect to temperature and water condition. In the former, all the regional $\delta^{18}\text{O}_{\text{TR}}$ chronologies were mainly governed by the July temperature over Korea. In the latter, the regional precipitation and SPEI-3 exerted more influences on the corresponding regional $\delta^{18}\text{O}_{\text{TR}}$ chronologies. The major influences of the local precipitation and SPEI-3 on the $\delta^{18}\text{O}$ in tree rings mainly come from the regional precipitation differences. In the three regions except NEC, the month affecting regional tree-ring oxygen chronologies shifted progressively later for higher latitudes of the regions. This is because the rain clouds that affect these regions move inland from the west of Japan to the center of Korea, changing the timing of their impact. Our results can serve as a reference for further studies about variations of rainfall in East Asia using $\delta^{18}\text{O}_{\text{TR}}$ chronology.

To investigate the effect of drought stress on $\delta^{18}\text{O}$ in tree rings, SPEI, calculated from 3-month-increment data was applied since the results from SPEI-3 were better than SPEI-1 in the correlation analysis of regional $\delta^{18}\text{O}_{\text{TR}}$ chronologies. The trees require time for photosynthesis to build tree rings using water. The higher correlations with SPEI-3 than SPEI-1 can be used as a scientific reference to improve our understanding of tree physiological process.

References

- Aggarwal, P. K., Alduchov, O. A., Froehlich, K. O., Araguas-Araguas, L. J., Sturchio, N. C., and Kurita, N. (2012). Stable isotopes in global precipitation: a unified interpretation based on atmospheric moisture residence time. *Geophys. Res. Lett.* 39:L11705. doi: 10.1029/2012GL051937
- Baker, J. C. A., Hunt, S. F. P., Clerici, S. J., Newton, R. J., Bottrell, S. H., Leng, M. J., et al. (2015). Oxygen isotopes in tree rings show good coherence between species and sites in Bolivia. *Glob. Planet. Chang.* 133, 298–308. doi: 10.1016/j.gloplacha.2015.09.008
- Barbour, M. M., Roden, J. S., Farquhar, G. D., and Ehleringer, J. R. (2004). Expressing leaf water and cellulose oxygen isotope ratios as enrichment above source water reveals evidence of a Péclet effect. *Oecologia* 138, 426–435. doi: 10.1007/s00442-003-1449-3
- Belmecheri, S., and Lavergne, A. (2020). Compiled records of atmospheric CO_2 concentrations and stable carbon isotopes to reconstruct climate and derive plant ecophysiological indices from tree rings. *Dendrochronologia* 63:125748. doi: 10.1016/j.dendro.2020.125748
- Bowen, G. J., and Wilkinson, B. (2002). Spatial distribution of $\delta^{18}\text{O}$ in meteoric precipitation. *Geology* 30, 315–318. doi: 10.1130/0091-7613(2002)030<0315:SDOIM>2.0.CO;2
- Brendel, O., Iannetta, P. P. M., and Stewart, D. (2000). A rapid and simple method to isolate pure alpha-cellulose. *Phytochem. Anal.* 11, 7–10. doi: 10.1002/(SICI)1099-1565(200001/02)11:1<7::AID-PCA488>3.0.CO;2-U
- Briffa, K., and Jones, P. D. (1990). "Basic chronology statistics and assessment" in *Method of dendrochronology*. eds. E. R. Cook and L. A. Kairiukstis (Dordrecht: Kluwer academic publishers). isbn:ISBN 978-0-7923-0586-6; 978-90-481-4060-2
- Büntgen, U. (2022). Scrutinizing tree-ring parameters for Holocene climate reconstructions. *WIREs Climate Change* 13:e778. doi: 10.1002/wcc.778
- Buras, A. (2017). A comment on the expressed population signal. *Dendrochronologia* 44: 130–132. doi: 10.1016/j.dendro.2017.03.005
- Chen, F., Man, W. M., Wang, S. J., Esper, E., Meko, D., Büntgen, U., et al. (2023). Southeast Asian ecological dependency on Tibetan plateau streamflow over the last millennium. *Nat. Geosci.* 16, 1151–1158. doi: 10.1038/s41561-023-01320-1
- Choi, E.-B., Kim, Y.-J., Park, J.-H., Park, C.-R., and Seo, J.-W. (2020b). Reconstruction of resin collection history of pine forests in Korea from tree-ring dating. *Sustain. For.* 12:9118. doi: 10.3390/su12219118
- Choi, E.-B., Sano, M., Park, J.-H., Kim, Y.-J., Li, Z., Nakatsuka, T., et al. (2020a). Synchronizations of tree-ring $\delta^{18}\text{O}$ time series within and between tree species and provinces in Korea: a case study using dominant tree species in high elevations. *J. Wood Sci.* 66:53. doi: 10.1186/s10086-020-01901-3
- Choi, S.-S., Moon, S.-E., and Ha, C.-H. (1997). Climatological characteristics of the Nopsae wind. *Asia-Pacific J. Atmos. Sci.* 33, 349–361. (written in Korean with abstract in English)

Data availability statement

The raw data supporting the conclusions of this article will be made available by the authors, without undue reservation.

Author contributions

E-BC: Data curation, Formal analysis, Investigation, Visualization, Writing – original draft, Writing – review & editing, Methodology. J-HP: Investigation, Methodology, Writing – review & editing. MS: Formal analysis, Writing – review & editing. TN: Writing – review & editing. J-WS: Project administration, Writing – review & editing.

Funding

The author(s) declare financial support was received for the research, authorship, and/or publication of this article. This research was supported by Basic Science Research Program through the National Research Foundation of Korea (NRF) funded by the Ministry of Education (2020R1I1A307194514).

Conflict of interest

The authors declare that the research was conducted in the absence of any commercial or financial relationships that could be construed as a potential conflict of interest.

Publisher's note

All claims expressed in this article are solely those of the authors and do not necessarily represent those of their affiliated organizations, or those of the publisher, the editors and the reviewers. Any product that may be evaluated in this article, or claim that may be made by its manufacturer, is not guaranteed or endorsed by the publisher.

- Cook, E. R., and Kairiukstis, L. A. (1990) *Methods of dendrochronology: Applications in the environmental sciences*. Dordrecht, The Netherlands Springer. ISBN 0792305868.
- Dansgaard, W. (1964). Stable isotopes in precipitation. *Tellus* 16, 436–468. doi: 10.1111/j.2153-3490.1964.tb00181.x
- Eriksson, E. (1965). Deuterium and oxygen-18 in precipitation and other natural waters: some theoretical considerations. *Tellus* 17, 498–512. doi: 10.3402/tellusa.v17i4.9160
- Farquhar, G. D., Ehleringer, J. R., and Hubick, K. T. (1989). Carbon isotope discrimination and photosynthesis. *Annu. Rev. Plant Physiol. Plant Mol. Biol.* 40, 503–537. doi: 10.1146/annurev.pp.40.060189.002443
- Fritts, H. (1976) *Tree rings and climate*. Amsterdam: Elsevier. ISBN 0323145280.
- Fritts, H. C., Vaganov, E. A., Sviderskaya, I. V., and Shashkin, A. V. (1991). Climatic variation and tree-ring structure in conifers: empirical and mechanistic models of tree-ring width, number of cells, cell size, cell-wall thickness and wood density. *Clim. Res.* 1, 97–116. doi: 10.3354/cr001097
- Green, J. W. (1963). “Wood cellulose” in *Methods in carbohydrate chemistry*. ed. R. L. Whistler (New York: Academic Press)
- Harris, I., Osborn, T. J., Jones, P., and Lister, D. (2020). Version 4 of the CRU TS monthly high-resolution gridded multivariate climate dataset. *Sci. Data* 7:109. doi: 10.1038/s41597-020-0453-3
- Hau, N.-X., Sano, M., Nakatsuka, T., Chen, S.-H., and Chen, I.-C. (2023). The modulation of Pacific decadal oscillation on ENSO-east Asian summer monsoon relationship over the past half-millennium. *Sci. Total Environ.* 857:159437. doi: 10.1016/j.scitotenv.2022.159437
- Haupt, M., Weigl, M., Grabner, M., and Boettger, T. (2011). A 400-year reconstruction of July relative air humidity for the Vienna region (eastern Austria) based on carbon and oxygen stable isotope ratios in tree-ring latewood cellulose of oaks (*Quercus petraea* Matt. Liebl.). *Climate Change* 105, 243–262. doi: 10.1007/s10584-010-9862-1
- Jayme, G. (1942). Preparation of holocellulose and cellulose with sodium chlorite. *Cellulose Chem. Technol.* 20, 43–49.
- Jia, Y., Lv, G., Guligena, H., Qin, L., Peng, Z., Abudurehman, R., et al. (2023). Differences in the responses of tree-ring stable carbon isotopes of *L. sibirica* and *P. Schrenkiana* to climate in the eastern Tianshan Mountains. *Forests* 14:1032. doi: 10.3390/f14051032
- Kagawa, A., Sano, M., Nakatsuka, T., Ikeda, T., and Kubo, S. (2015). An optimized method for stable isotope analysis of tree rings by extracting cellulose directly from cross-sectional laths. *Chem. Geol.* 393–394, 16–25. doi: 10.1016/j.chemgeo.2014.11.019
- Kim, Y.-J., Yoon, Y.-H., Mitsutani, T., Moon, W.-S., and Park, W.-K. (2013). Species identification and tree-ring dating of wood boxes excavated from the Shinan shipwreck, Korea. *Dendrochronologia* 31, 266–272. doi: 10.1016/j.dendro.2013.01.002
- Kim, Y., and Kim, M. K. (2013). A study of Foehn over Hong Cheon area of Gangwon province in South Korea. *Korean Geogr. Soc.* 48, 37–55. (written in Korean with abstract in English)
- Kirdyanov, A. V., Treydte, K. S., Nikolaev, A., Helle, G., and Schleser, G. H. (2008). Climate signals in tree-ring width, density and $\delta^{13}\text{C}$ from larches in eastern Siberia (Russia). *Chem. Geol.* 252, 31–41. doi: 10.1016/j.chemgeo.2008.01.023
- Kong, W.-S., Lee, S.-G., Park, H.-N., Lee, Y.-M., and Oh, S.-H. (2014). Time-spatial distribution of *Pinus* in the Korean peninsula. *Quat. Int.* 344, 43–52. doi: 10.1016/j.quaint.2014.03.038
- Korea Meteorological Administration (2020) *Korean climate change assessment report 2020: Climate change impact and adaptation*. Seoul: Korea Meteorological Administration. ISBN 9788993652604.
- Korea Meteorological Administration (2022) *White note on Changma*. Seoul: Korea Meteorological Administration. ISBN 9791192280202 (written in Korean).
- Kress, A., Saurer, M., Siegwolf, R. T. W., Frank, D. C., Esper, J., and Bugmann, H. (2010). A 350-year drought reconstruction from alpine tree ring stable isotopes. *Glob. Biogeochem. Cycles* 24:GB2011. doi: 10.1029/2009GB003613
- Kurita, N., Ichiyanagi, K., Matsumoto, J., Yamanaka, M. D., and Ohata, T. (2009). The relationship between the isotopic content of precipitation and the precipitation amount in tropical regions. *Journal of Geochemical Exploration* 102: 113–122. doi: 10.1016/j.gexplo.2009.03.002
- Larcher, W. (2003) *Physiological plant ecology*. Berlin, Heidelberg: Springer. ISBN 9783540435167.
- Leavitt, S. W., and Long, A. (1988). Stable carbon isotope chronologies from trees in the southwestern United States. *Glob. Biogeochem. Cycles* 2, 189–198. doi: 10.1029/GB002i003p00189
- Lee, H.-Y. (1994). The Nopsae; Foehn type wind over the Young Suh region of Central Korea. *Korean Geogr. Soc.* 29, 266–280. (written in Korean with abstract in English)
- Lee, J.-H., Jeong, H.-M., Sano, M., and Seo, J.-W. (2023). Investigating the potential of the tree-ring $\delta^{18}\text{O}$ time series of *Pinus thunbergia* in the dendrochronological study. *J. Conserv. Sci.* 39, 288–296. doi: 10.12654/JCS.2023.39.3.10
- Li, Q., Liu, Y., Nakatsuka, T., Zhan, Q.-B., Ohnishi, K., Sakai, A., et al. (2020). Oxygen stable isotopes of a network of shrubs and trees as high-resolution paleoclimatic proxies in northwestern China. *Agric. For. Meteorol.* 285–286:107929. doi: 10.1016/j.agrformet.2020.107929
- Li, Q., Liu, Y., Song, H., Liu, R., Cai, Q., Sun, C., et al. (2022). Sensitive climate response of tree-ring $\delta^{18}\text{O}$ to current warming in the Qinling Mountains along a climate boundary in China. *Clim. Dyn.* 60, 2597–2612. doi: 10.1007/s00382-022-06460-5
- Liu, J., Wang, B., Ding, Q., Kuang, X., Soon, W., and Zorita, E. (2009). Centennial variations of the global monsoon precipitation in the last millennium: results from ECHO-G model. *J. Clim.* 22, 2356–2371. doi: 10.1175/2008JCLI2353.1
- Loader, N. J., McCarroll, D., Miles, D., Young, G. H. F., Davies, D., and Ramsey, C. B. (2019). Tree-ring dating using oxygen isotopes: a master chronology for Central England. *J. Quat. Sci.* 34, 475–490. doi: 10.1002/jqs.3115
- Loader, N. J., McCarroll, D., Miles, D., Young, G. H. F., Davies, D., Ramsey, C. B., et al. (2021). Dating of non-oak species in the United Kingdom historical buildings archive using stable oxygen isotopes. *Dendrochronologia* 69:125862. doi: 10.1016/j.dendro.2021.125862
- Loader, N. J., Robertson, I., Barker, A. C., Switsur, V. R., and Waterhouse, J. S. (1997). An improved technique for the batch processing of small wholewood samples to α -cellulose. *Chem. Geol.* 136, 313–317. doi: 10.1016/S0009-2541(96)00133-7
- Loader, N. J., Santillo, P. M., Woodman-Ralph, J. P., Rolfe, J. E., Hall, M. A., Gagen, M., et al. (2008). Multiple stable isotopes from oak trees in southwestern Scotland and the potential for stable isotope dendroclimatology in maritime climatic regions. *Chem. Geol.* 252, 62–71. doi: 10.1016/j.chemgeo.2008.01.006
- Lopez-Saez, J., Corona, C., Arx, G., Fonti, P., Slamova, L., and Stoffel, M. (2023). Tree-ring anatomy of *Pinus cembra* trees opens new avenues for climate reconstructions in the European Alps. *Sci. Total Environ.* 855:158605. doi: 10.1016/j.scitotenv.2022.158605
- Mandy, B. F., Helle, G., Balting, D. F., Ballis, N., Schleser, G. H., and Cubasch, U. (2023). European tree-ring isotopes indicate unusual recent hydroclimate. *Commun. Earth Environ.* 4:26. doi: 10.1038/s43247-022-00648-7
- McCarroll, D., and Loader, N. J. (2004). Stable isotopes in tree rings. *Quat. Sci. Rev.* 23, 771–801. doi: 10.1016/j.quascirev.2003.06.017
- Miles, D., Loader, N., Young, G., McCarroll, D., Davies, D., Ramsey, C. B., et al. (2019). Stable isotope dating of historic buildings. *Vernac. Archit.* 50, 78–87. doi: 10.1080/03055477.2019.1660955
- Ministry of Land Infrastructure and Transport and National Geography Information Institute (2020) *The National Atlas of Korea 2*. Suwon: Ministry of Land Infrastructure and Transport. ISBN 9791129002990.
- National Institute of Meteorological Sciences (2018). *100 Years of Climate Change in the Korea*. Jeju: National Institute of Meteorological Sciences (written in Korean).
- Pandey, U., Nakatsuka, T., Mehrotra, N., Zhen, L., Kato, Y., Sano, M., et al. (2023). Tree-rings stable isotope ($\delta^{18}\text{O}$ and $\delta^2\text{H}$) based 368 years long term precipitation reconstruction of southeastern Kashmir Himalaya. *Sci. Total Environ.* 892:164640. doi: 10.1016/j.scitotenv.2023.164640
- Park, B. I. (2020). Types and characteristics of the Foehn phenomena over the Yeong-Seo region of Central Korea. *Korean Geogr. Soc.* 55, 67–81. (written in Korean with abstract in English)
- Park, C.-H., Lee, U.-C., Kim, S.-C., and Lee, K.-H. (2021). The relationship between tree-ring growths of *Pinus densiflora* and climate from three mountains in central region, the Republic of Korea. *Atmos.* 12:878. doi: 10.3390/atmos12070878
- Park, W.-K., Kim, Y.-J., Jeong, A. R., Kim, S. K., Oh, J. A., Park, S. Y., et al. (2010). Tree-ring dating and AMS wiggle matching of wooden statues at Neunggasa Temple in South Korea. *Radiocarbon* 52, 924–932. doi: 10.1017/S003822200046026
- Park, W.-K., Kim, Y.-J., Seo, J.-W., Lee, J.-H., and Wazny, T. (2007). Tree-ring dating of Sinnmun, the north gate of Kyungbok palace in Seoul. *Tree-Ring Res.* 63, 105–109. doi: 10.3959/1536-1098-63.2.105
- Poage, M. A., and Chamberlain, C. P. (2001). Empirical relationships between elevation and the stable isotope composition of precipitation and surface waters: consideration for studies of paleovegetation change. *Am. J. Sci.* 301, 1–15. doi: 10.2475/ajs.301.1.1
- Preechamart, S., Pumijumong, N., Bräuning, A., Muangsong, C., Cai, B., and Buajan, S. (2023). Inter-annual and intra-annual tree-ring oxygen isotope signals in response to monsoon rainfall in northwestern Thailand. *The Holocene* 33, 335–346. doi: 10.1177/09596836221138352
- Roden, J. (2008). Cross-dating of tree ring $\delta^{18}\text{O}$ and $\delta^{13}\text{C}$ time series. *Chem. Geol.* 252, 72–79. doi: 10.1016/j.chemgeo.2008.01.007
- Roden, J. S., and Ehleringer, J. R. (1999). Hydrogen and oxygen isotope ratios of tree-ring cellulose for riparian trees grown long-term under hydroponically controlled environments. *Oecologia* 121, 467–477. doi: 10.1007/s004420050953
- Roden, J. S., Lin, G., and Ehleringer, J. R. (2000). A mechanistic model for interpretation of hydrogen and oxygen isotope ratios in tree-ring cellulose. *Geochim. Cosmochim. Acta* 64, 21–35. doi: 10.1016/S0016-7037(99)00195-7
- Rozanski, K., Araguas-Araguas, L., and Gonfiantini, R. (1993). Relation between Long-term trends of Oxygen-18 isotope composition of precipitation and climate. *Science* 258, 981–985. doi: 10.1126/science.258.5084.981

- Sano, M., Li, Z., Murakami, Y., Jinno, M., Ura, Y., Kaneda, A., et al. (2022). Tree ring oxygen isotope dating of wood recovered from a canal in the ancient capital of Japan. *J. Archaeol. Sci. Rep.* 45:103626. doi: 10.1016/j.jasrep.2022.103626
- Sano, M., Tshering, P., Komori, J., Fujita, K., Xu, C., and Nakatsuka, T. (2013). May–September precipitation in the Bhutan Himalaya since 1743 as reconstructed from tree ring cellulose $\delta^{18}\text{O}$. *J. Geophys. Res. Atmos.* 118, 8399–8410. doi: 10.1002/jgrd.50664
- Saurer, M., Borella, S., and Leuenberger, M. (1997). $\delta^{18}\text{O}$ of tree rings of beech (*Fagus sylvatica*) as a record of $\delta^{18}\text{O}$ of the growing season precipitation. *Tellus* 49, 80–92. doi: 10.3402/tellusb.v49i1.15952
- Saurer, M., and Siegwolf, R. T. W. (2007). Human impacts on tree-ring growth reconstructed from stable isotopes. *Terrestrial Ecol.* 1, 49–62. doi: 10.1016/S1936-7961(07)01004-4
- Schweingruber, F. H. (1996) *Tree rings and environment: dendrochronology*. Berne: Paul Haupt AG Bern. ISBN 9783258054582.
- Seo, J.-W., Jeong, H. M., Sano, M., Choi, E. B. I., Park, J. H., Lee, K. H., et al. (2017). Establishing tree ring $\delta^{18}\text{O}$ chronologies for principle tree species (*T. cuspidata*, *P. koraiensis*, *A. koreana*, *Q. mongolica*) at subalpine zone in Mt. Jiri National Park and their correlations with the corresponding climate. *J. Korean Wood Sci. Technol.* 45, 667–670. doi: 10.5658/WOOD.2017.45.5.661, (written in Korean)
- Seo, J.-W., Sano, M., Joeng, H.-M., Lee, K.-H., Park, H.-C., Nakatsuka, T., et al. (2019). Oxygen isotope ratios of subalpine conifers in Jirisan National Park, Korea and their dendroclimatic potential. *Dendrochronologia* 57:125626. doi: 10.1016/j.dendro.2019.125626
- Shin, B. M., and Lee, S. H. (2023). The relationship between the variability of the Changma date and atmospheric index over Korea. *Korean Geogr. Soc.* 58, 287–303. (written in Korean with abstract in English)
- Siegwolf, R. T. W., Brooks, J. R., Roden, J., and Saurer, M. (2020) *Stable isotopes in tree rings: Inferring physiological, climatic and environmental responses*. Dordrecht, The Netherlands: Springer.
- Speer, J. H. (2010) *Fundamentals of tree-ring research*. Tucson, AZ: University of Arizona Press. ISBN 0816526842.
- Sternberg, L. S. L. O.-R. (2009). Oxygen stable isotope ratios of tree-ring cellulose: the next phase of understanding. *New Phytol.* 181, 553–562. doi: 10.1111/j.1469-8137.2008.02661.x
- The Academy of Korean Studies (2016) *Geography of Korea*. Seoul: Seoul selection. ISBN 9788997639670.
- Vuille, M., Bradley, R. S., Werner, M., Healy, R., and Keimig, F. (2003). Modeling the $\delta^{18}\text{O}$ in precipitation over the Americas: 2. Interannual variability and climatic controls. *J. Geophys. Res.* 108:4175. doi: 10.1029/2001JD002039
- Watanabe, Y., Katayama, Y., Li, Z., Nakatsuka, T., and Tazuru, S. (2023). Assessments of tree-ring intra-annual $\delta^{18}\text{O}$ record for reconstructing hydroclimate with high temporal resolution. *Geosci. Lett.* 10:28. doi: 10.1186/s40562-023-00282-x
- Wigley, T. M. L., Briffa, K. R., and Jones, P. D. (1984). On the average value of correlated time series, with applications in dendroclimatology and hydrometeorology. *J. Appl. Meteorol. Climatol.* 23, 201–213. doi: 10.1175/1520-0450(1984)023<0201:OTAVOC>2.0.CO;2
- Wise, L. E., Murphy, M., and Adieco, A. A. D. (1946). Chlorite holocellulose, its fractionation and bearing on summative wood analysis and on studies on the hemicelluloses. *Paper Trade J.* 122, 35–43.
- WMO. (1992) International meteorological vocabulary, 2, vol.182. World Meteorological Organization (WMO), Geneva. ISBN 978-92-63-02182-3.
- Xu, C., Zhao, Q., An, W., Wang, S., Tan, N., Sano, M., et al. (2021). Tree-ring oxygen isotope across monsoon Asia: common signal and local influence. *Quat. Sci. Rev.* 269:107156. doi: 10.1016/j.quascirev.2021.107156
- Xu, C., Zhu, H., Nakatsuka, T., Sano, M., Li, Z., Shi, F., et al. (2017). Sampling strategy and climatic implication of tree-ring cellulose oxygen isotopes of *Hippophae tibetana* and *Abies georgei* on the southeastern Tibetan plateau. *Int. J. Biometeorol.* 63, 679–686. doi: 10.1007/s00484-017-1365-6
- Xu, Y., Zhang, H., Chen, F., Wang, S., Hu, M., Hadad, M., et al. (2023). Drought reconstruction since 1976 CE based on tree-ring widths in the upper Heilongjiang (Amur) river basin in Northeast Asia and its linkage to Pacific Ocean climate variability. *Clim. Past* 19, 2079–2092. doi: 10.5194/cp-19-2079-2023
- Yakir, D., DeNiro, M. J., and Ephrath, J. E. (1990). Effects of water-stress on oxygen, hydrogen and carbon isotope ratios in two species of cotton plants. *Plant Cell Environ.* 13, 949–955. doi: 10.1111/j.1365-3040.1990.tb01985.x
- Young, G. H. F., Bale, R. J., Loader, N. J., McCarroll, D., Nayling, N., and Voutsden, N. (2012). Central England temperature since AD 1850: the potential of stable carbon isotopes in British oak trees to reconstruct past summer temperatures. *J. Quat. Sci.* 27, 606–614. doi: 10.1002/jqs.2554
- Young, G. H. F., Loader, N. J., McCarroll, D., Bale, R. J., Demmler, J. C., Miles, D., et al. (2015). Oxygen stable isotope ratios from British oak tree-rings provide a strong and consistent record of past changes in summer rainfall. *Clim. Dyn.* 45, 3609–3622. doi: 10.1007/s00382-015-2559-4



OPEN ACCESS

EDITED BY

Manfred J. Lexer,
University of Natural Resources and Life
Sciences Vienna, Austria

REVIEWED BY

Muhammad Ishtiaq,
Mirpur University of Science and Technology,
Pakistan
Mathias Neumann,
University of Natural Resources and Life
Sciences Vienna, Austria

*CORRESPONDENCE

Qian He
✉ heqian@scau.edu.cn
Quan Qiu
✉ qqiu@scau.edu.cn

RECEIVED 19 July 2023

ACCEPTED 11 April 2024

PUBLISHED 24 April 2024

CITATION

Guan Z, Zhang Q, Xu T, Chen D, Lu Y, Han Q,
Li N, Ma W, Wang J, Su Y, Li J, Qiu Q and
He Q (2024) Modeling branch attributes and
biomass for *Catalpa bungei* plantations under
various fertilization regimes.
Front. For. Glob. Change 7:1261310.
doi: 10.3389/ffgc.2024.1261310

COPYRIGHT

© 2024 Guan, Zhang, Xu, Chen, Lu, Han, Li,
Ma, Wang, Su, Li, Qiu and He. This is an open-
access article distributed under the terms of
the [Creative Commons Attribution License
\(CC BY\)](https://creativecommons.org/licenses/by/4.0/). The use, distribution or reproduction
in other forums is permitted, provided the
original author(s) and the copyright owner(s)
are credited and that the original publication
in this journal is cited, in accordance with
accepted academic practice. No use,
distribution or reproduction is permitted
which does not comply with these terms.

Modeling branch attributes and biomass for *Catalpa bungei* plantations under various fertilization regimes

Zhuizhui Guan^{1,2}, Qingbin Zhang¹, Tiaozi Xu², Dong Chen²,
Yizeng Lu³, Qingjun Han³, Ningning Li³, Wenjun Ma⁴,
Junhui Wang⁴, Yan Su², Jiyue Li², Quan Qiu^{2*} and Qian He^{2*}

¹Xinyang Agriculture and Forestry University, Xinyang, China, ²Guangdong Key Laboratory for Innovative Development and Utilization of Forest Plant Germplasm, College of Forestry and Landscape Architecture, South China Agricultural University, Guangzhou, China, ³Shandong Provincial Center of Forest and Grass Germplasm Resources, Institute of Resource Cultivation, Jinan, China, ⁴Research Institute of Forestry, Chinese Academy of Forestry, Beijing, China

The development and morphology of branches, a crucial step in producing high-quality large-diameter lumber, may be influenced by fertilization. The response of branch attributes to different fertilization regimes, however, is still poorly understood. The *Catalpa bungei* plantations, which had been growing for 6 years in northern China, were chosen to study how various fertilization measures affected branch attributes. The two fertilization techniques used were hole fertilization (HF) and water and fertilizer integration (WF), with no fertilization (CK) as a control. The quantity, density, morphology (e.g., diameter, length, and angle), and position (e.g., height and orientation) of branches, and organ biomass of 18 standard trees (total of 516 branches) were investigated. The results demonstrated a considerable increase in tree height, diameter at breast height (DBH), canopy ratio, branch quantity, and organ biomass following the addition of fertilizer. Both the maximum branch diameter and the number of branches rose with fertilization. Following fertilization, the number of branches rose by 16% (HF) and 28% (WF) compared to non-fertilized trees, while the maximum branch diameter increased by 3.5% (HF) and 17.3% (WF), respectively. WF led to an increase in the number of branches and largest branch diameter in comparison to CK and HF. The length, angle, and diameter of branches, however, were not affected significantly by different fertilization treatments. There were roughly equal amounts of branches in four orientations. The mixed-model analysis revealed that the number of branches was positively correlated with branch density and tree height. The branch diameter increased with the increase of branch length and angle. The branch length was negatively correlated with branch height and angle. The branch angle showed a larger angle at the bottom of the canopy. Tree height plus diameter at breast height combined, or just the diameter at breast height indicator alone, can both reliably predict the total biomass of trees. The branch models created in this research may offer some theoretical backing for understanding the crown dynamics of valuable tree species in northern China.

KEYWORDS

Catalpa bungei, fertilization, mixed-effects models, branch attributes, wood quality, integration of water and fertilizer

Introduction

The vigor and yield of trees are directly determined by the size, composition, and morphology of the tree canopy (Hein et al., 2007; Newton et al., 2012). The first-order branch, a vital component of the crown, mainly serves as the backbone of the tree. The crown shape is primarily determined by the length and spatial layout of the first-order branch. The evaluation and selection of appropriate management measures are potentially more accurate and biologically realistic via the quantitative simulation of the quantity, size, distribution, and growth of first-order branches, which can accurately forecast canopy dynamics, tree growth, and wood quality (Hein, 2008; Danescu et al., 2015; Wang et al., 2016, 2018).

Numerous studies have explored the branch attributes of various tree species, and, the majority of reports focus mostly on the linear and nonlinear models (Li, 2004; Liu et al., 2008; Courbet et al., 2012). For example, the branch models (e.g., diameter, length, angle, and number) are constructed directly with stand variables (e.g., site and density), tree variables (e.g., diameter at breast height, tree height, and crown length), as well as branch depth (Maguire et al., 1999; Courbet et al., 2007). These models have a high level of accuracy. The collinearity problem must be taken into account since variable components may autocorrelate. Furthermore, the model's forest interpretation is subpar (Hein et al., 2007; Jiang et al., 2012). Actually, the fundamental data used in forest management may follow a hierarchical pattern. As an illustration, consider the following categorization system: the stand covers the sample plot, the plot covers the sample tree, and the sample tree covers the branch (Wang et al., 2015, 2017, 2018). Therefore, the errors can not satisfy the assumption of independent distribution due to the situations of 'plot effect' or 'tree effect' in traditional modeling. As a result of the random selection of plots and trees, at least three effects should be included in the random errors (i.e., plots, trees, and branches).

The theoretical model (such as the nonlinear model) serves as the foundation for the mixed effect model. The fact that there is nesting in the data means that the mixed effects model can only be applied under this condition. The goal of mixed linear models, as opposed to general linear models, is to introduce random effects to create a better model for data interpretation. The theoretical model's parameters are updated to include the variable factors that have a meaningful relationship with the dependent variables. The model parameters that were built have strong ecological or forest implications (Gao et al., 2014). The mixed-effect models specify several covariance structures to describe the pertinent error scenario in order to reduce the error correlation and heterogeneity caused by the hierarchical structure data, increase the predictive power of models and illuminate the origin of variance components (Li and Tang, 2010).

In recent years, mixed models have been extensively utilized in forest investigation, such as diameter at breast height (Lei et al., 2009; Li, 2011), tree height (Fang and Bailey, 2001; Calegario et al., 2005), wood volume (Jiang et al., 2011), stem form (Jiang and Liu, 2011), and stand basal area (Li and Tang, 2010). Meredieu et al. (1998) established the length and angle models of *Pinus nigra* branches using a linear mixed model. Similarly, Beaulieu et al. (2011) developed the branch models of *Pinus banksiana* after considering the random impacts of the block, plot, and individual tree. Wang et al. (2018) created the generalized linear mixed models of live and dead branch numbers for *Betula alnoides* plantations. Dong et al. (2013) predicted the size of

first-order branches for *Pinus koraiensis* forests based on mixed-effect models. All of the relevant reports show that the mixed models outweigh traditional regression techniques when modeling the branch properties.

Until now, research has focused primarily on the effects of planting density (Wang et al., 2015, 2017), stand thinning (Weiskittel et al., 2007; Jia et al., 2021), and pruning (Pinkard, 2002; Wang and Zeng, 2016) on branch development, whereas reports on the effects of different fertilization regimes on branch attributes are scarce. Fertilization can regulate the growth of trees, which in turn can indirectly affect branch development. Chen (2020) discovered that various fertilization methods might drastically alter the branch diameter and length for seven-year-old *Tectona grandis* clones. Moreover, Briggs et al. (2008) noted that fertilizer intake had an impact on the branch diameter of coastal Douglas-fir plantings. As a result, we used the commercially valuable tree species *Catalpa bungei* originated from northern China as an example to investigate the effects of various fertilization measures, including water and fertilizer integration, hole fertilization, and no fertilization as a control, on branch attributes and tree biomass through branch dissection. The objectives of this study are addressed: First, create the mixed models that predict the quantity, diameter, angle, length of the branches, and tree biomass, respectively; second, explore whether the various fertilization regimes have an impact on the branch attributes. The hypothesis put forth in this study is that fertilization will, on the one hand, increase the biomass of trees, as well as the diameter and length of their branches, and will also significantly affect the branching angle of those branches; on the other hand, the branching properties of branches will be affected differently by different fertilization regimes. The findings of this study can be used to theoretically support branch development forecasts in broad-leaved trees in North China.

Materials and methods

Experimental plot and tree species

The study plots are situated in the Jujube Preservation Warehouse in Zhangqiu District, Shandong Province, China (36°25′-37°09′ N, 117°10′-117°35′ E). The research regions experience a moderate monsoon climate. The yearly average temperature is 12.8°C, with a maximum monthly temperature in July of 27.2°C and a minimum in January of -3.2°C. There is an average of 600.8 mm of precipitation, 2647.6 h of sunshine, and 192 days without frost throughout the entire year. The growing seasons of *C. bungei* forests last 130–150 days from May to September.

In March 2017, we established a pure forest with a row spacing of 3 × 4 m using a 2-year-old *C. bungei* clone ("9-1"). The total planting area was 0.8 ha with a total of 18 plots (384 m² for each plot), and 45 trees (5 rows × 9 columns) were planted in each plot. Since the planting of the trees, no tending had been done. After planting, *C. bungei* trees had an average height of 4.2 m and diameter at breast height (DBH) of 4.0 cm. Immediately following afforestation, the chemical composition of the soil was assessed, including its pH (7.67), organic matter content (19.64 g/kg), total nitrogen (0.91 g/kg), total phosphorus (0.53 g/kg), total potassium (16.70 g/kg), alkaline hydrolyzed nitrogen (81.88 mg/kg), available phosphorus (32.10 mg/

kg), and available potassium (176.82 mg/kg). The majority of the soil in the area is brown loam.

Field fertilization

Beginning in May 2018, we selected 9 plots at random and fertilized them as part of a split-plot experiment. Existing fertilization techniques included hole fertilization (HF) and water and fertilizer integration (WF), with no fertilization acting as a control. The HF approach was applied based on the previously fertilized forests of *C. bungei* (unpublished). The WF method was alluded to as being derived from the fertilization of fruits and crops in the agricultural ecosystem. Three plots were randomly selected for each fertilization treatment, and the distance between plots was around 6–8 m.

Early in May 2018, fertilization studies were carried out, with WF and HF applying the same quantity of fertilizers each year. In the first year, N (24 g/tree), P₂O₅ (8 g/tree), and K₂O (16 g/tree) were applied as fertilizers. Subsequently, the annual amount of fertilizers increased by 20% compared to the previous year. Every year in May, HF applied all of the fertilizers at once. We excavated a hole, with a size of 20 cm in diameter and 30 cm in depth in the south and north of each tree. Then the fertilizers were equally divided into 2 parts and placed into the holes. No water was added after covering the soil. WF divided its annual fertilizers into 12 portions that were distributed equally. Starting on May 1st, we fertilized once every 10 days. The fertilizers were correctly delivered close to the roots after being dissolved in 1000 L of water using an intelligent drip irrigation system (HN-BXE, Huinong Automation Corporation, China). Potassium sulfate was employed as the potassium fertilizer and urea as the nitrogen fertilizer for HF and WF. Calcium superphosphate was utilized as a phosphate fertilizer for HF, whereas ammonium dihydrogen phosphate was used for WF. All fertilizers were purchased on the Taobao website. The temperature and precipitation data from the nearby meteorological station for the years 2017 through 2022 were displayed in [Supplementary Figure S1](#).

Branch dissection and biomass determination

The standard tree represents the average level of trees in each sample plot, including their average height and DBH. Two standard trees were felled in each plot, and a total of 18 trees and 516 branches were collected in November 2021. In short, 6 trees were felled in each of the three treatments. The DBH and crown width (CW) were measured before being cut down. The tree height (TH) and the height of the crown base (HCB) were determined after felling. All branches (except dead branches) were dissected from the crown base to the top. The branch height (BH) (2.30–9.13 m), diameter (BD) (6.21–94.05 mm), angle (BA) (6.3–92.8°), length (BL) (0.45–5.10 m), orientation (BO) (0–355°), number of branches (NB) (20–39 branches), and density of the branches (DB) (3–6 branches·m⁻¹) were measured.

The DBH was the diameter of the trunk at 1.3 m. The CW was the mean of the east–west and north–south projections of the canopy. The TH was the vertical distance from the bottom to the top of the tree. The HCB was the vertical distance from the bottom of the trunk to the

crown base. The BH was the vertical distance from the base of the branch to the bottom of the trunk. The BD was the diameter at the base of the branch. The BA was the insertion angle between the branch and trunk pith. The BL was the distance between the base and the tip of the branch. The DB was the ratio of branch number to crown length. In addition, the trees were divided into the individual organ, including stems, branches, leaves, and roots. All of the roots were dug up with an excavator, and any soil that was left on top of the roots was then removed with a brush. The fresh weight of each organ was determined. Then, a small portion of each organ was collected, taken back to the laboratory at low temperature, and dried for water content determination.

Statistical analysis

The biomass was the difference between the fresh weight and water content of the organ. The total biomass of the tree was the sum of trunks, branches, leaves, and roots. The differences in branch attributes or organ biomass in different fertilization regimes were compared using a one-way analysis of variance (ANOVA) and Tukey's honestly significant difference test (Tukey's HSD). Since the data for the branch attributes of the investigated trees had a hierarchical structure, linear mixed-effects models ([Equations 1 and 2](#)) were used to assess the significance of variations in treatment for branch attributes at the tree and branch level.

$$y_{pt} = \mu + \mathcal{G}_F + \varphi_p + \varphi_{pt(\text{tree level})} \quad (1)$$

$$y_{ptbr} = \mu + \mathcal{G}_F + \varphi_p + \varphi_{pt} + \varphi_{ptbr(\text{branch level})} \quad (2)$$

Where y was observed value; μ was the overall mean; \mathcal{G}_F was the effect of fertilization regimes; φ_p , φ_{pt} , and φ_{ptbr} were the random effects for plot (p), tree (t), and branch (br), respectively.

The restricted maximum likelihood estimation (REML) was employed in the mixed-model analysis, and Tukey's HSD was utilized to conduct multiple range tests between treatments. Generalized linear mixed models (GLMM) were utilized for count variables (e.g., branch number) in the model-building process, and linear mixed models (LMM) were used for continuous variables (e.g., BD and BL). The following approaches were used to model the branch attributes. The multiple linear regression models were initially run for dependent variables with all pertinent independent variables to select potential factors. The prospective factors with statistical significance, a reasonable ecological explanation, and a variance inflation factor (VIF) that was not greater than three were then used to construct the mixed effects models. All of the above candidate and random components (such as plot and tree effects) were then evaluated using likelihood ratio tests (LRT) when a mixed effects model was constructed using the REML. Factors at a significance level of 0.05 were incorporated into models. Generalized linear models (GLM) or linear models (LM) were replaced in the absence of any discernible random factors. Lastly, the models were updated using the previously selected fixed and random components, and the best-fit models were picked from a range of variance functions primarily based on model simplicity and the Akaike Information Criterion (AIC).

Model performance was evaluated using the root mean squared error (RMSE), which was determined for each model on the original data scale. In the case of GLM, the predictive power R^2 was calculated as the squared correlation between observations and predictions. The marginal R^2 (R_m^2 , only the fixed effects) and conditional R^2 (R_c^2 , including the fixed and random effects) were measured for LMM. The associations between the dependent and all independent variables were expressed using simulation plots built on the fitting models. All statistical analyses and model building were performed using SPSS 25.0 for Windows (IBM-SPSS Inc., Chicago, IL, United States) (Table 1).

Results

Tree growth

The fertilizing regimes had minimal impact on the HCB and CD but markedly increased the TH, DBH, and CR (Table 2). The DBH grew by 7.8 and 19.5% and the TH increased by 1.9 and 8.2% for HF and WF in comparison to CK, respectively. HF and WF produced greater stems, branches, leaves, roots, and total biomass than CK (Table 3). WF dramatically enhanced the total biomass of each organ compared to other fertilizing methods. WF increased the stem biomass by 45.9%, branch biomass by 59.8%, leaf biomass by 63.8%, root biomass by 37.7%, and total biomass by 48.3% compared to CK, respectively. The rank of organ biomass in three fertilization regimes was: stem > root > branch > leaf. The fertilization techniques did not, however, have a significant impact on the allocation proportion of organ biomass.

Branch quantity and orientation

Amongst the three fertilization regimes, there was a noticeable difference in the total number of branches within the crown (Table 4). Most branches were in WF, and the fewest were in CK. Branch density did not considerably vary in response to fertilization regimes. The amount and percentage of branches at the four orientations for each fertilization treatment did not differ noticeably (Table 5). Thus, the four orientations of the branches within the crown were distributed roughly equally.

Branch diameter, length, and angle

Fertilization regimes had no discernible effect on the diameter, length, and angle of the *C. bungei* branches (Table 4). WF dramatically increased the biggest branch diameter compared to CK and HF. The height of the largest branch in WF was dramatically lowered than CK and HF.

Simulation of branch attributes and total biomass

Branch number

The number of branches (NB) was strongly correlated with the density of branches (DB), fertilization regimes (FR), and tree height (TH) (Equation 3). Parameter estimates, standard errors, and

TABLE 1 Summary of the abbreviation and symbol.

| Abbreviation | Indices implication | Precision |
|--------------------------|--|-----------|
| <i>Fertilization</i> | | |
| FR | Fertilization regime | / |
| CK | No fertilization | / |
| HF | Hole fertilization | / |
| WF | Integration of water and fertilizer | / |
| <i>Tree indices</i> | | |
| TH | Tree height | 0.01 m |
| DBH | Diameter at breast height | 0.01 cm |
| HCB | Height of crown base | 0.01 m |
| CR | Crown ratio | / |
| CD | Crown diameter | 0.01 m |
| <i>Branch indices</i> | | |
| BD | Branch diameter | 0.01 mm |
| BL | Branch length | 0.01 m |
| BA | Branch angle | 1° |
| BH | Branch height | 0.01 m |
| DB | Density of branch | / |
| NB | Number of branch | / |
| <i>Biomass indices</i> | | |
| LB | Leaf biomass | 0.01 kg |
| BB | Branch biomass | 0.01 kg |
| SB | Stem biomass | 0.01 kg |
| RB | Root biomass | 0.01 kg |
| TB | Total biomass | 0.01 kg |
| <i>Model descriptors</i> | | |
| a, b, c, d | Coefficients of fixed effect and intercept | / |
| p, pt., ptbr | Subscripts for plot, tree, and branch | / |
| α, β, γ | Variance component (random effect) | / |
| ln() | Natural log-link | / |
| RMSE | Root mean squared error | / |
| R_c^2, R_m^2 | Conditional and marginal R^2 | / |

statistical significance of the intercepts and predictors of the equation were displayed in Table 6.

$$\ln(\text{NB}) = a_0 + a_1 \times \text{DB} + a_2 \times \ln(\text{FR}) + a_3 \times \ln(\text{TH}) \quad (3)$$

The NB increased with the increase of DB (Figure 1A) and TH (Figure 1B). The NB under fertilization was higher than CK, and the NB in WF was larger than HF. A larger percentage of the overall variation was explained by the model ($R^2 = 0.804$). The accuracy of the model was likewise great (RMSE = 1.150).

TABLE 2 The sampled tree attributes of *Catalpa bungei*.

| Fertilization | TH (m) | DBH (cm) | HCB (m) | CD (m) | CR |
|---------------|----------------|----------------|---------------|---------------|----------------|
| CK | 8.98 ± 0.42 b | 12.57 ± 0.62 c | 3.51 ± 0.54 a | 3.15 ± 0.64 a | 0.61 ± 0.06 b |
| HF | 9.15 ± 0.30 ab | 13.55 ± 0.35 b | 3.06 ± 0.30 a | 3.32 ± 0.34 a | 0.66 ± 0.04 ab |
| WF | 9.72 ± 0.53 a | 15.02 ± 0.56 a | 2.91 ± 0.70 a | 3.69 ± 0.31 a | 0.70 ± 0.07 a |

Mean ± SD was shown. The different letters in the same column indicated significant differences between fertilization regimes at the 0.05 level (Tukey's HSD). CR = (TH - HCB)/TH. The abbreviations were referred to Table 1.

TABLE 3 Summary of biomass partitions of the felled *Catalpa bungei*.

| Biomass | CK | HF | WF |
|------------------|----------------|----------------|------------------|
| Stem (kg) | 40.13 ± 4.64 b | 47.09 ± 2.16 b | 58.55 ± 7.00 a |
| Stem ratio (%) | 46 ± 1 a | 48 ± 2 a | 45 ± 2 a |
| Branch (kg) | 16.10 ± 3.67 b | 17.98 ± 2.84 b | 25.73 ± 4.33 a |
| Branch ratio (%) | 19 ± 3 a | 18 ± 2 a | 20 ± 2 a |
| Leaf (kg) | 9.03 ± 1.62 b | 9.95 ± 1.72 b | 14.79 ± 0.98 a |
| Leaf ratio (%) | 10 ± 1 a | 10 ± 2 a | 12 ± 1 a |
| Root (kg) | 21.82 ± 2.73 b | 23.25 ± 2.91 b | 30.05 ± 1.81 a |
| Root ratio (%) | 25 ± 4 a | 24 ± 2 a | 23 ± 2 a |
| Total (kg) | 87.08 ± 9.93 b | 98.27 ± 5.26 b | 129.12 ± 12.21 a |

Mean ± SD was shown. The different letters in the same row indicated significant differences between fertilization regimes at the 0.05 level (Tukey's HSD).

Branch diameter

Branch diameter (BD) was closely associated with branch length (BL) and angle (BA) (Equation 4). Parameter estimates, standard errors, and statistical significance of the intercepts, fixed and random effects of the equation were presented in Table 6.

$$\ln(\text{BD}) = b_0 + b_1 \times \ln(\text{BL}) + b_2 \times \text{BA} + \alpha_{\text{ptbr}} \quad (4)$$

Branch diameter was positively correlated with branch length (Figure 2A) and angle (Figure 2B). Branch length had a higher impact on branch diameter than branch angle across the whole range of our dataset under consideration. The current model had a modestly low level of precision (RMSE = 9.300 mm), and it only adequately explained about 40% of the overall variance ($R_m^2 = 0.363$, $R_c^2 = 0.370$).

Branch length

The model showed that branch length (BL) was significantly correlated with branch diameter (BD), height (BH), and angle (BA) (Equation 5).

$$\ln(\text{BL}) = c_0 + c_1 \times \ln(\text{BD}) + c_2 \times \text{BH} + c_3 \times \text{BA} + \beta_{\text{ptbr}} \quad (5)$$

Across the whole range of the datasets we gathered, branch length increased as branch diameter did (Figure 3A), but it decreased when branch height and angle did (Figures 3B,C). Branch height and angle were less influential factors in determining branch length than branch diameter. The current model performed well in terms of prediction accuracy (RMSE = 0.882 m), accounting for around 50% of the overall variance ($R_m^2 = 0.453$, $R_c^2 = 0.457$).

TABLE 4 The branch attributes of *Catalpa bungei* undergoing three fertilization regimes.

| Branch attributes | Fertilization regimes | | |
|--|-----------------------|-----------------|-----------------|
| | CK | HF | WF |
| Branch number | 25 ± 5 b | 29 ± 4 ab | 32 ± 4 a |
| Branch density (branches·m ⁻¹) | 4.64 ± 0.67 a | 4.75 ± 0.63 a | 4.71 ± 0.72 a |
| Branch diameter (mm) | 23.21 ± 11.31 a | 23.24 ± 11.40 a | 24.73 ± 12.36 a |
| The largest branch diameter (mm) | 55.25 ± 15.01 b | 57.17 ± 12.42 b | 64.81 ± 15.68 a |
| Height of the largest branch (m) | 4.49 ± 0.93 a | 4.37 ± 0.87 ab | 3.65 ± 0.81 b |
| Branch length (m) | 1.94 ± 0.83 a | 1.91 ± 0.81 a | 2.10 ± 0.88 a |
| Branch angle (°) | 33 ± 15 a | 31 ± 15 a | 34 ± 15 a |

Mean ± SD was shown. The abbreviations saw Table 1. The different letters in the same row indicated significant differences between fertilization treatments at the 0.05 level (Tukey's HSD).

Branch angle

In our study, branch angle was significantly correlated with branch height (BH), diameter (BD), and length (BL) (Equation 6).

$$\ln(\text{BA}) = d_0 + d_1 \times \text{BH} + d_2 \times \ln(\text{BD}) + d_3 \times \ln(\text{BL}) + \gamma_{\text{pt}} + \gamma_{\text{ptbr}} \quad (6)$$

The branch angle increased as branch diameter increased (Figure 4B), but it reduced when branch height (Figure 4A) and length (Figure 4C) increased. The influence of branch diameter on branch angle was stronger than that of branch height and length across the entire range of our investigated datasets. The model had a good level of precision (RMSE = 5.8°), and it described a significant amount of the overall variation ($R_m^2 = 0.717$, $R_c^2 = 0.723$).

Total biomass

We developed the models that combined individual tree biomass and growth parameters such as tree height, DBH, crown width, and so on, and discovered that a single index (DBH) or two indexes (H and DBH) can better predicted biomass, with adj-R² reaching 0.95 (Table 7). The models of H-TB, CW-TB, and H:DBH-TB with adj-R² only ranging from 0.34 to 0.53 had lower predictive ability for TB.

Discussion

Tree growth and biomass

Our results showed that fertilization regimes (i.e., WF and HF) significantly increased the tree height, DBH, and organ biomass in the *C. bungei* forests compared to no fertilization. The fertility of the soil

TABLE 5 The branch quantity at four orientations of *Catalpa bungei* undergoing three fertilization regimes.

| Fertilization | East-North (0–90°) | | East-South (91–180°) | | West-South (181–270°) | | West-North (271–360°) | |
|---------------|--------------------|---------------|----------------------|---------------|-----------------------|---------------|-----------------------|---------------|
| | Number | Proportion | Number | Proportion | Number | Proportion | Number | Proportion |
| CK | 7 ± 3 a | 0.28 ± 0.12 a | 7 ± 2 a | 0.28 ± 0.08 a | 6 ± 2 a | 0.23 ± 0.06 a | 5 ± 2 a | 0.22 ± 0.10 a |
| HF | 8 ± 3 a | 0.28 ± 0.08 a | 8 ± 1 a | 0.27 ± 0.06 a | 7 ± 3 a | 0.24 ± 0.09 a | 6 ± 2 a | 0.22 ± 0.05 a |
| WF | 9 ± 3 a | 0.26 ± 0.09 a | 7 ± 2 a | 0.23 ± 0.06 a | 8 ± 3 a | 0.24 ± 0.06 a | 8 ± 1 a | 0.27 ± 0.05 a |

Mean ± SD was shown. The abbreviations saw Table 1. The different letters in the same column indicated significant differences between fertilization treatments at the 0.05 level (Tukey's HSD).

TABLE 6 Parameter estimates of fixed and random variables of the Equations (3–7).

| Equations | Response variables | Regression parameters | Predictor variables | Estimate | Standard error | Significance |
|-----------|--------------------|-----------------------|---------------------|----------|----------------|--------------|
| (3) | NB | a ₀ | Intercept | -0.116 | 1.013 | 0.910 |
| | | a ₁ | DB | 0.179 | 0.032 | <0.001 |
| | | a ₂ | FR | 0.121 | 0.053 | 0.038 |
| | | a ₃ | TH | 1.142 | 0.449 | 0.023 |
| (4) | BD | b ₀ | Intercept | 2.481 | 0.023 | <0.001 |
| | | b ₁ | BL | 0.909 | 0.017 | <0.001 |
| | | b ₂ | BA | 0.002 | 0.001 | 0.011 |
| | | α _{ptbr} | | 0.005 | 0.002 | 0.04 |
| (5) | BL | c ₀ | Intercept | -1.604 | 0.098 | <0.001 |
| | | c ₁ | BD | 0.830 | 0.021 | <0.001 |
| | | c ₂ | BH | -0.053 | 0.007 | <0.001 |
| | | c ₃ | BA | -0.002 | 0.001 | 0.003 |
| | | β _{ptbr} | | 0.005 | 0.002 | 0.016 |
| (6) | BA | d ₀ | Intercept | 3.487 | 0.278 | <0.001 |
| | | d ₁ | BH | -0.115 | 0.017 | <0.001 |
| | | d ₂ | BD | 0.218 | 0.098 | 0.026 |
| | | d ₃ | BL | -0.212 | 0.102 | 0.038 |
| | | γ _{pt} | | 0.005 | 0.001 | 0.047 |
| | | γ _{ptbr} | | 0.054 | 0.013 | <0.001 |

The abbreviations were referred to Table 1.

and availability of nutrients needed for plant growth are improved through soil fertilization (Tumushime et al., 2019; Yang and Karban, 2019; Li et al., 2021). In this study, the WF forests had greater tree growth and organ biomass than the HF forests did. Tree absorption and utilization for liquid fertilizer were superior to solid fertilizer, producing more biomass in the WF forests (Ma et al., 2019; Guan et al., 2022). The forest serves as a massive biomass carbon reservoir while also conserving water. Thus, WF forests may be recommended in terms of exhibiting greater water conductivity and carbon storage capabilities. Moreover, the DBH-TB model stated that it was possible to compute the total biomass of trees fairly quickly and efficiently, saving both time and labor, by precisely determining the DBH value.

Branch quantity

The H:D (i.e., TH: DBH) and crown ratio (i.e., CR) can be generally used as the indicators of tree vigor. The findings on the Scots pine and Norway spruce demonstrated that greater tree vigor increased the number of branches in a whorl (Kellomäki and Tuimala, 1981; Hein et al., 2007). Similarly, our results also indicated that fertilizer input obviously improved the CR and branch quantity

compared to non-fertilizer added. Furthermore, WF considerably increased the tree height and crown ratio compared to HF, which may result in an increase in branch number. However, our study was not partly in line with the reports on *Tectona grandis*, where the number of total branches was proved to be not affected by fertilization (Chen, 2020). Weiskittel et al. (2007) also found that the branch numbers of the coastal Douglas-fir were not related to the fertilizer input. But, instead, our results seemed to be in agreement with observations of a positive relationship between the number of branches and height growth in Norway spruce (Colin and Houllier, 1992; Klang and Ekö, 1999), and our study showed that fertilization increased the annual height growth of the stem. Another finding in our study was that the branch quantity in the WF forests was higher than that in the HF forests. These differences in the above studies might originate from the differences in fertilizer types, duration, and frequency in different fertilization regimes. In addition, the varying results among studies may also be potentially attributable to differences in soil attributes and species morphology/physiology.

The fertilized trees exhibited bigger crowns than the control trees due to their enhanced height and branch growth. The competition for

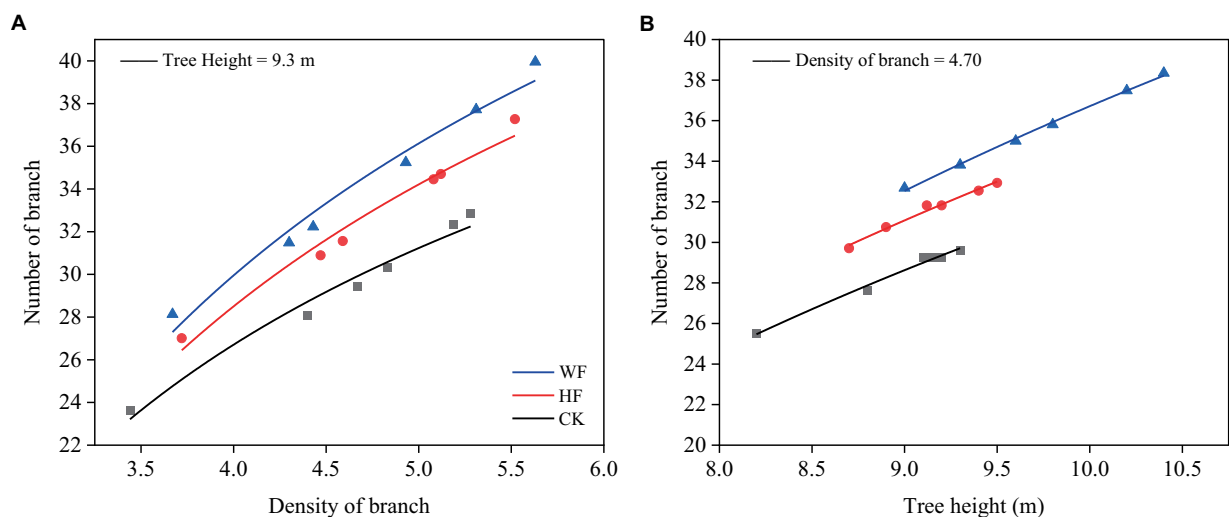


FIGURE 1 Relationships between branch number and branch density (A) and tree height (B). The abbreviations were referred to Table 1.

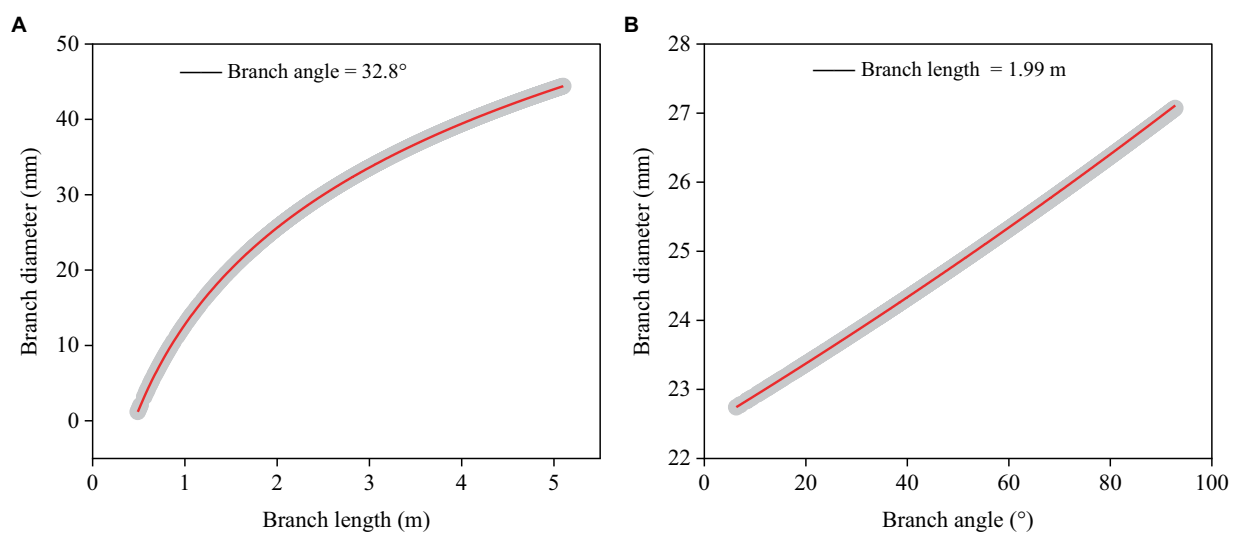


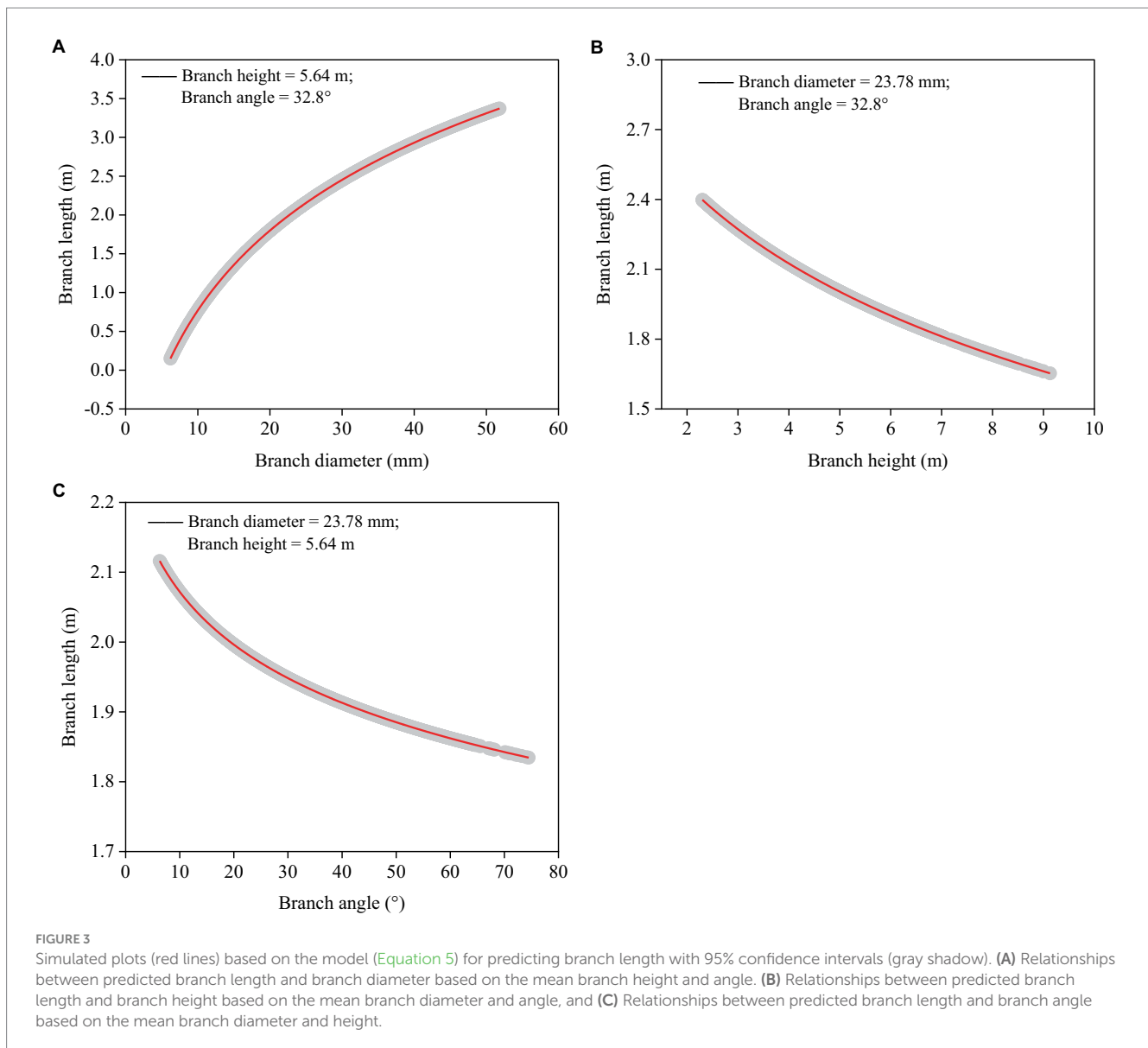
FIGURE 2 Simulated plots (red lines) based on the model (Equation 4) for predicting branch diameter with 95% confidence intervals (gray shadow). (A) Relationships between predicted branch diameter and branch length based on the mean branch angle. (B) Relationships between predicted branch diameter and branch angle based on the mean branch length.

light, thus, may be more intense in WF and HF stands. The base of the green crown was, however, lower in WF and HF forests than in non-fertilized forests, but the difference was small. This indicated that light limitations had not resulted in increased branch mortality at the bottom of the canopy in WF and HF stands. The fact that there were fewer living branches at the bottom of the canopy in control stands was probably the effect of low nutrient availability in non-fertilized stands.

Branch diameter

Branch characteristics, such as branch diameter, length, and angle, control the crown architecture and have a substantial impact on stem growth and knot development (Hein et al., 2008; Forrester et al., 2012;

Nelson et al., 2014). Our investigation found that fertilization schedules only increased the diameter of the largest branch but had no discernible impacts on the mean diameter and length of the branches. The results were partly different from the previous reports on *Tectona grandis* (Chen, 2020), *Pseudotsuga menziesii* (Briggs et al., 2008), as well as *Picea abies* (Mäkinen et al., 2001). These reports all concluded that fertilization had a positive effect on the branch size. Branch diameter was directly correlated with the age and size of the trees. The *C. bungei* species under investigation was young (i.e., 6 years old), hence the influence of fertilization on branch growth was not fully reflected. As a tree ages, the effect of fertilization on mean branch diameter would progressively become apparent; however, for the largest branch in the crown, as branches with large diameters were



also longer, competition effects between trees first became apparent on the larger branches. Furthermore, the position of the main branch on the stem is crucial to forest managers since it may shed with serious knot-related issues. Fertilization decreased the height of the biggest branch in the current study. That is to say, trees in the fertilization stands gave lower branches a preference for nutrients, which facilitated their rapid growth. Hence, pruning at the appropriate time improves the quality of the wood at the most desirable stem portion (e.g., below 6 m in the stem).

Branch angle

The angle at which the branches are attached to the stem has a significant impact on the wood's quality and the shape of the crown (Kantola and Mäkelä, 2004). On a particular tree, the factors of gravity, light availability, and reaction wood production dominate in determining branch angle. Also, the social position of the trees in the stand can significantly affect the branch angle (Maguire et al., 1994; Weiskittel et al., 2007). Hence, branch position inside the crown and branch diameter had a major role in determining branch angle in this

study. The models used in the current study demonstrated that as branch height fell near the crown base, branch angles became flatter.

Steep branch angles can prolong the time that branch stubs are occluded, which can result in severe wood defects including discoloration and knots (Hein, 2008; Danescu et al., 2015; Wang et al., 2015). In this study, fertilization did not seem to have much of an impact on the mean branch angle. The results had also been acknowledged by studies on *Picea abies* (Mäkinen et al., 2001) and *Tectona grandis* (Chen, 2020). However, research on Scots pine had indicated that branch angle was only marginally correlated with site fertility and stand structure (Mäkinen and Uusvaara, 1992). These different results might be properly explained by their differences in age, branching habits of species, and other compound effects. In our study, The tree-level variance component of the mixed model explained a moderate part of the total variation in branch angle, i.e., branch angles within a tree were correlated and the between-tree differences could not be completely explained by the fixed tree or stand variables. This may be the effect of the moderate heritability of the branch angle (Haapanen et al., 1997).

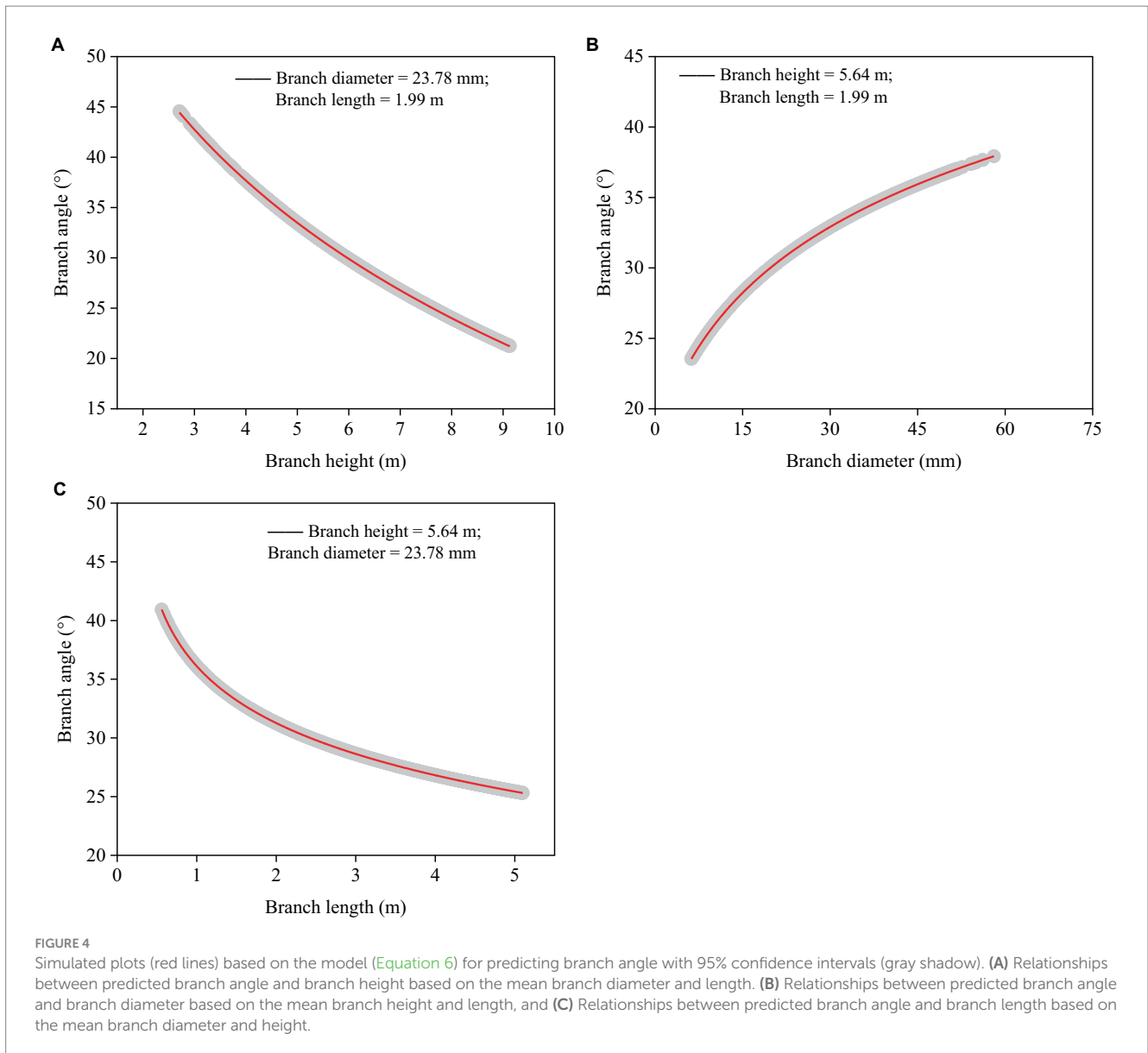


TABLE 7 The relationships between biomass of individual plant and growth index.

| Equations | | RSS | Adj- R^2 | F | p |
|-----------|---|---------|------------|--------|----------|
| (7) | $TB = -169.27 + 29.53 \times H$ | 3121.35 | 0.53 | 20.22 | 0.00036 |
| (8) | $TB = -132.40 + 17.30 \times DBH$ | 352.63 | 0.95 | 304.61 | <0.00001 |
| (9) | $TB = 17.32 + 25.83 \times CW$ | 4382.91 | 0.34 | 9.79 | 0.00647 |
| (10) | $TB = 318.21 - 314 \times (H:DBH)$ | 4054.34 | 0.39 | 11.88 | 0.00331 |
| (11) | $TB = -158.99 + 5.32 \times H + 15.64 \times DBH$ | 286.56 | 0.95 | 177.43 | <0.00001 |

H, DBH, CW, and H:DBH referred to tree height, diameter at breast height, crown width, and the ratio of H and DBH, respectively. TB, total biomass; RSS, residual sum of squares; Adj- R^2 , adjust R^2 .

Research limitation and prospect

The development of crown branches is influenced by a variety of factors, including site characteristics, stand density, management techniques, and tree growth potential. However, due to the limitations – a young stand age and a small number of sample trees – the models given are not suitable for widespread application. The impact of other aspects

must also be taken into account while creating a large-scale model. A future study based on more extensive data from various geographic regions is required to create models that might be broadly utilized.

Tree branches develop inconsistently at every age stage. The competition between branches for water, light, and nutrients intensifies as trees get older, which leads to natural pruning and inevitable disruption of the branch indexes. Furthermore, the size of

knots as well as the diameter, angle, and length of branches are significantly influenced by stand density. In the future, research on the development of large-diameter timber without knots in *C. bungei* plantations could focus on the importance of reasonable afforestation density and appropriate tending measures.

Conclusion

This study looked into the effects of several fertilization methods on the branch properties and tree growth. The biomass and development of *C. bungei* stands were positively impacted by fertilization. Water and fertilizer integration produced greater biomass and growth in comparison to hole fertilization. The number of live branches at age 6 years was greater on trees that had received HF and WF fertilization. Certain branch characteristics, like diameter, length, and angle, were not discovered to be significantly more sensitive to various fertilization regimes. Only the size and height of the largest branch, which was typically concerned with the quality of the wood at the lower stem section, were related to fertilization. With a high prediction accuracy and a clear understanding of the relationships and influencing variables between branch attributes, the mixed effect models of branches (including number, diameter, angle, and length) developed in this work might be utilized to forecast the dynamic evolution of the *C. bungei* crown. The established models could serve as a guide for producing high-quality wood from other valuable tree species in northern China.

Data availability statement

The original contributions presented in the study are included in the article/supplementary material, further inquiries can be directed to the corresponding authors.

Author contributions

ZG: Writing – original draft, Writing – review & editing. QZ: Conceptualization, Writing – original draft. TX: Conceptualization, Writing – original draft. DC: Data curation, Methodology, Writing – review & editing. YL: Formal analysis, Project administration, Writing – review & editing. QHa: Funding acquisition, Resources, Writing – review & editing. NL: Investigation, Software, Writing – review & editing. WM: Resources, Visualization, Writing – review & editing.

References

- Beaulieu, E., Schneider, R., Berninger, F., Ung, C., and Swift, D. E. (2011). Modeling jack pine branch characteristics in eastern Canada. *Forest Ecol. Manag.* 262, 1748–1757. doi: 10.1016/j.foreco.2011.06.054
- Briggs, D. G., Kantavichai, R., and Turnblom, E. C. (2008). Effect of precommercial thinning followed by a fertilization regime on branch diameter in coastal United States Douglas-fir plantations. *Can. J. For. Res.* 38, 1564–1575. doi: 10.1139/X07-199
- Calegario, N., Daniels, R. F., Maestri, R., and Neiva, R. (2005). Modeling dominant height growth based on nonlinear mixed-effects model: a clonal Eucalyptus plantation case study. *Forest Ecol. Manag.* 204, 11–21. doi: 10.1016/j.foreco.2004.07.051
- Chen, T. (2020). *Effects of Planting Density and Fertilization on the Growth and Branch Development of Teak (Tectona grandis L.f.) Clones. Dissertation.* Chinese Academy of Forestry, Beijing.
- Colin, F., and Houllier, F. (1992). Branchiness of Norway spruce in northeastern France: predicting the main crown characteristics from usual tree measurements. *Ann. Sci. For.* 49, 511–538. doi: 10.1051/forest:19920506
- Courbet, F., Hervé, J., Klein, E. K., and Colin, F. (2012). Diameter and death of whorl and interwhorl branches in atlas cedar (*Cedrus atlantica* Manetti): a model accounting for acrotony. *Ann. Forest Sci.* 69, 125–138. doi: 10.1007/s13595-011-0156-1
- Courbet, F., Sabatler, S., and Guédon, Y. (2007). Predicting the vertical location of branches along atlas cedar stem (*Cedrus atlantica* Manetti) in relation to annual shoot length. *Ann. Forest Sci.* 64, 707–718. doi: 10.1051/forest:2007051
- Danescu, A., Ehring, A., Bauhus, J., Albrecht, A., and Hein, S. (2015). Modelling discoloration and duration of branch occlusion following green pruning in *Acer*

JW: Resources, Visualization, Writing – review & editing. YS: Methodology, Supervision, Writing – review & editing. JL: Writing – review & editing. QQ: Writing – review & editing. QHe: Writing – review & editing.

Funding

The author(s) declare financial support was received for the research, authorship, and/or publication of this article. The research was supported by the National Key Research and Development Program of China (2017YFD0600604 and 2017YFD060060404).

Acknowledgments

The author thanks QH for her assistance in experimental design and revise. We also thank the Guangdong Key Laboratory for Innovative Development and Utilization of Forest Plant Germplasm, College of Forestry and Landscape Architecture, South China Agricultural University.

Conflict of interest

The authors declare that the research was conducted in the absence of any commercial or financial relationships that could be construed as a potential conflict of interest.

Publisher's note

All claims expressed in this article are solely those of the authors and do not necessarily represent those of their affiliated organizations, or those of the publisher, the editors and the reviewers. Any product that may be evaluated in this article, or claim that may be made by its manufacturer, is not guaranteed or endorsed by the publisher.

Supplementary material

The Supplementary material for this article can be found online at: <https://www.frontiersin.org/articles/10.3389/ffgc.2024.1261310/full#supplementary-material>

- pseudoplatanus* and *Fraxinus excelsior*. *Forest Ecol. Manag.* 335, 87–98. doi: 10.1016/j.foreco.2014.09.027
- Dong, L., Liu, Z., Li, F., and Jiang, L. (2013). Primary branch size of *Pinus koraiensis* plantation: a prediction based on linear mixed effect model. *Chin. J. Appl. Ecol.* 24, 2447–2456. doi: 10.13287/j.1001-9332.2013.0490
- Fang, Z., and Bailey, R. L. (2001). Nonlinear mixed effects modeling for slash pine dominant height growth following intensive silvicultural treatments. *For. Sci.* 47, 287–300. doi: 10.1046/j.1439-0329.2001.00240.x
- Forrester, D. I., Collopy, J. J., Beadle, C. L., and Baker, T. G. (2012). Interactive effects of simultaneously applied thinning, pruning and fertiliser application treatments on growth, biomass production and crown architecture in a young *Eucalyptus nitens* plantation. *Forest Ecol. Manag.* 267, 104–116. doi: 10.1016/j.foreco.2011.11.039
- Gao, Z., Wang, X., Li, H., and Zhang, P. (2014). An optimal model of the *Cunninghamia lanceolata* branch diameter in Fujian Province. *J. Northeast Forest. Univ.* 42, 23–27. doi: 10.13759/j.cnki.dlxb.20140721.018
- Guan, Z., Lu, Q., Lin, Y., Lin, D., Lu, Y., Han, Q., et al. (2022). Spatial variations and pools of non-structural carbohydrates in young *Catalpa bungei* undergoing different fertilization regimes. *Front. Plant Sci.* 13:1010178. doi: 10.3389/fpls.2022.1010178
- Haapanen, M., Velling, P., and Annala, M. (1997). Progeny trial estimates of genetic parameters for growth and quality traits in scots pine. *Silva Fenn.* 31, 3–12. doi: 10.14214/sf.a8506
- Hein, S. (2008). Knot attributes and occlusion of naturally pruned branches of *Fagus sylvatica*. *Forest Ecol. Manag.* 256, 2046–2057. doi: 10.1016/j.foreco.2008.07.033
- Hein, S., Makinen, H., Yue, C., and Kohnle, U. (2007). Modelling branch characteristics of Norway spruce from wide spacings in Germany. *Forest Ecol. Manag.* 242, 155–164. doi: 10.1016/j.foreco.2007.01.014
- Hein, S., Weiskittel, A. R., and Kohnle, U. (2008). Branch characteristics of widely spaced Douglas-fir in South-Western Germany: comparisons of modelling approaches and geographic regions. *Forest Ecol. Manag.* 256, 1064–1079. doi: 10.1016/j.foreco.2008.06.009
- Jia, W., Luo, T., and Li, F. (2021). Branch density model for *Pinus koraiensis* plantation based on thinning effects. *J. Beijing Forest. Univ.* 43, 10–21. doi: 10.12171/j.1000-1522.20200057
- Jiang, L., Du, S., and Li, F. (2011). Simulation of *Larix gmelinii* tree volume growth based on random effect. *Chin. J. Appl. Ecol.* 22, 2936–2969. doi: 10.13287/j.1001-9332.2011.0414
- Jiang, L., Li, F., and Zhang, R. (2012). Modeling branch diameter with linear mixed effects for Dahurian larch. *For. Res.* 25, 464–469. doi: 10.13275/j.cnki.lykxyj.2012.04.013
- Jiang, L., and Liu, R. (2011). A stem taper model with nonlinear mixed effects for Dahurian larch. *Sci. Silvae Sinicae* 19, 338–341. doi: 10.3724/SPJ.1011.2011.00338
- Kantola, A., and Mäkelä, A. (2004). Crown development in Norway spruce [*Picea abies* (L.) karst.]. *Trees* 18, 408–421. doi: 10.1007/s00468-004-0319-x
- Kellomäki, S., and Tuimala, A. (1981). Effect of stand density on branchiness of young scots pine. *Folia Forestalia* 478, 1–27.
- Klang, F., and Ekö, P. (1999). Tree properties and yield of *Picea abies* planted in shelterwoods. *Scand. J. Forest Res.* 14, 262–269. doi: 10.1080/02827589950152782
- Lei, X., Li, Y., and Xiang, W. (2009). Individual basal area growth model using multi-level linear mixed model with repeated measures. *Sci. Silvae Sinicae* 45, 74–79. doi: 10.1007/978-1-4020-9623-5_5
- Li, C. (2011). Using random intercept effects in DBH increment model of individual trees for fir plantation. *J. Beijing Forest. Univ.* 33, 7–12. doi: 10.13332/j.1000-1522.2011.04.022
- Li, C., and Tang, S. (2010). The basal area model of mixed stands of *Larix olgensis*, *Abies nephrolepis* and *Picea jezoensis* based on nonlinear mixed model. *Sci. Silvae Sinicae* 36, 474–477. doi: 10.3724/SPJ.1238.2010.00474
- Li, F. (2004). Modeling crown profile of *Larix olgensis* trees. *Sci. Silvae Sinicae* 32, 105–127. doi: 10.1016/j.jce.2003.10.003
- Li, Y., Liu, X., Fang, H., Shi, L., Yue, X., and Yang, Q. (2021). Exploring the coupling mode of irrigation method and fertilization rate for improving growth and water-fertilizer use efficiency of young mango tree. *Sci. Hortic Amsterdam* 286:110211. doi: 10.1016/j.scienta.2021.110211
- Liu, Z., Shu, Y., and Li, F. (2008). Modeling for primary branch length and branch diameter of Mongolian scots pine trees. *Bull. Botanical Res.* 28, 244–247.
- Ma, F., Liu, Y., Cui, J., Fan, H., Lu, Y., and Li, M. (2019). Review on the research progress of water and fertilizer integration. *Xinjiang Agric. Sci.* 56, 183–192. doi: 10.6048/j.issn.1001-4330.2019.01.022
- Maguire, D. A., Johnston, S. R., and Cahill, J. (1999). Predicting branch diameters on second-growth Douglas-fir from tree-level descriptors. *Can. J. For. Res.* 29, 1829–1840. doi: 10.1139/x99-147
- Maguire, D. A., Moeur, M., and Bennett, W. S. (1994). Models for describing basal diameter and vertical distribution of primary branches in young Douglas-fir. *Forest Ecol. Manag.* 63, 23–55. doi: 10.1016/0378-1127(94)90245-3
- Mäkinen, H., Saranpää, P., and Linder, S. (2001). Effect of nutrient optimization on branch characteristics in *Picea abies* (L.) karst. *Scand. J. For. Res.* 16, 354–362. doi: 10.1080/02827580120345
- Mäkinen, H., and Uusvaara, O. (1992). *Effect of Fertilization on the Branchiness and the Wood Quality of Scots Pine*. The Finnish Forest Research Institute, Folia Forestalia.
- Meredieu, C., Colin, F., and Hervé, J. (1998). Modelling branchiness of Corsican pine with mixed-effect models (*Pinus nigra* Arnold ssp. laricio (Poiret) Maire). *Ann. Forest Sci.* 55, 359–374. doi: 10.1051/forest:19980307
- Nelson, A. S., Weiskittel, A. R., and Wagner, R. G. (2014). Development of branch, crown, and vertical distribution leaf area models for contrasting hardwood species in Maine, USA. *Trees* 28, 17–30. doi: 10.1007/s00468-013-0926-5
- Newton, M., Lachenbruch, B., Robbins, J. M., and Cole, E. C. (2012). Branch diameter and longevity linked to plantation spacing and rectangularity in young Douglas-fir. *Forest Ecol. Manag.* 266, 75–82. doi: 10.1016/j.foreco.2011.11.009
- Pinkard, E. A. (2002). Effects of pattern and severity of pruning on growth and branch development of pre-canopy closure *Eucalyptus nitens*. *Forest Ecol. Manag.* 157, 217–230. doi: 10.1016/S0378-1127(00)00647-2
- Tumushime, I., Vogel, J. G., Minor, M. N., and Jokela, E. J. (2019). Effects of fertilization and competition control on tree growth and C, N, and P dynamics in a loblolly pine plantation in north Central Florida. *Soil Sci. Soc. Am. J.* 83, 242–251. doi: 10.2136/sssaj2018.08.0289
- Wang, C., Hein, S., Zhao, Z., Guo, J., and Zeng, J. (2016). Branch occlusion and discoloration of *Betula alnoides* under artificial and natural pruning. *Forest Ecol. Manag.* 375, 200–210. doi: 10.1016/j.foreco.2016.05.027
- Wang, C., Tang, C., Hein, S., Guo, J., Zhao, Z., and Zeng, J. (2018). Branch development of five-year-old *Betula alnoides* plantations in response to planting density. *Forests* 9:42. doi: 10.3390/f9010042
- Wang, C., and Zeng, J. (2016). Research advances in forest tree pruning. *World Forest. Res.* 29, 65–70. doi: 10.13348/j.cnki.sjlyyj.2016.03.006
- Wang, C., Zeng, J., Hein, S., Zhao, Z., Guo, J., and Zeng, J. (2017). Crown and branch attributes of mid-aged *Betula alnoides* plantations in response to planting density. *Scand. J. Forest Res.* 32, 679–687. doi: 10.1080/02827581.2016.1261936
- Wang, C., Zhao, Z., Hein, S., Zeng, J., Schuler, J., Guo, J., et al. (2015). Effect of planting density on knot attributes and branch occlusion of *Betula alnoides* under natural pruning in southern China. *Forests* 6, 1343–1361. doi: 10.3390/f6041343
- Weiskittel, A. R., Maguire, D. A., and Monserud, R. A. (2007). Modeling crown structural responses to competing vegetation control, thinning, fertilization, and Swiss needle cast in coastal Douglas-fir of the Pacific northwest, USA. *Forest Ecol. Manag.* 245, 96–109. doi: 10.1016/j.foreco.2007.04.002
- Yang, L. H., and Karban, R. (2019). The effects of pulsed fertilization and chronic herbivory by periodical cicadas on tree growth. *Ecology* 100:e2705. doi: 10.1002/ecy.2705

Frontiers in Forests and Global Change

Informs and promotes sustainable management
of the world's forests

An innovative journal that places forests at the
forefront of attention for scientists, policy makers
and the public. It advances our understanding of
how forests 'work', spanning from molecules to
ecosystems to the biosphere.

Discover the latest Research Topics

[See more →](#)

Frontiers

Avenue du Tribunal-Fédéral 34
1005 Lausanne, Switzerland
frontiersin.org

Contact us

+41 (0)21 510 17 00
frontiersin.org/about/contact

